High Resolution Rotational Spectroscopic Studies of the Dynamics and Conformations of Dispersion and Hydrogen Bonded Molecular Complexes

by

Bowei Wu

A thesis submitted in partial fulfillment of the requirements for the degree of

Doctor of Philosophy

Department of Chemistry
University of Alberta

Abstract

High resolution rotational spectra of non-covalently bonded molecular clusters produced in a supersonic jet expansion can provide detailed and rich information about their structure-energy relationship and dynamical behaviors. In this thesis, several non-covalently bonded molecular clusters which contain water and/or fluoroalcohols, two important types of solvents, were investigated using a cavity based and two chirped pulse (CP) Fourier transform microwave (FTMW) spectrometers. The experimental spectroscopic studies were aided by high level density-functional theory (DFT) calculations to reveal the complex conformational landscapes of the systems and to understand the effects of large amplitude motions in these systems. The specific results and conclusions of these systems are summarized below.

For pyrrole⋯water, we applied a recently developed semiempirical tight-binding quantum chemistry conformational searching program and DFT calculations to identify possible low energy conformers of the pyrrole-water complex which feature σ- and π-type hydrogen-bonding interactions. Rotational spectra of all monosubstituted ^{13}C isotopologues of pyrrole-water in their natural abundances were measured and assigned, including the ^{14}N nuclear quadrupole hyperfine splittings and water tunneling doublets. Moreover, the potential energy surface (PES) scans along the water-centered large

amplitude motions were also carried out and the interconversion paths among the four previously proposed pyrrole-water geometries identified. The theoretical investigation together with the additional ^{13}C experimental data allow one to confidently identify the ground state global minimum geometry and also estimate the water tunneling barrier.

Two other water-containing complexes, i.e., 1,1,1,3,3,3-hexafluoropropan-2-ol (HFIP)$\cdots$water 2,2,3,3,3-pentafluoro-1-propanol (PFP)$\cdots$water were also investigated using rotational spectroscopy. In the first case, a previously unidentified, higher energy conformer, namely *gauche* HFIP (HFIP$_g$)$\cdots$water was recognized. To confirm the identity of this new isomer, rotational spectra of seven of its deuterated species were also measured and analyzed. Both the experimental and theoretical pieces of evidence indicate that the intermolecular interaction with water preferentially stabilizes the HFIP$_g$ monomer configuration over the global minimum configuration, HFIP$_t$. In the second case, rotational spectra of two PFP$\cdots$water conformers, **PFP***G*+*g*+$\cdots$W$_H$ and **PFP***Tg*+$\cdots$W$_H$, and seven deuterated isotopologues of each, were assigned. Tunneling splittings were observed for both conformers and are attributed to the exchange of the bonded and non-bonded hydrogen atoms of water. Overall, these fluoroalcohol monohydrates exhibit even more complicated conformational landscapes and dynamics of water-centered large amplitude motions than pyrrole$\cdots$water. The large amplitude motions associated with the water subunits were examined in detail to explain the very different magnitudes of the experimental and theoretical permanent electric dipole moment components. The studies highlight the challenge in correctly identifying the conformers observed when large amplitude motions are involved.

The complexity of the conformational landscape increases noticeably when moving onto the PFP dimer. Nearly 80 stable, binary PFP geometries were identified in the theoretical search where ten of them are within a narrow energy window of ~1 kJ mol^{-1}, highlighting the structural diversity of the system. For the corresponding PFP monomer, the two most stable monomeric PFP mirror imaged pairs, i.e., **PFP***G+g+/G-g-* and **PFP***Tg+/Tg-* were observed and the associated large tunneling splittings in the rotational spectrum of **PFP***Tg+/Tg-* were analyzed in detail. The five most stable binary conformers predicted were also the ones observed experimentally. On the other hand, some other similarly low energy conformers were not observed. A combined kinetic and thermodynamic model was proposed to explain the observation or non-observation of low energy conformers, and the analysis was further verified by the 'argon test'. The non-covalent intermolecular interactions of PFP and its binary conformers are also discussed with the aid of quantum theory of atoms in molecule (QTAIM) and non-covalent interaction (NCI) analyses, as well as the effects of fluorination by comparing to 1-propanol and its dimers.

While the above molecular systems are mainly bound by hydrogen bonding interactions, we also investigated the HFIP⋯Ne and Ar binary complexes where the non-covalent intermolecular interactions are dominated by dispersion interactions. Rotational spectra of these two complexes including several isotopic species containing ^{20}Ne, ^{22}Ne, ^{40}Ar, ^{13}C, and hydroxyl D, were assigned. While multiple conformers were often detected in the hydrogen bonded systems reported above, only one isomer was detected for each species here, corresponding to the most stable one predicted. The QTAIM and electrostatic potential (ESP) calculations were employed to examine different rare gas binding sites at HFIP and the influence of fluorination since isopropanol⋯Ne and ⋯Ar, the non-fluorinated counter parts, exhibit much different binding topologies.

Preface

This thesis is based on the research work I have done at the University of Alberta between September 2017 and April 2022. The nature and extent of my contributions to the research work has been included in the thesis are briefly summarized below.

Chapter 3 of this thesis has been published as B. Wu, F. Xie. and Y. Xu, “The pyrrole-water complex: Multidimensional large amplitude dynamics and rotational spectra of its ^{13}C isotopologues", *J. Mol. Spectrosc.* **2020***, 374,* 111381*.* I was responsible for the data collection and further data analyses and wrote the first draft of the manuscript. Dr. Fan Xie assisted in the theoretical calculations and manuscript edits. Dr. Javix Thomas involved in the early stage of the calculations and Dr. Nathan A. Seifert helped with the 2–6 GHz CP-FTMW measurement. Professor Y. Xu was the supervisory author and was involved in the conceptualization, funding acquisition, supervision, and writing the draft and its review and editing.

Chapter 4 of this thesis has been published as as B. Wu, A. S. Hazrah, N. A. Seifert, S. Oswald, W. Jäger, Yunjie Xu, "A higher energy hexafluoroisopropanol⋯water isomer and its large amplitude motions: rotational spectra and DFT calculations", *J. Phys. Chem. A*. **2021**, *125*, 10401−10409. I was responsible for the data collection, assignment and analyses, original draft, review & editing. Arsh S. Harzrah contributed to data collection and analyses. Dr. Nathan A. Seifert helped with data collection and initial assignment. Dr. Sönke Oswald involved in initial calculation and data summary. Professor Wolfgang Jäger provided assistance in the experiments, funding acquisition, review and editing. Professor Yunjie Xu was the supervisory author and was involved in conceptualization, funding acquisition, supervision, analyses, original draft, review and editing.

Chapter 5 of this thesis has been published as B. Wu, N. A. Seifert, S. Oswald, W. Jäger, and Y. Xu, “Rotational Spectrum and Molecular Structures of the Binary Aggregates of 1,1,1,3,3,3-Hexafluoro-2-propanol with Ne and Ar”, *J. Phys. Chem. A.* **2021**, *125*, 5355-5364. I was responsible for the data collection, assignments, analyses, and writing the first draft of the manuscript and its review and editing. Dr. Nathan A. Seifert contributed to data collection and spectral assignment. Dr. Sönke Oswald contributed to calculation and data summary. Professor Wolfgang Jäger provided assistance in the experiments and took part in funding acquisition, review, and editing. Professor Yunjie Xu was the supervisory author and was involved in the conceptualization, funding acquisition, supervision, and writing the draft and its review and editing.

Chapter 6 of this thesis is the original draft contributed by Bowei Wu, Nathan A. Seifert, Aran Insausti, Jiarui Ma, Sönke Oswald, Wolfgang Jäger and Yunjie Xu on

“2,2,3,3,3-pentafluoro-1-propanol and its five dimers: structural diversity, conformational conversion, and tunneling motion”, and is planned to be submitted to *Phys. Chem. Chem. Phys.* I was responsible for the data collection, assignments and analyses, writing the first draft of the manuscript and its review and editing. Dr. Nathan A. Seifert contributed to data collection and spectral assignment. Aran Insausti contributed the spectral assignments of the **PFP***Tg+* monomer. Jiarui Ma contributed to data collection. Dr. Sönke Oswald contributed to calculation and data summary. Professor Wolfgang Jäger assisted in the experiments and took part in funding acquisition, review, and editing. Professor Yunjie Xu was the supervisory author and was involved in the conceptualization, funding acquisition, supervision, and writing the draft and its review and editing.

Chapter 7 of this thesis is the original draft contributed by B. Wu, N. A. Seifert, S. Oswald, W. Jäger, and Y. Xu, on “Rotational Spectroscopy of the 2,2,3,3,3-Pentafluoropropanol··· Water Complex: Conformations and Large Amplitude Motions” and is planned to be submitted to *ChemPhysChem.* I was responsible for the data collection, assignments and analyses, writing the first draft of the manuscript and its review and editing. Dr. Nathan A. Seifert and Dr. Sönke Oswald contributed to calculation and data summary. Professor Wolfgang Jäger provided assistance in the experiments and took part in funding acquisition, review, and editing. Professor Yunjie Xu was the supervisory author and was involved in the conceptualization, funding acquisition, supervision, and writing the draft and its review and editing.

Dedicated to:

My parents especially my loving mother

Acknowledgements

First of all, I thank my parents especially to my mother for her everlasting support, which greatly helped me to overcome the countless hard times I faced in Canada by myself, through my bridging MBA course in Langley, Vancouver in B.C., my M.Sc. in London, Ontario and PhD program in Edmonton, Alberta for a total time of 7 years.

I would like to appreciate my heartfelt thanks to several wonderful people who have helped me throughout my PhD program, by their heartwarming guidance and support.

" Man should venerate his mentor and be in touch with his friends."

(Xunzi, ancient Chinese scholar)

I express my deepest and sincerest gratitude from my heart to Prof. Yunjie Xu, who has been such patient, stimulative and supportive supervisor. She is so energetic and enthusiastic in academic research, and I may not be able to achieve my academic research goals so smoothly and confidently here in University of Alberta without her continuous supervising and guidance. I thank you for triggering my curiosity, persistence, wisdom and showing me the attitudes, clear logical thinking and methodology for completing excellent work. Along with her warm cares to me, all those would be the greatest gift in my future work and life.

I also would like to thank Prof. Wolfgang Jäger, for all his support in experimental techniques and critical thinking. I thank him for providing many valuable opportunities for academic discussions on scientific questions and practical tips and comments in giving good presentations.

I also express my sincere gratitude to Professor Yoram Apelblat and to the Chemistry Undergraduate Store technician, Dr. Margaret Sisley, for their help when I performed my TA laboratory duties.

I am grateful to Prof. Arthur Mar and Prof. Alex Brown for agreeing readily to be my supervisory committee members, and their helps during my hard times in 2021. I wish to express my deep gratitude also to Prof. Gabriel Hanna from the Physical/Computational Division, Prof. Li Liang from the Analytical Division, Department of Chemistry, University of Alberta, and Prof. Maria Eugenia Sanz from Department of Chemistry, King's Collage, London, U.K. for serving as the examiners in my defense. I am also grateful to Prof. Julianne M. Gibbs for her advising and assistance when I initially started my PhD program.

I also thank Dr. Sönke Oswald, who provided me great guidance in the initial days of my research work in 2018 when he was here for his visiting research work. I express my special thanks to Dr. Nathan A. Seifert, our post-doctoral alumnus, who assisted me a lot with the theories and techniques of the microwave instruments. Also, many thanks to Dr. Mattias Heger, the post-doctoral fellow in our group, who explained and provided many tips and assistance with the Python codes and programming.

I would like to express my gratitude to Dr. Tao Lu, who visited us from 2019 to 2020 for a year as a visiting PhD student. We had cooperated in many projects and special thanks to him for passing me his rich experiences in the microwave field.

I am also thankful to all my amazing friends and group members, Yanqing Yang (Ryan), Dr. Fan Xie, Arsh S. Hazrah, Molhamond, Guojie Li, Haolu Wang, Qian Yang, Jiarui Ma, Ziqi Li, Teng Cheong (Emily), Yan Li, Jiayi Li, and many others for all their friendship and support.

I am also much appreciating those graduate students who were in the same TA team with me and did me many favors. A special note of thanks to Jocelyn Sinclair and Ming Lv, who always supported me when I needed.

A special thanks to Rainey Lu who provided supreme touring trips for me when I was initially and lastly landed on Vancouver, B.C., keeping in touch during the time before my arrival and departure of Canada until now. There are not many chances to have such a good friend.

I also wish to acknowledge my uncle Y. Chai for his emotional supports to me.

This research is funded by the University of Alberta, the Natural Sciences and Engineering Research Council (NSERC) of Canada, the Canada Research Chairs Program, and the H. E. Gunning Research Fellowships. Access to the computing facilities of the Western Canada Research Grid (Westgrid), the Shared Hierarchical Academic Research Computing Network (SHARCNET: www.sharcnet.ca), and Compute/Calcul Canada is also acknowledged.

Table of Contents

List of Tables

List of Figures

List of Symbols

A, B, C	Rotational constants
ΔD_e	Relative raw dissociation energies
ΔD_0	Corrected dissociation energies
D_J, D_{JK}, D_K, d_1, d_2	Quartic distortion constants for Watson's S-reduction
E	Strength of external electric filed
E_{dist}	Deformation energies
E_{int}	Interaction energies
ΔE_{rot}	Rotational energy difference
ΔE_{conf}	Conformation energy
F	Effective rotational constant of a top
F_0	Internal rotor rotational constant of a top
H	Hamiltonian operator
H_0	Hamiltonian of the two-level system
H_{rot}	Rigid rotor Hamiltonian
$I_{\mathrm{a,b,c}}$	Moments of inertia along the a-, b-, and c-axes
J	Rotational quantum number
K	Projection of *J* onto the principal axis
K_{a}, (K_{c})	Quantum number at oblate (prolate) limit
K_B	Boltzmann constant
ΔN_0	Population difference
$P_{\mathrm{a,b,c}}$	Angular momentum on principal axes
P_{aa}, P_{bb}, P_{cc}	Planar Moments
S	Signal strength
S/N	Signal-to-noise ratio
T_{rot}	Rotational temperature
ν_{MW}	Microwave Frequency
β, γ	Euler angles

Δ_J, Δ_{JK}, Δ_K, δ_j, δ_k	Quartic distortion constants for Wartson's A-reduction
Θ	Bloch vector
$\mu_{a,b,c}$	Electric dipole moment components
μ_{ab}	Transition dipole moment
σ	Standard deviation
χ	Nuclear quadrupole coupling constant
ω	Transition frequency
Ω	Driving vector
$\hbar$	Reduced Planck constant

List of Abbreviations

a.u.	Arbitrary units
AWG	Arbitrary Waveform Generator
B3LYP	Becke, 3-parameter, Lee-Yang-Parr
BCP	Bond critical point
BSSE	Basis Set Superposition Energy
CP	Chirped Pulse
CREST	Conformer-Rotamer Ensemble Sampling Tool
D3BJ	Grimme's dispersion correction with Becke Johnson damping
DC	Direct Current
DFT	Density Functional Theory
ESP	ElectroStatic Potential maps
FID	Free Induction Decay
FTIR	Fourier Transform Infra-Red
FTMW	Fourier Transform Microwave Spectroscopy
FWHH	Full Width at Half Heigh
HF	Hartree-Fock
HFIP	2,2,2,3,3,3-hexafluoroisopropanol
LAM	Large Amplitude Motion
MW	Microwave
MP2	Møller-Plesset second order perturbation theory
NBO	Natural Bond-Order
NCI	Non-Covalent Interactions
NMR	Nuclear Magnetic Resonance
OSC	Oscilloscope
PES	Potential Energy Surface
PMIFST	Principal Moments of Inertia From STructure
PFP	2,2,3,3,3-pentafluoro-1-propanol
QTAIM	Quantum theory of atoms in molecules

QZVP	Quadruple Zeta Valence Polarization
RG	Rare Gas
ROA	Raman Optical Actively
RWA	Rotating Wave Approximation
STRFIT	STRucture FITting to rotational data
SMA	Sub-Miniature-A
TTL	Transistor-Transistor Logic
TWT	Traveling-wave tube amplifier
TZVP	Triple Zeta Valence Polarization
VCD	Vibrational Circular Dichroism
VMD	Visual Molecular Dynamics
xTB	A tight bonding semiempirical quantum chemical method
ZPE	Zero Point Vibrational Energy

Chapter 1

Introduction

“Nothing is softer or more flexible than water, yet nothing can resist it.” – Lao Tzu

1.1 General Overview

No one would deny that water is the most essential and vital substance on earth that help to facilitates everyday activities. Water creates and supports lives on the earth, but we still do not know a lot about the properties of water although water may have been the mostly studied substance.[1-3] For example, rotational spectroscopic studies reveal that when water aggregates, there are a diverse range of geometries that an aggregate can take on.[4-7] It would be interesting to probe how water interact with other molecules at the molecular level.

Meanwhile, in industries, fluoroalcohols are widely used as solvents in industry for organic syntheses and in many cases they also serve as catalysts to boost production efficiency. There are two sides of the story with regard to fluorinated alcohols: on one hand, they are widely regarded as remarkable catalysts[8] or even magical solvents[9,10] to boost industrial productions; on the other hand, fluoroalcohols are considered greenhouse pollutants with large global warming potentials because of their radiative activity in the mid-infrared region.[11,12] In addition, fluorinated alcohols are also often used as a peptide (or protein) co-solvent with water and show unusually interesting properties with great influence on the structural arrangement of a peptide (or protein).[10,14,15] For example, 2,2,2,3,3,3-Hexafluoroisopropanol (HFIP) can unfold the original structure of β-lactoglobulin, a predominantly β-sheet protein, and induce the formation of its α-helical structure.[16,17]

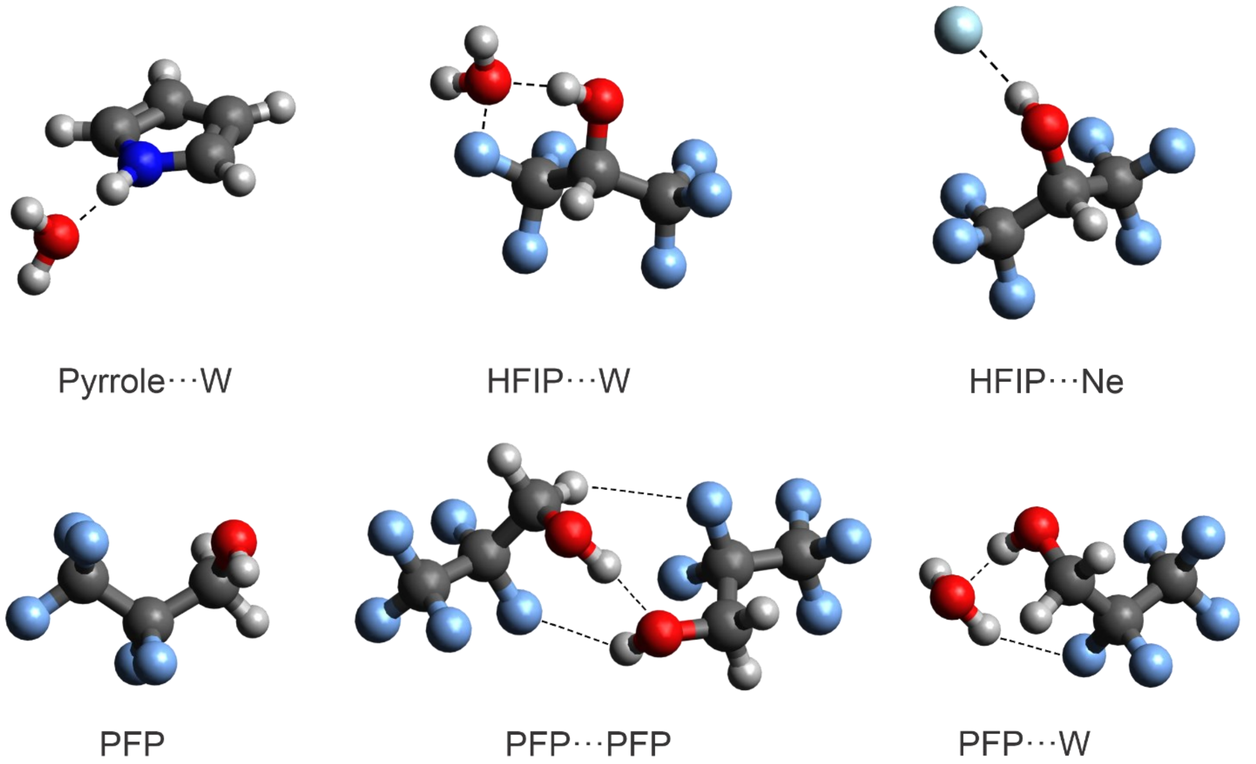

Pyrrole···W HFIP···W HFIP···Ne

PFP PFP···PFP PFP···W

Figure 1.1 Non-covalently bonded complexes investigated in this thesis.

Furthermore, the detailed mechanisms associated with the catalytic properties and the special co-solvent properties are so far not well understood. Some previous molecular dynamic studies[18] suggest that non-covalent interactions among fluoroalcohol molecules and with reactants or reaction intermediates are important for the catalytic properties of the fluoroalcohols. Thus, in this thesis, several fluoroalcohols and water are chosen as the main molecular targets. All the molecular systems investigated are summarized in Figure 1.1. The associated background information and the main motivation for studying these systems are described in the following subsections.

1.2. Studies of hydrogen-bonded fluoroalcohol aggregates using Fourier transform microwave spectroscopy

Hydrogen bonding interactions exist everywhere in the mother nature. It is one of the fundamental and critical interactions to make the earth filled with lives. One famous example is the double helix shape of DNA in living creatures are kept by hydrogen bonding interactions.[19] The hydrogen bonding interaction is relatively strong among the non-covalent intermolecular interactions in a general form of Y···H-X, where the Y and X are non-metal elements. Considering its importance in many fields of science, complexes involved with hydrogen bonding interaction have been intensively studied by many different spectroscopic techniques, such as Fourier-transform infrared (FTIR) spectroscopy,[20,21] solid-state and solution nuclear magnetic resonance (NMR) spectroscopy,[22-25] X-ray crystallography studies,[26,27] and Raman optical actively spectroscopy (ROA) [28,29] and VCD[30-33] spectroscopy in solution and in rare gas matrices.

Jet-cooled rotational spectroscopy has been used extensively to probe hydrogen bonding and other non-covalent interactions in isolated molecular clusters of the gas phase.[34-37] Because of its high sensitivity and high resolution, jet-cooled rotational spectroscopy can distinguish conformers with only minor structural differences, for example multiple conformers of the macrocycle gyclododecannone,[38] of propylene oxide homo- and heterochiral dimer [39] and trimer.[40] Our research group has worked on rotational spectroscopy of non-covalently bonded complexes which contain fluoroalcohols for many years, for example 2,2,2-trifluoroethanol (TFE)[41] and monofluoroethanol (MFE)[42] with propylene oxide, exploring transient chirality associated with these fluoroalcohols. Directly linked to the current thesis work are the jet-cooled rotational spectroscopic studies of hydrogen bonded aggregates of some simple fluoroalcohols such as binary,[43-

[45] ternary,[46-49] and tetrameric[50] clusters of 2,2,2-trifluoroethanol (TFE), monofluoroethanol (MFE), and HFIP, as well as their derivatives as such as 1-phenyl-2,2,2-trifluoroethanol and associated complexes.[51,52] In general, these studies focused on how hydrogen bonding interaction alters the conformational preference of the fluoroalcohols. Interestingly, often the abundances of the least stable or even non-stable monomeric unit in their isolated forms increase noticeably in the larger hydrogen bonded clusters, offering a glimpse of possible aggregations in the bulk phase. 2,2,3,3,3-pentafluoro-1-propanol (PFP), the system studied in this thesis, has a longer fluorocarbon chain and exhibits additional flexibility associated with the heavy atom frame. One main goal is to probe how the preferred conformations in the isolated PFP monomer change with the non-covalent interactions with another PFP molecule. This study may also provide some insight into the bulk property of PFP. In addition, we want to examine the conformational landscape of the binary PFP complex using conformer specific rotational spectroscopy and compare the experimental results with the structure-energy relationship predicted theoretically to benchmark theoretical calculations.

1.3. Rotational studies of the water-pyrrole and water-fluoroalcohol complexes

Complexes between water and (aromatic) organic molecules have also been a subject of considerably interest in the rotational spectroscopy community. For example, there has been many reports on the benzene···water dimer over the years to understand the nature of the interaction which features an O-H···π bond and the complicated dynamics associated with the dimer.[53,54] More recently, Melandri and co-workers reported that in the hexafluorobenzene···water dimer, the main interaction is replaced by a lone pair···π-hole bond.[55] Another recent focus is on the non-covalent interaction of water with volatile organic compounds such as pyruvic acid and limonene since such interactions may play a role in the formation of secondary organic aerosol.[56,57]

In my thesis research, I examined the binary complexes between water and three organic molecules, i.e., pyrrole, HFIP and PFP. The pyrrole-water complex was investigated in 1993 using Fourier transform microwave (FTMW) spectroscopy and only σ-hydrogen bonded complex was detected experimentally.[58] There was some ambiguity about the most stable geometry of this complex.

In the case of HFIP···water, one conformer was reported in a previous rotational spectroscopic study using a cavity-based Fourier transform microwave spectrometer.[60] Utilizing a broadband chirped pulsed Fourier transform microwave (CP-FTMW) spectrometer which was completed[59,60] during my PhD study, I aimed to explore the conformational space of this complex more completely taking advantage of the broadband scanning power of the CP-FTMW instrument[61] and the recently developed conformer search tools, such as the Conformer–Rotamer Ensemble Sampling Tool (CREST) developed by Grimme and co-workers.[62,63] These two main tools will be described in more detail in Chapter 2.

The PFP···water complex was investigated for the first time in this thesis. The main motivation was to examine the conformational space and identify the most stable conformers experimentally. Another motivation was to identify conformational conversion paths to explain the observation and non-observation of the conformers predicted. This is important to address the effect of a supersonic jet expansion on the relative abundances of different conformers and come up with some kinetic + thermodynamic models to adequately address the experimental abundant distributions.

Finally, a common scientific point to be addressed in all these water containing complexes is water-centered large amplitude motions (LAMs) including the tunneling motions. In the early high resolution spectroscopic studies of simple complexes containing rare gas atoms and/or linear molecules, extremely flexible behaviors were detected, for example in helium$_n$···OCS and in helium$_n$···N_2O,[64-66] in Ar-CO, and in CO-N_2[67-69] where there is often not a well-defined geometry associated with the ground vibrational state and different rotational constants were used to describe for different rotational K-levels and some signatures of LAMs are imbedded in the nuclear quadrupole coupling splittings.[70,71] The analysis of the nuclear quadrupole coupling constants was utilized in the pyrrole···water study to extract insight into the LAMs. The situations with the water containing complexes, such as HFIP···water and PFP···water, are somewhat different. While the heavy atom frames are generally fixed, the two water hydrogen atoms can experience very LAMs, leading to noticeable differences between the experimental and predicted permanent electric dipole moment components[72,73] and some small but not negligible changes in rotational constants. I applied potential energy scans along some of these flexible coordinates to understand how these properties are being affected by LAMs. A general goal here is to develop a strategy to deal with LAMs so that one can identify the correct conformers responsible for the observed rotational transitions.

1.4 Rotational studies of the rare gas···HFIP complexes

Rotational spectroscopy has been applied to examine van der Waals complexes containing only rare gas atoms[74-76] and rare gas atom with simple linear molecules [77-79] or high symmetric molecules.[80] More recently, several MW research groups have reported combined rotational spectroscopic and theoretical studies of rare gas atom with different fluoro-compounds such as 1,3-difluorobezene,[81] 3,3,3-trifluoro-1,2,-expoxypropane[82] and 3-fluoro-1,2,-epoxypropane.[83] One main goal is to evaluate the effects of fluorination on these very subtle interactions such as the preferred binding cites and to benchmark the ability of the current theoretical calculations in capturing the correct most stable geometry because the energy differences among different conformers tends to be quite small, often less than 1 kJ mol^{-1}. Another motivation is to evaluate the contribution of dispersion forces versus others in the van der Waals complexes. The study of HFIP···Ne and ···Ar was motivated by similar ideas including whether such weak interactions could change the conformational preference of HFIP.

1.5 Outline of the thesis

The present thesis is divided into six chapters. Chapter 1, the current chapter, describes the motivation for the studies of the molecular systems included in this thesis.

Chapter 2 introduces details of the theoretical and experimental methods used in the thesis research. These include a brief overview of rotational spectroscopy, the two Fourier transform microwave (FTMW) spectrometers used in the studies, as well as the theoretical calculation methods utilized in this thesis work.

Chapter 3 reports my first FTMW spectroscopic study on the dynamics of the pyrrole⋯water complex. The goal of this study is to identify the real global minimum geometry of the pyrrole⋯water complex and to identify the possible conversion paths between four different configurations of the complex reported before.

Chapter 4 focuses on rotational spectroscopic investigation of HFIP⋯water. It describes an interesting case where binding to water allows the detection of a previously not detected HFIP conformation to be observed. In addition, the effects of fluorination for the interactions between a (fluorinated) alcohol and water were also evaluated and discussed.

Chapter 5 describes the study of the HFIP⋯rare gas complexes with the goal to identify the most stable geometries and use the experimental results to benchmark the theoretical calculations. The isotopologues species of the HFIP⋯Ne complex were also studied to assist the identification of the most preferred geometry.

Chapter 6 presents the investigations on the PFP monomer and dimer. The pathways of transformation between two observed species and other unstable, high-energy conformers were also explored via carrying out 2-dimentional PES scans. As for the five PFP homodimers, their assignments were given, along with topology studies by conducting NCI and QTAIM analyses at high level of DFT theory.

Chapter 7 shows the research work on the PFP⋯water complex using both rotational spectroscopy and theoretical modeling. Rotational spectra of an extensive list of the deuterated species were measured and analyzed to help with the topology analyses. The electrostatic potential mappings of the different PFP configurations were utilized for identifying the preferred binding sites from water to PFP, also compared with non-fluorinated propanol counterpart.

Chapter 8, the final chapter of my thesis, summarizes the general conclusions of the thesis work, together with possible future work to extend current research projects.

Appendices (Supporting Information) are also attached to the end of this thesis. An up-to-date CV is also attached to the very end of the thesis.

References

1. Angell C.A. (1982) in *Water: A Comprehensive Treatise*, Prenum Press, New York, **1972,** *1*, 151.
2. Debenedetti, P. Stanley H., *Physics Today* **2003,** *56*,40–46.
3. Mishima, O.; Stanley, H. E., *Nature* **1998,** *396*, 329-335.
4. Pérez, C.; Lobsiger, S.; Seifert, N. A.; Zaleski, D. P.; Temelso, B.; Shields, G. C.; Kisiel, Z.; Pate, B. H., *Chem. Phys. Lett.* **2013,** *571*, 1-15.
5. Pérez, C.; Zaleski, D. P.; Seifert, N. A.; Temelso, B.; Shields, G. C.; Kisiel, Z.; Pate, B. H., *Angew. Chem. Int.* **2014,** *53*, 14368-14372. *Angew. Chem.* **2014,** *126*, 14596-14600.
6. Pérez, C.; Muckle, M. T.; Zaleski, D. P.; Seifert, N. A.; Temelso, B.; Shields, G. C.; Kisiel, Z.; Pate, B. H., *Science* **2012,** *336*, 897-901.
7. Evangelisti, L.; Perez, C.; Lobsiger, S.; Seifert, N. A.; Zaleski, D. P.; Pate, B.; Kisiel, Z.; Temelso, B.; Shields, G. C.， In *Deuterated water hexamer observed by chirped-pulse rotational spectroscopy*, 69th International Symposium on Molecular Spectroscopy, 2014; pFD12.
8. Wencel-Delord, J.; Colobert, F., *Org. Chem. Front.* **2016**, *3*, 394.
9. Colomer, I.; Chamberlain, A. E.; Haughey, M. B.; Donohoe, T. J., *Nat. Rev. Chem*. **2017**, *1*, 1-12.
10. Hong, D.-P.; Hoshino, M.; Kuboi, R.; Goto, Y., *J. Am. Chem. Soc.* **1999**, *121*, 8427-8433.
11. Godin, P. J.; Le Bris, K.; Strong, K., *J. Quant. Spectros. Radiat. Transf.* **2017**, *203*, 522-529.
12. Zhang, L.; Noda, I.; Czarnik-Matusewicz, B.; Wu, Y., *Anal. Sci*. **2007**, *23*, 901-905.
13. Godin, P. J.; Le Bris, K.; Strong, K., *J. Quant. Spectros. Radiat. Transf.* **2017**, *203*, 522-529.
14. Rajan, R.; Balaram, P., *Int. J. Pept. pROTein Res.* 1996, 48, 328-336
15. Narita, M.; Honda, S.; Umeyama, H.; Obana, S., *Bull. Chem. Soc. Jpn.* **1988**, *61*, 281-284.
16. Hirota, N.; Goto, Y.; Mizuno, K., *Protein Sci.* **1997**, *6*, 416-421.
17. Hirota, N.; Mizuno, K.; Goto, Y., *J. Mol. Biol.* **1998**, *275*, 365-378.
18. Xu, L.-H.; Fraser, G. T.; Lovas, F. J.; Suenram, R. D.; Gillies, C. W.; Warner, H. E.; Gillies, J. Z.; *J. Chem. Phys.* **1995**, *103*, 9541
19. Crick, F. H. C.; Watson, J. D.; Sciences, P., *Proc. R. Soc. A* **1954,** *223*, 80-96.
20. Chang, H.-C.; Jiang, J.-C.; Chen, T.-Y.; Wang, H.-S.; Li, L. Y.; Hung, W.-W.; Lin, S. H., *Phys. Chem. Chem. Phys.* **2013,** *15*, 12734-12741.
21. Tso, T. L.; Lee, E. K., *J. Phys. Chem.* **1985,** *89*, 1612-1618.

22. Martins, V.; Xu, J.; Wang, X.; Chen, K.; Hung, I.; Gan, Z.; Gervais, C.; Bonhomme, C.; Jiang, S.; Zheng, A., *J. Am. Chem. Soc.* **2020,** *142*, 14877-14889.

23. Chen, B.; Huang, Y., *J. Am. Chem. Soc.* **2006,** *128*, 6437-6446.

24. Scheiner, S.; Gu, Y.; Kar, T., *J. Mol. Struct. THEOCHEM* **2000,** *500*, 441-452.

25. Zhao, H.; Pan, Q.; Zhang, W.; Carmichael, I.; Serianni, A. S., *J. Org. Chem.* **2007,** *72*, 7071-7082.

26. Liu, Y.; Li, S.; Xu, J.; Zhang, H.; Guan, Y.; Jiang, H.; Huang, S.; Huang, H.; Wang, Z., *J. Cryst. Growth* **2018,** *18*, 1940-1943.

27. Reddy, T. R.; Reddy, L. S.; Reddy, G. R.; Yarbagi, K.; Lingappa, Y.; Rambabu, D.; Krishna, G. R.; Reddy, C. M.; Kumar, K. S.; Pal, M., *Green Chem.* **2012,** *14*, 1870-1872.

28. Kaminský, J.; Horáčková, F. k.; Biačková, N.; Hubáčková, T.; Socha, O. E.; Kubelka, J., *J. Phys. Chem. B* **2021**, *125*, 11350-11363

29. Han, W.-G.; Jalkanen, K.; Elstner, M.; Suhai, S., *J. Phys. Chem. B* **1998,** *102*, 2587-2602.

30. Yang, Y.; Cheramy, J., Xu, Y., *ChemPhysChem*, **2021**, *22*, 1336-1343.

31. Perera, A. S.; Cheramy, J.; Poopari, M. R.; Xu, Y., *Phys. Chem. Chem. Phys.* **2019**, *21*, 3574-3584.

32. Merten, C.; Berger, C. J.; McDonald, R.; Xu, Y., *Angew. Chem. Int. Ed.* **2014**, *53*, 9940–9943; *Angew. Chem.* **2014**, *126*, 10098−10101.

33. Merten, C.; Xu, Y., *Angew. Chem. Int. Ed.* **2013**, *52*, 2073−2076; *Angew. Chem.* **2013**, *125*, 2127−2130.

34. Becucci, M.; Melandri, S., *Chem. Rev.* **2016,** *116*, 5014-5037.

35. Xu, Y.; Van Wijngaarden, J.; Jäger, W., *Inter. Rev. Phys. Chem.* **2005**, *24*, 301−338.

36. Liu, X.; Xu, Y., High resolution microwave spectroscopy of chiral molecular contact pairs. *Chiral Recognition in the Gas Phase*, Ed. A. Zehnacker, CRC Press, Taylor&Francis Group, **2010**.

37. Jäger, W.; Xu, Y., Fourier transform microwave spectroscopy of doped helium clusters, in *Handbook of High-resolution Spectroscopy*, Eds M. Quack and F. Merkt, John Wiley and Sons, Chichester, **2011**.

38. Burevschi, E.; Sanz, M. E., *Molecules* **2021**, *26*, 5162

39. Su, Z.; Borho, N.; Xu, Y., *J. Am. Chem. Soc.* **2006**, *128*, 17126−17131.

40. Xie, F.; Fusè, M.; Hazrah, A. S.; Jäger, W.; Barone, V.; Xu, Y., *Angew. Chem. Int. Ed.* **2020**, *59*, 22427-22430; *Angew. Chem.* **2020,** *132*, 22613-22616.

41. Thomas, J.; Jäger, W.; Xu, Y., *Angew. Chem. Int. Ed.* **2014**, *53*, 7277−7280; *Angew. Chem.* **2014**, *126*, 7405−7408.

42. Borho, N.; Xu, Y., *J. Am. Chem. Soc.* **2008**, *130*, 5916−5921.

43. Thomas, J.; Xu, Y., *J. Phys. Chem. Lett.* **2014**, *5*, 1850−1855.

44. Liu, X.; Borho, N.; Xu, Y., *Chem. Eur. J.* **2009**, *15*, 270−277.

45. Scharge, T.; Häbery, T.; Suhm, M. A., *Phys. Chem. Chem. Phys.*, **2006**, *8*, 4664–4667.

46. Thomas, J.; Seifert, N. A.; Jäger, W.; Xu, Y., *Angew. Chem. Int. Ed.* **2017**, *56*, 6289-6293; *Angew. Chem.* **2017**, *129*, 6386-6390.

47. Thomas, J.; Liu, X.; Jäger, W.; Xu, Y., *Angew. Chem. Int. Ed.* **2015**, *54*, 11711-11715; *Angew. Chem.*

2015, *127*, 11877-11881.

48. Scharge, T.; Cézard, C.; Zielke, P.; Schuütz, A.; Emmeluth, C.; Suhm, M. A., *Phys. Chem. Chem. Phys.*, **2007**, *9*, 4472–4490.
49. Oswald, S.; Seifert, N. A.; Bohle, F.; Gawrilow, M.; Grimme, S.; Jäger, W.; Xu, Y.; Suhm, M. A., *Angew. Chem. Int. Ed.* **2019**, *58*, 5080-5084; *Angew. Chem.* **2019**, *131*, 5134-5138.
50. Seifert, N. A.; Thomas, J.; Jäger, W.; Xu, Y., *Phys. Chem. Chem. Phys.* **2018**, *20*, 27630-27637.
51. Carlson, C. D.; Seifert, N. A.; Heger, M.; Xie, F.; Thomas, J.; Xu, Y., *J. Mol. Spectrosc.* **2018**, *351*, 62-67.
52. Yang, Q.; Carlson, C. D.; Jäger, W.; Xu, Y., *J. Phys. Chem. A* **2022**, 126, 19, 2942–2949
53. Suzuki, S; Green, P.G.; Bumgarner, R.E.; Dasgupta, S.; Goddard 3rd, W.A.; Blake, G.A., *Science* **1992**, *257*, 942-946
54. Gutowsky, H.S.; Emilsson, T.; Arunan, E., *J. Chem. Phys.* **1993**, *99*, 4883-4893
55. Evangelisti, L.; Brendel, K.; Mäder, H.; Caminati, W.; Melandri S., *Angew. Chem. Int. Ed.* **2017**, *56*, 13699-13703; *Angew. Chem.* **2017**, *129*, 13887-13891.
56. Schnitzler, E. G.; Seifert, N. A.; Ghosh, S.; Thomas, J.; Xu, Y.; Jäger, W., *Phys. Chem. Chem. Phys.* **2017**, *19*, 4440-4446.
57. Murugachandran, I., Tang, J., Pena Calvo, I. P., Loru, D. & Sanz, M., *J. Phys. Chem. Lett.* **2021**, *12*, 1081–1086
58. Tubergen, M. J.; Andrews, A. M.; Kuczkowski, R. L., *J. Phys. Chem.* **1993,** *97*, 7451-7457.
59. Xie, F.; Ng, X.; Seifert, N. A.; Thomas, J.; Jäger, W.; Xu, Y., *J. Chem. Phys.* **2018**, *149*, 224306.
60. Xie, F.; Seifert, N. A.; Heger, M.; Thomas, J.; Jäger, W.; Xu, Y., *Phys. Chem. Chem. Phys.* **2019**, *21*, 15408-15416.
61. Pérez, C.; Lobsiger, S.; Seifert, N. A.; Zaleski, D. P.; Temelso, B.; Shields, G. C.; Kisiel, Z.; Pate, B. H., *Chem. Phys. Lett.*, **2013**, *571*, 1-15.
62. Grimme, S., *J. Chem. Theory. Comput.*, **2019**, *15*, 2847-2862.
63. Pracht, P.; Bohle, F.; Grimme, S., *Phys. Chem. Chem. Phys.*, **2020**, *22*, 7169-7192.
64. Xu, Y.; Jäger, W.; Tang, J.; McKellar, A. R. W., *Phys. Rev. Lett.* **2003**, *91*, 163401−163404.
65. Xu, Y.; Jäger, W., *J. Chem. Phys.* **2003**, *119*, 5457−5466.
66. Tang, J.; Xu, Y.; McKellar, A. R. W.; Jäger, W., *Science* **2002**, *297*, 2030−2033.
67. Xu, Y.; Civis, S.; McKellar, A. R. W.; König, S.; Haverlag, M.; Hilpert, G.; Havenith, M., *Mol. Phys.* **1996**, *87*, 1071–1082.
68. Xia, C.; McKellar, A. R. W.; Xu, Y., *J. Chem. Phys.* **2000**, *113*, 525–533.
69. Xu, Y.; Jäger, W., *J. Chem. Phys.* **2000**, *113*, 514–524.
70. Gordy, W.; Cook, R. L., *Techniques of Chemistry, Microwave Molecular Spectra*. Wiley: 1984.
71. De Leeluw, F.H.; Dymanus, A., *J. Mol. Spectrosc.* **1973**, *48*, 427-445,
72. Gall, J. T. A.; Thomas, J.; Xie, F.; Wang, Z.; Jäger, W.; Xu, Y., *Phys. Chem. Chem. Phys.* **2017**, *19*, 29508-29515.

73. Thomas, J.; Peña, I.; Carlson, C.; Yang, Y.; Jäger, W.; Xu, Y., *Phys. Chem. Chem. Phys.* **2020**, *22*, 23019-23027.

74. Grabow, J.-U.; Pine, A. S.; Fraser, G. T.; Lovas, F. J.; Suenram, R. D.; Emilsson, T.; Arunan, E.; Gutowsky, H. S., *J. Chem. Phys.* **1995**, *102*, 1181.

75. Jäger, W.; Xu, Y.; Gerry, M. C. L., *J. Chem. Phys.* **1993**, *99*, 919–927.

76. Xu, Y.; Jäger, W.; Gerry, M. C. L., *J. Chem. Phys.* **1994**, *100*, 4171–4180.

77. Novick, S.E.; Davies, P.; Harris, S.J.; Klemperer, W., *J. Chem. Phys.* **1973**, *59*, 2273-2279.

78. Xu, Y.; Jäger, W.; Ozier, I.; Gerry, M. C. L., *J. Chem. Phys.* **1993**, *98*, 3726–3731.

79. Jäger, W.; Xu, Y.; Heineking, N.; Gerry, M. C. L., *J. Chem. Phys.* **1993**, *99*, 7510–7520.

80. Janda, K.C., Bernstein, L.S.; Steed, J.M.; Novick, S.E.; Klemperer, W., *J. Am. Chem. Soc.* **1978**, *100*, 8074-8079.

81. Marshall, F. E.; Dorris, R.; Peebles, S. A.; Peebles, R. A.; Grubbs, G. S., *J. Phys. Chem. A* **2018**, *122*, 7385-7390.

82. Marshall, M. D.; Leung, H. O.;Wang, K.; Acha, M. D., *J. Phys. Chem. A* **2018***, 122*, 4670-4680.

83. Leung, H. O.; Marshall, M. D.; Stuart, D. J., *J. Phys. Chem. A* **2020**, *124*, 1798-1810.

Chapter 2

Experimental, Theoretical and Data Analysis Approaches

2.1 Introduction

This chapter will briefly introduce the principles of rotational spectroscopy, the two Fourier transform microwave spectrometers utilized during my graduate study, and theoretical approaches used, as well as some programs that facilitates the research work. In section 2.2, the theoretical treatment of rotational spectroscopy is only briefly introduced since its theoretical principles are well documented.[1-4] Section 2.3 highlights one important technique: a supersonic jet expansion that greatly reduces line congestion in a high-resolution rotational spectrum. The concept of several temperatures involved for rotational experiments are also discussed. Sections 2.4 presents the instrumentations of two types of Fourier transform microwave spectrometers utilized in my research. And section 2.5 discusses the theoretical calculation methods for conformer geometry optimizations and dynamic studies. In section 2.6, several programs facilitating the research work are summarized.

2.2 Rotational Spectroscopy

2.2.1 Semi-rigid Rotor Model

The semi-rigid rotor model is used to describe rotational spectra of molecules and clusters in the gas phase of which is the product by considering centrifugal distortions on the top of the rigid rotor model.[2] A simplest rigid rotor model can be regarded as a freely rotating diatomic molecule separated by a fixed distance. At the center of mass of this diatomic rigid rotor, the origin of a Cartesian coordinates is set up. Usually, the *z* axis is along the molecular axis while the *x* and *y* axis are arranged to follow the right-hand rule. To obtain the rotational eigenstates, i.e., rotational energy levels, one can solve the time-independent Schrödinger equation with the following rotational Hamiltonian:

$$H = \frac{J^2}{2I} \quad (Equation\ 2.2.1.2)$$

Here *J* represents the rotational angular momentum and in linear molecules, the principal moment of inertia have $I_z = 0$, $I_x = I_y = I$. The resulting energy eigenvalue *E(J)* can be expressed by:

$$E(J) = BJ(J+1) \quad (Equation\ 2.2.1.5)$$

and

$$B = \frac{\hbar^2}{2\mathrm{I}} = \frac{h^2}{8\pi^2 I} \quad (Equation\ 2.2.1.6)$$

where *B* is the rotational constants along *y* axis, and usually given in the unit of MHz:

$$B[MHz] = \frac{h^2}{8\pi^2 I} \times 10^{-6} \quad = \frac{505379}{I/(amu\ \text{Å}^2)} \quad (Equation\ 2.2.1.7)$$

For the diatomic molecule X-Y here used as the rigid rotor model, the moment of inertia I can be calculated using the expression below:

$$I = \mu r^2 \quad (Equation\ 2.2.1.8)$$

where the μ is the reduced mass:

$$\mu = \frac{m_N m_O}{m_N + m_O} \quad (Equation\ 2.2.1.9)$$

2.2.2 Non-linear Rotors

As for a general polyatomic molecule, its rotational Hamiltonian can be written as follow:

$$\hat{H}_{rot} = \frac{\hat{J}_a^2}{2I_A} + \frac{\hat{J}_b^2}{2I_B} + \frac{\hat{J}_c^2}{2I_C} \quad (Equation\ 2.2.2.1)$$

where the principal moment of inertia is defined as:

$$I_{xx} = \sum_{\alpha} m_\alpha\, r_{x,\alpha,\perp}^2 \ (Equation\ 2.2.2.2)$$

here m_α is the mass of atom α and $r_{x,\alpha,\perp}$ is the perpendicular distance to the *x* axis from atom α. All the off-diagonal elements of the moments of inertia are zero when the principal moment of inertia axis system is used and the principal inertia tensor ***I*** is defined as:

$$\mathbf{I} = \begin{pmatrix} I_{xx} & 0 & 0 \\ 0 & I_{yy} & 0 \\ 0 & 0 & I_{zz} \end{pmatrix} (Equation\ 2.2.2.3)$$

The *a*, *b*, and *c* axe labeling is decided according to the relative magnitudes of the principal moments of inertia of I_{xx}, I_{yy} and I_{zz}, where the I_C is always assigned to the largest one and I_A the smallest:

$$I_A \le I_B \le I_C \quad (Equation\ 2.2.2.4)$$

And the rotational constants can be expressed as:

$$A = \frac{h^2}{8\pi I_A};\ B = \frac{h^2}{8\pi I_B};\ C = \frac{h^2}{8\pi I_C} \quad (Equation\ 2.2.2.5)$$

Based on the magnitudes of principal moments of inertia, molecules can be categorized into five classes below:

- linear tops ($I_A = 0$, $I_B = I_C$), e.g., CO_2.
- spherical tops ($I_A = I_B = I_C$), e.g., CCl_4.
- oblate symmetric tops ($I_A = I_B \leq I_C$), e.g., NH_3.
- prolate symmetric tops ($I_A \leq I_B = I_C$), e.g., CH_3Cl.
- asymmetric tops ($I_A \leq I_B \leq I_C$).

The energy levels for linear-top and spherical-top molecules can be described by:

$$E(J) = \frac{\hbar}{2I} J(J+1) = BJ(J+1) \quad (Equation\ 2.2.2.6)$$

For symmetric-top rotors, an additional rotational quantum number K to describe the energy levels:

$E_o = BJ(J + 1) + (C - B)K_o^2$ for an oblate top (Equation 2.2.2.7);

$E_p = BJ(J + 1) + (A - B)K_p^2$ for a prolate top (Equation 2.2.2.8).

Most molecules fall into the asymmetric top category and their rotational Schrödinger equation no longer has an analytical solution. Their energies can be evaluated by expressing the rotational wavefunctions of an asymmetric top in the form of linear combinations of symmetric top wavefunctions, evaluate the energy matrix elements, and finally diagonalize the matrix to obtain the energy values.

2.2.3 Rotational Transitions

The energy levels for asymmetric tops can be denoted as $J_{K_aK_c}$, e.g., 1_{01}, where J is a good quantum number, corresponding to the total rotational angular momentum. K_a and

K_c correlate to K_p and K_o in the limit of the prolate and oblate top, respectively, and are no longer good quantum numbers.[2] A molecule must have a permanent electric dipole moment, μ, for its rotational spectrum to be detected. For different types of molecules, the quantum number selection rules are:

- for linear molecules: $\Delta J = \pm 1$, $\Delta M = 0$ or ± 1;
- for symmetric top molecules: $\Delta J = \pm 1$, $\Delta M = 0$ or ± 1, $\Delta K = 0$;
- for asymmetric top molecules: $\Delta J = \pm 1, 0$, $\Delta M = 0$ or ± 1;

and additionally, the selection rules for different types of transitions are:

- for *a*-type transitions: $\Delta K_a = 0$(even) and $\Delta K_c = \pm 1$(odd), e.g. 1_{01}-0_{00}
- for *b*-type transitions $\Delta K_a = \pm 1$(odd) and $\Delta K_c = \pm 1$(odd), e.g. 1_{11}-0_{00}
- for *c*-type transitions: $\Delta K_a = \pm 1$(odd) and $\Delta K_c = 0$(even), e.g. 1_{10}-0_{00}

The population difference between two levels of a rotational transition is the other key factor that affects the line intensity: a larger population difference gives rise to a larger intensity of a transition. The population difference of rotational energy levels follows the Boltzmann distribution,[5] which correlates to rotational temperature, T_t, and the energy difference, ΔE_{rot}, between given rotational energy levels:

$$\frac{N_{J+1}}{N_J} = \frac{g_{J+1}}{g_J} exp \frac{-\Delta E_{\mathrm{rot}}}{\mathrm{RT_t}} \quad (Equation\ 2.1.10)$$

Here, N_J is the population of the J-th rotational level, and N_{J+1} is the higher (J+1)-th energy level. ΔE_{rot} expresses the energy difference between two levels, and g_J is the degeneracy of J-th rotational level.

2.2.4 The Optical Bloch Equations

For the pulsed Fourier transform microwave spectroscopic techniques used in this thesis (see Section 2.5), it is helpful to apply the optical Bloch equations[6,7] to understand the intensity of rotational transitions, which is correlated to the macroscopic polarization upon molecule ensembles. The optical Bloch equations can help with the theoretical description of microwave spectroscopic techniques and explain how the electric dipole moments of the molecule ensembles interact with the pulsed, coherent microwave radiations. Since the Bloch equations are well documented,[8-12] only the solutions are summarized here.

For a simplified two-level system, in the presence of a pulsed external electromagnetic field under resonance condition, the solution of the Bloch equations can be vitalized using the Bloch vector diagrams (Figure 2.2.4). The energy difference ΔE between the two rotational energy levels, E_1 and E_2, can be expressed by $\Delta E = E_2 - E_1 = \hbar\omega_0$ with E_2 being the higher energy level, and ω_0 is the angular transition frequency. When the system is resonance with a continuous radiation, it coherently cycles between the ground and excited states, namely Rabi oscillation. The frequency of such cycles is called the Rabi frequency, which describes the strength of coupling between light and the molecule electric dipole moment. In Figure 2.2.4, let's apply a short pulse of radiation, say a π/2 pulse. At the initial time t=0, the population difference is ΔN_0. After the π/2 pulse, the population difference becomes zero, i.e., ΔN=0, and a superposition state is generated. Now the initial population difference ΔN_0 is converted to the macroscopic polarization in the XY polarization plane. The probability density $|\Psi|^2$ of the molecule ensemble now oscillates with the *transition frequency*, ω_0. If one applies a π pulse, from the Bloch vector diagram, one can see that a population inversion is achieved, i.e., $\Delta N = -\Delta N_0$.

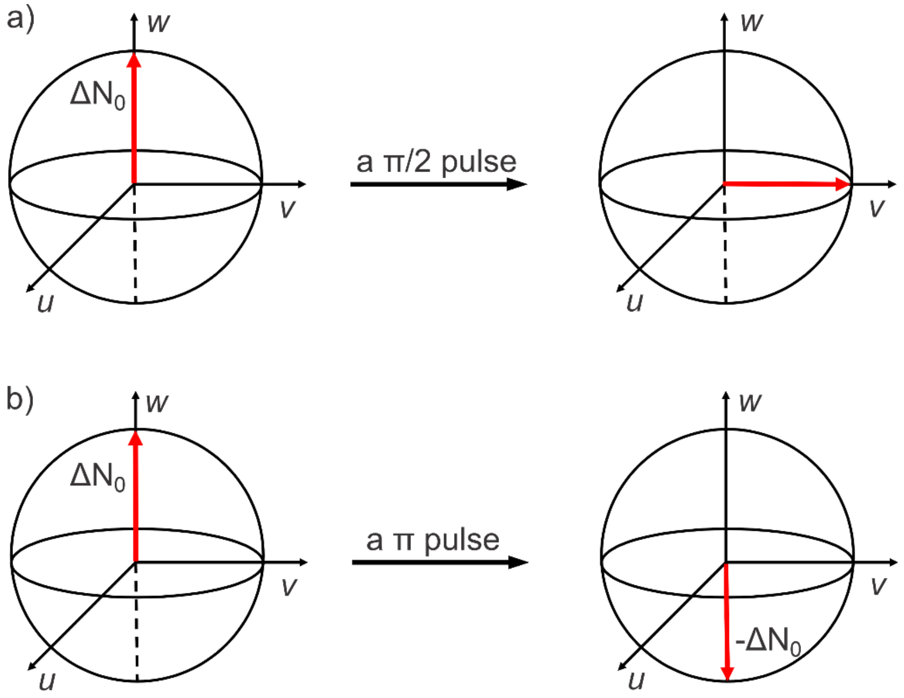

Figure 2.2.4 The time evolution diagram of the Bloch vector (Ref. 9) with the presence of an external electromagnetic field, initially, there is a population difference between two energy levels, ΔN_0. (a) after a π/2 pulse, a zero population difference between the two energy levels is achieved, as well as the maximum macroscopic polarization in the *uv* plane. (b) after a π pulse, a population inversion is generated and there is zero macroscopic polarization in the *uv* plane.

The optical Bloch equations can be directly employed to explain the principle of a cavity-based Fourier transform microwave spectrometer where usually a single resonance frequency is pulsed during the experiments. As for the experiments carried out using a chirped pulse Fourier transform microwave spectrometer, since the chirped pulses are swept over many frequencies very quickly, the concepts of π/2 pulse do not apply in those case anymore. But the optical Bloch equations still can be used to describe how the emission signals from coherent sample molecule ensembles are generated. The general description can be found in the review article by Park and Field.[13]

2.3 Supersonic Jet Expansion

Early microwave studies were conducted in 1940s and the Stark modulation technique was utilized.[14,15] The waveguide sample cell was used for early FTMW experiments, combined with the use of modulated electric field for the observations of microwave absorption spectra.[16] In a thermodynamic equilibrium environment, such as at room or high temperatures, the waveguide microwave experiment with static gas samples sealed in a long tube would quickly destroy the polarization coherence because of continuous collisions from other molecule in the waveguide tube. As a result, the lifetime of “the excited state” analytes is shortened, leading to a broader linewidth to the spectra. Because of the far smaller energy gaps between rotational energy levels than those between vibrational energy levels, a very broad population rotational distribution is present at room temperature, leading to very small population differences and weak rotational transition intensities. This is illustrated in *Figure 2.4.2* in a small temperature range from 0.5 to 5 K using a PFP conformer as an example. As one can see, even at 5 K, the rotational line intensity is significantly lower than at 0.5 K and also the density of lines increases drastically at 5 K, making it difficult to do spectral analyses.

Two types of important decay time involved with relaxation should be noted here. The spontaneous emission or collisions gives the T_1 time, determined by the excited state lifetime. Such de-population relaxation of the excited state would lead to equilibrium distribution. The polarization de-coherence, noted as the T_2 time, is resulted by a phase changing process where collisions from molecules/atoms would reset the coherent phase of the molecular wavefunctions without changing its population distribution. The lifetime of excited states in the waveguide experiments is greatly shortened by collisions. Thus, the supersonic jet expansion technique is introduced to create isolated sample molecules.

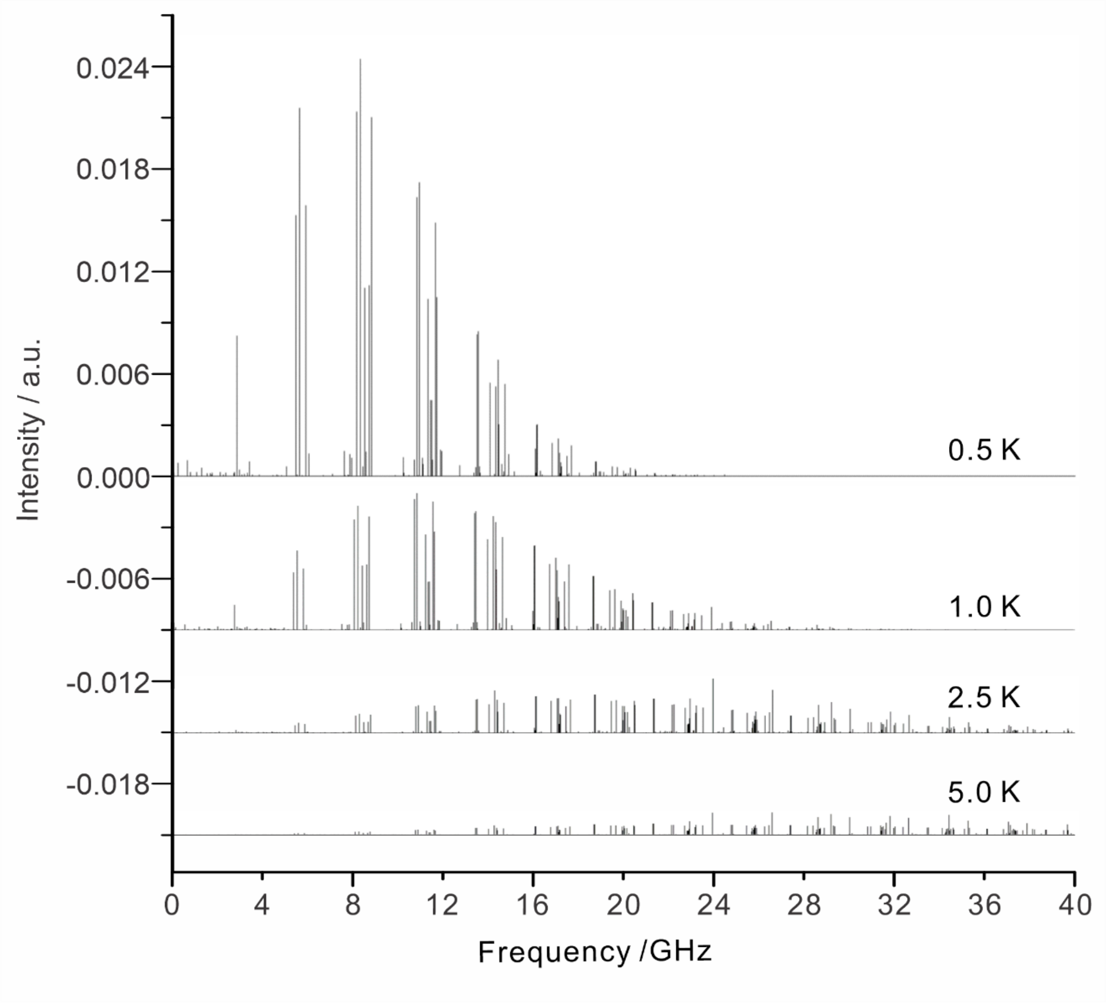

Figure 2.3.1 The figure compares simulated rotational spectra of the most abundant, global minimum energy **PFP***G+g+* monomer at different rotational temperatures involved in this thesis. The spectra are set at the same scale for better comparison. The rough line intensity ratios of the strongest line simulated at four rotational temperatures here, at 0.5 K, 1.0 K, 2.5 K and 5.0 K, respectively, are about 24:8:3:1. One can see the drastic decrease of simulated line intensities at higher rotational temperatures.

Kantrowitz and Gray firstly introduced the supersonic jet expansion in 1951,[17] which is used routinely in rotational spectroscopic experiments.[18] In a typical experiment using the supersonic jet expansion technique, a poppet in a nozzle controls the gas mixture expansion which travels adiabatically into a vacuum chamber kept at 10^{-6} to 10^{-7} Torr. When the poppet retreats back and the nozzle orifice opens for typically 500 to 800 μs, many collisions take place near the orifice. That is also when and where non-covalently bonded molecular complexes and clusters form. The design of this type of nozzle and orifice are shown in Figure 2.3.2, while the poppet is omitted for simplification. Once exit the nozzle hole, the molecules in the jet would remain in the collision-free environment until hitting the chamber wall or being evacuated by the pump. Under this condition, T_1 time takes over the control in the jet expansion experiments since the sample molecule ensembles are in coherence and isolated to each other, considered as “collision-free”. To form large molecule clusters, e.g. dimers, trimers or tetramers, more collisions are necessary to remove the excess energy released by the formation of the aggregates.

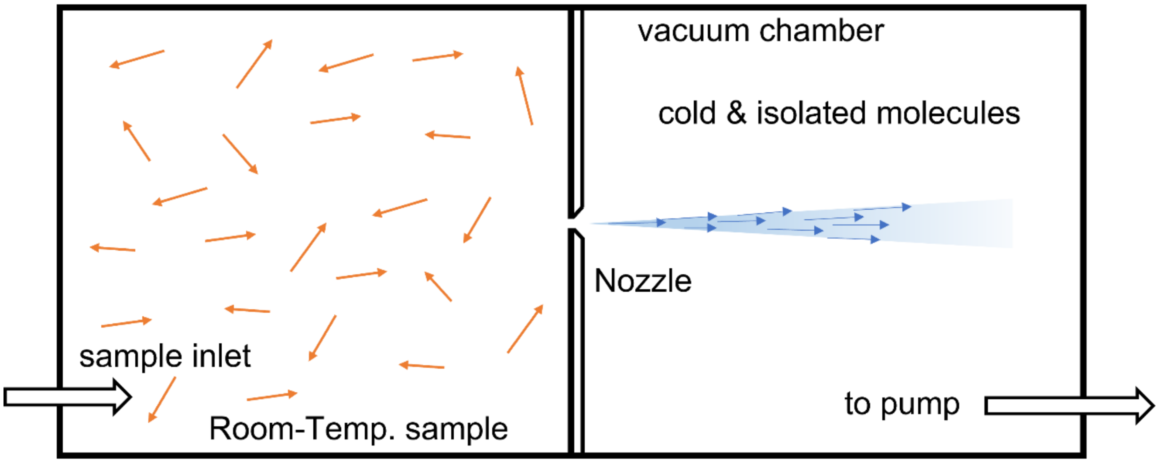

Figure 2.3.2 An overview of the principles of the supersonic jet expansion. The “hot” analyte molecule seeded in rare gas atmosphere at ~ 3 bars of room temperature are introduced into a vacuum chamber through a pulsed nozzle, giving almost paralleled, collision-free “cold” jet with rotational temperature at about 1 K.

In a supersonic jet expansion of rotational experiments, a gas mixture which typically contains a trace amount of the analyte gas sample with inert gas carrier such as helium and neon, is expanded into vacuum through a pinhole. The velocity distribution of the analyte molecule becomes nearly uniform, i.e., a collision-less flow.[19,20] There are several temperatures referred to in this thesis: translational (T_t), rotational (T_r), and vibrational (T_v) temperature.[21] The cooling efficiency for the first three motion types vary, in the order of translational > rotational > vibrational in generally. Because the vibrational energy levels are separated wider in energies than those of the rotational ones, the limited number of collisions happen at the exit of the pinhole is not enough to bring away the excess energy. As a result, high vibrational levels remain populated, leading to a high vibrational temperature.

2.4 Fourier Transform Microwave Spectrometers

Two different FTMW spectrometers were utilized in my graduate research. One of them is a Balle-Flygare[22-24] type cavity-FTMW spectrometer. The other is a broadband chirped-pulse FTMW spectrometer pioneered by Pate and co-workers.[25] Details of the cavity- and the chirped-pulse FTMW spectrometers employed in this work are introduced in the following sections.

2.4.1 Cavity- Fourier Transform Microwave Spectrometer

The details of the cavity-based FTMW spectrometer used for the research in this thesis have been published previously.[26,27] Its design was based on the original Balle-Flygare set up with some improvements where jet expansion travels parallel to the cavity axis.[28-32] The coaxial supersonic jet expansion with respect to the L-shape antenna and the chamber mirrors also generates two Doppler splitting components to each rotational transition, but the linewidth is much narrower than the perpendicular arrangement. The sensitivity and resolution achieved allow for the detection of the nuclear quadruple hyperfine structures in the Pyrrole⋯water and its ^{13}C isotopologues species at natural abundances in this thesis. The frequency uncertainty is ~ 2 kHz and the full linewidth at half height (FWHH) is about 10 kHz. Equipped with an “automatic step-scan” function and combined with the extraordinary resolution, the remarkable signal-to-noise ratio, the cavity-based FTMW spectrometer is capable of searching very weak signals of isotopologues rotational transitions from the noise level, greatly boost the research work. Moreover, most conveniently, the cavity-based FTMW spectrometer can be switched quickly between “stand-by” and “ready-to-go” modes. One can focus on searching transitions of interest “one by one”.

For this cavity-based instrument employed in this thesis, the time sequence are described below.

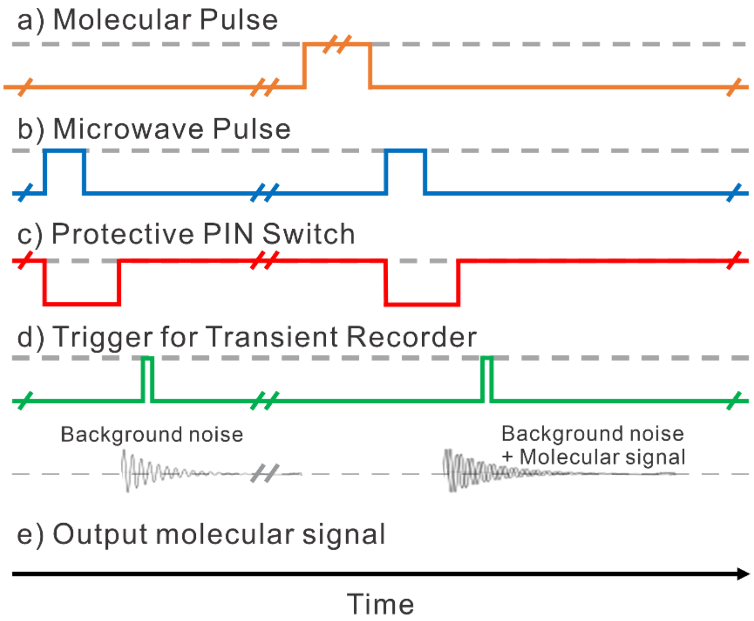

Figure 2.4.1 The timeline of typical pulse sequences applied to the acquisition cycles with a Balle-Flygare type cavity-based FTMW spectrometer. The crest square side on the dash line indicates “on” and continuous trough indicates “off” of corresponding pulses.

The cavity FTMW experiments are realized by the commanding a transistor-transistor logic (TTL) pulse sequences for the pulse generation and data acquisitions. The FID signals in the coherent phase are important to the averaging procedure: (a) an adjustable molecular pulse is launched in every second cycle to subtract background noises; (b) a short insertion before the MW excitation pulse is generated; (c) the protective PIN diode switch is notified by a pulse to block the fully amplified microwave-pulse from harming the sensitive detection electronics; (d) a trigger pulse is generated to start the molecular signal acquisition for an adapted, proper delay time (typically several μs) after the end of microwave-pulse.[33,34]

2.4.2 Chirped pulse Fourier transform microwave spectrometer

The traditional cavity-based FTMW spectrometer shows its advantages in high sensitivity and resolution, but the usage is limited because of its narrow-band nature making it time-consuming to scan a broad frequency coverage. Even with the help of an automatic step-scan, a measurement covering 100 MHz can easily take for overnight. Such experiments would waste precious analyte samples and Ne carrier gas. Thus, the need of employing a broadband chirped-pulse FTMW spectrometer to collect rotational spectra over a wide frequency range is indeed. The CP-FTMW instrument used in this thesis was designed based on a similar instrument by Pate and co-workers' work[34] has ~5 kHz frequency accuracy.[35-37]

According to the Standard Operation Procedure of the CP FTMW spectrometer used in our group,[38] the chirped pulse width is typically set to 1 or 4 μs, and the oscilloscope collects FID signals for 20 or 40 μs. The above measurement process would be repeated 6 times on every molecular pulse. Such multi-cycle probing sequences would allow for the deep averages of the analyte signals within one molecular pulse. Since the nozzle repetition rate for pulsing molecular jets is typically set at 2 Hz, meaning 12 frames per second. Thus, one can collect about one million FIDs for an "overnight" experiment before the analyte sample running out.[38] The other advantage respects the to CP FTMW spectrometer used in our group is that, the spectra band covers up to 12 GHz thanks to the side bands of the amplifier. The spectrometer works mainly over 2-6 GHz of microwave frequency where the line intensities and signal-to-noise ratios are well optimized. Some strong transitions could also be detected in the 6-12 GHz frequency, assisting the assignment work.

2.5 Theoretical Calculation Approaches

2.5.1 Gaussian 16

All electronic structure calculations conducted in this thesis work were carried out using the Gaussian 16 software package.[39] Gaussian 16 is a widely used, very powerful software package based on quantum mechanics fundamentals that predicts the molecular energies, geometries, vibrational frequencies, compound properties, reaction pathways and many other properties in variable chemical environments. A convenient viewing tool GaussView accompanies the usage of Gaussian 16, which allows one to visualize calculation results, presenting mapped surfaces and also carrying with many other useful features, for example showing animations of a coordinate scan file and vibrational motions. The electrostatic potential mapping figures presented in this thesis were visualized by using the GaussView software.

All common calculations were performed with the density functional theory (DFT). In this thesis, one of the widely used functionals is the B3LYP method[40,41] combined with Grimme's dispersion correction (D3)[42], Becke−Johnson damping (BJ)[43] to predict properties of the targeted molecules and clusters in the gas phase.

A basis set is a set of coded functions with approximations applied to simulate the atomic orbitals to describe the real wave functions. It is crucial to select a proper basis set in theoretical calculations because one needs to balance the calculation time and the prediction accuracies for a given molecular system in specific calculation tasks. For example, two of Weigend's split-valence basis sets def2-TZVP and def2-QZVP[44] are used with the B3LYP (Becke, 3-parameter, Lee-Yang-Parr)[40,41] hybrid functional in this thesis, in combination with the dispersion correction (D3)[42] and Becke-Johnson damping factor (BJ)[43] to describe non-covalent interactions such as hydrogen bonding interactions and dispersion interactions in this thesis. A significant calculation duration differences were noted between the triple zeta valence polarization (TZVP) and the quadruple zeta valence polarization (QZVP) basic sets[44] where the latter one requires roughly 12 times longer calculation time than that of the former one on the same calculation job. Generally, better agreements with the experimental data (see Supporting Information of Chapter 4-7) were obtained with QZVP versus TZVP, where the percentage errors up to about 10 times smaller than the latter one. ver. On the other hand, the *ab initio* calculations utilizing MP2 method of the Møller–Plesset perturbation theory takes even longer computing time than that with the def2-QZVP basic set. There is no clear improvements in the agreement with the experiment for the predicted spectroscopic data when compared to the def2-QZVP DFT approach. Thus, the B3LYP-D3(BJ) functional with def2-TZVP/QZVP basic sets were utilized for calculating non-covalent interaction systems in the current thesis. The def2-TZVP basic set was usually used for initial calculations of predicted rotational constants of the targeted species and one- and two-dimensional scans along the designated dihedral angles, while the def2-QZVP basic set were used to improve the agreement with the experimental results in most of the projects carried out in this thesis.

2.5.2 Conformational searching tool

CREST (conformer-rotamer ensemble sampling tool)[45,46] is a very useful conformation searching software package that allows one to find low energy conformers of the input molecule or clusters. This software package needs only simple input geometries and commands to set up simulation and screening conditions to meet the needs of specific requirements or conditions. For example, to search possible conformers of a monohydrate, one only needs to set up a coordination file that contains the monomer and the water molecule, leaving some distances between the two subunits. CREST would then sample the conformational space and output a detailed potential conformer list. All the output geometries are conveniently summarized in a txt file in increasing energy ordering. Inside CREST, repeated geometries were eliminated from the final list. Usually, the above conformational search procedure would be run for at least three times using input coordinate files with different relative positions of the subunits to search all possible conformations. In this case, the redundant structures from output files were eliminated using a Python script written in the group.[47] The resulting CREST candidates are submitted for subsequent DFT geometry optimization and harmonic frequency calculations. A list containing the spectroscopic parameters of all stable conformations would be obtained by ordering them from the lowest to the highest energy.

2.6 Other software packages used

2.6.1 Autofit

Autofit[48] is a software specially designed for assisting assignment of rotational spectra based on the initial input rotational constants and permanent electric dipole components, i.e., types of transitions and their intensities, and rotational temperature. This software was written based on SPFIT/SPCAT fitting packages.[49,50] Based on some initial assignment criteria selected by users, the program would select the transitions in the destinated frequency region, perform a fit, predict other (selected) transitions, and select these transitions from the experimental spectra, and perform a new fit, and finally list 100 best trial fits. Variable working options are available for users to customize searching conditions to utilize its powerful searching capabilities, especially from dense spectra. This software was mainly employed for identifying and giving assignments for different isotopologues of the water containing complexes from an extremely dense spectrum when traditional manual attempts were not successful.

2.6.2 Avogadro and Chimera

Avogadro[51] is a free, open-source molecule editor and visualizer that is mainly used for presenting molecular cluster geometries, e.g., isomer configurations in this thesis. It is capable to customize variable viewing effects and offer high quality image rendering process, as well as powerful embedded options for processing coordinate files, such as adding dummy atoms, center of mass and visualizing coordinates. A wide variable of file types can be read and saved by this software, playing an important role to bridge many other scientific software packages.

Chimera[52] is developed by University of California, San Francisco (UCSF) for the purposes of interactive visualization and molecular structure analysis. It also supports displaying density maps, trajectories, and sequence alignments. For commercial users, much better performance with large structures could be achieved, along with other new features. A paralleled program is called ChimeraX which includes a significant subset of Chimera features.

I also used Origin,[53] a data processing software, to aid the drawing of rotational spectra, potential energy surfaces of 1D curvatures, 2D contour plots and 3D stereo-viewings. The employments of the Origin software provide an accurate and straightforward way for understanding spectroscopic data and dynamic simulation results.

2.6.3 KRA, PMIFST, and STRFIT

KRA[54] program was developed for the calculations of single isotopic substituted coordinates using the standard Kraitchman's equations.[1] It is capable of calculations of on/off axis substitution in symmetric/asymmetric tops and general substitution in an asymmetric rotor. The two mostly used options are planar and non-planar substitution coordinates. Errors are presented in two ways: propagated uncertainties from experimental rotational constants, and the usually used Costain's error. On Kisiel’s website, the isotopic weights with good accuracies are summarized in tables for easy usage.

PMIFST program (Principal Moments of Inertia From STructure)[54] accepts Cartesians or internal coordinates of molecule files, and can be used as a fast method for predicting moments of inertia, rotational constants and planar moments. It is especially convenient for predicting isotopologues data based on the optimized parent geometry and allows 3D rotation for geometry viewing and checking. Some important parameters, such as bond lengths and angles can also be extracted from this program.

The STRFIT (STRucture FITting to rotational data) program[54] was originally developed for the determination of effective structures of H-bonding complexes, or partial geometries. It can also be used for complete geometry determination using many different types of input geometries. The input coordinates used in current thesis is the internal coordinates which associated with bond lengths, angles, and dihedral angles. Proper connection sequences of the target molecule cluster are necessary to obtain the best fitting results based on experimental rotational constants.

2.6.4 Pgopher and SPCAT/SPFIT

Pgopher[55] is a multifunctional program for spectral simulation and fitting. It can deal with rotational, vibrational, ro-vibrational and electronic spectra, capable of the treatments of linear molecules, and molecule clusters with symmetric and asymmetric tops and hyperfine structures such as nuclear quadrupole coupling hyperfine structures studied in this thesis. This program was developed with a graphical, user-friendly interface. One can easily drag and overlay numerical spectra from variable file sources for comparison and fitting simultaneously. There appears to be a bug in the program for fitting two states with Coriolis coupling. For such fitting, we utilized SPCAT/SPFIT by Pickett. [49,50]

The SPFIT/SPCAT[49,50] is the most widely used spectroscopic fitting and prediction program package developed by Pickett. The package does not have a graphical interface and is well known for its unfriendly formats for beginners, although there are various helping documents offered at several websites. The Autofit program employed in this thesis was coded based on the SPFIT/SPCAT package.

2.6.5 VMD+Multiwfn

The VMD software program[56] is a high-performance, cross-platform molecular graphics viewer, used for displaying static and dynamic structures, viewing sequence information, and for structure generation and dynamic analysis. Personalized exporting functions could help with drawing high-quality figures that meets the publication requirements. Combined with the utilization of the Multiwfn software[57], which analyzes and extracts useful information from calculated waveform file, variable interesting information could be presented, such as the QTAIM and NCI analyses data presented in this thesis.

References

1. Gordy, W.; Cook, R. L., *Techniques of Chemistry, Microwave Molecular Spectra*. Wiley: 1984.
2. Bernath, P. F., *Spectra of atoms and molecules*. Oxford university press: 2020.
3. Bauder, A., Fundamentals of rotational spectroscopy. *Handbook of High‐resolution Spectroscopy* **2011**.
4. Brown, J. M.; Brown, J. M.; Carrington, A., *Rotational spectroscopy of diatomic molecules*. Cambridge university press: **2003**.
5. McAfee Jr, K.; Hughes, R. H.; Wilson Jr, E. B., *Rev. Sci. Instrum.* **1949,** *20*, 821-826.
6. Hertel, I. V.; Schulz, C.-P., *Atoms, molecules and optical physics*. Springer: **2014**.
7. Universität Rostock, Lecture 17: Optical Bloch Equations. https://www.lkv.uni-rostock.de/storages/unirostock/Alle_MNF/Physik_Qms/Lehre_Scheel/quantenoptik/Quantenoptik-Vorlesung10.pdf.
8. Shun-Jin, W.; Cassing, W., *Ann. Phys.* **1985,** *159*, 328-350.
9. Blum, K., *Density matrix theory and applications*. Springer Science & Business Media: 2012; Vol. 64.
10. Von Neumann, J., Mathematisch-Physikalische Klasse, Wahrscheinlichkeitstheoretischer aufbau der quantenmechanik. Nachrichten von der Gesellschaft der Wissenschaften zu Göttingen, Mathematisch-Physikalische Klasse **1927,** *1927*, 245-272.
11. Allen, L.; Eberly, J. H., *Optical resonance and two-level atoms*. Courier Corporation: 1987; Vol. 28.
12. Arecchi, F.; Bonifacio, R., *IEEE J. Quantum Electron.* **1965,** *1*, 169-178.
13. Park, G.B.; Field, R.W., *J. Chem. Phys.* **2016**, *144*, 200901
14. McAfee Jr, K.; Hughes, R. H.; Wilson Jr, E. B., *Rev. Sci. Instrum.* **1949,** *20*, 821-826.
15. Hughes, R. H.; Wilson Jr, E. B., *Phys. Rev.* **1947,** *71*, 562.
16. Townes, C. H.; Schawlow, A. L., *Microwave spectroscopy*. Courier Corporation: 2013.
17. Kantrowitz, A.; Grey, J., *Rev. Sci. Instrum.* **1951,** *22*, 328-332.
18. Arunan, E.; Dev, S.; Mandal, P. K., *Appl. Spectrosc. Rev.* **2004,** *39*, 131-181.
19. Imasaka, T.; Moore, D. S.; Vo-Dinh, T., *J. Pure Appl. Chem.* **2003,** *75*, 975-998.
20. Even, U., *EPJ Tech. Instrum.* **2015,** *2,* 14.
21. Marrone, P. V., *Phys. Fluids* **1967,** *10*, 521-538.
22. Balle, T.; Flygare, W. J., *Rev. Sci. Instrum.* **1981,** *52*, 33-45.
23. Campbell, E.; Buxton, L.; Balle, T.; Flygare, W., *J. Chem. Phys.* **1981,** *74*, 813-828.
24. Campbell, E.; Buxton, L.; Balle, T.; Keenan, M.; Flygare, W. H., *J. Chem. Phys.* **1981,** *74*, 829-840.
25. Brown, G. G.; Dian, B. C.; Douglass, K. O.; Geyer, S. M.; Shipman, S. T.; Pate, B. H., *Rev. Sci. Instrum.* **2008,** *79*, 053103.
26. Xu, Y.; Jäger, W., *J. Chem. Phys.* **1997**, *107*, 4788–4796.
27. Xu, Y.; Jäger, W., *J. Chem. Phys.* **1997**, *106*, 7968–7980.
28. Grabow, J.-U., Fourier transform microwave spectroscopy measurement and instrumentation. *Handbook of High‐resolution Spectroscopy* **2011**.

29. Chuang, C.; Hawley, C.; Emilsson, T.; Gutowsky, H., *Rev. Sci. Instrum.* **1990,** *61*, 1629-1635.
30. Grabow, J.-U.; Stahl, W., *Z. Naturforsch. A* **1990,** *45*, 1043-1044.
31. Schnell, M.; Banser, D.; Grabow, J.-U., *Rev. Sci. Instrum.* **2004,** *75*, 2111-2115.
32. Andresen, U.; Dreizler, H.; Grabow, J.-U.; Stahl, W., *Rev. Sci. Instrum.* **1990,** *61*, 3694-3699.
33. http://www.chem.ualberta.ca/~jaeger/research/ftmw/ftmw.htm, access 2022 May
34. Pérez, C.; Lobsiger, S.; Seifert, N. A.; Zaleski, D. P.; Temelso, B.; Shields, G. C.; Kisiel, Z.; Pate, B. H., *Chem. Phys. Lett.* **2013,** *571*, 1-15.
35. Carlson, C. D.; Seifert, N. A.; Heger, M.; Xie, F.; Thomas, J.; Xu, Y., *J. Mol. Spectrosc.* **2018,** *351*, 62-67.
36. Seifert, N. A.; Thomas, J.; Jäger, W.; Xu, Y., *Phys. Chem. Chem. Phys.* **2018,** *20*, 27630-27637.
37. Xie, F.; Seifert, N. A.; Heger, M.; Thomas, J.; Jäger, W.; Xu, Y., *Phys. Chem. Chem. Phys.* **2019,** *21*, 15408-15416.
38. Seifert, N. A. *2-6 GHz Chirped-Pulse Fourier Transform Microwave (CP-FTMW) Spectrometer*: *Standard Operating Procedure / Tips & Tricks,* **2019**.
39. Frisch, M.; Trucks, G.; Schlegel, H.; Scuseria, G.; Robb, M.; Cheeseman, J.; Scalmani, G. J. R. A., 309 Barone, V.; Petersson, G.; Nakatsuji, H., et al. Gaussian 16. **2016,** *3*, 310.
40. Stephens, P. J.; Devlin, F. J.; Chabalowski, C. F.; Frisch, M. J., *J. Phys. Chem.* **1994,** *98*, 11623-11627.
41. Beck, A. D. *J. Chem. Phys.* **1993**, *98*, 1372-1377.
42. Grimme, S.; Antony, J.; Ehrlich, S.; Krieg, H. J., *J. Chem. Phys.* **2010,** *132*, 154104.
43. Grimme, S.; Ehrlich, S.; Goerigk, L., *J. Comput. Chem.* **2011,** *32*, 1456-1465.
44. Weigend, F.; Ahlrichs, R., *Phys. Chem. Chem. Phys.* **2005,** *7*, 3297-3305.
45. Pracht, P.; Bohle, F.; Grimme, S., *Phys. Chem. Chem. Phys.* **2020,** *22*, 7169-7192.
46. Grimme, S., *J.*, *Chem.Theory Comput.* **2019,** *15*, 2847-2862.
47. Wang, H.; Heger, M.; Al-Jabiri, M. H.; Xu, Y., *Molecules*, **2021**, 27, 38
48. Seifert, N. A.; Finneran, I. A.; Perez, C.; Zaleski, D. P.; Neill, J. L.; Steber, A. L.; Suenram, R. D.; Lesarri, A.; Shipman, S. T.; Pate, B. H., *J. Mol. Spectrosc.* **2015,** *312*, 13-21.
49. Pickett, H. M., *J. Mol. Spectrosc.* **1991,** *148*, 371-377.
50. Pickett, H. M., SPFIT/SPCAT Package, available at <http://spec.jpl.nasa.gov./>.
51. Hanwell, M. D.; Curtis, D. E.; Lonie, D. C.; Vandermeersch, T.; Zurek, E.; Hutchison, G. R., *J. Cheminformatics* **2012,** *4*, 17.
52. Pettersen, E. F.; Goddard, T. D.; Huang, C. C.; Couch, G. S.; Greenblatt, D. M.; Meng, E. C.; Ferrin, T. E., *J. Comput. Chem.* **2004,** *25*, 1605-1612.
53. May, R. A.; Stevenson, K. J., *Software review of Origin 8*. ACS Publications: 2009.
54. Kisiel, Z., PROSPE-Programs for rotational spectroscopy, in *Spectroscopy from Space*, Eds. J. Demaison, K. Sarka, E. A. Cohen, **2001**, pp. 91-106. Kluwer Academic Publishers, Dordrecht.
55. Western, C. M., *J. Quant. Spectrosc. Radiat. Transf.* **2017**, *186*, 221-242.
56. Humphrey, W.; Dalke, A.; Schulten, K., *J. Mol. Graph.* **1996**, *14*, 33-38.

57. Lu, T.; Chen, F., *J. Comput. Chem.* **2012,** *33*, 580-592.

Chapter 3

The pyrrole-water complex: Multidimensional large amplitude dynamics and rotational spectra of its ^{13}C isotopologues[1]

---

[1] This study has been published as B. Wu, F. Xie. and Y. Xu, "The pyrrole-water complex: Multidimensional large amplitude dynamics and rotational spectra of its ^{13}C isotopologues", *J. Mol. Spectrosc.* **2020,** *374,* 111381.

Abstract

The rotational spectrum of pyrrole-water was investigated before (*J. Phys. Chem.* **1993,** *97*, 7451.) In this work, we have applied a recently developed semiempirical tight-binding quantum chemistry program and DFT calculations to identify possible low energy conformers of the pyrrole-water complex which feature σ- and π-type hydrogen-bonding interactions. Using a cavity-based and two chirped pulse Fourier transform microwave spectrometers, we have measured and assigned all monosubstituted ^{13}C isotopologues of pyrrole-water in their natural abundances. The ^{14}N nuclear quadrupole hyperfine splittings and water tunneling doublets of these rarer isotopologues have also been observed and analyzed. Furthermore, we have carried out potential energy surface scans along possible paths of water large amplitude motions and identified all four previously proposed pyrrole-water geometries and correlated them to one global minimum and three transitions states. The theoretical investigation together with the additional ^{13}C experimental data allow one to confidently identify the ground state geometry and also estimate the water tunneling barrier.

Introduction

Pyrrole, a heterocyclic aromatic molecule, is an important building block of large biological molecules. To appreciate its role in larger biological systems, it is desirable to gain insight into its structural properties. Not surprisingly, its rotational spectrum was among the earliest organic molecules studied by microwave (MW) spectroscopy in order to determine its structure.[1,2] Furthermore, there is much interest in examining how pyrrole interacts with water, the natural environment for many biological molecules. In 1993, Tubergen et al.[3] reported the first rotational spectroscopic study of the pyrrole-water complex. The authors proposed four possible equilibrium geometries which they named *crossed*, *symmetric-crossed*, *hinged*, and *planar hinged* (vide infra), all featuring a σ-type NH···O hydrogen (H)-bond, although the available experimental and theoretical data at the time did not allow a conclusive determination of which one was the global minimum. In addition, the rotational transitions observed show ^{14}N nuclear quadrupole hyperfine patterns and tunneling doublets. Whether this tunneling splitting is due to the internal rotation of water about its C_2 axis or to an internal rotation about the NH···O H-bond which would exchange 3 pairs of equivalent hydrogens (1 pair on water and 2 pairs on pyrrole) were discussed although the specific tunneling path was not unambiguously determined.

Later on, several theoretical and spectroscopic studies of the pyrrole-water$_n$ complexes were reported.[4-7] One of them focused on theoretical investigation of charge-transfer driven femtosecond scale dynamics in the pyrrole-water$_{1,2}$ complexes.[5] Another one examined the σ- and π-type of H-bonds in the 1:1 pyrrole-water complex and in their 1:1 liquid mixture, in order to analyze similarities and differences of these H-bonds.[4] Matsumoto et al.[7] investigated the pyrrole-water complex using low resolution cavity ring down infrared spectroscopy and identified a 1:1 pyrrole-water complex which contains a σ-type H-bond, similar to that reported by Tubergen et al.[3] None of these studies, however, addressed the ambiguities raised in the Tubergen's report.[3]

In this study, we have systematically searched for possible low energy conformers of the pyrrole-water complex. We have extended the rotational transition measurements of the parent pyrrole-water complex reported[3] and performed a new study of all its ^{13}C isotopologues using chirped pulse-Fourier transform MW (CP-FTMW) and cavity-based FTMW spectroscopy. For the conformer observed experimentally, we have performed the potential energy surface (PES) scans along several possible water tunneling paths and applied higher level DFT calculations than before[3] to confirm the minimum or transition state nature of the geometries identified in the PES scans. All these efforts have allowed us to unambiguously establish the ground state geometry and the internal motion responsible for the tunneling splittings observed. Step-wise solvation studies of organic molecule-water$_n$ systems by rotational spectroscopy and theory have been reported, for example, for propylene oxide,[8] methyl lactate,[9] and more recently hydantoin[10] where considerable insight has been gained about the first few steps of solvation. The current study is the first step toward this goal for pyrrole.

Experimental

Three FTMW spectrometers have been used in the current study: a cavity-based Balle-Flygare[11] FTMW spectrometer in the 4-18 GHz region,[12,13] and two broadband CP-FTMW spectrometers. The details of the 7.7-18 GHz CP-FTMW instrument, similar to those reported earlier,[14,15] were described before.[16,17] The recently developed 2-6 GHz CP-FTMW spectrometer was constructed based on the design of a similar instrument by Pate and co-workers[18] and its details were reported in several recent publicaitons.[19-21] The accuracy and the full width at full height (FWHH) of the measurements are about 1 kHz and 10 kHz for the cavity instrument,[12,13] and ~5 kHz and ~125 kHz for the CP-FTMW instrument,[22] respectively.

Pyrrole (reagent grade, 98% purity) was purchased from Sigma-Aldrich and used without further purification. A gas mixture which contains about 0.1% pyrrole and 0.2% water in 4 bar neon was used for the cavity-based FTMW experiments or in 2.7 bar helium gas (research grade, Praxair) for the CP-FTMW experiments. Rotational spectra of all ^{13}C isotopologues of the pyrrole-water complex were measured in their natural abundances and all final frequency measurements were done with the cavity instrument.

Theoretical

To carry out systematic search for possible conformers of the pyrrole-water complex, we utilized a recently released quantum chemistry code called CREST, i.e. conformer-rotamer ensemble sampling tool,[23,24] developed by Grimme and co-workers. The code was designed to comprehensively explore the conformational flexibilities of molecular systems, from small systems to those containing hundreds or even thousands of atoms. Our research group has applied this code to successfully identify conformers of flexible organic molecules such as perillyl alcohol[19] and non-covalently bonded complexes such as hexafluoroisopropanol trimer[25] and homo-/heterochiral dimers of tetrahydro-2-furoic acid.[26] The subsequent geometry optimization and harmonic/anharmonic frequency calculations were carried out using the Gaussian 16 program package.[27] All calculations were performed with the B3LYP[28,29] functional, including D3 dispersion corrections[30] with the Becke-Johnson damping function,[31] and coupled to the def2-TZVP basis set.[32] To investigate the connection between different minimum geometries, a 2-dimensional (D) PES scan was carried out at the B3LYP-D3(BJ)/def2-TZVP level of theory. All energies reported are corrected by the zero-point energy (*ZPE*) and the basis set super position errors (*BSSE*s), calculated using the counterpoise procedure.[33] The keywords used in the calculations are provided in Point S1, Supporting Information. We used Avogadro[34] and UCSF Chimera[35] to visualize structures of the pyrrole-water complexes.

We utilized Kisiel's PMIFST, STRFIT and KRA programs[36] for the isotopic substitution and the structural fitting analyses. The Pgopher[37] program was used to obtain the final rotational spectroscopic fits.

Results and Discussions

1. Spectral analysis of pyrrole-water

Thirteen conformational candidates of pyrrole-water were identified by CREST,[23,24] although only three of them are within 20 kJ mol^{-1} from the global minimum. These three geometries were reoptimized and the final optimized geometries are shown in Figure 3.1. We name them Py$_{NH}$-W-I, Py$_{NH}$-W-II, and Py$_{\pi}$-W where Py$_{NH}$ and Py$_{\pi}$ indicate that pyrrole uses its NH to serve as the H-bond donor or utilizes its π-ring to serve as the H-bond acceptor, respectively. It turns out that Py$_{NH}$-W-I and -II are mirror images to each other and therefore we expect to see only one set of rotational transitions from them. We use Py$_{NH}$-W when referring to this conformer and keep the Py$_{NH}$-W-I and Py$_{NH}$-W-II labels for the later discussion of large amplitude motions. Py$_{\pi}$-W is ~2 kJ mol^{-1} higher in energy than the global minimum Py$_{NH}$-W after the *ZPE* and *BSSE* correction. The calculated rotational constants, quartic centrifugal distortion constants, and the permanent electric dipole moment components of Py$_{NH}$-W and Py$_{\pi}$-W are summarized in Table 3.1. Their atomic coordinates predicted are given in Table S3.1-S3.2, Supporting Information.

The rotational spectrum of the ^{12}C Py$_{NH}$-W complex was previously reported by Tubergen et al.[3] We have measured some additional *a*-type transitions with both ^{14}N nuclear quadrupole hyperfine structures and the tunneling doublets. The higher frequency tunneling components are noticeably stronger, about two to three times, than the lower ones, consistent with the previous report.[3] No *b*- or *c*-type transitions could be detected, despite substantial efforts. For consistency, we also remeasured all lines reported before. To fit the observed transitions, the Watson's semi-rigid rotor Hamiltonian in the *S*-reduction and I^r representation[38] including ^{14}N nuclear quadrupole hyperfine structures was used. The two tunneling components were fitted separately. The experimental spectroscopic constants obtained with the Pgopher program[37] are summarized in Table 3.1, while the observed transition frequencies are in Table S3.3, Supporting Information.

Since only *a*-type transitions were detected, *A* rotational constant is not as well determined as *B* and *C*. For the two tunneling states, *B* and *C* are quite similar whereas *A* differs significantly between these two tunneling states. The experimental *B* and *C* constants are about 1.8% smaller than the calculated ones at the equilibrium, whereas the average of *A*s of the two tunneling states is about 0.2% smaller than the DFT value. Such reductions are not surprising because the ground state structure is generally less compact than at the equilibrium.

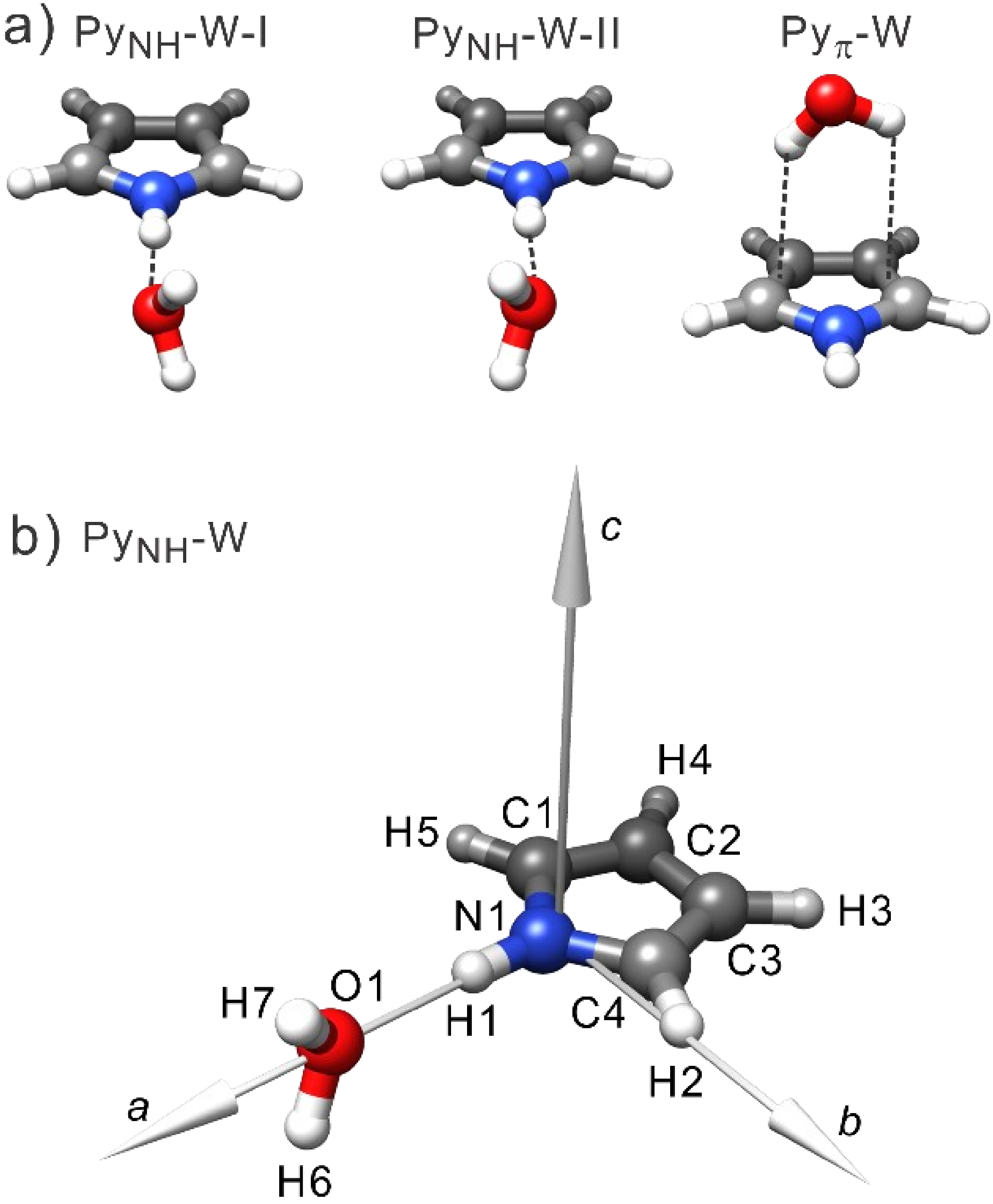

Figure 3.1. a) Optimized geometries of the pyrrole-water complex at the B3LYP-D3(BJ)/def2-TZVP level of theory. Py$_{NH}$-W-**I** and -**II** are mirror images to each other. b) The observed Py$_{NH}$-W conformer in its principal inertial axis system with atom numbering.

Table 3.1. Experimental and theoretical rotational constants, quartic centrifugal distortion constants, nuclear quadrupole coupling constants of the parent pyrrole-water complex.

Constants	Experiment			Theory[a]	
	^{12}C Py$_{NH}$-W			^{12}C Py$_{NH}$-W	^{12}C Py$_{\pi}$-W
	Upper	Lower	Average		
A / MHz	8949.12(25)	9035.68(24)	8992.27	9011.8	4517.8
B / MHz	1638.55735(70)	1638.45099(76)	1638.50433	1668.2	2580.9
C / MHz	1391.62362(67)	1391.23517(71)	1391.42919	1417.1	2578.6
D_J / kHz	0.5796(98)	0.713(11)	0.641	0.43621	4.5679
D_{Jk} / kHz	58.978(90)	60.238(84)	59.648	39.263	30.856
D_k[b] / kHz	-36.603 (fixed)	-36.603 (fixed)	-36.603	-36.603	-34.890
d_1 / kHz	-0.147(11)	-0.280(16)	-0.217	-0.0949	-0.0074
d_2[b] / kHz	-0.83855 (fixed)	-0.83855 (fixed)	-0.83855	-0.83855	0.00095
χ_{aa} / MHz	0.9104(27)	0.9186(27)	0.9147	0.9222	-2.7361
χ_{bb}-χ_{cc} / MHz	3.7534(48)	3.7697(66)	3.7613	3.7085	-0.2149
N[c]	58	43	N/A	N/A	N/A
σ[c] / kHz	3.5	2.8	N/A	N/A	N/A
$\|\mu_{a,b,c}\|$ / Debye	*a*-type only	*a*-type only	N/A	4.7, 0.9, 0.0	2.4, 0.1, 1.4

[a] The quartic centrifugal distortion constants were predicted with the anharmonic vibrational correction.

[b] Fixed to the calculated values of Py$_{NH}$-W during the fits.

[c] N is the number of hyperfine components included in the fit and σ is the standard deviation of the fit.

To predict the rotational transitions of the ^{13}C isotopologues, we scaled the calculated rotational constants with the factor used for the parent to reproduce the experimental rotational constants from their DFT values. Based on the equilibrium geometry of Py$_{NH}$-W (see Figure 3.1), one would expect four different ^{13}C substitution positions, C1, C2, C3, and C4, with the rotational constants of the substituted C1 and C4 species being similar and the same expected for C2 and C3. Despite extensive searches with the cavity-based and with the CP-FTMW instruments, only one set of rotational transitions could be attributed to C1/C4. The same can be said for C2/C3. This experimental evidence seems to suggest that the positions C1 and C4 are equivalent and the same for the C2 and C3 positions. We will come back to this point in the structural discussion.

Overall, 11 and 10 transition lines were detected for the upper and lower water tunneling states, respectively, with ^{13}C substitution at the C1/C4 sites, whereas 7 (upper) and 6 (lower) transitions lines were observed with ^{13}C substitution at the C2/C3 sites, respectively. These transition frequencies were fitted to the same Watson's Hamiltonian and the resulting spectroscopic constants are summarized in Table 3.2, while the related transition frequencies are listed in Table S3.4-S3.5, Supporting Information. A section of the broadband spectrum is presented in Figure 3.2, together with a zoom-in section showing the ^{14}N nuclear quadrupole hyperfine structures and water tunneling splitting of the ^{13}C isotopologues.

We were not able to detect rotational transitions of the Py$_{\pi}$-W complex with several attempts. Some possible reasons are: 1) Py$_{\pi}$-W is predicted to be ~5.3 kJ mol^{-1} less stable than Py$_{NH}$-W; 2) its μ_a, the strongest electric dipole component, is only about half of that of Py$_{NH}$-W. We also note that in the previous low resolution IR study,[7] only Py$_{NH}$-W was detected, but not Py$_{\pi}$-W.

Table 3.2. Experimental spectroscopic constants of the ^{13}C1/^{13}C4 and ^{13}C2/^{13}C3 isotopologues of Py$_{NH}$-W.

Constants[a]	^{13}C1/^{13}C4 Py$_{NH}$-W		^{13}C2/^{13}C3 Py$_{NH}$-W	
	Upper	Lower	Upper	Lower
A /MHz	8753.49(19)	8836.12(42)	8870.19(82)	8952.14(61)
B /MHz	1636.94827(42)	1636.8359(14)	1620.20102(82)	1620.09569(29)
C /MHz	1385.69953(37)	1385.3151(12)	1376.50853(89)	1376.12285(29)
D_J / kHz	0.4362 (fixed)[a]	0.4362 (fixed)[a]	0.4362 (fixed)[a]	0.4362 (fixed)[a]
D_{Jk} /kHz	60.13(18)	61.03(22)	52.74(59)	51.59(23)
D_k / kHz	-36.603 (fixed)[a]	-36.603 (fixed)[a]	-36.603 (fixed)[a]	-36.603 (fixed)[a]
d_1 / kHz	-0.09494 (fixed)[a]	-0.100(28)	-0.09494 (fixed)[a]	-0.09494 (fixed)[a]
d_2 / kHz	-0.83855 (fixed)[a]	-0.83855 (fixed)[a]	-0.83855 (fixed)[a]	-0.83855 (fixed)[a]
χ_{aa} / MHz	0.9091(26)	0.9081(49)	0.9178(35)	0.9155(11)
χ_{bb}-χ_{cc} / MHz	3.7792(75)	3.756(13)	3.7721(89)	3.7550(28)
N^b	31	27	23	15
σ^b / kHz	3.5	4.6	5.0	1.2

[a] Fixed to the calculated values of the ^{12}C Py$_{NH}$-W isotopologue.

[b] N is the number of hyperfine components included in the fit and σ is the standard deviation of the fit.

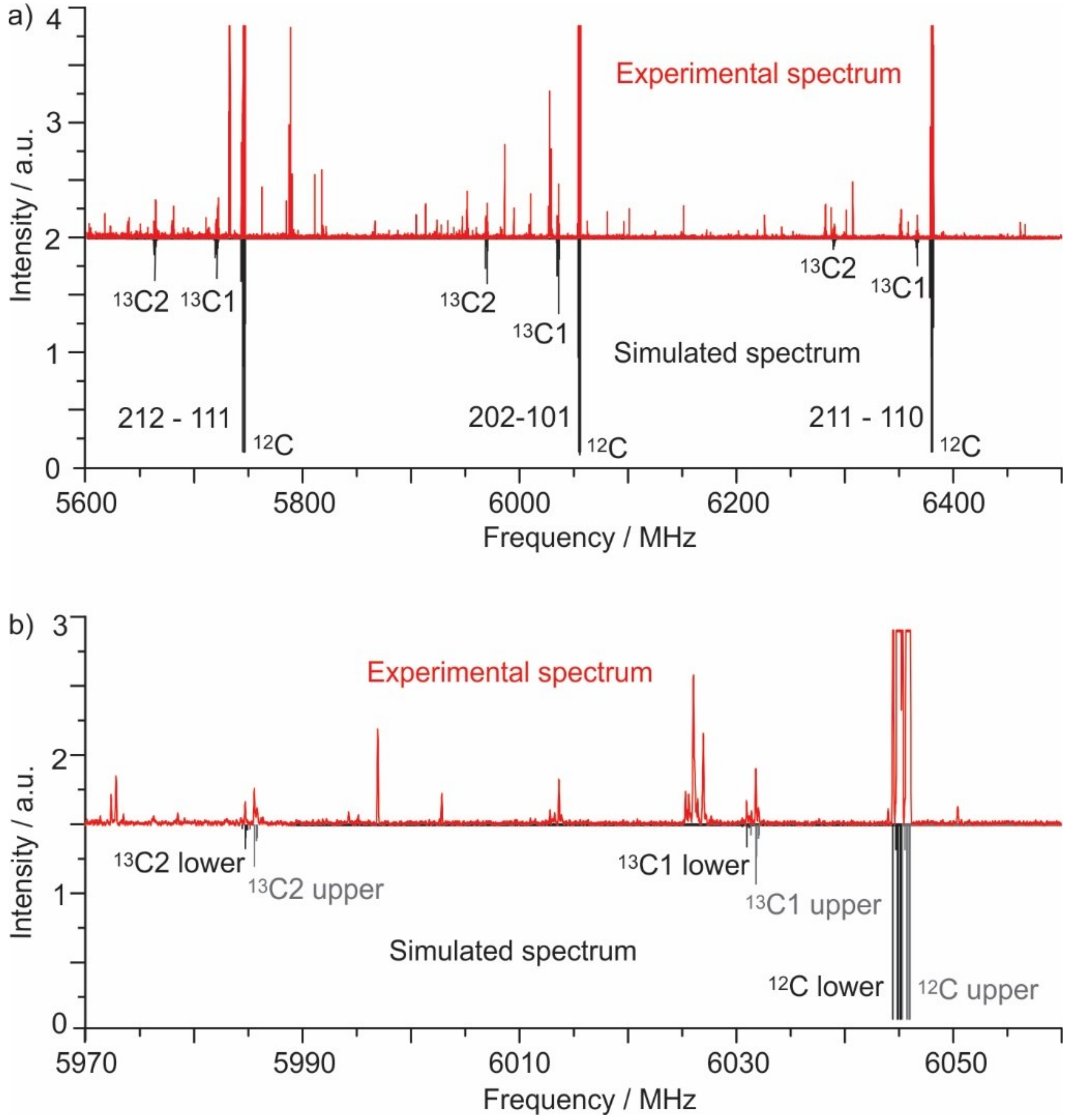

Figure 3.2. a) A section of the broadband rotational spectrum of Py_{NH}-W in the 5600-6500 MHz region. The ^{12}C Py_{NH}-W transitions are truncated to ~20% of its original intensities to provide a clearer view of the ^{13}C Py_{NH}-W transitions. The simulated spectra were generated using the spectroscopic constants obtained from the respective fits of the ^{12}C, ^{13}C1/^{13}C4 and ^{13}C2/^{13}C3 upper and lower tunneling states, the predicted dipole moment components, and a rotational temperature of 0.5 K. b) A zoom-in section of the 5970–6060 MHz region. The transitions of the lower water tunneling state are always lower in frequency than the corresponding ones of the upper tunneling state. Partially resolved ^{14}N nuclear quadrupole hyperfine splitting structures are visible.

2. The PES scan of Py$_{NH}$-W and its large amplitude motions

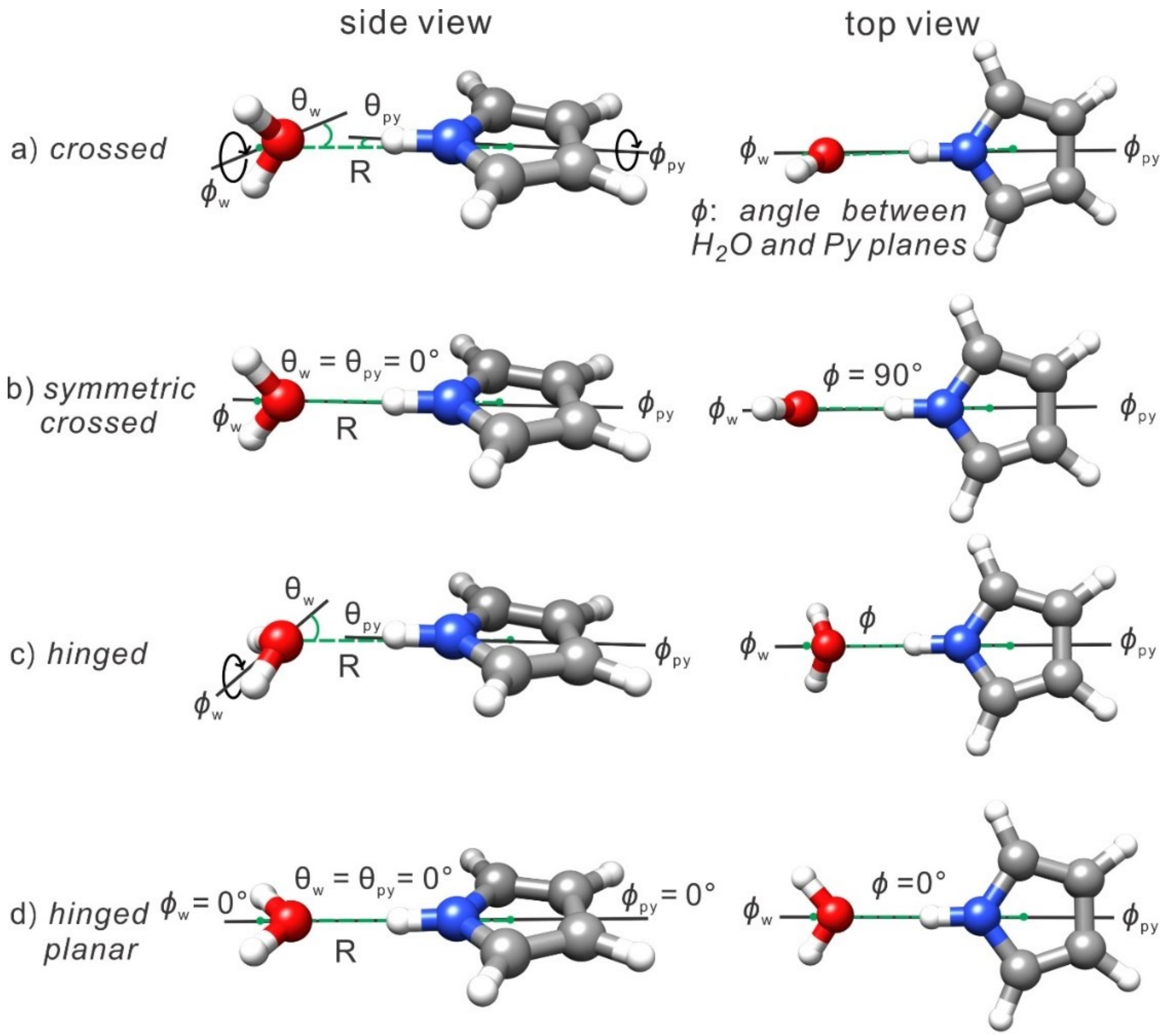

Figure 3.3. Four characteristic Py$_{NH}$-W geometries discussed in Ref. 3. The six structural parameters used to describe the relative positions of pyrrole and water in the complex are: R, the distance (green dashed line) between the centers of mass of pyrrole and of water (green dots); θ_{py}, the angle between the C_2 axis of pyrrole and R, θ_w. the angle between the C_2 axis of water and R; ϕ_{py} and ϕ_w are two angles which describe the rotation about the C_2 axis of pyrrole and of water, respectively; and finally, ϕ is the dihedral angle between ϕ_{py} and ϕ_w.

In the previous report of Py$_{NH}$-W,[3] four possible structures were proposed, i.e. *crossed*, *symmetric crossed*, *hinged*, and *planar hinged* (Figure 3.3). Generally, six intermolecular structural parameters are needed to describe the relative positions of the two monomeric subunits, assuming that the structures of the subunits remain very much the same as the respective isolated monomers. These coordinates are defined in Figure 3.3. The *crossed* structure in a) is the global minimum geometry of Py_{NH}-W (Figure 3.1) and the related *symmetric crossed* structure in b) has the pyrrole and water planes perpendicular to each other. The *hinged* structure in c) has two water H atoms above or below the pyrrole plane and the *hinged planar* structure d) corresponds to water and pyrrole in the same plane.

In recent studies of molecule-water complexes, multidimensional large amplitude motions have been identified theoretically and confirmed with experimental evidences, such as those in pyridine-water[39], glycidate-water[40], 2-fluoroethnaol-water.[22] Very often, these large amplitude motions can influence rotational transition selection rules, the magnitude of electric dipole moment components, and tunneling splitting patterns, as beautifully illustrated by Leopold and co-workers[39] in their work on pyridine-water. To better understand the relationship between the *hinged* and the *crossed* structures, we carried out a 2D PES scan along two water-centered motions starting from the *crossed* structure. The corresponding 3D and 2D presentations of the PES scans are depicted in Figure 3.4.

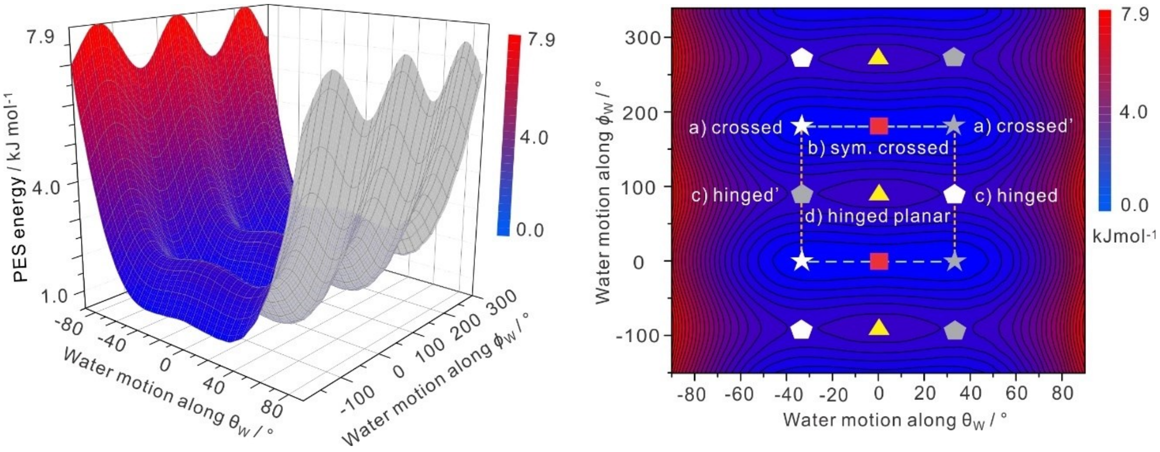

Figure 4. The 3D (left) and 2D (right) presentations of a rigid PES scan of Py_{NH}-W along two water motions, i.e. ϕ_w and θ_w defined in Figure 3. The global minima are the two *crossed* structures, i.e. Py_{NH}-W-**I** (white star) and Py_{NH}-W-**II** (gray star). The transition state (red square), corresponding to the *symmetric crossed* structure, connects the two global minima with the horizontal dashed line where the two H atoms of water flap from left to right and vice versa. Another minimum energy path (vertical dashed line) which connects Py_{NH}-W-**I** (white star) to the neighbouring Py_{NH}-W-**I** (white star) represents the water tunneling motion where the two water H atoms are exchanged. The associated transition states, marked as white or gray pentagons, have the *hinged* structure. The pink triangles between the white and gray pentagons correspond to the *hinged planar* structures.

As one can see from Figure 3.4, the PES is very shallow along the θ_w coordinate, near the pair of mirror-imaged global minima. Since the rigid step scans may not have enough accuracy to capture the real geometries at the global minima, the geometries at the two stars were reoptimized, resulting in the same $Py_{NH}W$-I and $Py_{NH}W$-II geometries identified in Figure 3.1. In addition, three transition state calculations were carried out at the other three geometries identified in Figure 3.4. One imaginary frequency was identified for each, confirming their transition state nature. The atomic coordinates obtained of these three transition state geometries are given in Table S3.6-S3.8, Supporting Information. For these four geometries, their energetic and other properties including the raw energies, *ZPE*, *BSSE*, and the *ZPE* and *BSSE* corrected relative energies, as well as whether an imaginary frequency was identified or not are summarized in Table S3.9, Supporting Information.

The *symmetric crossed* structure is identified as a transition state. It becomes about ~1.0 kJmol^{-1} *more stable* than the global minimum, i.e. the *crossed* structure, after applying the *ZPE* and *BSSE* corrections. This means that the *symmetric crossed* structure is actually below the ground vibrational state of the global minimum, indicating that the flapping motion of the two water H atoms, from left to right and vice verse along the θ_w internal coordinate, is actually a *barrierless*, large amplitude vibrational motion. Thus, the PES supports *only* one conformer whose average structure corresponds to the *symmetric crossed* structure (see Figure 3.3b)). Such an average structure would lead to a zero averaged μ_b value, explaining why no *b*-type transitions were observed even though μ_b was predicted to be ~0.9 Debye for Py_{NH}-W-I and Py_{NH}-W-II. Furthermore, the above analysis is also consistent with the experimental evidence that only one set of rotational transitions were obtained for the ^{13}C isotopologues at C1 and C4, and one set for ^{13}C at C2 and C3.

The other water motion, along the ϕ_w internal coordinate, interchanges the two equivalent H atoms of water, corresponding to the water tunneling motion. As mentioned above, the *hinged* structure turns out be a transition state with an imaginary vibrational frequency associated with interchanging the H-bonded and non-H-bonded H atoms of water. The tunneling barrier is estimated to be about 1.4 kJmol^{-1} after the *ZPE* and *BSSE* corrections.

How about the *hinged planar* structure? It is also a transition state structure and is essentially isoenergetic with the *hinged* structure after the *ZPE* and *BSSE* corrections (Table S3.9), consistent with the observation in Figure 3.4 that the PES along the θ_w coordinate in the valley region is extremely flat.

The exchanges of two equivalent water H atoms would lead to an intensity ratio of 3:1 for the tunneling doublets. Because of the ^{14}N hyperfine structures, it is difficult to accurately estimate the experimental intensity ratio between the upper and low frequency doublet pairs although a rough ratio of 3:1 or 2:1 was extracted, consistent with the nuclear spin statistical prediction. Similar doublet splittings were observed for the ^{13}C isotopologues. This provides additional evidence that the tunneling doublet pairs observed do not involve the internal motion of the pyrrole subunit.

3. The ^{14}N nuclear quadrupole coupling constants and the ground state structure

In the above discussion, we focused on large amplitude motions of water. The ^{14}N nuclear quadrupolar coupling constants of Py_{NH}-W can provide, in principle, information about the vibrational amplitude of the pyrrole subunit in the complex if the electric field gradient at the ^{14}N nucleus of pyrrole is not affected by complexation with water. In Table 3.3, we compare the χ_{aa}, χ_{bb}, and χ_{cc} values of the pyrrole monomer with those of the Py_{NH}-W complex where significant differences are noted. It is unlikely that such large changes are simply due to the large amplitude motion of the pyrrole subunit since it is much heavier than water. Indeed, the DFT χ_{aa}, χ_{bb}, and χ_{cc} values of the *crossed* and the *symmetric crossed* structures of Py_{NH}-W are very similar, indicating that the large amplitude motion of water has little effect on the ^{14}N nuclear coupling constants.

In Ref. 3, Tubergen et al. proposed that the H-bonding with water changes the electronic environment at ^{14}N as N-H acts as a proton donor and O of water as an accepter. Here, we examine the DFT ^{14}N coupling constant predictions where vibrational effects on these constants are not considered. If the electric field gradiences at ^{14}N were not significantly altered from the pyrrole monomer to the Py-W complex, one would expect the same ^{14}N

coupling constants for the monomer and the *symmetric crossed* structure of Py_{NH}-W since the directions of their *a*-, *b*- and *c*-principal inertial axes remain the same. This is clearly not the case: significant changes are predicted, indicating a noticeable electronic structural change upon complexation. Overall, the variation from the monomer to the complex is mostly captured by the DFT calculation and the experimental nuclear quadrupole coupling constants are well predicted, suggesting a small vibrational amplitude of the pyrrole subunit in Py_{NH}-W.

Table 3.3. Comparison of the ^{14}N nuclear quadrupolar coupling constants in the pyrrole monomer and in the Py_{NH}-W complex

Species	Exp./Cal.	χ_{aa}	χ_{bb}	χ_{cc}
Pyrrole[a]	Exp.	1.400(8)	1.300(8)	-2.799(11)
Pyrrole[b]	G16	1.5903	1.2336	-2.8238
^{12}C Py-W (*crossed*)[b]	G16	0.9218	1.3934	-2.3152
^{12}C Py-W (*sym. crossed*)[b]	G16	0.9268	1.3901	-2.3169
^{12}C Py-W	Exp. upper	0.9104(27)	1.4215(18)	-2.3319(30)
	Exp. lower	0.9186(27)	1.4256(25)	-2.3700(41)
^{13}C1/4 Py-W	Exp. upper	0.9091(26)	1.4351(28)	-2.3441(47)
	Exp. lower	0.9081(49)	1.4240(50)	-2.3320(80)
^{13}C2/3 Py-W	Exp. upper	0.9178(35)	1.4272(34)	-2.3449(55)
	Exp. lower	0.9155(11)	1.4198(11)	-2.3352(17)

[a] Reference 41.

[b] Calculated at the B3LYP-D3(BJ)/def2-TZVP level of theory.

We established in the previous section that the ground state average structure of Py_{NH}-W is *symmetric crossed*. Additional experimental supporting evidence for the *symmetric crossed* geometry can be found in the P_{cc} planar moment values of the isotopologues, summarized in Table 3.4. Even without the DFT calculations, one can already eliminate the *hinge planar* structure as the one observed because the much larger P_{cc} value of ^{14}N-D_3 Py_{NH}-W, compared to the others, indicates that the water H atoms are not in the same plane as pyrrole. The P_{cc} values of the lower tunneling states of the two ^{13}C (0.568(1) and 0.5744(3) amu Å^2), one ^{15}N (0.5752(23) amu Å^2), and ^{12}C parent (0.5608(7) amu Å^2)

isotopologues are very similar ranging from 0.56 to 0.57 amu Å^2, corresponding to the contribution of the two water H atoms. The P_{cc} values of the upper tunneling state for all isotopologues are all at ~0.87 amu Å^2. The consistent P_{cc} planar moment values of the aforementioned isotopologues indicate that the pyrrole ring is in the *ab*-plane. For comparison, the P_{cc} value of the ^{12}C, ^{13}C, and ^{15}N, and D isotopologues of pyrrole[39], a planar molecule, are -0.0080 amu Å^2. For Py$_{NH}$-W, the P_{bb} values of the ^{12}C, ^{15}N, and ^{14}N-D$_3$ isotopologues would be expected to be more or less the same for a *symmetric crossed* geometry. Indeed, the first two values are 55.3707(8) and 55.3764(23) amu Å^2 are very similar. The P_{bb} value of ^{14}N-D$_3$ is 55.4003(17) amu Å^2 and its slight variation from the other two can be attributed to the large amplitude motion of water along the θ_w coordinate since the deuterium substitution can modify the magnitude of this motion.

Table 3.4. Summary of the planar moments (amu Å^2) of the pyrrole monomer and the Py$_{NH}$-W complex

Species	State	P_{aa}	P_{bb}	P_{cc}
Pyrrole[a]	Ground state	56.153(10)	55.358(10)	-0.008(10)
^{12}C Py$_{NH}$-W	Upper tunneling	307.56(25)	55.6005(7)	0.8720(7)
	Lower tunneling	307.89(24)	55.3707(8)	0.5608(7)
^{13}C1/4 Py$_{NH}$-W	Upper tunneling	307.85(19)	56.8563(4)	0.8783(4)
	Lower tunneling	308.19(42)	56.6263(14)	0.5684(12)
^{13}C2/3 Py$_{NH}$-W	Upper tunneling	311.05(82)	56.0985(8)	0.8765(9)
	Lower tunneling	311.37(61)	55.8790(3)	0.5744(3)
^{15}N Py$_{NH}$-W[b]	Upper tunneling	307.6092(11)	55.5982(11)	0.8762(11)
	Lower tunneling	307.9315(23)	55.3764(23)	0.5752(23)
^{14}N-D$_3$ Py$_{NH}$-W[b]	Upper/lower tun.[b]	336.6734(17)	55.4003(17)	1.7112(17)

[a] Based on the rotational constants reported in Ref. 41.
[b] Based on the rotational constants reported in Ref. 3. ^{14}N-D$_3$ substitution corresponds pyrrole-1-*d*-D$_2$O and only the averaged rotational constants of the upper and lower tunnelling states are available.

With all the isotopologues studied, we employed the STRFIT program[36] to refine the effective intermolecular structural parameters of the pyrrole-water complex. The effective structural parameters of the pyrrole and water subunits were obtained using their rotational constants.[2,42] Theses monomeric structural parameters are listed in Table S3.10, Supporting Information. Since we have established that the average structure of Py_{NH}-W is *symmetric crossed*, in principle we need only one structural parameter, i.e. the distance *R* between the centre-of-masses of water and pyrrole, to describe the structure. On the other hand, the water subunit experiences a large amplitude vibrational motion along the θ_w coordinate (Figure 3.3), which is expected to modify the effective rotational constants. For this reason, we have adopted the same fitting parameters as in Ref. 3, which include *R* and also the amplitude of the water motion, angle θ_w. The fitted results for *R* and θ_w for the lower tunneling state are 4.2043(11) Å and 36.8(35) °, respectively. The corresponding atomic coordinates of the fitted geometry are given in Table S3.11, Supporting Information.

Conclusions

We have measured and assigned rotational spectra of all monosubstituted ^{13}C isotopologues of Py_{NH}-W in their natural abundances and extended the measurement of the ^{12}C parent species. The ^{14}N nuclear quadrupole hyperfine splittings and water tunneling doublets of the ^{13}C isotopologues were also observed and analyzed. We have performed PES scans along paths of possible water motions and identified all four previously proposed geometries, namely *crossed*, *symmetric-crossed*, *hinged* and *planar hinged*, and correlate them to one global minimum and three transitions states. The current theoretical and experimental data indicate that the vibrationally average ground state structure of Py_{NH}-W is *symmetric crossed*, and lead to the identification of the water tunneling path and an estimation of its barrier to be ~1.4 kJ mol^{-1}. The current study also paves the road for future investigation of step-wise solvation of pyrrole with several water molecules.

References

1. Nygaard, U.; Nielsen, J. T.; Kirchheiner, J.; Maltesen, G.; Rastrup-Andersen, J.; Sørensen, G. O., *J. Mol. Struct.* **1969,** *3*, 491-506.
2. Bak, B. R.; Christensen, D.; Hansen, L.; Rastrup‐Andersen, J., *J. Chem. Phys.* **1956,** *24*, 720-725.
3. Tubergen, M. J.; Andrews, A. M.; Kuczkowski, R. L., *J. Phys. Chem.* **1993,** *97*, 7451-7457.
4. Sobolewski, A. L.; Domcke, W., *Chem. Phys. Lett.* **2000,** *321*, 479-484.
5. Kumar, A.; Kołaski, M.; Kim, K. S., *J. Chem. Phys.* **2008,** *128*, 034304.
6. Gao, W.; Jiao, J.; Feng, H.; Xuan, X.; Chen, L., *J. Mol. Model.* **2013,** *19*, 1273-1283.
7. Matsumoto, Y.; Honma, K., *J. Chem. Phys.* **2009,** *130*, 054311.
8. Su, Z.; Xu, Y., *Angew. Chem. Int. Ed.* **2007,** *46*, 6163-6166; *Angew. Chem.* **2007**, *119*, 6275-6278.
9. Thomas, J.; Sukhorukov, O.; Jäger, W.; Xu, Y., *Angew. Chem. Int. Ed.* **2014**, *53*, 1156−1159; *Angew. Chem.* **2014**, *126*, 1175−1178.
10. Gruet, S.; Pérez, C.; Steber, A. L.; Schnell, M., *Phys. Chem. Chem. Phys.* **2018,** *20*, 5545-5552.
11. Balle, T.; Flygare, W., *Rev. Sci. Instrum.* **1981,** *52*, 33-45.
12. Xu, Y.; Jäger, W., *J. Chem. Phys.* **1997,** *106*, 7968-7980.
13. Xu, Y.; Wijngaarden, J. V.; Jäger, W., *Int. Rev. Phys. Chem.* **2005,** *24*, 301-338.
14. Brown, G. G.; Dian, B. C.; Douglass, K. O.; Geyer, S. M.; Pate, B. H., *J. Mol. Spectrosc.* **2006,** *238*, 200-212.
15. Grubbs, G. S.; Dewberry, C. T.; Etchison, K. C.; Kerr, K. E.; Cooke, S. A., *Rev. Sci. Instrum.* **2007,** *78*, 096106.
16. Dempster, S. P.; Sukhorukov, O.; Lei, Q. Y.; Jäger, W., *J. Chem. Phys.* **2012,** *137*, 174303.
17. Thomas, J.; Yiu, J.; Rebling, J.; Jäger, W.; Xu, Y., *J. Phys. Chem. A* **2013,** *117*, 13249-13254.
18. Pérez, C.; Lobsiger, S.; Seifert, N. A.; Zaleski, D. P.; Temelso, B.; Shields, G. C.; Kisiel, Z.; Pate, B. H., *Chem. Phys. Lett.* **2013,** *571*, 1-15.
19. Xie, F.; Seifert, N. A.; Heger, M.; Thomas, J.; Jäger, W.; Xu, Y.,. *Phys. Chem. Chem. Phys.* **2019,** *21*, 15408-15416.
20. Carlson, C. D.; Seifert, N. A.; Heger, M.; Xie, F.; Thomas, J.; Xu, Y., *J. Mol. Spectrosc.* **2018,** *351*, 62-67.
21. Seifert, N. A.; Thomas, J.; Jäger, W.; Xu, Y., *Phys. Chem. Chem. Phys.* **2018,** *20*, 27630-27637.
22. Huang, W.; Thomas, J.; Jäger, W.; Xu, Y., *Phys. Chem. Chem. Phys.* **2017,** *19*, 12221-12228.
23. Grimme, S., *J. Chem. Theory comput.* **2019,** *15*, 2847-2862.
24. Pracht, P.; Bohle, F.; Grimme, S., *Phys. Chem. Chem. Phys.* **2020,** *22*, 7169-7192.
25. Oswald, S.; Seifert, N. A.; Bohle, F.; Gawrilow, M.; Grimme, S.; Jäger, W.; Xu, Y.; Suhm, M. A., *Angew. Chem. Int. Ed.* **2019**, *58*, 5080-5084; *Angew. Chem.* **2019**, *131*, 5134-5138.
26. Xie, F.; Seifert, N. A.; Jaeger, W.; Xu, Y., *Angew. Chem. Int. Ed.* ***2020,*** *59, 15703-15710; Angew. Chem.* ***2020,*** *132,15833-15840.*

27. Frisch, M.; Trucks, G.; Schlegel, H.; Scuseria, G.; Robb, M.; Cheeseman, J.; Scalmani, G.; Barone, V.; Petersson, G.; Nakatsuji, H., Gaussian 16. *Revision A* **2016,** *3*.
28. Becke, A. D., Density-functional thermochemistry. III. The role of exact exchange. *J. Chem. Phys.* **1993,** *98*, 5648.
29. Stephens, P.; Devlin, F.; Chabalowski, C.; Frisch, M. J., *J. Phys. Chem.* **1994,** *98*, 11623-11627.
30. Grimme, S.; Ehrlich, S.; Goerigk, L., *J. Comput. Chem.* **2011,** *32*, 1456-1465.
31. Becke, A. D.; Johnson, E. R., A density-functional model of the dispersion interaction. *J. Chem. Phys.* **2005,** *123*, 154101.
32. Krishnan, R.; Binkley, J. S.; Seeger, R.; Pople, J. A., *J. Chem. Phys.* **1980,** *72*, 650-654.
33. Boys, S. F.; Bernardi, F., *Mol. Phys.* **1970,** *19*, 553-566.
34. Hanwell, M. D.; Curtis, D. E.; Lonie, D. C.; Vandermeersch, T.; Zurek, E.; Hutchison, G. R., *J. Cheminformatics* **2012,** *4*, 17.
35. Pettersen, E. F.; Goddard, T. D.; Huang, C. C.; Couch, G. S.; Greenblatt, D. M.; Meng, E. C.; Ferrin, T. E., *J. Comput. Chem.* **2004,** *25*, 1605-1612.
36. Kisiel, Z., PROSPE–Programs for rotational spectroscopy. *Spectroscopy from Space* **2001**, 91-106.
37. Western, C. M., PGOPHER: A program for simulating rotational, vibrational and electronic spectra. *J. Quant. Spectrosc. Radiat. Transfer* **2017,** *186*, 221-242.
38. Watson, *J. K. G., in Vibrational Spectra and Structure, Vol. 6 (Ed.: J. R. Durig), Elsevier, New York,* ***1977****, pp. 1- 89.*
39. Mackenzie, R. B.; Dewberry, C. T.; Cornelius, R. D.; Smith, C.; Leopold, K. R., *J. Phys. Chem. A* **2017,** *121*, 855-860.
40. Gall, J. T.; Thomas, J.; Xie, F.; Wang, Z.; Jäger, W.; Xu, Y., *Phys. Chem. Chem. Phys.* **2017,** *19*, 29508-29515.
41. Bolton, K.; Brown, R., *Aust. J. Phys.* **1974,** *27*, 143-146.
42. Császár, A. G.; Czakó, G.; Furtenbacher, T.; Tennyson, J.; Szalay, V.; Shirin, S. V.; Zobov, N. F.; Polyansky, O. L., *J. Chem. Phys.* **2005,** *122*, 214305.

Chapter 4

A higher energy hexafluoroisopropanol···water isomer and its large amplitude motions: rotational spectra and DFT calculations[1]

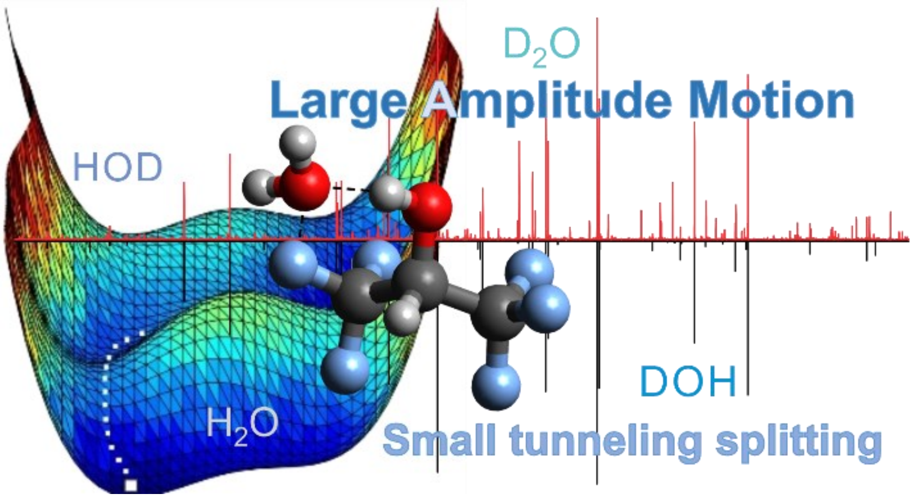

---

[1] This study has been published as B. Wu, A. S. Hazrah, N. A. Seifert, S. Oswald, W. Jäger, Yunjie Xu, "A higher energy hexafluoroisopropanol···water isomer and its large amplitude motions: rotational spectra and DFT calculations", *J. Phys. Chem. A*. **2021**, *125*, 10401−10409.

Abstract

Rotational spectra of the 1,1,1,3,3,3-hexafluoro-2-propanol (HFIP)···water complex were measured using a chirped pulse Fourier transform microwave spectrometer. The spectral analyses, aided by DFT calculations, reveal two HFIP···water isomers: one previously reported, *trans* HFIP ($HFIP_t$)···water (*Phys. Chem. Chem. Phys.* **2015,** *119*, 5650), and a new isomer, *gauche* HFIP ($HFIP_g$)···water. To confirm the identity of the new isomer, rotational spectra of seven of its deuterated species were also measured and analyzed. Both the experimental and theoretical evidence indicates that the intermolecular interaction with water preferentially stabilizes the $HFIP_g$ monomer configuration over the global minimum configuration, $HFIP_t$. The relative energy difference between these monomeric forms is 4.1 kJ mol^{-1} and decreases to 2.5 kJ mol^{-1} in the respective monohydrates at the B3LYP-D3(BJ)/def2-QZVP level of theory. Both rigid and relaxed potential energy surface scans were carried out to gain insights into the large amplitude water motions in $HFIP_g$···water. The non-observation of a water tunneling splitting in $HFIP_t$···water has been explained to be a result of a barrier-less (after zero-point-energy correction) pathway for the water motion, whereas in $HFIP_g$···water, a relatively large water tunneling barrier was identified as the cause of barely resolved water tunneling splittings. Non-covalent interaction (NCI) and quantum theory of atoms and molecules (QTAIM) analyses were used to evaluate the changes in $HFIP_g$···water when going from the minimum to the transition state in terms of attractive interactions such as the OH···H and OH···F contacts. The effect of fluorination is discussed by comparing the vastly different binding topologies of isopropanol···water and HFIP···water.

Introduction

1,1,1,3,3,3-hexafluoro-2-propanol (HFIP) is an important solvent widely used in (bio)organic syntheses. This is in part because it can act simultaneously as a proton donor and acceptor and in part because of some special properties associated with perfluorinated alcohols. For example, HFIP can help to stabilize the α-helix structures in proteins,[1-4] and also to dissolve some polymers at room temperature that are often hard to be dissolved using regular organic solvents.[5] HFIP, a fluorinated alcohol, is also considered to be a greenhouse gas.[6, 7] One main structural flexibility in HFIP is associated with the hydroxyl group orientation, i.e., the H-O-C-H dihedral angle τ. HFIP can take on *trans* (t, $\tau = 180°$), *gauche*+ (g+, $\tau = +60°$) and *gauche*- (g-, $\tau = -60°$) configurations.[8, 9] In the *trans* configuration of HFIP_t, the OH group points into the opposite direction of the central CH group, whereas they are on the same side of the carbon frame in the two *gauche*-forms of HFIP. In addition, the *g*+ and *g*- forms of HFIP are non-superimposable mirror images to each other and HFIP exhibits transient chirality. Since the *g*+ and *g*-forms would lead to the same rotational spectra, we simply name them as HFIP_g. The HFIP monomer had been investigated by Fourier transform microwave (FTMW)[8] spectroscopy in a supersonic jet expansion and by FT infrared (FTIR)[10, 11] spectroscopy in a static cell at room temperature and in a jet. While the fraction of HFIP_g is about 0.5 at room temperature, it decreases to essentially zero under jet conditions. In the FTMW study,[8] only the global minimum structure, HFIP_t, had been observed experimentally. Interestingly, HFIP_g had been detected in the HFIP dimer and trimer.[12] In particular, HFIP_g is the only monomeric subunit used in the global minimum structure of the HFIP trimer,[12] indicating that H-bonding interactions preferentially stabilize the *g*-form of HFIP in these cases. On the other hand, HFIP_t is the only subunit observed in the hydrogen bonded binary complex, HFIP···1,4 dioxane, in a recent FTMW study.[13] It is certainly of interest to investigate hydrogen bonding interactions between HFIP and water to gain further insight into the preference of the *trans* versus *gauche* forms of HFIP in these hydrogen bonded complexes.

In addition, detailed structural and energetics studies of the HFIP···water complex in the gas phase would be helpful for understanding properties of the HFIP+water co-solvent. A solution mixture of HFIP and water had been studied using X-ray, NMR and mass spectrometry,[14] where clusters of $\text{HFIP}\cdots\text{water}_n$ and HFIP oligomers were observed. Directly related to the current work is the previous FTMW spectroscopic report of the HFIP···water complex by Shahi and Arunan.[15] Only the global minimum structure, $\text{HFIP}_t\cdots$water, had been observed, along with three deuterated species, i.e., $\text{HFIP}_t\cdots\text{D}_2\text{O}$, $\text{HFIP}_t\cdots$HOD, and $\text{HFIP}_t(\text{OD})\cdots\text{H}_2\text{O}$ where (OD) indicates the deuteration of the alcohol OH group. In addition, no water tunneling splittings had been observed. These observations, together with a potential energy surface (PES) scan along a coordinate that exchanges the two equivalent hydrogen atoms of water, allowed the authors to establish that water rotates essentially freely about its C_2 axis in the monohydrate.

In the current study, we applied chirped pulse-FTMW (CP-FTMW) spectroscopy to study the HFIP⋯water complex, in combination with a systematic conformational search of its possible low energy structures using electronic structure calculations. In particular, we focused on the less stable HFIP_g⋯water isomer, and seven of its deuterated species. The water motion dynamics in HFIP_g⋯water is compared to that in HFIP_t⋯water. Further, the effect of hydrogen bonding interactions with water on the relative stability of the *trans* versus the *gauche* form of HFIP is also discussed.

Experimental and theoretical methods

A broadband 2-6 GHz CP-FTMW spectrometer was utilized for the measurements. The spectrometer was designed based on a similar instrument by Pate and co-workers[16] and its details were reported in several recent publications.[17, 18] Briefly, a 2 μs chirped pulse was generated with a 12 GS/s arbitrary waveform generator and amplified by a 400 W travelling wave tube amplifier. In a typical experiment, five frames of a 20 μs long free induction decay (FID) were collected in each molecular pulse, leading to a full width at half heigh (FWHH) of ~120 kHz. If a better resolution was needed crucial, 40 μs FID were collected instead of 20 μs, although with only two frames per molecular pulse. The FWHH in the latter case is ~60 kHz. The frequency accuracy is about 5 kHz.

HFIP (Sigma Aldrich, 99.9%) and deuterium oxide (Cambridge Isotope Laboratories, Inc. 99.5%) were used without further purification. Mixtures of 0.1% HFIP with 0.2% H_2O or D_2O in 5 bar of neon (Praxair, 99.999%) were used for the spectroscopic measurements.

An extensive search for possible low energy isomers of the HFIP monohydrate was carried out using Grimme's CREST software package.[19, 20] Further geometry optimizations and harmonic frequency calculations of the CREST candidates were carried out using the Gaussian 16 program package.[21] The B3LYP hybrid functional[22, 23] in combination with Grimme's dispersion correction (D3)[24] and Becke-Johnson damping factor (BJ),[25] and the def2-QZVP basis sets[26] were used. To investigate pathways of the water motions in the complex, 1- and 2-dimensional (1D and 2D) PES scans were carried out at the B3LYP-D3(BJ)/def2-QZVP level of theory.[26] All energies reported are zero-point energy (*ZPE*) and basis set superposition error (*BSSE*) corrected. The *BSSE* energy was calculated using the counterpoise procedure.[27] The keywords used in the calculations are provided in Point S1, Supporting Information (SI).

Rotational constants of the deuterated species were predicted using Kisiel's PMIFST (Principal Moments of Inertia From STructure) program and the KRA program was utilized for calculating isotopic substitution coordinates.[28] The Autofit program[29] was also utilized to assign rotational spectra of the deuterated isotopologues. The final rotational spectroscopic fits were performed using Pgopher.[30] Optimized structures of all complexes were visualized using Avogadro.[31] We carried out non-covalent interactions (NCI)[32] and Bader's quantum theory of atoms in molecules (QTAIM) analyses[33] using the Multiwfn[34] software package and visualized the results using VMD.[35]

Results and discussion

1. Searches of isomers

Six isomers of the HFIP monohydrate were found within an energy span of 30 kJ mol^{-1} and their atomic coordinates are listed in Table S4.1-S4.6, SI. To emphasize the different interaction sites on HFIP with water, we label the complexes as $\mathrm{HFIP}_t\cdots\mathrm{W_X}$ or $\mathrm{HFIP}_g\cdots\mathrm{W_X}$, where X is used to indicate a specific HFIP interaction site with water. In the conformational searches, four HFIP_t containing isomers were identified and these have water interaction sites at the acidic OH proton (H), the alcohol oxygen (O), the alkyl CH proton (C) and the CF_3 groups (F) of HFIP_t. Only two isomers were identified for HFIP_g which have interaction sites at the acidic OH proton (H) and at the CF_3 groups (F). Their predicted relative raw and *ZPE* corrected energies and binding energies, rotational constants, and electric dipole moment components at the B3LYP-D3(BJ)/def2-QZVP level of theory are listed in Table 4.1, with their respective geometries shown in Figure

3.1. Although only three monohydrate isomers had previously been reported at the MP2/6-311++G(d,p) level,[15] their energy ordering is consistent with the current calculation results.

Table 4.1. Spectroscopic properties of the isomers of the HFIP monohydrate at the B3LYP-D3(BJ)/def2-QZVP level of theory.

Species	ΔE_{raw} [a]	ΔE_0 [b]	ΔE_b [c]	A [d]	B [d]	C [d]	$\lvert\mu_a\rvert$ [e]	$\lvert\mu_b\rvert$ [e]	$\lvert\mu_c\rvert$ [e]
$HFIP_t$									
$\cdots W_H$	0.0	0.0	27.8	1152	975	708	0.4	1.1	1.6
$\cdots W_O$	16.1	14.3	13.5	1050	961	664	1.4	0.4	1.5
$\cdots W_C$	18.7	15.0	12.8	1220	833	702	1.9	1.1	1.2
$\cdots W_F$	29.6	25. 1	2.7	1048	1016	649	0.0	2.4	0.9
$HFIP_g$									
$\cdots W_H$	2.7	2.1	29.8	1268	827	627	4.6	1.8	1.0
$\cdots W_F$	33.9	28.9	3.1	1061	1008	66	1.4	4.2	1.1

[a] Relative raw electronic energy in kJ mol^{-1}.

[b] Relative energy including *ZPE* and *BSSE* energy corrections in kJ mol^{-1}.

[c] ΔE_b= - [(ΔE_0(HFIP$\cdots$W)-ΔE_0(HFIP)-ΔE_0(W)] in kJ mol^{-1} after the *ZPE* and *BSSE* corrections.

[d] Rotational constants in MHz.

[e] Magnitudes of the electric dipole moment components in Debye.

The global minimum isomer, $HFIP_t \cdots W_H$, is about 2.1 kJ mol^{-1} more stable than the next stable isomer, $HFIP_g \cdots W_H$, after *ZPE* and *BSSE* corrections. As in the case of the monohydrate of $HFIP_t$, the preferred binding site at $HFIP_g$ is also the acidic hydroxyl H atom which serves as a proton donor.

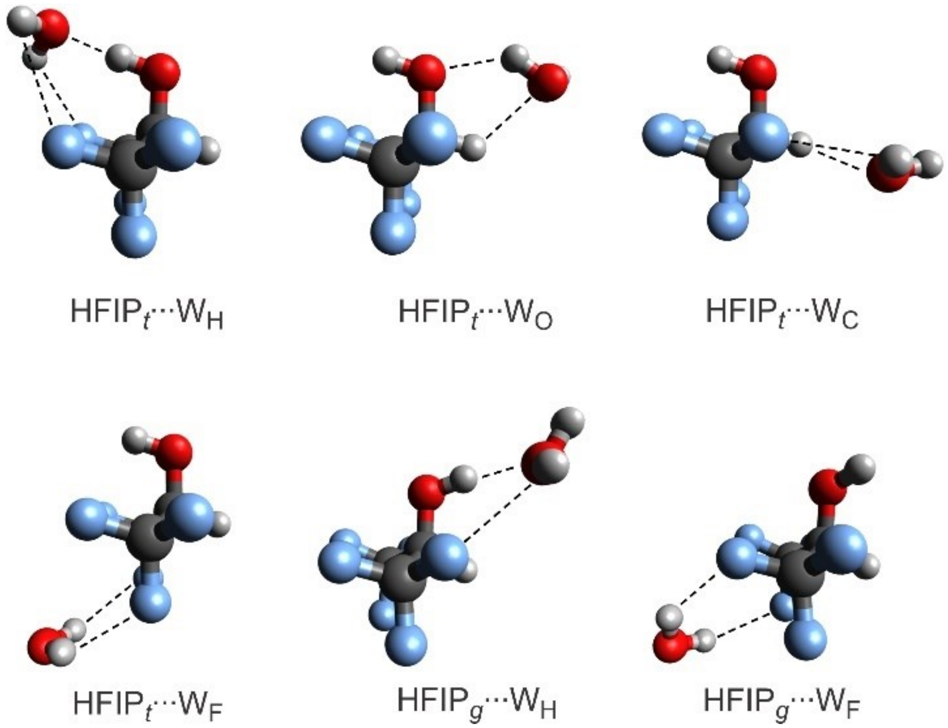
$\text{HFIP}_t\cdots\text{W}_\text{H}$ $\text{HFIP}_t\cdots\text{W}_\text{O}$ $\text{HFIP}_t\cdots\text{W}_\text{C}$

$\text{HFIP}_t\cdots\text{W}_\text{F}$ $\text{HFIP}_g\cdots\text{W}_\text{H}$ $\text{HFIP}_g\cdots\text{W}_\text{F}$

Figure 4.1. Geometries of the six most stable of isomers of the HFIP monohydrate at the B3LYP-D3(BJ)/def2-QZVP level of theory.

2. Spectroscopic assignments of $\text{HFIP}_\text{g}\cdots\text{W}_\text{H}$

After removing rotational transitions belonging to the HFIP monomer, dimer, trimer,[8, 12] and $\text{HFIP}_t\cdots\text{Ne}$[36] from the broadband spectrum, a new set of *a*-type transitions emerged, with comparable intensity to those belonging to $\text{HFIP}_t\cdots\text{W}_\text{H}$.[15] The reason for the relatively high intensity is that $\text{HFIP}_g\cdots\text{W}_\text{H}$, the less stable isomer, has a much larger predicted *a*-dipole moment component of 4.6 D than the $\mu_{a,b,c}$ dipole moment components of $\text{HFIP}_t\cdots\text{W}_\text{H}$ (≤ 1.8 D). The measured transitions frequencies were fitted using Watson's semi-rigid rotor Hamiltonian in the *A*-reduction and I^r representation.[37] The resulting spectroscopic constants are summarized in Table 4.2. Comparison of the experimental and theoretical rotational constants and the relative magnitudes of the *a*-, *b*- and *c*-dipole moment components suggests that the isomer is $\text{HFIP}_g\cdots\text{W}_\text{H}$. This is further confirmed by the deuterium isotopic data described below.

To investigate the deuterated species of HFIP$_g$⋯W$_H$, we let a gas cylinder containing D_2O and HFIP in Ne sit for >12 hours to allow deuterium exchange with the alcohol OH and residual H_2O. After removing transitions belonging to HFIP$_t$⋯W$_H$ and its three deuterium isotopologues[15] and the newly assigned HFIP$_g$⋯W$_H$ from the broadband spectrum, seven deuterated HFIP$_g$⋯W$_H$ isotopologues could be assigned with the aid of the autofit program.[29] Similar spectroscopic fits as for the parent species were carried out and the resulting spectroscopic constants are also summarized in Table 4.2. Attempts to measure the ^{13}C isotopologues of HFIP$_t$⋯W$_H$ and HFIP$_g$⋯W$_H$ using a cavity FTMW spectrometer[38] were not successful.

The atom numbering of HFIP$_g$⋯W$_H$ is shown in Figure 4.2. To clearly indicate which H is substituted, we use atomic numbering for the D substitution at water. For example, HFIP$_g$(OD)⋯HOD3 indicates deuteration of the alcohol hydroxyl group and of water at the H3 position. A section of the broadband spectrum showing these eight isotopologues is depicted in Figure 4.3, while the corresponding transition frequencies are listed in Table S4.7-S4.14, SI.

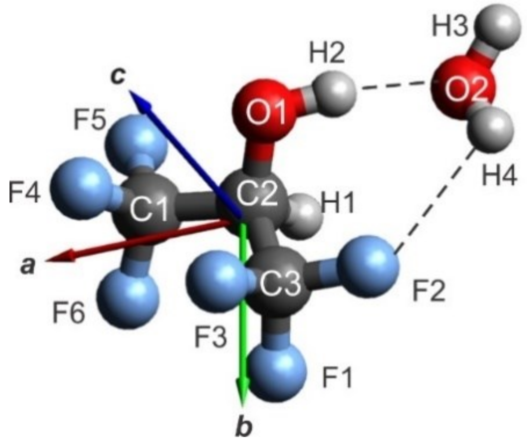

Figure 4.2. The atomic numbering of HFIP$_g$⋯W$_H$ in its principal inertial axis system. The intermolecular hydrogen bond and the close H⋯F contact between the two subunits are indicated with dashed lines.

Table 4.2. Experimental spectroscopic parameters of the $HFIP_g \cdots W_H$ isomer and seven deuterated isotopologues.

	$HFIP_g$				$HFIP_g(OD)$			
Parameter	H_2O	HOD4	HOD3	D_2O	H_2O	HOD4	HOD3	D_2O
A / MHz	1264.07887(82)	1262.90342(38)	1244.27575(32)	1244.06664(24)	1256.13582(43)	1255.12056(70)	1237.1723(27)	1237.05497(85)
B / MHz	835.05979(50)	817.04821(27)	817.56354(12)	800.07011(13)	831.87441(19)	813.996407(89)	814.36382(59)	797.01009(45)
C / MHz	632.58122(19)	622.31167(26)	618.05734(11)	608.29417(11)	629.03398(18)	618.91352(11)	614.75341(44)	605.12001(49)
Δ_J / kHz	0.1953(95)	0.1513(29)	0.1906 (fixed)[d]	0.1612(16)	0.1880 (fixed)[d]	0.1617(17)	0.1484(81)	0.1635(84)
Δ_{JK} / kHz	-0.326(40)	-0.222(14)	-0.359 (fixed)[d]	-0.272 (fixed)[d]	-0.325 (fixed)[d]	-0.247 (fixed)[d]	-0.143(36)	-0.278 (fixed)[d]
Δ_K / kHz	-6.29(14)	-6.19 (fixed)[d]	-6.76 (fixed)[d]	-6.66 (fixed)[d]	-6.17 (fixed)[d]	-6.10 (fixed)[d]	-5.72(48)	-4.934(37)
δ_J / kHz	0.0427(45)	0.0378(26)	0.0510 (fixed)[d]	0.0504(12)	0.0942(19)	0.0441 (fixed)[d]	0.0490(63)	0.0458 (fixed)[d]
δ_K / kHz	-0.737(43)	-0.687 (fixed)[f]	-0.567(18)	-0.913(12)	-0.715 (fixed)[d]	-0.652 (fixed)[d]	-0.733 (fixed)[d]	-0.479(73)
a-line no.[a]	36	31	22	21	22	23	19	19
b-line no.[a]	16	7	5	4	6	5	3	5
c-line no.[a]	6	2	1	0	0	1	0	1
N[b]	58	40	28	25	28	29	22	25
σ / kHz[c]	4.0	2.3	1.3	0.6	1.5	1.2	1.8	3.5

[a] Number of a particular type of transitions included in the fit.

[b] Total number of transitions included in the fit.

[c] Standard deviation of the fit.

[d] Centrifugal distortion constant values were fixed at the values obtained from the harmonic frequency calculations, scaled by the ratio of experimental versus calculated values for the parent species.

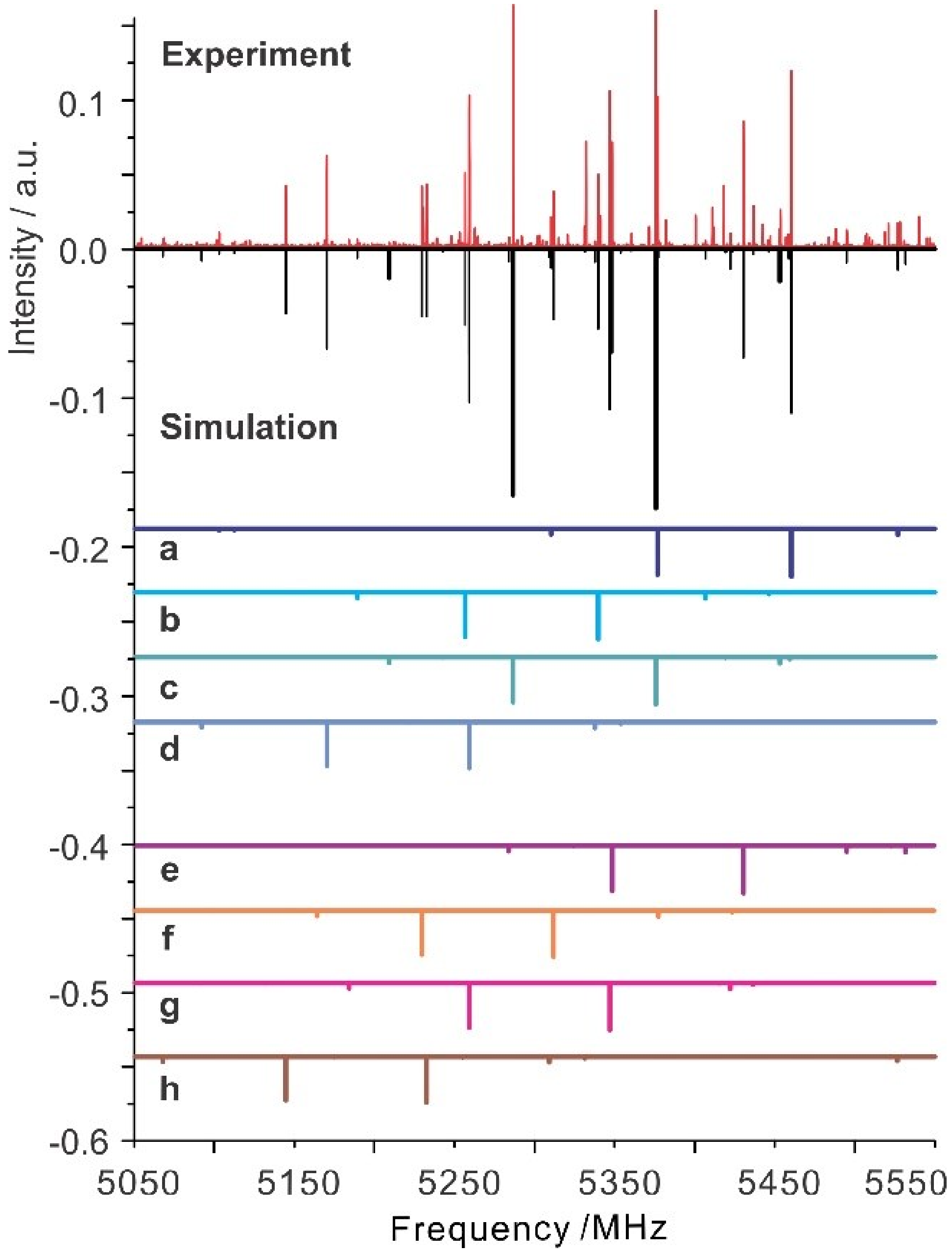

Figure 4.3. The experimental HFIP+D_2O spectrum and population weighted simulated spectra of the eight isotopologues of the $HFIP_g$ monohydrate: a) $HFIP_g\cdots H_2O$ (20%); b) $HFIP_g\cdots$HOD3 (7%); c) $HFIP_g\cdots$HOD4 (23%); d) $HFIP_g\cdots D_2O$ (11%); e) $HFIP_g$(OD)$\cdots H_2O$ (11%); f) $HFIP_g$(OD)$\cdots$HOD3 (7%); g) $HFIP_g$(OD)$\cdots$HOD4 (15%) and h) $HFIP_g$(OD)$\cdots D_2O$ (6%). In the individual spectra, the simulated line intensities of each species are normalized and their estimated experimental percentage abundances are given in the brackets above. All lines belonging to the HFIP monomers, dimers, HFIP$\cdots$Ne and $HFIP_t\cdots$water and their associated isotopologues were removed for clarity.

The predicted rotational constants obtained from the B3LYP-D3(BJ)/def2-QZVP results are compared to the experimental ones in Table S4.15, SI. Overall, very good agreement between experiment and theory is found, with the largest percentage errors being -0.71% for *A*, 0.85% for *B* and 0.63% for *C* rotational constants, confirming the identity of the carrier of the observed lines to be $\mathrm{HFIP}_g\cdots\mathrm{W_H}$.

3. Large amplitude motions associated with water

In this section, we examine possible large amplitude motions (LAM) which frequently accompany the free OH group of water, often observed in a range of monohydrates, such as pyridine⋯water,[39] methyl glycidate⋯water,[40] and 2-fluoroethanaol⋯ water.[41] In the previous study of $\mathrm{HFIP}_t\cdots\mathrm{W_H}$,[15] no water tunneling splitting had been observed experimentally. This was explained by a barrier-less rotational motion of the water subunit about its C_2 symmetry axis of the water molecule in the complex where two Hs of water are exchanged, i.e., the *ZPE* level is above the transition state of this motion. Even though the equilibrium $\mathrm{HFIP}_t\cdots\mathrm{W_H}$ structure does not have a symmetry plane and does have a predicted dipole moment component μ_a of 0.5 D, no *a*-type transitions could be detected because it averages to zero over this barrier-less water motion. Consequently, the vibrationally averaged structure has C_s symmetry with the *bc* plane being the symmetry plane, leading to only one, instead of two, $\mathrm{HFIP}_t\cdots\mathrm{HOD}$ isotopologue.

In the case of $\mathrm{HFIP}_g\cdots\mathrm{W_H}$, our initial CP-FTMW data recorded with a 20 μs FID also showed no water tunneling splittings. This prompted us to speculate that the water tunneling motion in $\mathrm{HFIP}_g\cdots\mathrm{W_H}$, might be barrier-less as in $\mathrm{HFIP}_t\cdots\mathrm{W_H}$ or nearly free as in the previously reported cases of the NH_3 internal rotation in ethanol⋯NH_3[42] and trifluoroethanol⋯NH_3,[43] where no splittings due to the NH_3 internal rotation were observed in the experimental spectra. On the other hand, Leopold and co-workers showed very different water LAM dynamics in pyridine⋯water[39] in comparison to those present in pyrrole⋯water,[44, 45] a structurally similar monohydrate. Since HFIP_g exhibits transient chirality, we also compared the situation with some previous examples of chiral monohydrates, such as propylene oxide⋯water[46] and methyl lactate⋯water.[47] Water serves both as a proton acceptor and donor in methyl lactate⋯water, forming a seven-membered intermolecular hydrogen bonded ring and quenching the water tunneling motion. In the monohydrate isomers of propylene oxide, water serves as a proton donor and has a free OH group, but no water tunneling splittings were detected in either syn- or anti- propylene oxide···water isomers.[46] Perhaps the low symmetry in $HFIP_g$ can also lead to much different water LAMs when compared to those in $HFIP_t \cdots W_H$.

To verify whether the tunneling barrier is non-existent as in $HFIP_t \cdots W_H$[15] or very high as in methyl lactate···water,[47] we decided to evaluate theoretically the hydrogen exchange pathway of water in $HFIP_g \cdots W_H$. To find a path along which the two H atoms of water exchange, we first carried out a simple 1D rigid scan about the water C_2 symmetry axis at the B3LYP-D3(BJ)/def2-QZVP level of theory. The scan produced an uncorrected barrier height of 19.2 kJ mol^{-1}. Our attempt to perform a relaxed scan along the same coordinate was not successful. This may be associated with the difficulty in defining the rotation about the C_2 axis while water moves during the scan.

Another possible hydrogen exchange path was proposed before for related systems such as 2-fluoroethanol···water,[41] and trifluoroethanol···water.[48] This path involves two motions: a) rotation of the water subunit about its intermolecular hydrogen bond to HFIP and b) a barrier-less wagging motion of the free hydroxyl group of water. Completion of these two motions allows the two H atoms of water to exchange and recovers the original minimum energy geometry. The corresponding motions for $HFIP_g \cdots W_H$ are depicted in Figure 4.4, together with the corresponding 1D rigid scans.

We also determined a 2D PES along the water wagging and rotation coordinates in an effort to identify the minimum energy path. The O1-H2-O2-H4 dihedral angle ϕ_2 was stepped in 10° increments, which corresponds to a rotation about the O2···H2-O1 intermolecular hydrogen bond and the H4-O2-H3-F1 dihedral angle ϕ_1 in 6° increments, corresponding to the wagging motion of the free H of water. Note that the surface is not periodic along the ϕ_2 axis because during rotation about the intermolecular bond, the free H atom (H3) is replaced by the H4 atom which has a close contact with the fluorine atom. Once the H3 and H4 exchange is complete, one needs therefore to use a new dihedral angle, H4-O2-H3-F2 (instead of H3-O2-H4-F2) to define the wagging motion. From the 1D scan along ϕ_1 and the 2D scan, one can see clearly that the wagging motion is barrierless. In the 2D scan, we also tentatively identify the minimum energy path along which H3 and H4 exchange their positions; the associated barrier is about ~7 kJ mol^{-1}.

In addition to the above rigid scans, we also performed a relaxed scan along the dihedral angle H4-O2-C2-C3 with a step size of 5°. A similar dihedral angle associated with the water tunneling motion was previously used for HFIP$_t$···W$_H$.[15] The result is shown in Figure 4.5. Interestingly, the PEC is highly asymmetric. A closer examination of the geometry variations along this dihedral angle coordinate is also provided in Figure 4.5. Starting from the global minimum (a), the energy climbs steeply as water rotates about the intermolecular hydrogen bond. At (b), we reach the transition state. As the system continues to evolve with the increasing dihedral angle, one arrives at point (c) where the original intermolecular H4···F2 contact is now replaced with H3···F2. Very interestingly, the subsequent dihedral angle increase appears to do little change to the H3···F2 contact. Rather, the free H4 atom moves from pointing down to pointing up, arriving finally at point (a′) whose geometry is equivalent to that at point (a), except that the positions of H3 and H4 are exchanged. In summary, by scanning along this particular dihedral angle, we essentially accomplish the two motions proposed in Figure 4.4 to complete the hydrogen exchange motion. The slight kink in the curve at (c) appears to signal a change in the type of motion.

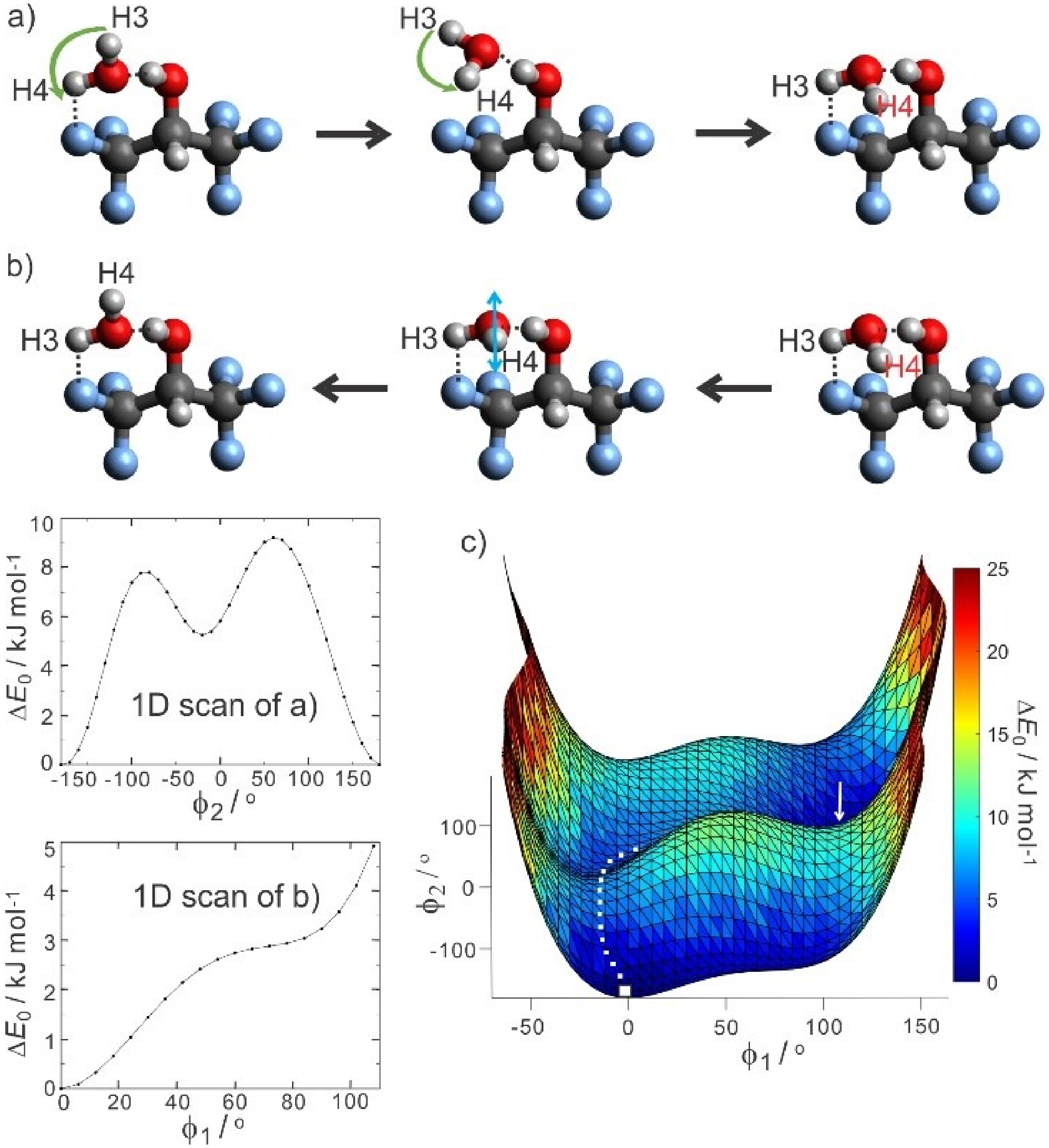

Figure 4.4. Two motions of water: a) a tunnelling motion of the water subunit where the interchange of two H atoms of water is facilitated. This is a rotation of the water subunit about its intermolecular hydrogen bond; b) a barrier-less wagging motion where the free hydrogen atom (H4) of water moves from pointing up to pointing down. Their corresponding 1D rigid PES scans along the dihedral angle ϕ_2, O1-H2-O2-H4. and along the dihedral angle ϕ_1, H4-O2-H3-F1, (see Figure 4.2 for atom numbering) are also provided. In the 1D scan of a), the water molecule continues to rotate a full 360°, beyond what is shown in the structures in the figure above. c) a 2D PES scan along the dihedral angles ϕ_1 and ϕ_2. The global minimum is indicated by a white square and the equivalent minimum where H3 and H4 are exchanged is indicated with a white arrow. The minimum energy path is tentatively indicated with the dashed line. All calculations were done at the B3LYP-D3(BJ)/def2-QZVP level of theory. See the text for discussions.

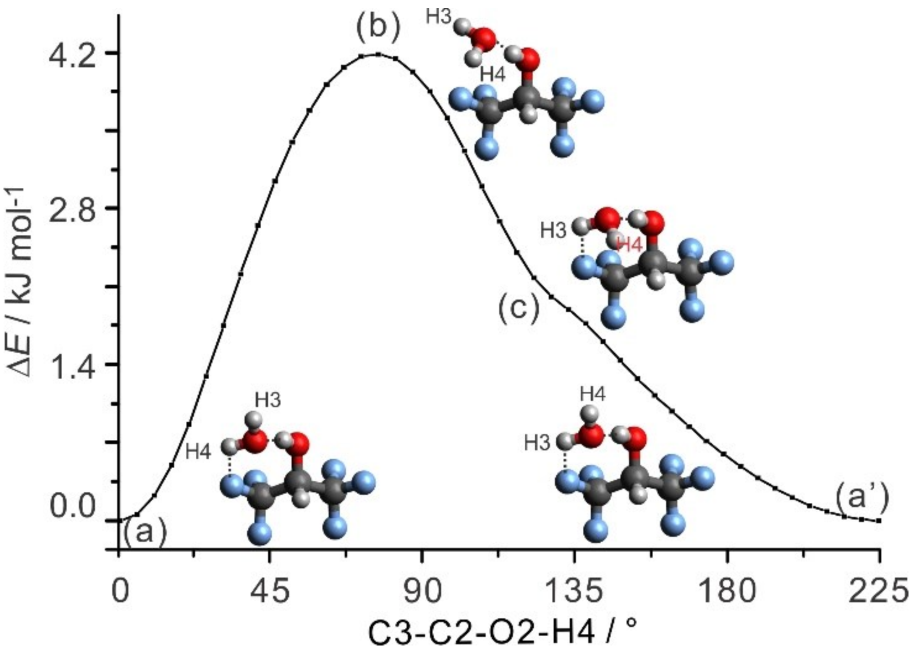

Figure 4.5. A relaxed 1D PES scan along the dihedral angle C3-C2-O2-H4 (see Figure 4.2 for atom numbering), for the water tunneling motion in $HFIP_g \cdots W_H$ at the B3LYP-D3(BJ)/def2-QZVP level of theory. The corresponding geometries at several points labelled as (a), (b), (c), and (a′) are provided. (a) and (a′) are the equivalent minimum energy geometries. See the text for discussions.

The transition state geometry (b) identified in the 1D relaxed scan was later confirmed by a transition state optimization calculation with a single imaginary frequency of -109 cm^{-1}, corresponding roughly to rotation of water about its intermolecular hydrogen bond. From the above calculations, a barrier height of ~ 3.3 or 4.2 kJ mol^{-1} was estimated with or without *ZPE* and *BSSE* correction, respectively.

To get a sense of the magnitude of the tunneling splitting one can anticipate with such a barrier height, we turn to the closely related system trifluoroethanol···water[48] where small water tunneling splittings of rotational transitions on the order of tens to some hundreds of kHz were observed experimentally. For comparison, we also performed water tunneling barrier calculations for trifluoroethanol···water and obtained a barrier height of 2.9 kJ mol^{-1} after *ZPE* and *BSSE* corrections at the same level of theory as for $HFIP_g \cdots W_H$. Overall, the situation with $HFIP_g \cdots W_H$ appears to be much different from $HFIP_t \cdots W_H$ and more similar to the trifluoroethanol···water[48] case where the attractive intermolecular contact between the H atom of water and the F-atom of the alcohol raises the tunneling barrier noticeably.

To verify experimentally the very narrow splittings anticipated, we performed additional chirped pulse measurements by extending the observation time from 20 μs to 40 μs. The longer observation time afforded us a better resolution and we were able to identify a narrow splitting pattern between two components with roughly 1:3 intensity ratio in some transitions. Most transitions show unresolved, slightly asymmetric line shapes. Some tunneling splitting/asymmetric line shape examples are provided in Figure S4.2, SI. Since the splittings are not well resolved in most transitions, we decided to keep the original experimental constants obtained based on the 20 μs spectra as they are in Table 4.2. Overall, the theoretical calculations and the additional experimental data confirm that the situation in $HFIP_g\cdots W_H$ is indeed similar to that of trifluoroethanol ⋯water, i.e., the water tunneling barrier is too high to produce well-resolved splitting, in direct contrast to the situation in $HFIP_t\cdots W_H$.

Furthermore, it is informative to note that unlike in the case of the $HFIP_t\cdots W_H$ where only one HOD isotopologue geometry has been observed, the HOD3 and HOD4 species in $HFIP_g\cdots W_H$ were detected as two different sets of transitions. This led to the detection of a total of eight isotopologues consisting of H_2O, HOD3, HOD4, and D_2O with $HFIP_g$ or $HFIP_g$(OD), respectively. Again, this is consistent with the fact that the water tunneling path has a barrier of about 3.3 kJ mol^{-1} in $HFIP_g\cdots W_H$, and is not barrier-less as in $HFIP_t\cdots W_H$. As a result, the HOD3 and HOD4 species in $HFIP_g\cdots W_H$ have different rotational constants.

We also carried out QTAIM and NCI analyses of the global minimum and the transition state geometries of $HFIP_g\cdots W_H$ to evaluate the intermolecular interactions within each geometry. The results are summarized in Figure S4.1, SI. From the QTAIM analysis, one can see that the main hydrogen bonding interaction strength decreases slightly from about 40.8 kJ mol^{-1} at the minimum to 39.2 kJ mol^{-1} at the transition state. The attractive interaction between the F2 atom to water is estimated to be ~5.3 kJ mol^{-1}, whereas no such bond was identified in the QTAIM analysis for the transition state. On the other hand, the NCI results show that the attractive interaction between F2 and water persists at the transition state although to a lesser degree compared to that at the minimum. In addition, the NCI analyses also confirm that the strong intermolecular hydrogen bond remains largely intact at the transition state. All these factors lead to a medium water tunneling barrier.

4. Deuteration effect and substitution structural parameters

From Figure 4.3, one can see that the intensity of the rotational transitions of $HFIP_g\cdots HOD3$ is about one third of that of $HFIP_g\cdots HOD4$. Similarly, the intensity of $HFIP_g(OD)\cdots HOD4$ is about half that of $HFIP_g(OD)\cdots HOD3$. This can be attributed to the lower ZPE when D4 is in close contact with F2 compared to the situation where D3 is free. Similar observations were reported previously, for example, in the studies of the fluorobenzene⋯water[49] and trifluoroethanol⋯water.[48] Indeed, the theoretical ZPE values show that the HOD4 species is about 0.1 kJ mol^{-1} more stable than the HOD3 species, consistent with the experimental observation.

Kraitchman's substitution coordinate analyses were also conducted using $HFIP_g\cdots H_2O$ and $HFIP_g\cdots HOD4$ as the parent species, together with other relevant isotopologues. The resulting coordinates are summarized in Table 4.3, along with the corresponding calculated equilibrium coordinates. In general, the experimental substitution coordinates of H2 (or D2), the alcohol hydroxy H atom, are in good agreement with the theoretical values, suggesting that this atom does not experience noticeable LAMs. The two H atoms of water, on the other hand, undergo LAMs, as discussed in the previous section. A closer examination of these LAMs indicates that these motions involve mainly changes in the *b*- and *c*-coordinates, leading to complicated averaging of these coordinates and large differences between their substitution and equilibrium coordinates. The variations in the substitution coordinates using either $HFIP_g\cdots H_2O$ or $HFIP_g\cdots HOD4$ as parent species are relatively small after taking into account the center-of-mass shift.

Table 4.3. Experimental substitution and calculated equilibrium coordinates of HFIP$_g$···W$_\mathrm{H}$.

Coord.	|Exp.|[a]	Theory[b]	Coord.	|Exp.|[a]	Theory[b]
	HFIP$_g$(OH)···H_2O as parent			HFIP$_g$(OD)···HOD4 as parent	
	H2			D2	
a	1.4560(10)	-1.4636	*a*	1.4652(10)	-1.4806
b	1.54223(98)	-1.6082	*b*	-1.5044(10)	-1.5534
c	0.4159(36)	0.4169	*c*	0. 4074(37)	0.4138
	H3			H3	
a	3.50517(43)	-3.6126	*a*	3.55368(43)	-3.6584
b	2.54051(59)	-2.6446	*b*	2.43982(62)	-2.5275
c	0.5361(28)	-0.1269	*c*	0.5144(30)	-0.1306
	H4			D4	
a	3.61246(42)	-3.5942	*a*	3.59693(42)	-3.5967
b	0.3374(45)	-1.1104	*b*	0.2362(64)	-0.9943
c	0.5229(29)	-0.2476	*c*	0.5040(30)	-0.2482

[a] Absolute experimental substitution coordinates with Costain errors in brackets. Atom numbering is provided in Figure 4.2. See the main text for discussions.

[b] Equilibrium coordinates of the parent species in its principal inertial axis system. The equilibrium geometry was optimized at the B3LYP(BJ)/def2-QZVP level.

In addition, we also calculated how deuteration affects the tunneling barrier heights. The largest difference is seen in the fully deuterated species HFIP$_g$(OD)···D_2O where the tunneling barrier increases by about 0.2 kJ mol^{-1}. No water tunneling splittings associated the D_2O isotopologues were observed, although some transitions are broadened, likely due to the unresolved D nuclear quadrupole coupling splitting.

5. Binding topologies and fluorination effects

As a monomer, HFIP$_g$ was found to be about 4~5 kJ mol^{-1} less stable than HFIP$_t$.[8] When interacting with a rare gas atom such as neon or argon, this energy gap is only slightly reduced where HFIP serves as a proton donor, playing a similar role as in the current case with water.[36] The interaction with water in the current study further reduces the energy gap to about 2.1 kJ mol^{-1}. Indeed, the binding energy of HFIP$_g$···W$_\mathrm{H}$ is predicted to be ~29.8 kJ mol^{-1}, larger than 27.8 kJ mol^{-1} of HFIP$_t$···W$_\mathrm{H}$ (see Table 4.1). This preferential stabilization of the HFIP$_g$ versus HFIP$_t$ monomer is one reason why

$HFIP_g \cdots W_H$ could be detected in the current experiment. Another reason for the detection of $HFIP_g \cdots W_H$ is the large electric dipole moment of this isomer in comparison to that of $HFIP_t \cdots W_H$. As a result, although $HFIP_t \cdots W_H$ is more abundant than $HFIP_g \cdots W_H$ in a jet expansion, the rotational spectrum of $HFIP_g \cdots W_H$ appears to be of similar intensity.

Based on the experimental intensities of $HFIP_g \cdots W_H$ versus $HFIP_t \cdots W_H$, a rotational temperature of 1 K, and their respective theoretical electric dipole components, their relative experimental abundance is estimated to be about 0.19. If we assume a conformational temperature of about 150 K,[50] an energy difference of 2.1 kJ mol^{-1}, similar to the theoretical value, was obtained. Hydrogen bonding interactions among fluoroalcohols have shown similar or even more drastic preferential stabilization of the less (or least) stable monomeric configuration in the case of trimers of 2-fluoroethanol,[17, 51] trifluoroethanol[52] and HFIP[12].

Finally, we comment on the effect of fluorination on the preferred binding topology by comparing the cases of $HFIP_g \cdots W_H$ and $HFIP_t \cdots W_H$ with that of isopropanol⋯water (IP⋯W).[53] As reported before, in IP⋯W IP has a strong preference to act as a proton acceptor, while water serves as a proton donor. Both IP⋯W isomers observed experimentally utilize a binding topology where IP serves as the proton acceptor and water as the donor. This is in direct contrast to the preferred binding topology in the HFIP⋯W complex. Clearly, the high electronegativity of the F atoms makes the hydroxyl O less negative and the hydroxyl H more positive in HFIP in comparison to IP. This greatly increases the proton donor ability and decreases the basicity of the acceptor O in HFIP with respect to IP. Similar observations were made in the previous FTIR study of IP and related fluorinated alcohols.[11] Second, the *gauche* form of the IP monomer is only about 0.1 kJ mol^{-1} more stable than its *trans*-form and both were detected in the previous rotational spectroscopic studies.[54-56] Interestingly, this preference persists or is even enhanced in its monohydrate, where the energy gap between the *trans* and the *gauche* form increases to 1.5 kJ mol^{-1}. Consequently, both observed IP⋯W isomers contain the *gauche* IP form, and none containing the *trans* IP monomer was detected. The situation with HFIP and its monohydrate is the opposite: $HFIP_t$ is much more stable than $HFIP_g$, and the energy gap between them is reduced rather than increased when going from the monomer to its monohydrate. As a result, the spectrum $HFIP_g\cdots W$ was observed even though the $HFIP_g$ monomer by itself could not be detected in the jet FTMW experiments.

Conclusions

Rotational spectra of the missing, higher energy isomer of the HFIP-water complex, i.e., $HFIP_g\cdots W_H$, and its seven deuterium isotopologues were recorded and analyzed. Interestingly, $HFIP_g\cdots W_H$ exhibits much different water LAM dynamics, compared to the previously reported global minimum isomer $HFIP_t\cdots W_H$.[15] We show that the absence of obvious water tunneling splittings in the initial 20 μs CP-FTMW spectra for both $HFIP_t\cdots W_H$ and $HFIP_g\cdots W_H$ has distinct different causes. In $HFIP_t\cdots W_H$, a barrier-less water tunneling motion has been used to explain the observation,[15] whereas in the case of $HFIP_g\cdots W_H$, a sizable barrier height of the water tunneling motion of ~ 3.3 kJ mol^{-1} was estimated. We have further demonstrated experimentally that this barrier indeed leads to fairly small splittings, not resolved in the initial 20 μs broadband spectrum but partially resolved in the 40 μs spectrum. Another point of interest is that hydrogen bonding with water preferentially stabilizes the $HIFP_g$ configuration over $HIFP_t$, facilitating the observation of the $HFIP_g$ monohydrate. Both the experimental estimate and the theoretical calculations indicate an energy disadvantage of 2.1 kJ mol^{-1} for $HFIP_g\cdots W_H$, much reduced compared to the energy difference of 4.1 kJ mol^{-1} between the $HFIP_g$ and HFIP*t* monomers. Finally, the significant influence of fluorination on the preferred binding topology between HFIP$\cdots$W and IP$\cdots$W is highlighted and discussed. The current study on the less stable $HFIP_g\cdots W_H$ isomer also paves the way for future rotational spectroscopic investigations of even larger solvation clusters of HFIP with several water molecules. Further insights into how hydrogen bonding with water influences the relative stability of the *gauche* versus *trans*-form of HFIP and the connection to the bulk properties of the HFIP+W co-solvent can be gained from such studies.

References

1. Hirota, N.; Goto, Y.; Mizuno, K., *Protein Sci.* **1997**, *6*, 416-421.
2. Hong, D.-P.; Hoshino, M.; Kuboi, R.; Goto, Y., *J. Am. Chem. Soc.* **1999**, *121*, 8427-8433.
3. Narita, M.; Honda, S.; Umeyama, H.; Obana, S., *Bull. Chem. Soc. Jpn.* **1988**, *61*, 281-284.
4. Hirota, N.; Mizuno, K.; Goto, Y., *J. Mol. Biol.* **1998**, *275*, 365-378.
5. Colomer, I.; Chamberlain, A. E.; Haughey, M. B.; Donohoe, T. J., *Nat. Rev. Chem*. **2017**, *1*, 1-12.
6. Godin, P. J.; Le Bris, K.; Strong, K., *J. Quant. Spectros. Radiat. Transf.* **2017**, *203*, 522-529.
7. Zhang, L.; Noda, I.; Czarnik-Matusewicz, B.; Wu, Y., *Anal. Sci*. **2007**, *23*, 901-905.
8. Shahi, A.; Arunan, E., *J. Phys. Chem. A* **2015**, *119*, 5650-5657.
9. Barnes, A.J.; Murto, J., *J. Chem. Soc., Faraday Trans. 2: Mol. Chem. Phys.* **1972**, *68*, 1642-1651.
10. Truax, D.R.; Wieser, H.; Lewis, P.N; Roche, R.S., *J. Am. Chem. Soc.* **1974**, *96*, 2327-2338.
11. Schaal, H.; Häber, T.; Suhm, M. A., *J. Phys. Chem. A* **2000**, *104*, 265-274.
12. Oswald, S.; Seifert, N. A.; Bohle, F.; Gawrilow, M.; Grimme, S.; Jäger, W.; Xu, Y.; Suhm, M. A., *Angew. Chem. Int. Ed.* **2019***, 58*, 5080-5084; *Angew. Chem.,* **2019**, *131*, 5134-5138.
13. Yang, Q.; Xie, F.; Lu, T.; Bui, N.; Jäger, W.; Xu, Y., *J. Mol. Spectrosc.* **2021**, *376*, 111408.
14. Yoshida, K.; Yamaguchi, T.; Adachi, T.; Otomo, T.; Matsuo, D.; Takamuku, T.; Nishi, N., *J. Chem. Phys.* **2003**, *119*, 6132-6142.
15. Shahi, A.; Arunan, E., *Phys. Chem. Chem. Phys.* **2015**, *17*, 24774-24782.
16. Pérez, C.; Lobsiger, S.; Seifert, N. A.; Zaleski, D. P.; Temelso, B.;Shields, G. C.; Kisiel, Z.; Pate, B. H., *Chem. Phys. Lett.* **2013**, *571*, 1-15.
17. Seifert, N. A.; Thomas, J.; Jäger, W.; Xu, Y., *Phys. Chem. Chem. Phys.* **2018**, *20*, 27630-27637.
18. Carlson, C. D.; Seifert, N. A.; Heger, M.; Xie, F.; Thomas, J.; Xu, Y., *J. Mol. Spectrosc.* **2018**, *351*, 62-67.
19. Grimme, S., *J. Chem. Theory Comput.* **2019**, *15*, 2847-2862.
20. Pracht, P.; Bohle, F.; Grimme, S., *Phys. Chem. Chem. Phys.* **2020**, *22*, 7169-7192.
21. Gaussian 16, Revision B.01, Frisch, M. J.; Trucks, G. W.; Schlegel, H. B.; Scuseria, G. E.; Robb, M. A.; Cheeseman, J. R.; Scalmani, G.; Barone, V.; Petersson, G. A.; Nakatsuji, H.; Li, X.; Caricato, M.; Marenich, A. V.; Bloino, J.; Janesko, B. G.; Gomperts, R.; Mennucci, B.; Hratchian, H. P.; Ortiz, J. V.; Izmaylov, A. F.; Sonnenberg, J. L.; Williams-Young, D.; Ding, F.; Lipparini, F.; Egidi, F.; Goings, J.; Peng, B.; Petrone, A.; Henderson, T.; Ranasinghe, D.; Zakrzewski, V. G.; Gao, J.; Rega, N.; Zheng, G.; Liang, W.; Hada, M.; Ehara, M.; Toyota, K.; Fukuda, R.; Hasegawa, J.; Ishida, M.; Nakajima, T.; Honda, Y.; Kitao, O.; Nakai, H.; Vreven, T.; Throssell, K.; Montgomery Jr., J. A.; Peralta, J. E.: Ogliaro, F.: Bearpark, M. J.: Heyd, J. J.: Brothers, E. N.; Kudin, K. N.; Staroverov, V. N.; Keith, T. A.; Kobayashi, R.; Normand, J.; Raghavachari, K.; Rendell, A. P.; Burant, J. C.; Iyengar, S. S.; Tomasi, J.; Cossi, M.; Millam, J. M.; Klene, M.; Adamo, C.; Cammi, R.; Ochterski, J. W.; Martin, R. L.; Morokuma, K.; Farkas, O.; Foresman, J. B.; Fox, D. J.; Gaussian 16, Revision A.03, Gaussian, Inc., Wallingford, CT, **2016.**

22. Stephens, P. J.; Devlin, F. J.; Chabalowski, C. F.; Frisch, M. J., *J. Phys. Chem.* **1994**, *98* (45), 11623-11627.

23. Beck, A. D. J. *J. Chem. Phys.* **1993**, *98*, 1372-1377.

24. Grimme, S.; Antony, J.; Ehrlich, S.; Krieg, H. J, *J. Chem. Phys.* **2010**, *132*, 154104.

25. Grimme, S.; Ehrlich, S.; Goerigk, L., *J. Comput. Chem.* **2011**, *32*, 1456-1465.

26. Weigend, F.; Ahlrichs, R., *Phys. Chem. Chem. Phys.* **2005**, *7*, 3297-3305.

27. Boys, S. F.; Bernardi, F., *Mol. Phys.* **1970**, *19*, 553-566.

28. Kisiel, Z., PROSPE–Programs for rotational spectroscopy, in Spectroscopy from Space, Eds. J. Demaison, K. Sarka, E. A. Cohen, **2001**, pp. 91-106. Kluwer Academic Publishers, Dordrecht.

29. Seifert, N. A.; Finneran, I. A.; Perez, C.; Zaleski, D. P.; Neill, J. L.; Steber, A. L.; Suenram, R. D.; Lesarri, A.; Shipman, S. T.; Pate, B. H., *J. Mol. Spectrosc.* **2015**, *312*, 13-21.

30. Western, C. M., *J. Quant. Spectrosc. Radiat. Transf.* **2017**, *186*, 221-242.

31. Hanwell, M.D.; Curtis, D.E.; Lonie, D.C., Vandermeersch, T.; Zurek, E.; Hutchison, G.R., *J. Cheminformatics* **2012**, 4, 17.

32. Johnson, E. R.; Keinan, S.; Mori-Sánchez, P.; Contreras-García, J.;Cohen, A. J.; Yang, W., *J. Am. Chem. Soc.* **2010**, *132*, 6498-6506.

33. Bader, R.F.W., Atoms in Molecules: A Quantum Theory, Oxford University Press, New York, **1990**.

34. Lu, T.; Chen, F., *J. Comput. Chem.*, **2012**, *33*, 580-592.

35. Humphrey, W.; Dalke, A.; Schulten, K., *J. Mol. Graph.* **1996**, *14*, 33-38.

36. Wu, B.; Seifert, N. A.; Oswald, S.; Jäger, W.; Xu, Y., *J. Phys. Chem. A* **2021**, *125*, 5355-5364.

37. Watson, J. K. G., in: During, J.R. (Ed.), Vibrational Spectra and Structure, vol. 6, Elsevier, New York, **1977**, pp. 1–89.

38. Xu, Y.; Jäger, W., *J. Chem. Phys.* **1997**, *107*, 4788-4796.

39. Mackenzie, R. B.; Dewberry, C. T.; Cornelius, R. D.; Smith, C.; Leopold, K. R., *J. Phys. Chem. A* **2017**, *121*, 855-860.

40. Gall, J. T.; Thomas, J.; Xie, F.; Wang, Z.; Jäger, W.; Xu, Y., *Phys. Chem. Chem. Phys.* **2017**, *19*, 29508-29515.

41. Huang, W.; Thomas, J.; Jäger, W.; Xu, Y., *Phys. Chem. Chem. Phys.* **2017**, *19*, 12221-12228.

42. Giuliano, B. M.; Favero, L. B.; Maris A.; Caminati, W., *Chem. Eur. J.* **2012**, *18*, 12759-12763.

43. Thomas, J.; Peña, I.; Carlson, C. D.; Yang, Y.; Jäger, W.; Xu, Y., *Phys. Chem. Chem. Phys.* **2020**, 22, 23019-23027.

44. Tubergen, M. J.; Andrews, A. M.; Kuczkowski, R. L., *J. Phys. Chem.* **1993**, *97*, 7451-7457.

45. Wu, B.; Xie, F.; Xu, Y., The pyrrole-water complex: *J. Mol. Spectrosc.* **2020,** *374*, 111381.

46. Su, Z.; Wen, Q.; Xu, Y., *J. Am. Chem. Soc.* **2006**, *128*, 655-6760.

47. Thomas, J.; Sukhorukov, O.; Jäger, W.; Xu, Y., *Angew. Chem. Int. Ed.*, **2014**, *53*, 1156-1159; *Angew. Chem.* **2014**, *12*, 1175-1178.

48. Thomas, J.; Xu, Y., *J. Chem. Phys.* **2014**, *140*, 204308/1-5.

49. Brendel, K.; Mäder, H.; Xu, Y.; Jäger, W., *J. Mol. Spectrosc.* **2011**, *268*, 47-52.

50. Xie, F.; Seifert, N. A.; Heger, M.; Thomas, J.; Jäger, W.; Xu, Y., *Phys. Chem. Chem. Phys.* **2019**, *21*, 15408-15416.

51. Thomas, J.; Liu, X.; Jäger, W.; Xu, Y., *Angew. Chem. Int. Ed.*, **2015,** *54*, 11711-11715. *Angew. Chem.* **2015**, *127*, 11877-11881.

52. Thomas, J.; Seifert, N. A.; Jäger, W.; Xu, Y., *Angew. Chem. Int. Ed.* **2017**, *56*, 6289-6293; *Angew. Chem.* **2017**, *129*, 6386–6390.

53. Evangelisti, L.; Gou, Q.; Feng, G.; Caminati, W.; Mead, G. J.; Finneran, I. A.; Carroll, P. B.; Blake, G. A., *Phys. Chem. Chem. Phys.* **2017**, *19*, 568-573.

54. Kondo, S.; Hirota, E. J., *J. Mol. Spectrosc.* **1970**, *34*, 97-107.

55. Hirota, E., *J. Phys. Chem.* **1979**, *83*, 1457-1465.

56. Inagaki, F.; Harada, I.; Shimanouchi, T. J., *J. Mol. Spectrosc.* **1973**, *46*, 381-396.

Chapter 5

Rotational Spectrum and Molecular Structures of the Binary Aggregates of 1,1,1,3,3,3-Hexafluoro-2-propanol with Ne and Ar[1]

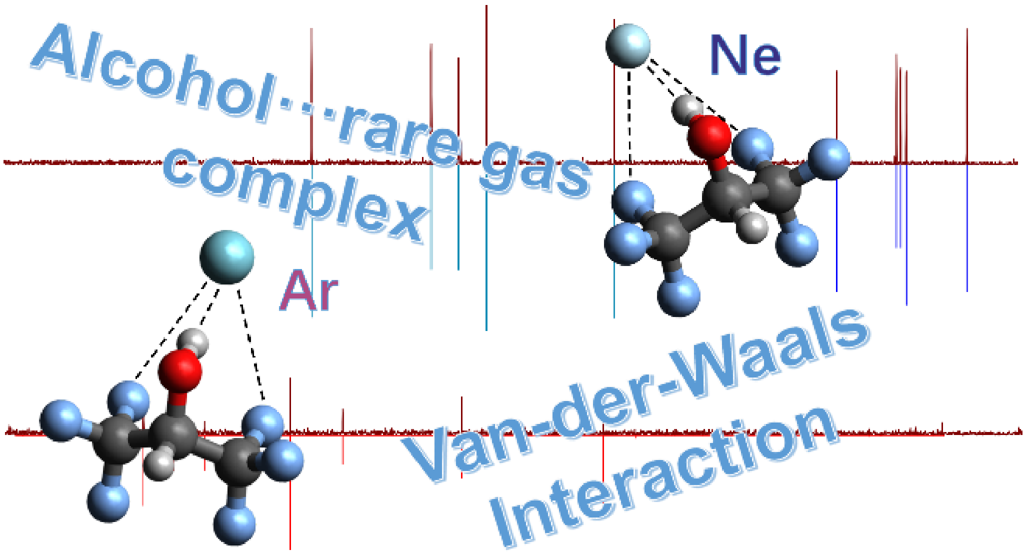

---

[1] This study has been published as B. Wu, N. A. Seifert, S. Oswald, W. Jäger, and Y. Xu, "Rotational Spectrum and Molecular Structures of the Binary Aggregates of 1,1,1,3,3,3-Hexafluoro-2-propanol with Ne and Ar", *J. Phys. Chem. A* **2021**, *125*, 5355-5364.

Abstract

The structures and binding topologies of two binary van der Waals complexes of 1,1,1,3,3,3-hexafluoro-2-propanol (HFIP)$\cdots$Ne and $\cdots$Ar were investigated. Rotational spectra of these two complexes including several isotopic species containing ^{20}Ne, ^{22}Ne, ^{40}Ar, ^{13}C, and hydroxyl D, were measured using a chirped pulse Fourier transform microwave spectrometer and a cavity-based Fourier transform microwave spectrometer. While HFIP were shown to exist in both the *gauche* and *trans* configurations based on previous reports, the rare gas atom is predicted to attach to HFIP in several different binding topologies, leading to a total of nine possible structural isomers for each complex. Only one isomer was detected for each species and it corresponds to the most stable one predicted, based on the comparison of the experimental rotational constants and electric dipole moment components with the theoretical predictions and on the isotopic data. We applied quantum theory of atoms and molecules (QTAIM) and electrostatic potential calculations to examine the different rare gas binding sites and to explore the nature of the interactions in these two complexes and several previously reported alcohol$\cdots$Ar complexes. The effects of fluorination are also discussed by comparison with the binary complexes of isopropanol$\cdots$Ne and $\cdots$Ar.

Introduction

1,1,1,3,3,3-hexafluoro-2-propanol (HFIP) is widely used as an organic solvent for chemical reactions and as a co-solvent for studies of peptides and proteins.[1, 2] It is a potent greenhouse gas and its global warming potential has been evaluated.[3] In this paper, we examine the preferred binding sites of HFIP to a rare gas atom, namely Ne or Ar, through use of rotational spectroscopy and quantum chemistry calculations. Rotational spectroscopy has been applied extensively for studies of non-covalent interactions[4,5] including van der Waals interactions involving rare gas atoms.[6,7] While earlier rotational spectroscopic studies focused on simpler rare gas atom containing van der Waals complexes such as pure rare gas clusters,[8] complexes with aromatic molecules,[9] and those with short linear molecules,[10] later studies have shifted to flexible binding partners with multiple bonding sites, and a wide variety of functionalized molecules such as fluorinated organics.[11-13] Here, rare gas atoms can be used as a tool to probe the electron density distribution of the molecular binding partner. So far, only a few rotational spectroscopic studies of complexes between an aliphatic alcohol and a rare gas atom have been reported, for example, methanol···Ar,[14] 2-butanol···Ar[15] and propargyl alcohol···Ar.[16]

HFIP has one important degree of flexibility, the H-O-C-H dihedral angle, which is related to the relative orientation of the OH group. This angle can take on 180°, 60° and -60°, corresponding to the *trans* (*t*), *gauche*+ (*g*+) and *gauche*- (*g*-) configuration, respectively.[17,18] The *g*+ and *g*- configurations are mirror images to each other with transient chirality, whereas *t* is an achiral form. Since *g*+ and *g*- would give rise to the same vibrational and rotational spectrum, for simplicity, we will label them as *g* only throughout the remaining text and use H_t and H_g to indicate the *trans* and *gauche* configurations of HFIP, respectively. The *g* conformer is ~4.0 kJ mol^{-1} less stable than the *t* conformer and only *t* was detected experimentally in the isolated form in a supersonic jet expansion.[17-19] Subsequently, several H-bonded complexes such as HFIP···H_2O, and the HFIP dimer and trimer were investigated using IR and microwave (MW) spectroscopies.[18,20,21] Interestingly, the H-bonding interactions with water and with itself appear to stabilize the *g*-form of HFIP in these complexes.[22] In the case of the HFIP trimer, the conformer consisting of three *g* subunits is the only one observed experimentally in a jet expansion.[21] It would be interesting to probe whether the weaker van der Waals interactions in HFIP···Ne and ···Ar may have similar effects on the relative stability of the *t* versus the *g* form.

In the previous MW study of propargyl alcohol⋯Ar,[16] a number of different types of intermolecular interactions, such as Ar⋯H-O, Ar⋯π and Ar⋯C contacts, were revealed. While HFIP has an OH functional group as propargyl alcohol, it also offers other possible binding sites. One goal of the current study is to identify the potential binding sites and evaluate their energetic preferences. In several recent rotational spectroscopic studies, the effects of fluorination on the van der Waals interactions between rare gas atoms and aromatic molecules such as benzene and oxirane derivatives[11,13] were investigated. For example, Leung and co-workers identified an unexpected structure of the 3-fluoro-1,2-epoxypropane⋯Ar binary complex,[13] noticeably different from that of 3,3,3-trifluoro-1,2-epoxypropane⋯Ar[23] but similar to that of propylene oxide⋯Ar.[11] It would be interesting to identify binding site preferences in HFIP⋯rare gas atom complexes and to compare results to those of the corresponding isopropanol (IP) containing complexes.

Experimental and theoretical methods

For the rotational spectroscopic measurements, a 2-6 GHz chirped pulse FTMW spectrometer[24-26] and a 4-18 GHz cavity-based FTMW spectrometer[27] were used. The frequency accuracies are about 5 kHz and 1 kHz for the former and latter instruments, respectively. The recently developed 2-6 GHz CP-FTMW spectrometer was constructed based on the design of a similar instrument by Pate and co-workers[28] and its details and some modifications were described in several recent publications.[24-26]

HFIP (Sigma Aldrich, 99.9%) was used without further purification. For the chirped pulse FTMW measurements of rotational spectra of HFIP-Ne (abbreviated as HNe) and HFIP-Ar (abbreviated as HAr), mixtures of 0.1% HFIP in 6 bar of neon (Praxair, 99.999%) or with the addition of 0.2% argon (Praxair, 99.998%) were used, respectively. For the measurements of the hydroxyl deuterated species, a gas mixture of 0.1% HFIP and 0.2% of D_2O (Cambridge Isotope Laboratories, Inc. 99.5%) in 8 bar of neon was prepared in a gas cylinder and left overnight to allow sufficient proton/deuterium exchange. For the cavity FTMW experiments, a mixture of 0.1% HFIP in 6 bar of neon (Praxair, 99.999%) or with the addition of 5% of argon and a total pressure of 8 bar were used for the HNe or HAr measurements, respectively. The measurements of the ^{13}C isotopic species of HFIP-Ne were obtained in natural abundance. For the searches of the hydroxyl deuterated species with the cavity FTMW spectrometer, the same sample conditions as for the chirped pulse FTMW experiments were used.

The conformer-rotamer ensemble sampling tool (CREST)[29,30] developed by Grimme and co-workers, was utilized for a comprehensive search of the possible structural candidates. Although CREST has been utilized for conformational searches of flexible organic molecules and hydrogen-bonded complexes, such as perillyl alcohol[24] and dimers of tetrahydro-2-furoic acid,[31] this code has rarely been used for conformational searches of rare gas⋯organic molecule van der Waals complexes. Many of the recent studies relied on potential energy scans along specific coordinates, or using previous experience with similar systems to identify the possible structures.[13,23,32] In a recent study of the propylene oxide trimer, which is bound dominantly by van der Waals and induction interactions, CREST failed to generate the structural candidate of the most stable heterochiral trimer.[33] It would be interesting to see how CREST performs with these very weakly bound systems involving rare gas atoms.

Geometry optimizations of the initial CREST candidates were carried out using the Gaussian 16 program package.[34] The B3LYP hybrid functional in combination with Grimme's dispersion correction (D3)[35], Becke-Johnson damping (BJ)[36] and the def2-QZVP basis set[37] were used for geometry optimizations and harmonic/anharmonic frequency calculations, as well as the predictions of isotopic ^{22}Ne, ^{13}C and hydroxyl D species. All energies reported are corrected for zero-point energy (*ZPE*) and the basis set superposition errors (*BSSE*s) which were calculated using the counterpoise procedure.[38] Bader‘s quantum theory of atoms and molecules (QTAIM) analyses were also used to provide insight into the associated van der Waals interactions,[39] The structures and QTAIM analyses were visualized using Avogadro[40], and VMD[41] with the Multiwfn[42] package, respectively. Kisiel’s PMIFST, STRFIT and KRA programs[43] were utilized for the isotopic substitution calculations and the structure fitting analyses, respectively. The PGOPHER[44] program was employed for spectral fitting.

Results and discussion

1. Structural search and calculations

As mentioned in the introduction, the HFIP monomer can take on either H_t or H_g configurations. The atomic coordinates of H_t and H_g are listed in Tables S5.1 and S5.2, Supporting Information (SI), respectively. The CREST searches resulted in sets of possible isomers for HNe and for HAr. Further DFT geometry optimization and harmonic frequency calculations led to nine stable structures for each species. From these structures, we identified four different HFIP binding sites to the rare gas atom. These are the acidic hydroxyl proton, the face formed by the CH proton and two F atoms, the face of the O atom and two F atoms, and finally the face of the CF_3 group, which are labelled as Ne_H, Ne_C, Ne_O, and Ne_F, respectively.

In the case of H_g, the two $-CF_3$ faces are different, and we label the one on the opposite side of OH with a prime, i.e. $H_gAr_{F'}$. The nine structures identified for HNe are shown in Figure 4.1; the corresponding side views and the corresponding geometries of the HAr complex are shown in Figures S1-S3, SI. The relative energies and calculated spectroscopic constants of all 9 structures of the HNe and HAr complexes are summarized in Table 5.1 and 5.2, respectively.

For the HFIP monomer, H_t is about 4 kJ mol^{-1} more stable than H_g.[17,18,20] This energy separation remains similar in the corresponding Ne and Ar complexes and we separate the structures into two groups: those containing H_t and those with H_g. The isomers within the H_tNe (or H_tAr) group or the H_gNe (or H_gAr) group are of very similar stability, within an energy window of less than 1.0 kJ mol^{-1} for the neon and ~2.5 kJ mol^{-1} for the argon complexes. It is interesting to note that the preference ordering of the rare gas binding sites is the same (i.e. H, C, O and F, in order of increasing energy) within the H_tNe, H_gNe,

H_tAr, and H_gAr groups. Note that H_gNe_F and $H_gNe_{F'}$ differ only in the relative OH orientation to the Ne···CF_3 subunit and have similar stabilities. The same can be said about H_gAr_F and $H_gAr_{F'}$. The global minimum structures of both HNe and HAr are those where the rare gas atom binds to the hydroxyl H atom in the H_tNe and H_tAr groups, i.e. H_tNe_H and H_tAr_H, respectively. The atomic coordinates of the most stable H_tNe_H and H_tAr_H isomers are listed in the SI in Tables S5.3 and S5.4, respectively.

Table 5.1: Properties of the conformers of the binary HNe complex predicted at the B3LYP-D3(BJ)/def2-QZVP level of theory.

Species	ΔE_e[a]	ΔE_0[b]	ΔE_b[c]	*A*[d]	*B*[d]	*C*[d]	$\lvert\mu_a\rvert$[e]	$\lvert\mu_b\rvert$[e]	$\lvert\mu_c\rvert$[e]
H_tNe_H	0.0	0.0	1.0	986.0	968.2	646.9	0.0	0.4	0.4
H_tNe_C	0.3	0.2	0.8	1033.6	948.0	676.9	0.0	0.2	0.5
H_tNe_O	0.4	0.3	0.7	1151.6	798.2	617.8	0.3	0..4	0.4
H_tNe_F	0.9	0.6	0.4	1875.8	589.5	541.3	0.1	0.6	0.0
H_gNe_H	4.7	4.0	1.1	1179.3	788.0	609.0	2.3	1.1	0.6
H_gNe_C	5.1	4.3	0.7	1037.2	927.6	670.1	0.6	1.3	2.1
H_gNe_O	5.4	4.5	0.5	1024.6	949.5	664.5	0.8	1.0	2.2
H_gNe_F	5.6	4.7	0.4	1874.7	591.3	541.0	1.5	1.3	1.5
$H_gNe_{F`}$	5.6	4.7	0.4	1894.0	588.3	539.9	0.5	1.8	1.7

[a] Relative electronic raw energy in kJ mol^{-1}.
[b] Relative energy including *ZPE* and *BSSE* energy corrections in kJ mol^{-1}.
[c] $\Delta E_b=-(\Delta E_{0(HFIP\text{-}Ne)}-\Delta E_{0(HFIP)}-\Delta E_{0(Ne)})$ in kJ mol^{-1} after *ZPE* and *BSSE* corrections.
[d] Rotational constants in MHz.
[e] Magnitudes of the electric dipole moment components in Debye.

Table 5.2: Properties of the conformers of the binary HAr complex predicted at the B3LYP-D3(BJ)/def2-QZVP level of theory.

Species	$\Delta E_e{}^a$	$\Delta E_0{}^b$	$\Delta E_b{}^c$	A^d	B^d	C^d	$\lvert\mu_a\rvert^e$	$\lvert\mu_b\rvert^e$	$\lvert\mu_c\rvert^e$
$\mathrm{H_tAr_H}$	0.0	0.0	3.6	966.1	625.3	469.8	0.6	0.0	0.4
$\mathrm{H_tAr_C}$	0.9	0.8	2.8	942.2	657.2	493.8	0.0	0.0	0.5
$\mathrm{H_tAr_O}$	1.2	1.1	2.5	1039.6	549.9	440.6	0.5	0.2	0.4
$\mathrm{H_tAr_F}$	2.5	2.2	1.4	1819.0	394.4	370.8	0.2	0.6	0.0
$\mathrm{H_gAr_H}$	4.6	3.9	3.7	1081.0	539.6	435.3	2.8	0.4	0.5
$\mathrm{H_gAr_C}$	5.8	5.0	2.6	949.3	640.0	487.2	1.1	1.2	1.9
$\mathrm{H_gAr_O}$	6.4	5.5	2.1	961.9	637.4	479.9	0.7	1.1	2.1
$\mathrm{H_gAr_F}$	7.2	6.3	1.4	1817.4	396.3	371.6	1.7	1.2	1.4
$\mathrm{H_gAr_F}$`	7.2	6.3	1.4	1838.2	394.1	370.6	0.4	1.9	1.6

[a] Relative electronic raw energy in kJ mol^{-1}.
[b] Relative energy including *ZPE* and *BSSE* energy corrections in kJ mol^{-1}.
[c] $\Delta E_b = -(\Delta E_{0(\mathrm{HFIP\text{-}Ne})} - \Delta E_{0(\mathrm{HFIP})} - \Delta E_{0(\mathrm{Ne})})$ in kJ mol^{-1} after *ZPE* and *BSSE* corrections.
[d] Rotational constants in MHz.
[e] Magnitudes of the electric dipole moment components in Debye.

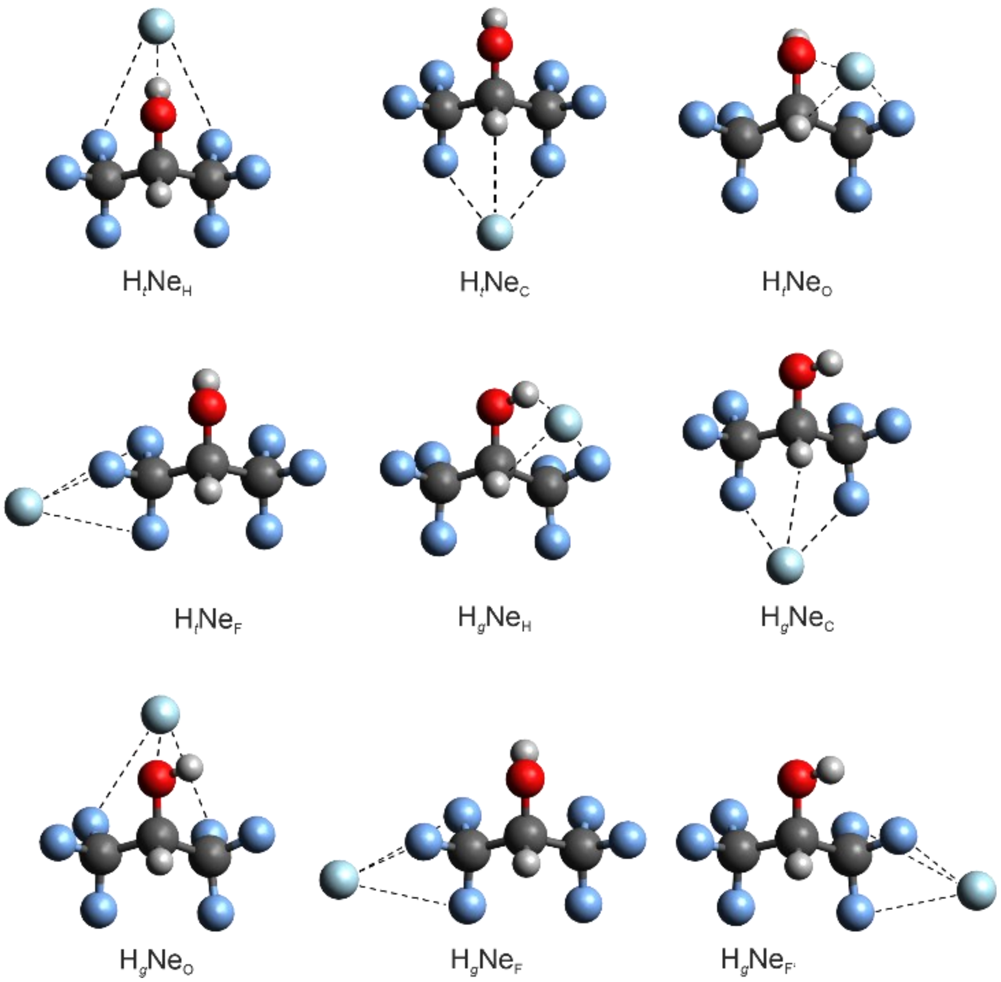

H_tNe_H H_tNe_C H_tNe_O

H_tNe_F H_gNe_H H_gNe_C

H_gNe_O H_gNe_F $H_gNe_{F'}$

Figure 5.1. Geometries of the nine isomers of HNe optimized at the B3LYP-D3(BJ)/def2-QZVP level of theory. In each case, the three closest intermolecular distances are indicated with dashed lines.

2. Assignments of the rotational spectra

The broadband rotational spectrum obtained with the HFIP + Ne mixture is very rich in transitions. After removing the transitions that belong to the HFIP monomer, dimer and trimer and the related rarer isotopologues, as well as HFIP$\cdots$$H_2O$,[18-20,22,45] some medium strength transitions remained. Two sets of transitions and each with two different types of transitions could eventually be assigned, and additional transitions were measured using the cavity-based FTMW instrument. The measured transition frequencies were fitted using Watson's semi-rigid rotor Hamiltonian in the *S*-reduction and I^r representation.[47] The resulting spectroscopic constants are summarized in Table 5.3.

Based on the comparison of the experimental and theoretical rotational constants and the relative magnitudes of the *a*-, *b*- and *c*-dipole moment components, we could confidently assign the carrier of one set of transitions to $H_t{}^{20}Ne_H$ and the carrier of the second set was later identified to be $H_t{}^{22}Ne_H$. Although *a*-type transition frequencies of $H_t{}^{20}Ne_H$ were well predicted, substantial efforts to measure them using the cavity FTMW instrument, which was used for systems of low electric dipole moments such as mixed rare gas clusters,[46] were not successful. This suggests that its *a*-dipole moment component is (nearly) zero. A section of the broadband spectrum, showing the transitions of $H_t{}^{20}Ne_H$ and $H_t{}^{22}Ne_H$ with surprisingly similar intensity, is depicted in Figure 5.2. Their relative experimental line intensities will be discussed later.

In the original assignment of the second set of transitions, we assigned *b*- and *c*-type transitions for the $H_t{}^{22}Ne_H$, in a similar manner as for $H_t{}^{20}Ne_H$. However, the PMIFST prediction indicates that replacing ^{20}Ne with ^{22}Ne results in an axis switching between the *a*- and *b*-principal inertial axes. This generated some confusion initially until we realized that switching the assignment from *b*-type to *a*-type caused very minor changes in the fitted spectroscopic constants. A subsequent planar moment analysis provided clear support for us to confidently associate the second set of transitions with $H_t{}^{22}Ne_H$.

With the high signal-to-noise ratio achieved for transitions of the ^{12}C isotopologue using the cavity FTMW spectrometer, we searched for, and observed all singly substituted ^{13}C isotopologues of $H_t{}^{20}Ne_H$ in their natural abundances. In total, 12 and 10 transitions were assigned for the ^{13}C substitution at the C2 and at the equivalent C1/C3 carbon sites (see Figure 5.3 for atom numbering), respectively. A roughly 2:1 intensity ratio was observed for the ^{13}C substitutions at C1/C3 versus at C2, although the lines from cavity FTMW experiments were weak. This indicates that the substitutions at the C1 and C3 sites are equivalent, an important indication of the *Cs* symmetry of the H_tNe_H complex which will be discussed further in the structure section.

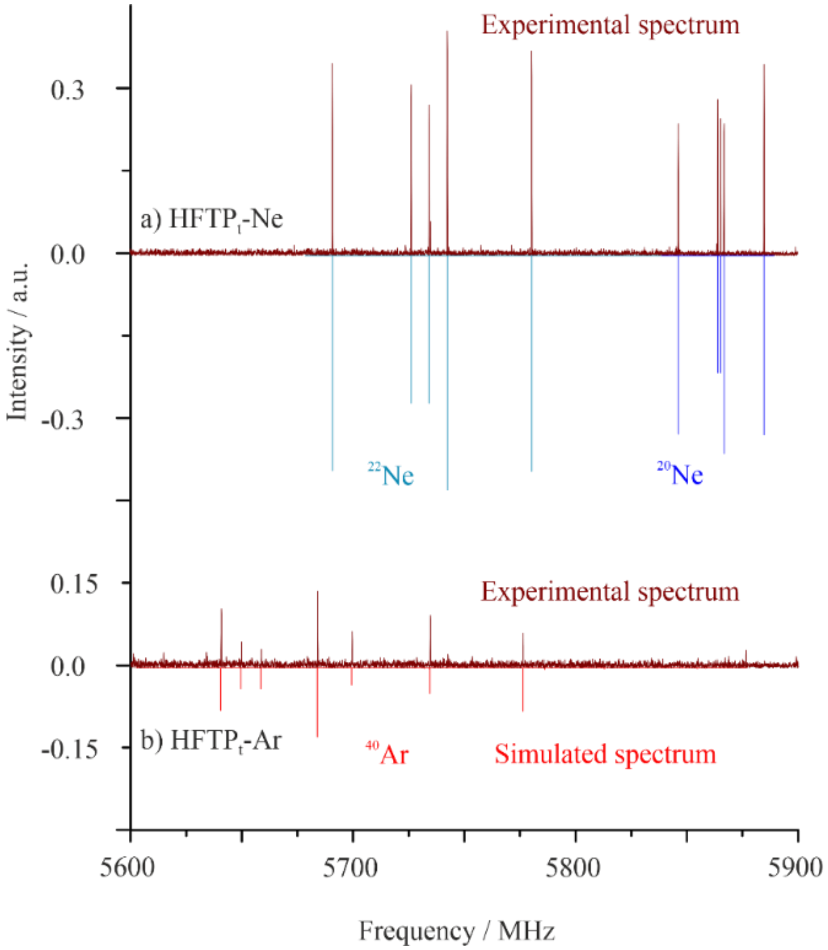

Figure 5.2. Experimental spectra of two sample mixtures: a) HFIP+Ne and b) HFIP+Ne+0.3%Ar. After the addition of the argon gas, nearly all transitions belonging to $H_t{}^{20}Ne$ and $H_t{}^{22}Ne$ disappeared. The known transitions of the HFIP monomer, dimer, trimer and HFIP-water are removed for clarity. The experimental spectroscopic constants, the calculated electric dipole moment components and a rotational temperature of 0.5 K were used for the spectral simulations.

To search for the deuterated (OD) H_tNe_H complex, we monitored the transitions of the (OD) H_t monomer and estimated its abundance to be about ~8% of the parent H_t. Our initial attempt to identify (OD) H_tNe_H transitions in the chirped spectrum was not successful, likely because of the competing formation of the (OD)$H_t\cdots H_2O$ complex. The (OD) H_tNe_H transition lines were eventually detected using the cavity FTMW spectrometer and the general intensity is comparable to or weaker than those of the ^{13}C isotopologues.

In total, 13 rotational lines of the deuterated (OD) H_t^{20}Ne$_H$ species were measured and assigned.

Because of the limited number of transitions obtained for the rarer isotopologues, we fixed some quartic centrifugal distortion constants using the scaled values of the parent isotopologue and the predicted ones obtained from the harmonic vibrational calculations. The resulting spectroscopic parameters of the rarer isotopologues of H_t^{20}Ne$_H$ are also listed in Table 5.3. All measured transition frequencies of the five H_tNe$_H$ isotopologues are summarized in Tables S5.5 to S5.9, SI.

The addition of 0.2% Ar gas to the sample mixture had a drastic effect on the appearance of the spectrum: transitions assigned to H_tNe$_H$ essentially disappeared and new transitions emerged, as illustrated in Figure 5.2b. Some *a*- and *c*-type transitions could be assigned, and additional transitions were measured using the cavity-based FTMW instrument. No *b*-type transitions could be detected, indicating a (nearly) zero *b*-dipole moment component. The fitted spectroscopic constants of the Ar complex are also summarized in Table 5.3.

H_tAr$_H$ sharing very similar binding orientations, all principal inertial axes are switched because the Ar mass is much larger than that of Ne, (see Figure 5.3). The measured transition frequencies of H_tAr$_H$ are summarized in Table S5.10, SI. We also searched for transitions of the ^{13}C isotopologues of H_t^{40}Ar$_H$ using the cavity instrument, but without success. This is perhaps not surprising since the experimental line intensity of H_t^{40}Ar$_H$ is in general noticeably weaker compared to H_t^{20}Ne$_H$ and H_t^{22}Ne$_H$. One main reason is that the peak of the Boltzmann distribution for pure rotational transitions of H_t^{40}Ar$_H$ is in a much lower frequency region where the sensitivity of the cavity-based instrument is sub-optimal.

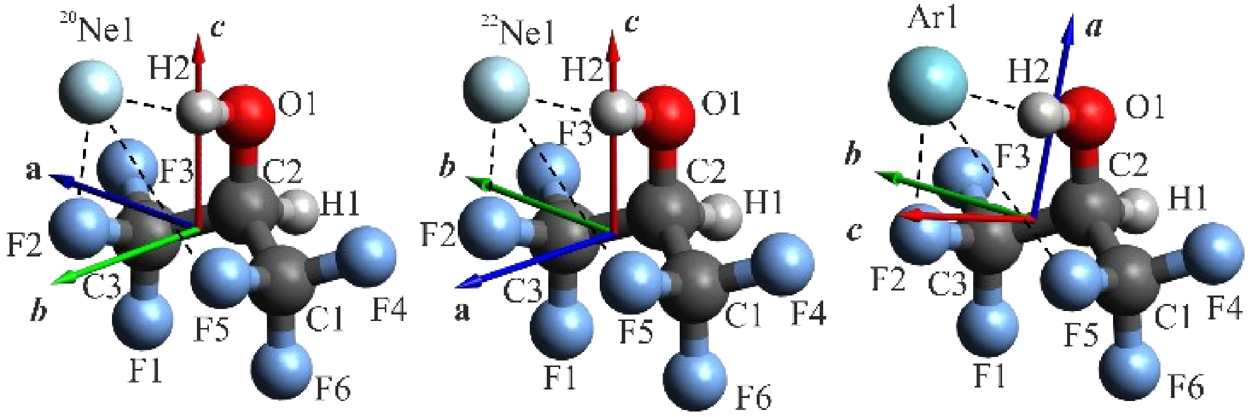

a) $H_t{}^{20}Ne_H$ b) $H_t{}^{22}Ne_H$ c) $H_t{}^{40}Ar_H$

Figure 5.3. Optimized geometries of a) $H_t{}^{20}Ne_H$, b) $H_t{}^{22}Ne_H$, and c) $H_t{}^{40}Ar_H$ at the B3LYP-D3(BJ)/def2-QZVP level of theory, with their atom numbering and their principal inertial axes. Note the axes switching in going from $H_t{}^{20}Ne_H$ to $H_t{}^{22}Ne_H$ and to $H_t{}^{40}Ar_H$.

The experimental rotational constants of $H_t{}^{20}Ne_H$ and $H_t{}^{40}Ar_H$ are compared with the theoretical ones calculated at several different levels of theory in Table S5.11, SI. Generally, the experimental rotational constants agree well with those obtained at the B3LYP-D3(BJ)/def2-QZVP level of theory, with errors of 0.20% and -0.68% for *A*, -0.31% and -1.37% for *B*, and -0.89% and -1.54% for *C*, respectively. In a recent study of pyrrole⋯$Ne_{1,2}$,[48] an error of 1.54% was reported at the CCSD/def2-TZVPP level, while much larger errors ranging from a few percentage points (CCSD/6-311++G(d,p) and MP2/6-311++G(2d,p)) to nearly ~20% (CCSD/aug-cc-pVTZ and MP2/aug-cc-pVTZ) were reported for the rotational constants of pyrrole⋯Ne_1. Those authors found that the errors in the rotational constants are in the range from 8 to 22% without the dispersion correction versus ~1% with the dispersion correction. We also tested a few more basis sets: TZVP, TZVPP and 6-311++G(2d,2p). The former two basis sets gave slightly worse performance with an error of ~3% for $H_t{}^{20}Ne_H$, and similarly good performance was obtained with the 6-311++G(2d,2p) basis set as with the QZVP basis set.

Table 5.3. Experimental spectroscopic parameters of the binary complexes of H_tNe_H and H_tAr_H.

Parameter	$H_t{}^{20}Ne_H$	$H_t{}^{22}Ne_H$	(^{13}C1/3) $H_t{}^{20}Ne_H$	(^{13}C2) $H_t{}^{20}Ne_H$	(OD) $H_t{}^{20}Ne_H$	$H_t{}^{40}Ar_H$
A^a	984.07286(23)	970.73755(24)	983.738(12)	982.030(45)	978.0695(16)	972.77323(13)
B^a	971.18792(23)	940.85049(24)	967.9983(93)	970.468(11)	969.2549(20)	633.958639(55)
C^a	652.68547(16)	633.59316(12)	651.072(15)	652.5274(19)	650.47805(80)	477.148302(55)
$D_J{}^a$	-1.3893(51)	-2.942(42)	-2.06(48)	-2.53(10)	-0.742(88)	0.25100(29)
$D_{JK}{}^a$	20.369(28)	16.592(26)	27.1(13)	39.1(13)	15.90(38)	4.1076(20)
$D_K{}^a$	-16.786(25)	-16.023(24)	-23.8(11)	-41.2(44)	-17.34(33)	-4.2195(38)
$d_1{}^a$	0.0742(19)	-0.3886(15)	0.07442 (fixed) [e]	0.07324 (fixed) [e]	-0.078(35)	-0.09576(18)
$d_2{}^a$	-0.9076(12)	-0.8262(10)	-1.004(91)	-1.095(56)	-0.825(20)	-0.08534(10)
a-line no.[b]	0	12	0	0	0	87
b-line no.[b]	48	0	2	5	5	0
c-line no.[b]	35	50	8	7	8	54
N [c]	83	62	10	12	13	141
σ [d]	3.3	2.1	5.5	5.5	1.6	2.0

[a] Rotational constants in MHz and quartic centrifugal distortion constants in kHz.
[b] Number of a particular type of transitions included in the fit.
[c] Total number of transitions included in the fit.
[d] Standard deviation of the fit in kHz.
[e] Centrifugal distortion constants were fixed at the product of the experimental distortion constant of the parent species and the ratio of the calculated distortion constant of the rare isotopologues versus that of parent at the harmonic vibrational level.

3. ZPE effects and large amplitude motions

Experimentally, the intensities of the transitions of $H_t{}^{22}Ne_H$ are about the same as those of $H_t{}^{20}Ne_H$ lines, as shown in Figure 5.2a. We attribute this to the lower *ZPE* of ^{22}Ne versus ^{20}Ne isotopologues. Because of the very weakly bound nature of the H_tN_H species, the binary complex undergoes repeated formation and dissociation processes in a jet expansion, leading to an enrichment of the heavier isotopologues with lower *ZPE*. A similar phenomenon was observed before, for example for Ne_2Kr,[8] and pyrrole···Ne.[48]

We assessed the population ratio of the $H_t{}^{20}Ne_H/{}^{22}Ne_H$ species to be roughly 1:1, based on the intensities of several strong *c*-type rotational transitions in the 2800 to 5900 MHz region. This population ratio indicates an enhancement factor of ~10 for the ^{22}Ne complex which has a natural abundance of 9.25% versus that of ^{20}Ne with a natural abundance of 90.48%. A cooling temperature of about 1 K between these two isotopologues can be estimated by using the Boltzmann distribution equation, slightly higher than the estimated rotational temperature of 0.3 K for these weakly bound complexes. Overall, this is expected since the binding energies of these complexes, although small, are generally larger than the rotational energy level gaps of the transitions observed.

While μ_b and μ_c of $H_t{}^{20}Ne_H$ are both predicted to be 0.4 D (Table 5.1), the comparison of the experimental versus predicted line intensities suggests a μ_b/μ_c ratio of about 0.7. From the structure of $H_t{}^{20}Ne_H$ in Figure 5.3a, one can see that the OH group contributes noticeably to the μ_b component of $H_t{}^{20}Ne_H$. The observed reduction in μ_b can be attributed to a large amplitude motion in which the hydroxyl H moves out of the *bc* plane, into the positive and to the negative *a*-axis directions. The same large amplitude motion would keep the average μ_a dipole moment component at zero as predicted. A corresponding argument can be made for the μ_a/μ_c ratio of $H_t{}^{22}Ne_H$, which experiences an axis switch between *a*- and *b*-axis compared to the $H_t{}^{20}Ne_H$ species, shown in Figure 5.3b.

4. Structure analyses

In Table 5.4, we compare the experimental and calculated planar moments of inertia of the binary complexes and the H_t monomer. As one can see, the calculated P_{aa} of H_t is essentially the same as P_{aa} of $H_t{}^{20}Ne_H$ and P_{bb} of $H_t{}^{22}Ne_H$ and $H_t{}^{40}Ar_H$. The corresponding experimental planar moments exhibit exactly the same behavior. All these observations confirm that the *bc* plane is the symmetry plane in the H_t monomer and in $H_t{}^{20}Ne_H$ and the *ac* plane is the symmetry plane in $H_t{}^{22}Ne_H$ and $H_t{}^{40}Ar_H$, and Ne or Ar are located in the symmetry plane. The non-observation of the *a*-type transitions in $H_t{}^{20}Ne_H$, and of *b*-type transitions in $H_t{}^{22}Ne_H$ and $H_t{}^{40}Ar_H$ in the experiments is consistent with the above theoretical predictions.

The structural parameters of the H_t monomer are only slightly changed in the binary complexes, as confirmed by the experimental planar moments P_{aa} or P_{bb}. Overall, the good agreement between the experimental and predicted rotational constants at the

QZVP level indicates that the actual structures of the H_tNe_H and H_tAr_H species are quite close to the theoretical ones.

Table 5.4. Calculated and experimental planar moments of $H_t{}^{20}Ne_H$, its rarer isotopologues, H_tAr_H and the H_t monomer.

	$H_t{}^{20}N_H$	$H_t{}^{22}Ne_H$	$(^{13}C2)H_t{}^{20}Ne_H$	$(^{13}C1/3)H_t{}^{20}Ne_H$	$(OD)H_t{}^{20}Ne_H$	$H_t{}^{40}Ar_H$	H_t
P_{aa}[a]	395.343	409.091	395.343	397.052	395.343	678.335	395.346
P_{bb}[a]	385.488	395.343	385.662	385.730	387.817	395.341	152.248
P_{cc}[a]	126.690	126.987	127.364	126.690	127.624	128.019	89.580
P_{aa}[b]	390.558	407.087	390.313	392.290	390.817	668.412	390.736[c]
P_{bb}[b]	383.755	390.559	384.182	383.936	386.118	390.761	151.318[c]
P_{cc}[b]	129.809	130.059	130.445	129.797	130.593	128.763	88.753[c]

[a] Calculated planar moments in amu Å^2 at the B3LYP-D3BJ/def2-QZVP level of theory.
[b] Experimental planar moments in amu Å^2.
[c] Calculated from the experimental constants reported in Ref. 19.

With the observation of five isotopologues of H_tNe_H, we used the STRFIT[43] program to refine the structural parameters, mainly those related to atoms directly involved in the bonding with Ne. During the fitting procedure, the symmetry plane discussed above was kept in place. We determined experimental H_t monomer structural parameters by fitting them to the experimental rotational constants reported in Ref. 19. The resulting main structural parameters of H_tNe_H and H_t are listed in Table 5.5, while a detailed list for each is provided in Table S5.12 and S5.13, respectively. The corresponding coordinates obtained from the STRFIT fit for H_tNe_H are summarized in Table S5.14, SI, together with those obtained from a Kraitchman analysis. The coordinates obtained from the STRFIT procedure for H_t are also provided in Table S5.15, SI for completeness. In general, the coordinates obtained for H_tNe_H from the STRFIT and the Kraitchman procedures are in good agreement with each other. We note that the $|a|$ substitution coordinates of H2, the hydroxyl H atom, and Ne, are 0.4079(37) and 0.107(14) Å, respectively. These values are not zero because of the expected large amplitude motions associated with the hydroxyl

H and neon atoms. The |*a*| substitution coordinate of ~0.4 Å of H2 suggests a relatively large amplitude wagging motion of OH about the *bc*-planes from the negative to the positive *a*-axis, consistent with the experimental observation that the *b*-electric dipole component is considerably smaller than predicted for H_tNe_H.

Table 5.5. Structural parameters from the STRFIT fit for the H_tNe_H complex and the H_t monomer.[a]

parameter	exp. [b]	theo. [c]	parameter	exp. [b]	theo. [c]
H_tNe_H					
C1/C3-C2 /Å	1.5673(83)	1.5405	H1-C2-C1 /°	105.69	106.87
C2-H1 /Å	1.0821	1.0889	H1-C2-C3 /°	105.69	106.87
C2-H2 /Å	1.9554	1.9445	H1-C1-H2 /°	140.25	136.37
Ne···H2 /Å	2.3392	2.3698	C1-C2-C3 /°	110.27	114.05
H2-O1 /Å	1.011(82)	0.964	C1/C3-C2-O1 /°	112.14(72)	110.58
H2-O1-C2 /°	106.3(28)	109.67	Ne···O1 /Å	3.348(33)	3.333
Ne···O1-C2 /°	109.48(17)	111.63	Ne···H2-O1 /°	175.47	177.24
H_t monomer[d]					
C1/C3-C2 /Å	1.5332(71)	1.5314	H1-C2-C1 /°	107.34(81)	107.18
C2-H1 /Å	1.082(17)	1.0922	H1-C2-C3 /°	107.34(81)	107.18
C2-H2 /Å	1.9729	1.9296	H1-C1-H2 /°	137.49	135.89
O1-C2 /Å	1.414(11)	1.3990	C1-C2-C3 /°	113.92	114.08
H2-O1 /Å	0.959(26)	0.9651	C1/C3-C2-O1 /°	108.86	110.31
H2-O1-C2 /°	111.04(52)	108.01	O1-C2-H1 /°	110.5(14)	107.50

[a] Bond lengths and angles are listed with four and two digits after the decimal points, respectively for consistency. These do not necessarily reflect their uncertainties. The atom numberings are provided in Figure 5.3.

[b] The structural parameters without error bars are directly read from the STRFIT output geometry.

[d] The experimental structural parameters are obtained by a fit to the experimental rotational constants reported in Ref. 19 and the theoretical parameters are obtained at the MP2/6-311++G(2d,2p) level of theory as in Ref. 19.

Based on the STRFIT results, the Ne···H distance of 2.3392 Å and the Ne···H-O angle of 175.47° were calculated from the fitted coordinates in Table S5.12. From the final STRFIT coordinates of the H_tNe_H complex, the H2-O1 distance is 1.011(82) Å, slightly longer than the corresponding monomer value of 0.959(26) Å. Also the C2-C1/C3 bond length is

1.5673(83) Å, slightly longer than the corepsonding monomer value at 1.5332(71) Å. These parameters suggest that the H_t subunit is a bit 'looser' in the complex than in the dimer. On the other hand, the H2-O1-C2 angle is 106.3(28)° in the H_tNe_H complex, smaller than 111.04(52)° in the monomer, to facilitate better contact of Ne with the H and F atoms in H_t.

Since no other alcohol···Ne complexes were reported before, we briefly compare the structural parameters for several alcohol···Ar complexes, for which DFT structures were reported to be close to the experimental ones. The Ar···H distance is the shortest at 2.61 Å in H_tAr_H, while the corresponding values are 2.82 Å in IP_tAr_H, 2.82 Å in *g*-propargyl···Ar,[16] 2.97 Å in 2-butanol···Ar,[15] and 2.80 Å in methanol···Ar.[14] The related Ar···H-O angle is most close to linear in H_tAr_H at 173.4°, followed by 166.2° in IP_tAr_H, 151.1° in methanol···Ar,[14] 145.2° in *g*-propargyl···Ar,[16] and 134.4° in 2-butanol···Ar.[15] Generally, one can relate the shortest Ar···H distance and largest Ar···H-O angle to the strongest bound binary alcohol···Ar complex, i.e. H_tAr_H (vide infra).

5. Binding topologies and effects of fluorination

To better understand the weak binding interactions between Ne/Ar with HFIP, we carried out QTAIM analyses,[38] and discuss the electrostatic potential (ESP) maps for these systems. Table 5.6 shows the bond critical points (BCPs) and bond paths associated with the non-covalent interactions in the four stable H_tNe and H_tAr isomers, as well as IP_tNe_H and IP_tAr_H for comparison. The corresponding energy values for all the non-covalent BCPs identified in these complexes are listed in Table 5.6 using an approximate formula reported before.[49] For completeness, similar analyses for H_g, H_gNe, and H_gAr are provided in Figure S5.4, SI.

In the H_tNe_H or H_tAr_H isomers, the strongest intermolecular bond energies are associated with the Ne (or Ar)···H-O bond, ranging from 2.9 kJ mol^{-1} for IP_tNe_H, 3.7 kJ mol^{-1} for IP_tAr_H, 5.2 kJ mol^{-1} for H_tNe_H, to 6.0 kJ mol^{-1} for H_tAr_H, demonstrating that fluorination nearly doubles the specific bond energies. At the same time, the Ne···H-O intermolecular distance increases by from 2.370 Å in $\mathrm{H}_{t}\mathrm{Ne}_{\mathrm{H}}$ to 2.606 Å in $\mathrm{IP}_{t}\mathrm{Ne}_{\mathrm{H}}$, and from 2.610 Å in $\mathrm{H}_{t}\mathrm{Ar}_{\mathrm{H}}$ to 2.825 Å in $\mathrm{IP}_{t}\mathrm{Ar}_{\mathrm{H}}$. We also note that replacing Ne with Ar increases the rare gas atom···H-O bond energies from 5.2 ($\mathrm{H}_{t}\mathrm{Ne}_{\mathrm{H}}$) to 6.0 ($\mathrm{H}_{t}\mathrm{Ar}_{\mathrm{H}}$) kJ mol^{-1} and from 2.9 ($\mathrm{IP}_{t}\mathrm{Ne}_{\mathrm{H}}$) to 3.7 ($\mathrm{IP}_{t}\mathrm{Ar}_{\mathrm{H}}$) kJ mol^{-1}. It is also important to recognize that not just the Ne/Ar···H-O bond energies are important, even in $\mathrm{H}_{t}\mathrm{Ne}_{\mathrm{H}}$ and $\mathrm{H}_{t}\mathrm{Ar}_{\mathrm{H}}$. Others intermolecular bond energies, such as those of Ne/Ar···F-C also contribute substantially, leading to a much larger binding energy difference from Ne to Ar. The sums of intermolecular bond energies are 5.2, 5.4, 3.9, 4.6 kJ mol^{-1}for $\mathrm{H}_{t}\mathrm{Ne}_{\mathrm{H}}$, $\mathrm{H}_{t}\mathrm{Ne}_{\mathrm{C}}$, $\mathrm{H}_{t}\mathrm{Ne}_{\mathrm{O}}$ and $\mathrm{H}_{t}\mathrm{Ne}_{\mathrm{F}}$, respectively, whereas the corresponding values are 9.2, 6.0, 4.3, 4.5 kJ mol^{-1} for $\mathrm{H}_{t}\mathrm{Ar}_{\mathrm{H}}$, $\mathrm{H}_{t}\mathrm{Ar}_{\mathrm{C}}$, $\mathrm{H}_{t}\mathrm{Ar}_{\mathrm{O}}$ and $\mathrm{H}_{t}\mathrm{Ar}_{\mathrm{F}}$, respectively. While these sums of energy values are only rough estimates based on an approximation,[49] they still reflect the same trend observed in the calculated DFT binding energies (see Table 5.1 and 5.2

Table 5.6. The intermolecular bond energies for all the non-covalent BCPs identified.

No.^{a}	Bond	$\mathrm{IP}_t\mathrm{Ne}_\mathrm{H}$	$\mathrm{IP}_t\mathrm{Ar}_\mathrm{H}$	No.^{a}	Bond	H_t	$\mathrm{H}_t\mathrm{Ne}_\mathrm{H}$	$\mathrm{H}_t\mathrm{Ar}_\mathrm{H}$
1	Ne/Ar···H-O	2.9^b	3.7^b	1	Ne/Ar···H-O	N/A	5.2^b	6.0^b
2	Ne/Ar···H-C	1.0^b	1.4^b	2	Ne/Ar···F-C	N/A	NA	1.6^b
3	Ne/Ar···H-C	1.0^b	1.4^b	3	Ne/Ar···F-C	N/A	NA	1.6^b
		NA	NA	4	F···F	12.8	12.8^b	12.9^b

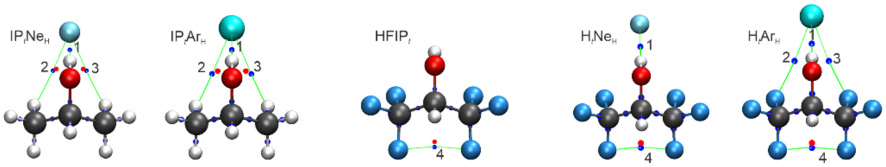

No.^{a}	Bond	$\mathrm{H}_t\mathrm{Ne}_\mathrm{C}$	$\mathrm{H}_t\mathrm{Ar}_\mathrm{C}$	Bond	$\mathrm{H}_t\mathrm{Ne}_\mathrm{O}$	$\mathrm{H}_t\mathrm{Ar}_\mathrm{O}$	Bond	$\mathrm{H}_t\mathrm{Ne}_\mathrm{F}$	$\mathrm{H}_t\mathrm{Ar}_\mathrm{F}$
1	Ne/Ar···H-C	2.4^b	2.8^b	Ne/Ar···H-C	2.5^b	2.9^b	Ne/Ar···F	1.6^b	1.5^b
2	Ne/Ar···F-C	1.5^b	1.6^b	Ne/Ar···F-C	1.4^b	1.4^b	Ne/Ar···F	1.5^b	1.5^b
3	Ne/Ar···F-C	1.5^b	1.6^b				Ne/Ar···F	1.5^b	1.5^b
4	F···F	12.8^b	12.9^b	F···F	12.8^b	12.9^b	F···F	12.8^b	12.8^b

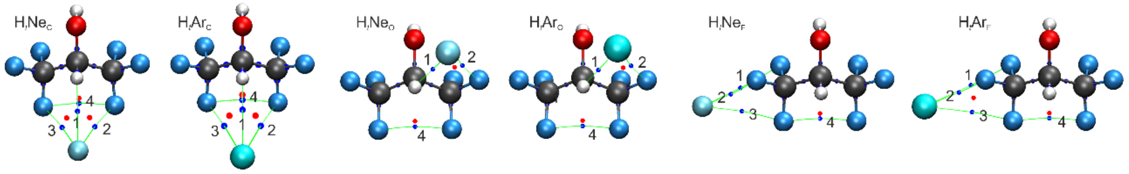

---

^{a} The numbers given are labels for the BCPs identified and correspond to the numbers provided in the related figures shown below.
^{b} The estimated bond energy values in kJ mol^{-1}. One digit after decimal point is provided for consistency in presentation. See the main text for details.

We also note that an intramolecular C-F⋯F-C BCP is identified for H_t, H_tNe and H_tAr, while it is not present in the corresponding H_g, H_gNe and H_gAr. This BCP is likely one reason why H_t and the related complexes are more stable than H_g and the associated complexes. In the study of the 2,2,2-triflouroethanol (TFE) trimers,[50] the shortest C-F⋯F-C binding distance in the TFE trimer I was identified to be 2.824 Å with a BCP energy of ~9.3 kJ mol^{-1}, comparable to the related distances of about 2.788 to 2.811 Å and a BCP energy of ~12.8 kJ mol^{-1} reported here for H_t, H_tNe, and H_tAr.

The electron density electrostatic potential (ESP) maps of the three monomers, H_t, H_g and IP_t are shown in Figure 5.4. It can be seen from Figure 5.4 that mostly positive regions, such as at the alcoholic H, but also negative regions such as at the F atom, can all serve as binding sites with the rare gas atoms. In both H_t and IP_t rare gas complexes, the alcoholic H region is the most positive ESP site and the rare gas⋯H-O bond has the largest bond energy value among all the intermolecular interactions.

Perhaps not surprisingly, it has been suggested in some earlier reports that rare gas atoms, for example helium atoms, tend to bind to the positive ESP site of a linear molecule like OCS in the ground state.[51] Later on, in some more complicated molecules such as 2,3,3,3-tetrafluoropropene, it was recognized that the Ar atom does not stay close to the purely negative or positive ESP area, but moves rather to a region of “moderate electron density”.[52] These statements may seem contradictory, mainly because they emphasize different situations. For example, there may be only one binding site available or multiple (nearby) binding sites possible simultaneously, or the nature of the intermolecular bond may be dominated by van der Waals or induction interactions. The QTAIM analyses indicate that while the rare gas⋯H-O bond has the largest bond energy, the preferred binding sites are generally based on where a rare gas atom can maximize the sum of binding energies of all possible contacts. Furthermore, the strengths of these contacts are not necessarily governed by the electrostatic potential but rather by the nature of the interactions which include electrostatic, induction, dispersion and exchange contributions.

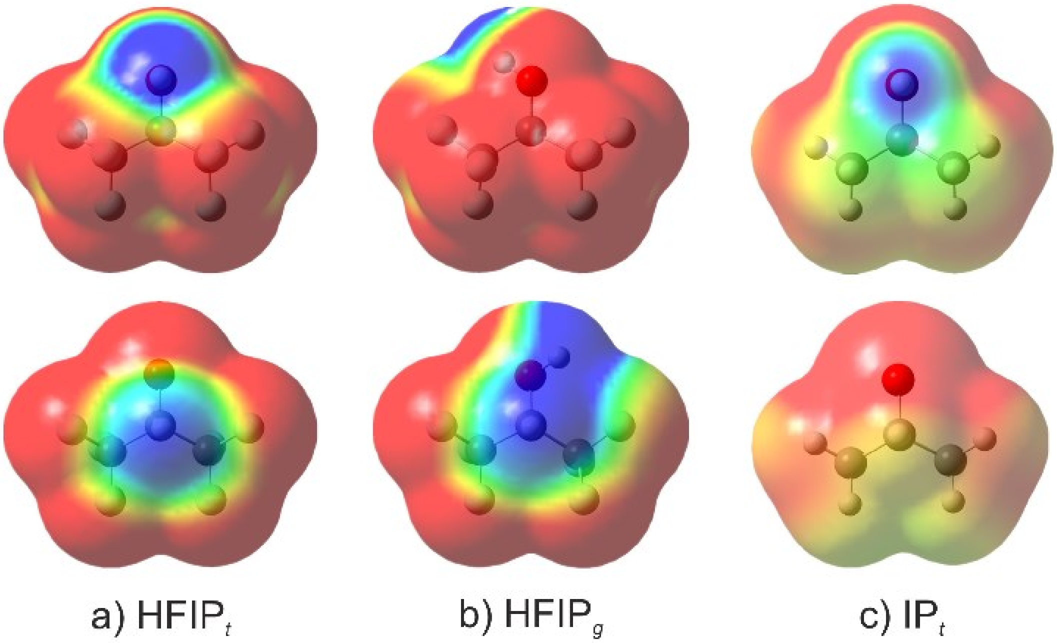

Figure 5.4. Electrostatic potential (ESP), mapped onto a total electron density isosurface for a) H_t, b) H_g and c) IP_t calculated at the B3LYP-D3(BJ)/def2-QZVP level of theory. Each is shown in two views: (top) the front view (center C-H pointing into the paper plane) and (bottom) rear view (center C-H pointing out of the paper plane). Red indicates negative electrostatic potential and blue positive electrostatic potential.

Conclusions

The van der Waals binding topologies between HFIP and Ne/Ar were explored using rotational spectroscopy, CREST, a new conformational search tool, DFT calculations, and QTAIM and ESP analyses. Nine isomers were identified for each binary species. Their non-covalent intermolecular interaction energies are quite similar, within an energy span of 0.6 kJ mol^{-1} for HNe and within 2.3 kJ mol^{-1} for HAr. Comparison of the experimental and theoretical planar moments and the electric dipole moment components allowed us to clearly identify the experimentally observed structure for HNe and for HAr to be the most stable isomers predicted, $H_t Ne_H$ and $H_t Ar_H$. Using the experimental $H_t Ne_H$ isotopic data, we refined the important van der Waals structural parameters, as well as some H_t

structural parameters. While binding with a rare gas atom has not altered the relative stability of the H_t and H_g configurations, the H_t subunit in the observed complex appears to be ′looser′ than in its isolated form. The similar intensities observed for $H_t{}^{20}Ne_H$ and $H_t{}^{22}Ne_H$ highlight the effect of ZPE for these very weakly bound binary complexes in a jet expansion. The QTAIM and ESP analyses emphasize the importance of maximizing the sum of interaction energies of all available contacts, suggesting that it is difficult to rationalize relative isomeric preference based on ESP or electrostatic/induction types of interactions alone. Finally, we show that fluorination from IP to HFIP increases the interaction energy of Ne/Ar···H-O significantly.

References

1. Narita, M.; Honda, S.; Umeyama, H.; Obana, S. *Bull. Chem. Soc. Jpn.* **1988**, *61*, 281-284.

2. Hong, D. P.; Hoshino, M.; Kuboi, R.; Goto, Y. *J. Am. Chem. Soc.* **1999**, *121*, 8427-8433.

3. Godin, P. J.; Le Bris, K.; Strong, K. *J. Quant. Spectros. Radiat. Transfer* **2017**, *203*, 522-529.

4. Becucci, M.; Melandri, S. *Chem. Rev.* **2016**, *116*, 5014-5037.

5. Juanes, M.; Saragi, R. T.; Caminati, W.; Lesarri, A. *Chem. Eur. J.* **2019**, *25*, 11402-11411.

6. Jäger, W.; Xu, Y. Fourier transform microwave spectroscopy of doped helium clusters. in *Handbook of High Resolution Spectroscopy, Foundamentals and Theory*, Eds. M. Quack and F. Merkt, **2011**, John Wiley Sons, Ltd.

7. Xu, Y.; Van Wijngaarden, J.; Jäger, W. *Int. Rev. Phys. Chem.* **2005**, *24*, 301-338.

8. Jäger, W.; Xu, Y.; Gerry, M. C. L. *J. Chem. Phys.* **1993**, *99*, 919-927.

9. Brupbacher, T.; Makarewicz, J.; Bauder, A. *J. Chem. Phys.* **1994**, *101*, 9736-9746.

10. Harris, S. J.; Janda, K. C.; Novick, S. E.; Klemperer, W. *J. Chem. Phys.* **1975**, *63*, 881-884.

11. Blanco, S.; Melandri, S.; Maris, A.; Caminati, W.; Velino, B.; Kisiel, Z. *Phys. Chem. Chem. Phys.* **2003**, *5*, 1359-1364.

12. Wilson, R. J.; Peebles, S. A.; Antolínez, S.; Sanz, M. E.; Kuczkowski, R. L. *J. Phys. Chem. A* **1998**, *102*, 10630-10635.

13. Leung, H. O.; Marshall, M. D.; Stuart, D. J. *J. Phys. Chem. A* **2020**, *124*, 1798-1810.

14. Tan, X. Q.; Sun, L. H.; Kuczkowski, R. L. *J. Mol. Spectrosc.* **1995**, *171*, 248-264.

15. King, A. K.; Howard, B. J. *J. Mol. Spectrosc.* **2002**, *214*, 97-102.

16. Mani, D.; Arunan, E. *ChemPhysChem.* **2013**, *14*, 754-763.

17. Durig, J. R.; Larsen, R. A.; Cox, F. O.; Van der Veken, B. J. *J. Mol. Struct.* **1988**, *172*, 183-201.

18. Schaal, H.; Häber, T.; Suhm, M. A. *J. Phys. Chem. A* **2000**, *104*, 265-274.

19. Shahi, A.; Arunan, E. *J. Phys. Chem. A* **2015**, *119*, 5650-5657.

20. Oswald, S.; Suhm, M. A. *Angew. Chem. Int. Ed.,* **2017***, 56*, 12672-12676; *Angew. Chem. Angew. Chem.* **2017,** 129**,** 12846.

21. Oswald, S.; Seifert, N. A.;Bohle, F.; Gawrilow, M.; Grimme, S.; Jäger, W.; Xu, Y.; Suhm, M. A. *Angew. Chem. Int. Ed.,* **2019***, 58*, 5080-5084; *Angew. Chem.* **2019**, *131*, 5134-5138.

22. Wu, B.; Hazrah, A. S.; Seifert, N. A.; Oswald, S.; Jäger, W.; Xu, Y., *J. Phys. Chem. A* **2021,** *125*, 10401-10409.

23. Marshall, M. D.; Leung, H. O.;Wang, K.; Acha, M. D. *J. Phys. Chem. A* **2018***, 122*, 4670-4680.

24. Xie, F.; Seifert, N. A.; Heger, M.; Thomas, J.; Jäger, W.; Xu, Y. *Phys. Chem. Chem. Phys.* **2019**, *21*, 15408-15416.

25. Carlson, C. D.; Seifert, N. A.; Heger, M.; Xie, F.; Thomas, J.; Xu, Y. *J. Mol. Spectrosc.* **2018**, *351*, 62-67.

26. Seifert, N. A.; Thomas, J.; Jäger, W.; Xu, Y. *Phys. Chem. Chem. Phys.* **2018**, *20*, 27630-27637.

27. Xu, Y.; Jäger, W. *J. Chem. Phys.* **1997**, *106*, 7968-7980.

28. Pérez, C.; Lobsiger, S.; Seifert, N. A.; Zaleski, D. P.; Temelso, B.; Shields, G. C.; Kisiel, Z.; Pate, B. H. *Chem. Phys. Lett.* **2013**, *571*, 1-15.

29. Grimme, S. *J. Chem. Theory Comput.* **2019**, *15*, 2847-2862.

30. Pracht, P.; Bohle, F.; Grimme, S. *Phys. Chem. Chem. Phys.* **2020**, *22*, 7169-7192.

31. Xie, F.; Seifert, N. A.; Jaeger, W.; Xu, Y. *Angew. Chem. Int. Ed.* **2020**, *59*, 15703-15710; *Angew. Chem.* **2020**, *132*, 15833-15840.

32. Marshall, F. E.; Dorris, R.; Peebles, S. A.; Peebles, R. A.; Grubbs, G. S. *J. Phys. Chem. A* **2018**, *122*, 7385-7390.

33. Xie, F.; Fusè, M.; Hazrah, A. S.; Jaeger, W.; Barone, V.; Xu, Y. *Angew. Chem. Int. Ed.,* **2020**, 59, 22427-22430; *Angew. Chem.* **2020,** *132*, 22613-22626.

34. Gaussian 16, Revision B.01, Frisch, M. J.; Trucks, G. W.; Schlegel, H. B.; Scuseria, G. E.; Robb, M. A.; Cheeseman, J. R.; Scalmani, G.; Barone, V.; Petersson, G. A.; Nakatsuji, H. et al., Gaussian, Inc., Wallingford, CT, **2016**.

35. Grimme, S.; Antony, J.; Ehrlich, S.; Krieg, H. *J. Chem. Phys.* **2010,** *132*, 154104.

36. Grimme, S.; Ehrlich, S.; Goerigk, L. *J. Comput. Chem.* **2011,** *32*, 1456-1465.

37. Weigend, F.; Ahlrichs, R. *Phys. Chem. Chem. Phys.* **2005,** *7*, 3297-3305.

38. Boys, S. F.; Bernardi, F. *Mol. Phys.* **1970,** *19*, 553-566.

39. Bader, R. F. W. Atoms in molecules: a quantum theory, Oxford University Press, New York, **1990**.

40. Hanwell, M. D.; Curtis, D. E.; Lonie, D. C., Vandermeersch, T.; Zurek, E.; Hutchison, G. R. *J. Cheminformatics*, **2012**, 4, 17.

41. Humphrey, W.; Dalke, A.; Schulten, K. *J. Mol. Graph.* 1996, 14: 33-38.

42. Lu, T.; Chen, F. *J. Comput. Chem.* 2012, 33, 580-592.

43. Kisiel, Z. PROSPE–Programs for rotational spectroscopy, in Spectroscopy from Space, Eds. J. Demaison, K. Sarka, E. A. Cohen, **2001**, pp. 91-106. Springer Science+Business Media Dordrecht.

44. Western, C. M. *J. Quant. Spectrosc. Radiat. Transf.* **2017,** *186*, 221-242.

45. Shahi, A.; Arunan, E. *Phys. Chem. Chem. Phys.* **2015,** *17*, 24774-24782.

46. Xu, Y.; Jäger, W. *J. Chem. Phys.* **1997,** *107*, 4788-4796.

47. Watson, J. K. G., in: During, J. R. (Ed.), Vibrational spectra and structure, vol. 6, Elsevier, New York, **1977**, pp. 1–89.

48. Peña, I.; Cabezas, C. *Phys. Chem. Chem. Phys.* **2020,** *22*, 25652-25660.

49. Mata, I.; Alkorta I.; Espinosa, E.; Molins, E. *Chem. Phys. Lett.* **2011,** *507*, 185-189.

50. Thomas, J.; Seifert, N. A.; Jäger, W.; Xu, Y. *Angew. Chem. Int. Ed.* **2017,** *56*, 6289-6293. *Angew. Chem.* **2017,** *129*, 6386–6390.

51. McKellar, A. R. W.; Xu, Y.; Jäger, W. *J. Phys. Chem. A* **2007,** *111*, 7329-7337.

52. Leung, H. O.; Marshall, M. D.; Wronkovich, M. A. *J. Mol. Spectrosc.* **2017,** *337*, 80-85.

Chapter 6

2,2,3,3,3-pentafluoro-1-propanol and its five dimers: structural diversity, conformational conversion, and tunneling motion[1]

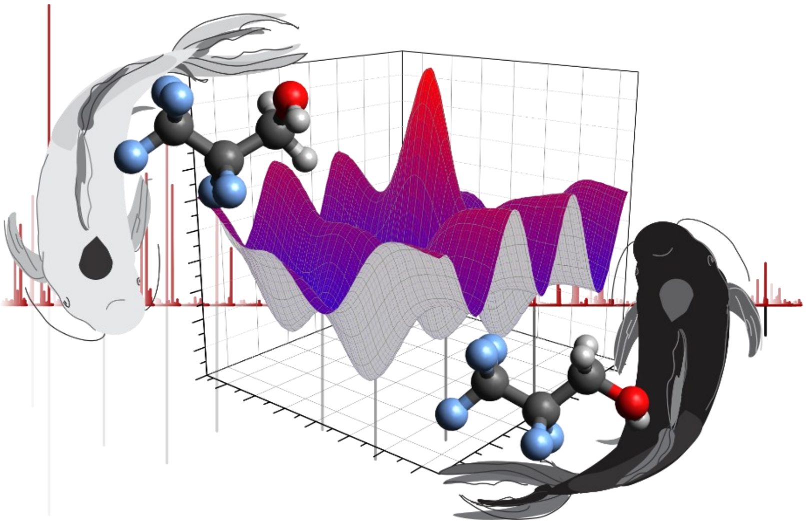

---

[1] This study is published as B. Wu, N. A. Seifert, Aran Insausti, Jiarui Ma, S. Oswald, W. Jäger, Y. Xu, "2,2,3,3,3-pentafluoro-1-propanol and its five dimers: structural diversity, conformational conversion, and tunneling motion". *Phys. Chem. Chem. Phys.*, **2022**, DOI:10.1039/D2CP01895K

Abstract

Rotational spectra of the 2,2,3,3,3-pentafluoro-1-propanol (PFP) were measured using cavity and chirped pulse Fourier transform microwave spectrometers. Of the nine possible PFP configurations which include four mirror-imaged pairs and an achiral conformer, the two most stable monomeric PFP imaged pairs, i.e., **PFP***G+g+/G-g-* and **PFP***Tg+/Tg-* were observed and assigned, along with the ^{13}C, ^{18}O and deuterated isotopologues of **PFP***G+g+/G-g-*. The rotational transitions of **PFP***Tg+/Tg-* exhibit large tunnelling splittings and were analyzed in detail. CREST, a recently developed conformational search tool, was used for systematic conformational searches of possible binary PFP conformers and the subsequent DFT calculations at the B3LYP-D3(BJ)/def2-QZVP level produced nearly 80 stable, binary PFP geometries, where ten of them are within a narrow energy window of ~1 kJ mol^{-1}, highlighting the structural diversity of the system. Rotational spectra of five $(PFP)_2$ conformers were assigned and were identified as the five most stable binary conformers predicted. A closer examination reveals that the assigned binary conformers are made exclusively of the two most stable PFP monomeric subunits observed experimentally. A combined kinetic and thermodynamic model was proposed to explain the observation or non-observation of low energy conformers, and the analysis was further verified by the 'argon test'. The non-covalent intermolecular interactions of PFP and its binary conformers are also discussed with the aid of quantum theory of atoms in molecule (QTAIM) and non-covalent interaction (NCI) analyses, as well as the effects of fluorination by comparing to 1-propanol and its dimers.

Introduction

The compound 2,2,3,3,3-pentafluoro-1-propanol (PFP) belongs to the family of fluoridated alcohols whose remarkable catalytical effects on C-H activation reactions have been reported in recent years.[1] It is also considered to be a potential replacement of hydrofluorocarbons which have large global warming potentials.[2] Characterizing the properties of the PFP monomer and its hydrogen-bonded adducts at the molecular level would be a crucial initial step in understanding the PFP aggregation behavior in the condensed phase and its role in the C-H activation mechanism. A closely related fluorinated alcohol is 1,1,1,3,3,3-hexaflouroisopropanol (HFIP) whose 'magical solvent effect' for the Pd-catalyzed C-H activation was very recently reviewed.[1] The main difference between HFIP and PFP is that the alcoholic hydroxyl group moves from the middle C to an end C atom. Structurally, the possible PFP conformations are determined by three dihedral angles, FCCC, CCCO, CCOH, corresponding approximately to the rotation of the trifluoromethyl (CF_3) group, the CH_2O group, and the hydroxyl (OH) group, respectively. HFIP, on the other hand, has only one flexible dihedral angle which is associated with the hydroxyl OH orientation. Jet-cooled rotational and infrared spectroscopic techniques have been utilized to probe the conformational landscape of HFIP monomer,[3] its dimer and trimer.[4] It is interesting to note that the achiral HFIP, i.e., *trans*-HFIP, dominates in the monomeric and dimeric forms, whereas the only observed HFIP trimer is made exclusively of three metastable chiral monomer (i.e., *gauche*-HFIP) units arranged into a strained OH⋯O hydrogen-bonded ring, which is reinforced by secondary CH⋯FC interactions. In the related binary,[5-7] ternary[8-10] and even tetrameric[11] clusters of 2,2,2-trifluoroethanol (TFE) and monofluoroethanol (MFE), the abundances of the least stable or even non-stable monomeric unit in their isolated forms increase noticeably in these clusters driven largely by the intermolecular hydrogen-bonding interactions. Such studies offer a gleam into the situation in the bulk phase, allowing one to appreciate the often very different conformational distributions of these important fluoroalcohol solvents in the isolated monomer and in the bulk phase. With a longer fluorocarbon chain than these previously studied fluoroalcohols, PFP offers additional flexibility associated with the heavy atom frame. It is of considerable interest to probe how the preferred conformations in the isolated PFP monomer change with the non-covalent interactions with a second PFP molecule.

Unlike its smaller counterparts mentioned above, no jet-cooled rotational or IR spectroscopic studies of the PFP monomer or dimer have been reported previously. The only combined experimental and theoretical study was carried out using liquid or solution samples where two most stable PFP conformers were tentatively identified from the observed FTIR/Raman features.[12] Jet-cooled rotational spectroscopic studies offer significant advantages in providing accurate geometric information and in distinguishing species with only minor structural differences. An additional advantage is the high-resolution capability which allows one to detect possible OH tunnelling dynamics in PFP, similar to what was reported in TFE[13] and cyclohexanol.[14] In the current study, we applied both cavity- and chirped pulse Fourier transform microwave spectroscopy, together with theoretical modelling, to probe the conformational landscapes of the PFP monomer and dimer and characterize potential large amplitude motions in PFP and non-covalent interactions in the PFP homodimers.

Methods

1. Experimental

A broadband 2-6 GHz chirped pulse Fourier transform microwave (CP-FTMW) spectrometer[15-17] with a measurement uncertainty of about 5-10 kHz was used for recording rotational spectra. This spectrometer was developed and constructed, based on a similar instrument designed by Pate and co-workers.[18] A 4-18 GHz cavity-based FTMW spectrometer[19] with a measurement accuracy of about 1 kHz was utilized for measuring additional transitions of several rare isotopologues of PFP. PFP (Sigma Aldrich, 99.9%) and D_2O (Cambridge Isotope Laboratories, Inc. 99.5%) were used without further purification. Sample mixtures of 0.1% PFP with 0.2% D_2O in 2 bars of neon (Praxair, 99.999%) or helium (Praxair, 99.998%) were prepared for the cavity and CP-FTMW measurements. We also performed the so-called “argon-test” by adding 5% Ar (Praxair, 99.998%) into the PFP+He mixture to investigate the conformational cooling properties of the binary PFP conformers. The ^{13}C and ^{18}O isotopic species were recorded in their natural abundances.

2. Computational

The conformer-rotamer ensemble sampling tool (CREST)[20,21] is a quantum chemistry code developed specifically for conformational searches of flexible organic molecules and has been used successfully for systems such as perillyl alcohol[15] and the dimer of tetrahydro-2-furoic acid.[22] On the other hand, it was recently reported that CREST failed to generate one main isomer of the propylene oxide trimer even though the geometry of the ternary isomer was derived from experimental spectra utilizing isotopic substitution.[23] We employed CREST for comprehensive isomer searches of the PFP monomer and its dimers. To ensure that the searches were complete, multiple runs with different starting geometries, which were thought to be separated by large conversion barriers, were used.

The CREST structural candidates were then re-optimized by employing the Gaussian16 program package.[24] The B3LYP hybrid functional, combined with Grimme's dispersion correction (D3)[25], Becke-Johnson damping (BJ)[26] and the def2-QZVP basis set,[27] was used for all geometry optimizations and harmonic frequency calculations. In addition, anharmonic calculations at the B3LYP-D3(BJ)/def2-QZVP level were also carried out for the isotopologues of the most stable PFP monomeric conformer to estimate the ro-vibrational contributions to the rotational constants, as well as geometry optimization and harmonic calculations at the MP2-cc-pVTZ, B3LYP-D3(BJ)/def2-TZVP, and PBE0-D3(BJ)/def2-TZVPD levels.

To investigate the energies corresponding to changes in the two dihedral angles, CCCO and CCOH in the PFP monomer, and to facilitate the experimental interpretation, some 1- and 2-dimensional (D) potential energy surface (PES) scans were also carried out at the B3LYP-D3(BJ)/def2-QZVP level of theory.[28] The corresponding results were visualized by the Origin 8 program.[29] All relative energies reported for the monomers were corrected for the zero-point energy (*ZPE*), and those of the PFP dimers were corrected for both *ZPE* and basis set super position errors (*BSSE*s) using the counterpoise procedure.[30] Kisiel's STRFIT, KRA, and EVAL programs[31] were utilized for the structural fitting analyses and the isotopic substitution coordinate calculations. The keywords used in the Gaussian calculations are provided in Point S1, Supporting Information (SI) and the Gaussian files of the five most stable PFP monomeric and ten PFP binary conformers are provided as a zip file.

Geometries of the PFP monomers and dimers were visualized using Avogadro.[32] Bader's quantum theory of atoms in molecules (QTAIM) analyses,[33] along with Johnson's non-covalent interaction (NCI) analyses[34] were also used to assist the intermolecular interaction topology analyses in the binary conformers, then visualized using the VMD[35] and Multiwfn[36] software packages. Finally, rotational transition fits were completed by using the Pgopher[37] program package and Pickett's SPFIT/SPCAT package.[1, 2]

Results and Discussion

1.The PFP monomer

Calculations

As mentioned before, the conformations of PFP are defined by the three dihedral angles FCCC, CCCO, and CCOH.[1] Our calculations indicate that only the *trans*-form (FCCC angle =180˚), i.e., the staggered conformation of CF_3 and CF_2H, is stable. For conciseness, we will use only the next two dihedral angles to label the different monomeric conformers. We use capital letters for the heavy atom frame configurations, corresponding to the CCCO angle *T* (180˚), *G+* (clockwise 60˚) and *G-* (anticlockwise 60˚) and *t*, *g+*, *g-* for the corresponding CCOH angle following the same nomenclature. For example, for a conformer like **PFP***G+g-*, **PFP** is the abbreviated name of the compound; the first capitalized *G+* indicates the heavy atom backbone configuration where the CCCO dihedral angle is in the *gauche+* (clockwise ~60°) configuration; the second lower case *g-* indicates the CCOH dihedral angle in the *gauche-* (anticlockwise ~60°) configuration. Overall, considering only the staggered PFP conformers, nine different conformations are expected, including four transiently chiral pairs (i.e., non-superimposable mirror-images), **PFP***G+g+*/*G-g-*, **PFP***Tg+*/*Tg-*, **PFP***G+g-*/*G-g+*, and **PFP***G+t*/*G-t*, and an achiral one, **PFP***Tt*. The predicted relative energies, rotational constants, and electric dipole moment components calculated at the B3LYP-D3(BJ)/def2-QZVP level of theory are listed in Table 6.1. The optimized geometries of the five PFP conformers are depicted in Figure 6.1 where each transiently chiral pair, such as **PFP***G+g+* and **PFP***G-g-*, are counted as one conformer since they give rise to the same rotational spectrum.

Rotational spectra of **PFP***G+g+/G-g-* and its isotopologues

The rotational transitions of the most stable **PFP***G+g+/G-g-* monomer dominate the experimental spectra observed with either neon or helium as carrier gas. It was also possible to observe the ^{18}O and three ^{13}C isotopologues of **PFP***G+g+/G-g-* in their natural abundances, as shown in Figure S6.1, SI. The rotational transitions of its deuterated acidic hydroxyl isotopologues were also assigned. The experimental rotational transitions were fitted using Watson's semi-rigid rotor Hamiltonian in the *S*-reduction and I^r representation[40] and the resulting spectroscopic constants of all the isotopologues are summarized in Table 6.2 and the transition frequencies are listed in Tables S6.1-S6.6, SI.

Table 6.1. Energies, rotational constants, and dipole moment components of PFP monomeric conformers at the B3LYP- D3(BJ)/def2-QZVP level of theory.[a]

Order[b]	Conformers	ΔE_{raw}	ΔE_0	ΔG	% [c]	*A*	*B*	*C*	$\lvert\mu_a\rvert$	$\lvert\mu_b\rvert$	$\lvert\mu_c\rvert$
I	**PFP***G+g+/G-g-*	0.0	0.0	0.0	44.5	2073.4	1507.6	1293.5	1.8	0.5	0.1
II	**PFP***Tg+/Tg-*	0.3	0.3	0.5	36.4	2533.8	1229.2	1188.4	0.5	1.3	1.0
III	**PFP***G+g−/G-g+*	2.7	2.6	2.9	13.8	2073.9	1503.9	1286.8	0.4	0.9	1.4
IV	**PFP***G+t/G-t*	8.7	7.4	6.4	3.4	2050.1	1540.7	1305.7	2.8	0.5	1.9
V	**PFP***Tt*	10.2	8.5	6.1	1.9	2535.4	1236.8	1191.8	1.3	3.1	0.0

[a] ΔE_{raw}, ΔE_0, and ΔG are the relative electronic raw energy, the relative energy including *ZPE* energy corrections, and the relative free energy at 298 K in kJ mol^{-1}; *A*, *B*, and *C* are the rotational constants in MHz; $\lvert\mu_{a,b,c}\rvert$ are the magnitudes of the electric dipole moment components in Debye.

[b] The relative stability ordering based on ΔE_0 with **I** being the most stable.

[c] Percentage abundance at 298 K based on the relative free energies.

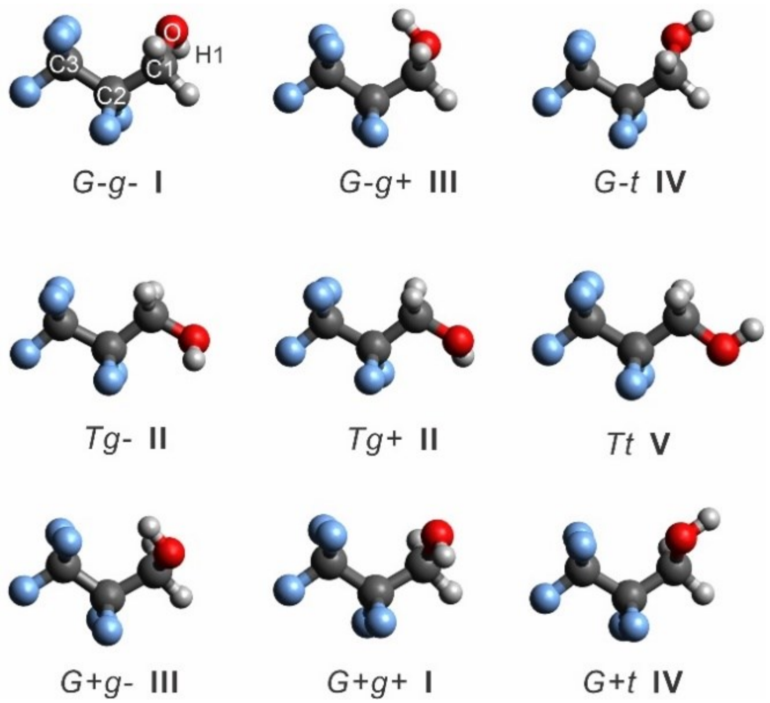

Figure 6.1. Nine configurations of the PFP monomer which include four transiently chiral mirror-imaged pairs: *G-g-*/*G+g+*, *G-g+*/*G+g-*, *G*-t/*G*+t, and *Tg-*/*Tg+*, and achiral *Tt*. The atomic numbers for the substituted atoms are shown in *G-g-*. The Roman numbers **I** to **V** indicate the relative stability of the five conformers with **I** being the most stable one. Please see the main text for the naming discussion.

Table 6.2. Experimental spectroscopic parameters of parent, ^{13}C, ^{18}O and D isotopologues of the **PFP***G+g+*/*G-g-* **I** monomer.

	Parent	^{13}C1	^{13}C2	^{13}C3	^{18}OH	OD
A /MHz	2086.35307(	2082.4323(21	2083.6572(17	2085.6190(27	2065.6546(60	2074.04612(6
B /MHz	1522.27266(	1507.87103(8	1521.60379(7	1519.10129(6	1481.31722(8	1492.56183(4
C /MHz	1305.09346(	1296.00364(8	1303.51040(6	1302.44608(6	1267.1137(10	1282.91088(4
D_J /kHz	0.316(12)	0.269(28)	0.272(24)	0.288(21)	0.309(28)	0.226(16)
D_{JK} /kHz	-0.9181(61)	-0.585(92)	-0.689(83)	-0.584(74)	-0.978 (fixed)	-0.802(24)
D_K /kHz	1.1680(89)	1.167 (fixed)[b]	1.174 (fixed)	1.136 (fixed)	1.252 (fixed)	1.207 (fixed)
d_1 /kHz	-0.01538(62)	-0.01534	-0.01539	-0.01480	-0.01595	-0.01597
d_2 /kHz	0.05555(47)	0.05484	0.05571	0.032(12)	0.087(16)	0.0179(26)
N[c]	92	18	20	19	14	38
σ /kHz[d]	3.5	4.8	4.4	3.6	4.2	3.6

[a] The errors are given in the unit of the last digits.

[b] Centrifugal distortion constant values were fixed at the calculated values obtained from the harmonic frequency calculations, scaled by the experimental versus calculated ratio for the parent species.

[c] N is the number of transitions included in the fit.

[d] σ is the standard deviation of the fit.

Rotation-tunnelling spectrum of **PFP***Tg+/Tg-*

Based on the initial semi-rigid rotor prediction, it appeared that the second strongest set of transitions belongs to **PFP***Tg+*/*Tg-* although there are additional splittings. We attribute the splittings to a tunnelling motion of the OH group that interconverts **PFP***Tg+* and *Tg-*. It quickly became obvious that the frequencies could not be fitted adequately using a semi-rigid rotor Hamiltonian as in high barrier OH tunnelling cases, such as TFE···*ortho* and *para* H_2O.[41] Based on previous experience with strong Coriolis coupling in CO-*para*N_2[42] and H_2O_2-formic acid,[43] we used frequency loops to identify *a*- and *b*-type transition in the ground and the excited states. We then used the relative intensities of the ground versus the excited state transitions to estimate the excited state band origin, i.e., $\Delta E_{1,0}$, in order to identify the cross-tunnelling *c*-type transitions which connect the ground and the excited states. In Figure S6.2, SI, two example spectra of **PFP***Tg+*/*Tg-* are depicted. The final spectroscopic fit was carried out using the SPFIT[1, 2] program with a Hamiltonian similar to that used for TFE[13] and cyclohexanol.[14] The resulting spectroscopic parameters are summarized in Table 6.3 and the related transition frequencies are listed in Table S6.7, SI. For the deuterated species of **PFP***Tg+*/*Tg-*, only very few tunnelling splitting transitions were identified. Because of the limited numbers of transitions, it was difficult to employ the frequency loop strategy efficiently and no further analyses were done for the deuterated species.

Interestingly, the OH proton tunnelling splitting of 7651.9002(32) MHz of the **PFP***Tg+*/*Tg-* monomer, is somewhat larger than that of the TFE monomer at 5868.6952(16) MHz.[13] To estimate the tunnelling barrier, we applied the Effective Barrier Height Model recommended for alcohols with electronegative substituents,[44] with the formula shown below.

$$ln\left(\frac{\Delta_{\mathrm{H}}\sqrt{\pi e}}{\omega_{0,H}hc}\right) = -0.333 \cdot \sqrt{(V_{0,H} - E_{0,H})/\mathrm{cm}^{-1}hc} + 1.85 \qquad (1)$$

where, Δ_H is the tunnelling splitting (i.e., $\Delta E_{1,0}$ in Table 6.3), $\omega_{0,\mathrm{H}}$ is the calculated harmonic torsional wavenumber, $E_{0,H}$ is the torsional *ZPE* of the minimum energy conformation and ($V_{0,H}$ - $E_{0,H}$) is the effective barrier height. The resulting effective tunnelling barriers ($V_{0,\mathrm{H}}$ - $E_{0,\mathrm{H}}$) based on equation (1) are 559 cm^{-1} (6.7 kJ mol^{-1}) and 612 cm^{-1} (7.3 kJ mol^{-1}) for **PFP***Tg+*/*Tg-* and TFE, respectively.

Table 6.3. Experimental spectroscopic parameters of **PFP***Tg+*/*Tg-* **II**.

PFP*Tg+*/*Tg-*	Ground state v=0	Excited state v=1
A /MHz	2552.1574(10)[a]	2552.13916(89)
B /MHz	1238.43417(57)	1238.43383(48)
C /MHz	1197.98670(46)	1197.99682(47)
D_J /kHz	0.056(13)s	
D_{JK} /kHz	0.165(40)	
D_K /kHz	0.060(54)	
d_1 /kHz	-0.002889 (fixed)[b]	
d_2 /kHz	0.000037 (fixed)[b]	
N[c]	103	
σ /kHz[c]	2.7	
$\Delta E_{1,0}$ /MHz[d]	7651.8987(32)	
F_{ac} /MHz[d]	12.88844(93)	
F_{bc} /MHz[d]	1.5346(37)	

[a] The errors are given in the unit of the last digits.

[b] The quartic centrifugal distortion constants (in kHz) are fixed at the values determined in the harmonic vibrational calculation.

[c] N is the number of transitions included in the fit, σ is the standard deviation of the fit. [d] $\Delta E_{1,0}$ is the band origin of the excited tunnelling state relative to the ground state, and F_{ac} and F_{bc} are the Coriolis coupling constants.

Conformational conversions and tunnelling motion

In the current experiment, four out of nine configurations were observed, i.e., two conformers (**PFP***G+g+*/*G-g-* and **PFP***Tg+*/*Tg-*) out of a total of five conformers shown in Figure 6.1. The relative experimental abundances were estimated to be about 60 % and 40 % for **PFP***G+g+*/*G-g-* and **PFP***Tg+*/*Tg-*, respectively. The Boltzmann factors for the five conformers at the source temperature, i.e., 298 K, using the ∆G values are 45%, 36%, 14%, 3%, and 2% from the most stable to the least stable (see Table 6.1). Since the rotational transitions of the ^{18}O isotopologue of **PFP***G+g+*/*G-g-* were observed experimentally in its natural abundance, one would expect to also detect the higher energy conformers, **PFP***G+g−/G-g+,* **PFP***G+t*/*G-t*, and **PFP***Tt*. Their non-observation is likely due to low interconversion barriers discussed below.

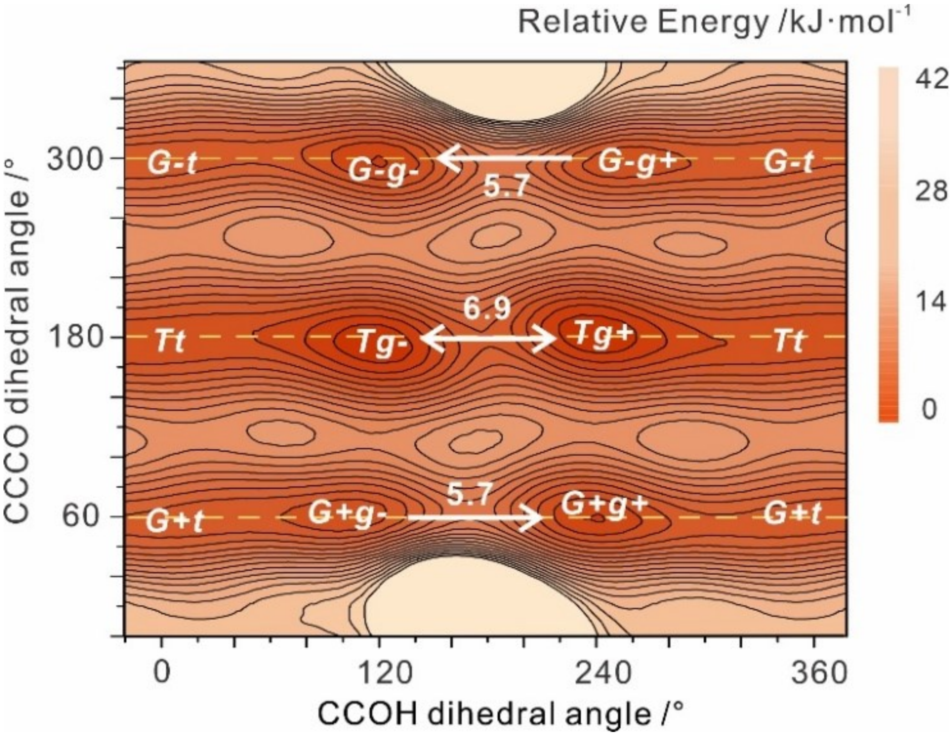

Figure 6.2. Potential energy surface from a rigid scan of PFP monomers at the B3LYP-D3(BJ)/def2-TZVP level of theory. The x- and y-axis correspond to the CCOH and CCCO dihedral angles which we chose to label as from 0-360 degree for simplicity. Some conversion barriers (single arrowed lines) from the high to low energy conformers obtained from the transition state calculations are indicated, as well as the tunnelling barrier (double arrowed line) between **PFP***Tg*- and *Tg*+, the mirror imaged pair (vide infra). The potential wells for **PFP***G*+*t*, **PFP***G*-*t* and **PFP***Tt* are extremely flat. See main text for discussions.

To evaluate the interconversion barriers, we carried out a rigid 2D-PES scan along the dihedral angles CCCO and CCOH and the result is shown in Figure 6.2. The 2D scan provides a general overview of the conformational landscape of the PFP monomer. To obtain a better estimate of the conformational conversion barriers, we also carried out transition state calculations. The calculated conversion barriers with *ZPE* correction are summarised in Figure S6.3, SI. A general trend emerges for the PFP conformers: the conversion barriers related to the changes of the heavy atom frame are high (> 11.7 kJ mol^{-1}) and can not be readily overcome in a jet expansion, whereas the conversion barriers related to the changes of the OH orientations are low (see Figure 6.2 and Figure S6.3) and can be easily overcome in a jet expansion. For example, the conversion barriers associated with a change in the heavy atom frame from **PFP***G*+*g*- to **PFP***G*-*g*-, from **PFP***G*-*g*+ to **PFP***Tg*+ and from **PFP***Tg*- to **PFP***G*-*g*- are estimated to be ~14.0, 11.7 and 13.3 kJ mol^{-1}, respectively (see Figure S6.3). The barrier from **PFP***G*-*g*+ to **PFP***G*-*g*-

is about 5.7 kJ mol^{-1}, and those from the *t*- to *g*-conformers with the same heavy atom frame (i.e., in the same row in Figure 6.2) are barrierless after *ZPE* correction (Figure S6.3). Consequently, one can treat the conformers in each row in Figure 6.2 separately, and only the lowest energy one in each row persists in a jet expansion, leading to the presence of **PFP***G+g+* (in row 3)/*G-g-* (in row 1) and **PFP***Tg+*/*Tg-* in row 2. Taking into account of the conformational cooling, the conformational abundances associated with *G+/G-* and *T* are 60% versus 40%, respectively, in good agreement with the experimental estimates reported above.

For the tunnelling between the mirror imaged pair, **PFP***Tg+* and **PFP***Tg-*, a relaxed 1D PES scan along the dihedral angle CCOH, at the B3LYP-D3BJ/def2-QZVP level, was also carried out and the result is depicted in Figure 6.3. As can be seen, **PFP***Tt* is only supported by an extremely shallow potential and its conversion to **PFP***Tg+*/*Tg-* becomes barrierless after *ZPE* correction (i.e., about 0.3 kJ mol^{-1} above the barrier). The transition state identified in Figure 6.3 has a single imaginary frequency at ~382 cm^{-1}, corresponding to the OH group tilting motion from *g*+ to *g*-between **PFP***Tg+* and **PFP***Tg-*. The corresponding *ZPE* corrected barriers are 6.9 and 7.2 kJ mol^{-1} (577 and 602 cm^{-1}) for **PFP***Tg+*/*Tg-* and TFE, respectively, in general agreement with the experimentally estimated barriers of 6.7 and 7.3 kJ mol^{-1} based on eq. (1).

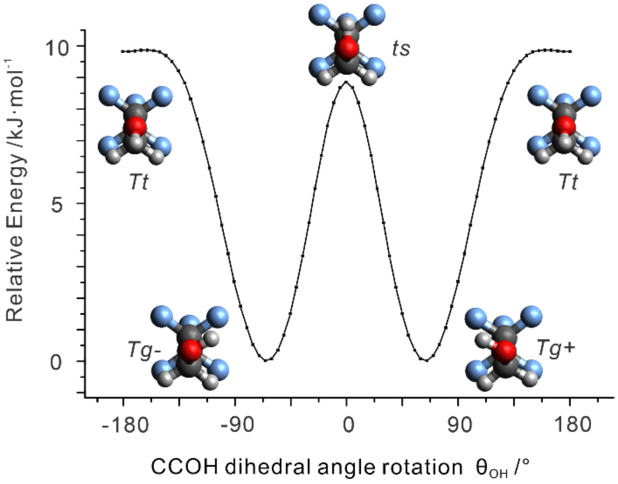

Figure 6.3. A fully relaxed PES scan along the OH flipping coordinate at the B3LYP-D3(BJ)/def2-QZVP level of theory. The geometries of the associated PFP conformers are given, as well as the transition state connecting the mirror imaged pair **PFP***Tg+*/*Tg-*. The tunnelling barrier between **PFP***Tg+*/*Tg-* was calculated to be ~ 6.9 kJ mol^{-1} after *ZPE* correction.

Comparison of the experimental and calculated rotational constants and a semi-experimental equilibrium structure

To compare the experimental and calculated rotational constants properly, the experimental rotational constants were corrected by the theoretical anharmonic vibrational contributions to obtain semi-experimental equilibrium constants.[45,46] Anharmonic calculations were carried out both at the B3LYP-D3(BJ)/def2-TZVP and def2-QZVP levels and similar corrections were obtained. Since the anharmonic corrections are not expected to change too much, for conciseness, we applied the anharmonic corrections at the def2-QZVP level for the following discussion. In Table 6.4, the experimental and semi-experimental equilibrium rotational constants are compared with the equilibrium rotational constants predicted for **PFP***G+g+*/*G-g-* at several levels of theory. The MP2/cc-pVTZ constants appear to give the best agreement with the semi-experimental equilibrium constants, while the PBE0-D3(BJ)/def2-TZVPD calculation gives the second best. The comparison in Table 6.4 also highlights some of the fortuitous cancellations in the DFT calculations. For example, the B3LYP equilibrium constants show good agreement with the experimental ground state rotational constants but the agreement gets much worse if one corrects for the anharmonic contribution.

The isotopic rotational constants of **PFP***G+g+*/*G-g-* were used to determine effective structural parameters using STRFIT and also the Kraitchman substitution coordinates. The results are summarized in Table S6.8-S6.10, SI. In addition, a fit of semi-experimental equilibrium structure (r_e^{SE}) parameters was carried out using STRFIT, starting with the MP2/cc-pVTZ structural parameters since those provide the best equilibrium rotational constants in comparison to the semi-experimental equilibrium ones. The r_e^{SE} result of **PFP***G+g+*/*G-g-* and a comparison to the effective and Kraitchman's results are summarized in Table S6.11-6.13, SI.

Table 6.4. Comparison of the experimental and semi-experimental equilibrium rotational constants (in MHz) with the equilibrium ones of **PFP***G+g+*/*G-g-* at several levels of theory.

Exp. and theoretical levels	A	B	C
Experimental[a]	2086.35307(32)	1522.27266(30)	1305.09346(30)
Semi-exp.-equilibrium[b]	2099.2391	1534.4976	1315.6848
MP2/cc-pVTZ	2088.2	1533.8	1314.5
PEB0-D3(BJ)/def2-TZVPD	2099.2	1520.1	1306.1
B3LYP-D3(BJ)/def2-QZVP	2073.6	1507.6	1293.5
B3LYP-D3(BJ)/def2-TZVP	2071.8	1510.6	1295.5

[a] The fitted experimental rotational constants from Table 6.2.

[b] Corrected for anharmonic contributions at the B3LYP-D3BJ/def2-QZVP level.

2. The PFP homodimer

Conformational searches

For the PFP homodimer, the CREST searches and the subsequent DFT calculations resulted in 78 conformers of the PFP homodimer which have no imaginary frequencies. The spectroscopic and energetic properties of these 78 binary PFP conformers are summarized in Table S6.13, SI. All the binary conformers feature an O-H···O intermolecular hydrogen bond. It is immediately obvious that the PFP homodimer exhibits an extremely rich structural diversity. Even within a fairly narrow relative energy window from 0 to 2 kJ mol^{-1}, there are 15 different predicted conformers. The related spectroscopic and energetic information of the 10 most stable binary conformers is given in Table 6.5 and the optimized geometries are depicted in Figure 6.4. Based solely on relative energy arguments and on experiments of other fluoroalcohol dimers observed before,[5,6] we should be able to detect transitions of all of these low energy conformers. Similar challenges were encountered in the recent rotational spectroscopic study of the cyclohexanol dimer[47] where the authors found many possible binary candidates in a narrow energy window and their predicted stability ordering varied depending on the levels of theory used, making it difficult to identify the carriers of the assigned sets of transitions.

To tackle the spectroscopic assignments, in particular the identification of the carriers, and to analyze the structure-energy relationship, it is important to have a systematic examination of composition of the binary conformers. Using the four pairs of monomeric

PFP enantiomers and one achiral PFP (see Table 6.1), one can build 16 homochiral and 16 heterochiral binary PFP complexes, in addition to 4 binary PFP conformers which contain the achiral **PFP***Tt* subunit, leading initially to 36 possible binary conformers. A further structural character to consider is that in each binary conformer, one subunit plays the role of the hydrogen bond donor, while the other one serves as the acceptor. This leads to 72 binary conformers just by considering the subunit composition alone. On the other hand, if the two subunits are the same in a homochiral binary conformer, such as **PFP***G+g+***PFP***G+g+,* or are of mirror images in a heterochiral binary conformer, such as **PFP***G+g+***PFP***G-g-,* switching the role of hydrogen bond donor versus acceptor results in the same binary conformer. Therefore, removing the 4 redundant homo- and 4 heterochiral conformers results in a total of 64 potential binary conformers, although some of them may not be a stable minimum. The more subtle fluorocarbon chain orientations introduce additional conformations.

For clarity, we name each binary conformer by its two subunits, such as **PFP***G+g+***PFP***Tg+*, starting with the hydrogen bond donor (**PFP***G+g+*) and then acceptor (**PFP***Tg+*). In addition, we consistently use the "+" enantiomer first in the hydrogen bond donor to avoid double counting or naming confusion. For example, **PFP***G-g-***PFP***Tg-* is mirror image to **PFP***G+g+***PFP***Tg+* and is not used in Table S6.18. Similarly, **PFP***G-g-***PFP***Tt* is mirror image to **PFP***G+g+***PFP***Tt* and is not listed. In a few cases where both donor and acceptor are the same, but the fluorocarbon chain orientations are different, we use additional numbers, such as _2 or _3, to indicate the higher energy binary conformers with the same composition, leading to a total of 78 conformers.

Rotational assignment of five binary PFP species

After removing all the assigned transitions of the PFP monomer and monohydrates,[48] five sets of rotational transitions were assigned and are attributed to the five lowest energy conformers of the PFP dimer based on good agreement between the experimental and theoretical rotational constants and the relative magnitudes of the electric dipole moment components. These are: **1 PFP***G+g+***PFP***Tg+*, **2 PFP***G+g+***PFP***G+g+*, **3 PFP***Tg+***PFP***Tg+,*

4 PFP*G+g+***PFP***G-g-,* and **5 PFP***G+g+***PFP***Tg-*. Their fitted spectroscopic parameters are summarized in Table 6.6.

All these five conformers have strong *a*-type transitions and we used the *a*-type transitions in the CP-FTMW spectrum to estimate a rotational temperature of ~ 1 K. These *a*-type transitions were also used to estimate the relative conformational abundances with the aid of the Pgopher software package. In Figure 6.5, the experimental line intensities are compared to the simulated line intensities of the five observed conformers using the experimental spectroscopic constants, the calculated *a*-type dipole moment components, a rotational temperature of 1 K and finally the estimated relative concentration of each conformer which is a feature implemented in Pgopher. The relative experimental abundances are **1** : **2** : **3** : **4** : **5** = 4.0 : 2.3 : 1.7 : 1.7 : 1.0.

A combined kinetic and thermodynamic model for the abundances of the binary species

If one assumes a purely thermodynamically controlled conformational distribution and uses a conformational temperature of ~40 K for hydrogen-bonded dimers,[49] the corresponding ratios are predicted at the B3LYP-(D3)BJ/def2-TZVP to be approximately 4.2 : 1.3 : 1.3 : 1.0 : 1.0, in reasonable agreement with the experimental estimated values. In a jet expansion, kinetically controlled processes are known to play a significant role in the formation of binary conformers.[50,51] We therefore also considered a different approach to estimate the abundances, which includes both kinetically and thermodynamically controlled processes. As discussed in the PFP monomer section, the barriers that separate different PFP conformers which have the same heavy atom frame but different OH orientations, are low and can be overcome in a jet expansion. Assuming the same is true in the formation of the binary PFP conformers and that the OH orientations can be easily optimized to maximize the intermolecular interaction energies, we can categorize the 78 binary conformers into three families according to the CCCO dihedral angle of the donor/acceptor PFP subunits: *GG* (including both homo- and heterochiral binary species), *GT/TG*, and *TT*. These three families have statistical weights of 38%, 47%, and 15%, based on the available abundances of monomeric *G* and *T* at the source temperature. Within each family, a thermodynamically controlled process is assumed with a conformational temperature of ~40 K. Such a combined approach gives the following abundance prediction for the first five binary conformers: 4.4 : 2.6 : 1.4 : 1.9 : 1.0, in better agreement with the experimental abundances than the purely thermodynamic model.

While the addition of Ar in the “Ar-test” experiments reduces the signal-to-noise ratios of the spectra of the binary PFP conformers overall, it was still possible to identify that only **5 PFP***G+g+***PFP***Tg-* experienced drastically more signal reduction. This appeared somewhat puzzling initially, since conformers **2-5** are very similar in energy (within 0.5 kJ mol^{-1}) (see Table 6.3). The observation can be understood using the proposed kinetic + thermodynamic model. The most stable *TT* conformer, **3 PFP***Tg+***PFP***Tg+*, survived the test because it is considered metastable and it does not cool to the lower energy conformers in other families. Of the two *GT* family conformers, **1 PFP***G+g+***PFP***Tg+* and **5 PFP***G+g+***PFP***Tg-*, the observed intensity of **5** reduced greatly while **1** remained with similar intensity. The reason is that **5** is about 0.5 kJ mol^{-1} less stable than **1**. Of the two *GG* family conformers, **2 PFP*G+g+*PFP*G+g+*** and **4 PFP*G+g+*PFP*G-g-*,** the cooling effect was not obvious because they are nearly iso-energetic (within 0.1 kJ mol^{-1}). Clearly, the purely thermodynamic model cannot explain the “Ar-test” results. The combined kinetic + thermodynamic model is particularly important in dealing with these conformers with very similar stability whose relative energy ranking may be (slightly) altered when calculated at a different level of theory.

Table 6.5. Energies, rotational constants, and dipole moment components of the ten most stable PFP homodimer conformations.[a]

Order[b]	Homodimers	ΔE_{raw}	ΔE_0	ΔE_b	*A*	*B*	*C*	$\lvert\mu_a\rvert$	$\lvert\mu_b\rvert$	$\lvert\mu_c\rvert$
I	**PFP**_G+g+_**PFP**_Tg+_	0.0	0.0	23.4	990.7	156.9	154.3	2.7	0.6	1.0
2	**PFP**_G+g+_**PFP**_G+g+_	0.7	0.4	22.8	848.5	171.1	167.2	2.0	1.1	0.3
3	**PFP**_Tg+_**PFP**_Tg+_	0.3	0.4	23.3	767.4	185.9	172.1	2.7	0.1	0.9
4	**PFP**_G+g+_**PFP**G-g-	1.1	0.5	22.6	793.7	191.5	184.0	2.4	1.6	0.1
5	**PFP**_G+g+_**PFP**_Tg-_	0.9	0.5	22.9	793.9	179.3	169.0	2.8	1.5	0.7
6	**PFP**_Tg+_**PFP**_G-g-_	1.0	0.6	22.8	679.3	229.4	202.9	2.6	1.2	0.3
7	**PFP**_Tg+_**PFP**_Tg-_	1.0	0.7	23.0	650.4	218.2	189.7	3.0	1.2	0.1
8	**PFP**_G+g+_**PFP**_Tg+__2	0.8	0.9	22.5	764.3	169.4	160.7	0.7	0.8	0.5
9	**PFP**_Tg+_**PFP**_G+g+_	1.3	0.9	22.5	724.2	187.1	180.5	2.1	0.6	0.6
10	**PFP**_G+g+_**PFP**_G+g+__2	0.9	1.0	22.2	834.6	161.4	155.5	0.6	1.0	0.3

[a] ΔE_{raw} is the relative electronic raw energy in kJ mol^{-1}; ΔE_0 is the relative energy including *ZPE* energy corrections in kJ mol^{-1}; ΔE_b is the estimated total binding energy and is calculated as: $-(\Delta E_{0(dimer)} - \Delta E_{0(monomer1)} - \Delta E_{0(monomer2)})$ in kJ mol^{-1} after *ZPE* and *BSSE* corrections; *A*, *B*, and *C* are the rotational constants in MHz; $|\mu_{a,b,c}|$ are the magnitudes of the electric dipole moment components in Debye predicted at the B3LYP- D3(BJ)/def2-QZVP level of theory.

[b] Energy ordering based on ΔE_0.

Table 6.6. Experimental spectroscopic parameters of the five experimentally observed PFP homodimers.

Parameter	**1 PFP**_G+g+_**PFP**_Tg+_	**2 PFP**_G+g+_**PFP**_G+g+_	**3 PFP**_Tg+_**PFP**_Tg+_	**4 PFP**_G+g+_**PFP**_G-g-_	**5 PFP**_G+g+_**PFP**_Tg-_
A /MHz	1004.085(42)[a]	856.092006(30)	762.75779(11)	793.383303(42)	792.34008(25)
B /MHz	156.688493(25)	170.1984584(95)	189.743434(11)	193.174419(19)	181.446954(58)
C /MHz	154.142180(25)	166.3157768(98)	174.955166(11)	185.243842(18)	170.539169(56)
D_J /kHz	0.0248568(97)	0.042520(14)	0.055729(14)	0.030442(24)	0.03392(10)
D_{JK} /kHz	-0.15978(17)	-0.11145(11)	-0.161511(59)	0.08306(11)	0.0371(17)
D_K /kHz	0.295388 (fixed)[b]	0.14697(81)	0.9639(74)	0.111792 (fixed)[b]	0.583032 (fixed)[b]
d_1 /kHz	-0.000545(22)	-0.001479(11)	-0.007274(14)	-0.001853(21)	-0.004626(76)
d_2 /kHz	0.001765(10)	0.0001211(44)	-0.0005790(71)	0.0006428(99)	0.000536(26)
N[c]	174	399	314	341	128
σ[d]	0.7	1.3	1.1	1.8	4.2

[a] The errors are given in the unit of the last digits.

[b] Centrifugal distortion constant values were fixed at the calculated values obtained from the harmonic frequency calculations.

[c] *N* is the number of transitions included in the fit.

[d] σ is the standard deviation of the fit.

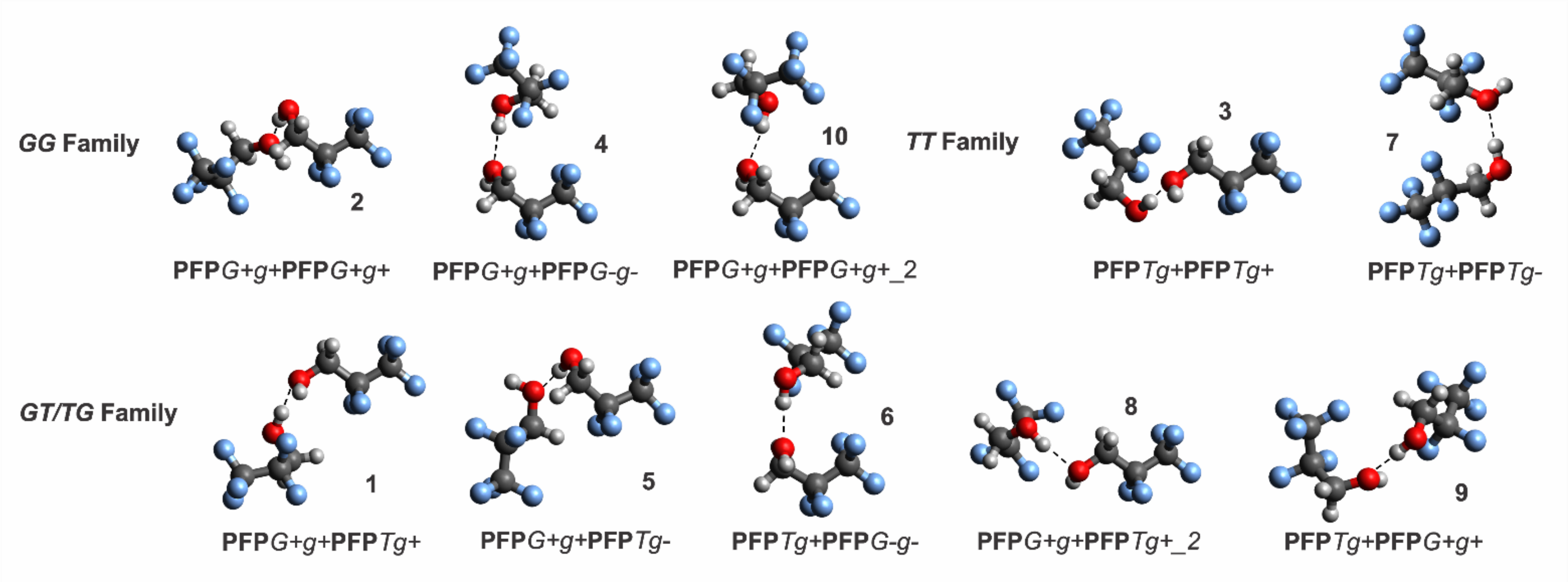

Figure 6.4. The ten most stable geometries of the **PFP** homodimer conformers optimized at the B3LYP-D3(BJ)/def2-QZVP level of theory. The relative stability ordering from **1** to **10** is also indicated in the figure. The conformers are grouped into three different conformational families based on the heavy atom framework of each subunit: *GG*, *GT*/*TG*, and *TT*. See the main text for discussion.

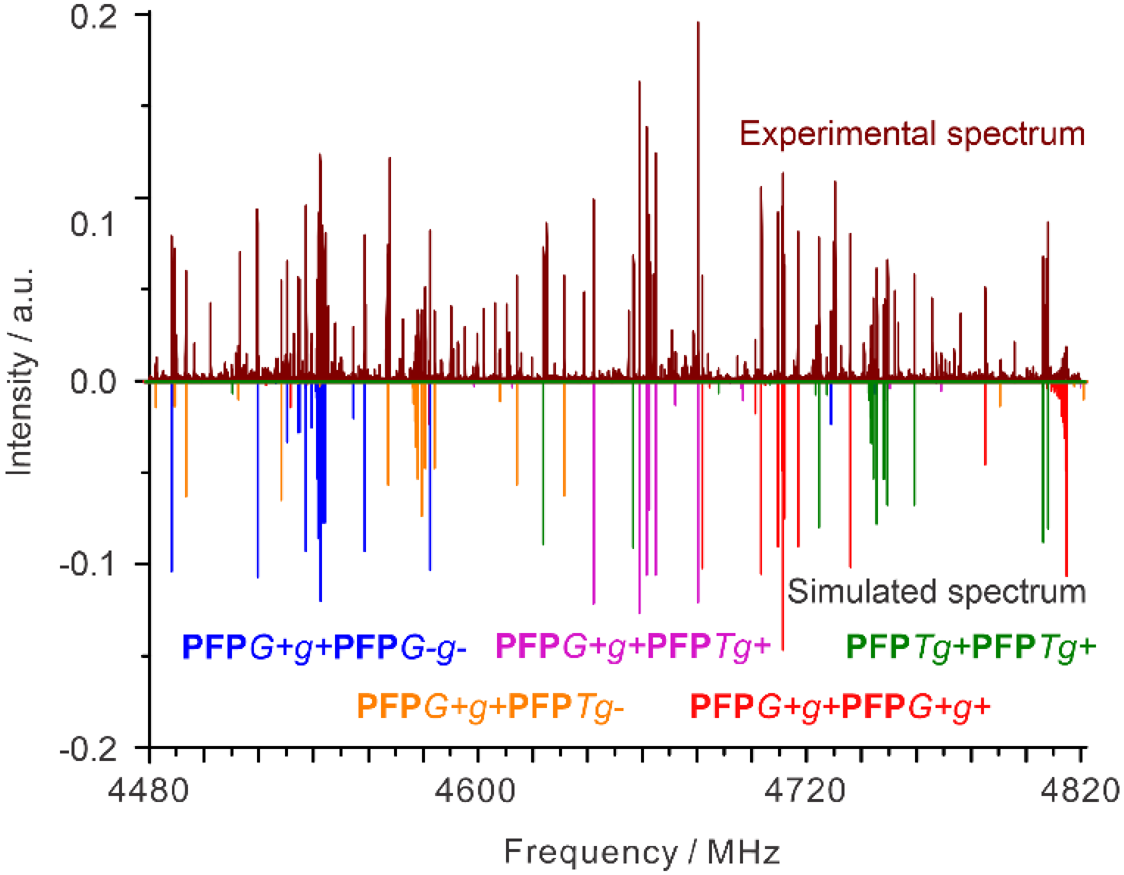

Figure 6.5. A section of the experimental PFP+Ne spectrum with transitions of five PFP homodimers, recorded with about 900 k free induction decays. The known transitions of the PFP monomeric conformers and its monohydrates (Ref 48) are removed for clarity. The experimental spectroscopic constants, the calculated electric dipole moment components and a rotational temperature of 1 K were used for the spectral simulations, as well as the concentration of each conformer. See the main text for discussions.

Non-covalent interactions and the effects of fluorination

In comparison to the PFP monomer, the non-fluorinated n-propanol (PrOH) monomer exists in five conformers, *G*+*t*/*G*-*t*, *G*+*g*+/*G*-*g*-, *G*+*g*-/*G*-*g*+, *Tt*, and *Tg*+/*Tg*- with a narrower energy window of about 0.6 kJ mol^{-1} from low to high energy.[52] In the same publication, the authors could only detect **PrOH***Gt* and **PrOH***Tt* under jet expansion conditions, confirming that *Gt* is the global minimum and *Tt* is more stable than *Tg*+/*Tg*-. The noticeably different distribution and stability ordering from the PFP monomeric conformers showcases the significant influence of fluorination. We further carried out QTAIM[29] and NCI[30] analyses for the five PFP and five PrOH monomeric conformers to evaluate and compare the strengths of different close molecular contacts. The results are summarized in Figure S6.4, SI. In the QTAIM analysis, only one intramolecular non-covalent interaction, i.e., the F···H-O contact in **PFP***G*+*g*-/*G*-*g*+, was identified, making it difficult to draw any conclusion about the stability of the PFP and PrOH conformers. The NCI analyses, on the other hand, identified multiple F···H-O and F···H-C weak attractive interactions. Some weak intramolecular F···F attractions were also spotted, similar to the situations reported previously in the HFIP_{g}-Ne/Ar cases[53] and in the TFE trimer.[8] A detailed analysis of the NCI results shows why the *g*-conformers of PFP are preferred over the *t*-conformers in both the *G* and *T* families: in all *g*-conformers of PFP, significant OH···F attractive interactions are present, whereas such attractive interactions are absent in all *t*-conformers of PFP. In fact, the *t*-conformers of PFP are unstable after *ZPE* correction (see Figure S6.3), and this likely comes from the repulsive interaction between the lone pair electrons of the O and F atoms. For PrOH, on the other hand, no such strong repulsion is present for the *t*-conformers. In addition, there is only a weak C-H···O attraction between the H atom of the CH_3 group and the hydroxyl O atom in the *G* family. These two factors lead to a much narrower energy window and preference for the *t*-conformers in PrOH.

Similar analyses were carried out for the five observed binary PFP conformers, with the results shown in Figure S6.5, SI. A recently reported formula was used to estimate the bond energies for all the non-covalent bond critical points identified.[54] In general, the O-H···O bond energies vary from 20.3 to 23.7 kJ mol^{-1}, while the O-H···F bond energies are about 7.7 to 8.1 kJ mol^{-1} and the weaker C-H···F bond range from 0.7 to 4.1 kJ mol^{-1}. The conformational distribution of binary PrOH conformers was analyzed for PrOH in solution based on the DFT calculations.[55] The study suggested that **PrOH***Tg*+**PrOH***G*+*g*- is the most favorable binary conformer at several different probe temperatures. It is interesting to note that this dimer is not made of the most stable monomeric subunits, likely because the energy gaps between the higher energy PrOH conformers and the global minimum are quite small, which can be easily compensated for by optimizing the intermolecular interactions.

Conclusions

The conformational landscapes of PFP and its hydrogen-bonded dimer have been investigated in considerable detail using rotational spectroscopy and theoretical calculations. The two most stable PFP monomeric conformers, **PFP***G+g+/G-g-* and **PFP***Tg+/Tg-*, were observed experimentally. Their relative experimental abundances could be satisfactorily explained by taking into account the conformational Boltzmann distribution at the source temperature and the subsequent conformational conversion in a jet expansion. A semi-experimental equilibrium structure was derived for **PFP***G+g+/G-g-* with the experimental isotopic data and theoretical anharmonic contributions, where the MP2 calculation provides the best agreement with the experiment. It is interesting to note that while the B3LYP calculations do not offer the best agreement with the semi-experimental equilibrium rotational constants, the fortuitous cancellation actually make the B3LYP rotational constants close to the effective ones obtained, greatly assisting the initial spectral assignment. The tunnelling splitting of **PFP***Tg+/Tg-* was analyzed and the corresponding tunnelling barrier was derived based on the experimental tunnelling splitting. The PFP dimer exhibits rich conformational diversity, and five binary PFP conformers were observed experimentally. A combined kinetic and thermodynamic model was developed to better explain the experimental abundances of these binary conformers. Among the PFP homodimers, the intermolecular interactions mainly consist of one O⋯H-O hydrogen-bonding interaction and several weaker F⋯H-C, F⋯H-O and F⋯F-C weak contacts, highlighting the importance of these weak interactions in determining the relative stabilities of the binary conformers.

References

1. Wencel-Delord, J.; Colobert, F., *Org. Chem. Front.*, **2016**, *3*, 394.
2. Godin, P. J.; Cabaj, A.; Xu, L.-H.; Le Bris, K.; Strong, K., *J. Quant. Spectrosc. Radiat. Transfer*, **2017**, *186*, 150-157.
3. Shahi, A.; Arunan, E., *J. Phys. Chem. A*, **2015**, *119*, 5650−5657.
4. Oswald, S.; Seifert, N. A.; Bohle, F.; Gawrilow, M.; Grimme, S.; Jäger, W.; Xu, Y.; Suhm, M. A., *Angew. Chem. Int. Ed.* **2019**, *58*, 5080-5084; *Angew. Chem.* **2019**, *131*, 5134-5138.
5. Thomas, J.; Xu, Y., *J. Phys. Chem. Lett.* **2014**, *5*, 1850−1855.
6. Liu, X.; Borho, N.; Xu, Y., *Chem. Eur. J.* **2009**, *15*, 270−277.
7. Scharge, T.; Häbery, T.; Suhm, M. A., *Phys. Chem. Chem. Phys.*, **2006**, *8*, 4664–4667.
8. Thomas, J.; Seifert, N. A.; Jäger, W.; Xu, Y., *Angew. Chem. Int. Ed.* **2017**, *56*, 6289-6293; *Angew. Chem.* **2017**, *129*, 6386-6390.
9. Thomas, J.; Liu, X.; Jäger, W.; Xu, Y., *Angew. Chem. Int. Ed.* **2015**, *54*, 11711-11715; *Angew. Chem.* **2015**, *127*, 11877-11881.
10. Scharge, T.; Cézard, C.; Zielke, P.; Schuütz, A.; Emmeluth, C.; Suhm, M. A., *Phys. Chem. Chem. Phys.*, **2007**, *9*, 4472–4490.
11. Seifert, N. A.; Thomas, J.; Jäger, W.; Xu, Y., *Phys. Chem. Chem. Phys.* **2018**, *20*, 27630-27637.
12. Badawi, H. M.; Förner, W., *Spectrochimi. Acta Part A: Mol. Biomol. Spectrosc.*, **2008**, *71*, 388-397.
13. Xu, L.-H.; Fraser, G. T.; Lovas, F. J.; Suenram, R. D.; Gillies, C. W.; Warner, H. E.; Gillies, J. Z.; *J. Chem. Phys.*, **1995**, *103*, 9541
14. Juanes, M.; Li, W.; Spada, L.; Evangelisti, L.; Lesarri, A.; Caminati, W., *Phys. Chem. Chem. Phys.*, **2019**, *21*, 3676
15. Xie, F.; Seifert, N. A.; Heger, M.; Thomas, J.; Jäger, W.; Xu, Y., *Phys. Chem. Chem. Phys.*, **2019**, *21*, 15408-15416.
16. Carlson, C. D.; Seifert, N. A.; Heger, M.; Xie, F.; Thomas, J.; Xu, Y., *J. Mol. Spectrosc.*, **2018**, *351*, 62-67.
17. Seifert, N. A.; Thomas, J.; Jäger, W.; Xu, Y., *Phys. Chem. Chem. Phys.*, **2018**, *20*, 27630-27637.
18. Pérez, C.; Lobsiger, S.; Seifert, N. A.; Zaleski, D. P.; Temelso, B.; Shields, G. C.; Kisiel, Z.; Pate, B. H., *Chem. Phys. Lett.*, **2013**, 571, 1-15.
19. Xu, Y.; Jäger, W., *J. Chem. Phys.*, **1997**, *107*, 4788-4706.
20. Grimme, S., *J. Chem. Theory. Comput.*, **2019**, *15*, 2847-2862.
21. Pracht, P.; Bohle, F.; Grimme, S., *Phys. Chem. Chem. Phys.*, **2020**, *22*, 7169-7192.
22. Xie, F.; Ng, X.; Seifert, N. A.; Thomas, J.; Jäger, W.; Xu, Y., *J. Chem. Phys.*, **2018**, *149*, 224306.
23. Xie, F.; Fusè, M.; Hazrah, A. S.; Jäger, W.; Barone, V.; Xu, Y., *Angew. Chem. Int. Ed.*, **2020**, *59*, 22427-22430; *Angew. Chem.*, **2020**, *132*, 22613-22626.

24. Frisch, M. J.; Trucks, G. W.; Schlegel, H. B.; et al., Gaussian 16. **2016**, *3*, 310. Full reference in Supporting Information.
25. Grimme, S.; Antony, J.; Ehrlich, S.; Krieg, H., *J. Chem. Phys.*, **2010**, *132*, 154104.
26. Grimme, S.; Ehrlich, S.; Goerigk, L., *J. Comput. Chem.*, **2011**, *32*, 1456-1465.
27. Weigend, F.; Ahlrichs, R., *Phys. Chem. Chem. Phys.*, **2005**, *7*, 3297-3305.
28. Berkessel, A.; Adrio, J. A.; Hüttenhain, D. J.; Neudörfl, M., *J. Am. Chem. Soc.* **2006**, *128*, 8421-8426
29. May, R. A.; Stevenson, K. J., Software review of Origin 8. ACS Publications: 2009.
30. Boys, S. F.; Bernardi, F., *Mol. Phys.*, **1970**, *19*, 553-566.
31. Kisiel, Z., PROSPE–Programs for rotational spectroscopy. In *Spectroscopy from Space*, Demaison, J.; Sarka, K.; Cohen, E. A., Eds., Kluwer Academic Publishers: Dordrecht, 2001, 91-106.
32. Hanwell, M. D.; Curtis, D. E.; Lonie, D. C.; Vandermeersch, T.; Zurek, E.; Hutchison, G. R., *J. Cheminf.*, **2012**, *4*, 17.
33. Bader, R.F.W., *Atoms in Molecules: A Quantum Theory*, Oxford University Press, New York, 1990.
34. Johnson, E. R.; Keinan, S.; Mori-Sánchez, P.; Contreras-García, J.; Cohen, A. J.; Yang, W., *J. Am. Chem. Soc.*, **2010**, *132*, 6498-6506.
35. Humphrey, W.; Dalke, A.; Schulten, K., *J. Mol. Graph.*, **1996**, *14*, 33-38.
36. Lu, T.; Chen, F., *J. Comput. Chem.*, **2012**, *33*, 580-592.
37. Western, C. M., *J. Quant. Spectrosc. Radiat. Transf.*, **2017**, *186*, 221-242.
38. Pickett, H. M., *J. Mol. Spectrosc.*, **1991**, *148*, 371-377.
39. Pickett, H. M., SPFIT/SPCAT Package, available at <http://spec.jpl.nasa.gov./>.
40. Watson, J. K. G., In *Vibrational Spectra and Structure*; J. R. During, Ed.; Elsevier: New York, **1977**, *6*, 1−89.
41. Thomas, J.; Xu, Y., *J. Chem. Phys.* **2014**, *140*, 234307/1-5.
42. Xu, Y.; Jäger, W., *J. Chem. Phys.*, **2000**, *113*, 514-524
43. Li, L. Y.; Seifert, N. A.; Xie, F.; Heger, M.; Xu, Y.; Jäger, W., *Phys. Chem. Chem. Phys.* **2018**, *20*, 21345-21351.
44. Medel, R., *Phys. Chem. Chem. Phys.*, **2021**, *23*, 17591-17605
45. Piccardo, M.; Penocchio, E.; Puzzarini, C.; Biczysko, M.; Barone, V., *J. Phys. Chem. A*, **2015**, *119*, 2058−2082
46. Vogt, N.; Demaison, J.; Rudolph, H. D.; Juanes, M.; Fernández, J.; Lesarri, A., *J. Chem. Phys*. **2018**, *148*, 064306
47. Juanes, M.; Usabiaga, I.; León, I.; Evangelisti, L.; Fernández, J. A.; Lesarri, A., *Angew. Chem. Int. Ed.*, *Angew. Chem. Int. Ed.* **2020**, *59* 14081-14085; *Angew. Chem.* **2020**, *132*, 14185-14189.
48. Wu, B.; Seifert, N. A.; Oswald, S.; Jäger, W.; Xu, Y., In International Symposium on Molecular Spectroscopy (Virtual): WA09, **2021**, June 21-25.
49. Borho, N.; Xu, Y., *Phys. Chem. Chem. Phys.* **2007**, *9*, 4514–4520.
50. Macario, A.; Blanco, S.; Thomas, J.; Xu, Y.; López, J. C., *J. Phys. Chem. A,* **2019**, *123*, 6772-6780.

51. Xie, F.; Seifert, N. A.; Jäger, W.; Xu, Y., *Angew. Chem. Int. Ed*. **2020**, *59*, 15703-15710; *Angew. Chem*. **2020**, *132*,15833-15840.

52. Kisiel, Z.; Dorosh, O.; Maeda, A.; Medvedev, I. R.; De Lucia, F. C.; Herbst, E. B.; Drouin, J.; Pearson, J. C.; Shipman, S. T., *Phys. Chem. Chem. Phys.*, **2010**, *12*, 8329-8339.

53. Wu, B.; Seifert, N. A.; Oswald, S.; Jäger, W.; Xu, Y., *J. Phys. Chem. A*, 2021, 125, 5355−5364.

54. Emamian, S.; Lu, T.; Kruse, H.; Emamian, H.; *J. Comput. Chem*. **2019**, *40*, 2868–2881

55. Doroshenko, I.; Vaskivskyi, Y.; Chernolevska, Y.; Meyliev, L.; Kuyliev, B., *Ukr. J. Phys.*, **2020**, *65*, 291-291.

Chapter 7

Rotational Spectroscopy of the 2,2,3,3,3-Pentafluoropropanol···Water Complex: Conformations and Large Amplitude Motions[1]

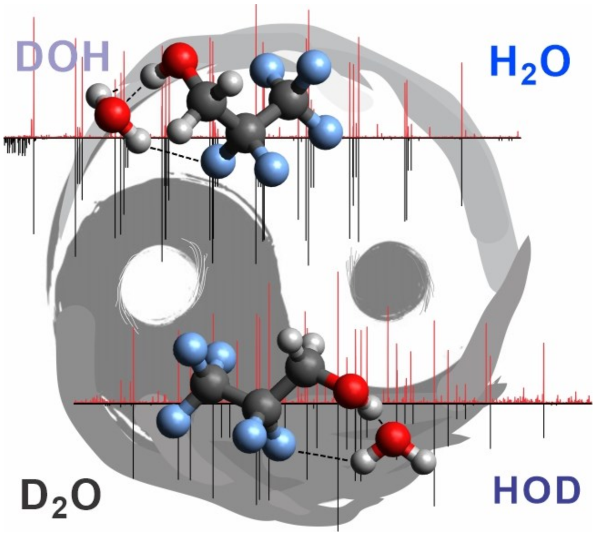

---

[1] This study is the draft submitted to *Phys.Chem.Phys.* as B. Wu, N. A. Seifert, S. Oswald, W. Jäger, Y. Xu, "Rotational Spectroscopy of the 2,2,3,3,3-Pentafluoropropanol··· Water Complex: Conformations and Large Amplitude Motions".

Abstract

2,2,3,3,3-pentafluoropropanol (PFP) can exist in five conformations defined by the CCCO and CCOH dihedral angles: four mirror-imaged pairs (*G+g+*/*G-g-*, *G+g-*/*G-g+*, *G+t*/*G-t*, *Tg+*/*Tg-*) and an achiral *Tt* form. In this study, we examined the conformational landscape of the PFP···water complex using chirped pulsed Fourier transform microwave spectroscopy and theoretical calculations. Rotational spectra of two PFP···water conformers, **PFP***G+g+*···W_H and **PFP***Tg+*···W_H, and seven deuterated isotopologues of each, were assigned. The tunneling splittings were observed for both conformers and were attributed to the exchange of the bonded and non-bonded hydrogen atoms of water. On the other hand, the tunneling splitting associated with the OH flipping motion in **PFP***Tg+/Tg-* appeared to be quenched upon hydrogen bonding with water. The large amplitude motions associated with the water subunits were examined in detail to explain the very different magnitudes of the experimental and theoretical permanent electric dipole moment components. The study highlights the challenge in correctly identify the conformers observed when large amplitude motions are involved. The quantum theory of atoms and molecules (QTAIM) and non-covalent interaction (NCI) analyses, as well as the electrostatic potential (ESP) calculations were also carried out to explore the nature of the non-covalent interactions and to appreciate the effects of fluorination on such interactions.

Introduction

2,2,3,3,3-pentafluoropropanol (PFP) is an important solvent for organic syntheses.[1] It is also considered to be greenhouse gas pollutant because it is radiatively active in the mid-infrared region.[2] Moreover, PFP + water mixture can be employed as a biodegradable firefighting foam.[3] For these reasons, understanding the non-covalent interactions between PFP and water in the gas phase at the molecular level is desirable. Such knowledge maybe helpful for developing more realistic estimate of the greenhouse effect because of the abundance of water in the atmosphere or improving the practical applications of the PFP + water mixture.

Jet-cooled rotational spectroscopy is highly sensitive to minor structural changes and can provide insight into structural-energetic relationship of the non-covalently bonded clusters.[4] In recent years, we have focused our attention on a series of fluoroalcohol containing hydrogen-bonded complexes, such as self-aggregates of monofluoroethanol (MFE),[5] trifluoroethanol (TFE),[6] and 1,1,1,3,3,3-Hexafluoro-2-propanol (HFIP).[7] One intriguing observation with these short chain fluoroalcohols is that the preferred conformation may alter greatly as the fluoroalcohol molecule aggregates. For example, in the cases of $(HFIP)_3$[8] and $(MFE)_4$,[5a] the ternary and quaternary conformers observed consist of exclusively the less stable monomeric conformations. Or in the case of $(TFE)_3$,[6b] the observed ternary conformers consist 30% *trans*-TFE which is unstable in its isolated form. The latter observation allows one to appreciate how *trans*-TFE becomes stabilized when going from the unstable monomer, i.e., 0%, to the liquid phase with 40% abundance.[9] More directly linked to the current study are the rotational spectroscopic investigations of MFE···water,[10] TFE···water,[11] and HFIP···water.[12] While the effects on hydrogen-bonding interaction on the conformational distributions of the fluoroalcohol molecules were less severe in the monohydrates than in their larger aggregates, it was possible to detect the less stable *gauche*-HFIP conformation in its monohydrate.[12b] In comparison to these short chain fluoroalcohols[7,13] which show only conformations associated with the OH pointing direction, PFP also exhibits interesting conformations related to the heavy atom frame.[14] It would be interesting to see how the conformational distribution of PFP varies with non-covalent interaction with water. Another point of interest is to investigate the possible large amplitude motions in the PFP monohydrate, for example, that associated with the OH tunneling motion in the PFP monomer.

In the current study, we applied chirped pulse Fourier transform microwave spectroscopy and *ab initio* calculations to characterize the hydrogen bonding interactions between PFP with water. Rotational spectra of two PFP⋯water conformers were assigned including their mono, di, and tri-deuterated species. The large amplitude motions associated with the water subunit led to tunneling splittings and other noticeable deviation from the equilibrium properties predicted. These phenomena were analyzed in detail.

Results and Discussion

1. Conformational searches and spectral assignments

The PFP monomer conformations are described by three dihedral angles (FCCC, CCCO and CCOH) which can display as the *trans* (~180°) or *gauche* (~±60°) forms.[14] Since the FCCC dihedral angle can take on only a *trans* (~180°) conformation for stable conformers, we name the PFP configuration using only two letters: the first upper-case (*G± or T*) describes the CCCO heavy atom frame, and the second lower-case (*g± or t*) indicates the OH pointing direction. The PFP monomer may take on five conformations with four pairs of mirror-images (*G+g+*/*G-g-*, *G+g-*/*G-g+*, *G+t*/*G-t*, and *Tg+*/*Tg-*) and an achiral *Tt*. Since the mirror-imaged pairs give the same rotational spectrum in the study of monohydrate, we will use just the first half of the notation for simplicity. For the monohydrate conformers, we also indicate the main contact site of PFP to water, using a similar scheme as for the HFIP⋯rare gas or water.[12b, 15] For example, **PFP***Tg+*⋯W_H indicates a PFP subunit with the CCCO at 180° (*T*) and the CCOH at +60° (*g+*), that water is hydrogen-bonded to the hydroxyl H of PFP. The subscript letter at W indicates that water binds to PFP at the acidic OH proton (H), the alcohol oxygen (O), the alkyl CH proton (C), and the CF_3 groups (F).

The conformer-rotamer ensemble sampling tool (CREST),[16] a powerful tool with quantum chemistry code developed by Grimme and co-workers, was employed for a comprehensive search of the possible PFP⋯W structural candidates. The subsequent DFT geometry optimization and harmonic frequency calculations produced 15 PFP⋯W conformers. The spectroscopic properties of the three most stable PFP⋯W conformers which contain **PFP***G+g+*, **PFP***Tg+* and **PFP***G+g-* are summarized in Table 7.1 and their geometries are shown in Figure 7.1. The 12 other conformers which contain the less stable **PFP***G+t* and **PFP***Tt* subunits, as well as structures where water serves as the hydrogen bond donor, are predicted to be at least 10 kJ mol^{-1} higher in energy than the first three. The coordinates of the three most stable conformers are given in Table S7.1-S3, Supporting Information (SI), while their spectroscopic and energetic properties are given in Table S7.4 and the conformational geometries of all 15 PFP⋯W conformers are depicted in Figure S7.1, SI.

Since these conformers all have strong *a*-type transitions, it was relatively straightforward to identify their spectral patterns. Only two most stable conformers, **PFP***G+g+*⋯W$_H$ and **PFP***Tg+*⋯W$_H$ were identified. Several attempts to identify **PFP***G+g-*⋯W$_H$ which is about 2.7 kJmol^{-1} higher in energy than the global minimum **PFP***G+g+*⋯W$_H$, were not successful. Some observed lines of **PFP***G+g+*⋯W$_H$ show apparent splitting doublets with ~3:1 intensity ratio, while others only give unresolved, asymmetric line shapes. Similar splittings were observed for **PFP***Tg+*⋯W$_H$. While in the **PFP***Tg+*/*Tg-*monomer, tunneling splittings associated with *Tg+* and *Tg-*, i.e., the OH flipping, were observed and analyze,[14] the current splittings were eventually attributed to the interchange of the bonded and non-bonded H atom of water (See section B). Some example spectra of the two assigned conformers are shown in Figure S7.2, SI, while some examples of tunneling splittings are depicted in Figure S7.3, SI.

Table 7.1. Relative raw (ΔE_e) and *ZPE* corrected (ΔE_0) energies and *ZPE* and *BSSE* corrected binding energy (ΔE_b) (in kJ mol^{-1}), rotational constants (in MHz), and electric dipole moment components (in Debye) of the three most stable PFP···W conformers at the B3LYP-D3(BJ)/def2-QZVP level of theory.

Conf.	ΔE_e	ΔE_0	ΔE_b	A	B	C	$\lvert\mu_a\rvert$	$\lvert\mu_b\rvert$	$\lvert\mu_c\rvert$
G+*g*+···W$_H$	0.0	0.0	24.9	1730.5	874.4	846.7	2.3	0.0	1.2
Tg+···W$_H$	0.8	0.8	24.4	1953.9	789.5	738.7	2.1	1.7	0.1
G+*g*-···W$_H$	3.0	2.7	24.9	1525.6	1075.7	831.5	3.3	1.3	0.6

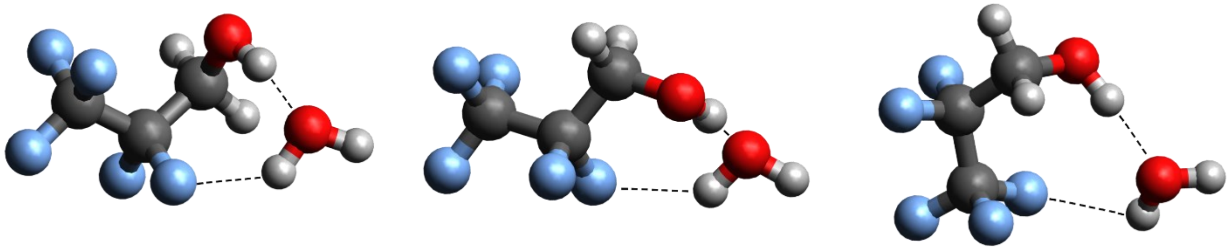

PFP*G*+*g*+···W$_H$ **PFP***Tg*+···W$_H$ **PFP***G*+*g*-···W$_H$

Figure 7.1. Optimized geometries of the three most stable isomers of the PFP···W conformers at the B3LYP-D3(BJ)/def2-QZVP level of theory. The close intermolecular contacts between H_2O and PFP are indicated with dashed lines.

To fit the experimental rotational transitions, the Watson's semi-rigid rotor Hamiltonian in the *S*-reduction and I^r representation[17] was used. The *ortho* and *para* spin species associated with the tunneling splittings were fitted separately, using the Pgopher[18] program. The experimental spectroscopic constants are listed in Table 7.2. We note that for **PFP***G*+*g*+···W$_H$, only very few lines show well resolved lines which were included in the fit of the *para* species, while most transitions exhibit unresolved, asymmetric line shapes. As a result, we had to fix the centrifugal distortion constants at the values of the *ortho* species (see Table 7.2). For **PFP***Tg*+···W$_H$, more transitions exhibit resolved splitting than **PFP***G*+*g*+···W$_H$, making it possible to fit the centrifugal distortion constants of the *para* species. The associated experimental transition frequencies of these two conformers are listed in Table S7.5-S7.8, SI.

Table 7.2. Experimental spectroscopic parameters of the *ortho* and *para* **PFP***G*+*g*+⋯W_H and **PFP***Tg*+⋯W_H.

Para.	**PFP***G*+*g*+(OH)⋯W_H		**PFP***Tg*+(OH)⋯W_H	
	ortho	*para*	*ortho*	*Para*
A [a]	1779.59208(15)	1779.5588(13)	1929.00680(24)	1929.0463(13)
B [a]	857.831515(74)	857.82237(78)	798.436174(81)	798.42382(92)
C [a]	829.818924(67)	829.8255(10)	741.438801(81)	741.42525 (94)
D_J [a]	0.48953(65)	fixed [d]	0.3382(10)	0.314(16)
D_{JK} [a]	-0.8202(27)	fixed [d]	-1.1239(29)	-1.116(11)
D_K [a]	3.1741(70)	fixed [d]	3.042(21)	3.205(75)
d_1 [a]	0.00742(59)	fixed [d]	-0.06572(39)	-0.0678(37)
d_2 [a]	0.00545(22)	fixed [d]	0.007846(97)	0.00874(85)
N [b]	104	9	87	28
σ [c]	1.0	5.1	1.1	3.8

[a] Rotational constants in MHz and quartic centrifugal distortion constants in kHz.
[b] Number of transitions included in the fit. [c] Standard deviation of the fit in kHz.
[d] Centrifugal distortion constants were fixed at those of the *ortho* species.

Further CP-FTMW experiments were carried out with a mixture of PFP+D_2O. Figure 7.2 shows **PFP***G*+*g*+⋯W_H and **PFP***Tg*+⋯W_H in their principal inertial axis systems with the atom numbering. After removing transitions belonging to the PFP monomer and dimer,[14] and the two newly assigned PFP⋯W parent species, seven **PFP***G*+*g*+⋯W_H and seven **PFP***Tg*+⋯W_H deuterated isotopologues were assigned by employing the autofit program[19] and by using the variations of the principal moments of inertia described in Section C. The simulations with the calculated deuterium nuclear quadrupole coupling constants indicate that the nuclear quadrupole coupling hyperfine structures are generally quite narrow in the *a*-type transitions but slightly more spread-out in the *b*-type transitions. In the experimental spectra, most splittings are not well resolved. Because of the complication associated with the D nuclear hyperfine structures, very few *para*-H_2O tunneling splittings could be tentatively identified in **PFP***G*+*g*+(OD)···H_2O and **PFP***Tg*+(OD)···H_2O and no tunneling splitting could be identified in the D_2O containing species. Therefore the water tunneling splittings were not analyzed in these deuterated isotopologues. The same semi-rigid rotor spectroscopic fitting procedure was used and the resulting spectroscopic constants are summarized in Table 7.3 and 7.4, and the transition frequencies are listed in Table S7.9-7.15 and S7.16-S7.22, SI, for the seven **PFP***G*+*g*+···W_H and seven **PFP***Tg*+···W_H deuterated isotopologues, respectively. An example broadband spectral section of **PFP***G*+*g*+···W_H and its deuterated species is depicted in Figure 7.3, while that of **PFP***Tg*+···W_H is provided in Figure S7.4, SI. The estimated population abundances of each species are also provided. "OD" in **PFP***G*+*g*+(OD)-HOD4 indicates the deuterated alcoholic hydroxyl group of the PFP subunit and "HOD4" stands for the mono-deuterated water where H4 is replaced deuterium. Attempts to measure the ^{13}C isotopologues of **PFP***G*+*g*+···W_H and **PFP***Tg*+···W_H using a cavity FTMW spectrometer[20] were not successful.

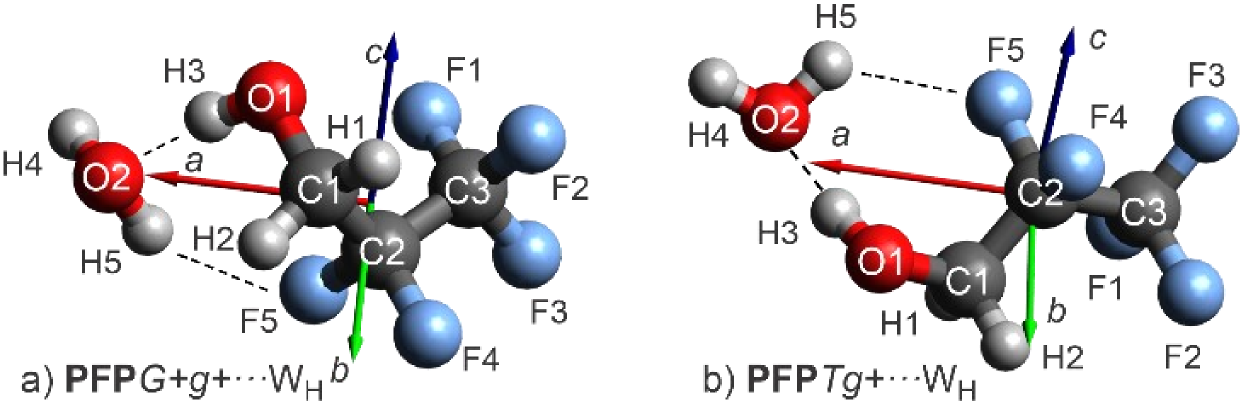

Figure 7.2. The two experimentally observed **PFP***G*+*g*+···W_H and **PFP***Tg*+···W_H in their corresponding principal inertial axis systems. The atomic numbering is also provided.

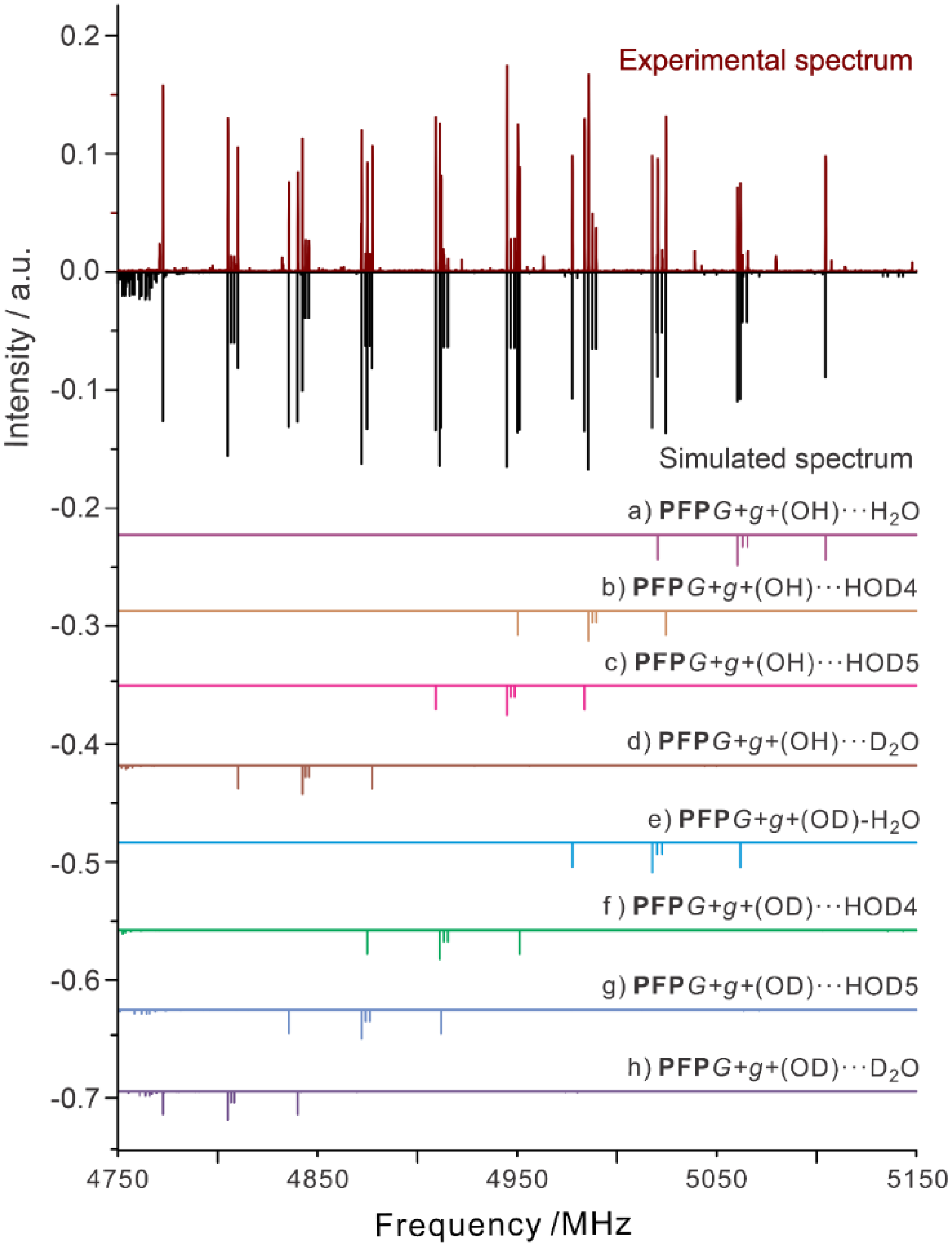

Figure 7.3. Top: the experimental **PFP***G*+*g*+···W_H spectrum and the overall simulated spectrum of all isotopologues. Bottom: the simulated individual spectrum of a) **PFP***G*+*g*+(OH)···H_2O parent 10%, b) **PFP***G*+*g*+(OH)···HOD4 12%, c) **PFP***G*+*g*+(OH)···HOD5 10%, d) **PFP***G*+*g*+(OH)···D_2O 16%, e) **PFP***G*+*g*+(OD)···H_2O 16%, f) **PFP***G*+*g*+(OD)···HOD4 10% and g) **PFP***G*+*g*+(OD)···HOD5 12%, h) **PFP***G*+*g*+(OD)···D_2O 14%. The estimated experimental percentage abundances are also indicated.

To assign the deuterated **PFP***G*+*g*+···W_H and **PFP***Tg*+···W_H species correctly, the experimental and theoretical values of the changes of the principal moments of inertia ($\Delta I_{a,b,c}$) from the parent species are compared in Table S7.5 and S7.6, SI. Since the water subunit undergoes large amplitude motions, such changes in the experiment can be difficult to capture reliably with the theoretical equilibrium predictions. The changes of the principal moments of inertia between the pair of **PFP***G*+*g*+(OH)···H_2O and **PFP***G*+*g*+(OD)···H_2O, **PFP***G*+*g*+(OH)···HOD4 and **PFP***G*+*g*+(OD)···HOD4, **PFP***G*+*g*+(OH)···HOD5 and **PFP***G*+*g*+(OD)···HOD5, and **PFP***G*+*g*+(OH)···D_2O and **PFP***G*+*g*+(OD)···D_2O are also compared in Table S7.5 and S7.6. These pairs were selected to minimize the effects of large amplitude motions of the water subunit, making it sensible to compare the theoretical and experimental principal moment of inertia changes for assigning the correct isotopologue.

Table 7.3. Experimental spectroscopic constants of **PFP***G*+*g*+ and its D isotopologues.[a]

Para.	**PFP***G*+*g*+(OH)			**PFP***G*+*g*+(OD)			
	HOD5	HOD4	D_2O	H_2O	HOD5	HOD4	D_2O
A	1767.90902(53)	1769.33719(53)	1761.94(19)	1774.8853(12)	1761.1212(13)	1765.2513(12)	1754.26360(32)
B	843.67884(16)	831.63443(16)	818.59815(23)	850.71978(19)	836.92878(28)	825.07674(37)	812.37083(18)
C	818.91815(15)	806.17643(11)	796.12088(23)	822.68913(17)	812.05566(24)	799.66254(32)	789.85967(18)
D_J	0.4657(18)	0.3785(22)	0.4846(32)	0.4353(14)	0.4725(34)	0.3332(62)	0.4564(25)
D_{JK}	-0.823(11)	-0.713(15)	-0.822(12)	-0.838 (fixed) [d]	-0.845(22)	-0.767 (fixed) [d]	-0.769 (fixed) [d]
D_K	3.137 (fixed) [d]	3.144 (fixed) [d]	3.093 (fixed) [d]	3.192 (fixed) [d]	2.79(12)	3.144 (fixed) [d]	3.112 (fixed) [d]
d_1	0.00796 (fixed) [d]	0.00724 (fixed) [d]	0.00698 (fixed) [d]	0.0098(19)	0.00661 (fixed) [d]	0.00724 (fixed) [d]	0.00673 (fixed) [d]
d_2	0.00669 (fixed) [d]	0.00553 (fixed) [d]	0.00638 (fixed) [d]	0.0041(14)	0.00769 (fixed) [d]	0.00553 (fixed) [d]	0.00631 (fixed) [d]
N [b]	33	23	25	21	40	22	38
σ [c]	1.5	1.3	2.0	0.7	2.4	2.2	2.2

Table 7.4. Experimental spectroscopic constants of **PFP***Tg*+···$\mathrm{W_H}$ and its D isotopologues.[a]

Para.	**PFP***Tg*+(OH)			**PFP***Tg*+(OD)			
	HOD5	HOD4	D_2O	H_2O	HOD5	HOD4	D_2O
A	1906.48061(63)	1914.6915(14)	1894.02578(42)	1927.06267(95)	1904.27250(36)	1912.5507(11)	1891.6444(10)
B	789.50918(35)	776.76865(54)	768.11063(25)	789.51564(39)	780.86080(18)	768.48934(56)	760.07321(69)
C	731.14049(33)	720.73723(52)	711.05101(21)	733.66826(38)	723.60553(19)	713.49350(56)	704.02395(53)
D_J	0.248(10)	0.269(13)	0.2680(40)	0.3082(100)	0.3096(37)	0.2786(83)	0.288(10)
D_{JK}	-1.058(19)	-1.164(74)	-0.964(14)	-1.159(28)	-1.1121(91)	-1.231(27)	-1.051(41)
D_K	2.882(62)	2.75(18)	2.820(54)	3.00(11)	3.073(49)	3.546(92)	3.129 (fixed)[d]
d_1	-0.0691 (fixed)[d]	-0.0675 (fixed)[d]	-0.0259(33)	-0.06268 (fixed)[d]	-0.0505(20)	-0.0927(85)	-0.0997(85)
d_2	0.00778 (fixed)[d]	0.00749 (fixed)[d]	0.00737 (fixed)[d]	0.007528 (fixed)[d]	0.00932(61)	0.007182 (fixed)[d]	0.007080 (fixed)[d]
N [b]	42	35	40	39	46	39	34
σ [c]	3.3	5.2	1.4	3.4	1.6	3.5	1.9

[a] The rotational constants are in MHz and the centrifugal distortion constants are in kHz.
[b] Number of transitions included in the fit.
[c] Standard deviation of the fit in kHz.
[d] Centrifugal distortion constant values were fixed at the calculated values obtained from the harmonic frequency calculations, scaled by the experiment/theory ratio of the parent species.

2. Large amplitude motions of the PFP···$\mathrm{W_H}$ conformers

To understand the origin of the water tunneling patterns observed, we carried out a similar 2D rigid scan as in $\mathrm{HFIP_g}$···$\mathrm{W_H}$,[12b] along the two water-centered motions. One of them is related to the rotation of water about the intermolecular hydrogen bond, i.e., along φ_1 = O1-H3-O2-H4, and the other associated with the flapping of the free water OH, i.e., along φ_2 = H4-O2-H5-F3. The two water motions and the resulting 2D PES for **PFP***G*+*g*+···$\mathrm{W_H}$ are presented in Figure S7.5, SI, together with the rigid 1D cuts along φ1 and φ2. The same for **PFP***Tg*+···$\mathrm{W_H}$ are in Figure S7.6, SI. The rigid 1D cuts along φ_2 for **PFP***G*+*g*+···$\mathrm{W_H}$ (Figure S7.5) and **PFP***Tg*+···$\mathrm{W_H}$ (Figure S7.6) correspond roughly to the flapping or wagging or flapping motion of water and already suggest a very low barrier which becomes barrierless after the consideration of *ZPE*. The rigid 1D cuts along φ_1, on the other hand, have a much higher barrier, indicating that it is necessary to include structural relaxation to properly account for the tunneling observed.

Following the examples of HFIP$_t$···W$_H$[12a] and HFIP$_g$···W$_H$,[12b] 1D relaxed scans along the dihedral angle H5-O2-C1-C2 were carried out for **PFP***G*+*g*+···W$_H$ and **PFP***Tg*+···W$_H$ with a step size of 5° to investigate the water tunneling motion. The resulting PESs of **PFP***G*+*g*+···W$_H$ and **PFP***Tg*+···W$_H$ are depicted in Figure 7.4 and Figure S7.7, respectively, showing quite similar PES shapes and barrier heights for both conformers. Interestingly, the 1D relaxed scans indicate that two distinct water motions are involved in completing the water tunneling event, very similar to those motions shown in Figure S7.5 and S7.6. First, water rotates about the intermolecular hydrogen bond where the weak contact between H5···F5 starts to break at (a), continues its rotation to the transition state (b) where the two water H atoms are roughly equal distance to the hydroxyl O of PFP, and eventually arrives at point (c) where the original intermolecular H5···F5 contact is now replaced by the H4···F5 contact. Second, with the H4···F5 contact remaining in intact, the free OH5 flaps up over a minor barrier to recover the original geometry. Please note that this minor barrier is actually barrierless after the *ZPE* correction as mentioned above. Interestingly, the kink in the PESs signals the change in the nature of the water motion from rotating about the intermolecular binding axis to a large amplitude motion of the free water OH group. The PFP···W$_H$ transitional states at (b) of each relax scan PES give a single imaginary frequency of -93 cm^{-1} and -108 cm^{-1} for **PFP***G*+*g*+···W$_H$ and **PFP***Tg*+···W$_H$, respectively, based on the transition state calculations. These are similar to -109 cm^{-1} for HFIP$_g$···W$_H$ and -104 cm^{-1} for TFE···water, calculated at the same level of theory in the current study. Based on the transitional state calculations, a barrier height of ~2.5 or 3.2 kJ mol^{-1} to **PFP***G*+*g*+···W$_H$ and of ~2.8 or 3.6 kJ mol^{-1} for **PFP***Tg*+···W$_H$ was estimated, respectively, with or without *ZPE* and *BSSE* corrections.

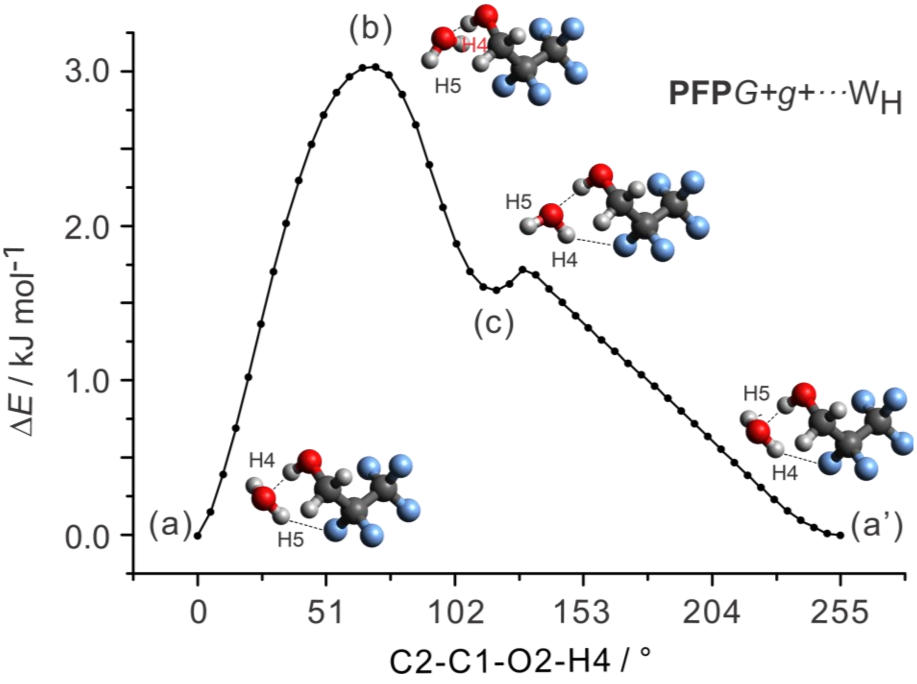

Figure 7.4. The relaxed 1D PES scan along the dihedral angle of C2-C1-O2-H4 (see Figure 7.2 for atom numbering) for **PFP***G*+*g*+···$\mathrm{W_H}$. (a) and (a′) are the equivalent minimum energy geometries. See the text for discussions.

One interesting, yet initially puzzling observation is that the experimental *b*- and *c*-type transitions of **PFP***G*+*g*+···$\mathrm{W_H}$ show similar intensity (Figure S7.8, SI), drastically different from the calculated ones based on μ_b = 0.0 D << μ_c = 1.2 D. To reproduce the experimental intensity pattern, one needs to change μ_b and μ_c to about 0.5 D relative to μ_a = 2.3 D. To gain insight into such large deviation, we calculated the dipole moment components at each geometry along the free OH large amplitude motion as shown in Figure 7.4 from c) to a'). The dipole moment component values at every 10° are summarized in Table S7.23, SI. The current situation is much more complicated than that of $\mathrm{HFIP}_t\cdots\mathrm{W_H}$[12a] where the barrierless, free OH flapping motion moves back and forth through a symmetry plane perpendicular to the *c*-axis, leading to an zero μ_c. For **PFP***G*+*g*+···$\mathrm{W_H}$, both μ_b and μ_c change drastically as the free OH flaps from down (at c)) to up (at a')) from about 2.2 D to 0.0 D and from -0.4 D to -1.2 D, respectively, while the percentage change in μ_a is much less dramatic. Form Table S7.23, one can appreciate how the averaged μ_b and μ_c dipole moments become about 0.5 D, as estimated experimentally, and much different from their equilibrium values of 0.0 D and 1.2 D (Table 7.1), respectively. The exact averaging depends on the associated wavefunctions (which are not currently available).

Similarly, for **PFP***Tg*+⋯W_H, the *c*-type transitions are much stronger than those predicted with μ_c = 0.1 D, while *a*- and *b*-types are roughly in agreement with the prediction. Rather its μ_c should be about 0.6 D to reproduce the relative intensity observed. The analogous, calculated dipole moment component values for **PFP***Tg*+⋯W_H are summarized in Table S7.24, SI, where μ_c change from -1.9 to -0.1 D, while μ_a and μ_b experience less dramatic percentage variations, consistent with the trend observed experimentally.

The above analyses highlight the challenge in identifying the correct conformer responsible for the assigned transitions when large amplitude motions are involved. Since the variation in the free water OH orientation typically does not bring about any significant change in the associated rotational constants, the relative magnitudes of the electric dipole moment components are usually used as a guard against mis-identification of the corresponding conformer. In this current study, the application of the second proof becomes more complicated because of the effects of the large amplitude motions. Actually, in the current study, we missed the global minimum structure initially even though the spectral assignment could still be moved forward with the erroneous geometry which turned out to be the structure corresponds to (c) in Figure 7.4. The study also showcases the power of the high resolution spectroscopy in differentiating these subtle differences, facilitating our understanding the effects of large amplitude motions.

3. Substitution parameters

Kraitchman's substitution coordinates of the deuterated **PFP***G*+*g*+⋯W_H and **PFP***Tg*+⋯W_H species were calculated using **PFP***G*+*g*+(OH)⋯H_2O and **PFP***G*+*g*+(OD)⋯D_2O as the parent species of the former, the **PFP***Tg*+ (OH)⋯H_2O and **PFP***Tg*+(OD)⋯D_2O being as the parents for the latter. The resulting substitutional coordinates, together with the theoretical equilibrium coordinates of the parent species of the two monohydrate species are summarized in Tables S7.25 and S7.26, SI, respectively.

The substitution coordinates obtained for these hydrogen atoms differ considerably from the equilibrium ones, especially for the free water H4 (D4). This is not surprising based on the large amplitude motion analyses in Section B. Indeed, such large amplitude motions also made it more difficult to assign the rotational spectra of various D-isotopologues based directly on the comparison of the calculated and experimental rotational constants. Rather, the changes in the principal moment of inertia moments upon substitution between the experiment and theory serves as a better discriminator. In some cases, it was even necessary to consider the substitution pairs such as OD···D_2O and OH···D_2O, OD···HOD5 and OH···HOD5, and OD···HOD4 and OH···HOD4 and compare the ΔI values between experiment and theory to finally confirm the identity of isotopologues, since such comparisons further reduce the influence of large amplitude motions by using the same water subunit isotopologue.

In the relative percentage abundances of the deuterated species of both conformers (Figure 7.3 and Figure S7.3), it is interesting to note that the HOD5 species always appear stronger than the corresponding HOD4 ones, even though the abundances of the subunits are the same. For example, **PFP***Tg*+(OH)···HOD5 has 13% versus **PFP***Tg*+(OH)···HOD4 which has 10%; **PFP***Tg*+(OD)···HOD5 has 17% versus **PFP***Tg*+(OD)···HOD4 which has 11%. Similar phenomena were observed for **PFP***G*+*g*+···W_H isotopologues. This is because the deuteration at H5 would result in a lower *ZPE* than at H4 since H5 has an attractive contact with F while H4 is free. Indeed, the *ZPE* calculations of the D species show that the HOD5 species is about 0.2 kJmol^{-1} lower in energy than the HOD4 species after *ZPE* correction for both **PFP***G*+*g*+···W_H and **PFP***Tg*+···W_H.

4. Binding topologies and fluorination effects

Based on the experimental intensity ratio between **PFP***G+g+*$\cdots$$W_H$ versus **PFP***Tg+*$\cdots$$W_H$, a rotational temperature of 1 K, and corresponding theoretical electric dipole components, the relative experimental abundance ratio between two monohydrate species is estimated to be about 10:7 or 59%:41% (See Figure S7.2), very similar to the experimental abundances (60%:40%) of the corresponding PFP monomeric subunits reported previously.[14] To give a quantitative estimate of the hydrogen bonding strength between water and PFP subunits in the observed **PFP***G+g+*$\cdots$$W_H$ and **PFP***Tg+*$\cdots$$W_H$, the QTAIM and NCI analyses were carried out with the results summarized in Figure S7.9, SI. The strong O-Hw$\cdots$O bond energies in **PFP***G+g+*$\cdots$$W_H$ and **PFP***Tg+*$\cdots$$W_H$ are estimated to be 27.0 and 26.7 kJ mol^{-1} and the medium strength O-Hw$\cdots$F bond energies are 5.4 and 5.2 kJ mol^{-1}, respectively, showing a similar preference for **PFP***G+g+*$\cdots$$W_H$ over **PFP***Tg+*$\cdots$$W_H$ as in Table 7.1.

The NCI analyses were also carried out for the two tunneling transition states for the two conformers observed (see Section B) and the results are also shown in Figure S7.9. The main O-$H_w$$\cdots$O bonding interactions decrease slightly by 0.4 and 0.6 kJ mol^{-1} in the corresponding transition configurations for **PFP***G+g+*$\cdots$$W_H$ **PFP***Tg+*$\cdots$$W_H$, respectively, while the O-$H_w$$\cdots$F bond energies drop to 2.2 and 2.0 kJ mol^{-1} in the transitional states, respectively. Clearly, all the major attractive interactions remain largely in contact at the transition states, consistent with the low tunneling barriers obtained.

Here we also compare the situation with the non-fluorinated *n*-propanol (PrOH) and its monohydrates (PrOH$\cdots$W). Rotational spectra of PrOH have been studied by several groups,[22] where all five monomeric PrOH conformers were detected experimentally. The corresponding energetic differences are much smaller (i.e., all within an energy window of ~ 0.6 kJ mol^{-1}) [22a] in comparison to PFP.[14] This difference can be attributed to the high electronegativity of the F atoms, facilitating additional attractive interactions between hydroxyl OH and F, as discussed above. The monohydrates of PrOH were reported by Blake and co-workers,[23] and two conformers **PrOH***Tg*$\cdots$W and **PrOH***Gg'*$\cdots$W, with water serving as the proton donor, were detected experimentally. In the PFP$\cdots$W case, water serves as a proton acceptor, in contrast to the PrOH···W case. Such different bonding topologies could be attributed mainly to the charge distribution region near the alcoholic H in PFP versus in PrOH, as visualized in the electrostatic potential (ESP) plots of the relevant PFP and PrOH monomeric conformations (see Figure S7.10, SI). In PFP, the positive hydroxyl H site is noticeably more positive compared to that of PrOH, thanks to the high electronegativity of the F atoms. On the other hand, the hydroxyl O in PrOH is more negative compared to that in PFP because of the electron withdrawing F atoms.

Conclusions

The rotational spectra of two stable PFP···water conformers, **PFP***G*+*g*+···W$_H$ and **PFP***Tg*+···W$_H$ were measured and analysed for the first time, along with seven deuterium isotopologues of each. The tunnelling splittings associated with the interchange of equivalent H atoms of H_2O were observed and fitted and their tunnelling barriers estimated theoretically to be of ~2.5 kJ mol^{-1} and ~2.8 kJ mol^{-1} for **PFP***G*+*g*+···W$_H$ and **PFP***Tg*+···W$_H$, respectively. Importantly, both **PFP***G*+*g*+···W$_H$ and **PFP***Tg*+···W$_H$ exhibit very large amplitude, barrierless motions associated with the free OH of water. Such motions not only alter the experimental relative intensities of the *b*- and *c*-type transitions substantially, but also making it more difficult to identify different deuterium isotopologues. The current study also points out the potential issues in identifying conformers based on the comparison of the experimental and theoretical spectroscopic properties when dealing molecular targets with some very flexible coordinates. Considerable care must be taken to properly identify the correct minimum geometries. In addition, the effects of fluorination are discussed by comparing the preferred conformations of PFP and PrOH and their monohydrates.

Experimental and Computational Methods

A broadband 2-6 GHz chirped pulse Fourier transform microwave (CP-FTMW) spectrometer,[5a,24] which was based on a similar design Pate and co-workers,[25] was used for recording rotational spectra. PFP (Sigma Aldrich, 99.9%), deuterium oxide (Cambridge

Isotope Laboratories, Inc. 99.5%) and distilled water were used without further purification. Mixtures of 0.1% PFP with 0.2% H_2O in 5 bars of neon (Praxair, 99.999%) were used. The deuterated species were measured under the same condition as for the normal water, but with D_2O.

The conformer-rotamer ensemble sampling tool (CREST),[16] a powerful tool with quantum chemistry code developed by Grimme and co-workers, was employed for a comprehensive search of the possible PFP⋯W structural candidates. CREST has been utilized for conformational searches of flexible organic molecules and hydrogen-bonded complexes, such as perillyl alcohol[26], dimers of tetrahydro-2-furoic acid[27] and $HFIP_g \cdots W_H$[12b] successfully, although a case of missing conformer was also reported in the study of the propylene oxide trimer study.[28]

Quantum chemical calculations of geometry optimizations were performed with the Gaussian16 program package[29] on those initial CREST candidates. The B3LYP hybrid functional[30] in combination with Grimme's dispersion correction (D3),[31] Becke-Johnson damping (BJ) and the def2-QZVP/TZVP basis sets[32] were used for geometry optimization, harmonic frequency, and transition state calculations. To investigate the potential energies corresponding to the motions of the PFP monohydrates, 1- and 2D PES scans were carried out at the B3LYP-D3(BJ)/def2-QZVP and TZVP level of theories, respectively. All energies reported are corrected by *ZPE* and *BSSE*s where the later were calculated using the counterpoise procedure.[33] The keywords used in the calculations are provided in Point S1, Supporting Information. Rotational constants of deuterated species were generated by PMFIST (Principal Moments of Inertia From STructure).[34] Rotational transition assignments and least-square fittings were done with Pgopher.[18] Geometry structures of all systems were visualized by Avogadro,[35] and the results from the NCI[36] and QTAIM[37] analyses were visualized by visual molecular dynamics (VMD)[38] after being processed by the Multiwfn[39] software packages. The ESP calculations were also visualized by Gaussian16 program package.[29]

References

1. a) Badawi, H. M.; Förner, W., *Spectrochimi. Acta Part A: Mol. Biomol. Spectrosc.* **2008**, *71*, 388-397; b) Wencel-Delord, J.; Colobert, F., *Org. Chem. Front.* **2016**, *3*, 394-400.
2. Godin, P. J.; Cabaj, A.; Xu, L.-H.; Le Bris, K.; Strong, K., *J. Quant. Spectrosc. Radiat. Transfer* **2017**, *186*, 150-157.
3. Bourgeois, A.; Bergendahl, J.; Rangwala, A., *Chemosphere* **2015**, *131*, 104-109.
4. a) Caminati, W.; Melandri, S.; Moreschini, P.; Favero, P. G., *Angew. Chem. Int. Ed.* **1999**, *38*, 2924-2925; *Angew. Chem.* **1999**,*38*,2924-2925; b) Melandri, S.; Consalvo, D.; Caminati, W.; Favero, P. G., *J. Chem. Phys.* **1999**, *111*, 3874-3879; c) Melandri, S., *Phys. Chem. Chem. Phys.* **2011**, *13*, 13901-13911; d) Murugachandran, S. I.; Tang, J.; Peña, I.; Loru, D.; Sanz, M. E., *J. Phys. Chem. Lett.* **2021**, *12*, 1081-1086.
5. a) Seifert, N. A.; Thomas, J.; Jäger, W.; Xu, Y., *Phys. Chem. Chem. Phys.* **2018**, *20*, 27630-27637; b) Thomas, J.; Liu, X.; Jäger, W.; Xu, Y., *Angew. Chem. Int. Ed.* **2015**, *54*, 11711-11715; *Angew. Chem.* **2015**, *127*, 11877-11881. ; c) Liu, X.; Borho, N.; Xu, Y., *Chem. Eur. J.* **2009**, *15*, 270-277.
6. a) Thomas, J.; Xu, Y., *J. Phys. Chem. Lett.* **2014**, *5*, 1850-1855; b) Thomas, J.; Seifert, N. A.; Jäger, W.; Xu, Y., *Angew. Chem. Int. Ed.* **2017**, *56*, 6289-6293; *Angew. Chem.* **2017**, *129*, 6386-6390.
7. Shahi, A.; Arunan, E., *J. Phys. Chem. A* **2015**, *119*, 5650-5657.
8. Oswald, S.; Seifert, N. A.; Bohle, F.; Gawrilow, M.; Grimme, S.; Jäger, W.; Xu, Y., Suhm, M. A., *Angew. Chem. Int. Ed.* **2019**, *58*, 5080-5084; *Angew. Chem.* **2019**, *131*, 5134-5138.
9. Bako, I.; Radnai, T.; Bellisent Funel, M. C., *J. Chem. Phys.* **2004**, *121*, 12472-12480.
10. Huang, W.; Thomas, J.; Jäger, W.; Xu, Y., *Phys. Chem. Chem. Phys.* **2017**, *19*, 12221-12228.
11. Thomas, J.; Xu, Y., *J. Chem. Phys.* **2014**, *140*, 234307/1-5.
12. a) Shahi, A.; Arunan, E., *Phys. Chem. Chem. Phys.* **2015**, *17*, 24774-24782; b) Wu, B.; Hazrah, A. S.; Seifert, N. A.; Oswald, S.; Jäger, W.; Xu, Y., *J. Phys. Chem. A* **2021,** *125*, 10401-10409.
13. a) Xu, L. H.; Fraser, G. T.; Lovas, F. J.; Suenram, R.; Gillies, C.; Warner, H.; Gillies, J., *J. Chem. Phys.* **1995**, *103*, 9541-9548.
14. Wu, B.; Seifert, N. A.; Insausti, A.; Ma, J.; S. Oswald, S.; Jäger, W.; Xu, Y., *Phys. Chem. Chem. Phys.* **2022**, DOI.org/10.1039/D2CP01895K.
15. B. Wu,; Hazrah, A. S.; Seifert, N. A.; Oswald, S.; Jäger, W.; Xu, Y., *J. Phys. Chem. A* **2021,** *125*, 5355-5364.
16. a) Grimme, S., *J. Chem. Theo. Comput.* **2019**, *15*, 2847-2862; b) Pracht, P.; Bohle, F.; Grimme, S., *Phys. Chem. Chem. Phys.* **2020**, *22*, 7169-7192.
17. Watson, J. K. G., Vibrational Spectra and Structure: A Series of Advances, Vol.6 (Ed.: J. R. Durig), Elsevier, New York, **1977**, p. 1.
18. Western, C. M., *J. Quant. Spectrosc. Radiat. Transf.* **2017**, *186*, 221-242.

19. Seifert, N. A.; Finneran, I.; Perez, A. C.; Zaleski, D. P.; Neill, J. L.; Steber, A. L.; Suenram, R. D.; Lesarri, A.; Shipman, S. T.; Pate, B. H., *J. Mol. Spectrosc.* **2015**, *312*, 13-21.
20. Xu, Y.; Jäger, W. *J. Chem. Phys.* **1997**, *107*, 4788-4796.
21. Borho, N.; Xu, Y., *Phys. Chem. Chem. Phys.* **2007**, *9*, 4514-4520.
22. a) Kisiel, Z.; Dorosh, O.; Maeda, A.; Medvedev, I. R.; De Lucia, F. C.; *Phys. Chem. Chem. Phys.* **2010**, *12*, 8329-8339; b) Maeda, A.; De Lucia, F. C.; Herbst, E.; Pearson, J. C.; Riccobono, J.; Trosell, E.; Bohn, R. K., *Astrophys. J. Suppl. Ser.* **2006**, *162*, 428; c) Dreizier, H.; Scappini, F.; *Z. Naturforsch. A* **1981**, *36*, 1187-1191; d) Kazimova, S. B., *J. Appl. Spectrosc.* **2016**, *82*, 1023-1027; e) Abdurakhmanov, A.; Veliyulin, E.; Ragimova, R.; Imanov, L.; *J. Struct. Chem.* **1981**, *22*, 28-33.
23. Mead, G. J.; Alonso, E. R.; Finneran, I. A.; Carroll, P. B.; Blake, G. A., *J. Mol. Spectrosc.* **2017**, *335*, 68-73.
24. Carlson, C. D.; Seifert, N. A.; Heger, M.; Xie, F.; Thomas, J.; Xu, Y., *J. Mol. Spectrosc.* **2018**, *351*, 62-67.
25. Pérez, C.; Lobsiger, S.; Seifert, N. A.; Zaleski, D. P.; Temelso, B.; Shields, G. C.; Kisiel, Z.; Pate, B. H., *Chem. Phys. Lett.* **2013**, *571*, 1-15.
26. Xie, F.; Seifert, N. A.; Heger, M.; Thomas, J.; Jäger, W. Xu, Y., *Phys. Chem. Chem. Phys.* **2019**, *21*, 15408-15416.
27. Xie, F.; Ng, X.; Seifert, N. A.; Thomas, J.; Jäger, W.; Xu, Y., *J. Chem. Phys.* **2018**, *149*, 224306/1-10.
28. Xie, F.; Fusè, M.; Hazrah, A. S.; Jäger, W.; Barone, V.; Xu, Y., *Angew. Chem. Int. Ed.* **2020,** *59*, 22427-22430; *Angew. Chem.* **2020**, *132*, 22613-22616.
29. Frisch, M. J.; Trucks, G. W.; Schlegel, H. B., et al., Gaussian 16, Revision C.01, **2016**. Full reference in Supporting Information.
30. a) Stephens, P. J.; Devlin, F. J.; Chabalowski, C. F.; Frisch M. J., *J. Phys. Chem.* **1994**, *98*, 11623-11627; b) Beck, A. D., *J. Chem. Phys.* **1993**, *98*, 5648-5646.
31. Grimme, S. Ehrlich, S.; Goerigk, L., *J. Comput. Chem.* **2011**, *32*, 1456-1465.
32. Weigend, F.; Ahlrichs, R., *Phys. Chem. Chem. Phys.* **2005**, *7*, 3297-3305.
33. Boys, F.; Bernardi, F., *Mol. Phys.*, **1970**, *19*, 553-566.
34. Kisiel, Z., PROSPE–Programs for rotational spectroscopy. In *Spectroscopy from Space*, Demaison, J.; Sarka, K.; Cohen, E. A., Eds., Kluwer Academic Publishers: Dordrecht, **2001**, 91-106.
35. Hanwell, M. D.; Curtis, D. E.; Lonie, D. C.; Vandermeersch, T.; Zurek, E.; Hutchison, G. R., *J. Cheminf.* **2012**, *4*, 17.
36. Johnson, E. R.; Keinan, S.; Mori-Sánchez, P.; Contreras-García, J.; Cohen, A. J.; Yang, W., *J. Am. Chem. Soc.* **2010**, *132*, 6498-6506.
37. Bader, R.F.W., *Atoms in Molecules: A Quantum Theory*, Oxford University Press, New York, **1990**.
38. Humphrey, W.; Dalke, A.; Schulten, K., *J. Mol. Graph.* **1996**, *14*, 33-38.
39. Lu, T.; Chen, F., *J. Comput. Chem.* **2012**, *33*, 580-592.

Chapter 8

Conclusions and Remarks

8.1 Conclusions and Future Work

During my PhD study period, I have investigated several non-covalently bonded molecule clusters which contain water and/or fluoroalcohols, two important types of solvents. These include the aromatic pyrrole monohydrate, HFIP and PFP monohydrate, PFP monomer and PFP dimer, as well as the PFP···Ne and Ar complexes using rotational spectroscopy and DFT calculations. These binary adducts and even the related monomeric systems present interesting conformational landscapes and exhibit large amplitude motions. Substantial details of these important aspects have been investigated in this thesis. Two chirped pulse and one cavity-based Fourier transform microwave spectrometers were employed through out these studies. Furthermore, high-level DFT theoretical calculations were applied in addition to some conformational searching tools.

To aid rotational spectroscopic assignments and identifications of the conformers detected experimentally, it is important to carry out a comprehensive conformational search in order to identify all possible low energy conformers. In my thesis work, we utilized CREST, a conformational search tool, and also carried out one dimensional and two dimensional scans manually along some specific coordinates to complete the conformational searches. The conformational searches provided the energy orderings of different conformational candidates and their spectroscopic constants such as rotational constants and dipole moment components. These predictions were used to generate simulated rotational spectra of the low energy geometries, and then assigned the rotational spectra of conformers detected. Big differences between the experimental and theoretical rotational constants and electric dipole moment components were detected in some systems, providing strong experimental evidences for the large amplitude motions (LAMs), revealing the flexible nature of the monohydrate, rare gas adducts and fluorinated alcohols. My work presented in this thesis has explored the effects brought on by the LAMs and compared them to those of similar species to provide comprehensive understandings of the dynamic motions of water. The specific results and conclusions obtained for these systems are summarized below.

8.1.1 The Pyrrole$_{NH}$⋯Water Monohydrate

The rotational spectra of all monosubstituted ^{13}C isotopologues of Py$_{NH}$⋯W in their natural abundances were measured and assigned in Chapter 3 by employing one cavity-based and one chirped-pulse Fourier transform microwave spectrometers. We also extended the rotational assignment of the ^{12}C parent species to higher J and K values. The ^{14}N nuclear quadrupole hyperfine splittings and water tunneling doublets of the ^{13}C isotopologues were also observed and analyzed. Combined with the PES scans along paths of possible water motions, the conversions between all four previously proposed geometries, namely crossed, symmetric-crossed, hinged and planar hinged were identified. These include a barrierless LAM motion where OH flips from one side to the other, and a water tunneling motion where the bonded and non-bonded water H atoms exchange. The current theoretical and experimental data indicate that the vibrationally average ground state structure of Py$_{NH}$⋯W is symmetric crossed by averaging two mirror imaged cross structures, leading to the identification of the water tunneling path, which further confirmed by the experimental nuclear quadrupolar coupling constants of the ^{14}N nucleus. The rough intensity ratio of 1:3 for the rotational transitions in the upper and lower tunneling states also confirm the existence of water tunneling motion. This study suggests the importance of constructing proper PES surfaces along possible water tunneling paths in order to connect the conformational minima via transitional state geometries. The current study also paves the road for future investigation of stepwise solvation of pyrrole with several water molecules.

8.1.2 The HFIP$_g$-Water$_H$ Monohydrate

In Chapter 4, the rotational spectra of the missing, higher energy isomer of the HFIP⋯water complex, i.e., HFIP$_g$⋯W$_H$, and its seven deuterium isotopologues were recorded and analyzed. Interestingly, HFIP$_g$⋯W$_H$ exhibits much different water LAM dynamics, compared to the previously reported global minimum isomer HFIP$_t$⋯W$_H$, by conducting fully relaxed and rigid PES scans in 1D and 2D forms. The non- observation of a water tunneling splitting in HFIP$_t$⋯water was explained as a result of a barrier-less (after zero-point-energy correction) pathway for the water motion,[15] whereas in $HFIP_g\cdots$water, a sizable barrier height (~ 3.3 kJ mol^{-1}) was identified as the cause of barely resolved water tunneling splittings. Moreover, the observation of $HFIP_g\cdots W_H$ monohydrate isomer reveals the fact that the hydrogen bonding with water preferentially stabilizes the less stable $HIFP_g$ configuration over the global minimum geometry $HIFP_t$. Both the experimental estimate and the theoretical calculations indicate an energy disadvantage between monohydrate isomers, $HFIP_g\cdots W_H$ and $HFIP_t\cdots W_H$, and between the $HFIP_g$ and $HFIP_t$ monomers is much reduced because of the complexation with water preferentially stabilize the less stable $HFIP_g$ configuration. The significant influence of fluorination on the preferred binding topology between HFIP⋯W and non-fluorinated IP⋯W is also highlighted and discussed.

8.1.3 The $HFIP_t$-Ne/Ar Rare Gas complexes

The rotational spectroscopy, along with several quantum mechanics analyses were employed for the investigation of the van der Waals binding topologies between HFIP and Ne/Ar as presented in Chapter 5. Nine low-energy binding topologies of the HFIP⋯Ne/Ar isomers were identified for each binary species within a small energy span. By utilizing the comparison of the experimental and theoretical rotational constants, the planar moments, and the electric dipole moment components, one could conclude that only the most stable isomers predicted, $HFIP_t\cdots Ne_H$ and $HFIP_t\cdots Ar_H$, were observed in the supersonic jet expansion. Important van der Waals structural parameters of the $HFIP_t\cdots Ne_H$ cluster were refined by using the experimental isotopic data, along with the $HFIP_t$ subunit structural parameters. Similar line intensities were observed for rotational transitions of $HFIP_t\cdots {}^{20}Ne_H$ and $HFIP_t\cdots {}^{22}Ne_H$, highlighting the isotopic effect of ZPE for these very weakly bound binary complexes where the more strongly binding strength of the $HFIP_t\cdots {}^{22}Ne_H$ isotopomer enriches its population abundance during the jet expansion process.

Moreover, the QTAIM and ESP analyses reveal that rare gas must take advantage of all available contacts with $HFIP_t$ subunit to maximize the sum of interaction energies in order to keep the loose binding interaction. The QTAIM analyses suggest that from IP to HFIP, the fluorination significantly increases the interaction energy of Ne/Ar···H−O. Meanwhile the ESP mapping reveals the relatively more positive hydroxyl H in HFIP, comparing to IP, provides the most suitable binding dock for rare gas. Thus, the comprehensive quantum chemical analyses are necessary to fully understand the binding topologies and preferences of the rare gas with respect to the fluorinated alcohol monomer.

8.1.4 The PFP Monomers and Dimers

The rotational spectra of two stable 2,2,3,3,3-pentafluoro-propan-1-ol (PFP) monomers, and five stable homodimer adducts were recorded using a cavity-based and a chirp pulsed rotational microwave spectrometer as introduced in Chapter 6 and were assigned. Two mirror-imaged monomeric pairs out of nine possible configurations, e.g., **PFP***G+g+/G-g-* and **PFP***Tg+/Tg-*, were observed experimentally. The experimental population abundances between the two monomers could be satisfactorily explained considering the conformational Boltzmann distribution at the source temperature and the subsequent conformational conversion in a jet expansion. For a better understanding of its dynamic geometry properties, the rigid 2-dimentional PES scans along possible paths of two important and flexible dihedral angles of the monomer configurations were carried out. The observation of several minor isotopologue data of **PFP***G+g+/G-g-* allows for the semi-experimental geometric structure refinement and the result was used for benchmarking current theoretical calculations. The results indicate that the MP2 calculation provides agreement with the best semi-experimental equilibrium structure. As for the **PFP***Tg+/Tg-* monomer, the OH tunneling splittings were analyzed in detail with the assignment of the cross-tunneling transitions between its ground and excited states. As for the five experimentally observed homodimers, the QTAIM and NCI analyses help with the understanding of the hydrogen bonding interactions between the two PFP monomer subunits. The experimental population abundances were also estimated of the five observed dimer adducts, together with an “Ar test” to investigate the conformational cooling properties. This project provides comprehensive and fundamental studies on the

PFP monomer and homodimers that would facilitate the future studies on larger PFP adducts, e.g., PFP monohydrates, PFP trimer and other aggregates.

8.1.5 The PFP···Water$_H$ Monohydrate Isomers

Two PFP···water monohydrate isomers, namely **PFP***G*+*g*+···W$_H$ and **PFP***Tg*+···W$_H$, were observed. They each contains the low-energy isomers of the **PFP** monomer. In addition, there 14 partially or fully deuterium isotopologues were also recorded and analyzed. Actually, the global minimum geometry of the **PFP***G*+*g*+···W$_H$ monohydrate was not identified in the early-stage conformational searches. Only by carrying out the relaxed scans along possible water motion coordinates, I could identify the real global minimum geometry, implying the importance of the PES relaxed scans. The observed rotational transitions show tunneling splitting patterns associated with the interchange of the equivalent H atoms of H_2O although but only a few ro-tunneling transitions are well resolved. By combining with some quantum mechanic calculations e.g., the QTAIM and NCI analyses, PES mappings, the topology features related to the water motions of the two PFP···water monohydrates were studied. The situations are similar to that in HFIP$_g$···W$_H$ described above. The LAM of the free water H atom not only significantly alters the electric dipole moments, but also brings challenges in assigning the proper carriers of the correct deuterated species due to large differences in the experimental and theoretical rotational constants. The fluorination effects were also investigated by comparing with the corresponding non-fluorinated propanol···water isomers. Based on the ESP mappings of the PFP and propanol monomers, the hydrogen bonding donor or acceptor roles of water play in each of the monohydrates could be well explained. In the PFP···water clusters, PFP donate its hydroxyl H to water whereas the propanol accepts H atom from water as the proton accepter. This is because the fluorine atoms would extract more electron density away from the hydroxyl H, making it more acidic in PFP compared to that in propanol.

8.2 Future Work

It would be very interesting to build on the present studies and move to larger water solvation clusters, such as Pyrrole⋯$(H_2O)_2$, HFIP⋯$(H_2O)_2$ / $(HFIP)_2$⋯H_2O, and PFP⋯$(H_2O)_2$ / $(PFP)_2$⋯H_2O ternary aggregates or even larger water containing clusters. These first few steps of explicit solvation are of importance in light of the on-going research effort to account for solvent effects in solution measurements. For example, in a recent work by our group we compared two different approaches to account for solvation effects, i.e., the cluster-in-a-liquid model which is based on explicit solvated clusters and ab initio molecular dynamic simulation. The rotational spectroscopic studies of sequential solvation can provide some additional experimental insight into the former model. The investigation of the larger fluoroalcohol aggregates with water is of considerable interest for understanding the properties of fluoroalcohol+water co-solvent, especially in light of that the molecular dynamics simulations suggest that larger fluoroalcohol aggregates exist in the co-solvent and play some important role in inducing folding and unfolding of polypeptides and proteins.

Moreover, one may also be interested in searching larger PFP homo-aggregates, e.g. trimers or even tetramers. The assignments could be quite challenging because the flexible nature and diverse conformational changes of the PFP monomer would bring numbers of conformations and the interconversions between conformations might be easy to complete. It would be interesting to see how many PFP trimer or tetramer aggregates could survive in the jet expansion and the relative population abundances among them.

These studies will be challenging because the larger systems are expected to exhibit a very complicated conformational landscape with many possible low energy conformers and also their rotational constants are much smaller than the related binary clusters, making their expected intensities much lower and their rotational spectra even denser. Nevertheless, the experience accumulated with the conformational searches and DFT optimized geometries can be helpful with these future studies.

One interesting finding of the current work is that large amplitude motions can influence the ground state properties, such as geometries and electric dipole moment components greatly, making them differ considerably from the theoretical equilibrium values. This also makes it quite challenging to identify the correct conformers responsible for the set of rotational transitions assigned. It is of considerable importance if one can properly account for large amplitude motions in estimating these properties. In the current thesis work, we used potential energy scans along some specific coordinates which correspond to the large amplitude motions of interest and calculated the associated structures and properties along the path to gain a general idea of the deviation. However, to properly account for the large amplitude motions and predict the actual ground state properties, input from theorists is needed. We may seek out theorists who are interested in this research direction.

Bibliography

1. Angell C.A. (1982) in *Water: A Comprehensive Treatise*, Prenum Press, New York, **1972,** *1*, 151.
2. Debenedetti, P. Stanley H., *Physics Today* **2003,** *56*,40–46.
3. Mishima, O.; Stanley, H. E., *Nature* **1998,** *396*, 329-335.
4. Pérez, C.; Lobsiger, S.; Seifert, N. A.; Zaleski, D. P.; Temelso, B.; Shields, G. C.; Kisiel, Z.; Pate, B. H., *Chem. Phys. Lett.* **2013,** *571*, 1-15.
5. Pérez, C.; Zaleski, D. P.; Seifert, N. A.; Temelso, B.; Shields, G. C.; Kisiel, Z.; Pate, B. H., *Angew. Chem. Int.* **2014,** *53*, 14368-14372. *Angew. Chem.* **2014,** *126*, 14596-14600.
6. Pérez, C.; Muckle, M. T.; Zaleski, D. P.; Seifert, N. A.; Temelso, B.; Shields, G. C.; Kisiel, Z.; Pate, B. H., *Science* **2012,** *336*, 897-901.
7. Evangelisti, L.; Perez, C.; Lobsiger, S.; Seifert, N. A.; Zaleski, D. P.; Pate, B.; Kisiel, Z.; Temelso, B.; Shields, G. C.， In *Deuterated water hexamer observed by chirped-pulse rotational spectroscopy*, 69th International Symposium on Molecular Spectroscopy, 2014; pFD12.
8. Wencel-Delord, J.; Colobert, F., *Org. Chem. Front.* **2016**, *3*, 394.
9. Colomer, I.; Chamberlain, A. E.; Haughey, M. B.; Donohoe, T. J., *Nat. Rev. Chem*. **2017**, *1*, 1-12.
10. Hong, D.-P.; Hoshino, M.; Kuboi, R.; Goto, Y., *J. Am. Chem. Soc.* **1999**, *121*, 8427-8433.
11. Godin, P. J.; Le Bris, K.; Strong, K., *J. Quant. Spectros. Radiat. Transf.* **2017**, *203*, 522-529.
12. Zhang, L.; Noda, I.; Czarnik-Matusewicz, B.; Wu, Y., *Anal. Sci*. **2007**, *23*, 901-905.
13. Godin, P. J.; Le Bris, K.; Strong, K., *J. Quant. Spectros. Radiat. Transf.* **2017**, *203*, 522-529.
14. Rajan, R.; Balaram, P., *Int. J. Pept. pROTein Res.* 1996, 48, 328-336
15. Narita, M.; Honda, S.; Umeyama, H.; Obana, S., *Bull. Chem. Soc. Jpn.* **1988**, *61*, 281-284.
16. Hirota, N.; Goto, Y.; Mizuno, K., *Protein Sci.* **1997**, *6*, 416-421.
17. Hirota, N.; Mizuno, K.; Goto, Y., *J. Mol. Biol.* **1998**, *275*, 365-378.
18. Xu, L.-H.; Fraser, G. T.; Lovas, F. J.; Suenram, R. D.; Gillies, C. W.; Warner, H. E.; Gillies, J. Z.; *J. Chem. Phys.* **1995**, *103*, 9541
19. Crick, F. H. C.; Watson, J. D.; Sciences, P., *Proc. R. Soc. A* **1954,** *223*, 80-96.
20. Chang, H.-C.; Jiang, J.-C.; Chen, T.-Y.; Wang, H.-S.; Li, L. Y.; Hung, W.-W.; Lin, S. H., *Phys. Chem. Chem. Phys.* **2013,** *15*, 12734-12741.
21. Tso, T. L.; Lee, E. K., *J. Phys. Chem.* **1985,** *89*, 1612-1618.
22. Martins, V.; Xu, J.; Wang, X.; Chen, K.; Hung, I.; Gan, Z.; Gervais, C.; Bonhomme, C.; Jiang, S.; Zheng, A., *J. Am. Chem. Soc.* **2020,** *142*, 14877-14889.
23. Chen, B.; Huang, Y., *J. Am. Chem. Soc.* **2006,** *128*, 6437-6446.
24. Scheiner, S.; Gu, Y.; Kar, T., *J. Mol. Struct. THEOCHEM* **2000,** *500*, 441-452.
25. Zhao, H.; Pan, Q.; Zhang, W.; Carmichael, I.; Serianni, A. S., *J. Org. Chem.* **2007,** *72*, 7071-7082.

26. Liu, Y.; Li, S.; Xu, J.; Zhang, H.; Guan, Y.; Jiang, H.; Huang, S.; Huang, H.; Wang, Z., *J. Cryst. Growth* **2018,** *18*, 1940-1943.

27. Reddy, T. R.; Reddy, L. S.; Reddy, G. R.; Yarbagi, K.; Lingappa, Y.; Rambabu, D.; Krishna, G. R.; Reddy, C. M.; Kumar, K. S.; Pal, M., *Green Chem.* **2012,** *14*, 1870-1872.

28. Kaminský, J.; Horáčková, F. k.; Biačková, N.; Hubáčková, T.; Socha, O. E.; Kubelka, J., *J. Phys. Chem. B* **2021**, *125*, 11350-11363

29. Han, W.-G.; Jalkanen, K.; Elstner, M.; Suhai, S., *J. Phys. Chem. B* **1998,** *102*, 2587-2602.

30. Yang, Y.; Cheramy, J., Xu, Y., *ChemPhysChem*, **2021**, *22*, 1336-1343.

31. Perera, A. S.; Cheramy, J.; Poopari, M. R.; Xu, Y., *Phys. Chem. Chem. Phys.* **2019**, *21*, 3574-3584.

32. Merten, C.; Berger, C. J.; McDonald, R.; Xu, Y., *Angew. Chem. Int. Ed.* **2014**, *53*, 9940–9943; *Angew. Chem.* **2014**, *126*, 10098−10101.

33. Merten, C.; Xu, Y., *Angew. Chem. Int. Ed.* **2013**, *52*, 2073−2076; *Angew. Chem.* **2013**, *125*, 2127−2130.

34. Becucci, M.; Melandri, S., *Chem. Rev.* **2016,** *116*, 5014-5037.

35. Xu, Y.; Van Wijngaarden, J.; Jäger, W., *Inter. Rev. Phys. Chem.* **2005**, *24*, 301−338.

36. Liu, X.; Xu, Y., High resolution microwave spectroscopy of chiral molecular contact pairs. *Chiral Recognition in the Gas Phase*, Ed. A. Zehnacker, CRC Press, Taylor&Francis Group, **2010**.

37. Jäger, W.; Xu, Y., Fourier transform microwave spectroscopy of doped helium clusters, in *Handbook of High-resolution Spectroscopy*, Eds M. Quack and F. Merkt, John Wiley and Sons, Chichester, **2011**.

38. Burevschi, E.; Sanz, M. E., *Molecules* **2021**, *26*, 5162

39. Su, Z.; Borho, N.; Xu, Y., *J. Am. Chem. Soc.* **2006**, *128*, 17126−17131.

40. Xie, F.; Fusè, M.; Hazrah, A. S.; Jäger, W.; Barone, V.; Xu, Y., *Angew. Chem. Int. Ed.* **2020**, *59*, 22427-22430; *Angew. Chem.* **2020,** *132*, 22613-22616.

41. Thomas, J.; Jäger, W.; Xu, Y., *Angew. Chem. Int. Ed.* **2014**, *53*, 7277−7280; *Angew. Chem.* **2014**, *126*, 7405−7408.

42. Borho, N.; Xu, Y., *J. Am. Chem. Soc.* **2008**, *130*, 5916−5921.

43. Thomas, J.; Xu, Y., *J. Phys. Chem. Lett.* **2014**, *5*, 1850−1855.

44. Liu, X.; Borho, N.; Xu, Y., *Chem. Eur. J.* **2009**, *15*, 270−277.

45. Scharge, T.; Häbery, T.; Suhm, M. A., *Phys. Chem. Chem. Phys.*, **2006**, *8*, 4664–4667.

46. Thomas, J.; Seifert, N. A.; Jäger, W.; Xu, Y., *Angew. Chem. Int. Ed.* **2017**, *56*, 6289-6293; *Angew. Chem.* **2017**, *129*, 6386-6390.

47. Thomas, J.; Liu, X.; Jäger, W.; Xu, Y., *Angew. Chem. Int. Ed.* **2015**, *54*, 11711-11715; *Angew. Chem.* **2015**, *127*, 11877-11881.

48. Scharge, T.; Cézard, C.; Zielke, P.; Schuütz, A.; Emmeluth, C.; Suhm, M. A., *Phys. Chem. Chem. Phys.*, **2007**, *9*, 4472–4490.

49. Oswald, S.; Seifert, N. A.; Bohle, F.; Gawrilow, M.; Grimme, S.; Jäger, W.; Xu, Y.; Suhm, M. A., *Angew. Chem. Int. Ed.* **2019**, *58*, 5080-5084; *Angew. Chem.* **2019**, *131*, 5134-5138.

50. Seifert, N. A.; Thomas, J.; Jäger, W.; Xu, Y., *Phys. Chem. Chem. Phys.* **2018**, *20*, 27630-27637.
51. Carlson, C. D.; Seifert, N. A.; Heger, M.; Xie, F.; Thomas, J.; Xu, Y., *J. Mol. Spectrosc.* **2018**, *351*, 62-67.
52. Yang, Q.; Carlson, C. D.; Jäger, W.; Xu, Y., *J. Phys. Chem. A* **2022**, 126, 19, 2942–2949
53. Suzuki, S; Green, P.G.; Bumgarner, R.E.; Dasgupta, S.; Goddard 3rd, W.A.; Blake, G.A., *Science* **1992**, *257*, 942-946
54. Gutowsky, H.S.; Emilsson, T.; Arunan, E., *J. Chem. Phys.* **1993**, *99*, 4883-4893
55. Evangelisti, L.; Brendel, K.; Mäder, H.; Caminati, W.; Melandri S., *Angew. Chem. Int. Ed.* **2017**, *56*, 13699-13703; *Angew. Chem.* **2017**, *129*, 13887-13891.
56. Schnitzler, E. G.; Seifert, N. A.; Ghosh, S.; Thomas, J.; Xu, Y.; Jäger, W., *Phys. Chem. Chem. Phys.* **2017**, *19*, 4440-4446.
57. Murugachandran, I., Tang, J., Pena Calvo, I. P., Loru, D. & Sanz, M., *J. Phys. Chem. Lett.* **2021**, *12*, 1081–1086
58. Tubergen, M. J.; Andrews, A. M.; Kuczkowski, R. L., *J. Phys. Chem.* **1993,** *97*, 7451-7457.
59. Xie, F.; Ng, X.; Seifert, N. A.; Thomas, J.; Jäger, W.; Xu, Y., *J. Chem. Phys.* **2018**, *149*, 224306.
60. Xie, F.; Seifert, N. A.; Heger, M.; Thomas, J.; Jäger, W.; Xu, Y., *Phys. Chem. Chem. Phys.* **2019**, *21*, 15408-15416.
61. Pérez, C.; Lobsiger, S.; Seifert, N. A.; Zaleski, D. P.; Temelso, B.; Shields, G. C.; Kisiel, Z.; Pate, B. H., *Chem. Phys. Lett.*, **2013**, *571*, 1-15.
62. Grimme, S., *J. Chem. Theory. Comput.*, **2019**, *15*, 2847-2862.
63. Pracht, P.; Bohle, F.; Grimme, S., *Phys. Chem. Chem. Phys.*, **2020**, *22*, 7169-7192.
64. Xu, Y.; Jäger, W.; Tang, J.; McKellar, A. R. W., *Phys. Rev. Lett.* **2003**, *91*, 163401−163404.
65. Xu, Y.; Jäger, W., *J. Chem. Phys.* **2003**, *119*, 5457−5466.
66. Tang, J.; Xu, Y.; McKellar, A. R. W.; Jäger, W., *Science* **2002**, *297*, 2030−2033.
67. Xu, Y.; Civis, S.; McKellar, A. R. W.; König, S.; Haverlag, M.; Hilpert, G.; Havenith, M., *Mol. Phys.* **1996**, *87*, 1071–1082.
68. Xia, C.; McKellar, A. R. W.; Xu, Y., *J. Chem. Phys.* **2000**, *113*, 525–533.
69. Xu, Y.; Jäger, W., *J. Chem. Phys.* **2000**, *113*, 514–524.
70. Gordy, W.; Cook, R. L., *Techniques of Chemistry, Microwave Molecular Spectra*. Wiley: 1984.
71. De Leeluw, F.H.; Dymanus, A., *J. Mol. Spectrosc.* **1973**, *48*, 427-445,
72. Gall, J. T. A.; Thomas, J.; Xie, F.; Wang, Z.; Jäger, W.; Xu, Y., *Phys. Chem. Chem. Phys.* **2017**, *19*, 29508-29515.
73. Thomas, J.; Peña, I.; Carlson, C.; Yang, Y.; Jäger, W.; Xu, Y., *Phys. Chem. Chem. Phys.* **2020**, *22*, 23019-23027.
74. Grabow, J.-U.; Pine, A. S.; Fraser, G. T.; Lovas, F. J.; Suenram, R. D.; Emilsson, T.; Arunan, E.; Gutowsky, H. S., *J. Chem. Phys.* **1995**, *102*, 1181.
75. Jäger, W.; Xu, Y.; Gerry, M. C. L., *J. Chem. Phys.* **1993**, *99*, 919–927.

76. Xu, Y.; Jäger, W.; Gerry, M. C. L., *J. Chem. Phys.* **1994**, *100*, 4171–4180.
77. Novick, S.E.; Davies, P.; Harris, S.J.; Klemperer, W., *J. Chem. Phys.* **1973**, *59*, 2273-2279.
78. Xu, Y.; Jäger, W.; Ozier, I.; Gerry, M. C. L., *J. Chem. Phys.* **1993**, *98*, 3726–3731.
79. Jäger, W.; Xu, Y.; Heineking, N.; Gerry, M. C. L., *J. Chem. Phys.* **1993**, *99*, 7510–7520.
80. Janda, K.C., Bernstein, L.S.; Steed, J.M.; Novick, S.E.; Klemperer, W., *J. Am. Chem. Soc.* **1978**, *100*, 8074-8079.
81. Marshall, F. E.; Dorris, R.; Peebles, S. A.; Peebles, R. A.; Grubbs, G. S., *J. Phys. Chem. A* **2018**, *122*, 7385-7390.
82. Marshall, M. D.; Leung, H. O.;Wang, K.; Acha, M. D., *J. Phys. Chem. A* **2018***, 122*, 4670-4680.
83. Leung, H. O.; Marshall, M. D.; Stuart, D. J., *J. Phys. Chem. A* **2020**, *124*, 1798-1810.
84. Bernath, P. F., *Spectra of atoms and molecules*. Oxford university press: 2020.
85. Bauder, A., Fundamentals of rotational spectroscopy. *Handbook of High‐resolution Spectroscopy* **2011**.
86. Brown, J. M.; Brown, J. M.; Carrington, A., *Rotational spectroscopy of diatomic molecules*. Cambridge university press: **2003**.
87. McAfee Jr, K.; Hughes, R. H.; Wilson Jr, E. B., *Rev. Sci. Instrum.* **1949,** *20*, 821-826.
88. Hertel, I. V.; Schulz, C.-P., *Atoms, molecules and optical physics*. Springer: **2014**.
89. Universität Rostock, Lecture 17: Optical Bloch Equations. https://www.lkv.uni-rostock.de/storages/unirostock/Alle_MNF/Physik_Qms/Lehre_Scheel/quantenoptik/Quantenoptik-Vorlesung10.pdf.
90. Shun-Jin, W.; Cassing, W., *Ann. Phys.* **1985,** *159*, 328-350.
91. Blum, K., *Density matrix theory and applications*. Springer Science & Business Media: 2012; Vol. 64.
92. Von Neumann, J., Mathematisch-Physikalische Klasse, Wahrscheinlichkeitstheoretischer aufbau der quantenmechanik. Nachrichten von der Gesellschaft der Wissenschaften zu Göttingen, Mathematisch-Physikalische Klasse **1927,** *1927*, 245-272.
93. Allen, L.; Eberly, J. H., *Optical resonance and two-level atoms*. Courier Corporation: 1987; Vol. 28.
94. Arecchi, F.; Bonifacio, R., *IEEE J. Quantum Electron.* **1965,** *1*, 169-178.
95. Park, G.B.; Field, R.W., *J. Chem. Phys.* **2016**, *144*, 200901
96. Hughes, R. H.; Wilson Jr, E. B., *Phys. Rev.* **1947,** *71*, 562.
97. Townes, C. H.; Schawlow, A. L., *Microwave spectroscopy*. Courier Corporation: 2013.
98. Kantrowitz, A.; Grey, J., *Rev. Sci. Instrum.* **1951,** *22*, 328-332.
99. Arunan, E.; Dev, S.; Mandal, P. K., *Appl. Spectrosc. Rev.* **2004,** *39*, 131-181.
100. Imasaka, T.; Moore, D. S.; Vo-Dinh, T., *J. Pure Appl. Chem.* **2003,** *75*, 975-998.
101. Even, U., *EPJ Tech. Instrum.* **2015,** *2,* 14.
102. Marrone, P. V., *Phys. Fluids* **1967,** *10*, 521-538.
103. Balle, T.; Flygare, W. J., *Rev. Sci. Instrum.* **1981,** *52*, 33-45.
104. Campbell, E.; Buxton, L.; Balle, T.; Flygare, W., *J. Chem. Phys.* **1981,** *74*, 813-828.
105. Campbell, E.; Buxton, L.; Balle, T.; Keenan, M.; Flygare, W. H., *J. Chem. Phys.* **1981,** *74*, 829-840.

106. Brown, G. G.; Dian, B. C.; Douglass, K. O.; Geyer, S. M.; Shipman, S. T.; Pate, B. H., *Rev. Sci. Instrum.* **2008,** *79*, 053103.

107. Xu, Y.; Jäger, W., *J. Chem. Phys.* **1997**, *107*, 4788–4796.

108. Xu, Y.; Jäger, W., *J. Chem. Phys.* **1997**, *106*, 7968–7980.

109. Grabow, J.-U., Fourier transform microwave spectroscopy measurement and instrumentation. *Handbook of High‐resolution Spectroscopy* **2011**.

110. Chuang, C.; Hawley, C.; Emilsson, T.; Gutowsky, H., *Rev. Sci. Instrum.* **1990,** *61*, 1629-1635.

111. Grabow, J.-U.; Stahl, W., *Z. Naturforsch. A* **1990,** *45*, 1043-1044.

112. Schnell, M.; Banser, D.; Grabow, J.-U., *Rev. Sci. Instrum.* **2004,** *75*, 2111-2115.

113. Andresen, U.; Dreizler, H.; Grabow, J.-U.; Stahl, W., *Rev. Sci. Instrum.* **1990,** *61*, 3694-3699.

114. http://www.chem.ualberta.ca/~jaeger/research/ftmw/ftmw.htm, access 2022 May

115. Seifert, N. A. *2-6 GHz Chirped-Pulse Fourier Transform Microwave (CP-FTMW) Spectrometer: Standard Operating Procedure / Tips & Tricks,* **2019**.

116. Gaussian 16, Revision B.01, Frisch, M. J.; Trucks, G. W.; Schlegel, H. B.; Scuseria, G. E.; Robb, M. A.; Cheeseman, J. R.; Scalmani, G.; Barone, V.; Petersson, G. A.; Nakatsuji, H.; Li, X.; Caricato, M.; Marenich, A. V.; Bloino, J.; Janesko, B. G.; Gomperts, R.; Mennucci, B.; Hratchian, H. P.; Ortiz, J. V.; Izmaylov, A. F.; Sonnenberg, J. L.; Williams-Young, D.; Ding, F.; Lipparini, F.; Egidi, F.; Goings, J.; Peng, B.; Petrone, A.; Henderson, T.; Ranasinghe, D.; Zakrzewski, V. G.; Gao, J.; Rega, N.; Zheng, G.; Liang, W.; Hada, M.; Ehara, M.; Toyota, K.; Fukuda, R.; Hasegawa, J.; Ishida, M.; Nakajima, T.; Honda, Y.; Kitao, O.; Nakai, H.; Vreven, T.; Throssell, K.; Montgomery Jr., J. A.; Peralta, J. E.: Ogliaro, F.: Bearpark, M. J.: Heyd, J. J.: Brothers, E. N.; Kudin, K. N.; Staroverov, V. N.; Keith, T. A.; Kobayashi, R.; Normand, J.; Raghavachari, K.; Rendell, A. P.; Burant, J. C.; Iyengar, S. S.; Tomasi, J.; Cossi, M.; Millam, J. M.; Klene, M.; Adamo, C.; Cammi, R.; Ochterski, J. W.; Martin, R. L.; Morokuma, K.; Farkas, O.; Foresman, J. B.; Fox, D. J.; Gaussian 16, Revision A.03, Gaussian, Inc., Wallingford, CT, **2016**.

117. Stephens, P. J.; Devlin, F. J.; Chabalowski, C. F.; Frisch, M. J., *J. Phys. Chem.* **1994,** *98*, 11623-11627.

118. Beck, A. D. *J. Chem. Phys.* **1993**, *98*, 1372-1377.

119. Grimme, S.; Antony, J.; Ehrlich, S.; Krieg, H. J., *J. Chem. Phys.* **2010,** *132*, 154104.

120. Grimme, S.; Ehrlich, S.; Goerigk, L., *J. Comput. Chem.* **2011,** *32*, 1456-1465.

121. Weigend, F.; Ahlrichs, R., *Phys. Chem. Chem. Phys.* **2005,** *7*, 3297-3305.

122. Wang, H.; Heger, M.; Al-Jabiri, M. H.; Xu, Y., *Molecules*, **2021**, 27, 38

123. Seifert, N. A.; Finneran, I. A.; Perez, C.; Zaleski, D. P.; Neill, J. L.; Steber, A. L.; Suenram, R. D.; Lesarri, A.; Shipman, S. T.; Pate, B. H., *J. Mol. Spectrosc.* **2015,** *312*, 13-21.

124. Pickett, H. M., *J. Mol. Spectrosc.* **1991,** *148*, 371-377.

125. Pickett, H. M., SPFIT/SPCAT Package, available at <http://spec.jpl.nasa.gov./>.

126. Hanwell, M. D.; Curtis, D. E.; Lonie, D. C.; Vandermeersch, T.; Zurek, E.; Hutchison, G. R., *J. Cheminformatics* **2012,** *4*, 17.

127. Pettersen, E. F.; Goddard, T. D.; Huang, C. C.; Couch, G. S.; Greenblatt, D. M.; Meng, E. C.; Ferrin, T. E., *J. Comput. Chem.* **2004,** *25*, 1605-1612.

128. May, R. A.; Stevenson, K. J., *Software review of Origin 8*. ACS Publications: 2009.

129. Kisiel, Z., PROSPE-Programs for rotational spectroscopy, in *Spectroscopy from Space*, Eds. J. Demaison, K. Sarka, E. A. Cohen, **2001**, pp. 91-106. Kluwer Academic Publishers, Dordrecht.

130. Western, C. M., *J. Quant. Spectrosc. Radiat. Transf.* **2017**, *186*, 221-242.

131. Humphrey, W.; Dalke, A.; Schulten, K., *J. Mol. Graph.* **1996**, *14*, 33-38.

132. Lu, T.; Chen, F., *J. Comput. Chem.* **2012,** *33*, 580-592.

133. Nygaard, U.; Nielsen, J. T.; Kirchheiner, J.; Maltesen, G.; Rastrup-Andersen, J.; Sørensen, G. O., *J. Mol. Struct.* **1969,** *3*, 491-506.

134. Bak, B. R.; Christensen, D.; Hansen, L.; Rastrup‐Andersen, J., *J. Chem. Phys.* **1956,** *24*, 720-725.

135. Sobolewski, A. L.; Domcke, W., *Chem. Phys. Lett.* **2000,** *321*, 479-484.

136. Kumar, A.; Kołaski, M.; Kim, K. S., *J. Chem. Phys.* **2008,** *128*, 034304.

137. Gao, W.; Jiao, J.; Feng, H.; Xuan, X.; Chen, L., *J. Mol. Model.* **2013,** *19*, 1273-1283.

138. Matsumoto, Y.; Honma, K., *J. Chem. Phys.* **2009,** *130*, 054311.

139. Thomas, J.; Sukhorukov, O.; Jäger, W.; Xu, Y., *Angew. Chem. Int. Ed.* **2014**, *53*, 1156−1159; *Angew. Chem.* **2014**, *126*, 1175−1178.

140. Gruet, S.; Pérez, C.; Steber, A. L.; Schnell, M., *Phys. Chem. Chem. Phys.* **2018,** *20*, 5545-5552.

141. Brown, G. G.; Dian, B. C.; Douglass, K. O.; Geyer, S. M.; Pate, B. H., *J. Mol. Spectrosc.* **2006,** *238*, 200-212.

142. Grubbs, G. S.; Dewberry, C. T.; Etchison, K. C.; Kerr, K. E.; Cooke, S. A., *Rev. Sci. Instrum.* **2007,** *78*, 096106.

143. Dempster, S. P.; Sukhorukov, O.; Lei, Q. Y.; Jäger, W., *J. Chem. Phys.* **2012,** *137*, 174303.

144. Thomas, J.; Yiu, J.; Rebling, J.; Jäger, W.; Xu, Y., *J. Phys. Chem. A* **2013,** *117*, 13249-13254.

145. Huang, W.; Thomas, J.; Jäger, W.; Xu, Y., *Phys. Chem. Chem. Phys.* **2017,** *19*, 12221-12228.

146. Xie, F.; Seifert, N. A.; Jaeger, W.; Xu, Y., *Angew. Chem. Int. Ed.* ***2020,*** *59, 15703-15710; Angew. Chem.* ***2020,*** *132,15833-15840.*

147. Becke, A. D., Density-functional thermochemistry. III. The role of exact exchange. *J. Chem. Phys.* **1993,** *98*, 5648.

148. Becke, A. D.; Johnson, E. R., A density-functional model of the dispersion interaction. *J. Chem. Phys.* **2005,** *123*, 154101.

149. Krishnan, R.; Binkley, J. S.; Seeger, R.; Pople, J. A., *J. Chem. Phys.* **1980,** *72*, 650-654.

150. Boys, S. F.; Bernardi, F., *Mol. Phys.* **1970,** *19*, 553-566.

151. Watson, *J. K. G., in Vibrational Spectra and Structure, Vol. 6 (Ed.: J. R. Durig), Elsevier, New York,* ***1977****, pp. 1- 89.*

152. Mackenzie, R. B.; Dewberry, C. T.; Cornelius, R. D.; Smith, C.; Leopold, K. R., *J. Phys. Chem. A* **2017,** *121*, 855-860.

153. Bolton, K.; Brown, R., *Aust. J. Phys.* **1974,** *27*, 143-146.

154. Császár, A. G.; Czakó, G.; Furtenbacher, T.; Tennyson, J.; Szalay, V.; Shirin, S. V.; Zobov, N. F.; Polyansky, O. L., *J. Chem. Phys.* **2005,** *122*, 214305.

155. Shahi, A.; Arunan, E., *J. Phys. Chem. A* **2015**, *119*, 5650-5657.

156. Barnes, A.J.; Murto, J., *J. Chem. Soc., Faraday Trans. 2: Mol. Chem. Phys.* **1972**, *68*, 1642-1651.

157. Truax, D.R.; Wieser, H.; Lewis, P.N; Roche, R.S., *J. Am. Chem. Soc.* **1974**, *96*, 2327-2338.

158. Schaal, H.; Häber, T.; Suhm, M. A., *J. Phys. Chem. A* **2000**, *104*, 265-274.

159. Yang, Q.; Xie, F.; Lu, T.; Bui, N.; Jäger, W.; Xu, Y., *J. Mol. Spectrosc.* **2021**, *376*, 111408.

160. Yoshida, K.; Yamaguchi, T.; Adachi, T.; Otomo, T.; Matsuo, D.; Takamuku, T.; Nishi, N., *J. Chem. Phys.* **2003**, *119*, 6132-6142.

161. Shahi, A.; Arunan, E., *Phys. Chem. Chem. Phys.* **2015**, *17*, 24774-24782.

162. Johnson, E. R.; Keinan, S.; Mori-Sánchez, P.; Contreras-García, J.;Cohen, A. J.; Yang, W., *J. Am. Chem. Soc.* **2010**, *132*, 6498-6506.

163. Bader, R.F.W., Atoms in Molecules: A Quantum Theory, Oxford University Press, New York, **1990**.

164. Wu, B.; Seifert, N. A.; Oswald, S.; Jäger, W.; Xu, Y., *J. Phys. Chem. A* **2021**, *125*, 5355-5364.

165. Giuliano, B. M.; Favero, L. B.; Maris A.; Caminati, W., *Chem. Eur. J.* **2012**, *18*, 12759-12763.

166. Wu, B.; Xie, F.; Xu, Y., The pyrrole-water complex: *J. Mol. Spectrosc.* **2020,** *374*, 111381.

167. Thomas, J.; Xu, Y., *J. Chem. Phys.* **2014**, *140*, 204308/1-5.

168. Brendel, K.; Mäder, H.; Xu, Y.; Jäger, W., *J. Mol. Spectrosc.* **2011**, *268*, 47-52.

169. Evangelisti, L.; Gou, Q.; Feng, G.; Caminati, W.; Mead, G. J.; Finneran, I. A.; Carroll, P. B.; Blake, G. A., *Phys. Chem. Chem. Phys.* **2017**, *19*, 568-573.

170. Kondo, S.; Hirota, E. J., *J. Mol. Spectrosc.* **1970**, *34*, 97-107.

171. Hirota, E., *J. Phys. Chem.* **1979**, *83*, 1457-1465.

172. Inagaki, F.; Harada, I.; Shimanouchi, T. J., *J. Mol. Spectrosc.* **1973**, *46*, 381-396.

173. Juanes, M.; Saragi, R. T.; Caminati, W.; Lesarri, A. *Chem. Eur. J.* **2019**, *25*, 11402-11411.

174. Jäger, W.; Xu, Y.; Gerry, M. C. L. *J. Chem. Phys.* **1993**, *99*, 919-927.

175. Brupbacher, T.; Makarewicz, J.; Bauder, A. *J. Chem. Phys.* **1994**, *101*, 9736-9746.

176. Harris, S. J.; Janda, K. C.; Novick, S. E.; Klemperer, W. *J. Chem. Phys.* **1975**, *63*, 881-884.

177. Blanco, S.; Melandri, S.; Maris, A.; Caminati, W.; Velino, B.; Kisiel, Z. *Phys. Chem. Chem. Phys.* **2003**, *5*, 1359-1364.

178. Wilson, R. J.; Peebles, S. A.; Antolínez, S.; Sanz, M. E.; Kuczkowski, R. L. *J. Phys. Chem. A* **1998**, *102*, 10630-10635.

179. Tan, X. Q.; Sun, L. H.; Kuczkowski, R. L. *J. Mol. Spectrosc.* **1995**, *171*, 248-264.

180. King, A. K.; Howard, B. J. *J. Mol. Spectrosc.* **2002**, *214*, 97-102.

181. Mani, D.; Arunan, E. *ChemPhysChem.* **2013**, *14*, 754-763.

182. Durig, J. R.; Larsen, R. A.; Cox, F. O.; Van der Veken, B. J. *J. Mol. Struct.* **1988**, *172*, 183-201.

183. Oswald, S.; Suhm, M. A. *Angew. Chem. Int. Ed.,* **2017***, 56*, 12672-12676; *Angew. Chem. Angew. Chem.* **2017,** 129**,** 12846.

184. B. Wu, A. S. Hazrah, N. A. Seifert, S. Oswald, W. Jäger, Y. Xu, *J. Phys. Chem. A*, **2021**, 125, 10401-10409.

185. Xu, Y.; Jäger, W. *J. Chem. Phys.* **1997,** *107*, 4788-4796.

186. Peña, I.; Cabezas, C. *Phys. Chem. Chem. Phys.* **2020,** *22*, 25652-25660.

187. Mata, I.; Alkorta I.; Espinosa, E.; Molins, E. *Chem. Phys. Lett.* **2011,** *507*, 185-189.

188. McKellar, A. R. W.; Xu, Y.; Jäger, W. *J. Phys. Chem. A* **2007,** *111*, 7329-7337.

189. Leung, H. O.; Marshall, M. D.; Wronkovich, M. A. *J. Mol. Spectrosc.* **2017,** *337*, 80-85.

190. Godin, P. J.; Cabaj, A.; Xu, L.-H.; Le Bris, K.; Strong, K., *J. Quant. Spectrosc. Radiat. Transfer*, **2017**, *186*, 150-157.

191. Badawi, H. M.; Förner, W., *Spectrochimi. Acta Part A: Mol. Biomol. Spectrosc.*, **2008**, *71*, 388-397.

192. Juanes, M.; Li, W.; Spada, L.; Evangelisti, L.; Lesarri, A.; Caminati, W., *Phys. Chem. Chem. Phys.*, **2019**, *21*, 3676

193. Xu, Y.; Jäger, W., *J. Chem. Phys.*, **1997**, *107*, 4788-4706.

194. Berkessel, A.; Adrio, J. A.; Hüttenhain, D. J.; Neudörfl, M., *J. Am. Chem. Soc.* **2006**, *128*, 8421-8426

195. Thomas, J.; Xu, Y., *J. Chem. Phys.* **2014**, *140*, 234307/1-5.

196. Xu, Y.; Jäger, W., *J. Chem. Phys.*, **2000**, *113*, 514-524

197. Li, L. Y.; Seifert, N. A.; Xie, F.; Heger, M.; Xu, Y.; Jäger, W., *Phys. Chem. Chem. Phys.* **2018**, *20*, 21345-21351.

198. Medel, R., *Phys. Chem. Chem. Phys.*, **2021**, *23*, 17591-17605

199. Piccardo, M.; Penocchio, E.; Puzzarini, C.; Biczysko, M.; Barone, V., *J. Phys. Chem. A*, **2015**, *119*, 2058−2082

200. Vogt, N.; Demaison, J.; Rudolph, H. D.; Juanes, M.; Fernández, J.; Lesarri, A., *J. Chem. Phys*. **2018**, *148*, 064306

201. Juanes, M.; Usabiaga, I.; León, I.; Evangelisti, L.; Fernández, J. A.; Lesarri, A., *Angew. Chem. Int. Ed.*, *Angew. Chem. Int. Ed.* **2020**, *59* 14081-14085; *Angew. Chem.* **2020**, *132*, 14185-14189.

202. Wu, B.; Seifert, N. A.; Oswald, S.; Jäger, W.; Xu, Y., In International Symposium on Molecular Spectroscopy (Virtual): WA09, **2021**, June 21-25.

203. Macario, A.; Blanco, S.; Thomas, J.; Xu, Y.; López, J. C., *J. Phys. Chem. A,* **2019**, *123*, 6772-6780.

204. Kisiel, Z.; Dorosh, O.; Maeda, A.; Medvedev, I. R.; De Lucia, F. C.; Herbst, E. B.; Drouin, J.; Pearson, J. C.; Shipman, S. T., *Phys. Chem. Chem. Phys.*, **2010**, *12*, 8329-8339.

205. Wu, B.; Seifert, N. A.; Oswald, S.; Jäger, W.; Xu, Y., *J. Phys. Chem. A*, 2021, 125, 5355−5364.

206. Emamian, S.; Lu, T.; Kruse, H.; Emamian, H.; *J. Comput. Chem*. **2019**, *40*, 2868–2881

207. Doroshenko, I.; Vaskivskyi, Y.; Chernolevska, Y.; Meyliev, L.; Kuyliev, B., *Ukr. J. Phys.*, **2020**, *65*, 291-291.

Appendix A

Supporting Information for Chapter 3

The pyrrole-water complex: Multidimensional large amplitude dynamics and rotational spectra of its ^{13}C isotopologues

Contents:

Point S3.1. Gaussian keywords used in the calculations.

Calculations	Employed keywords
Geometry optimization	opt, freq
Anharmonic distortions	Freq=(VCD,Anharmonic)
2D Rigid scan	scan
Transition state calculation	opt=(calcall,ts,noeigentest), scf=verytight, freq, int=grid=SuperFine density=current counterpoise=2
Common to all	output=pickett, empiricaldispersion=gd3bj, b3lyp, Def2-TZVP

Table S3.1. Atomic coordinates of the *crossed* structure of Py_{NH}-W[a]

Atom	Coordinates /Å		
	X	Y	Z
C1	-0.574703	-1.124770	0.000429
C2	-1.879192	-0.687063	-0.000654
C3	-1.846887	0.733629	-0.000636
C4	-0.523731	1.111000	0.000510
N1	0.239562	-0.025052	0.001087
H1	1.250376	-0.045702	0.002111
H2	-0.069963	2.087230	0.000845
H3	-2.693731	1.399525	-0.001378
H4	-2.755528	-1.313629	-0.001405
H5	-0.165219	-2.120245	0.000820
O1	3.218660	-0.032145	-0.000400
H6	3.730559	0.229768	-0.772650
H7	3.737127	0.230810	0.767089

[a] Optimized at the B3LYP-D3(BJ)/def2-TZVP level of theory. This is the global minimum. The atom numbering is in Figure 3.1.

Table S3.2. Atomic coordinates of Py$_{\pi}$-W^{a}

Atom	Coordinates /Å		
	X	Y	Z
C1	-0.603782	-1.180188	0.042883
C2	-0.608113	-0.378357	1.161269
C3	-0.687952	0.970263	0.716231
C4	-0.728404	0.946930	-0.65789
N1	-0.685973	-0.363619	-1.053567
H1	-0.644573	-0.676003	-2.006920
H2	-0.791877	1.745924	-1.376063
H3	-0.718733	1.852262	1.333437
H4	-0.568881	-0.720355	2.181777
H5	-0.557824	-2.250552	-0.058474
O1	2.530423	0.027149	-0.043288
H6	2.121046	0.893292	-0.145979
H7	1.826470	-0.493557	0.365585

[a] Optimized at the B3LYP-D3(BJ)/def2-TZVP level of theory. This is the second most stable conformer. The atom numbering is in Figure 3.1.

Table S3.3. Rotational transition frequencies of the ^{12}C Py$_{NH}$-W complex.

transitions		Lower tunneling doublet		Upper tunneling doublet	
$J'_{Ka\,Kc'}$ - $J''_{Ka''}$	F'-F''	freq (MHz)	obs-calc	freq (MHz)	obs-calc
101 – 000	0-1	3029.2249	0.0009		
	1-1	3029.9136	0.0006	3030.4103	0.0039
	2-1	3029.6372	-0.0002	3030.1342	0.0011
202 - 101	1-0	6053.4672	-0.0032	6054.4001	-0.0050
	1-1	6052.7778	-0.0037	6053.7251	0.0032
	2-1			6054.2077	-0.0006
	2-2	6053.5499	0.0028	6054.4788	-0.0028
	3-2	6053.2292	-0.0029	6054.1705	0.0016
211 - 110	1-0	6305.5020	0.0022	6306.2236	-0.0003
	1-1	6307.2612	0.0033	6307.9726	-0.0023
	2-1	6306.5499	0.0048	6307.2636	-0.0008
	2-2	6305.8380	-0.0038	6306.5644	-0.0004
	3-2	6306.3001	0.0001	6307.0257	0.0042
212 - 111	1-0	5812.0271	-0.0013		

	1-1	5810.9621	0.0027	5812.2363	-0.0039
	1-2	5811.3873	0.0003		
	2-1	5812.1317	0.0003	5813.4013	-0.0047
	2-2	5812.5574	-0.0016	5813.8318	-0.0004
	3-2	5811.8083	0.0028	5813.0802	-0.0025
303 - 202	2-1			9065.9345	0.0015
	2-2			9065.4424	-0.0042
	3-2	9064.6553	-0.0008	9065.9274	0.0014
	3-3			9066.2343	-0.0045
	4-3	9064.6113	-0.0024	9065.8855	0.0019
312 - 211	2-1			9456.4976	0.0000
	2-2	9455.4382	0.0021	9457.2021	-0.0060
	3-2			9456.6823	0.0023
	3-3	9455.6202	0.0006	9456.2260	0.0026
	4-3	9455.5545	0.0010	9456.6149	0.0006
313 - 212	2-1	8714.1309	-0.0007	8716.0083	-0.0031
	2-2			8714.8495	0.0040
	3-2	8714.1309	0.0046	8716.0083	0.0024
	3-3			8716.7537	-0.0017
	4-3	8714.0196	0.0041	8715.8984	0.0026
321 - 220	3-2	9112.0837	-0.0037	9113.8390	-0.0043
	4-3	9111.8188	-0.0048	9113.5805	-0.0016
322 - 221	2-1	9087.3096	-0.0014	9088.8417	0.0013
	2-2	9087.7689	0.0012	9089.2999	0.0039
	3-2	9087.7689	0.0012		
	3-3			9089.0087	0.0056
	4-3	9087.4737	0.0015	9089.0087	0.0056
404 - 303	3-2	12057.856	0.0025	12059.302	0.0063
	4-3	12057.879	-0.0036	12059.325	-0.0011
	5-4	12057.831	-0.0014	12059.276	0.0000
414 - 313	3-2	11611.841	-0.0031	11614.289	0.0007
	3-3			11613.126	-0.0017
	4-3	11611.841	0.0010	11614.286	-0.0024
	4-4			11615.150	0.0061
	5-4	11611.781	0.0018	11614.224	-0.0002
422 - 321	3-2	12172.549	0.0050	12175.123	-0.0014

	4-3	12172.650	-0.0091		
	5-4	12172.576	0.0047	12175.150	-0.0015
423 - 322	3-2	12111.836	0.0013	12113.844	0.0063
	4-3	12111.999	0.0008	12114.007	-0.0067
505 - 404	4-3			15028.725	0.0039
	5-4			15028.767	-0.0023
	6-5			15028.704	-0.0068
514 – 515	4-4			3701.6927	0.0039
	5-5			3700.1253	-0.0032
	6-6			3701.4254	-0.0007

The observed transitions are all weighted the same except those marked with [a] are weighted 1/2 and those with [b] are weighted with 1/3.

Table S3.4. Rotational transition frequencies of the $^{13}C1/^{13}C4$ Py_{NH}-W complex.

transitions		Lower tunneling doublet		Upper tunneling doublet	
$J'_{K_a K_c'}$ - J''_{K_a}	*F'-F''*	freq (MHz)	obs-calc	freq (MHz)	obs-calc
101 - 000	0-1	3021.6998	0.0045		
	1-1	3022.3751	-0.0013	3022.6002	-0.0004
	2-1	3022.1031	-0.0008	3022.8751	0.0018
202 - 101	1-0	6038.0237	0.0005	6038.9573	0.0006
	1-1	6037.3374	-0.0048	6038.2751	0.0002
	2-1	6037.8315	0.0033	6038.7618	-0.0002
	3-2	6037.7886	0.0004	6038.7223	0.0007
	2-2	6038.0959	-0.0047		
211 - 110	1-1	6296.5002	-0.0006	6297.2302	-0.0015
	2-1	6295.8007	0.0120	6296.5125	-0.0016
	2-2			6295.8114	0.0005
	3-2	6295.5505	0.0037	6296.2751	0.0030

212 - 111	1-0	5792.6569	0.0015 [a]	5793.9301	0.0032
	2-1	5792.7498	-0.0037	5794.0263	0.0035
	3-2	5792.4384	0.0073	5793.6999	0.0001
303 – 202	2-1			9041.8058	-0.0044
	2-2	9040.5067	-0.0034		
	3-2	9040.5510	-0.0026	9041.8058	0.0005
	4-3			9041.7631	0.0019
312 - 211	2-1			9440.1370	-0.0007
	3-2			9440.3205	-0.0006
	4-3			9440.2534	-0.0021
313 - 212	2-1			8686.7030	-0.0042
	3-2	8684.8392	0.0048	8686.7030	0.0018
	4-3	8684.7290	0.0046	8686.5900	-0.0009
321 - 220	2-1	9090.5931	-0.0057		
	3-2	9091.0156	0.0027		
	4-3	9090.7521	-0.0016	9092.5076	0.0031
404 - 303	3-2	12023.982	-0.0018		
	4-3	12024.008	-0.0073	12025.418	0.0073
	5-4	12023.961	-0.0033	12025.357	-0.0021
414 - 313	3-2			11574.791	-0.0077
	4-3	11572.367	-0.0052	11574.791	-0.0038
	5-4	11572.311	0.0001	11574.730	-0.0042
505 – 404	4-3			14983.582	-0.0056
	5-4			14983.644	0.0046
	6-5	14982.263	0.0071	14983.579	0.0010

The observed transitions are all weighted the same except those marked with [a] are weighted ½.

Table S3.5. Rotational transition frequencies of the ^{13}C2/^{13}C3 Py$_{NH}$-W complex.

transitions		Lower tunneling doublet		Upper tunneling doublet	
$J'_{Ka\ Kc'}$ - J''_{Ka}	*F'-F''*	freq (MHz)	obs-calc	freq (MHz)	obs-calc
101 - 000	0-1			2996.2534	0.0045
	1-1	2996.4449	-0.0008	2996.9405	0.0032
	2-1	2996.1724	0.0014	2996.6688	0.0069
202 - 101	1-0	5986.6497	0.0008	5987.5763	-0.0022
	1-1	5985.9615	-0.0008	5986.8868	-0.0033
	2-1	5986.4499	-0.0007	5987.3753	-0.0047
	3-2	5986.4123	0.0009	5987.3379	-0.0025
211 - 110	1-0	6235.3746	0.0006		
	1-1	6237.1255	0.0001		
	2-1	6236.4139	-0.0015	6237.1132	0.0001
	2-2			6236.4103	0.0007
	3-2	6236.1686	-0.0026	6236.8655	-0.0028
212 - 111	1-0	5748.3735	0.0005	5749.6299	-0.0021
	1-1			5748.5599	-0.0019
	2-1	5748.4748	-0.0011	5749.7353	0.0011
	2-2			5750.1618	-0.0005
	3-2	5748.1503	-0.0008	5749.4099	0.0013
303 - 202	2-1	8964.7106	-0.0006	8965.9715	-0.0019
	3-2			8965.9715	0.0054
	4-3	8964.6619	0.0005	8965.9249	0.0013
313 - 212	2-1	8618.6409	-0.0017	8620.5717	-0.0026
	3-2			8620.5717	0.0028
	4-3			8620.4682	0.0100
404 - 303	3-2			11926.537	-0.0024
	4-3			11926.567	-0.0015

The observed transitions are all weighted the same except those marked with ^{a} are weighted ½.

Table S3.6. Atom coordinates of the *symmetric crossed* structure of $\mathrm{Py}_{\mathrm{NH}}$-W.[a]

Atom	Coordinates /Å		
	X	Y	Z
C1	0.549709	1.118195	0.000000
C2	1.863862	0.710532	0.000000
C3	1.863855	-0.710538	0.000000
C4	0.549699	-1.118205	0.000000
N1	-0.239166	0.000007	0.000000
H1	-1.249796	0.000008	0.000000
H2	0.117709	-2.104157	0.000000
H3	2.725629	-1.356992	0.000000
H4	2.725638	1.356988	0.000000
H5	0.117728	2.104173	0.000000
O1	-3.214006	0.000017	0.000000
H6	-3.790486	-0.000110	-0.770700
H7	-3.790486	-0.000110	0.770700

[a] Optimized at the B3LYP-D3(BJ)/def2-TZVP level of theory with “scf=verytight int=grid=SuperFine”. This is a transition state with one imaginary frequency at 96 cm^{-1}. The atom numbering is in Figure 3.1.

Table S1.7. Atom coordinates of the *hinged* structure of $\mathrm{Py}_{\mathrm{NH}}$-W.[a]

Atom	Coordinates /Å		
	X	Y	Z
C1	0.553164	-1.117970	-0.028050
C2	1.865340	-0.710390	0.044619
C3	1.865340	0.710390	0.044619
C4	0.553164	1.117970	-0.028050
N1	-0.234700	0.000000	-0.072680
H1	-1.245050	0.000000	-0.115670
H2	0.123615	2.104720	-0.054990
H3	2.725816	1.356900	0.090278
H4	2.725816	-1.356900	0.090278
H5	0.123615	-2.104720	-0.054990
O1	-3.241670	0.000000	-0.007140
H6	-3.669270	0.767820	0.386939
H7	-3.669270	-0.767820	0.386939

[a] Optimized at the B3LYP-D3(BJ)/def2-TZVP level of theory with “scf=verytight int=grid=SuperFine”. This is a transition state with one imaginary frequency at 85 cm^{-1}. The atom numbering is in Figure 3.1.

Table S3.8. Atom coordinates of the *planar hinged* structure of Py_{NH}-W.[a]

Atom	Coordinates /Å		
	X	Y	Z
C1	0.549678	-1.118200	0.000005
C2	0.549711	1.118210	0.000017
C3	1.863863	0.710524	-0.000011
C4	1.863847	-0.710556	-0.000016
N1	-0.239175	0.000018	0.000021
H1	-1.249795	0.000035	0.000041
H2	0.117738	2.104179	0.000024
H3	2.725651	1.356957	-0.000023
H4	2.725609	-1.357013	-0.000034
H5	0.117671	-2.104151	0.000008
O6	-3.213985	0.000009	-0.000010
H6	-3.790465	-0.000240	0.770690
H7	-3.790385	0.000094	-0.770770

[a] Optimized at the B3LYP-D3(BJ)/def2-TZVP level of theory with “scf=verytight int=grid=SuperFine”. This is a transition state with one imaginary frequency at 96 cm^{-1}. The atom numbering is in Figure 3.1.

Table S3.9. Energetic and other properties of the four geometries of Py_{NH}-W.[a]

Geometry	*crossed*	*sym. crossed*	*hinged*	*planar hinged*
Imaginary frequency	none	one	one	one
Raw Energy/ Hartree	-286.74011	-286.74007	-286.73945	-286.73945
ZPE correction/ Hartree	0.10551	0.10519	0.10541	0.10541
BSSE correction/ Hartree	0.00083	0.00072	0.00079	0.00079
Corrected energy/ Hartree	-286.63377	-286.63416	-286.63325	-286.63325
$\Delta E_{corr.}$/ Hartree [b]	0.0000	-0.00039	0.00052	0.00052
$\Delta E_{corr.}$/ kJ·mol^{-1} [b]	0.0	-1.0	1.4	1.4

[a] Calculated at the B3LYP-D3(BJ)/def2-TZVP level of theory.

[b] Relative energies corrected for both *ZPE* and *BSSE*.

Table S3.10. Effective structural parameters from SRFTIT of the pyrrole and water monomers.[a]

Distance	/ Å	Angle	/ °
		Pyrrole monomer	
N1-C1=N1-C4	1.3766(24)	N1-C1-C2 = N1-C4-C3	107.82(17)
C1-C2 (C4-C3)	1.3797(30)	C1-C2-C3= C4-C3-C2[b]	107.36
C(2)-C(3)[b]	1.4271	C1-N1-C4	109.64(23)
N1-H1	0.9931(21)	H1-N1-C1=H1-N1-C4	125.18(13)
C1-H5=C4-H2	1.0737(15)	H2-C4-N1=H5-C1-N1	121.76(96)
C2-H4=C3-H3	1.0750(17)	H2-C4-C3=H5-C1-C2[b]	130.42
		Water	
O1-H6=O1-H7	0.9654(21)	H6-O1-H7	104.68(45)

[a] Effective structural parameters obtained the fits to the effective rotational constants of several pyrrole isotopologues in Ref. 3 and several water isotopologues Ref. 42. The atom numbering is shown in Figure 3.1.

[b] Parameters calculated from the corresponding geometries obtained in the STRFIT fits.

Table S3.11. Atomic coordinates of $\mathrm{Py_{NH}}$-W (lower tunneling state) based on the STRFIT geometry.[a]

Atom	Coordinates /Å		
	X	Y	Z
C1	0.560031	-1.124490	0.000000
C2	1.876438	-0.711296	0.000000
C3	1.874733	0.715763	0.000000
C4	0.557342	1.125809	0.000000
N1	-0.234463	-0.000288	0.000000
H1	-1.227532	-0.001475	0.000000
H2	0.135531	2.113225	0.000000
H3	2.729785	1.367365	0.000000
H4	2.733045	-1.360853	0.000000
H5	0.140582	-2.112911	0.000000
X_{py}	0.890426	0.001062	0.000000
X_w	-3.313873	-0.003984	0.000000
O1	-3.261051	-0.043424	0.000000
H6	-3.733681	0.309469	0.764231
H7	-3.733681	0.309469	-0.764230

[a] Fitted to the effective rotational constants of the lower tunneling states of all isotopologues of $\mathrm{Py_{NH}}$-W. The atom numbering is given in Figure 3.1. X_{py} and X_w are the centre-of-mass of pyrrole and water, respectively.

Appendix B

Supporting Information for Chapter 4

A higher energy hexafluoroisopropanol···water isomer and its large amplitude motions: rotational spectra and DFT calculations

Contents:

Point S4.1. Gaussian keywords used in the calculations.

Calculations	Employed keywords
Geometry optimization	Freq, fopt=(verytight,MaxCycles=200), int=superfine, output=picket
Harmonic calculation	Freq=(VCD,VibRot)
Transition calculation	opt=(calcall,ts,noeigentest), scf=verytight, int=grid=SuperFine
Rigid PES scan	scan
BSSE correction	density=current, counterpoise=2
Common to all	b3lyp, Def2-QZVP, empiricaldispersion=gd3bj, output=picket

Table S4.1. Cartesian coordinates (in Å) of $\mathrm{HFIP}_{t}\cdots\mathrm{W}_{\mathrm{H}}$.

Atom	X	Y	Z
C	1.307284	0.415189	0.013517
C	0.012821	0.208002	0.825906
H	0.037234	0.954517	1.620819
C	-1.270550	0.493168	0.019978
F	2.368575	0.209222	0.804202
F	1.401999	-0.448393	-1.019216
F	1.403778	1.656132	-0.484320
F	-1.285756	1.728350	-0.498723
F	-2.337589	0.371212	0.818396
F	-1.432262	-0.378668	-1.001165
O	-0.024623	-1.044123	1.415480
H	-0.059627	-1.756576	0.743799
O	-0.150629	-3.089546	-0.442671
H	0.701741	-3.252514	-0.856434
H	-0.726488	-2.784776	-1.150318

Table S4.2. Cartesian coordinates (in Å) of $\mathrm{HFIP}_t\cdots\mathrm{W}_\mathrm{O}$.

Atom	X	Y	Z
C	1.379701	0.087231	-0.086456
C	-0.125374	0.380039	0.028207
H	-0.398511	1.039746	-0.794049
C	-1.02075	-0.866766	-0.066321
F	2.060163	1.239771	-0.100856
F	1.817981	-0.62804	0.970001
F	1.685111	-0.587656	-1.199562
F	-0.822647	-1.552967	-1.196520
F	-2.308076	-0.494565	-0.030336
F	-0.813001	-1.700311	0.972291
O	-0.393367	1.077774	1.215211
H	-0.144104	0.540844	1.975474
O	-1.439339	3.150945	-0.492196
H	-2.359888	3.413585	-0.559633
H	-1.321903	2.846069	0.414111

Table S4.3. Cartesian coordinates (in Å) of $\mathrm{HFIP}_t\cdots\mathrm{W}_\mathrm{C}$.

Atom	X	Y	Z
C	0.929366	0.771500	0.092867
C	0.001397	-0.322650	-0.461909
H	0.455900	-1.277057	-0.199164
C	-1.415676	-0.299314	0.133456
F	2.171241	0.594321	-0.397710
F	0.526349	2.000295	-0.285477
F	1.015512	0.755619	1.425784
F	-1.415091	-0.372427	1.469376
F	-2.114581	-1.342928	-0.334448
F	-2.078737	0.821114	-0.221466
O	-0.053599	-0.246961	-1.857745
H	-0.456372	0.588416	-2.119375
O	2.314902	-2.415684	0.219734
H	3.003422	-1.827943	-0.103099
H	2.610528	-3.303497	0.004925

Table S4.4. Cartesian coordinates (in Å) of HFIP$_t$···W$_F$.

Atom	X	Y	Z
C	-1.293593	0.276052	0.122834
C	0.000000	1.089587	0.317719
H	0.000000	1.442961	1.347766
C	1.293593	0.276052	0.122834
F	-2.349968	1.039618	0.422049
F	-1.428053	-0.132848	-1.149421
F	-1.339143	-0.809743	0.914484
F	1.339143	-0.809743	0.914484
F	2.349968	1.039618	0.422049
F	1.428053	-0.132848	-1.149421
O	0.000000	2.211107	-0.511629
H	0.000000	1.933812	-1.434923
O	0.000000	-3.501935	-0.352580
H	-0.759586	-3.047890	0.020088
H	0.759586	-3.047890	0.020088

Table S4.5. Cartesian coordinates (in Å) of HFIP$_g$···W$_H$.

Atom	X	Y	Z
C	-0.671926	1.007676	0.000671
C	-0.08268	-0.402811	-0.204535
H	-0.320683	-0.680681	-1.235338
C	1.448847	-0.446327	-0.092266
F	-2.024924	0.920377	-0.038938
F	-0.343010	1.551405	1.173828
F	-0.306746	1.853850	-0.973521
F	2.024626	0.443191	-0.920367
F	1.885741	-1.666284	-0.442313
F	1.879161	-0.195454	1.147283
O	-0.597074	-1.292189	0.729591
H	-1.463574	-1.608241	0.416884
O	-3.057002	-1.898904	-0.368081
H	-3.594199	-1.110402	-0.247582
H	-3.612571	-2.644564	-0.126939

Table S4.6. Cartesian coordinates (in Å) of HFIP$_g$···W$_F$.

Atom	X	Y	Z
C	-1.316195	0.091418	0.135722
C	-0.156816	1.101685	0.240530
H	-0.217728	1.531984	1.244375
C	1.233926	0.459369	0.129852
F	-2.473876	0.783656	0.084643
F	-1.252596	-0.669043	-0.964631
F	-1.370310	-0.713181	1.201479
F	1.364069	-0.546031	1.018767
F	2.173407	1.370428	0.406158
F	1.474969	-0.034070	-1.085883
O	-0.232377	2.061213	-0.770821
H	-1.021762	2.596523	-0.650301
O	0.524875	-3.430456	-0.382171
H	-0.000253	-2.855152	-0.943800
H	1.034165	-2.833011	0.170819

Table S4.7. Rotational transition frequencies of the parent HFIP$_g$···W$_H$ complex.

J'	*K*$_a$'	*K*$_c$'	*J"*	*K*$_a$"	*K*$_c$"	Obs/ MHz	Cal/ MHz	Obs - Cal/ MHz
1	1	0	0	0	0	2099.1506	2099.1461	0.0045
3	2	2	3	0	3	2379.6005	2379.5919	0.0086
4	2	3	4	1	4	2678.6373	2678.6356	0.0017
2	1	2	1	1	1	2732.7892	2732.7969	-0.0077
4	2	3	4	0	4	2745.1754	2745.1685	0.0069
2	0	2	1	0	1	2878.7894	2878.7928	-0.0034

2	1	1	1	1	0	3137.7613	3137.7572	0.0041
2	1	2	1	0	1	3161.8254	3161.8216	0.0038
5	2	4	5	1	5	3226.2879	3226.2836	0.0043
5	2	4	5	0	5	3252.6667	3252.6637	0.0030
2	1	1	1	0	1	3769.2622	3769.2631	-0.0009
6	2	5	6	1	6	3848.5638	3848.5651	-0.0013
6	2	5	6	0	6	3858.3002	3858.3068	-0.0066
5	1	4	4	3	1	3890.3253	3890.3271	-0.0018
3	0	3	2	1	2	3917.9118	3917.9139	-0.0021
3	1	3	2	1	2	4067.6901	4067.6879	0.0022
3	0	3	2	0	2	4200.9385	4200.9427	-0.0042
3	1	3	2	0	2	4350.7123	4350.7167	-0.0044
3	2	2	2	2	1	4402.9074	4402.9098	-0.0024
2	2	1	1	1	0	4424.9105	4424.9118	-0.0013
2	2	0	1	1	0	4481.3885	4481.3947	-0.0062
3	2	1	2	2	0	4604.8751	4604.8690	0.0061
2	2	1	1	1	1	4627.3895	4627.3930	-0.0035
3	1	2	2	1	1	4664.7999	4664.8046	-0.0047
2	2	0	1	1	1	4683.8748	4683.8759	-0.0011
4	1	3	3	2	1	4844.7106	4844.7088	0.0018
4	1	3	3	2	2	5103.1508	5103.1510	-0.0002
2	2	0	1	0	1	5112.9011	5112.9006	0.0005
4	0	4	3	1	3	5310.3882	5310.3875	0.0007
4	1	4	3	1	3	5376.9252	5376.9205	0.0047
4	0	4	3	0	3	5460.1631	5460.1616	0.0015

4	1	4	3	0	3	5526.6885	5526.6945	-0.0060
3	2	2	2	1	1	5690.0631	5690.0643	-0.0012
4	2	3	3	2	2	5825.7388	5825.7381	0.0007
3	2	1	2	1	1	5948.5001	5948.5065	-0.0064
4	3	2	3	3	1	5959.1752	5959.1816	-0.0064
4	3	1	3	3	0	6017.5999	6017.5956	0.0043
4	1	3	3	1	2	6128.4128	6128.4107	0.0021
4	2	2	3	2	1	6234.5363	6234.5386	-0.0023
3	2	2	2	1	2	6297.4998	6297.5058	-0.0060
5	0	5	4	1	4	6639.4368	6639.4310	0.0058
5	1	5	4	1	4	6665.8129	6665.8111	0.0018
5	0	5	4	0	4	6705.9655	6705.9639	0.0016
5	1	5	4	0	4	6732.3504	6732.3440	0.0064
5	1	4	4	2	3	6775.7257	6775.7216	0.0041
4	2	3	3	1	2	6851.0006	6850.9978	0.0028
5	2	4	4	2	3	7213.4614	7213.4591	0.0023
5	3	3	4	3	2	7449.4626	7449.4662	-0.0036
5	1	4	4	1	3	7498.3127	7498.3088	0.0039
5	3	2	4	3	1	7629.1254	7629.1228	0.0026
5	2	3	4	2	2	7833.6249	7833.6279	-0.0030
6	1	6	5	1	5	7941.9865	7941.9845	0.0020
6	0	6	5	0	5	7958.6252	7958.6230	0.0022
6	2	5	5	2	4	8564.2622	8564.2661	-0.0039
6	1	5	5	1	4	8775.0114	8775.0071	0.0043
7	1	6	6	1	5	10005.5754	10005.5754	0.0000

8	1	8	7	1	7	10478.3132	10478.3154	-0.0022
8	0	8	7	0	7	10480.5745	10480.5781	-0.0036

Table S4.8. Rotational transition frequencies of HFIP$_g$(OH)···HOD4.

J'	K_a'	K_c'	J''	K_a''	K_c''	Obs/ MHz	Cal/ MHz	Obs - Cal/ MHz
2	1	2	1	1	1	2683.9768	2683.9777	-0.0009
2	0	2	1	0	1	2827.5618	2827.5618	0.0000
2	1	1	1	1	0	3073.4551	3073.4539	0.0012
3	1	3	2	1	2	3997.2793	3997.2805	-0.0012
3	0	3	2	0	2	4133.0909	4133.0911	-0.0002
3	1	3	2	0	2	4299.5549	4299.5571	-0.0022
3	2	2	2	2	1	4318.0673	4318.0686	-0.0013
2	2	1	1	1	0	4411.1144	4411.1137	0.0007
3	2	1	2	2	0	4503.0410	4503.0408	0.0002
3	1	2	2	1	1	4572.7381	4572.7369	0.0012
2	2	1	1	1	1	4605.8554	4605.8527	0.0027
2	2	0	1	1	1	4657.0091	4657.0058	0.0033
4	1	3	3	2	2	4932.6373	4932.6345	0.0028
4	0	4	3	1	3	5209.2566	5209.2594	-0.0028
4	1	4	3	1	3	5286.6044	5286.6053	-0.0009

4	0	4	3	0	3	5375.7263	5375.7253	0.0010
4	2	3	3	2	2	5716.9378	5716.9361	0.0017
4	3	2	3	3	1	5838.7448	5838.7452	-0.0004
4	3	1	3	3	0	5888.6613	5888.6623	-0.0010
3	2	1	2	1	1	5891.8508	5891.8537	-0.0029
4	1	3	3	1	2	6015.6285	6015.6260	0.0025
4	2	2	3	2	1	6097.3761	6097.3775	-0.0014
5	0	5	4	1	4	6524.1675	6524.1686	-0.0011
5	1	5	4	1	4	6556.2501	6556.2507	-0.0006
5	0	5	4	0	4	6601.5127	6601.5145	-0.0018
5	1	5	4	0	4	6633.6008	6633.5967	0.0041
5	2	4	4	2	3	7083.7503	7083.7449	0.0054
5	3	3	4	3	2	7300.9597	7300.9618	-0.0021
5	4	2	4	4	1	7309.7501	7309.7471	0.0030
5	4	1	4	4	0	7319.3121	7319.3118	0.0003
5	1	4	4	1	3	7373.7379	7373.7351	0.0028
4	2	2	3	1	2	7416.4897	7416.4943	-0.0046
5	3	2	4	3	1	7456.9787	7456.9790	-0.0003
5	2	3	4	2	2	7669.3856	7669.3894	-0.0038
6	1	6	5	1	5	7813.0379	7813.0403	-0.0024
6	0	6	5	0	5	7832.7371	7832.7369	0.0002
6	2	5	5	2	4	8416.1861	8416.1855	0.0006
6	1	5	5	1	4	8641.6255	8641.6233	0.0022
6	3	4	5	3	3	8743.4132	8743.4179	-0.0047
6	3	3	5	3	2	9081.6752	9081.6731	0.0021

Table S4.9. Rotational transition frequencies of $HFIP_g(OH)\cdots HOD3$.

J'	*K*a'	*K*c'	*J"*	*K*a"	*K*c"	Obs/ MHz	Cal/ MHz	Obs - Cal/ MHz
2	1	2	1	1	1	2671.7289	2671.7303	-0.0014
2	0	2	1	0	1	2815.9835	2815.9837	-0.0002
2	1	1	1	1	0	3070.7448	3070.7439	0.0009
3	1	3	2	1	2	3976.7555	3976.7559	-0.0004
3	0	3	2	0	2	4109.0058	4109.006	-0.0002
3	2	2	2	2	1	4306.8502	4306.8507	-0.0005
2	2	1	1	1	0	4350.9874	4350.9868	0.0006
2	2	0	1	1	0	4406.2372	4406.2388	-0.0016
3	2	1	2	2	0	4504.6866	4504.6867	-0.0001
3	1	2	2	1	1	4565.2582	4565.2563	0.0019
4	0	4	3	1	3	5189.4861	5189.4875	-0.0014
4	1	4	3	1	3	5256.5876	5256.5857	0.0019
4	0	4	3	0	3	5339.7005	5339.7026	-0.0021
4	1	4	3	0	3	5406.8032	5406.8008	0.0024
4	2	3	3	2	2	5698.6502	5698.6513	-0.0011
4	3	2	3	3	1	5829.3103	5829.3086	0.0017
4	3	1	3	3	0	5886.0496	5886.0507	-0.0011
4	1	3	3	1	2	5997.8502	5997.8513	-0.0011
4	2	2	3	2	1	6099.8899	6099.889	0.0009
5	0	5	4	1	4	6489.6027	6489.6034	-0.0007
5	1	5	4	1	4	6516.3537	6516.3549	-0.0012
5	0	5	4	0	4	6556.7003	6556.7016	-0.0013

5	1	5	4	0	4	6583.4543	6583.4531	0.0012
5	2	4	4	2	3	7056.0752	7056.0761	-0.0009
5	3	3	4	3	2	7287.3923	7287.3933	-0.001
5	4	1	4	4	0	7311.5505	7311.5502	0.0003
5	1	4	4	1	3	7338.7749	7338.7728	0.0021
6	0	6	5	0	5	7780.3358	7780.3344	0.0014

Table S4.10. Rotational transition frequencies of the parent $\mathrm{HFIP}_g\mathrm{(OH)\cdots D_2O}$.

J'	K_a'	K_c'	J''	K_a''	K_c''	Obs/ MHz	Cal/ MHz	Obs - Cal/ MHz
2	0	2	1	0	1	2766.7869	2766.786	0.0009
2	1	1	1	1	0	3008.5032	3008.5025	0.0007
3	1	3	2	1	2	3909.3926	3909.3935	-0.0009
3	0	3	2	0	2	4044.2192	4044.2202	-0.0010
3	2	2	2	2	1	4225.0814	4225.082	-0.0006
3	2	1	2	2	0	4405.9374	4405.9372	0.0002
3	1	2	2	1	1	4476.2572	4476.2565	0.0007
4	1	4	3	1	3	5170.3293	5170.3293	0.0000
4	0	4	3	0	3	5259.4186	5259.4187	-0.0001
4	1	4	3	0	3	5337.6661	5337.6651	0.0010
4	2	3	3	2	2	5593.9241	5593.9242	-0.0001
4	3	2	3	3	1	5712.9776	5712.9779	-0.0003
4	3	1	3	3	0	5761.2964	5761.2969	-0.0005

4	1	3	3	1	2	5889.1031	5889.1028	0.0003
4	2	2	3	2	1	5966.7396	5966.7391	0.0005
3	2	1	2	1	2	6363.3001	6363.3005	-0.0004
5	0	5	4	1	4	6379.2106	6379.211	-0.0004
5	1	5	4	1	4	6411.8753	6411.8758	-0.0005
5	0	5	4	0	4	6457.4582	6457.4574	0.0008
5	1	5	4	0	4	6490.1226	6490.1222	0.0004
5	2	4	4	2	3	6931.4316	6931.4326	-0.0010
5	1	4	4	1	3	7219.2253	7219.2254	-0.0001
5	1	4	4	1	3	7219.2258	7219.2254	0.0004
5	3	2	4	3	1	7295.3253	7295.3252	0.0001
5	3	2	4	3	1	7295.3254	7295.3252	0.0002

Table S4.11. Rotational transition frequencies of HFIP$_g$(OD)$\cdots$H$_2$O.

J'	K_a'	K_c'	J''	K_a''	K_c''	Obs/ MHz	Cal/ MHz	Obs - Cal/ MHz
2	1	2	1	1	1	2718.9699	2718.9718	-0.0019
2	0	2	1	0	1	2864.6632	2864.6635	-0.0003
2	1	1	1	1	0	3124.6504	3124.6524	-0.0020
3	1	3	2	1	2	4046.6135	4046.6124	0.0011
3	0	3	2	0	2	4178.7702	4178.7727	-0.0025
3	2	2	2	2	1	4382.7137	4382.7127	0.0010
2	2	1	1	1	0	4397.5354	4397.5341	0.0013

3	2	1	2	2	0	4586.6425	4586.6449	-0.0024
3	1	2	2	1	1	4644.5688	4644.5682	0.0006
4	0	4	3	1	3	5283.8923	5283.8911	0.0012
4	1	4	3	1	3	5348.4411	5348.4390	0.0021
4	0	4	3	0	3	5430.3052	5430.3062	-0.0010
4	1	4	3	0	3	5494.8526	5494.8541	-0.0015
4	2	3	3	2	2	5798.2678	5798.2668	0.0010
4	3	2	3	3	1	5933.0949	5933.0955	-0.0006
4	3	1	3	3	0	5992.7574	5992.7601	-0.0027
4	1	3	3	1	2	6100.1007	6100.0994	0.0013
4	2	2	3	2	1	6209.9438	6209.9417	0.0021
5	0	5	4	1	4	6604.5261	6604.5272	-0.0011
5	1	5	4	1	4	6629.9286	6629.9267	0.0019
5	0	5	4	0	4	6669.0751	6669.0752	-0.0001
5	1	5	4	0	4	6694.4746	6694.4746	0.0000
4	2	3	3	1	2	6809.2913	6809.2930	-0.0017
5	2	4	4	2	3	7178.3582	7178.3586	-0.0004
5	3	3	4	3	2	7416.4745	7416.4745	0.0000
5	1	4	4	1	3	7460.8582	7460.8559	0.0023
6	1	6	5	1	5	7898.8001	7898.8011	-0.0010
6	0	6	5	0	5	7914.8915	7914.8907	0.0008

Table S4.12. Rotational transition frequencies of HFIP$_g$(OD)···HOD4.

J'	*K*a'	*K*c'	*J"*	*K*a"	*K*c"	Obs/ MHz	Cal/ MHz	Obs - Cal/ MHz
2	0	2	1	0	1	2814.0697	2814.0692	0.0005
2	1	1	1	1	0	3060.9001	3060.8997	0.0004
3	1	3	2	1	2	3977.1038	3977.1039	-0.0001
3	0	3	2	0	2	4111.9274	4111.9263	0.0011
3	1	3	2	0	2	4274.8942	4274.8959	-0.0017
3	2	2	2	2	1	4298.7171	4298.7182	-0.0011
3	2	1	2	2	0	4485.5035	4485.5043	-0.0008
3	1	2	2	1	1	4553.4037	4553.4023	0.0014
4	0	4	3	1	3	5184.1553	5184.1564	-0.0011
4	1	4	3	1	3	5259.3393	5259.3404	-0.0011
4	0	4	3	0	3	5347.1267	5347.126	0.0007
4	1	4	3	0	3	5422.3092	5422.31	-0.0008
3	1	2	2	0	2	5436.4468	5436.4476	-0.0008
4	2	3	3	2	2	5690.6511	5690.6526	-0.0015
4	3	2	3	3	1	5813.7168	5813.7162	0.0006
4	3	1	3	3	0	5864.6897	5864.6895	0.0002
4	1	3	3	1	2	5988.6877	5988.6865	0.0012
4	2	2	3	2	1	6073.8515	6073.85	0.0015
5	0	5	4	1	4	6490.9121	6490.913	-0.0009
5	1	5	4	1	4	6521.8754	6521.8757	-0.0003
5	0	5	4	0	4	6566.1002	6566.0971	0.0031
5	1	5	4	0	4	6597.0603	6597.0597	0.0006

5	2	4	4	2	3	7050.2004	7050.1985	0.0019
5	3	3	4	3	2	7269.3657	7269.3663	-0.0006
5	4	1	4	4	0	7288.6609	7288.6621	-0.0012
5	1	4	4	1	3	7338.1707	7338.1702	0.0005
6	1	6	5	1	5	7771.6289	7771.6302	-0.0013
6	0	6	5	0	5	7790.7246	7790.7236	0.001
6	2	5	5	2	4	8375.1255	8375.1265	-0.001

Table S4.13. Rotational transition frequencies of HFIP$_g$(OD)···HOD3.

J’	K_a’	K_c’	*J”*	K_a”	K_c”	Obs/ MHz	Cal/ MHz	Obs - Cal/ MHz
2	0	2	1	0	1	2802.5334	2802.5331	0.0003
3	1	3	2	1	2	3956.8614	3956.8625	-0.0011
3	0	3	2	0	2	4088.1988	4088.1977	0.0011
3	2	2	2	2	1	4287.3413	4287.3391	0.0022
3	2	1	2	2	0	4486.4752	4486.477	-0.0018
3	1	2	2	1	1	4545.5123	4545.5141	-0.0018
4	0	4	3	1	3	5164.2741	5164.2738	0.0003
4	1	4	3	1	3	5229.8129	5229.8123	0.0006
4	0	4	3	0	3	5311.8372	5311.8372	0.0000
4	1	4	3	0	3	5377.3746	5377.3757	-0.0011
4	2	3	3	2	2	5672.2685	5672.2715	-0.0030
4	3	2	3	3	1	5803.8495	5803.8469	0.0026

4	3	1	3	3	0	5861.4611	5861.4622	-0.0011
4	1	3	3	1	2	5970.6253	5970.6252	0.0001
4	2	2	3	2	1	6075.3368	6075.3339	0.0029
5	1	5	4	1	4	6482.7125	6482.7139	-0.0014
5	0	5	4	0	4	6522.2753	6522.2716	0.0037
5	1	5	4	0	4	6548.2511	6548.2524	-0.0013
5	2	4	4	2	3	7022.5878	7022.5902	-0.0024
5	3	3	4	3	2	7255.2876	7255.2878	-0.0002
5	1	4	4	1	3	7303.3378	7303.3361	0.0017
5	2	3	4	2	2	7634.0151	7634.0158	-0.0007

Table S4.14. Rotational transition frequencies of HFIP$_g$(OD)⋯D$_2$O.

J'	K_a'	K_c'	*J"*	K_a"	K_c"	Obs/ MHz	Cal/ MHz	Obs - Cal/ MHz
2	0	2	1	0	1	2753.9137	2753.9136	0.0001
3	1	3	2	1	2	3890.3128	3890.315	-0.0022
3	0	3	2	0	2	4024.3002	4024.2957	0.0045
3	2	2	2	2	1	4206.3748	4206.3793	-0.0045
3	2	1	2	2	0	4388.4619	4388.4563	0.0056
3	1	2	2	1	1	4457.3772	4457.3774	-0.0002
2	2	1	1	1	1	4508.2506	4508.2507	-0.0001
7	5	2	7	4	3	4508.3497	4508.3502	-0.0005
4	1	4	3	1	3	5144.6503	5144.6526	-0.0023

4	0	4	3	0	3	5232.6619	5232.6602	0.0017
3	2	2	2	1	1	5526.5879	5526.5919	-0.0040
4	2	3	3	2	2	5568.6596	5568.6612	-0.0016
4	3	2	3	3	1	5688.5507	5688.5556	-0.0049
4	3	1	3	3	0	5737.6145	5737.6201	-0.0056
4	1	3	3	1	2	5863.1327	5863.1304	0.0023
4	2	2	3	2	1	5943.2748	5943.2684	0.0064
5	0	5	4	1	4	6347.8354	6347.8319	0.0035
5	1	5	4	1	4	6379.6002	6379.5987	0.0015
5	0	5	4	0	4	6424.3499	6424.3453	0.0046
5	1	5	4	0	4	6456.1122	6456.1121	0.0001
5	2	4	4	2	3	6899.3848	6899.3888	-0.004
3	3	0	2	2	1	6923.4998	6923.4958	0.0040
5	1	4	4	1	3	7185.4493	7185.4553	-0.006
5	3	2	4	3	1	7266.6262	7266.6247	0.0015
6	0	6	5	0	5	7621.3581	7621.358	0.0001

Table S4.15. Percentage errors in the calculated rotational constants of HFIP$_g$···W$_H$ and its deuterated isotopologues species.

Isotopologues	*A /MHz*	(% [a])	*B /MHz*	(% [a])	*C/MHz*	(% [a])
HFIP$_g$···H_2O	1273.1	-0.71	828.4	0.80	630.0	0.41
HFIP$_g$···HOD4	1269.2	-0.50	811.3	0.71	619.3	0.49
HFIP$_g$···HOD3	1252.2	-0.63	810.6	0.86	614.7	0.54
HFIP$_g$···D_2O	1249.4	-0.43	794.0	0.76	604.6	0.61
HFIP$_g$(OD)···H_2O	1264.2	-0.64	825.3	0.80	626.3	0.44
HFIP$_g$(OD)···HOD4	1260.6	-0.43	808.2	0.72	615.7	0.52
HFIP$_g$(OD)···HOD3	1244.3	-0.57	807.4	0.86	611.3	0.56
HFIP$_g$(OD)···D_2O	1241.8	-0.38	791.0	0.76	601.3	0.64

[a] The percentage error = 100 *(exp. – calc.) / exp.

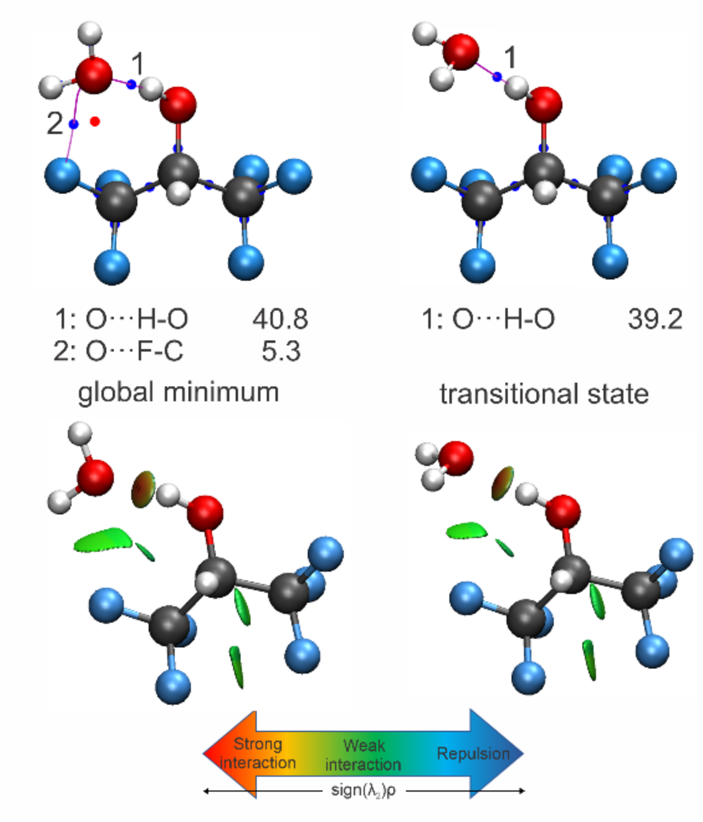

Figure S4.1. The QTAIM and NCI results of the HFIP$_g$···W$_H$ minimum and its water tunneling transition state at the B3LYP-D3(BJ)/def2-QZVP level of theory. The iso-surface value is set at 0.65. The bond energy values are in kJ mol^{-1}.

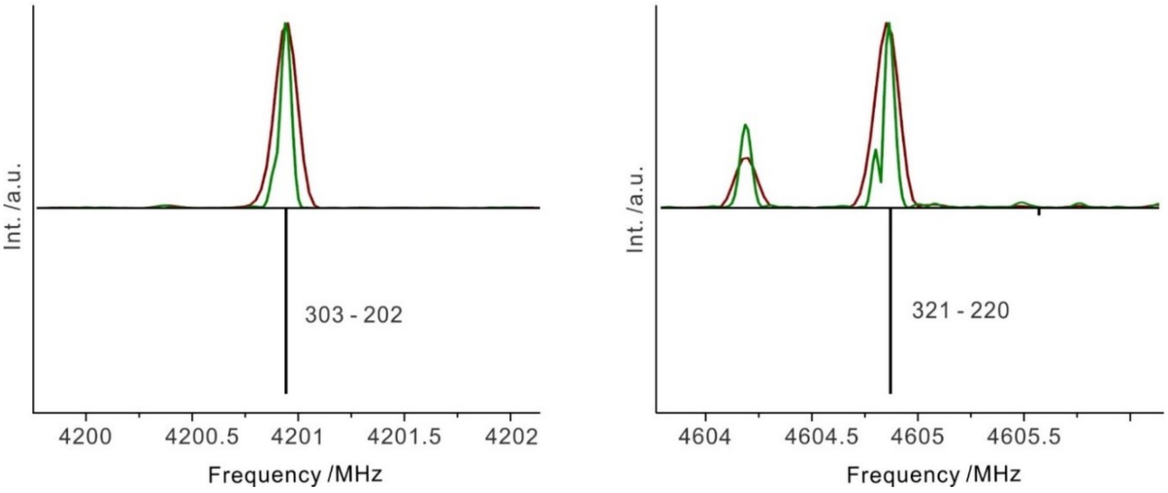

Figure S4.2. Comparison of the experimental CP-FTMW spectra recorded with an FID detection time of 20 µs (brown) and 40 µs (green). With the longer observation time, one can observe the asymmetric line shape in 303–202 or the narrow splitting in 321–220 of the HFIP$_g$···W$_H$ parent species.

Appendix C

Supporting Information for Chapter 5

Rotational Spectrum and Molecular Structures of the Binary Aggregates of 1,1,1,3,3,3-Hexafluoro-2-propanol with Ne and Ar

Contents:

Table S5.1. Calculated Cartesian coordinates (in Å) of the H_t monomer.[a]

		H_t	
C1	1.292429	0.124938	0.050627
C2	0.000000	-0.560617	0.533028
C3	-1.292429	0.124938	0.050627
H1	0.000000	-0.507149	1.620621
H2	0.000000	-1.992854	-0.781684
F1	-1.339815	1.420509	0.381455
F2	-1.424287	0.028154	-1.285803
F3	-2.350720	-0.479987	0.606593
F4	2.350720	-0.479987	0.606593
F5	1.424287	0.028154	-1.285803
F6	1.339815	1.420509	0.381455
O1	0.000000	-1.910490	0.178610

[a] Optimized at the B3LYP-D3(BJ)/def2-QZVP level of theory with "scf=verytight, int=grid=UltraFine".

Table S5.2. Calculated Cartesian coordinates (in Å) of the H_g monomer.[a]

		H_g	
C1	-1.285019	0.125568	-0.035575
C2	0.003933	-0.565819	-0.519837
C3	1.292476	0.118647	-0.040130
H1	0.001804	-0.483973	-1.610746
H2	-0.664332	-2.388426	-0.456783
F1	1.288992	1.420112	-0.371267
F2	1.462461	0.023590	1.279742
F3	2.348554	-0.452837	-0.637490
F4	-2.334643	-0.646162	-0.404179
F5	-1.340153	0.275902	1.288162
F6	-1.449226	1.324734	-0.607183
O1	0.061724	-1.888363	-0.073576

[a] Optimized at the B3LYP-D3(BJ)/def2-QZVP level of theory with "scf=verytight, int=grid=UltraFine".

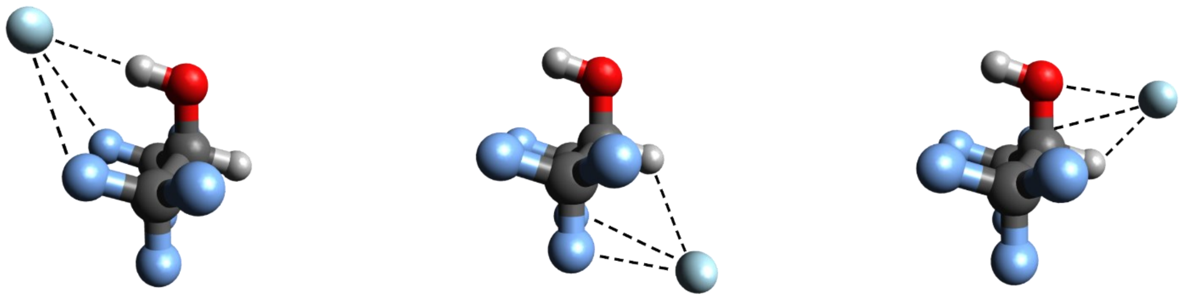

H_tNe_H H_tNe_C H_tNe_O

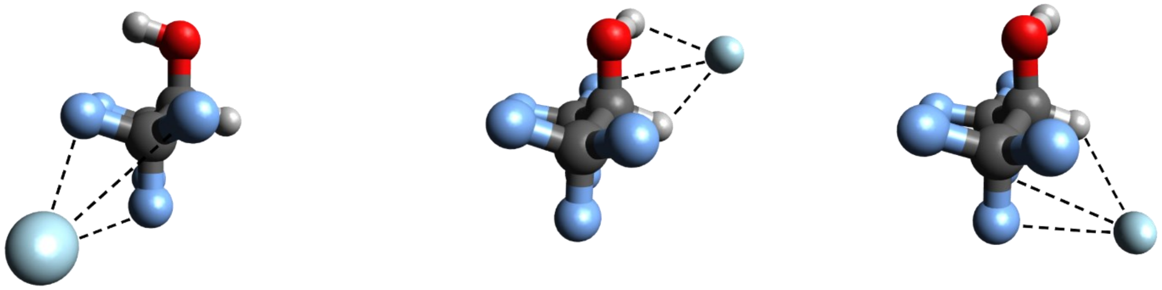

H_tNe_F H_gNe_H H_gNe_C

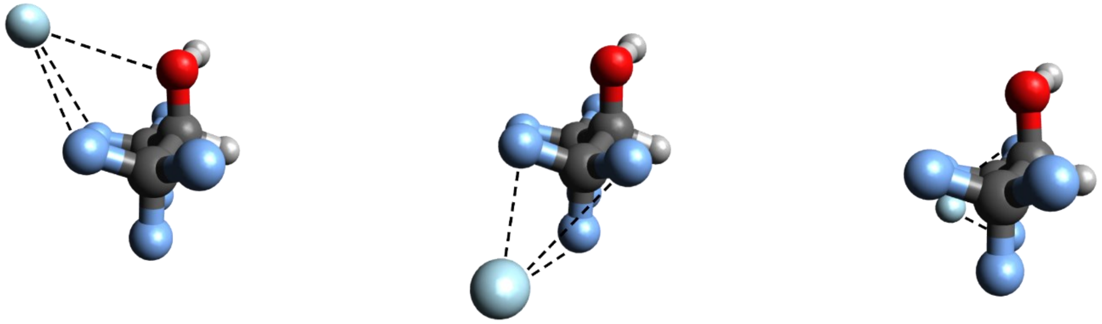

H_gNe_O H_gNe_F $H_gNe_{F'}$

Figure S5.2. Side views of the nine isomers of the HNe complex optimized at the B3LYP-D3(BJ)/def2-QZVP level of theory. The three closest intermolecular distances are indicated with dashed lines. The Ne atom may look bigger of smaller in size because of its position relative to the *trans* or *gauche* forms of the HFIP subunit which is fixed in space, if it is closer or further away to the reader's eyes, respectively.

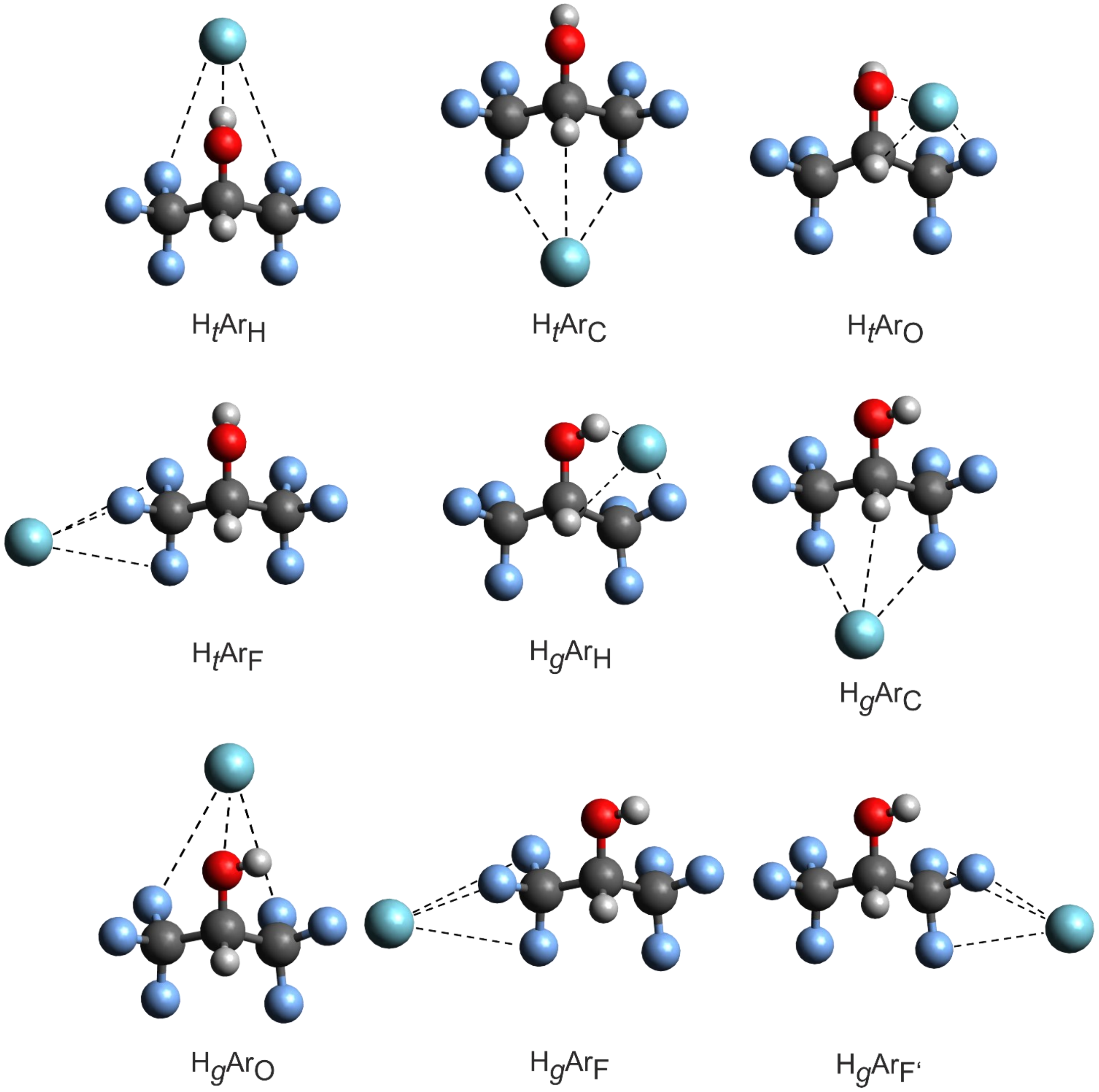

$\mathrm{H}_t\mathrm{Ar}_\mathrm{H}$ $\mathrm{H}_t\mathrm{Ar}_\mathrm{C}$ $\mathrm{H}_t\mathrm{Ar}_\mathrm{O}$

$\mathrm{H}_t\mathrm{Ar}_\mathrm{F}$ $\mathrm{H}_g\mathrm{Ar}_\mathrm{H}$ $\mathrm{H}_g\mathrm{Ar}_\mathrm{C}$

$\mathrm{H}_g\mathrm{Ar}_\mathrm{O}$ $\mathrm{H}_g\mathrm{Ar}_\mathrm{F}$ $\mathrm{H}_g\mathrm{Ar}_{\mathrm{F'}}$

Figure S5.2. Nine isomers of the HAr complex optimized at the B3LYP-D3(BJ)/def2-QZVP level of theory. The three closest intermolecular distances are indicated with dashed lines.

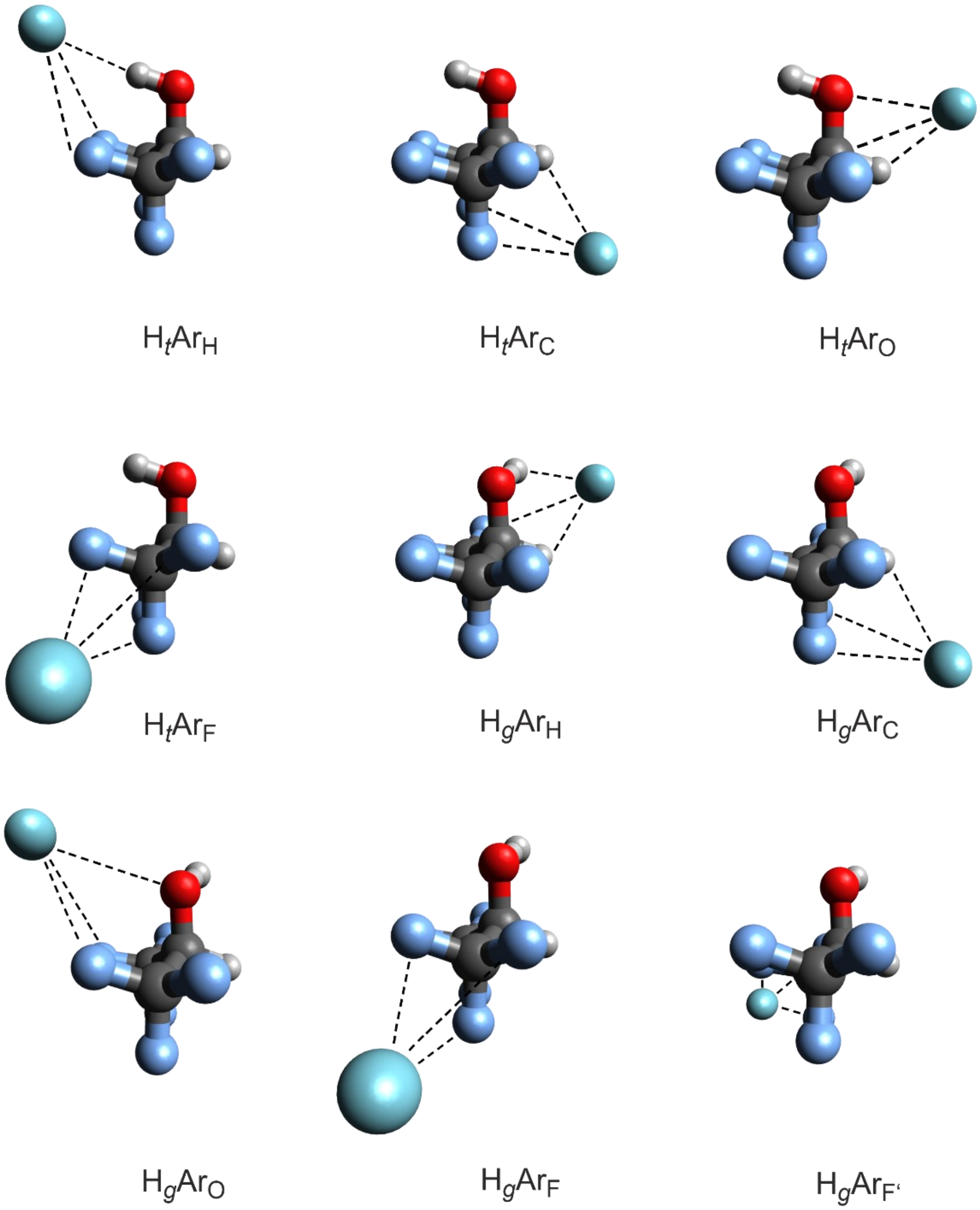

H_tAr_H H_tAr_C H_tAr_O

H_tAr_F H_gAr_H H_gAr_C

H_gAr_O H_gAr_F $H_gAr_{F'}$

Figure S5.3. Side views of the nine isomers of the HAr complex optimized at the B3LYP-D3(BJ)/def2-QZVP level of theory. The three closest intermolecular distances are indicated with dashed lines. The Ar atom may look bigger of smaller in size because of its position relative to the *trans* or *gauche* forms of the HFIP subunit which is fixed in space, if it is closer or further away to the reader's eyes, respectively.

Table S5.3. Calculated Cartesian coordinates (in Å) of the $\mathrm{H}_t\mathrm{Ne}_\mathrm{H}$ complex.[a]

$\mathrm{H}_t\mathrm{Ne}_\mathrm{H}$			
C1	1.292301	0.533198	-0.008359
C2	0.000000	0.41548	0.821770
C3	-1.292301	0.533198	-0.008359
H1	0.000000	1.246016	1.526031
H2	0.000000	-1.523451	0.968777
F1	-1.339634	1.661788	-0.725691
F2	-1.424656	-0.506479	-0.853485
F3	-2.350719	0.524154	0.813100
F4	2.350719	0.524154	0.813100
F5	1.424656	-0.506479	-0.853485
F6	1.339634	1.661788	-0.725691
O1	0.000000	-0.765824	1.564451
Ne1	0.000000	-3.454697	-0.404640

[a] Optimized at the B3LYP-D3(BJ)/def2-QZVP level of theory with “scf=verytight, int=grid=UltraFine”.

Table S5.4. Calculated Cartesian coordinates (in Å) of the $\mathrm{H}_t\mathrm{Ar}_\mathrm{H}$ complex.[a]

$\mathrm{H}_t\mathrm{Ar}_\mathrm{H}$			
C1	0.922174	1.292002	0.018424
C2	0.844570	0.000000	-0.816916
C3	0.922174	-1.292002	0.018424
H1	1.709723	0.000000	-1.478330
H2	-1.085591	0.000000	-1.062508
F1	2.017409	-1.340148	0.786136
F2	-0.154307	-1.423243	0.816043
F3	0.949301	-2.350993	-0.802016
F4	0.949301	2.350993	-0.802016
F5	-0.154307	1.423243	0.816043
F6	2.017409	1.340148	0.786136
O1	-0.297299	0.000000	-1.617877
Ar1	-3.378254	0.000000	0.185068

[a] Optimized at the B3LYP-D3(BJ)/def2-QZVP level of theory with “scf=verytight, int=grid= UltraFine”.

Table S5.5. Experimental rotational transitions of $H_t{}^{20}Ne_H$.

J'	K_a'	K_c'	J''	K_a''	K_c''	Obs/ MHz	Cal/ MHz	Obs - Cal/ MHz
5	2	4	5	1	5	2923.1752	2923.1799	-0.0047
2	0	2	1	1	1	2928.8753	2928.8707	0.0046
2	1	2	1	0	1	2942.0631	2942.0660	-0.0029
2	2	1	1	1	0	3604.7751	3604.7738	0.0013
2	1	1	1	0	1	3897.5751	3897.5783	-0.0032
2	2	0	1	1	0	3910.7882	3910.7903	-0.0021
2	2	1	1	1	1	3923.2754	3923.2767	-0.0013
2	2	0	1	1	1	4229.2872	4229.2932	-0.0060
3	0	3	2	1	2	4240.7599	4240.7607	-0.0008
3	1	3	2	0	2	4241.1004	4241.0989	0.0015
3	1	2	2	2	1	4869.7002	4869.7011	-0.0009
3	2	2	2	1	1	4909.9252	4909.9279	-0.0027
4	0	4	3	1	3	5546.1901	5546.1909	-0.0008
4	1	4	3	0	3	5546.1953	5546.1945	0.0008
3	3	1	2	2	0	5578.9133	5578.9152	-0.0019
3	2	1	2	1	1	5846.4498	5846.4453	0.0045
3	1	2	2	0	2	5864.1004	5864.1072	-0.0068
3	2	2	2	1	2	5865.4375	5865.4402	-0.0027
3	3	0	2	2	0	5866.9501	5866.9424	0.0077
3	3	1	2	2	1	5884.9248	5884.9316	-0.0068
3	3	0	1	1	1	6172.9627	6172.9589	0.0038
4	1	3	3	2	2	6195.0902	6195.0904	-0.0002
4	2	3	3	1	2	6196.7819	6196.7831	-0.0012
4	2	2	3	3	1	6801.8801	6801.8790	0.0011
5	0	5	4	1	4	6851.4035	6851.4044	-0.0009
5	1	5	4	0	4	6851.4035	6851.4044	-0.0009
4	3	2	3	2	1	6883.9015	6883.9003	0.0012

5	2	4	4	1	3	7501.0057	7501.0089	-0.0032
4	4	1	3	3	0	7558.5742	7558.5719	0.0023
4	3	1	3	2	1	7795.4098	7795.4083	0.0015
4	2	2	3	1	2	7817.1097	7817.1095	0.0002
4	1	3	3	0	3	7819.7840	7819.7699	0.0141
4	2	3	3	1	3	7819.7901	7819.7913	-0.0012
4	3	2	3	2	2	7820.4169	7820.4176	-0.0007
4	4	0	3	3	0	7823.9812	7823.9822	-0.0010
4	4	1	3	3	1	7846.5980	7846.5992	-0.0012
4	4	0	3	3	1	8112.0083	8112.0095	-0.0012
5	2	3	4	3	2	8148.4402	8148.4393	0.0009
5	3	3	4	2	2	8153.5141	8153.5144	-0.0003
6	1	6	5	0	5	8156.5451	8156.5449	0.0002
5	3	2	4	4	1	8723.9955	8723.9922	0.0033
4	3	1	3	2	2	8731.9182	8731.9257	-0.0075
6	2	5	5	1	4	8806.0468	8806.0465	0.0003
4	4	1	3	1	2	8861.8304	8861.8297	0.0007
5	4	2	4	3	1	8863.7403	8863.7385	0.0018
6	2	4	5	3	3	9455.5351	9455.5356	-0.0005
6	3	4	5	2	3	9455.6365	9455.6344	0.0021
7	0	7	6	1	6	9461.5908	9461.5992	-0.0084
5	5	1	4	4	0	9542.8641	9542.8614	0.0027
5	4	1	4	3	1	9744.5030	9744.5036	-0.0006
5	3	2	4	2	2	9768.7130	9768.7124	0.0006
5	2	3	4	1	3	9773.7669	9773.7666	0.0003
5	3	3	4	2	3	9773.8404	9773.8408	-0.0004
5	1	4	4	0	4	9774.5856	9774.5845	0.0011
5	2	4	4	1	4	9774.5856	9774.5844	0.0012
5	4	2	4	3	2	9775.2469	9775.2465	0.0004
5	5	0	4	4	0	9782.1534	9782.1543	-0.0009

5	5	1	4	4	1	9808.2715	9808.2717	-0.0002
5	5	0	4	4	1	10047.5688	10047.5645	0.0043
6	3	3	5	4	2	10100.3099	10100.3114	-0.0015
7	1	6	6	2	5	10111.0179	10111.0173	0.0006
7	2	6	6	1	5	10111.0179	10111.0173	0.0006
6	4	3	5	3	2	10112.1172	10112.1160	0.0012
7	2	5	6	3	4	10760.3654	10760.3664	-0.0010
7	3	5	6	2	4	10760.3654	10760.3658	-0.0004
8	1	8	7	0	7	10766.5558	10766.5532	0.0026
8	0	8	7	1	7	10766.5558	10766.5532	0.0026
7	3	4	6	4	3	11409.8187	11409.8214	-0.0027
7	4	4	6	3	3	11410.1142	11410.1143	-0.0001
8	2	7	7	1	6	11415.8851	11415.8853	-0.0002
8	1	7	7	2	6	11415.8851	11415.8853	-0.0002
6	6	1	5	5	0	11530.6378	11530.6393	-0.0015
6	5	1	5	4	1	11693.7702	11693.7704	-0.0002
6	4	2	5	3	2	11718.6735	11718.6723	0.0012
6	3	3	5	2	3	11727.1169	11727.1186	-0.0017
6	4	3	5	3	3	11727.3156	11727.3140	0.0016
6	2	4	5	1	4	11728.3910	11728.3924	-0.0014
6	3	4	5	2	4	11728.3910	11728.3920	-0.0010
6	2	5	5	1	5	11729.2282	11729.2265	0.0017
6	1	5	5	0	5	11729.2282	11729.2265	0.0017
6	5	2	5	4	2	11729.8842	11729.8856	-0.0014
6	6	0	5	5	0	11741.6303	11741.6309	-0.0006
6	6	1	5	5	1	11769.9326	11769.9321	0.0005

Table S5.6. Experimental rotational transitions of $\mathrm{H_t{}^{22}Ne_{H.}}$

J'	K_a'	K_c'	*J"*	K_a"	K_c"	Obs/ MHz	Cal/ MHz	Obs - Cal/ MHz
2	1	2	1	1	1	2841.5889	2841.5855	0.0034
2	0	2	1	0	1	2869.4324	2869.4289	0.0035
2	1	1	1	1	0	3456.0749	3456.0752	-0.0003
2	1	1	1	0	1	3793.2002	3793.2009	-0.0007
2	2	0	1	1	0	3825.1405	3825.1401	0.0004
2	2	1	1	1	1	3852.9647	3852.9662	-0.0015
3	1	3	2	1	2	4122.4389	4122.4414	-0.0025
3	0	3	2	0	2	4124.3879	4124.3871	0.0008
2	2	0	1	0	1	4162.2633	4162.2658	-0.0025
3	2	2	2	2	1	4723.0429	4723.0438	-0.0009
3	1	2	2	1	1	4802.6004	4802.5971	0.0033
3	2	1	2	2	0	5321.8623	5321.8608	0.0015
4	0	4	3	1	3	5390.4002	5390.4033	-0.0031
4	1	4	3	0	3	5390.4895	5390.4881	0.0014
3	2	1	2	1	1	5690.9253	5690.9257	-0.0004
3	1	2	2	0	2	5726.3694	5726.3691	0.0003
3	2	2	2	1	2	5734.4255	5734.4246	0.0009
3	3	0	2	2	0	5742.6504	5742.6513	-0.0009
3	3	1	2	2	1	5780.5504	5780.5471	0.0033
4	2	3	3	2	2	6029.9497	6029.9478	0.0019
4	1	3	3	1	2	6039.4571	6039.4558	0.0013
3	3	0	2	1	1	6111.7171	6111.7161	0.001
5	0	5	4	1	4	6657.4579	6657.457	0.0009
5	1	5	4	0	4	6657.4579	6657.4596	-0.0017
4	3	1	3	2	1	7590.1235	7590.1223	0.0012
4	2	2	3	1	2	7627.2968	7627.2968	0.0000
4	1	3	3	0	3	7641.4379	7641.4379	0.0000

4	3	2	3	2	2	7647.0533	7647.0548	-0.0015
4	4	0	3	3	0	7665.7525	7665.7534	-0.0009
4	4	1	3	3	1	7709.3369	7709.3383	-0.0014
6	1	6	5	0	5	7924.4056	7924.4062	-0.0006
6	0	6	5	1	5	7924.4056	7924.4061	-0.0005
6	1	5	5	2	4	8567.9368	8567.9348	0.0020
6	2	5	5	1	4	8567.9512	8567.9586	-0.0074
7	0	7	6	1	6	9191.2697	9191.2692	0.0005
7	1	7	6	0	6	9191.2697	9191.2693	0.0004
5	4	1	4	3	1	9491.4886	9491.4881	0.0005
5	3	2	4	2	2	9522.6499	9522.6511	-0.0012
5	2	3	4	1	3	9548.6966	9548.696	0.0006
5	3	3	4	2	3	9550.4143	9550.4148	-0.0005
5	1	4	4	0	4	9552.423	9552.4234	-0.0004
5	2	4	4	1	4	9552.4447	9552.4439	0.0008
5	4	2	4	3	2	9560.6767	9560.6771	-0.0004
5	5	0	4	4	0	9595.3196	9595.3207	-0.0011
5	5	1	4	4	1	9639.5725	9639.5732	-0.0007
7	1	6	6	2	5	9834.6834	9834.6823	0.0011
7	2	6	6	1	5	9834.6834	9834.683	0.0004
8	1	8	7	0	7	10458.0321	10458.0319	0.0002
8	0	8	7	1	7	10458.0321	10458.0319	0.0002
7	2	5	6	3	4	10478.2741	10478.268	0.0061
7	3	5	6	2	4	10478.3822	10478.3874	-0.0052
6	5	1	5	4	1	11395.8908	11395.8903	0.0005
6	4	2	5	3	2	11413.0663	11413.0666	-0.0003
6	3	3	5	2	3	11453.4194	11453.4181	0.0013
6	4	3	5	3	3	11457.9563	11457.9591	-0.0028
6	2	4	5	1	4	11460.4907	11460.4901	0.0006
6	3	4	5	2	4	11460.5809	11460.5823	-0.0014

6	2	5	5	1	5	11462.9225	11462.9223	0.0002
6	1	5	5	0	5	11462.9225	11462.9217	0.0008
6	5	2	5	4	2	11475.5359	11475.5342	0.0017
6	6	0	5	5	0	11530.9711	11530.9708	0.0003
6	6	1	5	5	1	11571.3598	11571.3591	0.0007

Table S5.7. Experimental rotational transitions of $^{13}C1/3-H_t{}^{20}Ne_{H.}$

J'	K_a'	K_c'	J''	K_a''	K_c''	Obs/ MHz	Cal/ MHz	Obs - Cal/ MHz
4	1	4	3	0	3	5532.9996	5532.9991	0.0005
4	0	4	3	1	3	5532.9996	5532.9989	0.0007
3	3	0	2	2	0	5856.3401	5856.3401	0.0000
5	1	5	4	0	4	6834.8532	6834.8532	0.0000
5	0	5	4	1	4	6834.8532	6834.8532	0.0000
5	1	4	4	2	3	7484.6861	7484.6872	-0.0012
4	1	3	3	0	3	7808.3800	7808.3799	0.0001
4	2	3	3	1	3	7808.3800	7808.3812	-0.0012
5	2	4	4	1	4	9760.0701	9760.0695	0.0006
5	1	4	4	0	4	9760.0701	9760.0695	0.0006

Table S5.8. Experimental rotational transitions of ^{13}C2-H$_t$^{20}Ne$_H$.

J’	*K*$_a$’	*K*$_c$’	*J*”	*K*$_a$”	*K*$_c$”	Obs/ MHz	Cal/ MHz	Obs - Cal/ MHz
4	1	4	3	0	3	5543.7308	5543.7311	-0.0003
4	0	4	3	1	3	5543.7308	5543.7316	-0.0008
3	3	0	2	2	0	5856.3418	5856.3418	0.0000
5	1	5	4	0	4	6848.6601	6848.6594	0.0007
5	0	5	4	1	4	6848.6601	6848.6593	0.0008
4	2	3	3	1	3	7808.2857	7808.2874	-0.0017
4	1	3	3	0	3	7808.2857	7808.284	0.0017
5	2	4	4	1	4	9760.0742	9760.0742	0.0000
5	1	4	4	0	4	9760.0742	9760.0742	0.0000
6	0	6	5	1	5	8153.5147	8153.515	-0.0003
6	1	6	5	0	5	8153.5147	8153.515	-0.0003

Table S5.9. Experimental rotational transitions of H$_t$-OD-^{20}Ne$_H$.

J’	*K*$_a$’	*K*$_c$’	*J*”	*K*$_a$”	*K*$_c$”	Obs/ MHz	Cal/ MHz	Obs - Cal/ MHz
2	2	0	1	1	0	3894.7742	3894.7706	0.0036
2	2	1	1	1	1	3903.4144	3903.4169	-0.0025
4	1	4	3	0	3	5526.8056	5526.8058	-0.0002
4	0	4	3	1	3	5526.8056	5526.8059	-0.0003
3	3	1	2	2	0	5545.0717	5545.0702	0.0015
3	2	1	2	1	1	5828.6444	5828.6431	0.0013
3	2	2	2	1	2	5841.7416	5841.7418	-0.0002

3	3	0	2	2	0	5842.5198	5842.5231	-0.0033
3	1	2	2	0	2	5841.2101	5841.2103	-0.0002
3	3	1	2	2	1	5855.2005	5855.2003	0.0002
5	0	5	4	1	4	6827.5864	6827.5863	0.0001
5	1	5	4	0	4	6827.5864	6827.5863	0.0001
4	4	0	3	3	0	7790.7251	7790.7249	0.0002

Table S5.10. Experimental rotational transitions of $H_t{}^{40}Ar_H$.

J'	K_a'	K_c'	J''	K_a''	K_c''	Obs/ MHz	Cal/ MHz	Obs - Cal/ MHz
2	1	1	1	0	1	2874.6138	2874.6172	-0.0034
3	1	3	2	1	2	3073.9998	3074.0019	-0.0021
3	0	3	2	0	2	3178.7684	3178.7676	0.0008
3	2	2	2	2	1	3333.2096	3333.2033	0.0063
2	2	0	1	1	0	3438.5251	3438.5206	0.0045
3	2	1	2	2	0	3487.7146	3487.7130	0.0016
3	1	2	2	1	1	3536.6754	3536.6710	0.0044
2	2	1	1	1	1	3552.2504	3552.2448	0.0056
4	1	4	3	1	3	4062.8752	4062.8795	-0.0043
4	0	4	3	0	3	4129.1504	4129.1474	0.0030
3	1	2	2	0	2	4232.1755	4232.1717	0.0038
4	2	3	3	2	2	4410.1123	4410.1091	0.0032
4	3	2	3	3	1	4511.9253	4511.9228	0.0025
3	2	1	2	1	1	4547.2367	4547.2369	-0.0002
4	3	1	3	3	0	4555.8255	4555.8364	-0.0109
5	1	4	4	2	2	4595.5663	4595.5648	0.0015

4	1	3	3	1	2	4646.1618	4646.1582	0.0036
4	2	2	3	2	1	4724.1377	4724.1390	-0.0013
3	2	2	2	1	2	4820.0635	4820.0660	-0.0025
5	1	5	4	1	4	5035.9624	5035.9572	0.0052
5	0	5	4	0	4	5068.3371	5068.3367	0.0004
3	3	0	2	2	0	5408.0376	5408.0375	0.0001
3	3	1	2	2	1	5443.3873	5443.3816	0.0057
5	2	4	4	2	3	5460.1638	5460.1651	-0.0013
5	3	3	4	3	2	5640.7253	5640.7272	-0.0019
5	4	2	4	4	1	5649.8748	5649.8728	0.0020
5	4	1	4	4	0	5658.7156	5658.7211	-0.0055
5	1	4	4	1	3	5684.1121	5684.1116	0.0005
4	1	3	3	0	3	5699.5631	5699.5623	0.0008
4	2	2	3	1	2	5734.7002	5734.7050	-0.0048
5	3	2	4	3	1	5776.3753	5776.3760	-0.0007
5	2	3	4	2	2	5938.3115	5938.3074	0.0041
6	1	6	5	1	5	5999.0369	5999.0357	0.0012
6	0	6	5	0	5	6012.6138	6012.6148	-0.0010
4	2	3	3	1	3	6156.1749	6156.1732	0.0017
4	3	1	3	2	1	6476.1626	6476.1609	0.0017
6	2	5	5	2	4	6481.8363	6481.8359	0.0004
4	3	2	3	2	2	6622.1004	6622.1011	-0.0007
6	1	5	5	1	4	6649.6167	6649.6182	-0.0015
6	3	4	5	3	3	6752.0026	6752.0030	-0.0004
6	5	2	5	5	1	6776.1625	6776.1624	0.0001
6	5	1	5	5	0	6777.6527	6777.6505	0.0022
6	4	3	5	4	2	6801.0537	6801.0534	0.0003
6	4	2	5	4	1	6838.2925	6838.2925	0.0000
7	1	7	6	1	6	6956.8824	6956.8836	-0.0012
7	0	7	6	0	6	6962.0908	6962.0917	-0.0009

5	2	3	4	1	3	7026.8529	7026.8542	-0.0013
6	3	3	5	3	2	7040.6293	7040.6290	0.0003
6	2	4	5	2	3	7098.2435	7098.2444	-0.0009
5	1	4	4	0	4	7254.5276	7254.5266	0.0010
4	4	0	3	3	0	7368.2538	7368.2547	-0.0009
4	4	1	3	3	1	7374.8496	7374.8508	-0.0012
7	2	6	6	2	5	7478.0644	7478.0654	-0.0010
5	3	2	4	2	2	7528.3966	7528.3978	-0.0012
5	2	4	4	1	4	7553.4599	7553.4588	0.0011
7	1	6	6	1	5	7577.6665	7577.6677	-0.0012
7	3	5	6	3	4	7836.7125	7836.7130	-0.0005
5	3	3	4	3	3	7852.7191	7852.7192	-0.0001
8	1	8	7	1	7	7912.3640	7912.3649	-0.0009
8	0	8	7	0	7	7914.2511	7914.2523	-0.0012
7	5	3	6	5	2	7931.5513	7931.5490	0.0023
7	5	2	6	5	1	7939.3791	7939.3777	0.0014
7	4	4	6	4	3	7950.8265	7950.8271	-0.0006
7	4	3	6	4	2	8060.7598	8060.7594	0.0004
7	2	5	6	2	4	8182.9911	8182.9920	-0.0009
7	3	4	6	3	3	8305.5071	8305.5077	-0.0006
6	2	4	5	1	4	8440.9876	8440.9870	0.0006
8	2	7	7	2	6	8455.1595	8455.1595	-0.0000
5	4	1	4	3	1	8471.1381	8471.1394	-0.0013
8	1	7	7	1	6	8504.5979	8504.5988	-0.0009
5	4	2	4	3	2	8512.8006	8512.8008	-0.0002
6	3	3	5	2	3	8630.7192	8630.7195	-0.0003
6	1	5	5	0	5	8835.8078	8835.8080	-0.0002
9	1	9	8	1	8	8866.8741	8866.8758	-0.0017
9	0	9	8	0	8	8867.5326	8867.5335	-0.0009
8	3	6	7	3	5	8889.9664	8889.9655	0.0009

6	2	5	5	1	5	8999.3366	8999.3375	-0.0009
8	4	5	7	4	4	9088.4879	9088.4888	-0.0009
8	5	4	7	5	3	9094.5625	9094.5614	0.0011
8	5	3	7	5	2	9123.6981	9123.6983	-0.0002
6	3	4	5	2	4	9144.5563	9144.5571	-0.0008
8	2	6	7	2	5	9181.5999	9181.6007	-0.0008
8	2	6	7	2	5	9181.5999	9181.6007	-0.0008
5	5	0	4	4	0	9316.7858	9316.7870	-0.0012
5	5	1	4	4	1	9317.7793	9317.7794	-0.0001
8	4	4	7	4	3	9334.3838	9334.3832	0.0006
9	2	8	8	2	7	9420.1525	9420.1534	-0.0009
9	1	8	8	1	7	9441.9607	9441.9602	0.0005
8	3	5	7	3	4	9522.6552	9522.6541	0.0011
6	4	2	5	3	2	9533.0560	9533.0559	0.0001
6	4	3	5	3	3	9673.1263	9673.1271	-0.0008
10	1	10	9	1	9	9821.0054	9821.0043	0.0011
10	0	10	9	0	9	9821.2273	9821.2269	0.0004
7	3	4	6	2	4	9837.9825	9837.9828	-0.0003
9	3	7	8	3	6	9911.8612	9911.8622	-0.0010
6	3	3	5	1	4	9973.4609	9973.4620	-0.0011
7	2	5	6	1	5	9974.3610	9974.3608	0.0002
9	2	7	8	2	6	10113.3252	10113.3254	-0.0002
9	4	6	8	4	5	10203.1380	10203.1389	-0.0009
9	6	4	8	6	3	10217.6026	10217.6019	0.0007
9	6	3	8	6	2	10223.8538	10223.8523	0.0015
9	5	5	8	5	4	10259.8298	10259.8308	-0.0010
9	5	4	8	5	3	10344.2306	10344.2312	-0.0006
10	2	9	9	2	8	10378.6192	10378.6184	0.0008
10	1	9	9	1	8	10387.5235	10387.5236	-0.0001
7	1	6	6	0	6	10400.8619	10400.8609	0.0010

6	5	1	5	4	1	10435.7164	10435.7164	0.0000
6	5	2	5	4	2	10444.0683	10444.0690	-0.0007
7	2	6	6	1	6	10478.3663	10478.3672	-0.0009
7	3	5	6	2	5	10499.4333	10499.4342	-0.0009
7	4	3	6	3	3	10553.1859	10553.1863	-0.0004
9	4	5	8	4	4	10634.9180	10634.9180	0.0000
9	3	6	8	3	5	10662.8844	10662.8835	0.0009
11	1	11	10	1	10	10774.9709	10774.9709	0.0000
11	0	11	10	0	10	10775.0452	10775.0446	0.0006
7	4	4	6	3	4	10871.9511	10871.9511	0.0000
10	3	8	9	3	7	10907.0639	10907.0629	0.0010
10	2	8	9	2	7	11022.5714	11022.5722	-0.0008
8	3	5	7	2	5	11177.6436	11177.6448	-0.0012
6	6	0	5	5	0	11262.7102	11262.7105	-0.0003
6	6	1	5	5	1	11262.8453	11262.8442	0.0011
10	4	7	9	4	6	11286.7635	11286.7627	0.0008
11	2	10	10	2	9	11334.0113	11334.0122	-0.0009
11	1	10	10	1	9	11337.4593	11337.4593	0.0000
10	6	5	9	6	4	11389.5519	11389.5541	-0.0022
10	6	4	9	6	3	11411.3062	11411.3046	0.0016
10	5	6	9	5	5	11418.2378	11418.2379	-0.0001
7	5	2	6	4	2	11536.8025	11536.8017	0.0008
7	5	3	6	4	3	11574.5654	11574.5645	0.0009
8	2	6	7	1	6	11578.2961	11578.2938	0.0023
8	4	4	7	3	4	11582.0624	11582.0618	0.0006
10	5	5	9	5	4	11615.1807	11615.1832	-0.0025
10	3	7	9	3	6	11709.7635	11709.7623	0.0012
12	0	12	11	0	11	11728.8735	11728.8731	0.0004
11	3	9	10	3	8	11882.8596	11882.8585	0.0011
10	4	6	9	4	5	11909.1879	11909.1868	0.0011

8	3	6	7	2	6	11911.3336	11911.3343	-0.0007
11	2	9	10	2	8	11940.3620	11940.3610	0.0010
8	1	7	7	0	7	11943.3667	11943.3681	-0.0014
8	2	7	7	1	7	11976.6421	11976.6431	-0.0010
8	4	5	7	3	5	12123.7272	12123.7269	0.0003

Table S5.11. Experimental and calculated rotational constants of the H_tNe_H, H_tAr_H, IP_tNe_H, and IP_tAr_H complexes.

Species		*A* /MHz	Error	*B* /MHz	Error	*C* /MHz	Error
H_tNe_H	Level of theory / Experimental	984.073	-	971.188	-	652.685	-
	B3LYP-D3BJ/def2-QZVP	986.0438	0.20%	968.1865	-0.31%	646.8769	-0.89%
	B3LYP-D3BJ/def2-TZVP	1015.4702	3.19%	963.7546	-0.76%	662.1733	1.45%
	B3LYP-D3B/def2-TZVPP	1015.4702	3.19%	963.7546	-0.76%	662.1733	1.45%
	B3LYP-D3BJ/6-311++G(2d,2p)	990.4455	0.65%	971.8777	0.07%	649.9646	-0.42%
	B3LYP/6-311++G(2d,2p)	985.4197	0.14%	889.8877	-8.37%	597.3209	-8.48%
H_tAr_H	Level of theory / Experimental	972.7732	-	633.9586	-	477.1483	-
	B3LYP-D3BJ/def2-QZVP	966.1262	-0.68%	625.2937	-1.37%	469.7972	-1.54%
	B3LYP-D3BJ/def2-TZVP	964.4390	-0.86%	634.3432	0.06%	475.7316	-0.30%
	B3LYP-D3B/def2-TZVPP	965.2089	-0.78%	635.9242	0.31%	476.3340	-0.17%
	B3LYP-D3BJ/6-311++G(2d,2p)	969.1935	-0.37%	624.9433	-1.42%	470.3286	-1.43%
	B3LYP/6-311++G(2d,2p)	991.8637	1.96%	494.7566	-21.96%	387.9167	-18.30%
IP_tNe_H	B3LYP-D3BJ/def2-QZVP	4875.2795	-	1972.6759	-	1930.8224	-
IP_tAr_H	B3LYP-D3BJ/def2-QZVP	4861.6282	-	1210.5264	-	1195.4454	-

Table S5.12. Structural parameters of H_tNe_H.

parameter	exp. [a]	theo. [b]
C1/C3-C2 /Å	1.5673(83)	1.5405
C2-O1 /Å	1.4140	1.3954
C2-H1 /Å	1.0821	1.0889
C2···H2 /Å	1.9554	1.9445
C2···Ne1 /Å	4.0451	4.0599
Ne···H2 /Å	2.3392	2.3698
Ne···O1 /Å	3.348(33)	3.3328
H2-O1 /Å	1.011(82)	0.9638
F5/2-C1/3 /Å	1.3445	1.3464
F4/F3-C1/C3 /Å	1.3374	1.3398
F6/F1-C1/C3 /Å	1.3358	1.3381
∠Ne···O1-C2 /°	109.48(17)	111.627
∠Ne···O1-C2-H1 /°	180.0000	180.0000
∠Ne···H2-O1 /°	175.467	177.243
∠H2-O1-C2 /°	106.3(28)	109.667
∠H1-C2-C1 /°	105.692	106.872
∠H1-C2-C3 /°	105.692	106.872
∠H1-C2···H2 /°	140.248	135.368
∠C1-C2-C3 /°	110.270	114.050
∠C1/C3-C2-O1 /°	112.14(72)	110.580
∠F5/2-C1/3-C2 /°	110.858	111.206
∠F4/F3-C1/3-C2 /°	109.344	109.378
∠F6/F1-C1/3-C2 /°	112.479	112.520
∠H2-O1-C2-H1 /°	180.0000	180.0000
∠H2-O1-C2-C1 /°	-62.3547	-63.649
∠H2-O1-C2-C3 /°	62.3547	63.649
∠H1-C1···H2···Ne /°	180.0000	180.0000

[a] Obtained from the STRFIT described in the main text.

[b] Calculated at the B3LYP-D3(BJ)/def2-QZVP level of theory.

Table S5.13. Structural parameters of H_t

parameter	exp. [a]	theo. [b]
C1/C3-C2 /Å	1.5332(71)	1.5314
O1-C2 /Å	1.414(11)	1.3990
H1-C2 /Å	1.08S2(17)	1.0922
C2···H2 /Å	1.9729	1.9296
H2-O1 /Å	0.959(26)	0.9651
F5/2-C1/3 /Å	1.3445	1.3445
F4/F3-C1/C3 /Å	1.3374	1.3374
F6/F1-C1/C3 /Å	1.3358	1.3358
∠H2-O1-C2 /°	111.04(52)	108.005
∠H1-C2-C1 /°	107.34(81)	107.177
∠H1-C2-C3 /°	107.34(81)	107.177
∠H1-C2-O1 /°	110.5(14)	107.489
∠H1-C2···H2 /°	137.487	135.893
∠C1-C2-C3 /°	113.920	114.075
∠C1/C3-C2-O1 /°	108.857	110.310
∠F5/2-C1/3-C2 /°	110.858	110.858
∠F4/F3-C1/3-C2 /°	109.344	109.344
∠F6/F1-C1/3-C2 /°	112.479	112.479
∠H2-O1-C2-H1 /°	180.0000	180.0000
∠H2-O1-C2-C1 /°	-62.355	-63.463
∠H2-O1-C2-C3 /°	62.355	63.463

[a] Obtained from the STRFIT described in the main text.

[b] Calculated at the MP2/6-311++G(2d,p)) level of theory as in Ref. 19.

.

Table S5.14. The atomic coordinates obtained of H_tNe_H

Atom	*a* (Å)	*b* (Å)	*c* (Å)
(i) From the STRFIT			
C1	-1.28597(29)	0.53304(99)	-0.0072(20)
C2	0.00000^{a}	0.394(30)	1.531(22)
C3	1.28597(29)	0.53304(99)	-0.0072(20)
H1	0.00000^{a}	1.257(38)	1.531(22)
H2	0.00000^{a}	-1.559(43)	0.997(67)
O1	0.00000^{a}	-0.801(39)	1.6342(45)
F1	-1.298(15)	1.665(12)	-0.717(22)
F2	-1.3940(49)	-0.501(15)	-0.860(17)
F3	-2.3678(50)	0.5254(54)	0.7790(46)
F4	2.3678(50)	0.5254(54)	0.7790(46)
F5	1.3940(49)	-0.501(15)	-0.860(17)
F6	1.298(15)	1.665(12)	-0.717(22)
Ne1	0.00000^{a}	-3.4319(91)	-0.4352(95)
(ii) Substitution coordinates^{b}			
^{13}C1	-1.2980(40)	0.488(13)	Nonphysical
^{13}C2	Nonphysical	0.6472(94)	0.7970(79)
^{13}C3	1.2979(40)	0.488(13)	Nonphysical
^{2}H2	±0.4079(37)	-1.5642(10)	0.8873(18)
^{22}Ne	±0.107(14)	-3.43123(44)	-0.3721(40)

[a] Atoms that are fixed in the *bc*-plane as predicted theoretically.

[b] The signs for the substitution coordinates are assigned based on the theoretical structure. The Costain errors are quoted here. The "±" are used because these coordinates are 0 in the theoretical structure. These values are associated with the large amplitude motions discussed in the main text.

Table S5.15 Coordinates (in Å) for the H_t monomer

		MP2[a]	
C1	-1.284899	0.125962	-0.051816
C2	0.000000	-0.550656	-0.538090
C3	1.284899	0.125962	-0.051816
H1	0.000000	-1.960440	0.779368
H2	0.000000	-0.496697	-1.628957
F1	1.334990	1.420604	-0.377094
F2	1.405259	0.021432	1.283239
F3	2.341261	-0.480987	-0.603448
F4	-2.341261	-0.480987	-0.603448
F5	-1.405259	0.021432	1.283239
F6	-1.334990	1.420604	-0.377094
O1	0.000000	-1.904083	-0.184096
		Calculated from the STRFIT result[b]	
C1	-1.285264	-0.127671	0.055452
C2	0.000000	0.530416	0.570915
C3	1.285264	-0.127671	0.055452
H1	0.000000	0.437273	1.648984
H2	0.000000	1.892475	0.191311
F1	1.365059	-1.419775	0.384865
F2	1.371078	-0.027337	-1.282589
F3	2.344489	0.499376	0.578367
F4	-2.344489	0.499376	0.578367
F5	-1.371078	-0.027337	-1.282589
F6	-1.365059	-1.419775	0.384865
O1	0.000000	1.892475	0.191311

[a] Optimized at the MP2/6-311++G(d,p) level of theory as in Ref. 19.
[b] Calculated from the STRFIT result which was obtained by fitting to the experimental rotational constants reported in Ref. 19.

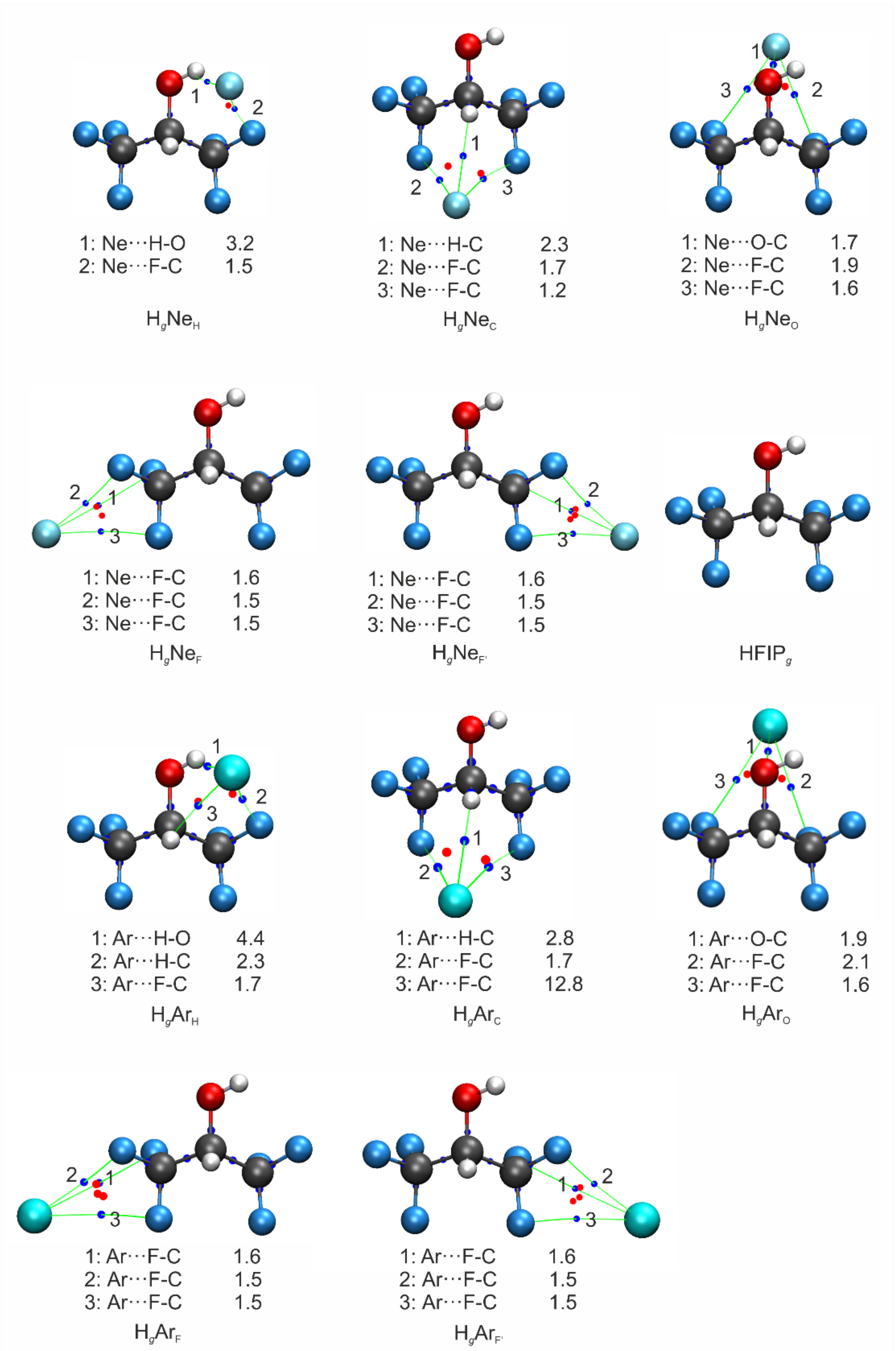

1: Ne···H-O 3.2
2: Ne···F-C 1.5

H_gNe_H

1: Ne···H-C 2.3
2: Ne···F-C 1.7
3: Ne···F-C 1.2

H_gNe_C

1: Ne···O-C 1.7
2: Ne···F-C 1.9
3: Ne···F-C 1.6

H_gNe_O

1: Ne···F-C 1.6
2: Ne···F-C 1.5
3: Ne···F-C 1.5

H_gNe_F

1: Ne···F-C 1.6
2: Ne···F-C 1.5
3: Ne···F-C 1.5

$H_gNe_{F'}$

$HFIP_g$

1: Ar···H-O 4.4
2: Ar···H-C 2.3
3: Ar···F-C 1.7

H_gAr_H

1: Ar···H-C 2.8
2: Ar···F-C 1.7
3: Ar···F-C 12.8

H_gAr_C

1: Ar···O-C 1.9
2: Ar···F-C 2.1
3: Ar···F-C 1.6

H_gAr_O

1: Ar···F-C 1.6
2: Ar···F-C 1.5
3: Ar···F-C 1.5

H_gAr_F

1: Ar···F-C 1.6
2: Ar···F-C 1.5
3: Ar···F-C 1.5

$H_gAr_{F'}$

Figure S5.4. QTAIM results of the H_g monomer and the five H_gNe and five H_gAr conformers calculated at the B3LYP-D3(BJ)/def2-QZVP level of theory. The blue dots with number labels are the bond critical points and the corresponding non-covalent bond energies are also provided in kJ mol^{-1}. The green lines represent the corresponding bond paths and the red dots are the ring critical points.

Appendix D

Supporting Information for Chapter 6

2,2,3,3,3-pentafluoro-1-propanol and its dimers: structural diversity, conformational conversion, and tunneling motion

Contents

Point S6.1. Gaussian keywords used in the calculations.

Calculations	Employed keywords
Geometry optimization	Freq, fopt=(verytight,MaxCycles=200), int=SuperFine; empiricaldispersion=gd3bj
Harmonic calculation	Freq=(VCD,VibRot), or Freq=(savenormalmodes,VibRot)
	B3LYP, Def2-QZVP, empiricaldispersion=gd3bj; PBE1PBE, Def2-TZVPD, empiricaldispersion=gd3bj; MP2, cc-pVTZ
Anharmonic calculations	Freq=Anharmonic, fopt=tight, int=SuperFine (for TZVP); and fopt=verytight, (for QZVP)
Transition calculation	opt=(calcall,ts,noeigentest), scf=verytight, int=grid=SuperFine
Rigid PES scan	scan
BSSE correction	density=current, counterpoise=2
Common keywords	output=picket

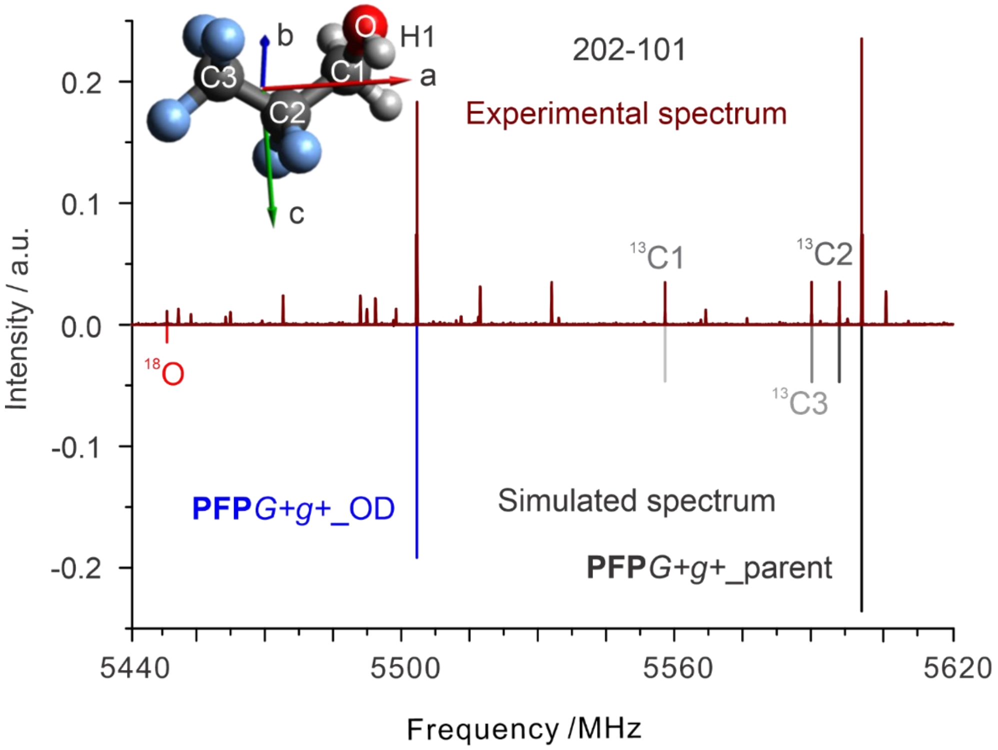

Figure S6.1. Experimental spectra of the **PFP***G*+*g*+/**PFP***G*-*g*- monomer and isotopologues species of its 2,0,2-1,0,1 transition of the PFP+D_2O mixture in the Ne atmosphere. The experimental spectroscopic constants, the calculated electric dipole moment components and a rotational temperature of 0.5 K were used for the spectral simulations. The experimental spectra were recorded by averaging about 900 k free induction decays.

Table S6.1. Rotational transition frequencies of the parent **PFP***G*+*g*+ monomer.

J'	K_a'	K_c'	J''	K_a''	K_c''	Obs/ MHz	Cal/ MHz	Obs - Cal/ MHz
4	1	3	4	1	4	2118.1766	2118.1757	0.0009
4	1	3	4	0	4	2234.4507	2234.4470	0.0037
2	2	1	2	1	2	2343.7751	2343.7759	-0.0008
5	3	2	5	2	3	2669.1246	2669.1171	0.0075
3	2	2	3	1	3	2698.7252	2698.7308	-0.0056
2	2	1	2	0	2	2742.2867	2742.2813	0.0054
1	0	1	0	0	0	2827.3625	2827.3649	-0.0024
4	3	2	4	2	2	2875.5745	2875.5743	0.0002
4	3	1	4	2	2	2929.1759	2929.1783	-0.0024
3	2	2	3	0	3	2932.0002	2931.9996	0.0006
3	2	1	3	1	3	2940.0504	2940.0449	0.0055
5	1	4	5	1	5	3057.9251	3057.9234	0.0017
5	1	4	5	0	5	3109.7134	3109.7116	0.0018
3	3	1	3	2	1	3151.2002	3151.1982	0.0020
3	3	0	3	2	1	3159.1253	3159.1271	-0.0018
4	2	3	4	1	4	3176.1133	3176.1103	0.0030
4	2	3	4	0	4	3292.3845	3292.3816	0.0029
7	2	5	7	1	6	3323.4127	3323.4166	-0.0039
1	1	1	0	0	0	3391.4452	3391.4460	-0.0008
3	3	1	3	2	2	3392.5119	3392.5124	-0.0005
3	3	0	3	2	2	3400.4417	3400.4413	0.0004
8	4	4	8	3	5	3504.7134	3504.7115	0.0019
4	3	2	4	2	3	3516.9767	3516.9731	0.0036
4	3	1	4	2	3	3570.5764	3570.5771	-0.0007
1	1	0	0	0	0	3608.6252	3608.6251	0.0001
5	3	3	5	2	4	3741.7379	3741.7370	0.0009
5	2	4	5	1	5	3765.1378	3765.1347	0.0031
7	4	3	7	3	4	3852.1488	3852.1447	0.0041
6	1	5	6	1	6	4031.1306	4031.1310	-0.0004
6	1	5	6	0	6	4052.5756	4052.5796	-0.0040
6	4	2	6	3	3	4199.5003	4199.4997	0.0006
5	4	2	5	3	2	4440.3648	4440.3667	-0.0019
6	2	5	6	1	6	4445.0748	4445.0748	0.0000
5	4	1	5	3	2	4449.2129	4449.2107	0.0022

6	2	5	6	0	6	4466.5241	4466.5234	0.0007
4	3	2	4	1	3	4574.9098	4574.9077	0.0021
4	4	1	4	3	1	4582.8165	4582.8174	-0.0009
4	4	0	4	3	1	4583.8245	4583.8225	0.0020
4	4	1	4	3	2	4636.4252	4636.4213	0.0039
4	4	0	4	3	2	4637.4252	4637.4265	-0.0013
5	4	2	5	3	3	4639.9873	4639.9885	-0.0012
5	4	1	5	3	3	4648.8374	4648.8325	0.0049
6	4	3	6	3	4	4685.3709	4685.3729	-0.0020
3	3	1	3	1	2	4796.0998	4796.1013	-0.0015
2	0	2	1	1	0	4821.8646	4821.8626	0.0020
7	1	6	7	0	7	4984.0842	4984.0838	0.0004
2	0	2	1	1	1	5039.0416	5039.0417	-0.0001
7	2	6	7	1	7	5190.2748	5190.2741	0.0007
7	2	6	7	0	7	5198.7375	5198.7372	0.0003
9	2	7	9	1	8	5298.6371	5298.6385	-0.0014
2	1	2	1	1	1	5437.5501	5437.5471	0.0030
3	0	3	2	2	0	5498.4876	5498.4794	0.0082
2	0	2	1	0	1	5603.1252	5603.1228	0.0024
16	7	10	16	6	10	5607.0499	5607.0505	-0.0006
3	1	3	2	2	0	5731.7499	5731.7482	0.0017
7	5	2	7	4	3	5744.0115	5744.0109	0.0006
3	1	3	2	2	1	5783.3512	5783.3501	0.0011
2	1	1	1	1	0	5871.9007	5871.9045	-0.0038
6	5	2	6	4	2	5872.9503	5872.9495	0.0008
6	5	1	6	4	2	5874.1992	5874.1928	0.0064
7	5	3	7	4	4	5882.1009	5882.1059	-0.0050
6	5	2	6	4	3	5915.4113	5915.4108	0.0005
6	5	1	6	4	3	5916.6501	5916.6541	-0.0040
5	5	1	5	4	2	5948.6377	5948.6388	-0.0011
5	5	0	5	4	2	5948.7518	5948.7538	-0.0020
2	1	2	1	0	1	6001.6258	6001.6282	-0.0024
3	3	0	3	1	3	6099.1759	6099.1720	0.0039
2	1	1	1	0	1	6653.1624	6653.1647	-0.0023
3	1	2	2	2	1	7078.5005	7078.4920	0.0085
2	2	1	1	1	0	7564.1377	7564.1439	-0.0062
2	2	1	1	1	1	7781.3249	7781.3230	0.0019

2	2	0	1	1	1	7832.9249	7832.9250	-0.0001
3	0	3	2	1	2	7893.8624	7893.8572	0.0052
3	1	3	2	1	2	8127.1255	8127.1261	-0.0006
3	0	3	2	0	2	8292.3626	8292.3627	-0.0001
3	1	3	2	0	2	8525.6366	8525.6315	0.0051
3	2	1	2	2	0	8671.7874	8671.7931	-0.0057
3	1	2	2	1	1	8770.7373	8770.7314	0.0059
3	2	2	2	1	1	10174.3128	10174.3204	-0.0076
4	1	3	3	2	2	10210.7759	10210.7678	0.0081
4	1	4	3	1	3	10791.3235	10791.3229	0.0006
4	0	4	3	0	3	10908.3154	10908.3204	-0.0050
4	1	4	3	0	3	11024.5874	11024.5917	-0.0043
3	2	1	2	1	2	11067.1631	11067.1710	-0.0079
4	2	3	3	2	2	11268.7021	11268.7024	-0.0003
4	3	2	3	3	1	11393.1709	11393.1632	0.0077
4	3	1	3	3	0	11438.8359	11438.8382	-0.0023
3	2	1	2	0	2	11465.6751	11465.6764	-0.0013
4	1	3	3	1	2	11614.3506	11614.3567	-0.0061
4	2	2	3	2	1	11668.7858	11668.7870	-0.0012
3	3	1	2	2	0	11822.9882	11822.9913	-0.0031
3	3	0	2	2	1	11882.5215	11882.5222	-0.0007

Table S6.2. Rotational transition frequencies of the ^{13}C1 **PFP***G*+*g*+ monomer.

J'	K_a'	K_c'	J''	K_a''	K_c''	Obs/ MHz	Cal/ MHz	Obs - Cal/ MHz
1	0	1	0	0	0	2821.5499	2821.5462	0.0037
2	0	2	1	1	1	5025.3692	5025.3719	-0.0027
2	0	2	1	0	1	5591.8859	5591.8897	-0.0038
2	1	2	1	1	1	5426.4317	5426.4331	-0.0014
2	1	1	1	1	0	5859.7439	5859.7426	0.0013
3	1	3	2	1	2	8110.6692	8110.6716	-0.0024
3	0	3	2	0	2	8276.2352	8276.2370	-0.0018
3	2	2	2	2	1	8464.6249	8464.6220	0.0029
3	2	1	2	2	0	8653.0074	8653.0022	0.0052
3	1	2	2	1	1	8752.8158	8752.8132	0.0026

2	1	2	1	0	1	5992.9497	5992.9509	-0.0012
1	1	1	0	0	0	3388.0637	3388.0640	-0.0003
4	1	4	3	1	3	10769.6749	10769.6654	0.0095
4	0	4	3	0	3	10887.3503	10887.3543	-0.0040
4	2	3	3	2	2	11245.7507	11245.7536	-0.0029
4	1	3	3	1	2	11591.2039	11591.2043	-0.0004
4	2	2	3	2	1	11643.5418	11643.5450	-0.0032
4	3	2	3	3	1	11369.3098	11369.3063	0.0035
4	3	1	3	3	0	11414.3763	11414.3807	-0.0044

Table S6.3. Rotational transition frequencies of the ^{13}C2 **PFP***G+g+* monomer.

J’	K_a’	K_c’	*J*”	K_a”	K_c”	Obs/ MHz	Cal/ MHz	Obs - Cal/ MHz
1	0	1	0	0	0	2821.5499	2821.5462	0.0037
1	1	1	0	0	0	3388.0637	3388.0646	-0.0009
2	0	2	1	1	1	5025.3692	5025.3712	-0.0020
2	1	2	1	1	1	5426.4317	5426.4332	-0.0015
2	0	2	1	0	1	5591.8859	5591.8897	-0.0038
2	1	1	1	1	0	5859.7439	5859.7424	0.0015
2	1	2	1	0	1	5992.9497	5992.9517	-0.0020
3	1	3	2	1	2	8110.6692	8110.6720	-0.0028
3	0	3	2	0	2	8276.2352	8276.2373	-0.0021
3	2	2	2	2	1	8464.6249	8464.6199	0.0050
3	2	1	2	2	0	8653.0074	8653.0040	0.0034
3	1	2	2	1	1	8752.8158	8752.8125	0.0033
4	1	4	3	1	3	10769.6749	10769.6672	0.0077
4	0	4	3	0	3	10887.3503	10887.3560	-0.0057
4	2	3	3	2	2	11245.7507	11245.7481	0.0026
4	3	2	3	3	1	11369.3098	11369.3053	0.0045
4	3	1	3	3	0	11414.3763	11414.3834	-0.0071
4	1	3	3	1	2	11591.2039	11591.2014	0.0025
4	2	2	3	2	1	11643.5418	11643.5482	-0.0064

Table S6.4. Rotational transition frequencies of the ^{13}C3 **PFP***G*+*g*+ monomer.

J'	K_a'	K_c'	*J"*	K_a"	K_c"	Obs/ MHz	Cal/ MHz	Obs - Cal/ MHz
1	0	1	0	0	0	2803.8751	2803.8736	0.0015
4	2	3	4	0	4	3294.7262	3294.7250	0.0012
2	0	2	1	1	1	4984.5821	4984.5749	0.0072
2	1	2	1	1	1	5395.8754	5395.8762	-0.0008
2	0	2	1	0	1	5559.1334	5559.1362	-0.0028
2	1	1	1	1	0	5819.6126	5819.6100	0.0026
3	1	3	2	1	2	8066.2327	8066.2370	-0.0043
3	0	3	2	0	2	8231.9672	8231.9752	-0.0080
3	2	2	2	2	1	8411.6093	8411.6038	0.0055
3	2	1	2	2	0	8591.2359	8591.2341	0.0018
3	1	2	2	1	1	8694.6374	8694.6407	-0.0033
4	1	4	3	1	3	10712.3142	10712.3188	-0.0046
4	0	4	3	0	3	10832.6252	10832.6183	0.0069
4	2	3	3	2	2	11177.1461	11177.1363	0.0098
4	3	2	3	3	1	11294.8546	11294.8569	-0.0023
4	3	1	3	3	0	11336.4269	11336.4306	-0.0037
4	1	3	3	1	2	11518.2085	11518.2068	0.0017
4	2	2	3	2	1	11559.0900	11559.0952	-0.0052

Table S6.5. Rotational transition frequencies of the ^{18}O **PFP***G*+*g*+ monomer.

J'	K_a'	K_c'	*J"*	K_a"	K_c"	Obs/ MHz	Cal/ MHz	Obs - Cal/ MHz
1	0	1	0	0	0	2748.4296	2748.4297	-0.0001
2	1	2	1	1	1	5282.6485	5282.6530	-0.0045
2	0	2	1	0	1	5447.9456	5447.9479	-0.0023
2	1	1	1	1	0	5711.0621	5711.0589	0.0032
2	1	2	1	0	1	5866.9892	5866.9912	-0.0020
3	1	3	2	1	2	7896.2145	7896.2196	-0.0051
3	0	3	2	0	2	8064.4076	8064.4088	-0.0012
3	2	2	2	2	1	8245.2788	8245.2747	0.0041
3	2	1	2	2	0	8426.1497	8426.1421	0.0076

3	1	2	2	1	1	8531.6242	8531.6232	0.0010
4	1	4	3	1	3	10485.3052	10485.3058	-0.0006
4	0	4	3	0	3	10607.8009	10607.7935	0.0074
4	2	3	3	2	2	10955.1228	10955.1252	-0.0024
4	2	2	3	2	1	11340.1359	11340.1423	-0.0064

Table S6.6. Rotational transition frequencies of **PFP***G*+*g*+ (OD) monomer.

J'	K_a'	K_c'	J''	K_a''	K_c''	Obs/ MHz	Cal/ MHz	Obs - Cal/ MHz
1	0	1	0	0	0	2775.4753	2775.4718	0.0035
2	2	1	2	0	2	2792.4624	2792.4586	0.0038
3	2	2	3	0	3	2967.4377	2967.4336	0.0041
5	1	4	5	1	5	2970.0485	2970.0515	-0.0030
4	3	1	4	2	2	3023.6855	3023.6874	-0.0019
4	2	3	4	1	4	3174.2238	3174.2185	0.0053
3	3	0	3	2	1	3243.0107	3243.0098	0.0009
4	2	3	4	0	4	3304.6794	3304.6782	0.0012
1	1	1	0	0	0	3356.9505	3356.9566	-0.0061
3	3	1	3	2	2	3458.3393	3458.3375	0.0018
1	1	0	0	0	0	3566.6067	3566.6074	-0.0007
4	3	2	4	2	3	3572.9503	3572.9555	-0.0052
5	2	4	5	1	5	3742.9258	3742.9273	-0.0015
5	3	3	5	2	4	3781.2447	3781.2479	-0.0032
5	2	4	5	0	5	3803.1582	3803.1566	0.0016
6	1	5	6	1	6	3933.5895	3933.5924	-0.0029
5	3	3	5	1	4	4554.1207	4554.1236	-0.0029
4	4	0	4	3	1	4691.3615	4691.3578	0.0037
4	3	2	4	1	3	4697.1863	4697.1925	-0.0062
2	0	2	1	1	0	4712.5872	4712.5826	0.0046
4	4	1	4	3	2	4737.0556	4737.0518	0.0038
5	4	2	5	3	3	4737.8015	4737.7989	0.0026
2	0	2	1	1	1	4922.2332	4922.2334	-0.0002
2	1	2	1	1	1	5341.2953	5341.2910	0.0043
2	0	2	1	0	1	5503.7124	5503.7182	-0.0058
2	1	1	1	1	0	5760.5932	5760.5918	0.0014

2	1	2	1	0	1	5922.7751	5922.7757	-0.0006
2	2	1	1	1	0	7505.0417	7505.0412	0.0005
3	1	3	2	1	2	7985.1005	7985.1069	-0.0064
3	0	3	2	0	2	8151.4335	8151.4363	-0.0028
3	2	2	2	2	1	8326.4173	8326.4113	0.0060
3	2	1	2	2	0	8501.3749	8501.3722	0.0027
3	1	2	2	1	1	8607.2001	8607.2022	-0.0021
4	1	4	3	1	3	10605.1499	10605.1507	-0.0008
4	0	4	3	0	3	10727.4135	10727.4192	-0.0057
4	2	3	3	2	2	11064.6656	11064.6638	0.0018
4	3	2	3	3	1	11179.2853	11179.2818	0.0035
4	1	3	3	1	2	11404.0869	11404.0852	0.0017

Table S6.7. Rotational transition frequencies of the **PFP***Tg*+ monomer. The ground state is noted as "0" and "1" for the excited states.

J'	K_a'	K_c'	stat	J''	K_a''	K_c''	stat	Obs/ MHz	Cal/ MHz	Obs - Cal/ MHz
1	0	1	0	0	0	0	0	2436.3895	2436.4022	-0.0127
5	0	5	0	4	1	3	1	2962.0498	2962.0471	0.0027
4	2	3	0	3	3	0	0	3077.6048	3077.6022	0.0026
4	2	2	0	3	3	1	0	3091.8937	3091.8950	-0.0013
6	1	6	1	6	2	4	0	3167.1012	3167.1018	-0.0006
3	1	3	0	2	2	0	0	3184.6473	3184.6494	-0.0021
3	1	3	1	2	2	0	1	3185.6693	3185.6715	-0.0022
6	1	5	0	5	2	3	1	3318.5042	3318.5020	0.0023
5	1	5	1	5	2	3	0	3319.1439	3319.1410	0.0029
3	1	2	0	2	2	1	0	3428.0946	3428.0945	0.0001
3	1	3	1	3	2	1	0	3526.1166	3526.1152	0.0014
2	0	2	0	1	1	1	0	3558.1396	3558.1380	0.0016
2	0	2	1	1	1	1	1	3558.3332	3558.3305	0.0027
2	1	2	1	2	2	0	0	3589.3117	3589.3089	0.0028
3	2	1	0	2	1	1	1	3601.2569	3601.2576	-0.0007
4	1	3	0	3	0	3	1	3630.8305	3630.8301	0.0004
1	1	1	0	0	0	0	0	3750.1398	3750.1432	-0.0034
1	1	1	1	0	0	0	1	3750.1398	3750.1357	0.0041

4	2	2	0	4	1	3	0	3813.3126	3813.3087	0.0039
4	2	2	1	4	1	3	1	3828.0002	3828.0003	-0.0001
3	2	1	0	3	1	2	0	3884.7715	3884.7721	-0.0006
3	2	1	1	3	1	2	1	3891.0456	3891.0462	-0.0006
2	2	0	1	2	1	1	1	3941.7009	3941.7013	-0.0004
2	2	0	0	2	1	1	0	3941.9003	3941.9019	-0.0016
5	1	4	1	5	2	4	0	3958.0753	3958.0807	-0.0054
2	2	1	0	2	1	2	0	4062.2089	4062.2098	-0.0009
6	1	5	1	6	2	5	0	4080.1371	4080.1357	0.0014
3	2	2	0	3	1	3	0	4122.5122	4122.5106	0.0016
3	2	2	1	3	1	3	1	4129.1326	4129.1313	0.0013
1	1	0	1	2	0	2	0	4134.2127	4134.2086	0.0041
4	2	3	0	4	1	4	0	4203.1221	4203.1189	0.0032
4	2	3	1	4	1	4	1	4218.7051	4218.7041	0.0010
2	2	0	1	3	1	2	0	4225.2147	4225.2158	-0.0011
5	2	4	0	5	1	5	0	4304.1645	4304.1626	0.0019
5	2	4	1	5	1	5	1	4331.0607	4331.0597	0.0010
5	5	0	0	5	4	2	1	4364.9799	4364.9798	0.0001
5	5	1	0	5	4	1	1	4364.9799	4364.9784	0.0015
8	1	7	1	8	2	7	0	4381.2747	4381.2740	0.0007
6	2	5	0	6	1	6	0	4425.7402	4425.7385	0.0017
7	2	6	0	7	1	7	0	4567.8628	4567.8671	-0.0043
2	1	2	0	1	1	1	0	4832.2625	4832.2619	0.0006
2	1	2	1	1	1	1	1	4832.8413	4832.8409	0.0004
2	0	2	0	1	0	1	0	4871.8797	4871.8790	0.0007
2	0	2	1	1	0	1	1	4872.0127	4872.0094	0.0033
2	1	1	0	1	1	0	0	4913.0999	4913.1003	-0.0004
2	1	1	1	1	1	0	1	4913.7369	4913.7341	0.0028
6	0	6	0	5	1	4	1	5268.5113	5268.5143	-0.0030
5	2	4	0	4	3	1	0	5516.7739	5516.7716	0.0024
4	1	4	1	3	2	1	1	5530.3004	5530.3031	-0.0027
4	1	4	0	3	2	1	0	5535.4219	5535.4139	0.0080
5	2	3	0	4	3	2	0	5550.2375	5550.2418	-0.0043
4	1	3	0	3	2	2	0	5944.2252	5944.2251	0.0001
4	2	2	0	3	1	2	1	5984.0328	5984.0340	-0.0012
3	0	3	1	2	1	2	1	6031.2382	6031.2462	-0.0080
3	0	3	0	2	1	2	0	6031.3855	6031.3837	0.0018

2	1	2	0	1	0	1	0	6146.0007	6146.0029	-0.0022
2	1	2	1	1	0	1	1	6146.5181	6146.5198	-0.0017
5	1	4	0	4	0	4	1	6172.4253	6172.4255	-0.0002
4	2	3	0	3	1	3	1	6212.4183	6212.4175	0.0008
3	3	0	0	2	2	0	1	6320.4875	6320.4868	0.0007
3	3	1	0	2	2	1	1	6321.3562	6321.3563	-0.0001
1	0	1	1	1	1	1	0	6338.2127	6338.2123	0.0004
2	0	2	1	2	1	2	0	6377.9626	6377.9598	0.0028
3	0	3	1	3	1	3	0	6435.9016	6435.9057	-0.0041
4	0	4	1	4	1	4	0	6510.0377	6510.0383	-0.0006
6	3	3	0	6	2	4	0	6592.3502	6592.3471	0.0031
5	0	5	1	5	1	5	0	6597.7049	6597.7033	0.0016
5	3	2	1	5	2	3	1	6601.6811	6601.6790	0.0021
5	3	2	0	5	2	3	0	6624.6394	6624.6415	-0.0021
4	3	1	1	4	2	2	1	6635.6835	6635.6827	0.0008
4	3	1	0	4	2	2	0	6646.7004	6646.6990	0.0014
4	3	2	1	4	2	3	1	6649.0732	6649.0734	-0.0002
5	3	3	0	5	2	4	0	6656.5402	6656.5463	-0.0061
3	3	0	1	3	2	1	1	6659.5035	6659.5069	-0.0034
4	3	2	0	4	2	3	0	6660.6243	6660.6242	0.0001
3	3	0	0	3	2	1	0	6660.9304	6660.9305	-0.0001
3	3	1	1	3	2	2	1	6664.0365	6664.0384	-0.0019
3	3	1	0	3	2	2	0	6665.6372	6665.6388	-0.0016
6	0	6	1	6	1	6	0	6695.6826	6695.6826	0.0000
7	0	7	1	7	1	7	0	6800.3514	6800.3507	0.0007
3	1	3	0	2	1	2	0	7247.8108	7247.8107	0.0001
3	1	3	1	2	1	2	1	7248.7242	7248.7215	0.0027
3	0	3	0	2	0	2	0	7305.5082	7305.5076	0.0006
3	0	3	1	2	0	2	1	7305.7547	7305.7565	-0.0018
3	2	2	0	2	2	1	0	7308.1116	7308.1115	0.0001
3	2	1	0	2	2	0	0	7311.9151	7311.9151	0.0000
4	0	4	0	3	1	3	0	8519.9516	8519.9538	-0.0022
3	1	3	0	2	0	2	0	8521.9333	8521.9346	-0.0013
2	2	1	0	1	1	0	0	8854.0524	8854.0506	0.0018
2	2	1	1	1	1	0	1	8854.5206	8854.5190	0.0016
3	1	3	1	3	0	3	0	8869.8096	8869.8080	0.0016
2	2	0	0	1	1	1	0	8895.4214	8895.4232	-0.0018

2	2	0	1	1	1	1	1	8895.8941	8895.8908	0.0033
2	1	2	1	2	0	2	0	8926.5913	8926.5941	-0.0028
1	1	1	1	1	0	1	0	8965.6325	8965.6322	0.0003
4	1	4	0	3	1	3	0	9662.6775	9662.6796	-0.0021
4	1	4	0	3	0	3	0	10879.1038	10879.1066	-0.0028
5	0	5	0	4	1	4	0	11020.9114	11020.9116	-0.0002
2	0	2	1	1	1	0	0	11169.8001	11169.8007	-0.0006
3	2	2	0	2	1	1	0	11249.0635	11249.0618	0.0017
3	2	2	1	2	1	1	1	11256.5034	11256.5041	-0.0007
3	2	1	0	2	1	2	0	11375.0828	11375.0764	0.0064
1	1	0	1	0	0	0	0	11442.4868	11442.4898	-0.0030

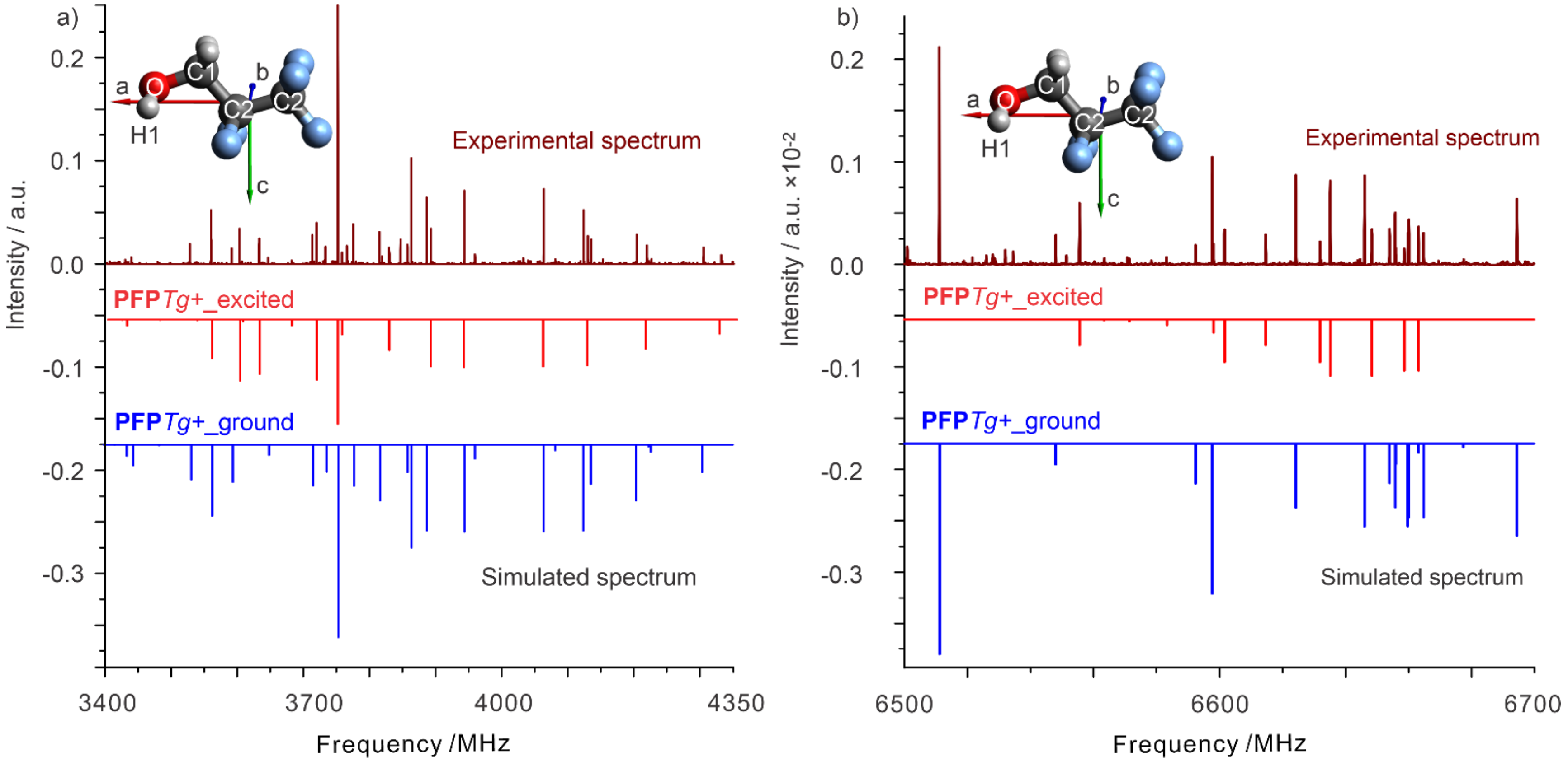

Figure S6.2. Experimental spectra of **PFP***Tg*+/**PFP***Tg*- monomer transitions measured using neon as a carrier gas. The ground state transitions are presented in blue and those of excited state in red. The known transitions of the **PFP***G*+*g*+/**PFP***G*-*g*- monomer and the PFP monohydrate species are removed for clarity. The experimental spectroscopic constants, the calculated electric dipole moment components, and a rotational temperature of 0.6 K were used for the spectral simulations. Please note that the b) 6.5-6.7 GHz is outside the usual operational range of the TWT and the power is lower at the higher frequency end. The experimental spectra were recorded by averaging about 900 k free induction decays.

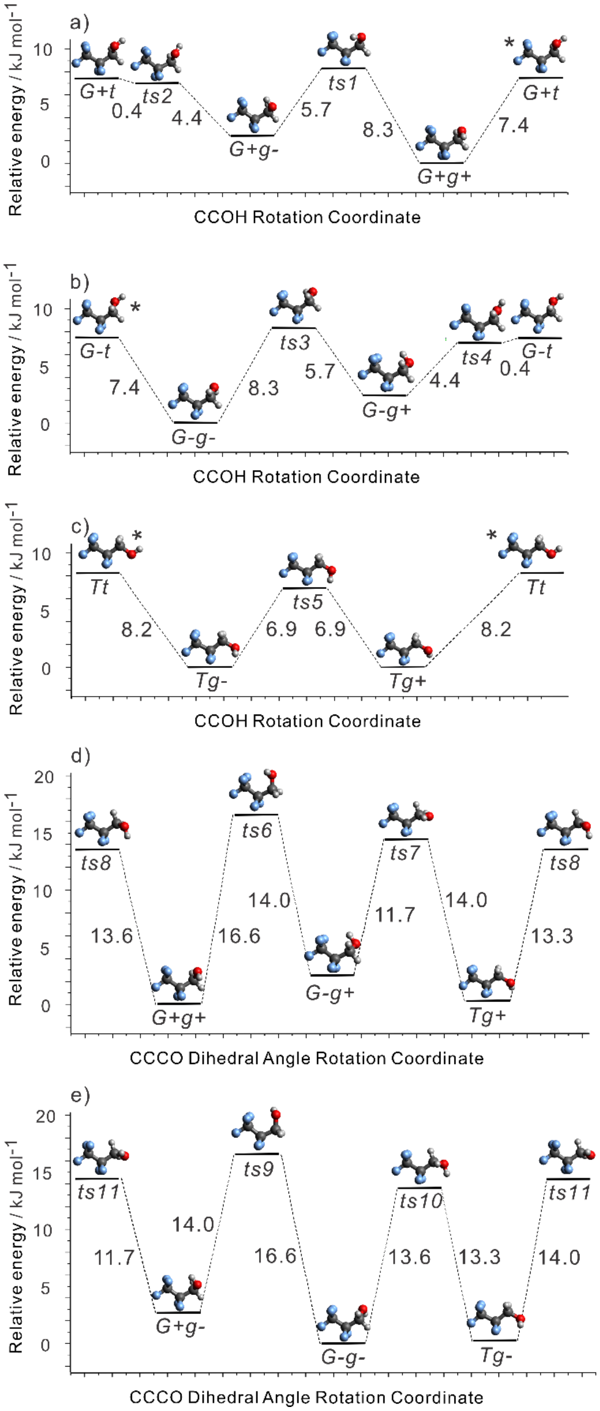

Figure S6.3. The interconversion barriers after *ZPE* corrections in kJ mol^{-1} of the **PFP** conformers at the B3LYP-D3(BJ)/def2-QZVP level. * indicates that the *t*-conformers are unstable, i.e., above the nearby transition states (see also Figure 4 in the main text).

Table S6.8. Experimental Kraitchman's coordinates (in Å) in the principal inertia axis of **PFP***G+g+*/*G-g-*.

Atom	*a*	*b*	*c*
^{13}C1	1.64862(91)[i]	-0.025(60)	0.6826(22)
^{13}C2	0.3892(39)	-0.5664(27)	0.0 [ii]
^{13}C3	-0.8365(18)	0.3012(50)	0.0
^{18}O1	2.12666(71)	1.1634113)	0.0
^{2}H1	2.42133(62)	0.8965(17)	-0.8446(18)

[i] Costain errors in units of the least significant digits are given in brackets.
[ii] Non-physical value and set to 0.0.

Table S6.9. The r_o structural parameters obtained from the STRFIT fit for **PFP***G+g+*/*G-g-*.[a]

parameter	exp. [b]	theo. [c]	Parameter	exp. [b]	theo. [c]
C1-C2 /Å	1.5448(34)	1.5247	H1-O1-C1 /°	105.1(25)	109.42
C2-C3 /Å	1.483(11)	1.5504	O1-C1-C2 /°	119.1(21)	113.32
C1-O1 /Å	1.334(35)	1.4038	H1-O1-C1-C2 /°	69.0(23)	62.92
H1-O1 /Å	0.892(39)	0.9615	O1-C1-C2-C3 /°	59.2(25)	63.34

[a] Bond lengths and angles are listed with four and two digits after the decimal points, respectively for consistency. These do not necessarily reflect their uncertainties. The atom numberings are provided in Figure 1.
[b] Structural parameters without error bars are directly read from the STRFIT output geometry.
[c] The equilibrium geometry at the B3LYP-D3(BJ)/def2-QZVP level of theory.

Table S6.10. Experimental r_0 coordinates (in Å) of **PFP***G-g-* monomer in the principal inertia axis based on the STRFIT geometry.[a]

Atom	*a*	*b*	*c*
C1	-1.648(17)	-0.057(16)	0.584(42)
H2	-1.431(37)	-0.393(44)	1.596(48)
H3	-2.393(15)	0.742(18)	0.637(35)
C2	-0.4262(52)	0.5645(22)	0.0181(19)
F1	-0.137(15)	1.679(21)	0.738(36)
F2	-0.662(30)	0.949(38)	-1.2693(45)
C3	0.8444(26)	-0.3141(32)	0.0075(11)
F3	0.708(15)	-1.352(22)	-0.819(33)
F4	1.083(28)	-0.779(37)	1.2427(93)
F5	1.9029(86)	0.401(11)	-0.385(41)
O1	-2.1231(74)	-1.1752(91)	0.0338(83)
H1	-2.430(14)	-0.928(35)	-0.766(35)

[a] The experimental rotational constants were used and some structural parameters were fixed at the values obtained at the B3LYP-D3BJ/def2-QZVP level.

Table S6.11. The r_e^{SE} geometry parameters obtained from the STRFIT fit for **PFP***G+g+*/*G-g-*.[a]

parameter	semi-exp. [b]	theo. [c]	Parameter	semi-exp. [b]	theo. [c]
C1-C2 /Å	1.5192(21)	1.5148	H1-O1-C1 /°	107.16(50)	107.82
C2-C3 /Å	1.54609(73)	1.5378	O1-C1-C2 /°	113.61(40)	112.99
C1-O1 /Å	1.3985(77)	1.4041	H1-O1-C1-C2 /°	65.43(45)	61.03
H1-O1 /Å	0.9560(87)	0.9624	O1-C1-C2-C3 /°	62.66(43)	62.63

[a] Bond lengths and angles are listed with four and two digits after the decimal points, respectively for consistency. These do not necessarily reflect their uncertainties. The atom numberings are in Figure 1.

[b] Structural parameters without error bars are directly read from the STRFIT output geometry.

[c] The equilibrium structural parameters at the MP2/cc-pVTZ level of theory.

Table S6.12. The r_e^{SE} coordinates (in Å) of **PFP***G*+*g*+/*G*-*g*- in its principal inertia axis.[a]

Atom	*a*	*b*	*c*
C1	-1.6511(37)	-0.0164(36)	0.6726(83)
H2	-2.3892(34)	0.7890(38)	0.6961(68)
H3	-1.4070(81)	-0.2922(93)	1.6941(89)
C2	-0.4150(11)	0.57638(44)	0.01799(35)
F1	-0.6916(62)	0.8885(77)	-1.27503(40)
F2	-0.0897(27)	1.7175(37)	0.6670(75)
C3	0.84404(58)	-0.32092(69)	0.01168(23)
F3	0.6698(28)	-1.3890(41)	-0.7583(70)
F4	1.8916(20)	0.3619(24)	-0.4443(80)
F5	1.1114(58)	-0.7260(76)	1.2555(14)
O1	-2.1258(16)	-1.1668(19)	0.0345(17)
H1	-2.4234(31)	-0.9044(79)	-0.8354(76)

[a] The semi-experimental equilibrium rotational constants were used. Some structural parameters were fixed at the values obtained at the MP2/cc-pVTZ level. See the main text for details.

Table S6.13. Comparison of the experimental bond lengths (in Å), angles (˚) and dihedral angle (˚) with the theoretical predictions at the indicated level of theory.

Atom	r_0	r_s	r_e^{SE}	MP2[a]	PBE[b]	B3LYP[c]
C1-C2 /Å	1.5448(34)	1.531(21)	1.5192(21)	1.51480	1.51906	1.52472
C2-C3 /Å	1.483(11)	1.5017(48)	1.54609(73)	1.53779	1.54484	1.55044
C1-O1 /Å	1.334(35)	1.452(49)	1.3985(77)	1.40409	1.39434	1.40379
H1-O1 /Å	0.892(39)	0.9337(18)	0.9560(87)	0.96240	0.96191	0.96149
H1-O1-C1 /°	105.1(25)	107.1(13)	107.16(50)	107.815	109.119	109.417
O1-C1-C2 /°	119.1(21)	110.5(15)	113.61(40)	112.994	113.407	113.320
H1-O1-C1-C2 /°	69.0(23)	67.1(20)	65.43(45)	61.027	62.111	62.919
O1-C1-C2-C3 /°	59.2(25)	63.6(15)	62.66(43)	62.634	64.144	63.337

[a] At the MP2/cc-pVTZ level of theory.
[b] At the PBE1PBE-D3BJ/def2-TZVPD level of theory.
[c] At the B3LYP-D3BJ/def2-QZVP level of theory.

Table S6.14. Full list of the properties of the for 2,2,3,3,3-pentafluoro-1-propanol homodimer conformations predicted at the B3LYP- D3(BJ)/def2-QZVP level of theory.

#	Homodimers	ΔE_{raw} [a]	ΔE_0 [b]	ΔE_b [c]	*A* [d]	*B* [d]	*C* [d]	$\lvert\mu_a\rvert$ [e]	$\lvert\mu_b\rvert$ [e]	$\lvert\mu_c\rvert$ [e]
I	**PFP**G+g+**PFP**Tg+	0.0	0.0	23.4	990.7	156.9	154.3	2.7	0.6	1.0
2	**PFP**G+g+**PFP**G+g+	0.7	0.4	22.8	848.5	171.1	167.2	2.0	1.1	0.3
3	**PFP**Tg+**PFP**Tg+	0.3	0.4	23.3	767.4	185.9	172.1	2.7	0.1	0.9
4	**PFP**G+g+**PFP**G-g-	1.1	0.5	22.6	793.7	191.5	184.0	2.4	1.6	0.1
5	**PFP**G+g+**PFP**Tg-	0.9	0.5	22.9	793.9	179.3	169.0	2.8	-1.5	-0.7
6	**PFP**Tg+**PFP**G-g-	1.0	0.6	22.8	679.3	229.4	202.9	2.6	1.2	0.3
7	**PFP**Tg+**PFP**Tg-	1.0	0.7	23.0	650.4	218.2	189.7	3.0	1.2	0.1
8	**PFP**G+g+**PFP**Tg+	0.8	0.9	22.5	764.3	169.4	160.7	0.7	0.8	0.5
9	**PFP**Tg+**PFP**G+g+	1.3	0.9	22.5	724.2	187.1	180.5	2.1	0.6	0.6
10	**PFP**G+g+**PFP**G+g+_2	0.9	1.0	22.2	834.6	161.4	155.5	0.6	1.0	0.3
11	**PFP**G+g+**PFP**G-g-_2	1.4	1.0	22.1	715.3	194.3	189.6	0.9	2.2	0.7
12	**PFP**G+g+**PFP**G+g+_3	1.7	1.4	21.7	714.1	215.9	200.5	1.4	3.5	0.3
13	**PFP**G+g+**PFP**Tg-_2	1.7	1.5	22.0	715.4	176.3	164.6	0.6	1.8	1.0
14	**PFP**G+g+**PFP**Tg+_2	2.0	1.7	21.7	709.7	202.1	185.6	1.1	2.6	1.9
15	**PFP**G+g+**PFP**G-g-_3	2.2	1.8	21.3	738.4	197.5	188.5	1.2	3.3	0.4
16	**PFP**G+g+**PFP**Tg-_3	2.3	2.1	-21.3	830.5	175.7	167.8	1.4	2.9	1.2
17	**PFP**G+g+**PFP**G-g+	2.3	2.1	-23.6	830.0	187.1	177.3	2.8	0.3	1.2
18	**PFP**Tg+**PFP**G-g+	2.3	2.3	-23.8	680.3	225.6	200.3	2.8	0.0	0.8
19	**PFP**Tg+**PFP**G+g+_2	2.8	2.5	-20.9	806.0	141.8	138.0	0.9	0.6	0.5
20	**PFP**G+g-**PFP**Tg-	3.0	2.6	-23.4	825.5	182.1	178.1	3.3	0.1	1.4
21	**PFP**Tg+**PFP**G+g+_3	3.0	2.6	-20.8	810.8	173.5	171.3	0.7	3.4	1.0
22	**PFP**Tg+**PFP**Tg+_2	3.0	2.8	-21.0	963.1	122.7	120.1	0.5	0.7	0.4
23	**PFP**Tg+**PFP**G-g-_2	3.3	2.9	-20.5	877.9	156.9	151.5	0.5	2.3	2.5
24	**PFP**Tg+ **PFP**Tg+_2	3.3	2.9	-20.8	813.6	153.6	146.6	1.0	1.1	3.3
25	**PFP**G+g+**PFP**G+g-	3.4	3.0	-22.8	925.5	164.9	160.6	3.1	1.0	0.8
26	**PFP**G+g-**PFP**G-g-	3.6	3.0	-22.7	736.8	200.5	196.5	2.7	1.0	1.0
27	**PFP**Tg+**PFP**Tg-_2	3.2	3.0	-20.7	835.0	146.3	142.3	1.0	0.8	0.3
28	**PFP**G+g+**PFP**G-g-_4	2.9	3.1	-22.7	718.6	196.3	185.4	0.7	0.9	0.2
29	**PFP**Tg+**PFP**Tg-_3	3.3	3.1	-20.7	1031.9	133.6	132.0	1.0	1.1	3.1
30	**PFP**Tg+**PFP**G+g-_2	3.6	3.3	-22.7	762.4	190.6	176.4	3.3	0.7	0.2
31	**PFP**G+g+**PFP**G+g-_2	3.6	3.5	-22.3	715.1	215.3	200.0	1.4	2.3	2.1
32	**PFP**G+g-**PFP**Tg+	4.1	3.6	-22.5	721.2	207.8	192.8	3.2	1.0	1.1
33	**PFP**G+g+ **PFP**Tg-_2	4.1	3.8	-19.7	790.9	157.7	155.9	0.0	0.3	1.8
34	**PFP**G+g+**PFP**G+g-_3	4.3	4.0	-21.7	839.0	157.7	153.8	1.3	1.8	0.7

35	PFPG+g-PFPG+g+	4.9	4.1	-21.6	715.5	209.1	208.4	2.7	1.4	0.2
36	PFPG+g-PFPG+g+_2	4.7	4.2	-21.5	745.1	207.1	190.6	2.1	2.1	0.6
37	PFPG+g+PFPG-g+_2	4.6	4.3	-21.5	833.4	178.8	170.7	1.7	2.7	1.5
38	PFPG+g-PFPG+g-	5.1	4.7	-23.7	725.6	216.4	200.5	3.4	0.4	1.1
39	PFPG+g-PFPTg-_2	4.7	4.7	-21.3	852.1	157.3	152.1	0.3	0.4	0.7
40	PFPG+g-PFPG-g-_2	4.7	4.7	-21.3	870.9	158.8	151.8	0.4	0.3	0.6
41	PFPG+g-PFPG-g-_3	5.3	4.8	-21.0	754.1	198.6	196.4	1.3	0.4	3.7
42	PFPTg+PFPG+g-	5.0	4.8	-21.3	834.4	167.3	160.6	0.8	0.9	3.1
43	PFPTg+PFPG-g+_2	5.1	4.8	-21.2	786.8	149.0	140.0	0.6	0.7	0.2
44	PFPTg+PFPG-g-_3	5.3	4.9	-18.5	859.0	146.2	138.9	0.0	0.8	1.5
45	PFPTg+PFPTg-_4	5.2	4.9	-18.8	718.8	161.4	148.4	0.3	1.0	1.3
46	PFPG+g-PFPG+g+_3	5.6	5.0	-20.7	799.6	176.2	166.5	1.3	2.0	2.8
47	PFPG+g-PFPTg-_2	5.6	5.1	-21.0	788.4	183.7	170.6	1.8	1.3	3.5
48	PFPG+g-PFPG+g+_4	5.7	5.1	-20.6	776.0	193.7	188.7	1.4	1.4	3.3
49	PFPTg+PFPG-g+_3	5.3	5.2	-20.9	770.9	171.0	158.0	0.9	0.6	0.7
50	PFPG+g-PFPTg+_2	5.7	5.3	-20.7	903.9	169.7	163.4	1.8	0.7	3.4
51	PFPTg+PFPG-g+_4	5.7	5.4	-20.7	963.4	143.7	141.5	1.4	0.7	3.3
52	PFPG+g-PFPTg+_3	6.0	5.7	-20.4	816.7	158.5	153.7	1.2	0.5	1.7
53	PFPG+g-PFPG-g+	6.6	6.1	-22.3	809.6	190.3	182.9	3.4	0.1	1.2
54	PFPG+g+PFPG+t	7.3	6.2	-26.1	883.3	180.0	177.1	0.2	0.5	2.0
55	PFPG+g-PFPG+g-_2	6.7	6.8	-21.5	790.8	185.4	170.4	0.4	0.2	0.7
56	PFPTg+PFPG+t	8.2	7.1	-25.5	846.9	174.6	167.2	0.4	1.0	2.0
57	PFPG+g+PFPG-t	7.8	7.2	-25.2	876.2	161.4	156.9	1.1	0.6	1.6
58	PFPG+g-PFPG-g+_2	7.7	7.2	-21.2	790.4	178.8	168.3	1.7	0.0	3.3
59	PFPTg+PFPG-t	9.0	7.3	-25.4	793.6	169.2	161.3	1.2	0.3	2.7
60	PFPG+g-PFPG+g-_3	8.0	7.5	-20.9	866.3	173.7	165.1	2.2	0.6	3.5
61	PFPG+g+PFPG+t_2	8.5	7.6	-24.7	800.7	177.8	174.8	1.4	0.9	1.1
62	PFPTg+PFPTt	9.0	7.8	-26.0	706.2	193.8	175.7	0.9	0.7	2.0
63	PFPG+g+PFPTt	8.5	7.8	-25.6	818.4	165.6	158.0	1.1	0.2	1.6
64	PFPG+g-PFPG-g+_3	8.0	7.8	-20.6	778.0	182.7	169.0	0.9	0.2	1.9
65	PFPG+g-PFPG-t	9.2	8.3	-26.7	817.2	191.1	183.9	1.0	2.8	0.5
66	PFPTg+PFPG-t_2	9.7	8.4	-24.3	722.6	209.4	198.6	-0.6	0.7	1.7
67	PFPTg+PFPG-t_3	9.9	8.6	-24.1	896.7	145.5	141.0	0.1	1.9	0.6
68	PFPG+tPFPG+g+	10.4	9.0	-16.7	739.7	210.3	192.0	3.9	2.8	0.8
69	PFPG+g-PFPTt	10.2	9.1	-33.6	779.4	187.2	182.5	1.6	2.1	1.5
70	PFPTg+PFPTt_2	10.4	9.2	-24.5	1080.5	123.0	121.9	0.2	2.0	0.8
71	PFPG+g-PFPG+t	10.9	9.3	-25.7	764.8	188.7	187.8	2.0	1.2	2.6
72	PFPG+g-PFPG+t_2	10.8	9.8	-25.2	743.9	213.0	202.6	0.8	2.1	0.8

73	**PFP***G*+*g*-**PFP***Tt*_2	13.2	12.3	-30.4	863.8	163.5	158.3	0.0	2.0	2.3
74	**PFP***G*+*g*+**PFP***G*-*t*_2	16.7	14.1	-18.3	707.2	214.7	202.1	3.3	4.2	1.6
75	**PFP***G*+*g*+**PFP***Tt*_2	17.1	15.0	-18.5	737.4	193.6	180.3	3.0	4.5	0.9
76	**PFP***G*+*t* **PFP***G*-*t*	18.8	16.4	-25.2	767.7	164.2	161.0	5.4	2.4	2.2
77	**PFP***G*+*t***PFP***G*+*t*	18.9	16.6	-25.0	806.6	156.6	153.6	5.1	3.1	1.3
78	**PFP***G*+*t* **PFP***G*-*t*_2	21.1	18.8	-22.8	865.7	154.2	145.6	2.9	2.3	0.6

Table S6.15. Rotational transition frequencies of the **PFP***G*+*g*+**PFP***Tg*+ homodimer.

J'	K_a'	K_c'	*J"*	K_a"	K_c"	Obs/ MHz	Cal/ MHz	Obs - Cal/ MHz
5	1	5	4	1	4	1547.7504	1547.7511	-0.0007
5	0	5	4	0	4	1554.0237	1554.0248	-0.0011
5	3	3	4	3	2	1554.1742	1554.1747	-0.0005
5	3	2	4	3	1	1554.1742	1554.1749	-0.0007
5	4	2	4	4	1	1554.1783	1554.1792	-0.0009
5	4	1	4	4	0	1554.1783	1554.1792	-0.0009
5	2	3	4	2	2	1554.2502	1554.2495	0.0007
5	1	4	4	1	3	1560.4817	1560.4821	-0.0004
6	1	6	5	1	5	1857.2792	1857.2794	-0.0002
6	0	6	5	0	5	1864.7596	1864.7598	-0.0002
6	2	5	5	2	4	1864.9428	1864.9433	-0.0005
6	3	3	5	3	2	1865.0113	1865.0113	0.0000
6	3	4	5	3	3	1865.0113	1865.0109	0.0004
6	4	3	5	4	2	1865.0130	1865.0128	0.0002
6	4	2	5	4	1	1865.0130	1865.0128	0.0002
6	5	2	5	5	1	1865.0251	1865.0253	-0.0002
6	5	1	5	5	0	1865.0251	1865.0253	-0.0002
6	2	4	5	2	3	1865.1463	1865.1459	0.0004
6	1	5	5	1	4	1872.5552	1872.5557	-0.0005
4	1	3	3	0	3	2096.4035	2096.4031	0.0004
7	1	7	6	1	6	2166.7959	2166.7957	0.0002
7	0	7	6	0	6	2175.4569	2175.4567	0.0002
7	2	6	6	2	5	2175.7438	2175.7435	0.0003
7	3	5	6	3	4	2175.8486	2175.8477	0.0009
7	3	4	6	3	3	2175.8486	2175.8487	-0.0001

7	2	5	6	2	4	2176.0674	2176.0675	-0.0001
7	1	6	6	1	5	2184.6170	2184.6169	0.0001
5	1	4	4	0	4	2413.6276	2413.6271	0.0005
8	1	8	7	1	7	2476.2999	2476.2981	0.0018
8	0	8	7	0	7	2486.1093	2486.1091	0.0002
8	2	7	7	2	6	2486.5326	2486.5327	-0.0001
8	4	5	7	4	4	2486.6753	2486.6757	-0.0004
8	4	4	7	4	3	2486.6753	2486.6757	-0.0004
8	3	5	7	3	4	2486.6863	2486.6872	-0.0009
8	3	6	7	3	5	2486.6863	2486.6852	0.0011
8	5	4	7	5	3	2486.6863	2486.6870	-0.0007
8	5	3	7	5	2	2486.6863	2486.6870	-0.0007
8	6	3	7	6	2	2486.7095	2486.7096	-0.0001
8	6	2	7	6	1	2486.7095	2486.7096	-0.0001
8	2	6	7	2	5	2487.0187	2487.0187	0.0000
8	1	7	7	1	6	2496.6631	2496.6634	-0.0003
6	1	5	5	0	5	2732.1585	2732.1581	0.0004
9	1	9	8	1	8	2785.7853	2785.7848	0.0005
9	0	9	8	0	8	2796.7118	2796.7109	0.0009
9	2	8	8	2	7	2797.3096	2797.3094	0.0002
9	4	6	8	4	5	2797.5041	2797.5047	-0.0006
9	4	5	8	4	4	2797.5041	2797.5047	-0.0006
9	5	4	8	5	3	2797.5131	2797.5137	-0.0006
9	5	5	8	5	4	2797.5131	2797.5137	-0.0006
9	3	7	8	3	6	2797.5237	2797.5233	0.0004
9	3	6	8	3	5	2797.5265	2797.5270	-0.0005
9	6	3	8	6	2	2797.5378	2797.5371	0.0007
9	6	4	8	6	3	2797.5378	2797.5371	0.0007
9	2	7	8	2	6	2798.0028	2798.0034	-0.0006
9	1	8	8	1	7	2808.6939	2808.6932	0.0007
12	0	12	11	1	11	2968.6564	2968.6566	-0.0002
7	1	7	6	0	6	2980.7249	2980.7232	0.0017
7	1	6	6	0	6	3052.0161	3052.0152	0.0009
13	0	13	12	1	11	3094.4809	3094.4799	0.0010
10	1	10	9	1	9	3095.2543	3095.2539	0.0004
10	0	10	9	0	9	3107.2561	3107.2557	0.0004
10	2	9	9	2	8	3108.0723	3108.0720	0.0003

10	4	6	9	4	5	3108.3319	3108.3318	0.0001
10	4	7	9	4	6	3108.3319	3108.3318	0.0001
10	5	6	9	5	5	3108.3373	3108.3371	0.0002
10	5	5	9	5	4	3108.3373	3108.3371	0.0002
10	3	8	9	3	7	3108.3612	3108.3620	-0.0008
10	6	5	9	6	4	3108.3612	3108.3606	0.0006
10	6	4	9	6	3	3108.3612	3108.3606	0.0006
10	3	7	9	3	6	3108.3683	3108.3685	-0.0002
10	2	8	9	2	7	3109.0253	3109.0258	-0.0005
10	1	9	9	1	8	3120.7035	3120.7039	-0.0004
8	1	8	7	0	7	3281.5645	3281.5646	-0.0001
8	1	7	7	0	7	3373.2244	3373.2219	0.0025
14	0	14	13	1	12	3386.6249	3386.6255	-0.0006
11	1	11	10	1	10	3404.7049	3404.7036	0.0013
11	0	11	10	0	10	3417.7375	3417.7375	0.0000
11	2	10	10	2	9	3418.8197	3418.8190	0.0007
11	4	7	10	4	6	3419.1566	3419.1568	-0.0002
11	5	7	10	5	6	3419.1566	3419.1569	-0.0003
11	4	8	10	4	7	3419.1566	3419.1567	-0.0001
11	5	6	10	5	5	3419.1566	3419.1569	-0.0003
11	3	8	10	3	7	3419.2118	3419.2118	0.0000
11	2	9	10	2	8	3420.0885	3420.0898	-0.0013
11	1	10	10	1	9	3432.6942	3432.6934	0.0008
3	2	2	2	1	1	3475.6751	3475.6742	0.0009
3	2	1	2	1	1	3475.7031	3475.7032	-0.0001
15	0	15	14	1	13	3677.0296	3677.0302	-0.0006
9	1	8	8	0	8	3695.8044	3695.8059	-0.0015
12	1	12	11	1	11	3714.1342	3714.1321	0.0021
12	0	12	11	0	11	3728.1501	3728.1503	-0.0002
12	2	11	11	2	10	3729.5478	3729.5488	-0.0010
12	5	7	11	5	6	3729.9723	3729.9728	-0.0005
12	5	8	11	5	7	3729.9723	3729.9728	-0.0005
12	4	8	11	4	7	3729.9785	3729.9794	-0.0009
12	4	9	11	4	8	3729.9785	3729.9793	-0.0008
12	6	6	11	6	5	3729.9924	3729.9940	-0.0016
12	6	7	11	6	6	3729.9924	3729.9940	-0.0016
12	3	10	11	3	9	3730.0406	3730.0412	-0.0006

12	3	9	11	3	8	3730.0582	3730.0575	0.0007
12	2	10	11	2	9	3731.1995	3731.1994	0.0001
12	1	11	11	1	10	3744.6613	3744.6594	0.0019
10	1	10	9	0	9	3879.7854	3879.7834	0.0020
10	1	9	9	0	9	4019.7999	4019.7990	0.0009
13	1	13	12	1	12	4023.5364	4023.5375	-0.0011
13	0	13	12	0	12	4038.4883	4038.4881	0.0002
13	2	12	12	2	11	4040.2611	4040.2599	0.0012
13	5	9	12	5	8	4040.7841	4040.7843	-0.0002
13	5	8	12	5	7	4040.7841	4040.7843	-0.0002
13	4	9	12	4	8	4040.8005	4040.7994	0.0011
13	4	10	12	4	9	4040.8005	4040.7993	0.0012
13	3	11	12	3	10	4040.8806	4040.8814	-0.0008
13	2	11	12	2	10	4042.3603	4042.3583	0.0020
13	1	12	12	1	11	4056.5999	4056.5995	0.0004
18	3	16	18	2	16	4311.9884	4311.9898	-0.0014
17	3	15	17	2	15	4315.9212	4315.9200	0.0012
16	3	14	16	2	14	4319.2337	4319.2341	-0.0004
14	1	14	13	1	13	4332.9164	4332.9184	-0.0020
11	3	8	11	2	10	4332.9164	4332.9158	0.0006
20	3	17	20	2	19	4344.6631	4344.6636	-0.0005
11	1	10	10	0	10	4345.2372	4345.2366	0.0006
14	0	14	13	0	13	4348.7445	4348.7452	-0.0007
14	2	13	13	2	12	4350.9506	4350.9507	-0.0001
14	2	12	13	2	11	4353.5711	4353.5702	0.0009
14	1	13	13	1	12	4368.5121	4368.5114	0.0007
6	2	5	5	1	5	4431.0751	4431.0760	-0.0009
17	0	17	16	1	16	4598.3176	4598.3197	-0.0021
15	1	15	14	1	14	4642.2746	4642.2729	0.0017
15	0	15	14	0	14	4658.9158	4658.9161	-0.0003
15	2	14	14	2	13	4661.6199	4661.6196	0.0003
15	4	11	14	4	10	4662.4316	4662.4310	0.0006
15	4	12	14	4	11	4662.4316	4662.4307	0.0009
15	7	8	14	7	7	4662.4422	4662.4419	0.0003
15	7	9	14	7	8	4662.4422	4662.4419	0.0003
15	2	13	14	2	12	4664.8384	4664.8382	0.0002
12	1	11	11	0	11	4672.1581	4672.1584	-0.0003

15	1	14	14	1	13	4680.3907	4680.3928	-0.0021
7	2	6	6	1	6	4749.5386	4749.5401	-0.0015
18	0	18	17	1	17	4926.2831	4926.2839	-0.0008
16	1	16	15	1	15	4951.5993	4951.5996	-0.0003
16	0	16	15	0	15	4968.9937	4968.9956	-0.0019
16	2	15	15	2	14	4972.2645	4972.2652	-0.0007
16	5	12	15	5	11	4973.1893	4973.1892	0.0001
16	5	11	15	5	10	4973.1893	4973.1892	0.0001
16	6	10	15	6	9	4973.1941	4973.1941	0.0000
16	6	11	15	6	10	4973.1941	4973.1941	0.0000
16	7	10	15	7	9	4973.2314	4973.2311	0.0003
16	7	9	15	7	8	4973.2314	4973.2311	0.0003
16	4	13	15	4	12	4973.2425	4973.2417	0.0008
16	4	12	15	4	11	4973.2425	4973.2421	0.0004
16	3	14	15	3	13	4973.3995	4973.4019	-0.0024
16	3	13	15	3	12	4973.4708	4973.4713	-0.0005
16	2	14	15	2	13	4976.1649	4976.1657	-0.0008
16	1	15	15	1	14	4992.2416	4992.2410	0.0006
13	1	12	12	0	12	5000.6072	5000.6077	-0.0005
14	1	14	13	0	13	5063.4414	5063.4434	-0.0020
9	5	4	10	4	6	5234.2559	5234.2564	-0.0005
9	5	4	10	4	7	5234.2559	5234.2565	-0.0006
9	5	5	10	4	7	5234.2559	5234.2565	-0.0006
9	5	5	10	4	6	5234.2559	5234.2564	-0.0005
17	1	17	16	1	16	5260.8945	5260.8968	-0.0023
17	0	17	16	0	16	5278.9783	5278.9788	-0.0005
17	2	16	16	2	15	5282.8854	5282.8858	-0.0004
17	5	12	16	5	11	5283.9791	5283.9798	-0.0007
17	6	11	16	6	10	5283.9791	5283.9777	0.0014
17	6	12	16	6	11	5283.9791	5283.9777	0.0014
17	5	13	16	5	12	5283.9791	5283.9798	-0.0007
17	7	10	16	7	9	5284.0119	5284.0125	-0.0006
17	7	11	16	7	10	5284.0119	5284.0125	-0.0006
17	4	13	16	4	12	5284.0514	5284.0499	0.0015
17	4	13	16	4	12	5284.0514	5284.0499	0.0015
17	4	14	16	4	13	5284.0514	5284.0491	0.0023
17	3	15	16	3	14	5284.2405	5284.2411	-0.0006

17	3	14	16	3	13	5284.3351	5284.3352	-0.0001
17	2	15	16	2	14	5287.5563	5287.5553	0.0010
9	2	7	8	1	7	5300.5392	5300.5404	-0.0012
17	1	16	16	1	15	5304.0525	5304.0535	-0.001
14	1	13	13	0	13	5330.6316	5330.6311	0.0005
15	1	15	14	0	14	5356.9734	5356.9711	0.0023
9	2	8	8	1	8	5390.2871	5390.2883	-0.0012
8	5	3	9	4	5	5545.0754	5545.0746	0.0008
8	5	4	9	4	5	5545.0754	5545.0746	0.0008
8	5	4	9	4	6	5545.0754	5545.0746	0.0008
8	5	3	9	4	6	5545.0754	5545.0746	0.0008
18	1	18	17	1	17	5570.1609	5570.1632	-0.0023
18	0	18	17	0	17	5588.8602	5588.8610	-0.0008
18	2	17	17	2	16	5593.4813	5593.4799	0.0014
18	5	14	17	5	13	5594.7624	5594.7642	-0.0018
18	5	13	17	5	12	5594.7624	5594.7642	-0.0018
18	3	16	17	3	15	5595.0783	5595.0792	-0.0009
18	3	15	17	3	14	5595.2067	5595.2045	0.0022
18	2	16	17	2	15	5599.0096	5599.0094	0.0002
18	1	17	17	1	16	5615.8274	5615.8278	-0.0004
16	1	16	15	0	15	5649.6539	5649.6546	-0.0007
7	5	3	8	4	5	5855.8921	5855.8923	-0.0002
7	5	3	8	4	4	5855.8921	5855.8923	-0.0002
7	5	2	8	4	4	5855.8921	5855.8923	-0.0002
7	5	2	8	4	5	5855.8921	5855.8923	-0.0002
19	1	19	18	1	18	5879.4001	5879.3973	0.0028
19	0	19	18	0	18	5898.6361	5898.6383	-0.0022
19	2	18	18	2	17	5904.0467	5904.046	0.0007
19	6	13	18	6	12	5905.5219	5905.5219	0.0000
19	6	14	18	6	13	5905.5219	5905.5219	0.0000
19	4	16	18	4	15	5905.6555	5905.6527	0.0028
19	4	15	18	4	14	5905.6555	5905.6543	0.0012
19	3	17	18	3	16	5905.9143	5905.9157	-0.0014
19	3	16	18	3	15	5906.0802	5906.0800	0.0002
19	2	17	18	2	16	5910.5295	5910.5300	-0.0005
19	1	18	18	1	17	5927.5621	5927.5612	0.0009
16	1	15	15	0	15	5995.6054	5995.6036	0.0018

20	1	20	19	1	19	6188.5998	6188.5977	0.0021
20	0	20	19	0	19	6208.3048	6208.3070	-0.0022
20	2	19	19	2	18	6214.5827	6214.5825	0.0002
20	5	15	19	5	14	6216.3127	6216.3131	-0.0004
20	5	16	19	5	15	6216.3127	6216.3131	-0.0004
20	4	16	19	4	15	6216.4497	6216.4506	-0.0009
20	4	17	19	4	16	6216.4497	6216.4484	0.0013
20	3	18	19	3	17	6216.7507	6216.7500	0.0007
20	3	17	19	3	16	6216.9629	6216.9626	0.0003
20	2	18	19	2	17	6222.1192	6222.1187	0.0005
20	1	19	19	1	18	6239.2499	6239.2510	-0.0011

Table S6.16. Rotational transition frequencies of the **PFP***G*+*g*+**PFP***G*+*g*+ homodimer.

J’	K_a’	K_c’	*J*”	K_a”	K_c”	Obs/ MHz	Cal/ MHz	Obs - Cal/ MHz
5	1	4	4	1	3	1692.1842	1692.1846	-0.0004
14	2	12	14	1	13	1892.3407	1892.3395	0.0012
6	1	6	5	1	5	2007.2750	2007.2730	0.0020
6	0	6	5	0	5	2018.4760	2018.4738	0.0022
6	2	5	5	2	4	2018.9797	2018.9800	-0.0003
6	4	3	5	4	2	2019.1249	2019.1259	-0.0010
6	5	1	5	5	0	2019.1249	2019.1232	0.0017
6	5	2	5	5	1	2019.1249	2019.1232	0.0017
6	4	2	5	4	1	2019.1249	2019.1260	-0.0011
6	3	4	5	3	3	2019.1513	2019.1499	0.0014
6	3	3	5	3	2	2019.1513	2019.1523	-0.0010
6	2	4	5	2	3	2019.5544	2019.5551	-0.0007
6	2	4	6	1	5	2024.0249	2024.0263	-0.0014
6	1	5	5	1	4	2030.5623	2030.5641	-0.0018
4	2	3	4	1	4	2082.9547	2082.9521	0.0026
5	2	4	5	1	5	2092.6932	2092.6963	-0.0031
5	1	5	4	0	4	2341.4008	2341.4013	-0.0005
7	1	7	6	1	6	2341.7434	2341.7425	0.0009
7	0	7	6	0	6	2354.6222	2354.6220	0.0002
7	2	6	6	2	5	2355.4160	2355.4196	-0.0036

7	2	5	6	2	4	2356.3410	2356.3392	0.0018
7	1	6	6	1	5	2368.9140	2368.9118	0.0022
9	0	9	8	1	8	2405.9095	2405.9095	0.0000
6	1	6	5	0	5	2666.4509	2666.4530	-0.0020
8	1	8	7	1	7	2676.1745	2676.1777	-0.0032
8	0	8	7	0	7	2690.6492	2690.6489	0.0003
8	2	7	7	2	6	2691.8322	2691.8329	-0.0007
8	6	2	7	6	1	2692.1523	2692.1530	-0.0007
8	5	3	7	5	2	2692.1523	2692.1517	0.0006
8	5	4	7	5	3	2692.1523	2692.1517	0.0006
8	6	3	7	6	2	2692.1523	2692.1530	-0.0007
8	4	4	7	4	3	2692.1708	2692.1707	0.0001
8	4	5	7	4	4	2692.1708	2692.1707	0.0001
8	3	6	7	3	5	2692.2345	2692.2346	-0.0001
8	3	5	7	3	4	2692.2455	2692.2455	0.0000
8	2	6	7	2	5	2693.2106	2693.2112	-0.0006
8	1	7	7	1	6	2707.2218	2707.2221	-0.0003
2	2	1	1	1	0	2734.5922	2734.5907	0.0015
2	2	1	1	1	1	2738.4768	2738.4734	0.0034
2	2	0	1	1	1	2738.492	2738.4898	0.0022
10	0	10	9	1	9	2757.6115	2757.6088	0.0027
7	1	7	6	0	6	2989.7209	2989.7218	-0.0009
9	1	9	8	1	8	3010.5744	3010.5739	0.0005
9	0	9	8	0	8	3026.5362	3026.5380	-0.0018
9	6	4	8	6	3	3028.6583	3028.6580	0.0003
9	6	3	8	6	2	3028.6583	3028.658	0.0003
9	5	5	8	5	4	3028.6627	3028.6621	0.0006
9	5	4	8	5	3	3028.6627	3028.6621	0.0006
9	7	3	8	7	2	3028.6687	3028.6687	0.0000
9	7	2	8	7	1	3028.6687	3028.6687	0.0000
9	4	5	8	4	4	3028.6951	3028.6940	0.0011
9	4	6	8	4	5	3028.6951	3028.6939	0.0012
9	3	7	8	3	6	3028.7859	3028.7864	-0.0005
9	3	6	8	3	5	3028.8058	3028.8065	-0.0007
9	2	7	8	2	6	3030.1843	3030.1828	0.0015
9	1	8	8	1	7	3045.4892	3045.4893	-0.0001
3	2	2	2	1	1	3067.2245	3067.2213	0.0032

3	2	1	2	1	2	3078.9504	3078.9514	-0.0010
7	1	6	6	0	6	3098.4206	3098.4184	0.0022
11	0	11	10	1	10	3110.5206	3110.5208	-0.0002
8	1	8	7	0	7	3311.2767	3311.2775	-0.0008
10	1	10	9	1	9	3344.9260	3344.9269	-0.0009
10	0	10	9	0	9	3362.2766	3362.2732	0.0034
10	2	9	9	2	8	3364.5643	3364.5655	-0.0012
10	6	5	9	6	4	3365.1576	3365.1581	-0.0005
10	6	4	9	6	3	3365.1576	3365.1581	-0.0005
10	7	4	9	7	3	3365.1659	3365.1659	0.0000
10	7	3	9	7	2	3365.1659	3365.1659	0.0000
10	5	6	9	5	5	3365.1699	3365.1695	0.0004
10	5	5	9	5	4	3365.1699	3365.1695	0.0004
10	8	2	9	8	1	3365.1859	3365.1858	0.0001
10	8	3	9	8	2	3365.1859	3365.1858	0.0001
10	4	7	9	4	6	3365.2186	3365.2178	0.0008
10	4	6	9	4	5	3365.2186	3365.2180	0.0006
10	3	8	9	3	7	3365.3440	3365.3449	-0.0009
10	3	7	9	3	6	3365.3794	3365.3793	0.0001
10	2	8	9	2	7	3367.2630	3367.2654	-0.0024
10	1	9	9	1	8	3383.7040	3383.7074	-0.0034
4	2	3	3	1	2	3397.9084	3397.9057	0.0027
15	3	12	15	2	13	3412.4134	3412.4138	-0.0004
14	3	11	14	2	12	3418.5862	3418.5859	0.0003
4	2	2	3	1	3	3421.4479	3421.4480	-0.0001
13	3	10	13	2	11	3423.6509	3423.6529	-0.0020
12	3	9	12	2	10	3427.7417	3427.7417	0.0000
11	3	8	11	2	9	3430.9761	3430.9774	-0.0013
10	3	7	10	2	8	3433.4798	3433.4807	-0.0009
9	3	6	9	2	7	3435.3668	3435.3668	0.0000
8	3	6	8	2	6	3436.7238	3436.7230	0.0008
8	3	5	8	2	6	3436.7419	3436.7431	-0.0012
7	3	5	7	2	5	3437.6996	3437.6995	0.0001
7	3	4	7	2	5	3437.7082	3437.7087	-0.0005
6	3	4	6	2	4	3438.3493	3438.3495	-0.0002
6	3	3	6	2	4	3438.3535	3438.3532	0.0003
5	3	3	5	2	3	3438.7551	3438.7547	0.0004

5	3	2	5	2	3	3438.7551	3438.7559	-0.0008
4	3	2	4	2	2	3438.9878	3438.9852	0.0026
4	3	1	4	2	2	3438.9878	3438.9855	0.0023
5	3	2	5	2	4	3439.3311	3439.3313	-0.0002
5	3	3	5	2	4	3439.3311	3439.3301	0.0010
6	3	4	6	2	5	3439.5018	3439.5000	0.0018
6	3	3	6	2	5	3439.5018	3439.5036	-0.0018
7	3	5	7	2	6	3439.7694	3439.7696	-0.0002
7	3	4	7	2	6	3439.7789	3439.7788	0.0001
8	3	6	8	2	7	3440.1709	3440.1713	-0.0004
9	3	7	9	2	8	3440.7418	3440.7417	0.0001
10	3	8	10	2	9	3441.5211	3441.5211	0.0000
11	3	9	11	2	10	3442.5535	3442.5540	-0.0005
12	3	10	12	2	11	3443.8894	3443.8883	0.0011
13	3	11	13	2	12	3445.5748	3445.5753	-0.0005
14	3	12	14	2	13	3447.6695	3447.6694	0.0001
15	3	13	15	2	14	3450.2276	3450.2280	-0.0004
8	1	7	7	0	7	3451.0163	3451.0186	-0.0023
16	3	14	16	2	15	3453.3107	3453.3108	-0.0001
17	3	15	17	2	16	3456.9792	3456.9800	-0.0008
18	3	16	18	2	17	3461.2982	3461.2997	-0.0015
12	0	12	11	1	11	3464.5096	3464.5093	0.0003
19	3	17	19	2	18	3466.3355	3466.3357	-0.0002
20	3	18	20	2	19	3472.1557	3472.1550	0.0007
9	1	9	8	0	8	3631.1998	3631.2024	-0.0026
11	1	11	10	1	10	3679.2328	3679.2325	0.0003
11	0	11	10	0	10	3697.8386	3697.839	-0.0004
11	2	10	10	2	9	3700.8746	3700.8773	-0.0027
11	6	5	10	6	4	3701.6523	3701.6527	-0.0004
11	6	6	10	6	5	3701.6523	3701.6527	-0.0004
11	7	4	10	7	3	3701.6567	3701.6564	0.0003
11	7	5	10	7	4	3701.6567	3701.6564	0.0003
11	5	6	10	5	5	3701.6753	3701.6735	0.0018
11	5	7	10	5	6	3701.6753	3701.6735	0.0018
11	4	8	10	4	7	3701.7426	3701.7424	0.0002
11	4	7	10	4	6	3701.7426	3701.7427	-0.0001
11	3	9	10	3	8	3701.9066	3701.9102	-0.0036

11	3	8	10	3	7	3701.9651	3701.9662	-0.0011
11	2	9	10	2	8	3704.4686	3704.4695	-0.0009
11	1	10	10	1	9	3721.8702	3721.8703	-0.0001
5	2	4	4	1	3	3726.6449	3726.6446	0.0003
5	2	4	4	1	4	3765.4691	3765.4699	-0.0008
5	2	3	4	1	4	3766.0442	3766.0453	-0.0011
13	0	13	12	1	12	3819.4314	3819.4285	0.0029
6	5	2	7	4	4	3834.8055	3834.8051	0.0004
6	5	1	7	4	4	3834.8055	3834.8051	0.0004
6	5	2	7	4	3	3834.8055	3834.8051	0.0004
6	5	1	7	4	3	3834.8055	3834.8051	0.0004
19	1	19	18	2	16	3872.7705	3872.7702	0.0003
14	7	8	15	6	10	3894.1702	3894.1703	-0.0001
14	7	7	15	6	10	3894.1702	3894.1703	-0.0001
14	7	8	15	6	9	3894.1702	3894.1703	-0.0001
14	7	7	15	6	9	3894.1702	3894.1703	-0.0001
17	1	16	16	2	14	3895.1622	3895.1629	-0.0007
10	1	10	9	0	9	3949.5886	3949.5913	-0.0027
12	1	12	11	1	11	4013.4868	4013.4869	-0.0001
12	0	12	11	0	11	4033.2204	4033.2210	-0.0006
12	2	11	11	2	10	4037.1467	4037.1479	-0.0012
12	7	6	11	7	5	4038.1406	4038.1394	0.0012
12	7	5	11	7	4	4038.1406	4038.1394	0.0012
12	6	6	11	6	5	4038.1406	4038.1412	-0.0006
12	6	7	11	6	6	4038.1406	4038.1412	-0.0006
12	8	5	11	8	4	4038.1557	4038.1561	-0.0004
12	8	4	11	8	3	4038.1557	4038.1561	-0.0004
12	5	8	11	5	7	4038.1737	4038.1738	-0.0001
12	5	7	11	5	6	4038.1737	4038.1738	-0.0001
12	4	9	11	4	8	4038.2688	4038.2677	0.0011
12	4	8	11	4	7	4038.2688	4038.2683	0.0005
12	3	10	11	3	9	4038.4821	4038.4821	0.0000
12	3	9	11	3	8	4038.5691	4038.5691	0.0000
12	2	10	11	2	9	4041.8046	4041.8048	-0.0002
6	2	5	5	1	4	4053.4424	4053.4399	0.0025
12	1	11	11	1	10	4059.9713	4059.9716	-0.0003
6	2	4	5	1	5	4112.8253	4112.8267	-0.0014

10	1	9	9	0	9	4163.0263	4163.0284	-0.0021
14	0	14	13	1	13	4175.1237	4175.1249	-0.0012
11	1	11	10	0	10	4266.5482	4266.5507	-0.0025
13	1	13	12	1	12	4347.689	4347.6863	0.0027
13	2	12	12	2	11	4373.3757	4373.3734	0.0023
13	7	7	12	7	6	4374.6143	4374.6143	0.0000
13	7	6	12	7	5	4374.6143	4374.6143	0.0000
13	6	7	12	6	6	4374.6232	4374.6231	0.0001
13	6	8	12	6	7	4374.6232	4374.6231	0.0001
13	8	5	12	8	4	4374.6279	4374.6279	0.0000
13	8	6	12	8	5	4374.6279	4374.6279	0.0000
13	5	9	12	5	8	4374.6718	4374.6700	0.0018
13	5	8	12	5	7	4374.6718	4374.6700	0.0018
13	4	10	12	4	9	4374.7962	4374.7938	0.0024
13	4	9	12	4	8	4374.7962	4374.7949	0.0013
13	3	11	12	3	10	4375.063	4375.0604	0.0026
13	3	10	12	3	9	4375.1922	4375.1908	0.0014
7	2	6	6	1	5	4378.2959	4378.2954	0.0005
13	2	11	12	2	10	4379.2793	4379.2797	-0.0004
13	1	12	12	1	11	4398.0046	4398.0048	-0.0002
3	3	1	2	2	0	4448.7061	4448.7062	-0.0001
3	3	0	2	2	0	4448.7061	4448.7062	-0.0001
3	3	0	2	2	1	4448.7227	4448.7227	0.0000
3	3	1	2	2	1	4448.7227	4448.7226	0.0001
7	2	5	6	1	6	4461.8928	4461.8929	-0.0001
15	0	15	14	1	14	4531.4382	4531.4385	-0.0003
12	1	12	11	0	11	4582.1961	4582.1986	-0.0025
14	1	14	13	1	13	4681.8250	4681.8272	-0.0022
8	2	7	7	1	6	4701.2166	4701.2165	0.0001
14	0	14	13	0	13	4703.3831	4703.3827	0.0004
14	2	13	13	2	12	4709.5478	4709.5503	-0.0025
14	7	7	13	7	6	4711.0798	4711.0803	-0.0005
14	7	8	13	7	7	4711.0798	4711.0803	-0.0005
14	8	7	13	8	6	4711.0901	4711.0898	0.0003
14	8	6	13	8	5	4711.0901	4711.0898	0.0003
14	6	8	13	6	7	4711.0974	4711.0978	-0.0004
14	6	9	13	6	8	4711.0974	4711.0978	-0.0004

14	9	6	13	9	5	4711.1177	4711.1176	0.0001
14	9	5	13	9	4	4711.1177	4711.1176	0.0001
14	5	9	13	5	8	4711.1631	4711.1619	0.0012
14	5	10	13	5	9	4711.1631	4711.1619	0.0012
14	4	11	13	4	10	4711.3222	4711.3207	0.0015
14	4	10	13	4	9	4711.3222	4711.3226	-0.0004
14	3	12	13	3	11	4711.6438	4711.6444	-0.0006
14	3	11	13	3	10	4711.8346	4711.8339	0.0007
14	2	12	13	2	11	4716.9007	4716.9009	-0.0002
14	1	13	13	1	12	4735.9606	4735.9628	-0.0022
4	3	2	3	2	1	4785.1868	4785.1865	0.0003
4	3	1	3	2	1	4785.1868	4785.1868	0.0000
4	3	2	3	2	2	4785.2697	4785.2687	0.0010
4	3	1	3	2	2	4785.2697	4785.2690	0.0007
20	4	16	20	3	17	4805.9052	4805.9056	-0.0004
18	4	14	18	3	15	4809.2241	4809.2242	-0.0001
20	4	17	20	3	18	4810.1935	4810.1931	0.0004
17	4	13	17	3	14	4810.4631	4810.4628	0.0003
19	4	16	19	3	17	4810.8983	4810.8979	0.0004
16	4	12	16	3	13	4811.4733	4811.4728	0.0005
18	4	15	18	3	16	4811.5435	4811.5425	0.0010
17	4	14	17	3	15	4812.1215	4812.1229	-0.0014
15	4	11	15	3	12	4812.2891	4812.2878	0.0013
16	4	13	16	3	14	4812.6366	4812.6375	-0.0009
14	4	11	14	3	11	4812.9328	4812.9336	-0.0008
14	4	10	14	3	11	4812.9376	4812.9377	-0.0001
15	4	12	15	3	13	4813.0863	4813.0864	-0.0001
8	2	6	7	1	7	4813.3591	4813.3616	-0.0025
13	4	9	13	3	10	4813.4488	4813.4491	-0.0003
14	4	11	14	3	12	4813.4711	4813.4711	0.0000
11	4	8	11	3	9	4814.2761	4814.2758	0.0003
11	4	7	11	3	9	4814.2761	4814.2765	-0.0004
10	4	7	10	3	7	4814.3691	4814.369	0.0001
10	4	6	10	3	7	4814.3691	4814.3693	-0.0002
10	4	6	10	3	8	4814.4438	4814.444	-0.0002
10	4	7	10	3	8	4814.4438	4814.4437	0.0001
9	4	6	9	3	7	4814.5705	4814.5708	-0.0003

9	4	5	9	3	7	4814.5705	4814.5709	-0.0004
8	4	5	8	3	5	4814.6431	4814.6431	0.0000
8	4	4	8	3	5	4814.6431	4814.6432	-0.0001
6	4	2	6	3	3	4814.7646	4814.7646	0.0000
6	4	3	6	3	3	4814.7646	4814.7646	0.0000
6	4	2	6	3	4	4814.7682	4814.7682	0.0000
6	4	3	6	3	4	4814.7682	4814.7682	0.0000
4	4	0	4	3	2	4814.8039	4814.8039	0.0000
4	4	1	4	3	1	4814.8039	4814.8036	0.0003
4	4	0	4	3	1	4814.8039	4814.8036	0.0003
4	4	1	4	3	2	4814.8039	4814.8039	0.0000
16	0	16	15	1	15	4888.2054	4888.2048	0.0006
13	1	13	12	0	12	4896.6652	4896.6639	0.0013
15	1	15	14	1	14	5015.9073	5015.9065	0.0008
9	2	8	8	1	7	5022.2124	5022.2104	0.0020
15	0	15	14	0	14	5038.1379	5038.1408	-0.0029
15	2	14	14	2	13	5045.6757	5045.6747	0.0010
15	7	9	14	7	8	5047.5372	5047.5368	0.0004
15	7	8	14	7	7	5047.5372	5047.5368	0.0004
15	8	8	14	8	7	5047.5411	5047.5411	0.0000
15	8	7	14	8	6	5047.5411	5047.5411	0.0000
15	6	9	14	6	8	5047.5661	5047.5648	0.0013
15	6	10	14	6	9	5047.5661	5047.5648	0.0013
15	5	11	14	5	10	5047.6499	5047.6490	0.0009
15	5	10	14	5	9	5047.6499	5047.6490	0.0009
15	4	12	14	4	11	5047.8499	5047.8485	0.0014
15	4	11	14	4	10	5047.8499	5047.8515	-0.0016
15	3	13	14	3	12	5048.2322	5048.2333	-0.0011
15	3	12	14	3	11	5048.5003	5048.5015	-0.0012
15	2	13	14	2	12	5054.6759	5054.6736	0.0023
15	1	14	14	1	13	5073.8375	5073.8386	-0.0011
5	3	3	4	2	2	5121.5979	5121.6012	-0.0033
5	3	2	4	2	2	5121.5994	5121.6024	-0.0030
5	3	3	4	2	3	5121.8492	5121.8478	0.0014
5	3	2	4	2	3	5121.8492	5121.8491	0.0001
9	2	7	8	1	8	5167.3662	5167.3667	-0.0005
14	1	14	13	0	13	5210.0839	5210.0850	-0.0011

17	0	17	16	1	16	5245.2597	5245.2572	0.0025
10	2	9	9	1	8	5341.2901	5341.2866	0.0035
16	1	16	15	1	15	5349.9222	5349.9212	0.0010
16	0	16	15	0	15	5372.6760	5372.6729	0.0031
16	2	15	15	2	14	5381.7415	5381.7431	-0.0016
16	8	8	15	8	7	5383.9809	5383.9810	-0.0001
16	8	9	15	8	8	5383.9809	5383.9810	-0.0001
16	7	9	15	7	8	5383.9824	5383.9831	-0.0007
16	7	10	15	7	9	5383.9832	5383.9831	0.0000
16	5	12	15	5	11	5384.1314	5384.1311	0.0003
16	5	11	15	5	10	5384.1314	5384.1311	0.0003
16	4	12	15	4	11	5384.3798	5384.3819	-0.0021
16	4	13	15	4	12	5384.3798	5384.3771	0.0027
16	3	14	15	3	13	5384.8258	5384.8259	-0.0001
16	3	13	15	3	12	5385.1975	5385.1969	0.0006
16	2	14	15	2	13	5392.6003	5392.6005	-0.0002
16	1	15	15	1	14	5411.6256	5411.6247	0.0009
6	3	4	5	2	3	5457.9042	5457.9046	-0.0004
6	3	3	5	2	3	5457.9084	5457.9082	0.0002
6	3	4	5	2	4	5458.4803	5458.4799	0.0004
6	3	3	5	2	4	5458.4837	5458.4836	0.0001
15	1	15	14	0	14	5522.6101	5522.6089	0.0012
10	2	8	9	1	9	5524.0571	5524.0581	-0.0010
10	2	8	9	1	9	5524.0571	5524.0581	-0.0010
18	0	18	17	1	17	5602.4274	5602.4290	-0.0016
11	2	10	10	1	9	5658.4556	5658.4564	-0.0008
17	1	17	16	1	16	5683.8688	5683.8686	0.0002
17	0	17	16	0	16	5706.9760	5706.9736	0.0024
17	2	16	16	2	15	5717.7500	5717.7518	-0.0018
17	7	11	16	7	10	5720.4167	5720.4186	-0.0019
17	7	10	16	7	9	5720.4167	5720.4186	-0.0019
17	6	12	16	6	11	5720.4749	5720.4734	0.0015
17	6	11	16	6	10	5720.4749	5720.4734	0.0015
17	5	12	16	5	11	5720.6081	5720.6078	0.0003
17	5	13	16	5	12	5720.6081	5720.6077	0.0004
17	4	14	16	4	13	5720.9072	5720.9064	0.0008
17	4	13	16	4	12	5720.9135	5720.9138	-0.0003

17	3	15	16	3	14	5721.4209	5721.4210	-0.0001
17	3	14	16	3	13	5721.9239	5721.9238	0.0001
17	2	15	16	2	14	5730.6822	5730.6820	0.0002
17	1	16	16	1	15	5749.3120	5749.3133	-0.0013
7	3	5	6	2	4	5794.0375	5794.0388	-0.0013
7	3	5	6	2	5	5795.1899	5795.1892	0.0007
7	3	4	6	2	5	5795.1983	5795.1983	0.0000
16	1	16	15	0	15	5834.3876	5834.3893	-0.0017
11	2	9	10	1	10	5883.6022	5883.6007	0.0015
19	0	19	18	1	18	5959.5543	5959.5563	-0.0020
12	2	11	11	1	10	5973.7346	5973.7340	0.0006
18	1	18	17	1	17	6017.7464	6017.7464	0.0000
18	0	18	17	0	17	6041.0380	6041.0404	-0.0024
18	2	17	17	2	16	6053.6964	6053.6973	-0.0009
18	8	10	17	8	9	6056.8241	6056.8236	0.0005
18	8	11	17	8	10	6056.8241	6056.8236	0.0005
18	9	9	17	9	8	6056.8388	6056.8380	0.0008
18	9	10	17	9	9	6056.8388	6056.8380	0.0008
18	7	12	17	7	11	6056.8438	6056.8425	0.0013
18	7	11	17	7	10	6056.8438	6056.8425	0.0013
18	6	12	17	6	11	6056.9143	6056.9138	0.0005
18	6	13	17	6	12	6056.9143	6056.9138	0.0005
18	5	13	17	5	12	6057.0773	6057.0787	-0.0014
18	5	14	17	5	13	6057.0773	6057.0787	-0.0014
18	4	15	17	4	14	6057.4365	6057.4365	0.0000
18	4	14	17	4	13	6057.4475	6057.4476	-0.0001
18	3	16	17	3	15	6058.0187	6058.0170	0.0017
18	3	15	17	3	14	6058.6877	6058.6862	0.0015
18	2	16	17	2	15	6068.915	6068.9157	-0.0007
18	1	17	17	1	16	6086.8968	6086.8963	0.0005
8	3	6	7	2	5	6129.9341	6129.9341	0.0000
8	3	5	7	2	5	6129.9541	6129.9542	-0.0001
8	3	6	7	2	6	6132.0048	6132.0042	0.0006
8	3	5	7	2	6	6132.0254	6132.0243	0.0011
17	1	17	16	0	16	6145.5826	6145.5850	-0.0024
4	4	1	3	3	1	6160.8909	6160.8907	0.0002
4	4	1	3	3	0	6160.8909	6160.8907	0.0002

4	4	0	3	3	0	6160.8909	6160.8907	0.0002
4	4	0	3	3	1	6160.8909	6160.8907	0.0002
12	2	10	11	1	11	6246.1709	6246.1730	-0.0021
13	2	12	12	1	11	6287.1365	6287.1357	0.0008
19	1	19	18	1	18	6351.5501	6351.5523	-0.0022
19	0	19	18	0	18	6374.8755	6374.8737	0.0018
19	2	18	18	2	17	6389.5747	6389.5758	-0.0011
19	8	11	18	8	10	6393.2239	6393.2246	-0.0007
19	8	12	18	8	11	6393.2239	6393.2246	-0.0007
19	7	12	18	7	11	6393.2533	6393.2542	-0.0009
19	7	13	18	7	12	6393.2533	6393.2542	-0.0009
19	6	14	18	6	13	6393.3447	6393.3443	0.0004
19	6	13	18	6	12	6393.3447	6393.3443	0.0004
19	5	14	18	5	13	6393.5437	6393.5436	0.0001
19	5	15	18	5	14	6393.5437	6393.5435	0.0002
19	4	16	18	4	15	6393.9669	6393.9673	-0.0004
19	4	15	18	4	14	6393.9829	6393.9835	-0.0006
19	3	17	18	3	16	6394.6137	6394.6118	0.0019
19	3	16	18	3	15	6395.4892	6395.4885	0.0007
19	2	17	18	2	16	6407.2973	6407.2964	0.0009
19	1	18	18	1	17	6424.3645	6424.3652	-0.0007
9	3	7	8	2	6	6465.5073	6465.5093	-0.0020
5	4	2	4	3	2	6497.4081	6497.4082	-0.0001
5	4	1	4	3	1	6497.4081	6497.4079	0.0002
5	4	2	4	3	1	6497.4081	6497.4079	0.0002
5	4	1	4	3	2	6497.4081	6497.4082	-0.0001
20	1	20	19	1	19	6685.2871	6685.2845	0.0026
20	0	20	19	0	19	6708.4752	6708.4764	-0.0012
20	2	19	19	2	18	6725.3861	6725.3840	0.0021
20	6	14	19	6	13	6729.7624	6729.7643	-0.0019
20	6	15	19	6	14	6729.7624	6729.7643	-0.0019
20	5	15	19	5	14	6729.9989	6730.0021	-0.0032
20	5	16	19	5	15	6729.9989	6730.0018	-0.0029
20	4	17	19	4	16	6730.499	6730.4985	0.0005
20	4	16	19	4	15	6730.5228	6730.5218	0.0010
20	3	17	19	3	16	6732.3375	6732.3354	0.0021
20	1	19	19	1	18	6761.7128	6761.7112	0.0016

6	4	2	5	3	3	6833.9174	6833.9181	-0.0007
6	4	3	5	3	2	6833.9174	6833.9169	0.0005
6	4	3	5	3	3	6833.9174	6833.9181	-0.0007
6	4	2	5	3	2	6833.9174	6833.9169	0.0005
6	4	3	5	3	2	6833.9176	6833.9169	0.0007
6	4	3	5	3	3	6833.9176	6833.9181	-0.0005
6	4	2	5	3	2	6833.9176	6833.9169	0.0007
6	4	2	5	3	3	6833.9176	6833.9181	-0.0005
7	4	3	6	3	4	7170.4168	7170.4163	0.0005

Table S6.17. Rotational transition frequencies of the **PFP***G*+*g*+**PFP***G*-*g*- homodimer.

J'	K_a'	K_c'	J''	K_a''	K_c''	Obs/ MHz	Cal/ MHz	Obs - Cal/ MHz
5	0	5	4	0	4	1890.5178	1890.5179	-0.0001
5	4	2	4	4	1	1892.2365	1892.2362	0.0003
5	4	1	4	4	0	1892.2365	1892.2362	0.0003
5	3	3	4	3	2	1892.3315	1892.3318	-0.0003
5	3	2	4	3	1	1892.3434	1892.3419	0.0015
5	2	3	4	2	2	1893.4575	1893.4579	-0.0004
5	1	4	4	1	3	1911.5501	1911.5483	0.0018
4	1	4	3	0	3	2078.3412	2078.3405	0.0007
11	2	10	11	1	11	2078.4078	2078.4121	-0.0043
7	0	7	6	1	6	2119.3551	2119.3574	-0.0023
6	1	6	5	1	5	2246.0844	2246.0883	-0.0039
6	0	6	5	0	5	2267.7601	2267.7608	-0.0007
6	2	5	5	2	4	2270.1257	2270.1275	-0.0018
6	5	1	5	5	0	2270.6529	2270.6534	-0.0005
6	5	2	5	5	1	2270.6529	2270.6534	-0.0005
6	4	2	5	4	1	2270.7331	2270.7326	0.0005
6	4	3	5	4	2	2270.7331	2270.7326	0.0005
6	3	4	5	3	3	2270.8907	2270.8900	0.0007
6	3	3	5	3	2	2270.9168	2270.917	-0.0002
6	2	4	5	2	3	2272.8505	2272.8513	-0.0008
6	1	5	5	1	4	2293.6303	2293.6277	0.0026

17	2	16	17	1	17	2436.4199	2436.4216	-0.0017
5	1	5	4	0	4	2437.3762	2437.3745	0.0017
8	0	8	7	1	7	2520.0031	2520.0060	-0.0029
7	1	7	6	1	6	2620.1428	2620.1441	-0.0013
7	0	7	6	0	6	2644.5389	2644.5415	-0.0026
7	2	6	6	2	5	2648.2736	2648.2735	0.0001
7	6	2	6	6	1	2649.0619	2649.0627	-0.0008
7	6	1	6	6	0	2649.0619	2649.0627	-0.0008
7	5	2	6	5	1	2649.1354	2649.1339	0.0015
7	5	3	6	5	2	2649.1354	2649.1339	0.0015
7	4	3	6	4	2	2649.2586	2649.25600	0.0026
7	4	4	6	4	3	2649.2586	2649.2557	0.0029
7	3	5	6	3	4	2649.4925	2649.4941	-0.0016
7	3	4	6	3	3	2649.5573	2649.5547	0.0026
7	2	5	6	2	4	2652.6197	2652.6201	-0.0004
7	1	6	6	1	5	2675.5756	2675.5770	-0.0014
6	1	6	5	0	5	2792.9486	2792.9449	0.0037
9	0	9	8	1	8	2922.3877	2922.3896	-0.0019
14	3	11	14	2	12	2929.5863	2929.5900	-0.0037
13	3	10	13	2	11	2950.8703	2950.8722	-0.0019
12	3	9	12	2	10	2968.5528	2968.5553	-0.0025
11	3	8	11	2	9	2982.8936	2982.8937	-0.0001
8	1	8	7	1	7	2994.0697	2994.0716	-0.0019
10	3	7	10	2	8	2994.2135	2994.2119	0.0016
9	3	6	9	2	7	3002.8836	3002.8797	0.0039
8	3	5	8	2	6	3009.2908	3009.2901	0.0007
7	3	4	7	2	5	3013.8369	3013.8381	-0.0012
6	3	3	6	2	4	3016.9041	3016.9035	0.0006
5	3	2	5	2	3	3018.8409	3018.8378	0.0031
4	3	1	4	2	2	3019.9561	3019.9539	0.0022
3	3	0	3	2	1	3020.5179	3020.5190	-0.0011
8	0	8	7	0	7	3020.7911	3020.7927	-0.0016
4	3	2	4	2	3	3021.1211	3021.1210	0.0001
5	3	3	5	2	4	3021.5548	3021.5538	0.0010
6	3	4	6	2	5	3022.3148	3022.3164	-0.0016
7	3	5	7	2	6	3023.5394	3023.5370	0.0024
8	3	6	8	2	7	3025.3613	3025.3618	-0.0005

8	2	7	7	2	6	3026.3217	3026.3234	-0.0017
8	5	4	7	5	3	3027.6302	3027.6320	-0.0018
8	5	3	7	5	2	3027.6302	3027.6320	-0.0018
8	4	5	7	4	4	3027.8095	3027.8100	-0.0005
8	4	4	7	4	3	3027.8095	3027.8108	-0.0013
9	3	7	9	2	8	3027.9525	3027.9530	-0.0005
8	3	6	7	3	5	3028.1475	3028.1482	-0.0007
8	3	5	7	3	4	3028.2715	3028.2692	0.0023
10	3	8	10	2	9	3031.4852	3031.4874	-0.0022
11	3	9	11	2	10	3036.1538	3036.1540	-0.0002
12	3	10	12	2	11	3042.1522	3042.1523	-0.0001
13	3	11	13	2	12	3049.6886	3049.6897	-0.0011
8	1	7	7	1	6	3057.3735	3057.3709	0.0026
15	3	13	15	2	14	3070.2346	3070.2382	-0.0036
16	3	14	16	2	15	3083.6859	3083.6835	0.0024
17	3	15	17	2	16	3099.5312	3099.5318	-0.0006
18	3	16	18	2	17	3117.9951	3117.9955	-0.0004
19	3	17	19	2	18	3139.2816	3139.2816	0.0000
7	1	7	6	0	6	3145.3276	3145.3282	-0.0006
10	0	10	9	1	9	3326.0163	3326.0142	0.0021
9	1	9	8	1	8	3367.8551	3367.8571	-0.0020
9	0	9	8	0	8	3396.4566	3396.4553	0.0013
9	2	8	8	2	7	3404.2627	3404.2635	-0.0008
9	7	3	8	7	2	3405.9171	3405.9169	0.0002
9	7	2	8	7	1	3405.9171	3405.9169	0.0002
9	6	4	8	6	3	3406.0111	3406.0097	0.0014
9	6	3	8	6	2	3406.0111	3406.0097	0.0014
9	5	4	8	5	3	3406.1503	3406.1503	0.0000
9	5	5	8	5	4	3406.1503	3406.1503	0.0000
9	4	6	8	4	5	3406.4001	3406.3999	0.0002
9	4	5	8	4	4	3406.4001	3406.4018	-0.0017
9	3	7	8	3	6	3406.8542	3406.8548	-0.0006
9	3	6	8	3	5	3407.0758	3407.0765	-0.0007
9	2	7	8	2	6	3413.4864	3413.4869	-0.0005
9	1	8	8	1	7	3438.9856	3438.9823	0.0033
8	1	8	7	0	7	3494.8584	3494.8584	0.0000
11	0	11	10	1	10	3730.3613	3730.3649	-0.0036

10	1	10	9	1	9	3741.4875	3741.4884	-0.0009
10	0	10	9	0	9	3771.4777	3771.4817	-0.0040
10	2	9	9	2	8	3782.0799	3782.0804	-0.0005
10	8	3	9	8	2	3784.2907	3784.2911	-0.0004
10	8	2	9	8	1	3784.2907	3784.2911	-0.0004
10	7	4	9	7	3	3784.3801	3784.3805	-0.0004
10	7	3	9	7	2	3784.3801	3784.3805	-0.0004
10	6	4	9	6	3	3784.5043	3784.5027	0.0016
10	6	5	9	6	4	3784.5043	3784.5027	0.0016
10	5	5	9	5	4	3784.6898	3784.6913	-0.0015
10	5	6	9	5	5	3784.6898	3784.6913	-0.0015
10	4	7	9	4	6	3785.0314	3785.0294	0.0020
10	4	6	9	4	5	3785.0314	3785.0337	-0.0023
10	3	8	9	3	7	3785.6159	3785.6148	0.0011
10	3	7	9	3	6	3785.9962	3785.9943	0.0019
10	2	8	9	2	7	3794.6652	3794.6622	0.0030
10	1	9	9	1	8	3820.3831	3820.3819	0.0012
9	1	9	8	0	8	3841.9186	3841.9228	-0.0042
14	1	13	13	2	12	3880.0187	3880.0185	0.0002
6	2	5	5	1	4	4023.4117	4023.4112	0.0005
11	1	11	10	1	10	4114.9544	4114.9554	-0.0010
12	0	12	11	1	11	4134.9232	4134.9219	0.0013
11	0	11	10	0	10	4145.8371	4145.8391	-0.0020
3	3	1	2	2	0	4156.0804	4156.0801	0.0003
3	3	0	2	2	1	4156.1603	4156.1587	0.0016
11	2	10	10	2	9	4159.7629	4159.7606	0.0023
11	9	2	10	9	1	4162.6499	4162.6503	-0.0004
11	9	3	10	9	2	4162.6499	4162.6503	-0.0004
11	8	4	10	8	3	4162.7388	4162.7397	-0.0009
11	8	3	10	8	2	4162.7388	4162.7397	-0.0009
11	7	4	10	7	3	4162.8527	4162.8530	-0.0003
11	7	5	10	7	4	4162.8527	4162.8530	-0.0003
11	6	5	10	6	4	4163.0115	4163.0107	0.0008
11	6	6	10	6	5	4163.0115	4163.0107	0.0008
11	5	6	10	5	5	4163.2574	4163.2575	-0.0001
11	5	7	10	5	6	4163.2574	4163.2575	-0.0001
11	4	8	10	4	7	4163.7021	4163.7029	-0.0008

11	4	7	10	4	6	4163.7111	4163.7113	-0.0002
11	3	9	10	3	8	4164.4283	4164.4272	0.0011
11	3	8	10	3	7	4165.0434	4165.0429	0.0005
11	2	9	10	2	8	4176.3618	4176.3610	0.0008
18	4	14	18	3	15	4194.3123	4194.3120	0.0003
11	1	10	10	1	9	4201.5383	4201.5385	-0.0002
15	1	14	14	2	13	4311.1868	4311.1881	-0.0013
12	1	12	11	1	11	4488.2483	4488.2498	-0.0015
12	0	12	11	0	11	4519.5128	4519.5125	0.0003
11	1	11	10	0	10	4530.4296	4530.4296	0.0000
4	3	2	3	2	1	4534.3327	4534.3324	0.0003
4	3	1	3	2	2	4534.7255	4534.7260	-0.0005
12	2	11	11	2	10	4537.2909	4537.2908	0.0001
13	0	13	12	1	12	4539.1791	4539.1792	-0.0001
12	10	2	11	10	1	4540.9921	4540.9926	-0.0005
12	10	3	11	10	2	4540.9921	4540.9926	-0.0005
12	9	3	11	9	2	4541.0852	4541.0843	0.0009
12	9	4	11	9	3	4541.0852	4541.0843	0.0009
12	8	5	11	8	4	4541.1939	4541.1940	-0.0001
12	8	4	11	8	3	4541.1939	4541.1940	-0.0001
12	7	6	11	7	5	4541.3371	4541.3353	0.0018
12	7	5	11	7	4	4541.3371	4541.3353	0.0018
12	6	7	11	6	6	4541.5368	4541.5351	0.0017
12	6	6	11	6	5	4541.5368	4541.5351	0.0017
12	5	7	11	5	6	4541.8516	4541.8515	0.0001
12	5	8	11	5	7	4541.8516	4541.8514	0.0002
12	4	9	11	4	8	4542.4223	4542.4242	-0.0019
12	4	8	11	4	7	4542.4395	4542.4400	-0.0005
12	3	10	11	3	9	4543.2899	4543.2891	0.0008
12	3	9	11	3	8	4544.2433	4544.2448	-0.0015
12	2	10	11	2	9	4558.5833	4558.5832	0.0001
12	1	11	11	1	10	4582.4175	4582.4182	-0.0007
13	1	13	12	1	12	4861.3646	4861.3653	-0.0007
13	0	13	12	0	12	4892.5082	4892.5071	0.0011
5	3	3	4	2	2	4912.2823	4912.2823	0.0000
5	3	2	4	2	3	4913.4651	4913.4662	-0.0011
13	2	12	12	2	11	4914.6583	4914.6581	0.0002

13	10	4	12	10	3	4919.4122	4919.4118	0.0004
13	10	3	12	10	2	4919.4122	4919.4118	0.0004
13	9	4	12	9	3	4919.5218	4919.5213	0.0005
13	9	5	12	9	4	4919.5218	4919.5213	0.0005
13	8	5	12	8	4	4919.6516	4919.6544	-0.0028
13	8	6	12	8	5	4919.6516	4919.6544	-0.0028
13	7	6	12	7	5	4919.8269	4919.8285	-0.0016
13	7	7	12	7	6	4919.8269	4919.8285	-0.0016
13	6	7	12	6	6	4920.0768	4920.0776	-0.0008
13	6	8	12	6	7	4920.0768	4920.0776	-0.0008
13	5	9	12	5	8	4920.4757	4920.4756	0.0001
13	5	8	12	5	7	4920.4757	4920.4759	-0.0002
13	4	10	12	4	9	4921.1942	4921.1970	-0.0028
13	4	9	12	4	8	4921.2258	4921.2251	0.0007
13	3	11	12	3	10	4922.1952	4922.1955	-0.0003
13	3	10	12	3	9	4923.6254	4923.6250	0.0004
13	2	11	12	2	10	4941.3067	4941.3080	-0.0013
14	0	14	13	1	13	4942.6639	4942.6630	0.0009
13	1	12	12	1	11	4962.9843	4962.9846	-0.0003
8	2	6	7	1	7	4966.9739	4966.9738	0.0001
9	2	8	8	1	7	5075.6966	5075.6960	0.0006
17	1	16	16	2	15	5180.3792	5180.3797	-0.0005
14	1	14	13	1	13	5234.2968	5234.2978	-0.0010
14	0	14	13	0	13	5264.8491	5264.8491	0.0000
6	3	4	5	2	3	5289.7146	5289.7144	0.0002
14	2	13	13	2	12	5291.8502	5291.8497	0.0005
6	3	3	5	2	4	5292.4852	5292.4842	0.0010
14	11	4	13	11	3	5297.7189	5297.7198	-0.0009
14	11	3	13	11	2	5297.7189	5297.7198	-0.0009
14	10	4	13	10	3	5297.8326	5297.8317	0.0009
14	10	5	13	10	4	5297.8326	5297.8317	0.0009
14	9	6	13	9	5	5297.9612	5297.9615	-0.0003
14	9	5	13	9	4	5297.9612	5297.9615	-0.0003
14	8	7	13	8	6	5298.1213	5298.1213	0.0000
14	8	6	13	8	5	5298.1217	5298.1213	0.0004
14	7	8	13	7	7	5298.3358	5298.3332	0.0026
14	7	7	13	7	6	5298.3358	5298.3332	0.0026

14	6	9	13	6	8	5298.6406	5298.6396	0.0010
14	6	8	13	6	7	5298.6406	5298.6396	0.0010
14	5	10	13	5	9	5299.1329	5299.1326	0.0003
14	5	9	13	5	8	5299.1329	5299.1332	-0.0003
14	3	12	13	3	11	5301.1396	5301.1395	0.0001
14	3	11	13	3	10	5303.2111	5303.2113	-0.0002
14	2	12	13	2	11	5324.4948	5324.4935	0.0013
14	1	13	13	1	12	5343.2002	5343.1989	0.0013
15	0	15	14	1	14	5344.9507	5344.9497	0.0010
10	2	9	9	1	8	5418.7947	5418.7941	0.0006
15	1	15	14	1	14	5607.0427	5607.0449	-0.0022
18	1	17	17	2	16	5617.7958	5617.7977	-0.0019
15	0	15	14	0	14	5636.5851	5636.5844	0.0007
7	3	5	6	2	4	5666.3574	5666.3572	0.0002
15	2	14	14	2	13	5668.8542	5668.8533	0.0009
7	3	4	6	2	5	5671.9118	5671.9115	0.0003
15	11	4	14	11	3	5676.1212	5676.1226	-0.0014
15	11	5	14	11	4	5676.1212	5676.1226	-0.0014
15	10	5	14	10	4	5676.2537	5676.2524	0.0013
15	10	6	14	10	5	5676.2537	5676.2524	0.0013
15	9	7	14	9	6	5676.4055	5676.4050	0.0005
15	9	6	14	9	5	5676.4055	5676.4050	0.0005
15	8	8	14	8	7	5676.5964	5676.5954	0.0010
15	8	7	14	8	6	5676.5964	5676.5954	0.0010
15	7	9	14	7	8	5676.8518	5676.8505	0.0013
15	7	8	14	7	7	5676.8518	5676.8505	0.0013
15	6	9	14	6	8	5677.2238	5677.2226	0.0012
15	6	10	14	6	9	5677.2238	5677.2226	0.0012
15	5	11	14	5	10	5677.8266	5677.8250	0.0016
15	5	10	14	5	9	5677.8266	5677.8260	0.0006
15	4	12	14	4	11	5678.9114	5678.9107	0.0007
15	4	11	14	4	10	5678.9889	5678.9886	0.0003
15	3	13	14	3	12	5680.1116	5680.1120	-0.0004
15	3	12	14	3	11	5683.0342	5683.0340	0.0002
15	2	13	14	2	12	5708.0765	5708.0774	-0.0009
15	1	14	14	1	13	5723.0186	5723.0192	-0.0006
16	0	16	15	1	15	5745.6823	5745.6804	0.0019

11	2	10	10	1	9	5758.1735	5758.1728	0.0007
16	1	16	15	1	15	5979.6066	5979.6065	0.0001
16	0	16	15	0	15	6007.7756	6007.7756	0.0000
8	3	6	7	2	5	6041.8851	6041.8853	-0.0002
16	2	15	15	2	14	6045.6595	6045.6569	0.0026
8	3	5	7	2	6	6051.9077	6051.9072	0.0005
16	12	4	15	12	3	6054.3914	6054.3917	-0.0003
16	12	5	15	12	4	6054.3914	6054.3917	-0.0003
16	11	6	15	11	5	6054.5249	6054.5241	0.0008
16	11	5	15	11	4	6054.5249	6054.5241	0.0008
16	10	7	15	10	6	6054.6761	6054.6741	0.0020
16	10	6	15	10	5	6054.6761	6054.6741	0.0020
16	9	7	15	9	6	6054.8503	6054.8523	-0.0020
16	9	8	15	9	7	6054.8503	6054.8523	-0.0020
16	8	8	15	8	7	6055.0752	6055.0771	-0.0019
16	8	9	15	8	8	6055.0752	6055.0771	-0.0019
16	7	9	15	7	8	6055.3808	6055.3812	-0.0004
16	7	10	15	7	9	6055.3808	6055.3812	-0.0004
16	6	11	15	6	10	6055.8284	6055.8282	0.0002
16	6	10	15	6	9	6055.8284	6055.8282	0.0002
16	5	12	15	5	11	6056.5559	6056.5551	0.0008
16	5	11	15	5	10	6056.5559	6056.5571	-0.0012
16	4	13	15	4	12	6057.8575	6057.8573	0.0002
16	4	12	15	4	11	6057.9804	6057.9805	-0.0001
16	3	14	15	3	13	6059.1005	6059.1023	-0.0018
16	3	13	15	3	12	6063.1254	6063.1257	-0.0003
16	2	14	15	2	13	6091.9803	6091.9801	0.0002
12	2	11	11	1	10	6093.9251	6093.9251	0.0000
16	1	15	15	1	14	6102.4043	6102.4017	0.0026
17	0	17	16	1	16	6144.5714	6144.5716	-0.0002
17	1	17	16	1	16	6351.9853	6351.9841	0.0012
17	0	17	16	0	16	6378.4964	6378.4977	-0.0013
9	3	7	8	2	6	6415.9225	6415.9230	-0.0005
17	2	16	16	2	15	6422.2503	6422.2492	0.0011
13	2	12	12	1	11	6426.1645	6426.1650	-0.0005
9	3	6	8	2	7	6432.6605	6432.6602	0.0003
17	11	6	16	11	5	6432.9254	6432.9244	0.0010

17	11	7	16	11	6	6432.9254	6432.9244	0.0010
17	10	7	16	10	6	6433.0945	6433.0966	-0.0021
17	10	8	16	10	7	6433.0945	6433.0966	-0.0021
17	9	8	16	9	7	6433.3052	6433.3035	0.0017
17	9	9	16	9	8	6433.3052	6433.3035	0.0017
17	8	10	16	8	9	6433.5652	6433.5669	-0.0017
17	8	9	16	8	8	6433.5652	6433.5669	-0.0017
17	7	11	16	7	10	6433.9266	6433.9263	0.0003
17	7	10	16	7	9	6433.9266	6433.9263	0.0003
17	6	11	16	6	10	6434.4578	6434.4578	0.0000
17	6	12	16	6	11	6434.4578	6434.4577	0.0001
17	5	13	16	5	12	6435.3255	6435.3257	-0.0002
17	5	12	16	5	11	6435.3287	6435.3290	-0.0003
17	4	14	16	4	13	6436.8678	6436.8667	0.0011
17	4	13	16	4	12	6437.0558	6437.0558	0.0000
17	3	15	16	3	14	6438.0972	6438.0975	-0.0003
17	3	14	16	3	13	6443.5203	6443.5212	-0.0009
17	2	15	16	2	14	6476.1114	6476.1089	0.0025
17	1	16	16	1	15	6481.3009	6481.3001	0.0008
18	0	18	17	1	17	6541.4205	6541.4196	0.0009
17	1	17	16	0	16	6585.9079	6585.9103	-0.0024
18	1	18	17	1	17	6724.1827	6724.1809	0.0018
18	0	18	17	0	17	6748.8327	6748.8321	0.0006
14	2	13	13	1	12	6755.0291	6755.0301	-0.0010
18	2	17	17	2	16	6798.6196	6798.6195	0.0001
18	7	12	17	7	11	6812.4884	6812.4866	0.0018
18	7	11	17	7	10	6812.4884	6812.4866	0.0018
18	6	12	17	6	11	6813.1108	6813.1130	-0.0022
18	6	13	17	6	12	6813.1108	6813.1129	-0.0021
18	5	14	17	5	13	6814.1376	6814.1390	-0.0014
18	5	13	17	5	12	6814.1438	6814.1446	-0.0008
18	4	15	17	4	14	6815.9400	6815.9404	-0.0004
18	4	14	17	4	13	6816.2223	6816.2233	-0.0010
18	3	16	17	3	15	6817.0824	6817.0832	-0.0008
18	3	15	17	3	14	6824.2548	6824.2563	-0.0015
18	1	17	17	1	16	6859.6707	6859.6673	0.0034
18	2	16	17	2	15	6860.3624	6860.3637	-0.0013

19	1	19	18	1	18	7096.1995	7096.2017	-0.0022
19	0	19	18	0	18	7118.8596	7118.8610	-0.0014
13	2	11	12	1	12	7144.7546	7144.7527	0.0019
11	3	9	10	2	8	7157.8158	7157.8158	0.0000
19	2	18	18	2	17	7174.7579	7174.7576	0.0003
19	6	13	18	6	12	7191.7986	7191.7953	0.0033
19	6	14	18	6	13	7191.7986	7191.7952	0.0034
19	5	15	18	5	14	7192.9950	7192.9976	-0.0026
19	5	14	18	5	13	7193.0046	7193.0069	-0.0023
19	3	16	18	3	15	7205.3662	7205.3671	-0.0009
19	1	18	18	1	17	7237.4539	7237.4553	-0.0014
19	1	19	18	0	18	7278.9622	7278.9631	-0.0009
20	1	20	19	1	19	7468.0533	7468.0525	0.0008
20	0	20	19	0	19	7488.6635	7488.6624	0.0011

Table S6.18. Rotational transition frequencies of the **PFP***G*+*g*+**PFP***Tg*- homodimer.

J’	K_a’	K_c’	*J*”	K_a”	K_c”	Obs/ MHz	Cal/ MHz	Obs - Cal/ MHz
6	1	6	5	1	5	2078.0416	2078.0412	0.0004
6	0	6	5	0	5	2106.8438	2106.8487	-0.0049
6	2	5	5	2	4	2111.2251	2111.2323	-0.0072
6	3	4	5	3	3	2112.6405	2112.6450	-0.0045
6	3	3	5	3	2	2112.7068	2112.7124	-0.0056
6	2	4	5	2	3	2116.2631	2116.2727	-0.0096
6	1	5	5	1	4	2143.4046	2143.4149	-0.0103
11	2	10	11	1	11	2216.6591	2216.6524	0.0067
5	1	5	4	0	4	2295.6553	2295.6597	-0.0044
7	1	7	6	1	6	2423.8601	2423.8576	0.0025
7	0	7	6	0	6	2455.8326	2455.8328	-0.0002
7	2	6	6	2	5	2462.7261	2462.7259	0.0002
7	3	5	6	3	4	2464.9905	2464.9787	0.0118
7	3	4	6	3	3	2465.1392	2465.1301	0.0091
7	2	5	6	2	4	2470.7578	2470.7519	0.0059

7	1	6	6	1	5	2500.0613	2500.0513	0.0100
6	1	6	5	0	5	2616.6717	2616.6751	-0.0034
8	1	8	7	1	7	2769.4501	2769.4485	0.0016
8	0	8	7	0	7	2803.8747	2803.8702	0.0045
8	2	7	7	2	6	2814.0500	2814.0452	0.0048
8	3	6	7	3	5	2817.4054	2817.4006	0.0048
8	3	5	7	3	4	2817.7092	2817.7030	0.0062
8	2	6	7	2	5	2826.0043	2825.9973	0.0070
8	1	7	7	1	6	2856.3896	2856.3940	-0.0044
9	1	9	8	1	8	3114.7879	3114.7929	-0.0050
9	0	9	8	0	8	3150.8764	3150.8788	-0.0024
9	2	8	8	2	7	3165.1749	3165.1658	0.0091
9	5	4	8	5	3	3168.7001	3168.7064	-0.0063
9	5	5	8	5	4	3168.7065	3168.7064	0.0001
9	3	7	8	3	6	3169.9139	3169.9122	0.0017
9	3	6	8	3	5	3170.4667	3170.4657	0.0010
9	2	7	8	2	6	3182.0628	3182.0649	-0.0021
9	1	8	8	1	7	3212.3890	3212.3886	0.0004
4	2	3	3	1	2	3224.2138	3224.2211	-0.0073
8	1	8	7	0	7	3247.2969	3247.2998	-0.0029
18	3	16	18	2	17	3254.1338	3254.1332	0.0006
17	3	14	17	2	16	3266.8303	3266.8314	-0.0011
4	2	3	3	1	3	3289.6618	3289.6664	-0.0046
4	2	2	3	1	3	3291.8323	3291.8373	-0.0050
14	1	13	13	2	11	3424.2687	3424.2714	-0.0027
20	3	17	20	2	19	3445.5515	3445.5509	0.0006
10	1	10	9	1	9	3459.8742	3459.8737	0.0005
10	0	10	9	0	9	3496.8001	3496.8103	-0.0102
10	2	9	9	2	8	3516.0665	3516.0635	0.0030
10	3	8	9	3	7	3522.5166	3522.5108	0.0058
10	3	7	9	3	6	3523.4656	3523.4574	0.0082
10	2	8	9	2	7	3538.9756	3538.9762	-0.0006
5	2	4	4	1	3	3554.3613	3554.3534	0.0079
5	2	3	4	1	3	3559.4101	3559.4130	-0.0029
10	1	9	9	1	8	3567.9723	3567.9759	-0.0036
5	2	4	4	1	4	3663.4155	3663.4213	-0.0058
5	2	3	4	1	4	3668.4752	3668.4809	-0.0057

11	1	11	10	1	10	3804.6754	3804.6782	-0.0028
11	0	11	10	0	10	3841.6534	3841.6572	-0.0038
11	2	10	10	2	9	3866.7253	3866.7144	0.0109
10	1	10	9	0	9	3867.2088	3867.2173	-0.0085
11	3	9	10	3	8	3875.1927	3875.1896	0.0031
11	3	8	10	3	7	3876.7241	3876.7231	0.0010
6	2	5	5	1	4	3879.0626	3879.0511	0.0115
11	2	9	10	2	8	3896.7065	3896.7114	-0.0049
11	1	10	10	1	9	3923.0801	3923.0913	-0.0112
12	1	12	11	1	11	4149.1904	4149.1982	-0.0078
11	1	11	10	0	10	4175.0882	4175.0852	0.0030
12	0	12	11	0	11	4185.4546	4185.4569	-0.0023
12	2	11	11	2	10	4217.0984	4217.0955	0.0029
12	3	10	11	3	9	4227.9489	4227.9373	0.0116
12	3	9	11	3	8	4230.3227	4230.3129	0.0098
12	2	10	11	2	9	4255.2008	4255.2052	-0.0044
12	1	11	11	1	10	4277.6643	4277.6647	-0.0004
7	2	6	6	1	6	4427.3174	4427.3143	0.0031
7	2	5	6	1	6	4445.4369	4445.4404	-0.0035
12	1	12	11	0	11	4482.6303	4482.6262	0.0041
13	1	13	12	1	12	4493.4246	4493.4296	-0.0050
13	0	13	12	0	12	4528.2825	4528.2898	-0.0073
13	2	12	12	2	11	4567.1868	4567.1843	0.0025
13	3	11	12	3	10	4580.7409	4580.7384	0.0025
13	3	10	12	3	9	4584.2883	4584.2829	0.0054
13	2	11	12	2	10	4614.3418	4614.3484	-0.0066
13	1	12	12	1	11	4631.6214	4631.6202	0.0012
13	1	13	12	0	12	4790.6004	4790.5989	0.0015
8	2	7	7	1	7	4817.5038	4817.5019	0.0019
14	1	14	13	1	13	4837.3673	4837.3727	-0.0054
8	2	6	7	1	7	4847.5759	4847.5801	-0.0042
14	0	14	13	0	13	4870.2738	4870.2729	0.0009
14	2	13	13	2	12	4916.9612	4916.9594	0.0018
14	7	8	13	7	7	4929.0915	4929.0917	-0.0002
14	7	7	13	7	6	4929.0915	4929.0917	-0.0002
14	3	12	13	3	11	4933.5745	4933.5732	0.0013
14	3	11	13	3	10	4938.6952	4938.6940	0.0012

14	2	12	13	2	11	4973.9917	4973.9934	-0.0017
14	1	13	13	1	12	4984.8729	4984.8769	-0.0040
14	1	14	13	0	13	5099.6831	5099.6817	0.0014
15	1	15	14	1	14	5181.0278	5181.0315	-0.0037
9	2	8	8	1	8	5213.2255	5213.2192	0.0063
9	2	7	8	1	8	5260.1966	5260.1965	0.0001
15	2	14	14	2	13	5266.3924	5266.4004	-0.0080
15	3	13	14	3	12	5286.4192	5286.4179	0.0013
15	3	12	14	3	11	5293.6238	5293.6114	0.0124
15	1	14	14	1	13	5337.3434	5337.3495	-0.0061
15	1	15	14	0	14	5410.4503	5410.4403	0.0100
16	1	16	15	1	15	5524.4023	5524.4137	-0.0114
16	0	16	15	0	15	5552.2682	5552.2684	-0.0002
16	2	15	15	2	14	5615.4871	5615.4885	-0.0014
16	6	11	15	6	10	5634.3852	5634.3829	0.0023
16	6	10	15	6	9	5634.3852	5634.3830	0.0022
16	3	14	15	3	13	5639.2451	5639.2456	-0.0005
16	3	13	15	3	12	5649.1019	5649.1021	-0.0002
10	2	8	9	1	9	5684.3788	5684.3798	-0.0010
16	1	15	15	1	14	5688.9479	5688.9508	-0.0029
17	0	17	16	0	16	5892.5752	5892.5838	-0.0086
17	2	16	16	2	15	5964.2032	5964.2065	-0.0033
17	4	14	16	4	13	5991.1179	5991.1135	0.0044
17	4	13	16	4	12	5991.7468	5991.7460	0.0008
17	3	15	16	3	14	5992.0254	5992.0261	-0.0007
17	3	14	16	3	13	6005.2272	6005.2326	-0.0054
18	4	15	17	4	14	6344.3496	6344.3430	0.0066
18	3	16	17	3	15	6344.7349	6344.7270	0.0079
18	4	14	17	4	13	6345.2928	6345.2874	0.0054
18	1	18	17	0	17	6356.3859	6356.3776	0.0083
19	9	10	18	9	9	6689.1961	6689.2021	-0.0060
19	9	11	18	9	10	6689.1961	6689.2021	-0.0060
19	8	12	18	8	11	6689.7857	6689.7875	-0.0018
19	8	11	18	8	10	6689.7857	6689.7875	-0.0018
19	6	13	18	6	12	6691.9395	6691.9370	0.0025
19	6	14	18	6	13	6691.9395	6691.9363	0.0032
19	3	17	18	3	16	6697.3056	6697.3141	-0.0085

19	4	16	18	4	15	6697.6859	6697.6806	0.0053
19	4	15	18	4	14	6699.062	6699.0584	0.0036
6	1	6	5	1	5	2078.0416	2078.0412	0.0004
6	0	6	5	0	5	2106.8438	2106.8487	-0.0049
6	2	5	5	2	4	2111.2251	2111.2323	-0.0072
6	3	4	5	3	3	2112.6405	2112.6450	-0.0045
6	3	3	5	3	2	2112.7068	2112.7124	-0.0056
6	2	4	5	2	3	2116.2631	2116.2727	-0.0096
6	1	5	5	1	4	2143.4046	2143.4149	-0.0103
11	2	10	11	1	11	2216.6591	2216.6524	0.0067
5	1	5	4	0	4	2295.6553	2295.6597	-0.0044
7	1	7	6	1	6	2423.8601	2423.8576	0.0025
7	0	7	6	0	6	2455.8326	2455.8328	-0.0002
7	2	6	6	2	5	2462.7261	2462.7259	0.0002
7	3	5	6	3	4	2464.9905	2464.9787	0.0118
7	3	4	6	3	3	2465.1392	2465.1301	0.0091
7	2	5	6	2	4	2470.7578	2470.7519	0.0059
7	1	6	6	1	5	2500.0613	2500.0513	0.0100
6	1	6	5	0	5	2616.6717	2616.6751	-0.0034
8	1	8	7	1	7	2769.4501	2769.4485	0.0016
8	0	8	7	0	7	2803.8747	2803.8702	0.0045
8	2	7	7	2	6	2814.0500	2814.0452	0.0048
8	3	6	7	3	5	2817.4054	2817.4006	0.0048
8	3	5	7	3	4	2817.7092	2817.7030	0.0062
8	2	6	7	2	5	2826.0043	2825.9973	0.0070
8	1	7	7	1	6	2856.3896	2856.3940	-0.0044
9	1	9	8	1	8	3114.7879	3114.7929	-0.005
9	0	9	8	0	8	3150.8764	3150.8788	-0.0024
9	2	8	8	2	7	3165.1749	3165.1658	0.0091
9	5	4	8	5	3	3168.7001	3168.7064	-0.0063
9	5	5	8	5	4	3168.7065	3168.7064	0.0001
9	3	7	8	3	6	3169.9139	3169.9122	0.0017
9	3	6	8	3	5	3170.4667	3170.4657	0.0010
9	2	7	8	2	6	3182.0628	3182.0649	-0.0021
9	1	8	8	1	7	3212.3890	3212.3886	0.0004
4	2	3	3	1	2	3224.2138	3224.2211	-0.0073
8	1	8	7	0	7	3247.2969	3247.2998	-0.0029

18	3	16	18	2	17	3254.1338	3254.1332	0.0006
17	3	14	17	2	16	3266.8303	3266.8314	-0.0011
4	2	3	3	1	3	3289.6618	3289.6664	-0.0046
4	2	2	3	1	3	3291.8323	3291.8373	-0.0050
14	1	13	13	2	11	3424.2687	3424.2714	-0.0027
20	3	17	20	2	19	3445.5515	3445.5509	0.0006
10	1	10	9	1	9	3459.8742	3459.8737	0.0005
10	0	10	9	0	9	3496.8001	3496.8103	-0.0102
10	2	9	9	2	8	3516.0665	3516.0635	0.0030
10	3	8	9	3	7	3522.5166	3522.5108	0.0058
10	3	7	9	3	6	3523.4656	3523.4574	0.0082
10	2	8	9	2	7	3538.9756	3538.9762	-0.0006
5	2	4	4	1	3	3554.3613	3554.3534	0.0079
5	2	3	4	1	3	3559.4101	3559.4130	-0.0029
10	1	9	9	1	8	3567.9723	3567.9759	-0.0036
5	2	4	4	1	4	3663.4155	3663.4213	-0.0058
5	2	3	4	1	4	3668.4752	3668.4809	-0.0057
11	1	11	10	1	10	3804.6754	3804.6782	-0.0028
11	0	11	10	0	10	3841.6534	3841.6572	-0.0038
11	2	10	10	2	9	3866.7253	3866.7144	0.0109
10	1	10	9	0	9	3867.2088	3867.2173	-0.0085
11	3	9	10	3	8	3875.1927	3875.1896	0.0031
11	3	8	10	3	7	3876.7241	3876.7231	0.0010
6	2	5	5	1	4	3879.0626	3879.0511	0.0115
11	2	9	10	2	8	3896.7065	3896.7114	-0.0049
11	1	10	10	1	9	3923.0801	3923.0913	-0.0112
12	1	12	11	1	11	4149.1904	4149.1982	-0.0078
11	1	11	10	0	10	4175.0882	4175.0852	0.0030
12	0	12	11	0	11	4185.4546	4185.4569	-0.0023
12	2	11	11	2	10	4217.0984	4217.0955	0.0029
12	3	10	11	3	9	4227.9489	4227.9373	0.0116
12	3	9	11	3	8	4230.3227	4230.3129	0.0098
12	2	10	11	2	9	4255.2008	4255.2052	-0.0044
12	1	11	11	1	10	4277.6643	4277.6647	-0.0004
7	2	6	6	1	6	4427.3174	4427.3143	0.0031
7	2	5	6	1	6	4445.4369	4445.4404	-0.0035
12	1	12	11	0	11	4482.6303	4482.6262	0.0041

13	1	13	12	1	12	4493.4246	4493.4296	-0.0050
13	0	13	12	0	12	4528.2825	4528.2898	-0.0073
13	2	12	12	2	11	4567.1868	4567.1843	0.0025
13	3	11	12	3	10	4580.7409	4580.7384	0.0025
13	3	10	12	3	9	4584.2883	4584.2829	0.0054
13	2	11	12	2	10	4614.3418	4614.3484	-0.0066
13	1	12	12	1	11	4631.6214	4631.6202	0.0012
13	1	13	12	0	12	4790.6004	4790.5989	0.0015
8	2	7	7	1	7	4817.5038	4817.5019	0.0019
14	1	14	13	1	13	4837.3673	4837.3727	-0.0054
8	2	6	7	1	7	4847.5759	4847.5801	-0.0042
14	0	14	13	0	13	4870.2738	4870.2729	0.0009
14	2	13	13	2	12	4916.9612	4916.9594	0.0018
14	7	8	13	7	7	4929.0915	4929.0917	-0.0002
14	7	7	13	7	6	4929.0915	4929.0917	-0.0002
14	3	12	13	3	11	4933.5745	4933.5732	0.0013
14	3	11	13	3	10	4938.6952	4938.6940	0.0012
14	2	12	13	2	11	4973.9917	4973.9934	-0.0017
14	1	13	13	1	12	4984.8729	4984.8769	-0.0040
14	1	14	13	0	13	5099.6831	5099.6817	0.0014
15	1	15	14	1	14	5181.0278	5181.0315	-0.0037
9	2	8	8	1	8	5213.2255	5213.2192	0.0063
9	2	7	8	1	8	5260.1966	5260.1965	0.0001
15	2	14	14	2	13	5266.3924	5266.4004	-0.0080
15	3	13	14	3	12	5286.4192	5286.4179	0.0013
15	3	12	14	3	11	5293.6238	5293.6114	0.0124
15	1	14	14	1	13	5337.3434	5337.3495	-0.0061
15	1	15	14	0	14	5410.4503	5410.4403	0.0100
16	1	16	15	1	15	5524.4023	5524.4137	-0.0114
16	0	16	15	0	15	5552.2682	5552.2684	-0.0002
16	2	15	15	2	14	5615.4871	5615.4885	-0.0014
16	6	11	15	6	10	5634.3852	5634.3829	0.0023
16	6	10	15	6	9	5634.3852	5634.3830	0.0022
16	3	14	15	3	13	5639.2451	5639.2456	-0.0005
16	3	13	15	3	12	5649.1019	5649.1021	-0.0002
10	2	8	9	1	9	5684.3788	5684.3798	-0.0010
16	1	15	15	1	14	5688.9479	5688.9508	-0.0029

17	0	17	16	0	16	5892.5752	5892.5838	-0.0086
17	2	16	16	2	15	5964.2032	5964.2065	-0.0033
17	4	14	16	4	13	5991.1179	5991.1135	0.0044
17	4	13	16	4	12	5991.7468	5991.7460	0.0008
17	3	15	16	3	14	5992.0254	5992.0261	-0.0007
17	3	14	16	3	13	6005.2272	6005.2326	-0.0054
18	4	15	17	4	14	6344.3496	6344.3430	0.0066
18	3	16	17	3	15	6344.7349	6344.7270	0.0079
18	4	14	17	4	13	6345.2928	6345.2874	0.0054
18	1	18	17	0	17	6356.3859	6356.3776	0.0083
19	9	10	18	9	9	6689.1961	6689.2021	-0.0060
19	9	11	18	9	10	6689.1961	6689.2021	-0.0060
19	8	12	18	8	11	6689.7857	6689.7875	-0.0018
19	8	11	18	8	10	6689.7857	6689.7875	-0.0018
19	6	13	18	6	12	6691.9395	6691.9370	0.0025
19	6	14	18	6	13	6691.9395	6691.9363	0.0032
19	3	17	18	3	16	6697.3056	6697.3141	-0.0085
19	4	16	18	4	15	6697.6859	6697.6806	0.0053
19	4	15	18	4	14	6699.0620	6699.0584	0.0036

Table S6.19. Rotational transition frequencies of the **PFP***Tg*+**PFP***Tg*+ homodimer.

J’	K_a’	K_c’	*J*”	K_a”	K_c”	Obs/ MHz	Cal/ MHz	Obs - Cal/ MHz
5	2	4	4	2	3	1822.8436	1822.8441	-0.0005
5	4	1	4	4	0	1824.1194	1824.1191	0.0003
5	4	2	4	4	1	1824.1194	1824.1188	0.0006
5	3	3	4	3	2	1824.4157	1824.4158	-0.0001
5	3	2	4	3	1	1824.4879	1824.4866	0.0013
5	2	3	4	2	2	1828.4627	1828.4626	0.0001
6	1	6	5	1	5	2141.6195	2141.6198	-0.0003
6	0	6	5	0	5	2178.3675	2178.3682	-0.0007
6	2	5	5	2	4	2186.8803	2186.8807	-0.0004
6	5	2	5	5	1	2188.9004	2188.8983	0.0021
6	5	1	5	5	0	2188.9004	2188.8983	0.0021
6	4	3	5	4	2	2189.1351	2189.1346	0.0005
6	4	2	5	4	1	2189.1351	2189.1358	-0.0007

6	3	4	5	3	3	2189.6225	2189.6216	0.0009
6	3	3	5	3	2	2189.8112	2189.8101	0.0011
6	2	4	5	2	3	2196.6552	2196.6537	0.0015
6	1	5	5	1	4	2230.1466	2230.1482	-0.0016
7	1	7	6	1	6	2497.5667	2497.5675	-0.0008
7	0	7	6	0	6	2537.3250	2537.3231	0.0019
7	2	6	6	2	5	2550.6263	2550.6278	-0.0015
7	6	1	6	6	0	2553.6851	2553.6863	-0.0012
7	6	2	6	6	1	2553.6851	2553.6863	-0.0012
7	5	3	6	5	2	2553.8733	2553.8729	0.0004
7	5	2	6	5	1	2553.8733	2553.8729	0.0004
7	4	4	6	4	3	2554.255	2554.2545	0.0005
7	4	3	6	4	2	2554.2585	2554.2585	0.0000
7	3	5	6	3	4	2554.9762	2554.9738	0.0024
7	3	4	6	3	3	2555.3958	2555.3974	-0.0016
7	2	5	6	2	4	2566.1109	2566.1129	-0.0020
7	1	6	6	1	5	2600.6397	2600.6418	-0.0021
8	1	8	7	1	7	2853.1032	2853.1033	-0.0001
8	0	8	7	0	7	2894.5688	2894.5691	-0.0003
8	2	7	7	2	6	2914.0370	2914.0381	-0.0011
8	7	2	7	7	1	2918.4797	2918.4803	-0.0006
8	7	1	7	7	0	2918.4797	2918.4803	-0.0006
8	6	3	7	6	2	2918.6342	2918.6332	0.0010
8	6	2	7	6	1	2918.6342	2918.6332	0.0010
8	5	4	7	5	3	2918.9207	2918.9204	0.0003
8	5	3	7	5	2	2918.9207	2918.9205	0.0002
8	4	5	7	4	4	2919.4943	2919.4949	-0.0006
8	4	4	7	4	3	2919.5063	2919.5059	0.0004
8	3	6	7	3	5	2920.4719	2920.4735	-0.0016
8	3	5	7	3	4	2921.3175	2921.3186	-0.0011
15	2	13	14	3	11	2927.4618	2927.4623	-0.0005
9	3	6	9	2	8	2930.1817	2930.1821	-0.0004
8	2	6	7	2	5	2936.9284	2936.9303	-0.0019
8	1	7	7	1	6	2970.5357	2970.5344	0.0013
16	1	16	15	2	14	3021.1349	3021.1345	0.0004
13	3	10	13	2	12	3026.7665	3026.7665	0.0000
4	2	2	3	1	2	3159.8280	3159.8278	0.0002

9	1	9	8	1	8	3208.1987	3208.1982	0.0006
4	2	3	3	1	3	3244.3218	3244.3212	0.0006
9	0	9	8	0	8	3250.0499	3250.0510	-0.0011
9	2	8	8	2	7	3277.0653	3277.0649	0.0004
9	8	1	8	8	0	3283.2802	3283.2796	0.0006
9	8	2	8	8	1	3283.2802	3283.2796	0.0006
9	7	2	8	7	1	3283.4077	3283.4062	0.0015
9	7	3	8	7	2	3283.4077	3283.4062	0.0015
9	6	4	8	6	3	3283.6342	3283.6339	0.0003
9	6	3	8	6	2	3283.6342	3283.6339	0.0003
9	5	5	8	5	4	3284.0502	3284.0514	-0.0012
9	5	4	8	5	3	3284.0502	3284.0516	-0.0014
9	4	6	8	4	5	3284.8709	3284.8716	-0.0007
9	4	5	8	4	4	3284.8979	3284.8980	-0.0001
9	3	7	8	3	6	3286.1118	3286.1117	0.0001
9	3	6	8	3	5	3287.6562	3287.6558	0.0004
9	2	7	8	2	6	3309.1090	3309.1091	-0.0001
9	1	8	8	1	7	3339.7042	3339.7058	-0.0016
7	1	6	6	0	6	3351.5649	3351.5647	0.0002
5	2	3	4	1	3	3500.5076	3500.5096	-0.0020
10	1	10	9	1	9	3562.8352	3562.8333	0.0019
10	0	10	9	0	9	3603.8130	3603.8148	-0.0018
5	2	4	4	1	4	3638.5136	3638.5136	0.0000
10	2	9	9	2	8	3639.6630	3639.6631	-0.0001
10	8	2	9	8	1	3648.1890	3648.1879	0.0011
10	8	3	9	8	2	3648.1890	3648.1879	0.0011
10	7	4	9	7	3	3648.3757	3648.3729	0.0028
10	7	3	9	7	2	3648.3757	3648.3729	0.0028
10	6	5	9	6	4	3648.6980	3648.6951	0.0029
10	6	4	9	6	3	3648.6980	3648.6952	0.0028
10	5	5	9	5	4	3649.2760	3649.2768	-0.0008
10	5	6	9	5	5	3649.2760	3649.2762	-0.0002
10	4	7	9	4	6	3650.4003	3650.3990	0.0013
10	4	6	9	4	5	3650.4583	3650.4560	0.0023
10	3	8	9	3	7	3651.8706	3651.8696	0.0010
10	3	7	9	3	6	3654.5042	3654.5038	0.0004
10	2	8	9	2	7	3682.5520	3682.5497	0.0023

10	1	9	9	1	8	3708.0238	3708.0229	0.0009
6	2	4	5	1	4	3838.0031	3838.0014	0.0016
11	1	11	10	1	10	3917.0002	3917.0003	-0.0001
11	0	11	10	0	10	3956.0112	3956.0086	0.0026
3	3	0	2	2	0	3995.9802	3995.9789	0.0013
3	3	1	2	2	1	3996.2577	3996.2581	-0.0004
11	2	10	10	2	9	4001.7870	4001.7890	-0.0020
11	9	3	10	9	2	4012.9763	4012.9768	-0.0005
11	9	2	10	9	1	4012.9763	4012.9768	-0.0005
11	8	4	10	8	3	4013.1284	4013.1276	0.0008
11	8	3	10	8	2	4013.1284	4013.1276	0.0008
11	7	4	10	7	3	4013.3843	4013.3850	-0.0007
11	7	5	10	7	4	4013.3843	4013.3850	-0.0007
11	6	6	10	6	5	4013.8249	4013.8237	0.0012
11	6	5	10	6	4	4013.8249	4013.8237	0.0012
11	5	6	10	5	5	4014.6054	4014.6067	-0.0013
11	5	7	10	5	6	4014.6054	4014.6052	0.0002
11	4	8	10	4	7	4016.0887	4016.0898	-0.0011
11	4	7	10	4	6	4016.2014	4016.2037	-0.0023
11	3	9	10	3	8	4017.7180	4017.7179	0.0001
11	3	8	10	3	7	4021.9712	4021.9706	0.0006
11	2	9	10	2	8	4057.0478	4057.0483	-0.0005
11	1	10	10	1	9	4075.3389	4075.3396	-0.0007
7	2	5	6	1	5	4173.9641	4173.9661	-0.0020
18	0	18	17	1	16	4183.4154	4183.4165	-0.0011
9	1	8	8	0	8	4229.9121	4229.9126	-0.0005
12	1	12	11	1	11	4270.7003	4270.7002	0.0001
12	0	12	11	0	11	4306.8637	4306.865	-0.0013
4	3	1	3	2	1	4360.1226	4360.1229	-0.0003
4	3	2	3	2	2	4361.5127	4361.5112	0.0015
12	2	11	11	2	10	4363.3990	4363.4010	-0.0020
12	10	2	11	10	1	4377.7723	4377.7722	0.0001
12	10	3	11	10	2	4377.7723	4377.7722	0.0001
12	9	4	11	9	3	4377.8925	4377.8934	-0.0009
12	9	3	11	9	2	4377.8925	4377.8934	-0.0009
12	8	4	11	8	3	4378.1018	4378.1017	0.0001
12	8	5	11	8	4	4378.1018	4378.1017	0.0001

12	7	6	11	7	5	4378.4461	4378.4469	-0.0008
12	7	5	11	7	4	4378.4461	4378.4469	-0.0008
12	6	7	11	6	6	4379.0253	4379.0262	-0.0009
12	6	6	11	6	5	4379.0253	4379.0262	-0.0009
12	5	8	11	5	7	4380.0486	4380.0488	-0.0002
12	5	7	11	5	6	4380.0519	4380.0522	-0.0003
12	4	9	11	4	8	4381.9559	4381.9549	0.0010
12	4	8	11	4	7	4382.1669	4382.1677	-0.0008
12	3	10	11	3	9	4383.6180	4383.6179	0.0001
12	3	9	11	3	8	4390.1780	4390.1759	0.0021
16	1	15	15	2	13	4391.4757	4391.4765	-0.0008
12	2	10	11	2	9	4432.3136	4432.3132	0.0004
12	1	11	11	1	10	4441.4963	4441.4974	-0.0011
8	2	6	7	1	6	4510.2555	4510.2545	0.0010
13	1	13	12	1	12	4623.9424	4623.9434	-0.0010
13	0	13	12	0	12	4656.6675	4656.6687	-0.0012
10	1	9	9	0	9	4687.8833	4687.8846	-0.0013
5	3	2	4	2	2	4723.2245	4723.2250	-0.0005
13	2	12	12	2	11	4724.4609	4724.4608	0.0001
5	3	3	4	2	3	4727.3605	4727.3614	-0.0009
13	9	4	12	9	3	4742.8375	4742.8363	0.0012
13	9	5	12	9	4	4742.8375	4742.8363	0.0012
13	8	5	12	8	4	4743.1125	4743.1135	-0.0010
13	8	6	12	8	5	4743.1125	4743.1135	-0.0010
13	7	6	12	7	5	4743.5626	4743.5634	-0.0008
13	7	7	12	7	6	4743.5626	4743.5634	-0.0008
13	6	8	12	6	7	4744.3120	4744.3095	0.0025
13	6	7	12	6	6	4744.3120	4744.3095	0.0025
13	5	9	12	5	8	4745.6168	4745.6172	-0.0004
13	5	8	12	5	7	4745.6243	4745.6244	-0.0001
13	4	10	12	4	9	4748.0020	4748.0017	0.0003
13	4	9	12	4	8	4748.3782	4748.3789	-0.0007
13	3	11	12	3	10	4749.5225	4749.5217	0.0008
13	3	10	12	3	9	4759.2486	4759.2480	0.0006
13	1	12	12	1	11	4806.3295	4806.3295	0.0000
13	2	11	12	2	10	4807.9965	4807.9968	-0.0003
9	2	7	8	1	7	4848.8277	4848.8292	-0.0015

8	2	7	7	1	7	4865.5748	4865.5743	0.0005
14	1	14	13	1	13	4976.7475	4976.7480	-0.0005
14	0	14	13	0	13	5005.7163	5005.7171	-0.0008
6	3	3	5	2	3	5084.5730	5084.5726	0.0004
14	2	13	13	2	12	5084.9336	5084.9333	0.0003
6	3	4	5	2	4	5094.1386	5094.1389	-0.0003
14	11	4	13	11	3	5107.4497	5107.4508	-0.0011
14	11	3	13	11	2	5107.4497	5107.4508	-0.0011
14	10	5	13	10	4	5107.5854	5107.5838	0.0016
14	10	4	13	10	3	5107.5854	5107.5838	0.0016
14	9	5	13	9	4	5107.8094	5107.8074	0.0020
14	9	6	13	9	5	5107.8094	5107.8074	0.0020
14	8	7	13	8	6	5108.1642	5108.1660	-0.0018
14	8	6	13	8	5	5108.1642	5108.1660	-0.0018
14	7	8	13	7	7	5108.7385	5108.7388	-0.0003
14	7	7	13	7	6	5108.7385	5108.7388	-0.0003
14	6	9	13	6	8	5109.6801	5109.6803	-0.0002
14	6	8	13	6	7	5109.6801	5109.6805	-0.0004
14	5	10	13	5	9	5111.3201	5111.3206	-0.0005
14	5	9	13	5	8	5111.3353	5111.3350	0.0003
14	4	11	13	4	10	5114.2349	5114.2347	0.0002
14	4	10	13	4	9	5114.8733	5114.8730	0.0003
14	3	12	13	3	11	5115.3742	5115.3739	0.0003
14	3	11	13	3	10	5129.3173	5129.3178	-0.0005
11	1	10	10	0	10	5159.4092	5159.4093	-0.0001
14	1	13	13	1	12	5169.6651	5169.6658	-0.0007
14	2	12	13	2	11	5183.7346	5183.7338	0.0008
10	2	8	9	1	8	5191.6753	5191.6731	0.0022
15	1	15	14	1	14	5329.1379	5329.1384	-0.0005
15	0	15	14	0	14	5354.2852	5354.2844	0.0008
7	3	4	6	2	4	5443.3158	5443.3163	-0.0005
15	2	14	14	2	13	5444.7865	5444.7880	-0.0015
7	3	5	6	2	5	5462.2312	5462.2320	-0.0008
15	12	4	14	12	3	5472.2411	5472.2408	0.0003
15	12	3	14	12	2	5472.2411	5472.2408	0.0003
15	11	5	14	11	4	5472.3403	5472.3418	-0.0015
15	11	4	14	11	3	5472.3403	5472.3418	-0.0015

15	10	5	14	10	4	5472.5189	5472.5205	-0.0016
15	10	6	14	10	5	5472.5204	5472.5205	0.0000
15	9	6	14	9	5	5472.8094	5472.8091	0.0003
15	9	7	14	9	6	5472.8094	5472.8091	0.0003
15	8	7	14	8	6	5473.2613	5473.2623	-0.0010
15	8	8	14	8	7	5473.2613	5473.2623	-0.0010
15	7	9	14	7	8	5473.9778	5473.9777	0.0001
15	7	8	14	7	7	5473.9778	5473.9777	0.0001
15	6	9	14	6	8	5475.1462	5475.1460	0.0002
15	6	10	14	6	9	5475.1462	5475.1455	0.0007
15	5	11	14	5	10	5477.1686	5477.1688	-0.0002
15	5	10	14	5	9	5477.1960	5477.1961	-0.0001
15	4	12	14	4	11	5480.6535	5480.6534	0.0001
15	3	13	14	3	12	5481.1119	5481.1130	-0.0011
15	4	11	14	4	10	5481.6909	5481.6923	-0.0014
15	3	12	14	3	11	5500.5079	5500.5086	-0.0007
4	4	1	3	3	1	5521.5485	5521.5499	-0.0014
4	4	0	3	3	0	5521.5485	5521.5466	0.0019
15	1	14	14	1	13	5531.3422	5531.3432	-0.0010
11	2	9	10	1	9	5540.7002	5540.6984	0.0018
15	2	13	14	2	12	5559.1741	5559.1752	-0.0011
16	1	16	15	1	15	5681.1423	5681.1440	-0.0017
16	0	16	15	0	15	5702.5997	5702.5983	0.0014
8	3	5	7	2	5	5798.5214	5798.5221	-0.0007
16	2	15	15	2	14	5803.9983	5803.9992	-0.0009
8	3	6	7	2	6	5832.0764	5832.0776	-0.0012
16	12	5	15	12	4	5837.1071	5837.1089	-0.0018
16	12	4	15	12	3	5837.1071	5837.1089	-0.0018
16	11	5	15	11	4	5837.2486	5837.2479	0.0007
16	11	6	15	11	5	5837.2486	5837.2479	0.0007
16	10	6	15	10	5	5837.4802	5837.4797	0.0005
16	10	7	15	10	6	5837.4802	5837.4797	0.0005
16	9	7	15	9	6	5837.8453	5837.8435	0.0018
16	9	8	15	9	7	5837.8453	5837.8435	0.0018
16	8	8	15	8	7	5838.4048	5838.4056	-0.0008
16	8	9	15	8	8	5838.4048	5838.4056	-0.0008
16	7	10	15	7	9	5839.2870	5839.2848	0.0022

16	7	9	15	7	8	5839.2870	5839.2848	0.0022
16	6	11	15	6	10	5840.7130	5840.7120	0.0010
16	6	10	15	6	9	5840.7130	5840.7129	0.0001
16	3	14	15	3	13	5846.6750	5846.6730	0.0020
16	4	13	15	4	12	5847.2521	5847.2525	-0.0004
16	4	12	15	4	11	5848.8853	5848.8867	-0.0014
16	3	13	15	3	12	5872.9250	5872.9229	0.0021
16	1	15	15	1	14	5891.2177	5891.2184	-0.0007
12	2	10	11	1	10	5897.6729	5897.6720	0.0009
16	2	14	15	2	13	5934.0113	5934.0115	-0.0002
17	1	17	16	1	16	6032.7986	6032.7973	0.0013
17	0	17	16	0	16	6050.8291	6050.8296	-0.0005
9	3	6	8	2	6	6149.2492	6149.2476	0.0016
17	2	16	16	2	15	6162.5472	6162.5475	-0.0003
17	12	6	16	12	5	6201.9883	6201.9870	0.0013
17	12	5	16	12	4	6201.9883	6201.9870	0.0013
17	11	7	16	11	6	6202.1694	6202.1700	-0.0006
17	11	6	16	11	5	6202.1694	6202.1700	-0.0006
17	10	7	16	10	6	6202.4629	6202.4629	0.0000
17	10	8	16	10	7	6202.4629	6202.4629	0.0000
17	9	9	16	9	8	6202.9127	6202.9127	0.0000
17	9	8	16	9	7	6202.9127	6202.9127	0.0000
17	8	10	16	8	9	6203.5985	6203.5991	-0.0006
17	8	9	16	8	8	6203.5985	6203.5991	-0.0006
9	3	7	8	2	7	6204.1501	6204.1512	-0.0011
17	7	11	16	7	10	6204.6644	6204.6645	-0.0001
17	7	10	16	7	9	6204.6644	6204.6645	-0.0001
17	6	11	16	6	10	6206.3871	6206.3883	-0.0012
17	6	12	16	6	11	6206.3871	6206.3866	0.0005
17	5	13	16	5	12	6209.3369	6209.3370	-0.0001
17	5	12	16	5	11	6209.4227	6209.4233	-0.0006
17	3	15	16	3	14	6211.9850	6211.9851	-0.0001
17	4	14	16	4	13	6214.0197	6214.0209	-0.0012
17	4	13	16	4	12	6216.5146	6216.5151	-0.0005
17	3	14	16	3	13	6246.6247	6246.6254	-0.0007
17	1	16	16	1	15	6249.1865	6249.1853	0.0012
13	2	11	12	1	11	6264.1702	6264.1714	-0.0012

17	2	15	16	2	14	6307.9791	6307.9804	-0.0013
18	1	18	17	1	17	6384.1334	6384.1323	0.0011
18	0	18	17	0	17	6399.0951	6399.0936	0.0015
10	3	7	9	2	7	6494.6413	6494.6423	-0.0010
18	2	17	17	2	16	6520.4192	6520.4197	-0.0005
18	12	7	17	12	6	6566.8751	6566.8757	-0.0006
18	12	6	17	12	5	6566.8751	6566.8757	-0.0006
18	11	8	17	11	7	6567.1085	6567.1091	-0.0006
18	11	7	17	11	6	6567.1085	6567.1091	-0.0006
18	10	9	17	10	8	6567.4715	6567.4716	-0.0001
18	10	8	17	10	7	6567.4715	6567.4716	-0.0001
18	9	10	17	9	9	6568.0189	6568.0190	-0.0001
18	9	9	17	9	8	6568.0189	6568.0190	-0.0001
18	8	10	17	8	9	6568.8446	6568.8458	-0.0012
18	8	11	17	8	10	6568.8446	6568.8458	-0.0012
18	7	12	17	7	11	6570.1215	6570.1215	0.0000
18	7	11	17	7	10	6570.1215	6570.1216	-0.0001
18	6	13	17	6	12	6572.1759	6572.1762	-0.0003
18	6	12	17	6	11	6572.1802	6572.1796	0.0006
18	5	14	17	5	13	6575.6748	6575.6740	0.0008
18	5	13	17	5	12	6575.8195	6575.8194	0.0001
18	3	16	17	3	15	6576.9806	6576.9801	0.0005
10	3	8	9	2	8	6578.9563	6578.9558	0.0005
18	4	15	17	4	14	6580.9413	6580.9408	0.0005
18	4	14	17	4	13	6584.6463	6584.6463	0.0000
18	1	17	17	1	16	6605.1925	6605.1926	-0.0001
12	2	11	11	1	11	6606.3573	6606.3573	0.0000
18	3	15	17	3	14	6621.6229	6621.6238	-0.0009
18	2	16	17	2	15	6680.8646	6680.8651	-0.0005
19	1	19	18	1	18	6735.1836	6735.1835	0.0001
11	3	8	10	2	8	6834.0635	6834.0632	0.0003
19	2	18	18	2	17	6877.6103	6877.6098	0.0005
19	7	12	18	7	11	6935.6617	6935.6606	0.0011
19	7	13	18	7	12	6935.6617	6935.6605	0.0012
19	6	14	18	6	13	6938.0886	6938.0879	0.0007
19	6	13	18	6	12	6938.0938	6938.0940	-0.0002
19	4	16	18	4	15	6947.9889	6947.9873	0.0016

19	4	15	18	4	14	6953.3603	6953.3602	0.0001
19	1	18	18	1	17	6959.2624	6959.2608	0.0016
19	3	16	18	3	15	6997.8517	6997.8521	-0.0004
19	2	17	18	2	16	7052.4839	7052.4839	0.0000
20	3	18	19	3	17	7305.7473	7305.7469	0.0004

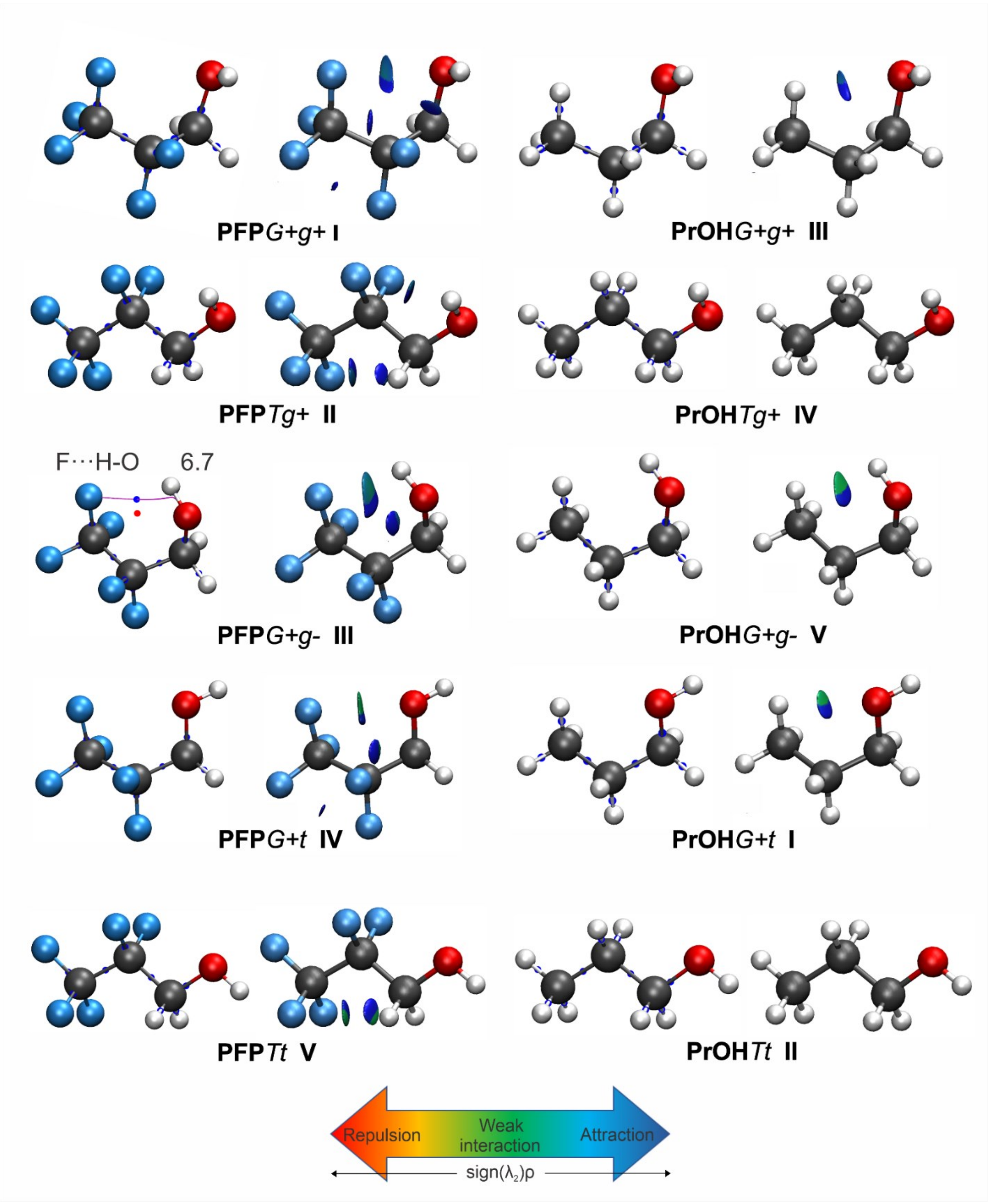

Figure S6.4. The intramolecular forces for all the non-covalent BCPs identified and non-covalent interaction analyses of the all possible PFP and PrOH monomers calculated at the B3LYP-D3(BJ)/def2-QZVP level of theory. The bond energy is in kJmol^{-1}. **I** to **V** indicate the relative stability with **I** being the most stable.

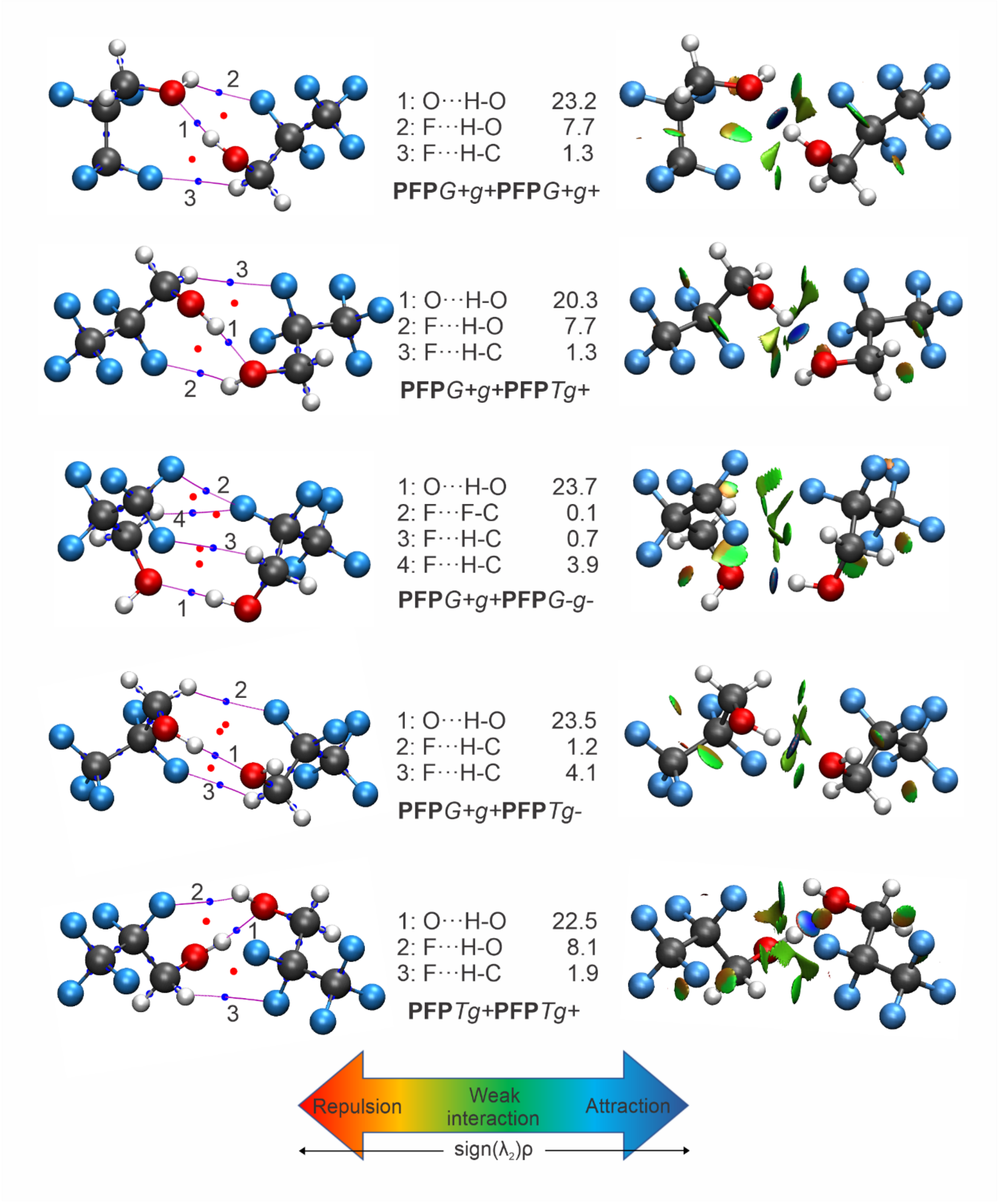

Figure S6.5. The intermolecular bond energies (in kJmol^{-1}) for all the non-covalent BCPs identified and the NCI analyses of the five observed PFP homodimers calculated at the B3LYP-D3(BJ)/def2-QZVP level of theory.

Table S6.20. Calculated Cartesian coordinates (in Å) of the **PFP***G+g+* monomer.[a]

PFP*G+g+*			
C	-0.848530	-0.317980	0.011580
C	0.419966	0.573498	0.019323
C	1.658090	-0.021540	0.680939
H	2.395782	0.785755	0.713654
H	1.407996	-0.301430	1.701188
O	2.136216	-1.171300	0.032801
H	2.411544	-0.943840	-0.859900
F	-0.678450	-1.395130	-0.756080
F	-1.897980	0.367603	-0.450910
F	-1.125190	-0.721890	1.260188
F	0.699598	0.888078	-1.278370
F	0.097207	1.724056	0.665453

[a] Optimized at the B3LYP-D3(BJ)/def2-QZVP level of theory with “scf=verytight, int= SuperFine”.

Table S6.21. Calculated Cartesian coordinates (in Å) of the **PFP***G-g-* monomer.[a]

PFP*G-g-*			
C	-0.848452	0.318052	0.011574
C	0.419900	-0.573616	0.019307
C	1.658359	0.021382	0.680405
O	2.135990	1.171589	0.032753
F	-0.678302	1.394841	-0.756495
F	-1.898101	-0.367616	-0.450444
F	-1.124863	0.722502	1.260116
F	0.699039	-0.888670	-1.278424
F	0.097345	-1.723865	0.665997
H	2.396185	-0.785867	0.712276
H	1.408878	0.300432	1.701081
H	2.411762	0.944516	-0.859976

[a] Optimized at the B3LYP-D3(BJ)/def2-QZVP level of theory with “scf=verytight, int= SuperFine”.

Table S6.22. Calculated Cartesian coordinates (in Å) of the **PFP***Tg*+ monomer.[a]

PFP*Tg*+			
C	1.037547	0.164538	0.003834
C	-0.455000	-0.244780	-0.019720
C	-1.415470	0.938403	-0.086120
H	-1.167040	1.626919	0.725416
H	-1.268250	1.449400	-1.034490
O	-2.753670	0.514261	-0.042200
H	-2.925540	0.090156	0.803553
F	1.332724	0.877356	-1.093110
F	1.831612	-0.903710	0.042892
F	1.294109	0.925273	1.078106
F	-0.633070	-1.078550	-1.070910
F	-0.696560	-0.963350	1.116741

[a] Optimized at the B3LYP-D3(BJ)/def2-QZVP level of theory with “scf=verytight, int= SuperFine”.

Table S6.23. Calculated Cartesian coordinates (in Å) of the **PFP***Tg*- monomer.[a]

PFP*Tg*-			
C	1.037547	0.164539	-0.003835
C	-0.454998	-0.244783	0.019721
C	-1.415474	0.938403	0.086112
H	-1.268252	1.449402	1.034484
H	-1.167036	1.626918	-0.725421
O	-2.753668	0.514261	0.042194
H	-2.925542	0.090158	-0.803557
F	1.294109	0.925268	-1.078110
F	1.831612	-0.903707	-0.042888
F	1.332725	0.877362	1.093107
F	-0.696555	-0.963351	-1.116736
F	-0.633073	-1.078547	1.070910

[a] Optimized at the B3LYP-D3(BJ)/def2-QZVP level of theory with “scf=verytight, int= SuperFine”.

Table S6.24. Calculated Cartesian coordinates (in Å) of the **PFP***G+g-* monomer.[a]

PFP*G+g-*			
C	0.851237	-0.310775	-0.012350
C	-0.415846	0.580523	-0.006279
C	-1.643167	-0.031788	-0.682813
H	-2.384600	0.763937	-0.726355
H	-1.368554	-0.301108	-1.705449
O	-2.219148	-1.094603	0.030665
H	-1.640782	-1.861378	0.009691
F	0.607893	-1.476131	0.615731
F	1.872470	0.287219	0.594344
F	1.207352	-0.593318	-1.273818
F	-0.680336	0.903340	1.280073
F	-0.090053	1.724332	-0.670606

[a] Optimized at the B3LYP-D3(BJ)/def2-QZVP level of theory with “scf=verytight, int= SuperFine”.

Table S6.25. Calculated Cartesian coordinates (in Å) of the **PFP***G-g+* monomer.[a]

PFP*G-g+*			
C	-0.851239	-0.310775	-0.012350
C	0.415847	0.580520	-0.006279
C	1.643163	-0.031790	-0.682819
H	1.368545	-0.301121	-1.705450
H	2.384595	0.763935	-0.726372
O	2.219154	-1.094597	0.030665
H	1.640797	-1.861380	0.009697
F	-1.207363	-0.593303	-1.273818
F	-1.872466	0.287216	0.594359
F	-0.607894	-1.476137	0.615717
F	0.090053	1.724332	-0.670601
F	0.680342	0.903333	1.280073

[a] Optimized at the B3LYP-D3(BJ)/def2-QZVP level of theory with “scf=verytight, int= SuperFine”.

Table S6.26. Calculated Cartesian coordinates (in Å) of the **PFP***G+t* monomer.[a]

PFP*G+t*			
C	-0.832964	-0.319594	0.012167
C	0.431664	0.582281	0.002787
C	1.677174	-0.015644	0.635725
H	2.445734	0.759831	0.570365
H	1.454842	-0.205747	1.687895
O	2.031695	-1.187321	-0.061440
H	2.808063	-1.575377	0.347122
F	-0.706325	-1.350555	-0.819450
F	-1.906689	0.387839	-0.352818
F	-1.042884	-0.791976	1.252168
F	0.662906	0.944226	-1.281203
F	0.120729	1.708218	0.703830

[a] Optimized at the B3LYP-D3(BJ)/def2-QZVP level of theory with “scf=verytight, int= SuperFine”.

Table S6.27. Calculated Cartesian coordinates (in Å) of the **PFP***G-t* monomer.[a]

PFP*G-t*			
C	-0.832964	-0.319594	-0.012167
C	0.431664	0.582281	-0.002787
C	1.677174	-0.015644	-0.635725
H	1.454842	-0.205747	-1.687895
H	2.445734	0.759831	-0.570365
O	2.031695	-1.187321	0.061440
H	2.808063	-1.575377	-0.347122
F	-1.042884	-0.791976	-1.252168
F	-1.906689	0.387839	0.352818
F	-0.706325	-1.350555	0.819450
F	0.120729	1.708218	-0.703830
F	0.662906	0.944226	1.281203

[a] Optimized at the B3LYP-D3(BJ)/def2-QZVP level of theory with “scf=verytight, int= SuperFine”.

Table S6.28. Calculated Cartesian coordinates (in Å) of the **PFP***Tt* monomer.[a]

PFP*Tt*			
C	-1.032160	-0.165734	0.000000
C	0.462425	0.249200	0.000000
C	1.403706	-0.944863	0.000000
H	1.186705	-1.541388	0.889496
H	1.186705	-1.541388	-0.889496
O	2.720318	-0.443595	0.000000
H	3.336185	-1.179108	0.000000
F	-1.311273	-0.902909	-1.085701
F	-1.823910	0.904087	0.000000
F	-1.311273	-0.902909	1.085701
F	0.663277	1.022684	-1.095217
F	0.663277	1.022684	1.095217

[a] Optimized at the B3LYP-D3(BJ)/def2-QZVP level of theory with “scf=verytight, int= SuperFine”.

Table S6.29. Calculated Cartesian coordinates (in Å) of the **PFP***G*+*g*+**PFP***Tg*+ homodimer.[a]

PFP*G*+*g*+**PFP***Tg*+			
C	3.729720	0.076570	-0.161130
C	2.347440	-0.548200	0.160400
C	1.603400	0.038160	1.356980
H	0.688550	-0.552810	1.457500
H	2.217930	-0.132550	2.238860
O	1.361250	1.410210	1.251310
H	0.644640	1.559540	0.616540
F	3.606830	1.323500	-0.614550
F	4.361800	-0.647260	-1.092670
F	4.487710	0.092440	0.943960
F	1.592710	-0.435300	-0.982120
F	2.542990	-1.873250	0.379170
C	-3.900920	-0.183100	0.013650
C	-2.373810	0.059960	-0.052550
C	-1.986330	1.341170	-0.782270
H	-2.428400	1.322510	-1.779560
H	-2.386170	2.190730	-0.235020
O	-0.586400	1.491830	-0.829500
H	-0.192590	0.798200	-1.370230
F	-4.497880	0.842370	0.636880
F	-4.181070	-1.304950	0.671440
F	-4.405830	-0.273670	-1.224570
F	-1.903620	0.073180	1.220290
F	-1.812090	-1.010940	-0.680170

[a] Optimized at the B3LYP-D3(BJ)/def2-QZVP level of theory with “scf=verytight, int= SuperFine”.

Table S6.30. Calculated Cartesian coordinates (in Å) of the **PFP**_G_+_g_+**PFP**_G_+_g_+ homodimer.[a]

PFP_G_+_g_+**PFP**_G_+_g_+			
C	3.035440	0.754690	0.047280
C	2.961630	-0.778490	-0.171370
C	2.120290	-1.559140	0.832930
H	2.299290	-2.616140	0.623260
H	2.471910	-1.339340	1.837260
O	0.752940	-1.232260	0.779740
H	0.375930	-1.477030	-0.071810
F	1.838590	1.323200	-0.139140
F	3.900580	1.309360	-0.801320
F	3.436860	1.015010	1.298550
F	2.483230	-0.986360	-1.429080
F	4.232630	-1.251170	-0.121200
C	-3.582010	-0.262530	0.093760
C	-2.305450	0.427110	-0.453330
C	-1.549460	1.321620	0.524740
H	-0.714660	1.742100	-0.043380
H	-2.215480	2.135330	0.805020
O	-1.146620	0.668300	1.692010
H	-0.424310	0.056000	1.488040
F	-3.281340	-1.197300	0.995100
F	-4.259270	-0.845070	-0.902710
F	-4.379540	0.648700	0.667230
F	-1.490050	-0.574190	-0.921460
F	-2.675130	1.173240	-1.525070

[a] Optimized at the B3LYP-D3(BJ)/def2-QZVP level of theory with “scf=verytight, int= SuperFine”.

Table S6.31. Calculated Cartesian coordinates (in Å) of the **PFP***Tg*+**PFP***Tg*+ homodimer.[a]

PFP*Tg*+**PFP***Tg*+			
C	3.071510	-0.973160	0.030120
C	2.541050	0.478630	-0.052940
C	1.759070	0.919700	1.182880
H	0.954210	0.200540	1.349220
H	2.439400	0.877810	2.031860
O	1.295550	2.233130	1.061480
H	0.513040	2.241850	0.490780
F	3.881680	-1.105520	1.089760
F	3.752770	-1.303530	-1.067350
F	2.052520	-1.832920	0.171330
F	3.598160	1.288710	-0.280770
F	1.743760	0.538060	-1.172000
C	-3.579760	-0.477620	0.071720
C	-2.156460	0.119080	-0.044590
C	-2.108280	1.457670	-0.772750
H	-2.575360	1.339640	-1.751710
H	-2.671970	2.188540	-0.198990
O	-0.785270	1.930310	-0.873840
H	-0.266310	1.353890	-1.445680
F	-4.379250	0.377580	0.724490
F	-3.564050	-1.634400	0.728440
F	-4.092730	-0.683720	-1.149190
F	-1.657640	0.239990	1.212170
F	-1.380910	-0.787400	-0.701850

[a] Optimized at the B3LYP-D3(BJ)/def2-QZVP level of theory with "scf=verytight, int= SuperFine".

Table S6.32. Calculated Cartesian coordinates (in Å) of the **PFP***G+g+***PFP***G-g-* homodimer.[a]

PFP*G+g+***PFP***G-g-*			
C	-2.589040	-0.812800	-0.259700
C	-2.920480	0.505530	0.485300
C	-1.736280	1.403530	0.825760
H	-0.983800	0.825760	1.353190
H	-2.121810	2.177040	1.493580
O	-1.122000	1.951670	-0.319570
H	-1.750720	2.498260	-0.800140
F	-1.708310	-1.526550	0.451060
F	-3.690830	-1.543330	-0.432150
F	-2.056350	-0.561170	-1.461900
F	-3.548570	0.166620	1.638000
F	-3.805270	1.196820	-0.289360
C	3.411740	0.126930	0.312800
C	2.069950	-0.512520	-0.127940
C	1.550240	-0.108430	-1.504190
H	0.658240	-0.718390	-1.674540
H	2.301290	-0.389410	-2.239920
O	1.308160	1.262330	-1.625160
H	0.500890	1.492950	-1.142080
F	3.281840	1.436100	0.525960
F	3.848560	-0.439890	1.443830
F	4.339130	-0.063350	-0.636870
F	1.149660	-0.203370	0.835740
F	2.242560	-1.860430	-0.108090

[a] Optimized at the B3LYP-D3(BJ)/def2-QZVP level of theory with “scf=verytight, int= SuperFine”.

Table S6.33. Calculated Cartesian coordinates (in Å) of the **PFP***G+g+***PFP***Tg-* homodimer.[a]

PFP*G+g+***PFP***Tg-*			
C	3.357080	0.747320	-0.144490
C	2.454400	-0.483300	0.113090
C	1.634620	-0.907230	-1.099020
H	0.943830	-0.110330	-1.355630
H	2.311950	-1.080200	-1.936350
O	0.861450	-2.051510	-0.804710
H	1.438920	-2.797840	-0.617450
F	4.225540	0.480450	-1.130680
F	4.041890	1.076920	0.947810
F	2.606880	1.792050	-0.515490
F	3.262110	-1.514260	0.497170
F	1.648980	-0.191230	1.163530
C	-3.489240	0.259420	-0.348650
C	-2.168000	0.352520	0.457200
C	-1.803270	-0.867780	1.297200
H	-0.899760	-0.588580	1.846510
H	-2.605300	-1.028060	2.015160
O	-1.648590	-2.035030	0.544490
H	-0.807470	-2.005420	0.064490
F	-3.399260	-0.635030	-1.332400
F	-3.790040	1.446630	-0.888840
F	-4.493620	-0.097100	0.465230
F	-1.174970	0.625300	-0.443090
F	-2.275980	1.428350	1.281030

[a] Optimized at the B3LYP-D3(BJ)/def2-QZVP level of theory with "scf=verytight, int= SuperFine".

Table S6.34. Calculated Cartesian coordinates (in Å) of the **PFP***Tg*+**PFP***G*-*g*- homodimer.[a]

PFP*Tg*+**PFP***G*-*g*-			
C	2.806832	0.846839	0.015407
C	2.231178	-0.581134	0.171862
C	1.777815	-1.210872	-1.143225
H	1.077653	-0.523224	-1.623448
H	2.653742	-1.315238	-1.781110
O	1.231990	-2.481673	-0.938000
H	0.333360	-2.389106	-0.589240
F	3.865596	0.827166	-0.807530
F	3.193389	1.345798	1.189855
F	1.884643	1.666418	-0.509895
F	3.177692	-1.336968	0.775992
F	1.174377	-0.490753	1.037162
C	-2.098820	0.914237	-0.352999
C	-2.859601	-0.211605	0.392400
C	-2.008606	-1.352508	0.940901
H	-1.184432	-0.945710	1.518582
H	-2.658575	-1.925826	1.605590
O	-1.454998	-2.154538	-0.078752
H	-2.157676	-2.559015	-0.595936
F	-1.188105	1.459479	0.459493
F	-2.943534	1.867126	-0.749162
F	-1.470465	0.431574	-1.432394
F	-3.519194	0.369007	1.425038
F	-3.788446	-0.715761	-0.470181

[a] Optimized at the B3LYP-D3(BJ)/def2-QZVP level of theory with “scf=verytight, int= SuperFine”.

Table S6.35. Calculated Cartesian coordinates (in Å) of the **PFP***Tg*+**PFP***Tg-*-homodimer.[a]

PFP*Tg*+**PFP***Tg-*			
C	2.784998	-1.017757	-0.195764
C	2.374298	0.400867	0.266754
C	2.015699	1.343178	-0.880299
H	1.254701	0.855377	-1.493256
H	2.910470	1.483626	-1.484275
O	1.608039	2.593898	-0.406023
H	0.693844	2.536421	-0.091223
F	3.842856	-0.945443	-1.016959
F	3.107158	-1.791981	0.841100
F	1.777755	-1.600610	-0.861920
F	3.392342	0.897745	1.007695
F	1.302903	0.248427	1.105050
C	-2.979972	-0.867619	0.195869
C	-2.245081	0.414604	-0.263910
C	-1.765610	1.292171	0.885396
H	-1.030825	0.744317	1.466687
H	-2.619265	1.534181	1.519861
O	-1.128901	2.453708	0.396285
H	-1.760470	2.995182	-0.086768
F	-4.061194	-0.541897	0.919212
F	-3.369565	-1.597163	-0.846496
F	-2.168483	-1.607117	0.961596
F	-3.106855	1.125732	-1.048122
F	-1.207479	0.035513	-1.049076

[a] Optimized at the B3LYP-D3(BJ)/def2-QZVP level of theory with “scf=verytight, int= SuperFine”.

Table S6.36. Calculated Cartesian coordinates (in Å) of the **PFP***G*+*g*+**PFP***Tg*+_2 homodimer.[a]

PFP*G*+*g*+**PFP***Tg*+_2			
C	-2.865509	0.992373	0.094425
C	-3.019903	-0.496635	-0.312545
C	-3.000570	-1.510330	0.827089
H	-3.109394	-2.491080	0.352299
H	-3.880431	-1.330376	1.441384
O	-1.874291	-1.417404	1.648523
H	-1.076365	-1.653924	1.147415
F	-1.621408	1.250782	0.515895
F	-3.122639	1.790414	-0.945593
F	-3.720495	1.289933	1.078740
F	-2.013103	-0.761634	-1.208289
F	-4.192312	-0.616465	-0.983085
C	3.551853	0.620876	0.171990
C	2.588995	-0.508564	-0.269360
C	1.360783	-0.642170	0.621518
H	0.870869	0.329547	0.697129
H	1.677121	-0.958285	1.611706
O	0.487454	-1.634788	0.121226
H	0.145651	-1.352653	-0.734496
F	3.965536	0.399439	1.428170
F	4.617049	0.682078	-0.623425
F	2.924048	1.803923	0.139316
F	3.295515	-1.662418	-0.300435
F	2.194801	-0.235296	-1.546508

[a] Optimized at the B3LYP-D3(BJ)/def2-QZVP level of theory with “scf=verytight, int= SuperFine”.

Table S6.37. Calculated Cartesian coordinates (in Å) of the **PFP***Tg*+**PFP***G*+*g*+ homodimer.[a]

PFP*Tg*+**PFP***G*+*g*+			
C	-2.739748	0.637634	0.627747
C	-2.908603	-0.176048	-0.681235
C	-2.427007	-1.622383	-0.638563
H	-2.916289	-2.135036	0.185095
H	-2.751430	-2.078648	-1.576636
O	-1.038284	-1.735821	-0.445497
H	-0.557201	-1.354037	-1.186987
F	-3.309208	-0.019934	1.646731
F	-3.318492	1.832868	0.516231
F	-1.445620	0.821019	0.914307
F	-4.231338	-0.176052	-0.984263
F	-2.250193	0.497021	-1.664779
C	3.195689	0.798238	-0.172401
C	2.442451	-0.537409	0.039253
C	1.676101	-0.609365	1.358451
H	2.401037	-0.513482	2.164938
H	0.997082	0.245046	1.400126
O	1.018528	-1.833294	1.511699
H	0.236752	-1.851714	0.940660
F	2.332572	1.824568	-0.166308
F	3.851232	0.805908	-1.333252
F	4.079755	0.988513	0.816880
F	1.579617	-0.670849	-1.022301
F	3.346448	-1.537024	-0.059943

[a] Optimized at the B3LYP-D3(BJ)/def2-QZVP level of theory with “scf=verytight, int= SuperFine”.

Table S6.38. Calculated Cartesian coordinates (in Å) of the **PFP***G*+*g*+**PFP***G*+*g*+_2 homodimer.[a]

PFP*G*+*g*+**PFP***G*+*g*+_2			
C	-3.727415	-0.308831	0.109245
C	-2.525232	0.651043	-0.087458
C	-1.325974	0.081001	-0.833896
H	-0.641819	0.914921	-1.003961
H	-1.654729	-0.304924	-1.794694
O	-0.708141	-0.981721	-0.137968
H	-0.343440	-0.650166	0.690024
F	-3.408286	-1.320933	0.917741
F	-4.764084	0.344434	0.638002
F	-4.102033	-0.811293	-1.076407
F	-2.135971	1.071663	1.148636
F	-2.980001	1.729389	-0.773900
C	3.152835	0.781512	-0.169822
C	2.933955	-0.629242	0.437241
C	2.736638	-1.766600	-0.559816
H	2.583438	-2.666713	0.044738
H	3.666280	-1.882618	-1.113151
O	1.711456	-1.540422	-1.481706
H	0.854518	-1.509144	-1.025584
F	2.026224	1.249097	-0.721295
F	3.537376	1.642943	0.776118
F	4.101724	0.733811	-1.110883
F	1.848062	-0.528854	1.272728
F	4.009210	-0.910976	1.213460

[a] Optimized at the B3LYP-D3(BJ)/def2-QZVP level of theory with “scf=verytight, int= SuperFine”.

Gaussian 16, Revision C.01, M. J. Frisch, G. W. Trucks, H. B. Schlegel, G. E. Scuseria, M. A. Robb, J. R. Cheeseman, G. Scalmani, V. Barone, G. A. Petersson, H. Nakatsuji, X. Li, M. Caricato, A. V. Marenich, J. Bloino, B. G. Janesko, R. Gomperts, B. Mennucci, H. P. Hratchian, J. V. Ortiz, A. F. Izmaylov, J. L. Sonnenberg, D. Williams-Young, F. Ding, F. Lipparini, F. Egidi, J. Goings, B. Peng, A. Petrone, T. Henderson, D. Ranasinghe, V. G. Zakrzewski, J. Gao, N. Rega, G. Zheng, W. Liang, M. Hada, M. Ehara, K. Toyota, R. Fukuda, J. Hasegawa, M. Ishida, T. Nakajima, Y. Honda, O. Kitao, H. Nakai, T. Vreven, K. Throssell, J. A. Montgomery, Jr., J. E. Peralta, F. Ogliaro, M. J. Bearpark, J. J. Heyd, E. N. Brothers, K. N. Kudin, V. N. Staroverov, T. A. Keith, R. Kobayashi, J. Normand, K. Raghavachari, A. P. Rendell, J. C. Burant, S. S. Iyengar, J. Tomasi, M. Cossi, J. M. Millam, M. Klene, C. Adamo, R. Cammi, J. W. Ochterski, R. L. Martin, K. Morokuma, O. Farkas, J. B. Foresman, and D. J. Fox, Gaussian, Inc., Wallingford CT, **2016**.

Appendix E

Supporting Information for Chapter 7

Rotational Spectroscopy of the 2,2,3,3,3-Pentafluoropropanol··· Water Complex: Conformations and Large Amplitude Motions

Contents:

Point S7.1. Gaussian keywords used in the calculations.

Calculations	Employed keywords
Geometry optimization	Freq, fopt=(verytight,MaxCycles=200), int=superfine, output=picket
Harmonic calculation	Freq=(VCD,VibRot)
Transition calculation	opt=(calcall,ts,noeigentest), scf=verytight, int=grid=SuperFine
Rigid PES scan	scan
BSSE correction	density=current, counterpoise=2
Common to all	b3lyp, Def2-QZVP, empiricaldispersion=gd3bj, output=picket

Table S7.1. Cartesian coordinates (in Å) of **PFP***G*+*g*+···W_H complex.

Atom	x	y	z
C	-1.129861	-0.436462	-0.144782
C	-0.088394	0.681688	0.119712
C	0.808404	0.491595	1.340079
H	1.443345	1.382589	1.380672
H	0.166824	0.490827	2.219482
O	1.534687	-0.699911	1.323644
H	2.253953	-0.627068	0.673435
F	-0.541590	-1.567186	-0.536880
F	-1.985734	-0.058584	-1.102200
F	-1.829981	-0.680181	0.971212
F	0.664914	0.792512	-1.021703
F	-0.772879	1.846265	0.261074
O	3.408204	-0.265360	-0.724407
H	3.939155	-0.977484	-1.089913
H	2.803815	0.003420	-1.423129

Table S7.2. Cartesian coordinates (in Å) of **PFP***Tg+*···W_H complex.

Atom	x	y	z
C	1.307284	0.415189	0.013517
C	0.012821	0.208002	0.825906
H	0.037234	0.954517	1.620819
C	-1.270550	0.493168	0.019978
F	2.368575	0.209222	0.804202
F	1.401999	-0.448393	-1.019216
F	1.403778	1.656132	-0.484320
F	-1.285756	1.728350	-0.498723
F	-2.337589	0.371212	0.818396
F	-1.432262	-0.378668	-1.001165
O	-0.024623	-1.044123	1.415480
H	-0.059627	-1.756576	0.743799
O	-0.150629	-3.089546	-0.442671
H	0.701741	-3.252514	-0.856434
H	-0.726488	-2.784776	-1.150318

Table S7.3. Cartesian coordinates (in Å) of **PFP***G+g-*···W_H complex.

Atom	x	y	z
C	-0.431326	0.837586	0.050078
C	-0.740303	-0.674253	-0.089468
C	0.408905	-1.556064	-0.581362
H	-0.034722	-2.542237	-0.723622
H	0.724594	-1.180466	-1.557163
O	1.461564	-1.666216	0.329710
H	2.105521	-0.957137	0.171611
F	0.498415	1.059474	0.995913
F	-1.525046	1.524716	0.379509
F	0.040934	1.322837	-1.108496
F	-1.201322	-1.099759	1.110592
F	-1.763129	-0.771060	-0.988063
O	3.187436	0.482087	-0.210863
H	2.844556	1.241065	0.269726
H	4.122496	0.430439	0.002856

Table S7.4. Relative raw energy (ΔE_e), ZPE and BSSE corrected energies (ΔE_0) and binding energy ($\triangle E_b$) (in kJ mol-1), rotational constants (in MHz), and electric dipole moment components (in Debye) of the 15 CREST identified PFP···W monohydrate conformers calculated at the B3LYP-D3(BJ)/def2-QZVP level of theory.

Conformations	ΔE_e	ΔE_0	ΔE_b	*A*	*B*	*C*	$\lvert\mu_a\rvert$	$\lvert\mu_b\rvert$	$\lvert\mu_c\rvert$
I **PFP**G+g+···W_H	0.0	0.0	24.9	1730.5	874.4	846.7	2.3	0.0	1.2
II **PFP**Tg+···W_H	0.8	0.8	24.4	1953.9	789.5	738.7	2.1	1.7	0.1
III **PFP**G+g-···W_H	3.1	2.7	24.9	1525.6	1075.7	831.5	3.3	1.3	0.6
IV **PFP**G+g+···W_C	12.3	11.5	13.4	1508.7	1034.3	827.7	0.5	1.5	1.1
V **PFP**Tg+···W_C	12.7	11.9	13.3	1861.5	780.2	714.8	0.7	1.9	0.2
VI **PFP**G+g-···W_C	15.2	13.9	13.7	2062.7	702.8	651.8	0.3	1.5	0.1
VII 2_**PFP**G+g+···W_C	19.2	15.3	9.7	1731.7	876.2	745.1	2.4	0.7	0.6
VIII **PFP**G+t···W_C	20.5	18.3	14.1	1924.5	803.3	753.0	0.7	0.6	1.4
IX **PFP**G+g-···W_C	22.4	18.4	9.1	1333.4	1033.7	871.3	1.5	1.6	1.0
X **PFP**G+g+···W_F	25.8	21.3	3.6	1619.3	906.6	745.5	2.8	0.7	0.0
XI **PFP**Tg+···W_F	26.0	21.6	3.6	1277.1	1052.9	733.4	3.4	1.7	0.8
XII 2_**PFP**G+t···W_C	27.2	22.7	9.7	1729.7	867.8	742.0	2.2	0.7	0.7
XIII **PFP**G+g-···W_F	28.9	24.2	3.4	1638.6	896.5	740.0	3.3	1.1	0.9
XIV **PFP**G+t···W_F	33.7	28.2	4.2	1632.8	905.6	801.8	3.2	1.0	1.4
XV **PFP**Tt···W_F	35.4	29.1	4.3	1293.8	1039.4	732.3	5.1	1.7	0.5

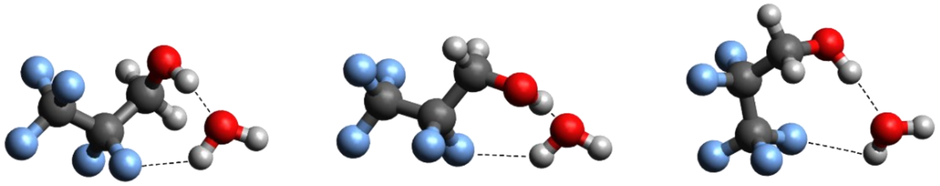

I PFP*G+g+*···W$_H$ **II PFP***Tg+*···W$_H$ **III PFP***G+g-*···W$_H$

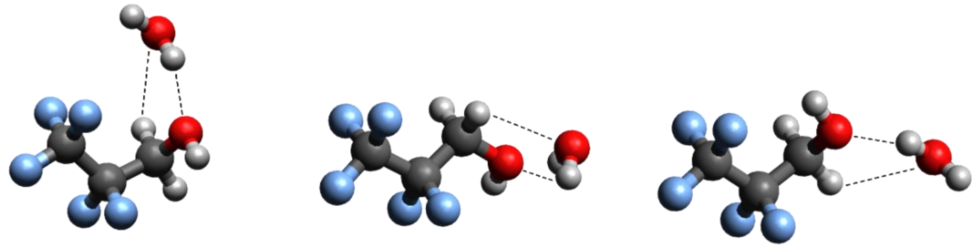

IV PFP*G+g+*···W$_C$ **V PFP***Tg+*···W$_C$ **VI PFP***G+g-*···W$_C$

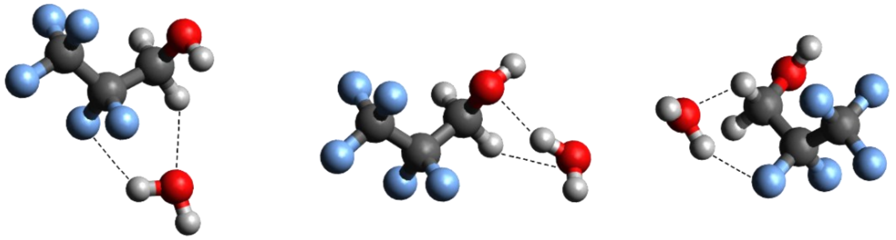

VII 2_PFP*G+g+*···W$_C$ **VIII PFP***G+t*···W$_C$ **IX PFP***G+g-*···W$_C$

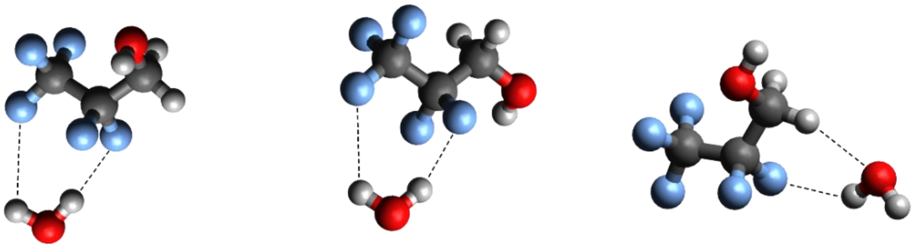

X PFP*G+g+*···W$_F$ **XI PFP***Tg+*···W$_F$ **XII 2_PFP***G+t*···W$_C$

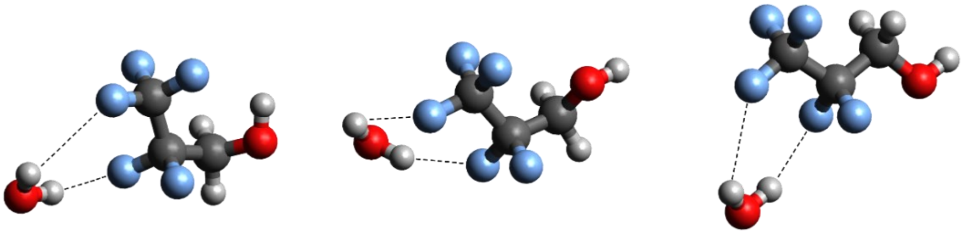

XIII PFP*G+g-*···W$_F$ **XIV PFP***G+t*···W$_F$ **XV PFP***Tt*···W$_F$

Figure S7.1. Geometries of 15 PFP···W monohydrate species identified using CREST and the subsequent DFT calculations with I being the most stable and XV the least stable one.

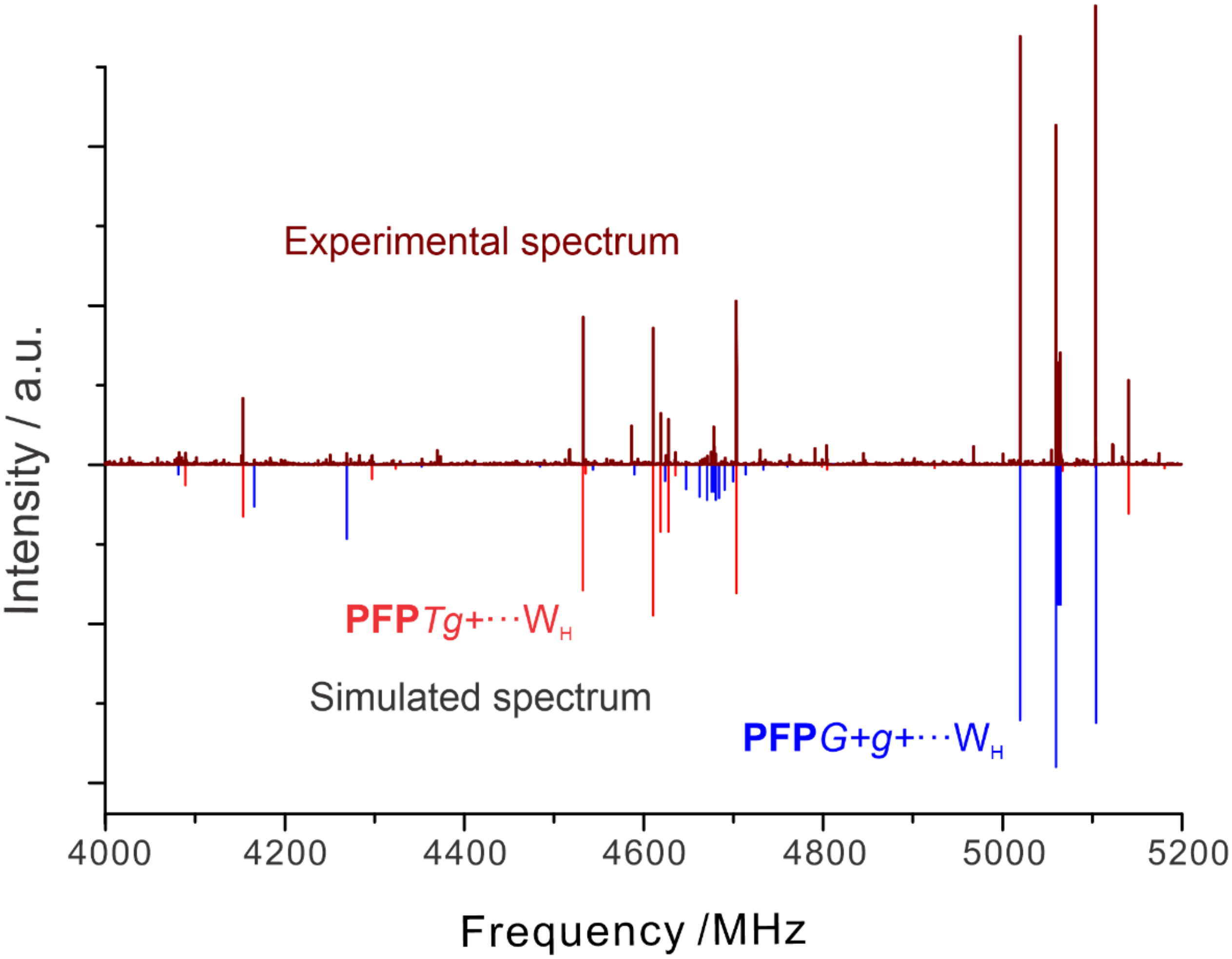

Figure S7.2. The broadband experimental spectrum of PFP+H_2O and the simulated spectra of where **PFP***G*+*g*+···W_H (in blue) and **PFP***Tg*+···W_H (in red) where the experimental spectroscopic constants, the calculated electric dipole moment components and a rotational temperature of 1 K, and a relative population abundance of 10:7 were used for the spectral simulations. The known transitions of PFP monomers and dimers are removed for clarity. Please note that some transition intensities do not match the experimental ones. For example, the experimental intensities of the *c*-type transitions at ~4166.0 MHz and 4269.0 MHz (blue) are much weaker than the predicted. These are due to the large amplitude motions discussed in the main text.

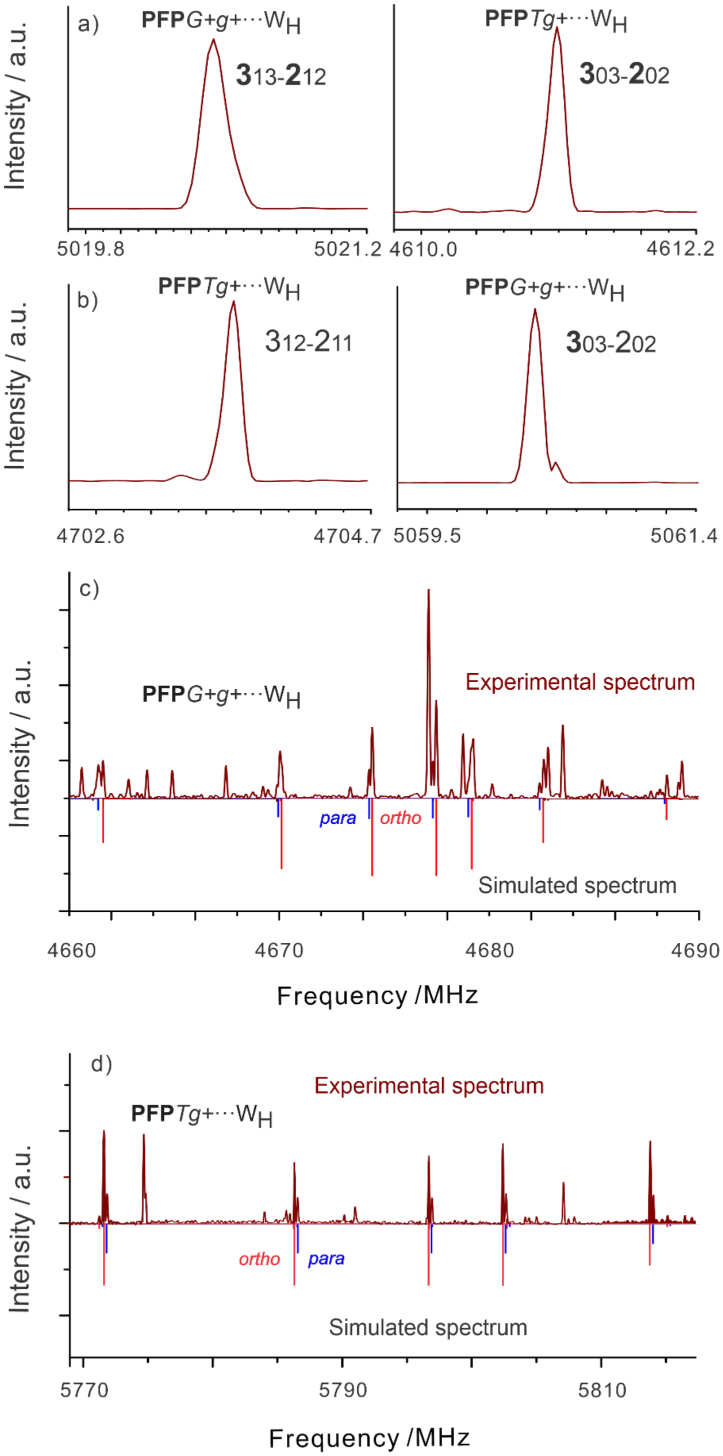

Figure S7.3. The ortho- and para-components of **PFP***G*+*g*+···$\mathrm{W_H}$ and **PFP***Tg*+···$\mathrm{W_H}$ in the experimental CP-FTMW spectra. These two components are largely unresolved for the *a*-type transitions as shown in a) and b) and generally better resolved in the higher K, *b*-type transitions ash shown in c) and d).

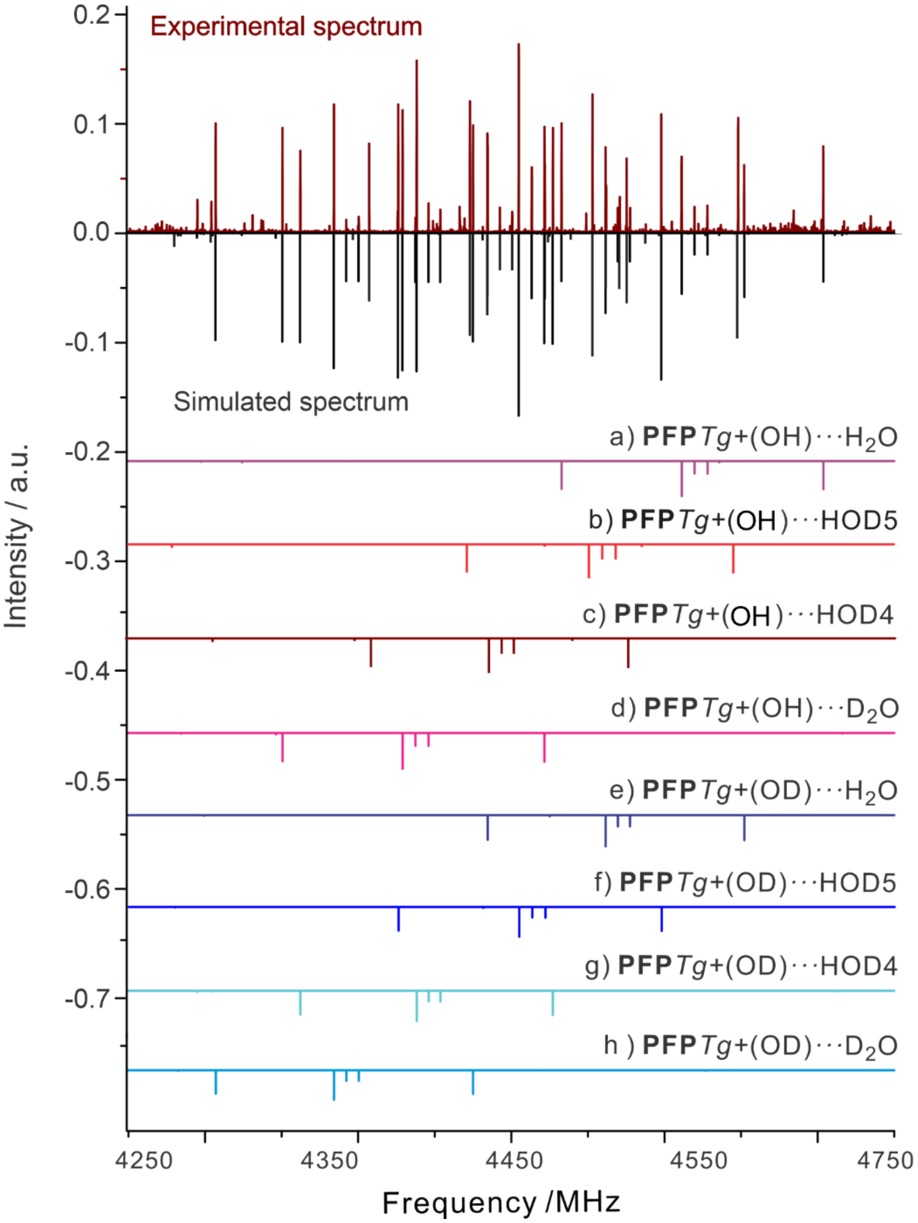

Figure S7.4. Top: the experimental and the overall simulated spectra of the **PFP***Tg*+···W parent and deuterated isotopologues, using the experimental spectroscopic constants, calculated *a*-type permanent electric dipole moment components, a rotational temperature of 1 K, and the percentage abundances of each species indicated below. Bottom: the simulated individual spectra of a) **PFP***Tg*+(OH)···H$_2$O parent, 10%; b) **PFP***Tg*+(OH)···HOD5, 13%; c) **PFP***Tg*+(OH)···HOD4, 10%; d) **PFP***Tg*+(OH)···D$_2$O, 12%; e) **PFP***Tg*+(OD)···H$_2$O, 8%; f) **PFP***Tg*+(OD)···HOD5, 17%; g) **PFP***Tg*+(OD)···HOD4, 11%, and h) **PFP***Tg*+(OD)···D$_2$O 19%.

Table S7.5. Rotational transition frequencies of the parent *ortho*-**PFP***G*+*g*+···W$_H$ complex.

J'	K_a'	K_c'	J''	K_a''	K_c''	Obs/ MHz	Cal/ MHz	Obs - Cal/ MHz	Weight
1	0	1	0	0	0	1687.6489	1687.6485	0.0004	1
5	2	4	5	1	4	2599.8635	2599.8620	0.0015	2
1	1	1	0	0	0	2609.4083	2609.4075	0.0008	2
5	2	3	5	1	4	2621.7647	2621.7640	0.0007	2
1	1	0	0	0	0	2637.4207	2637.4201	0.0006	2
4	2	3	4	1	3	2668.4249	2668.4273	-0.0024	2
4	2	2	4	1	3	2677.8398	2677.8426	-0.0028	2
3	2	2	3	1	2	2723.6429	2723.6406	0.0023	2
3	2	1	3	1	2	2726.7855	2726.7839	0.0016	2
2	2	1	2	1	1	2765.2482	2765.2485	-0.0003	2
2	2	0	2	1	1	2765.8752	2765.8776	-0.0024	2
2	2	0	2	1	2	2849.9125	2849.9159	-0.0034	2
3	2	2	3	1	3	2891.7059	2891.7094	-0.0035	2
3	2	1	3	1	3	2894.8537	2894.8528	0.0009	2
4	2	3	4	1	4	2948.4978	2948.4973	0.0005	2
4	2	2	4	1	4	2957.9128	2957.9126	0.0002	2
5	2	4	5	1	5	3019.8185	3019.8169	0.0016	2
5	2	3	5	1	5	3041.7170	3041.7189	-0.0019	2
6	2	5	6	1	6	3105.8449	3105.8453	-0.0004	2
6	2	4	6	1	6	3149.4226	3149.4207	0.0019	2
7	2	6	7	1	7	3206.7503	3206.7506	-0.0003	2
2	1	2	1	1	1	3347.2751	3347.2757	-0.0006	1
2	0	2	1	0	1	3374.6559	3374.6564	-0.0005	1
2	1	1	1	1	0	3403.3001	3403.3013	-0.0012	1
5	2	3	4	3	1	3777.6596	3777.6588	0.0008	2
5	2	3	4	3	2	3777.7161	3777.7206	-0.0045	2
4	1	4	3	2	1	3798.3721	3798.3715	0.0006	2
4	1	4	3	2	2	3801.5128	3801.5149	-0.0021	2
4	1	3	3	2	1	4078.4435	4078.4415	0.0020	2
4	1	3	3	2	2	4081.5855	4081.5849	0.0006	2
3	0	3	2	1	2	4166.0020	4166.0069	-0.0049	2
2	1	2	1	0	1	4269.0353	4269.0347	0.0006	2
2	1	1	1	0	1	4353.0735	4353.0730	0.0005	2

7	3	4	7	2	5	4624.1150	4624.1179	-0.0029	2
6	3	3	6	2	4	4647.5973	4647.5971	0.0002	2
5	3	2	5	2	3	4662.6730	4662.6781	-0.0051	2
4	3	2	4	2	2	4671.4084	4671.4061	0.0023	2
4	3	1	4	2	2	4671.4687	4671.4680	0.0007	2
3	3	0	3	2	1	4675.9334	4675.9320	0.0014	2
4	3	2	4	2	3	4680.8205	4680.8215	-0.0010	2
6	3	4	6	2	5	4690.4322	4690.4312	0.0010	2
7	3	5	7	2	6	4700.0660	4700.0669	-0.0009	2
7	3	4	7	2	6	4701.9140	4701.9174	-0.0034	2
8	3	6	8	2	7	4714.2870	4714.2855	0.0015	2
3	1	3	2	1	2	5020.4953	5020.4950	0.0003	1
3	0	3	2	0	2	5060.3837	5060.3852	-0.0015	1
3	2	2	2	2	1	5062.9172	5062.9176	-0.0004	1
3	2	1	2	2	0	5065.4315	5065.4319	-0.0004	1
3	1	2	2	1	1	5104.5255	5104.5255	0.0000	1
5	1	5	4	2	2	5407.4035	5407.4079	-0.0044	2
4	0	4	3	1	3	5889.7196	5889.7189	0.0007	2
3	1	3	2	0	2	5914.8754	5914.8733	0.0021	2
3	1	2	2	0	2	6082.9425	6082.9421	0.0004	2
2	2	1	1	1	0	6168.5504	6168.5498	0.0006	2
2	2	0	1	1	0	6169.1808	6169.1789	0.0019	2
2	2	1	1	1	1	6196.5632	6196.5624	0.0008	2
2	2	0	1	1	1	6197.1898	6197.1915	-0.0017	2
7	4	4	7	3	4	6543.8433	6543.8432	0.0001	2
7	4	3	7	3	4	6543.8605	6543.8603	0.0002	2
7	4	4	7	3	5	6545.6938	6545.6937	0.0001	2
7	4	3	7	3	5	6545.7119	6545.7108	0.0011	2
6	4	3	6	3	3	6546.4323	6546.4300	0.0023	2
6	4	2	6	3	3	6546.4323	6546.4347	-0.0024	2
6	4	3	6	3	4	6547.1735	6547.1713	0.0022	2
6	4	2	6	3	4	6547.1735	6547.1760	-0.0025	2
5	4	1	5	3	2	6547.9343	6547.9346	-0.0003	2
5	4	2	5	3	2	6547.9343	6547.9336	0.0007	2
5	4	2	5	3	3	6548.1808	6548.1810	-0.0002	2

5	4	1	5	3	3	6548.1808	6548.1819	-0.0011	2
4	4	0	4	3	1	6548.7346	6548.7345	0.0001	2
4	4	1	4	3	1	6548.7346	6548.7344	0.0002	2
4	4	1	4	3	2	6548.7966	6548.7963	0.0003	2
4	4	0	4	3	2	6548.7966	6548.7964	0.0002	2
4	1	4	3	1	3	6693.2258	6693.2243	0.0015	1
4	0	4	3	0	3	6744.2081	6744.2070	0.0011	1
4	2	3	3	2	2	6750.0113	6750.0122	-0.0009	1
4	2	2	3	2	1	6756.2832	6756.2841	-0.0009	1
4	1	3	3	1	2	6805.2255	6805.2254	0.0001	1
4	1	4	3	0	3	7547.7131	7547.7124	0.0007	2
5	1	5	4	1	4	8365.3213	8365.3205	0.0008	1
5	0	5	4	0	4	8425.5261	8425.5252	0.0009	1
5	2	4	4	2	3	8436.6404	8436.6402	0.0002	1
5	4	2	4	4	1	8439.5364	8439.5361	0.0003	1
5	4	1	4	4	0	8439.5364	8439.5370	-0.0006	1
5	3	3	4	3	2	8440.1527	8440.1514	0.0013	2
5	3	2	4	3	1	8440.3374	8440.3369	0.0005	2
5	2	3	4	2	2	8449.1259	8449.1268	-0.0009	1
5	1	4	4	1	3	8505.2051	8505.2054	-0.0003	1
5	1	5	4	0	4	9168.8257	9168.8259	-0.0002	1
6	1	6	5	1	5	10036.6595	10036.6571	0.0024	1
6	0	6	5	0	5	10103.8129	10103.8117	0.0012	1
6	2	5	5	2	4	10122.6866	10122.6854	0.0012	1
6	4	2	5	4	1	10127.7774	10127.7779	-0.0005	2
6	4	3	5	4	2	10127.7774	10127.7742	0.0032	2
6	3	4	5	3	3	10128.7842	10128.7838	0.0004	2
6	3	3	5	3	2	10129.2787	10129.2778	0.0009	2
6	2	4	5	2	3	10144.3594	10144.3589	0.0005	1
6	1	5	5	1	4	10204.2501	10204.2514	-0.0013	1
7	1	7	6	1	6	11707.1251	11707.1274	-0.0023	1
7	0	7	6	0	6	11778.6595	11778.6596	-0.0001	1
7	2	6	6	2	5	11808.0327	11808.0328	-0.0001	1
7	3	5	6	3	4	11817.6698	11817.6685	0.0013	2
7	3	4	6	3	3	11818.7797	11818.7777	0.0020	2

7	1	6	6	1	5	11902.1256	11902.1267	-0.0011	1

Table S7.6. Rotational transition frequencies of the parent *para*-**PFP***G*+*g*+···W$_H$ complex.

J’	K_a’	K_c’	*J*”	K_a”	K_c”	Obs/ MHz	Cal/ MHz	Obs - Cal/ MHz	Weight
3	2	2	3	1	3	2891.5600	2891.5656	-0.0056	1
4	2	3	4	1	4	2948.3150	2948.3212	-0.0062	1
5	2	4	5	1	5	3019.5940	3019.6002	-0.0062	1
6	2	5	6	1	6	3105.5885	3105.5793	0.0092	1
4	1	3	3	2	2	4081.5930	4081.5939	-0.0009	1
3	0	3	2	1	2	4166.0160	4166.0111	0.0049	2
3	3	0	3	2	1	4675.7756	4675.7748	0.0008	1
3	3	1	3	2	2	4678.9117	4678.9060	0.0057	1
5	3	3	5	2	4	4684.1650	4684.1666	-0.0016	1

Table S7.7. Rotational transition frequencies of the parent *ortho*-**PFP***Tg*+···W$_H$ complex.

J'	*K*$_a$'	*K*$_c$'	*J"*	*K*$_a$"	*K*$_c$"	Obs/ MHz	Cal/ MHz	Obs - Cal/ MHz	Weight
1	1	1	0	0	0	2670.4433	2670.4437	-0.0004	1
8	2	6	8	1	7	2915.0750	2915.0756	-0.0006	2
10	2	8	10	1	9	2937.4834	2937.4839	-0.0005	2
4	1	3	3	2	2	2961.4913	2961.4925	-0.0012	2
7	2	5	7	1	6	2963.9707	2963.9717	-0.0010	2
2	1	2	1	1	1	3022.7497	3022.7484	0.0013	1
6	2	4	6	1	5	3039.7969	3039.7961	0.0008	1
2	0	2	1	0	1	3077.6392	3077.6380	0.0012	1
5	2	3	5	1	4	3131.4293	3131.4295	-0.0002	1
2	1	1	1	1	0	3136.7401	3136.7389	0.0012	1
4	2	2	4	1	3	3227.6487	3227.6477	0.0010	1
3	2	1	3	1	2	3318.0447	3318.0451	-0.0004	2
2	2	0	2	1	1	3393.7907	3393.7901	0.0006	2
6	2	5	5	3	2	3414.5127	3414.5100	0.0027	2
3	0	3	2	1	2	3535.5256	3535.5233	0.0023	2
6	2	4	5	3	3	3558.8874	3558.8855	0.0019	2
2	2	1	2	1	2	3562.6752	3562.6760	-0.0008	2
3	2	2	3	1	3	3649.4755	3649.4742	0.0013	2
5	1	5	4	2	2	3750.8352	3750.8324	0.0028	2
4	2	3	4	1	4	3765.9001	3765.9025	-0.0024	2
5	2	4	5	1	5	3912.4203	3912.4198	0.0005	2
6	2	5	6	1	6	4089.4366	4089.4365	0.0001	2
2	1	2	1	0	1	4153.3191	4153.3184	0.0007	2
7	2	6	7	1	7	4297.2251	4297.2222	0.0029	2
3	1	3	2	1	2	4532.8158	4532.8165	-0.0007	1
8	2	7	8	1	8	4535.8136	4535.8144	-0.0008	1
3	0	3	2	0	2	4611.2026	4611.2037	-0.0011	1
3	2	2	2	2	1	4619.6138	4619.6146	-0.0008	1
3	2	1	2	2	0	4628.0001	4628.0008	-0.0007	1
5	1	4	4	2	3	4635.6503	4635.6481	0.0022	2
3	1	2	2	1	1	4703.7463	4703.7459	0.0004	1
9	2	8	9	1	9	4804.9377	4804.9361	0.0016	2

7	2	6	6	3	3	4924.9215	4924.9187	0.0028	2
6	1	6	5	2	3	5067.6252	5067.6286	-0.0034	2
4	0	4	3	1	3	5141.2841	5141.2833	0.0008	2
7	2	5	6	3	4	5181.1496	5181.1490	0.0006	2
10	3	7	10	2	8	5247.5504	5247.5488	0.0016	2
9	3	6	9	2	7	5396.9128	5396.9143	-0.0015	2
8	3	5	8	2	6	5523.0495	5523.0449	0.0046	2
3	1	3	2	0	2	5608.4954	5608.4969	-0.0015	2
7	3	4	7	2	5	5622.2615	5622.2660	-0.0045	2
6	3	3	6	2	4	5694.4754	5694.4796	-0.0042	2
5	3	2	5	2	3	5742.5502	5742.5551	-0.0049	2
4	3	1	4	2	2	5771.2609	5771.2599	0.0010	2
3	3	0	3	2	1	5786.0694	5786.0678	0.0016	2
3	3	1	3	2	2	5796.5064	5796.5070	-0.0006	2
4	3	2	4	2	3	5802.2499	5802.2481	0.0018	2
5	3	3	5	2	4	5813.7003	5813.6991	0.0012	2
6	3	4	6	2	5	5833.4499	5833.4503	-0.0004	2
7	3	5	7	2	6	5864.3622	5864.3621	0.0001	2
8	3	6	8	2	7	5909.4504	5909.4454	0.0050	2
3	1	2	2	0	2	5950.4127	5950.4137	-0.0010	2
9	3	7	9	2	8	5971.7379	5971.7382	-0.0003	2
4	1	4	3	1	3	6041.3846	6041.3846	0.0000	1
4	0	4	3	0	3	6138.5749	6138.5765	-0.0016	1
4	2	3	3	2	2	6157.8121	6157.8128	-0.0007	1
4	3	2	3	3	1	6163.5501	6163.5540	-0.0039	2
4	3	1	3	3	0	6163.8437	6163.8446	-0.0009	2
4	2	2	3	2	1	6178.6514	6178.6525	-0.0011	1
4	1	3	3	1	2	6269.0492	6269.0499	-0.0007	1
2	2	1	1	1	0	6528.4252	6528.4276	-0.0024	2
2	2	0	1	1	0	6530.5255	6530.5290	-0.0035	2
2	2	1	1	1	1	6585.4257	6585.4244	0.0013	2
2	2	0	1	1	1	6587.5268	6587.5259	0.0009	2
5	0	5	4	1	4	6757.9344	6757.9340	0.0004	2
4	1	4	3	0	3	7038.6806	7038.6778	0.0028	2
5	1	5	4	1	4	7548.0653	7548.0623	0.0030	2

5	0	5	4	0	4	7658.0384	7658.0352	0.0032	2
5	3	3	4	3	2	7706.0297	7706.0305	-0.0008	3
5	3	2	4	3	1	7707.0434	7707.0454	-0.0020	3
5	2	3	4	2	2	7735.7509	7735.7502	0.0007	2
5	1	4	4	1	3	7831.9707	7831.9684	0.0023	2
3	2	2	2	1	1	8011.3059	8011.3033	0.0026	2
5	1	5	4	0	4	8448.1629	8448.1635	-0.0006	2
6	1	6	5	1	5	9052.5501	9052.5464	0.0037	2
6	0	6	5	0	5	9168.4174	9168.4140	0.0034	2
6	2	5	5	2	4	9229.5613	9229.5631	-0.0018	2
6	3	4	5	3	3	9249.3126	9249.3142	-0.0016	2
4	2	2	3	1	3	9838.6127	9838.6144	-0.0017	2
6	1	6	5	0	5	9842.6751	9842.6747	0.0004	2
7	0	7	6	1	6	9995.1502	9995.1525	-0.0023	2
3	3	1	2	2	0	10414.0257	10414.0201	0.0056	2
7	1	7	6	1	6	10554.6319	10554.6341	-0.0022	2
7	2	5	6	2	4	10871.5755	10871.5777	-0.0022	2
7	1	6	6	1	5	10947.4008	10947.4020	-0.0012	2
4	3	2	3	2	1	11949.5752	11949.5733	0.0019	2
4	3	1	3	2	2	11960.3997	11960.4001	-0.0004	2

Table S7.8. Rotational transition frequencies of the parent *para*-**PFP***Tg*+··$\mathrm{W_H}$ complex.

J’	K_a’	K_c’	*J*”	K_a”	K_c”	Obs/ MHz	Cal/ MHz	Obs - Cal/ MHz	Weight
6	2	4	6	1	5	3039.9470	3039.9407	0.0063	1
5	2	3	5	1	4	3131.5740	3131.5767	-0.0027	1
4	2	2	4	1	3	3227.8010	3227.7972	0.0038	1
3	2	1	3	1	2	3318.1940	3318.1966	-0.0026	1
2	2	0	2	1	1	3393.9450	3393.9433	0.0017	1
3	0	3	2	1	2	3535.4010	3535.3976	0.0034	2
2	2	1	2	1	2	3562.8380	3562.8327	0.0053	1
3	2	2	3	1	3	3649.6260	3649.6322	-0.0062	1
4	2	3	4	1	4	3766.0580	3766.0619	-0.0039	1

5	2	4	5	1	5	3912.5790	3912.5804	-0.0014	1
6	2	5	6	1	6	4089.6001	4089.5977	0.0024	1
5	1	4	4	2	3	4635.3890	4635.3833	0.0057	1
4	0	4	3	1	2	4799.2110	4799.2137	-0.0027	1
6	1	6	5	2	3	5067.3300	5067.3309	-0.0009	1
8	3	5	8	2	6	5523.2950	5523.2953	-0.0003	1
7	3	4	7	2	5	5622.5160	5622.5162	-0.0002	1
6	3	3	6	2	4	5694.7320	5694.7299	0.0021	1
5	3	2	5	2	3	5742.8040	5742.8057	-0.0017	2
4	3	1	4	2	2	5771.5115	5771.5109	0.0006	1
3	3	0	3	2	1	5786.3191	5786.3192	-0.0001	1
3	3	1	3	2	2	5796.7550	5796.7585	-0.0035	1
4	3	2	4	2	3	5802.5070	5802.4996	0.0074	1
5	3	3	5	2	4	5813.9440	5813.9504	-0.0064	1
6	3	4	6	2	5	5833.7038	5833.7015	0.0023	1
7	3	5	7	2	6	5864.6182	5864.6131	0.0051	1
8	3	6	8	2	7	5909.6890	5909.6961	-0.0071	1
9	3	7	9	2	8	5971.9890	5971.9880	0.0010	1
5	0	5	4	1	4	6757.7670	6757.7700	-0.0030	1

Table S7.9. Rotational transition frequencies of **PFP***G*+*g*+ (OH)···HOD5.

J'	K_a'	K_c'	J''	K_a''	K_c''	Obs/ MHz	Cal/ MHz	Obs - Cal/ MHz	Weight
1	0	1	0	0	0	1662.5961	1662.5951	0.0010	3
2	1	2	1	1	1	3300.4191	3300.4214	-0.0023	1
2	0	2	1	0	1	3324.6878	3324.6882	-0.0004	1
2	1	1	1	1	0	3349.9453	3349.9433	0.0020	1
5	3	2	5	2	3	4670.3879	4670.3917	-0.0038	3
4	3	1	4	2	2	4677.2685	4677.2703	-0.0018	3
3	3	0	3	2	1	4680.7558	4680.7541	0.0017	3
3	3	1	3	2	2	4683.2054	4683.2027	0.0027	3
3	3	0	3	2	2	4683.2122	4683.2088	0.0034	5
3	1	3	2	1	2	4950.2969	4950.2999	-0.0030	1

3	0	3	2	0	2	4985.7795	4985.7784	0.0011	1
3	2	2	2	2	1	4987.7621	4987.7598	0.0023	1
3	2	1	2	2	0	4989.7251	4989.7234	0.0017	1
3	1	2	2	1	1	5024.5788	5024.5776	0.0012	1
4	1	4	3	1	3	6599.7873	6599.7881	-0.0008	1
4	0	4	3	0	3	6645.3711	6645.3713	-0.0002	1
4	2	3	3	2	2	6649.9129	6649.9116	0.0013	1
4	3	2	3	3	1	6651.2909	6651.2918	-0.0009	1
4	3	1	3	3	0	6651.3281	6651.3284	-0.0003	1
4	2	2	3	2	1	6654.8111	6654.8122	-0.0011	1
4	1	3	3	1	2	6698.7999	6698.7984	0.0015	1
5	1	5	4	1	4	8248.7684	8248.7700	-0.0016	1
5	0	5	4	0	4	8302.9902	8302.9918	-0.0016	1
5	2	4	4	2	3	8311.6904	8311.6909	-0.0005	1
5	3	3	4	3	2	8314.4503	8314.4504	-0.0001	1
5	2	3	4	2	2	8321.4579	8321.4571	0.0008	1
5	1	4	4	1	3	8372.4529	8372.4534	-0.0005	1
6	1	6	5	1	5	9897.1456	9897.1410	0.0046	1
6	0	6	5	0	5	9958.2062	9958.2069	-0.0007	1
6	3	4	5	3	3	9977.7992	9977.8004	-0.0012	1
6	3	3	5	3	2	9978.1429	9978.1414	0.0015	1
6	2	4	5	2	3	9989.9861	9989.9865	-0.0004	1
6	1	5	5	1	4	10045.3757	10045.3778	-0.0021	1

Table S7.10. Rotational transition frequencies of **PFP***G*+*g*+ (OH)···HOD4.

J’	K_a’	K_c’	*J*”	K_a”	K_c”	Obs/ MHz	Cal/ MHz	Obs - Cal/ MHz	Weight
2	1	2	1	1	1	3250.1544	3250.1542	0.0002	1
2	0	2	1	0	1	3275.0991	3275.0982	0.0009	1
2	1	1	1	1	0	3301.0721	3301.0707	0.0014	1
8	2	7	8	1	8	3318.7666	3318.7671	-0.0005	1

5	2	4	4	3	1	3433.9615	3433.9622	-0.0007	2
5	2	4	4	3	2	3434.0067	3434.0072	-0.0005	2
3	1	3	2	1	2	4874.8918	4874.8917	0.0001	1
3	0	3	2	0	2	4911.3481	4911.3475	0.0006	1
3	2	2	2	2	1	4913.4081	4913.4083	-0.0002	1
3	2	1	2	2	0	4915.4522	4915.4535	-0.0013	1
3	1	2	2	1	1	4951.2629	4951.2609	0.0020	1
4	1	4	3	1	3	6499.2285	6499.2306	-0.0021	1
4	0	4	3	0	3	6546.0426	6546.0450	-0.0024	1
4	2	3	3	2	2	6550.7692	6550.7702	-0.0010	1
4	3	2	3	3	1	6552.2045	6552.2016	0.0029	1
4	3	1	3	3	0	6552.2404	6552.2402	0.0002	1
4	2	2	3	2	1	6555.8728	6555.8743	-0.0015	1
4	1	3	3	1	2	6601.0287	6601.0278	0.0009	1
5	1	5	4	1	4	8123.0513	8123.0526	-0.0013	1
5	0	5	4	0	4	8178.7004	8178.6990	0.0014	1
5	1	4	4	1	3	8250.2152	8250.2151	0.0001	1
6	0	6	5	0	5	9808.8641	9808.8627	0.0014	1
6	1	5	5	1	4	9898.6525	9898.6531	-0.0006	1

Table S7.11. Rotational transition frequencies of the parent **PFP***G*+*g*+ (OH)···D_2O.

J’	K_a’	K_c’	*J*”	K_a”	K_c”	Obs/ MHz	Cal/ MHz	Obs - Cal/ MHz	Weight
2	1	2	1	1	1	3206.9507	3206.9483	0.0024	1
2	0	2	1	0	1	3229.0257	3229.0256	0.0001	1
2	1	1	1	1	0	3251.9007	3251.9033	-0.0026	1
3	1	3	2	1	2	4810.1503	4810.1471	0.0032	1
3	0	3	2	0	2	4842.5168	4842.5179	-0.0011	1
3	2	2	2	2	1	4844.1249	4844.1239	0.0010	1
3	2	1	2	2	0	4845.7132	4845.7120	0.0012	1
3	1	2	2	1	1	4877.5752	4877.5760	-0.0008	1

4	1	4	3	1	3	6413.0228	6413.0215	0.0013	1
4	0	4	3	0	3	6454.7867	6454.7902	-0.0035	1
4	2	3	3	2	2	6458.4664	6458.4681	-0.0017	1
4	3	2	3	3	1	6459.5929	6459.5921	0.0008	1
4	3	1	3	3	0	6459.6186	6459.6184	0.0002	1
4	2	2	3	2	1	6462.4326	6462.4329	-0.0003	1
4	1	3	3	1	2	6502.9076	6502.9078	-0.0002	1
5	1	5	4	1	4	8015.4754	8015.4733	0.0021	1
5	0	5	4	0	4	8065.4498	8065.4514	-0.0016	1
5	4	2	4	4	1	8074.3653	8074.3664	-0.0011	1
5	4	1	4	4	0	8074.3653	8074.3668	-0.0015	1
5	3	3	4	3	2	8074.7483	8074.7456	0.0027	1
5	3	2	4	3	1	8074.8401	8074.8379	0.0022	1
5	2	3	4	2	2	8080.4043	8080.4079	-0.0036	1
5	1	4	4	1	3	8127.7752	8127.7745	0.0007	1
6	1	6	5	1	5	9617.4105	9617.4131	-0.0026	1
6	1	5	5	1	4	9752.0462	9752.0430	0.0032	1

Table S7.12. Rotational transition frequencies of **PFP***G*+*g*+ (OD)···H_2O.

J’	K_a’	K_c’	*J*”	K_a”	K_c”	Obs/ MHz	Cal/ MHz	Obs - Cal/ MHz	Weight
2	1	2	1	1	1	3318.7751	3318.7763	-0.0012	1
2	0	2	1	0	1	3346.1755	3346.1759	-0.0004	1
2	1	1	1	1	0	3374.8377	3374.8382	-0.0005	1
3	1	3	2	1	2	4977.7504	4977.7495	0.0009	1
3	0	3	2	0	2	5017.6703	5017.6697	0.0006	1
3	2	2	2	2	1	5020.1997	5020.1995	0.0002	1
3	2	1	2	2	0	5022.7096	5022.7103	-0.0007	1
3	1	2	2	1	1	5061.8342	5061.8348	-0.0006	1
3	1	2	2	0	2	6042.6918	6042.6918	0.0000	1
4	1	4	3	1	3	6636.2372	6636.2370	0.0002	1
4	0	4	3	0	3	6687.2618	6687.2627	-0.0009	1
4	2	3	3	2	2	6693.0621	6693.0615	0.0006	1

4	2	2	3	2	1	6699.3254	6699.3249	0.0005	1
4	1	3	3	1	2	6748.3127	6748.3118	0.0009	1
5	0	5	4	0	4	8354.3608	8354.3601	0.0007	1
5	2	4	4	2	3	8365.4624	8365.4628	-0.0004	1
5	3	3	4	3	2	8368.9707	8368.9702	0.0005	1
5	3	2	4	3	1	8369.1535	8369.1550	-0.0015	1
5	1	4	4	1	3	8434.0757	8434.0753	0.0004	1
6	1	6	5	1	5	9951.2046	9951.2042	0.0004	1
6	0	6	5	0	5	10018.4345	10018.4352	-0.0007	1

Table S7.13. Rotational transition frequencies of **PFP***G*+*g*+ (OD)···HOD5.

J'	K_a'	K_c'	J''	K_a''	K_c''	Obs/ MHz	Cal/ MHz	Obs - Cal/ MHz	Weight
2	1	2	1	1	1	3273.0877	3273.0838	0.0039	1
2	0	2	1	0	1	3297.4607	3297.4584	0.0023	1
2	1	1	1	1	0	3322.8271	3322.8305	-0.0034	1
3	0	3	2	1	1	3970.4938	3970.4857	0.0081	2
3	0	3	2	1	2	4045.0998	4045.1056	-0.0058	2
2	1	2	1	0	1	4197.2838	4197.2750	0.0088	2
2	1	1	1	0	1	4271.8914	4271.8950	-0.0036	2
5	3	3	5	2	3	4670.2255	4670.2235	0.0020	2
5	3	2	5	2	3	4670.3907	4670.3965	-0.0058	2
5	3	3	5	2	4	4687.5007	4687.4995	0.0012	2
5	3	2	5	2	4	4687.6753	4687.6725	0.0028	2
3	1	3	2	1	2	4909.2928	4909.2903	0.0025	1
3	0	3	2	0	2	4944.9249	4944.9222	0.0027	1
3	2	2	2	2	1	4946.9205	4946.9219	-0.0014	1
3	2	1	2	2	0	4948.9041	4948.9033	0.0008	1
3	1	2	2	1	1	4983.9035	4983.9051	-0.0016	1
4	0	4	3	1	2	5577.4607	5577.4556	0.0051	2
4	0	4	3	1	3	5726.6856	5726.6904	-0.0048	2
3	1	3	2	0	2	5809.1106	5809.1069	0.0037	2
3	1	2	2	0	2	5958.3388	5958.3417	-0.0029	2

2	2	1	1	1	0	6095.3784	6095.3806	-0.0022	2
2	2	0	1	1	0	6095.8821	6095.8762	0.0059	2
2	2	1	1	1	1	6120.2502	6120.2538	-0.0036	2
2	2	0	1	1	1	6120.7478	6120.7494	-0.0016	2
4	1	4	3	1	3	6545.1008	6545.1029	-0.0021	1
4	0	4	3	0	3	6590.8755	6590.8750	0.0005	1
4	2	3	3	2	2	6595.4563	6595.4569	-0.0006	1
4	3	2	3	3	1	6596.8497	6596.8501	-0.0004	1
4	3	1	3	3	0	6596.8878	6596.8872	0.0006	1
4	2	2	3	2	1	6600.4002	6600.4018	-0.0016	1
4	1	3	3	1	2	6644.5612	6644.5623	-0.0011	1
5	1	5	4	1	4	8180.4006	8180.4045	-0.0039	1
5	0	5	4	0	4	8234.8338	8234.8376	-0.0038	1
5	2	4	4	2	3	8243.6137	8243.6157	-0.0020	1
5	3	3	4	3	2	8246.4012	8246.4007	0.0005	1
5	2	3	4	2	2	8253.4738	8253.4699	0.0039	1
5	1	4	4	1	3	8304.6501	8304.6481	0.0020	1
6	2	5	5	2	4	9891.3017	9891.3047	-0.0030	1
6	2	4	5	2	3	9908.4398	9908.4383	0.0015	1
6	1	5	5	1	4	9964.0002	9963.9960	0.0042	1

Table S7.14. Rotational transition frequencies of **PFP***G*+*g*+(OD)···HOD4.

J'	K_a'	K_c'	J''	K_a''	K_c''	Obs/ MHz	Cal/ MHz	Obs - Cal/ MHz	Weight
2	1	2	1	1	1	3224.0582	3224.0565	0.0017	1
2	0	2	1	0	1	3248.9627	3248.9596	0.0031	1
2	1	1	1	1	0	3274.8849	3274.8854	-0.0005	1
3	1	3	2	1	2	4835.7513	4835.7498	0.0015	1
3	0	3	2	0	2	4872.1507	4872.1500	0.0007	1
3	2	2	2	2	1	4874.1968	4874.1997	-0.0029	1
3	2	1	2	2	0	4876.2287	4876.2327	-0.0040	1
3	1	2	2	1	1	4911.9891	4911.9876	0.0015	1
2	2	1	1	1	0	6095.3773	6095.3754	0.0019	3

2	2	0	1	1	0	6095.8872	6095.8840	0.0032	3
2	2	1	1	1	1	6120.7838	6120.7897	-0.0059	3
2	2	0	1	1	1	6121.2988	6121.2983	0.0005	3
4	1	4	3	1	3	6447.0499	6447.0499	0.0000	1
4	0	4	3	0	3	6493.8025	6493.8009	0.0016	1
4	2	3	3	2	2	6498.5005	6498.4996	0.0009	1
4	3	2	3	3	1	6499.9212	6499.9249	-0.0037	1
4	3	1	3	3	0	6499.9599	6499.9631	-0.0032	1
4	2	2	3	2	1	6503.5738	6503.5732	0.0006	1
4	1	3	3	1	2	6548.6752	6548.6722	0.0030	1
5	0	5	4	0	4	8113.4269	8113.4243	0.0026	1
5	2	3	4	2	2	8132.5352	8132.5385	-0.0033	1
5	1	4	4	1	3	8184.7864	8184.7849	0.0015	1

Table S7.15. Rotational transition frequencies of **PFP***G*+*g*+ (OD)···D_2O.

J'	*K*$_a$'	*K*$_c$'	*J"*	*K*$_a$"	*K*$_c$"	Obs/ MHz	Cal/ MHz	Obs - Cal/ MHz	Weight
1	1	0	0	0	0	2566.6302	2566.6311	-0.0009	1
3	2	2	3	1	3	2927.2032	2927.2068	-0.0036	1
3	2	1	3	1	3	2929.1996	2929.2010	-0.0014	1
2	1	2	1	1	1	3181.9366	3181.9381	-0.0015	1
2	0	2	1	0	1	3204.0472	3204.0477	-0.0005	1
2	1	1	1	1	0	3226.9571	3226.9609	-0.0038	1
3	0	3	2	1	1	3817.7346	3817.7326	0.0020	1
3	0	3	2	1	2	3885.2701	3885.2666	0.0035	1
2	1	1	1	0	1	4191.3647	4191.3632	0.0015	1
3	1	3	2	1	2	4772.6294	4772.6324	-0.0030	1
3	0	3	2	0	2	4805.0493	4805.0482	0.0011	1
3	2	2	2	2	1	4806.6609	4806.6601	0.0008	1
3	2	1	2	2	0	4808.2536	4808.2553	-0.0017	1
3	1	2	2	1	1	4840.1629	4840.1628	0.0001	1
4	0	4	3	1	2	5382.3985	5382.3953	0.0032	1
4	0	4	3	1	3	5517.4613	5517.4597	0.0016	1

2	2	1	1	1	0	6052.6087	6052.6059	0.0028	1
2	2	0	1	1	0	6053.0067	6053.0050	0.0017	1
2	2	1	1	1	1	6075.1185	6075.1171	0.0014	1
2	2	0	1	1	1	6075.5185	6075.5162	0.0023	1
4	1	4	3	1	3	6363.0001	6363.003	-0.0029	1
4	0	4	3	0	3	6404.8256	6404.8255	0.0001	1
4	2	3	3	2	2	6408.5143	6408.5181	-0.0038	1
4	3	2	3	3	1	6409.6417	6409.6449	-0.0032	1
4	3	1	3	3	0	6409.6691	6409.6715	-0.0024	1
4	2	2	3	2	1	6412.5014	6412.5008	0.0006	1
4	1	3	3	1	2	6453.0287	6453.0245	0.0042	1
5	1	5	4	1	4	7952.9503	7952.9522	-0.0019	1
5	0	5	4	0	4	8002.9881	8002.9873	0.0008	1
5	2	4	4	2	3	8010.0639	8010.0660	-0.0021	1
5	3	3	4	3	2	8012.3176	8012.3182	-0.0006	1
5	3	2	4	3	1	8012.4095	8012.4111	-0.0016	1
5	2	3	4	2	2	8018.0099	8018.0087	0.0012	1
5	1	4	4	1	3	8065.4217	8065.4218	-0.0001	1
6	1	6	5	1	5	9542.3905	9542.3908	-0.0003	1
6	0	6	5	0	5	9599.1722	9599.1692	0.0030	1
6	2	5	5	2	4	9611.2251	9611.2263	-0.0012	1
6	2	4	5	2	3	9625.0563	9625.0549	0.0014	1

Table S7.16. Rotational transition frequencies of **PFP***Tg*+(OH)···HOD5.

J'	K_a'	K_c'	J''	K_a''	K_c''	Obs/ MHz	Cal/ MHz	Obs - Cal/ MHz	Weight
1	1	1	0	0	0	2637.6130	2637.6191	-0.0061	1
4	1	3	3	2	2	2929.9060	2929.9109	-0.0049	1
2	1	2	1	1	1	2982.9200	2982.9248	-0.0048	1
2	0	2	1	0	1	3039.0650	3039.0630	0.0020	1
5	2	3	5	1	4	3087.2060	3087.2039	0.0021	1
2	1	1	1	1	0	3099.6720	3099.6665	0.0055	1
4	2	2	4	1	3	3184.1390	3184.1379	0.0011	1

3	2	1	3	1	2	3275.8860	3275.8876	-0.0016	1
2	2	0	2	1	1	3353.1120	3353.1160	-0.0040	1
3	0	3	2	1	2	3492.2020	3492.1975	0.0045	1
2	2	1	2	1	2	3526.0030	3525.9986	0.0044	1
2	2	0	2	1	2	3528.2340	3528.2270	0.0070	2
3	2	2	3	1	3	3614.9500	3614.9453	0.0047	1
4	2	3	4	1	4	3734.2870	3734.2936	-0.0066	1
2	1	2	1	0	1	4099.8950	4099.8952	-0.0002	1
2	1	1	1	0	1	4275.0130	4275.0061	0.0069	2
3	1	3	2	1	2	4472.9980	4473.0009	-0.0029	1
3	0	3	2	0	2	4553.0290	4553.0296	-0.0006	1
3	2	2	2	2	1	4561.9480	4561.9476	0.0004	1
3	2	1	2	2	0	4570.8430	4570.8402	0.0028	1
3	1	2	2	1	1	4648.0700	4648.0686	0.0014	1
4	0	4	3	1	3	5079.6390	5079.6378	0.0012	1
3	1	3	2	0	2	5533.8330	5533.8331	-0.0001	1
5	3	2	5	2	3	5674.8780	5674.8763	0.0017	1
4	3	1	4	2	2	5705.2596	5705.2590	0.0006	1
3	3	0	3	2	1	5720.9510	5720.9544	-0.0034	1
3	3	1	3	2	2	5732.0220	5732.0222	-0.0002	1
4	3	2	4	2	3	5738.1010	5738.1006	0.0004	1
5	3	3	5	2	4	5750.2250	5750.2234	0.0016	1
6	3	4	6	2	5	5771.1250	5771.1266	-0.0016	1
3	1	2	2	0	2	5884.0230	5884.0117	0.0113	2
4	1	4	3	1	3	5961.4890	5961.4866	0.0024	1
4	0	4	3	0	3	6060.4390	6060.4412	-0.0022	1
4	2	3	3	2	2	6080.8310	6080.8349	-0.0039	1
4	3	2	3	3	1	6086.9130	6086.9133	-0.0003	1
4	3	1	3	3	0	6087.2330	6087.2324	0.0006	1
4	2	2	3	2	1	6102.9260	6102.9279	-0.0019	1
4	1	3	3	1	2	6194.6760	6194.6776	-0.0016	1
2	2	1	1	1	0	6450.5480	6450.5542	-0.0062	1
2	2	0	1	1	1	6511.1560	6511.1518	0.0042	1
5	0	5	4	1	4	6677.6500	6677.6469	0.0031	1
4	1	4	3	0	3	6942.2910	6942.2901	0.0009	1

Table S7.17. Rotational transition frequencies of **PFP***Tg*+(OH)···HOD4.

J'	*K*$_a$'	*K*$_c$'	*J"*	*K*$_a$"	*K*$_c$"	Obs/ MHz	Cal/ MHz	Obs - Cal/ MHz	Weight
2	0	2	1	0	1	2992.9850	2992.9844	0.0006	1
2	1	1	1	1	0	3051.0470	3051.0414	0.0056	1
3	1	3	2	1	2	4407.1980	4407.2014	-0.0034	1
3	2	2	2	2	1	4492.5170	4492.5166	0.0004	1
3	2	1	2	2	0	4500.5800	4500.5748	0.0052	1
3	1	2	2	1	1	4575.2680	4575.2646	0.0034	1
4	0	4	3	0	3	5969.9180	5969.9203	-0.0023	1
2	1	2	1	1	1	2938.9650	2938.9743	-0.0093	1
3	0	3	2	0	2	4484.4260	4484.4305	-0.0045	1
4	2	3	3	2	2	5988.4190	5988.4211	-0.0021	1
4	2	2	3	2	1	6008.4470	6008.4548	-0.0078	1
4	1	3	3	1	2	6097.8610	6097.8663	-0.0053	1
4	1	4	3	1	3	5873.9860	5873.9790	0.0070	1
5	1	5	4	1	4	7338.9310	7338.9256	0.0054	1
5	0	5	4	0	4	7447.7780	7447.7793	-0.0013	1
4	0	4	3	1	3	4963.2460	4963.2373	0.0087	1
2	1	2	1	0	1	4076.8870	4076.8964	-0.0094	1
4	2	3	4	1	4	3781.6000	3781.6020	-0.0020	1
3	2	2	3	1	3	3667.1580	3667.1599	-0.0019	1
2	2	1	2	1	2	3581.8620	3581.8448	0.0172	2
2	2	0	2	1	1	3415.7500	3415.7645	-0.0145	2
3	0	3	2	1	2	3400.5210	3400.5184	0.0026	1
3	2	1	3	1	2	3341.0700	3341.0747	-0.0047	1
4	2	2	4	1	3	3251.6800	3251.6631	0.0169	2
5	2	3	5	1	4	3156.0350	3156.0303	0.0047	2
1	1	1	0	0	0	2635.4250	2635.4270	-0.0020	1
3	1	3	2	0	2	5491.1110	5491.1135	-0.0025	1
4	3	1	4	2	2	5806.5470	5806.5535	-0.0065	2
3	3	1	3	2	2	5830.8170	5830.8234	-0.0064	2
4	3	2	4	2	3	5836.3460	5836.3459	0.0001	2
5	3	3	5	2	4	5847.3710	5847.3657	0.0053	2
2	2	1	1	1	0	6464.7890	6464.7871	0.0019	1

2	2	0	1	1	1	6522.8480	6522.8378	0.0102	1
5	0	5	4	1	4	6537.0330	6537.0375	-0.0045	1
4	1	4	3	0	3	6880.6640	6880.6620	0.0020	1

Table S7.18. Rotational transition frequencies of the parent **PFP***Tg*+(OH)···D_2O.

J'	K_a'	K_c'	J''	K_a''	K_c''	Obs/ MHz	Cal/ MHz	Obs - Cal/ MHz	Weight
1	1	1	0	0	0	2605.0756	2605.0749	0.0007	1
2	1	2	1	1	1	2901.2627	2901.2598	0.0029	1
2	0	2	1	0	1	2956.2003	2956.2005	-0.0002	1
2	1	1	1	1	0	3015.3766	3015.3773	-0.0007	1
5	2	3	5	1	3	3117.5607	3117.5549	0.0058	2
4	2	2	4	1	2	3213.6611	3213.6633	-0.0022	2
3	2	1	3	1	2	3304.0552	3304.0511	0.0041	2
3	0	3	2	1	2	3358.0512	3358.0453	0.0059	2
5	1	5	4	2	2	3460.4024	3460.4046	-0.0022	2
2	2	1	2	1	3	3548.8979	3548.8983	-0.0004	2
3	2	2	3	1	4	3635.8005	3635.7992	0.0013	2
4	2	3	4	1	5	3752.3755	3752.3731	0.0024	2
5	2	4	5	1	1	3899.0827	3899.0848	-0.0021	2
2	1	2	1	0	6	4027.1693	4027.1741	-0.0048	2
6	2	5	6	1	2	4076.3489	4076.3502	-0.0013	2
3	1	3	2	1	2	4350.5756	4350.5774	-0.0018	1
3	0	3	2	0	1	4429.0188	4429.0189	-0.0001	1
3	2	2	2	2	0	4437.4784	4437.4784	0.0000	1
3	2	1	2	2	1	4445.9183	4445.9169	0.0014	1
3	1	2	2	1	3	4521.7018	4521.7017	0.0001	1
4	0	4	3	1	2	4903.0785	4903.0787	-0.0002	1
3	1	3	2	0	3	5421.5504	5421.5510	-0.0006	1
6	3	3	6	2	2	5670.7358	5670.7410	-0.0052	2
5	3	2	5	2	3	5719.0997	5719.1024	-0.0027	2
4	3	1	4	2	4	5747.9872	5747.9882	-0.0010	2
4	3	2	4	2	3	5779.1710	5779.1679	0.0031	2

5	3	3	5	2	5	5790.6814	5790.6811	0.0003	2
4	1	4	3	1	3	5798.3884	5798.3883	0.0001	1
6	3	4	6	2	2	5810.5487	5810.5435	0.0052	2
4	0	4	3	0	1	5895.6109	5895.6109	0.0000	1
4	2	3	3	2	0	5914.9607	5914.9622	-0.0015	1
4	3	1	3	3	1	5921.0246	5921.0260	-0.0014	1
4	2	2	3	2	2	5935.9343	5935.9318	0.0025	1
4	1	3	3	1	0	6026.3197	6026.3196	0.0001	1
2	2	1	1	1	1	6393.0971	6393.0986	-0.0015	1
2	2	0	1	1	4	6452.2721	6452.2726	-0.0005	1
5	0	5	4	1	3	6458.9377	6458.9386	-0.0009	1
4	1	4	3	0	4	6790.9213	6790.9205	0.0008	1
5	1	5	4	1	4	7244.3001	7244.3004	-0.0003	1
5	0	5	4	0	4	7354.2497	7354.2482	0.0015	1

Table S7.19. Rotational transition frequencies of **PFP** *Tg*+ (OD)···H_2O.

J’	K_a’	K_c’	*J*”	K_a”	K_c”	Obs/ MHz	Cal/ MHz	Obs - Cal/ MHz	Weight
1	1	1	0	0	0	2660.7272	2660.7293	-0.0021	1
2	1	2	1	1	1	2990.5149	2990.5172	-0.0023	1
2	0	2	1	0	1	3044.3554	3044.3518	0.0036	1
2	1	1	1	1	0	3102.2057	3102.2079	-0.0022	1
5	2	3	5	1	4	3155.6145	3155.6040	0.0105	2
4	2	2	4	1	3	3251.0123	3251.0093	0.0030	2
3	2	1	3	1	2	3340.1625	3340.1666	-0.0041	2
2	2	0	2	1	1	3414.6172	3414.6255	-0.0083	2
3	0	3	2	1	2	3477.8103	3477.7997	0.0106	2
2	2	1	2	1	2	3580.1689	3580.1566	0.0123	2
3	2	2	3	1	3	3665.1861	3665.1731	0.0130	2
4	2	3	4	1	4	3779.2001	3779.1968	0.0033	2

5	2	4	5	1	5	3922.6619	3922.6716	-0.0097	2
2	1	2	1	0	1	4128.0652	4128.0638	0.0014	1
3	1	3	2	1	2	4484.5257	4484.5291	-0.0034	1
3	0	3	2	0	2	4561.5112	4561.5117	-0.0005	1
3	2	2	2	2	1	4569.5501	4569.5455	0.0046	1
3	2	1	2	2	0	4577.5556	4577.5536	0.0020	1
3	1	2	2	1	1	4652.0096	4652.0126	-0.0030	1
4	0	4	3	1	3	5066.0251	5066.0241	0.0010	1
3	1	3	2	0	2	5568.2407	5568.2410	-0.0003	1
5	3	2	5	2	3	5776.8998	5776.8886	0.0112	2
4	3	1	4	2	2	5804.3407	5804.3443	-0.0036	2
3	3	0	3	2	1	5818.4989	5818.4914	0.0075	2
3	3	1	3	2	2	5828.4642	5828.4609	0.0033	2
4	3	2	4	2	3	5833.9476	5833.9494	-0.0018	2
5	3	3	5	2	4	5844.8802	5844.8990	-0.0188	2
6	3	4	6	2	5	5863.7947	5863.7943	0.0004	2
4	1	4	3	1	3	5977.1074	5977.1075	-0.0001	1
4	0	4	3	0	3	6072.7503	6072.7534	-0.0031	1
4	2	3	3	2	2	6091.1336	6091.1313	0.0023	1
4	3	2	3	3	1	6096.6173	6096.6198	-0.0025	1
4	3	1	3	3	0	6096.8925	6096.8902	0.0023	1
4	2	2	3	2	1	6111.0356	6111.0373	-0.0017	1
4	1	3	3	1	2	6200.1976	6200.1946	0.0030	1
2	2	1	1	1	0	6514.8251	6514.8270	-0.0019	1
2	2	0	1	1	1	6572.6796	6572.6803	-0.0007	1
5	0	5	4	1	4	6665.3330	6665.3328	0.0003	1
5	1	5	4	1	4	7467.8757	7467.8768	-0.0011	1

Table S7.20. Rotational transition frequencies of **PFP***Tg*+(OD)···HOD5.

J'	K_a'	K_c'	*J"*	K_a"	K_c"	Obs/ MHz	Cal/ MHz	Obs - Cal/ MHz	Weight
1	1	1	0	0	0	2627.8754	2627.8761	-0.0007	1
7	2	5	7	1	6	2943.3998	2943.3991	0.0007	1
2	1	2	1	1	1	2951.6750	2951.6735	0.0015	1
2	0	2	1	0	1	3006.7921	3006.7897	0.0024	1
6	2	4	6	1	5	3018.3754	3018.3746	0.0008	1
2	1	1	1	1	0	3066.1829	3066.1808	0.0021	1
5	2	3	5	1	4	3109.6258	3109.6241	0.0017	1
4	2	2	4	1	3	3205.8003	3205.7993	0.0010	1
3	2	1	3	1	2	3296.3599	3296.3587	0.0012	1
2	2	0	2	1	1	3372.3454	3372.3442	0.0012	1
3	0	3	2	1	2	3436.5598	3436.5584	0.0014	1
2	2	1	2	1	2	3541.9711	3541.9728	-0.0017	1
3	2	2	3	1	3	3629.1764	3629.1785	-0.0021	1
4	2	3	4	1	4	3746.1592	3746.1614	-0.0022	1
5	2	4	5	1	5	3893.3869	3893.3863	0.0006	1
6	2	5	6	1	6	4071.2695	4071.2674	0.0021	1
2	1	2	1	0	1	4075.0824	4075.0846	-0.0022	1
3	1	3	2	1	2	4426.1876	4426.1856	0.0020	1
5	1	4	4	2	3	4481.4392	4481.4404	-0.0012	1
3	0	3	2	0	2	4504.8523	4504.8534	-0.0011	1
3	2	2	2	2	1	4513.3905	4513.3913	-0.0008	1
3	2	1	2	2	0	4521.9045	4521.9053	-0.0008	1
3	1	2	2	1	1	4597.8904	4597.8908	-0.0004	1
4	0	4	3	1	3	5007.0102	5007.0075	0.0027	1
3	1	3	2	0	2	5494.4782	5494.4805	-0.0023	1
6	3	3	6	2	4	5657.8862	5657.8841	0.0021	3
5	3	2	5	2	3	5706.6228	5706.6235	-0.0007	3
4	3	1	4	2	2	5735.7472	5735.7461	0.0011	3
3	3	0	3	2	1	5750.7763	5750.7762	0.0001	3
3	3	1	3	2	2	5761.3720	5761.3740	-0.0020	3
4	3	2	4	2	3	5767.1988	5767.2005	-0.0017	3
5	3	3	5	2	4	5778.8167	5778.8204	-0.0037	3

6	3	4	6	2	5	5798.8528	5798.8598	-0.0070	3
4	1	4	3	1	3	5899.1749	5899.1770	-0.0021	1
4	0	4	3	0	3	5996.6363	5996.6347	0.0016	1
4	2	3	3	2	2	6016.1577	6016.1599	-0.0022	1
4	3	2	3	3	1	6021.9860	6021.9864	-0.0004	1
4	3	1	3	3	0	6022.2827	6022.2846	-0.0019	1
4	2	2	3	2	1	6037.3122	6037.3147	-0.0025	1
4	1	3	3	1	2	6127.8755	6127.8741	0.0014	1
6	1	5	5	2	4	6143.7473	6143.7476	-0.0003	1
2	2	1	1	1	0	6436.3913	6436.3915	-0.0002	1
2	2	0	1	1	1	6495.7817	6495.7799	0.0018	1
5	0	5	4	1	4	6588.2276	6588.2244	0.0032	1
4	1	4	3	0	3	6888.8037	6888.8042	-0.0005	1
5	0	5	4	0	4	7480.3945	7480.3940	0.0005	1

Table S7.21. Rotational transition frequencies of **PFP***Tg*+(OD)···HOD4.

J'	K_a'	K_c'	J''	K_a''	K_c''	Obs/ MHz	Cal/ MHz	Obs - Cal/ MHz	Weight
2	1	2	1	1	1	2908.9667	2908.9697	-0.0030	1
2	0	2	1	0	1	2962.0202	2962.0219	-0.0017	1
2	1	1	1	1	0	3018.9502	3018.9544	-0.0042	1
6	2	4	6	1	5	3085.8101	3085.8210	-0.0109	2
5	2	3	5	1	4	3177.5257	3177.5327	-0.0070	2
4	2	2	4	1	3	3272.3386	3272.3442	-0.0056	2
3	2	1	3	1	2	3360.5921	3360.5849	0.0072	2
2	2	0	2	1	1	3434.1003	3434.0908	0.0095	2
3	2	2	3	1	3	3680.8318	3680.8294	0.0024	2
4	2	3	4	1	4	3793.0752	3793.0677	0.0075	3
5	2	4	5	1	5	3934.2772	3934.2805	-0.0033	2
2	1	2	1	0	1	4053.0241	4053.0297	-0.0056	1
5	1	4	4	2	3	4294.8296	4294.8309	-0.0013	1
3	1	3	2	1	2	4362.2546	4362.2538	0.0008	1
3	0	3	2	0	2	4438.2004	4438.1945	0.0059	1

3	2	2	2	2	1	4445.9486	4445.9485	0.0001	1
3	2	1	2	2	0	4453.6754	4453.6723	0.0031	1
3	1	2	2	1	1	4527.1753	4527.1782	-0.0029	1
4	0	4	3	1	3	4893.5909	4893.5881	0.0028	1
3	1	3	2	0	2	5453.2635	5453.2616	0.0019	1
4	1	4	3	1	3	5814.1631	5814.1562	0.0069	1
4	3	1	4	2	2	5835.5637	5835.5650	-0.0013	1
3	3	0	3	2	1	5849.2121	5849.2137	-0.0016	1
3	3	1	3	2	2	5858.8263	5858.8301	-0.0038	1
4	3	2	4	2	3	5864.1358	5864.1293	0.0065	1
5	3	3	5	2	4	5874.7009	5874.7013	-0.0004	1
4	0	4	3	0	3	5908.6501	5908.6552	-0.0051	1
4	2	3	3	2	2	5926.3871	5926.3945	-0.0074	1
4	3	2	3	3	1	5931.6903	5931.6936	-0.0033	1
4	3	1	3	3	0	5931.9543	5931.9488	0.0055	1
4	2	2	3	2	1	5945.6006	5945.5976	0.0030	1
4	1	3	3	1	2	6033.8366	6033.8383	-0.0017	1
2	2	1	1	1	0	6451.1137	6451.1101	0.0036	1
5	0	5	4	1	4	6451.2228	6451.2223	0.0005	1
2	2	0	1	1	1	6508.0387	6508.0395	-0.0008	1
4	1	4	3	0	3	6829.2241	6829.2232	0.0009	1
5	0	5	4	0	4	7371.7874	7371.7903	-0.0029	1
5	2	4	4	2	3	7405.5262	7405.5257	0.0005	1
5	2	3	4	2	2	7443.5053	7443.5014	0.0039	1
5	1	4	4	1	3	7538.3103	7538.3130	-0.0027	1

Table S7.22. Rotational transition frequencies of **PFP***Tg*+(OD)···D_2O.

J'	K_a'	K_c'	*J"*	K_a"	K_c"	Obs/ MHz	Cal/ MHz	Obs - Cal/ MHz	Weight
2	1	2	1	1	1	2872.1498	2872.1466	0.0032	1
2	0	2	1	0	1	2926.1543	2926.1553	-0.0010	1
2	1	1	1	1	0	2984.2323	2984.2336	-0.0013	1
3	0	3	2	1	2	3306.5998	3306.6054	-0.0056	2

3	2	1	3	1	2	3322.0916	3322.0915	0.0001	2
2	2	1	2	1	2	3562.8355	3562.8353	0.0002	2
3	2	2	3	1	3	3648.1594	3648.1599	-0.0005	1
4	2	3	4	1	4	3762.6001	3762.5993	0.0008	1
5	2	4	5	1	5	3906.6004	3906.5986	0.0018	1
2	1	2	1	0	1	4003.7056	4003.7073	-0.0017	1
6	2	5	6	1	6	4080.5576	4080.5583	-0.0007	2
5	1	4	4	2	3	4248.5362	4248.5355	0.0007	2
3	1	3	2	1	2	4306.9637	4306.9600	0.0037	1
3	0	3	2	0	2	4384.1554	4384.1574	-0.0020	1
3	2	2	2	2	1	4392.2825	4392.2846	-0.0021	1
3	2	1	2	2	0	4400.3952	4400.3925	0.0027	1
3	1	2	2	1	1	4475.0351	4475.0358	-0.0007	1
3	1	3	2	0	2	5384.5133	5384.5120	0.0013	1
3	1	2	2	0	2	5720.7197	5720.7200	-0.0003	2
4	1	4	3	1	3	5740.3289	5740.3257	0.0032	1
4	0	4	3	0	3	5836.1724	5836.1730	-0.0006	1

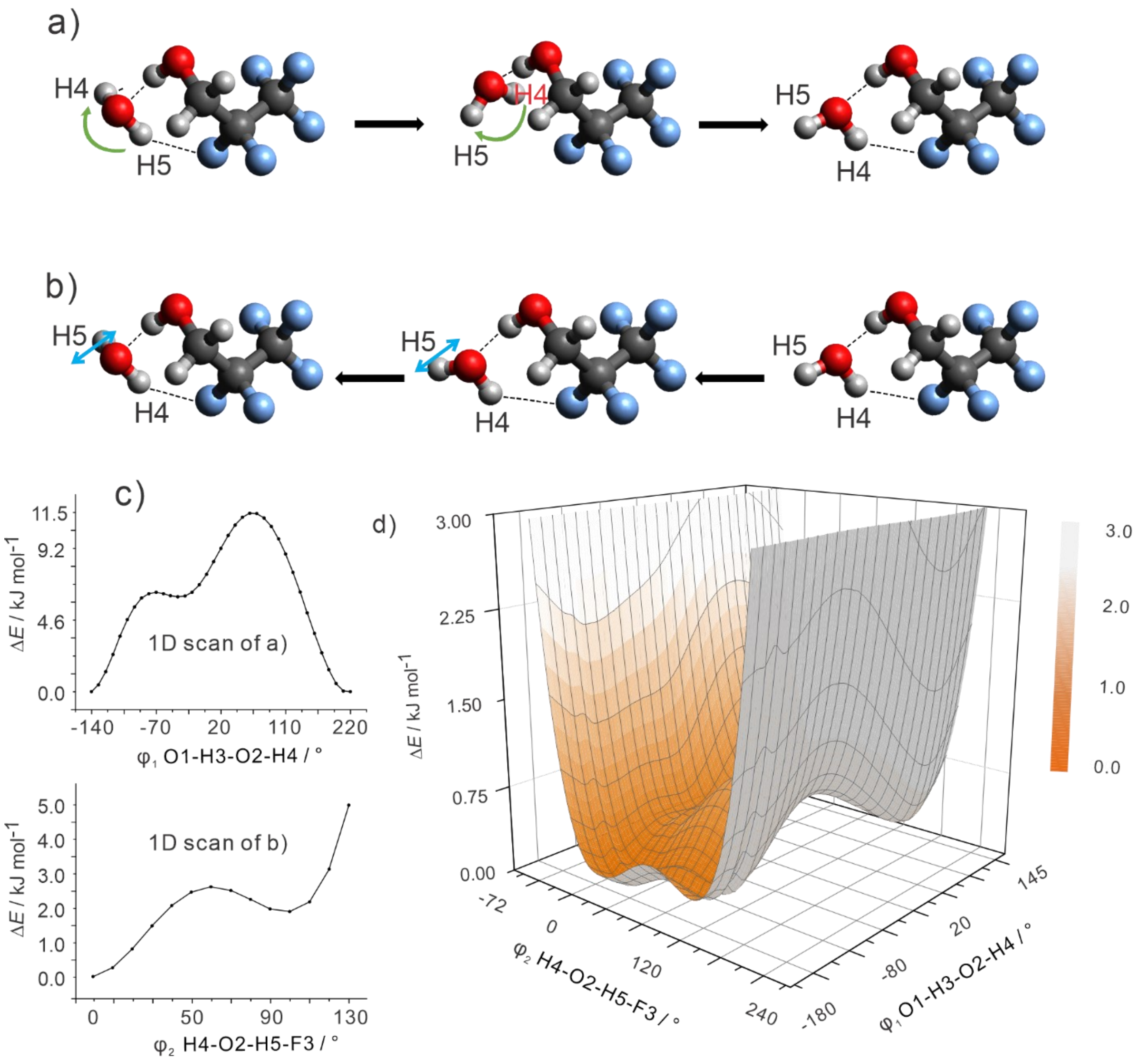

Figure S7.5. The two water-centered motions of **PFP***G*+*g*+···W$_{H}$ which exchange the two equivalent H atoms of the water subunit: a) rotation about the intermolecular hydrogen bond and b) wagging of the free OH of water from down to up, returning to the original geometry. c) 1D cut along φ$_1$ = H5-O2-H3-O1 dihedral angle and along φ$_2$ = H4-O2-H5-F3 dihedral angle. d) The 3D presentation of the 2D rigid PES scans associated with two water motions shown in a) and b) along φ$_1$ and φ$_2$ at the B3LYP-D3(BJ)/def2-QZVP level. After applying *ZPE* and *BSSE* energy corrections, the wagging motion is barrierless.

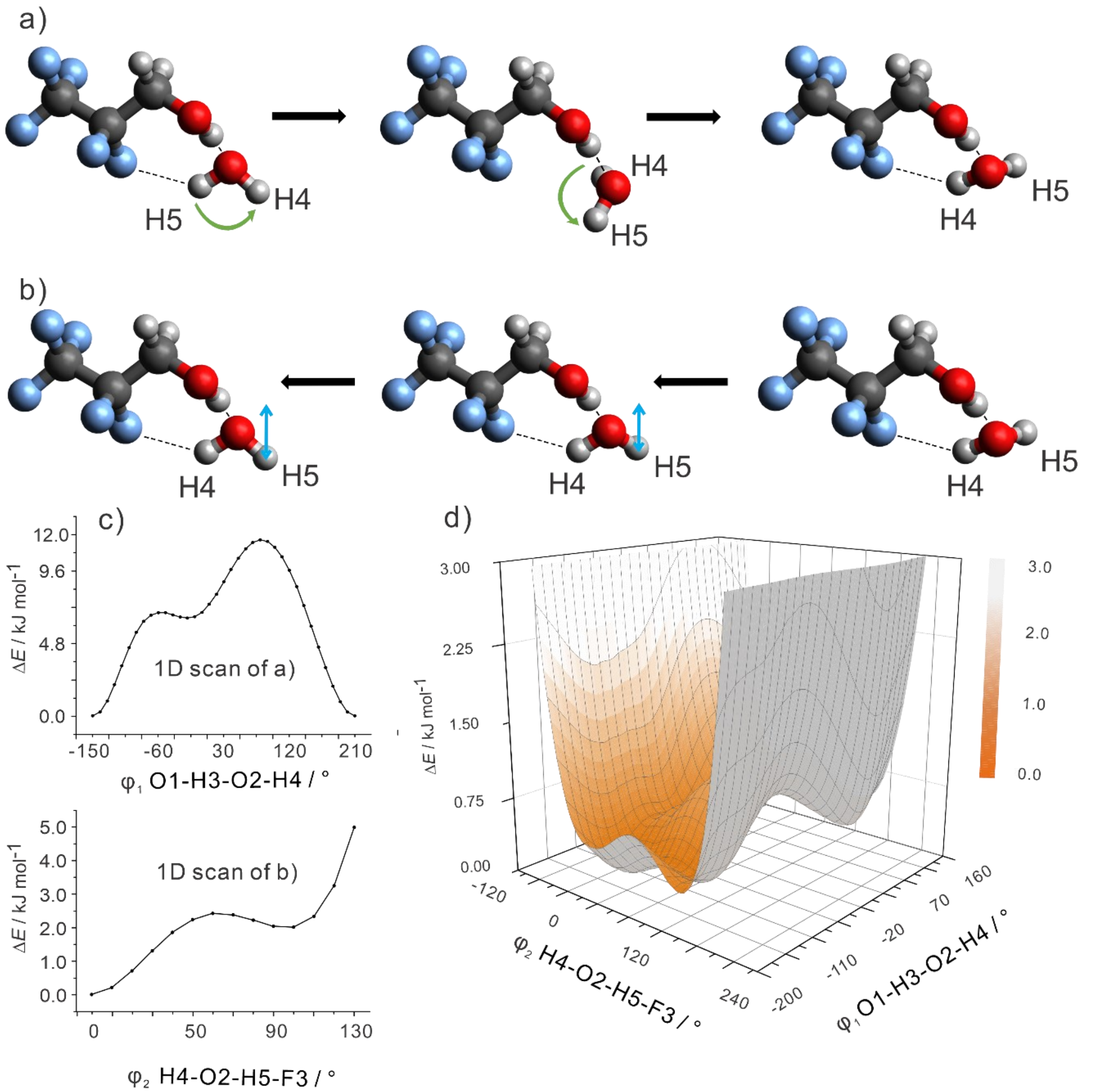

Figure S7.6. The two water-centered motions of **PFP***Tg*+···W_H which exchange the two equivalent H atoms of the water subunit: a) rotation about the intermolecular hydrogen bond and b) wagging of the free OH of water from down to up, returning to the original geometry. c) 1D cut along φ_1 = H5-O2-H3-O1 dihedral angle and along φ_2 = H4-O2-H5-F3 dihedral angle. d) The 3D presentation of the 2D rigid PES scans associated with two water motions shown in a) and b) along φ_1 and φ_2 at the B3LYP-D3(BJ)/def2-QZVP level. After applying *ZPE* and *BSSE* energy corrections, the wagging motion is barrierless.

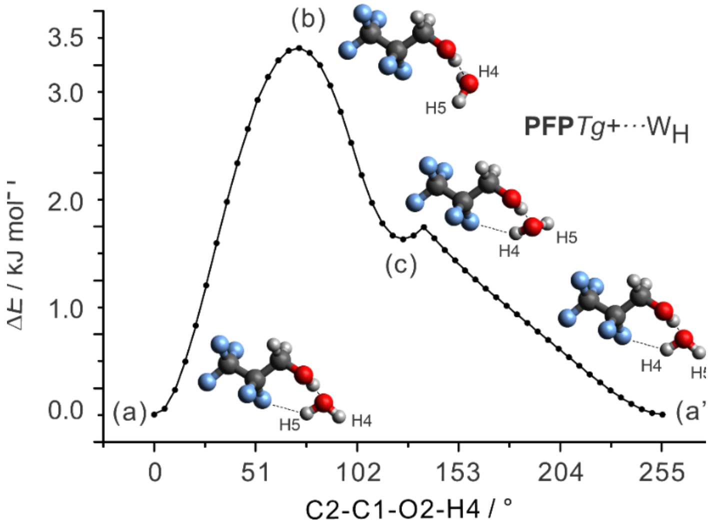

Figure S7.7. The relaxed 1D PES scan along the dihedral angle of C2-C1-O2-H4 (see Figure 2 for atom numbering) for **PFP***Tg*+···W$_\mathrm{H}$. (a) and (a′) are the equivalent minimum energy geometries. See the text for discussions.

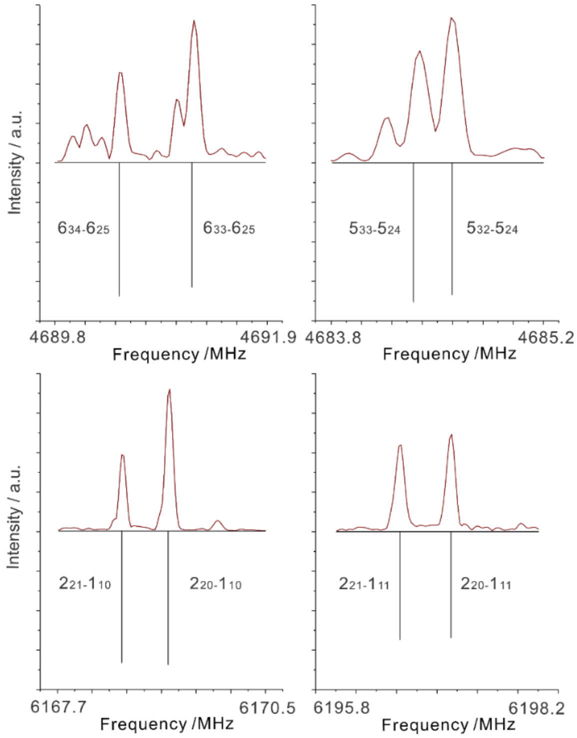

Figure S7.8. Sections of broadband rotational spectra of the **PFP***G*+*g*+···W$_\mathrm{H}$ species whose *b*- and *c*-type lines with similar intensities, despite the drastically different calculated μ_b (0.0 D) and μ_c (1.7 D) dipole moment components. The simulated line intensities of these transitions shown are done with the estimated $\mu_b = \mu_c = 0.5$ D.

Table S7.23. Predicted dipole moment components of **PFP***G*+*g*+⋯W at a 10° stepwise based on the relaxed scan shown in Figure 4 at the B3LYP-D3(BJ)/def2-QZVP level of theory.

Points	Angle /°	Dipole moments			Points	Angle /°	Dipole moments		
		μ_a	μ_b	μ_c			μ_a	μ_b	μ_c
1	12.46	2.2	0.1	-1.3	14	142.46	3.2	1.5	-0.7
2	22.46	2.0	0.1	-1.3	15	152.46	3.2	1.4	-0.8
3	32.46	1.8	0.1	-1.4	16	162.46	3.2	1.3	-0.8
4	42.46	1.6	0.2	-1.5	17	172.46	3.2	1.2	-0.9
5	52.46	1.5	0.3	-1.6	18	182.46	3.2	1.1	-1.0
6	62.46	1.6	0.5	-1.7	19	192.46	3.2	0.9	-1.0
7	72.46	1.7	0.8	-1.7	20	202.46	3.2	0.8	-1.1
8	82.46	1.9	1.1	-1.7	21	212.46	3.1	0.6	-1.1
9	92.46	2.1	1.6	-1.5	22	222.46	3.0	0.5	-1.2
10	102.46	2.4	2.0	-1.0	23	232.46	2.9	0.3	-1.2
11	112.46	2.6	2.2	-0.6	24	242.46	2.7	0.2	-1.2
12	122.46	2.9	2.2	-0.4	25	252.46	2.5	0.1	-1.2
13	132.46	3.2	2.0	-0.5	26	262.46	2.2	0.0	-1.2

Table S7.24. Predicted dipole moments of the **PFP***Tg*+(OH)···W monohydrate species calculated at a 10° stepwise of an H_2O internal rotational relaxed scan based on Figure 2 ii) at the B3LYP-D3(BJ)/def2-QZVP level of theory.

Points	Angle /°	Dipole moments			Points	Angle /°	Dipole moments		
		μ_a	μ_b	μ_c			μ_a	μ_b	μ_c
1	5.33	2.1	-1.7	-0.1	14	135.33	1.7	-2.8	-1.8
2	15.33	1.9	-1.8	-0.1	15	145.33	1.9	-2.7	-0.8
3	25.33	1.7	-1.8	-0.1	16	155.33	2.0	-2.7	-0.7
4	35.33	1.4	-1.8	-0.2	17	165.33	2.1	-2.6	-0.6
5	45.33	1.3	-1.9	-0.3	18	175.33	2.2	-2.5	-0.6
6	55.33	1.2	-2.1	-0.4	19	185.33	2.3	-2.5	-0.5
7	65.33	1.1	-2.2	-0.6	20	195.33	2.3	-2.4	-0.5
8	75.33	1.0	-2.3	-0.9	21	205.33	2.4	-2.3	-0.4
9	85.33	0.9	-2.4	-1.2	22	215.33	2.4	-2.2	-0.3
10	95.33	0.8	-2.5	-1.4	23	225.33	2.4	-2.0	-0.3
11	105.33	0.8	-2.6	-1.7	24	235.33	2.3	-1.9	-0.2
12	115.33	1.0	-2.6	-1.8	25	245.33	2.2	-1.8	-0.1
13	125.33	1.3	-2.7	-1.9	26	255.33	2.0	-1.7	-0.1

Table S7.25. Experimental substitution and calculated equilibrium coordinates of **PFP**G+g+···W_H.

Coord.	|Exp.| [a]	Theory[b]	Coord.	|Exp.| [a]	Theory[b]
PFPg+g+(OH)···H_2O as parent			PFPg+g+ (OD)···D_2O as parent		
	H3			D3	
a	2.16865(69)	2.2485	*a*	2.0560(38)	2.1909
b	0.7449(20)	-0.5989	*b*	0.8832(90)	-0.5269
c	0.4561 (33)	0.6907	*c*	0.670(11)	0.7638
	H4			D4	
a	4.15430(36)	3.8808	*a*	3.52325(43)	3.8663
b	0.6861(22)	-1.0382	*b*	0.7251(21)	-0.9961
c	1.1230(13)	-1.0956	*c*	1.3482(11)	-0.9742
	H5			D5	
a	2.82701(53)	2.8155	*a*	2.78843(54)	2.7898
b	0.2167(69)	0.0234	*b*	0.1728(88)	0.0355
c	1.3682(11)	-1.4113	*c*	1.3064(12)	-1.3462

[a] Absolute experimental substitution coordinates with Costain errors in brackets. Atom numbering is provided in Figure 7.2. See the main text for discussions.

[b] Equilibrium coordinates of the parent species in its principal inertial axis system. The equilibrium geometry was optimized at the B3LYP(BJ)/def2-QZVP level.

Table S7.26. Experimental substitution and calculated equilibrium coordinates of **PFP**_Tg_+···W$_H$.

Coord.	|Exp.| [a]	Theory[b]	Coord.	|Exp.| [a]	Theory[b]
PFP_Tg_+(OH)···H$_2$O as parent			PFP_Tg_+(OD)···D$_2$O as parent		
	H3			D3	
a	2.65193(57)	2.6681	*a*	2.60645(58)	2.5972
b	0.4106(H37)	0.5646	*b*	0.4799(32)	0.6352
c	0.3162(48)	-0.3328	*c*	0.3109(49)	-0.3282
	H4			D4	
a	4.18394(37)	4.3536	*a*	4.19227(36)	4.3173
b	1.4238(11)	-1.1645	*b*	1.2862(12)	-1.0748
c	0.141(11)	0.2321	*c*	0.147(10)	0.1885
	H5			D5	
a	2.59993(59)	2.8808	*a*	2.63123(58)	2.8524
b	1.67199(91)	-1.51928	*b*	1.58997(96)	-1.4640
c	0.5909(26)	0.49338	*c*	0.5593(27)	0.4451

[a] Absolute experimental substitution coordinates with Costain errors in brackets. Atom numbering is provided in Figure 7.2. See the main text for discussions.

[b] Equilibrium coordinates of the parent species in its principal inertial axis system. The equilibrium geometry was optimized at the B3LYP(BJ)/def2-QZVP level.

Table S7.27. Predicted (at the B3LYP-D3(BJ)/def2-QZVP level) and experimental rotational constants and the principal moments of inertia of the *ortho*-parent **PFP***G*+*g*+(OH)···W isotopologues.

PFP*G*+*g*+		Water H_2O						Relative to
		A^a	B^a	C^a	I_a^b	I_b^b	I_c^b	
exp	i) OH	1779.5924	857.8316	829.8191	283.9858	589.1355	609.0231	-
cal		1730.5354	874.4153	846.7463	292.0362	577.9622	596.8482	
		A^a	B^a	C^a	ΔI_a^c	ΔI_b^c	ΔI_c^c	
exp	ii) OD	1774.8853	850.7198	822.6891	0.7531	4.9250	5.2782	To i)
cal		1725.6155	866.1235	839.0263	0.8326	5.5331	5.4917	
		Water HOD5						
		A^a	B^a	C^a	ΔI_a^c	ΔI_b^c	ΔI_c^c	
exp	iii) OH	1767.9090	843.6788	818.9182	1.8767	9.8828	8.1070	To i)
cal		1718.9129	859.7049	835.6644	1.9746	9.8895	7.9149	
exp	iv) OD	1761.1212	836.9288	812.0556	1.1018	4.8312	5.2152	To iii)
cal		1713.7599	851.7835	828.2958	0.8840	5.4669	5.3800	
		Water HOD4						
		A^a	B^a	C^a	ΔI_a^c	ΔI_b^c	ΔI_c^c	
exp	v) OH	1769.3373	831.6345	806.1763	1.6460	18.5582	17.8609	To i)
cal		1718.5511	849.8526	823.8469	2.0365	16.7044	16.5898	
exp	vi) OD	1765.2513	825.0767	799.6625	0.6611	4.8300	5.1064	To v)
cal		1713.6439	842.0432	816.7989	0.8421	5.5151	5.2933	
		Water D_2O						
		A^a	B^a	C^a	ΔI_a^c	ΔI_b^c	ΔI_c^c	
exp	vii) OH	1761.9400	818.5982	796.1209	2.8452	28.2358	25.7788	To i)
cal		1707.7588	836.1579	813.3943	3.8949	26.4440	24.4728	
exp	viii) OD	1754.2636	812.3708	789.8597	1.2551	4.7325	5.0321	To vii)
cal		1702.6196	828.6795	806.6690	0.8932	5.4544	5.1800	

[a] Rotational constants in MHz.
[b] Principal moments of inertia in amu Å^2.
[c] Differences in pricipal moments of inertia to the parent species.

Table S7.28. Predicted (at the B3LYP-D3(BJ)/def2-QZVP level) and experimental rotational constants and the principal moments of inertia of the ortho-parent **PFP***Tg*+(OH)···W isotopologues.

PFP*Tg*+		**Water H_2O**						Relative to
		A[a]	B[a]	C[a]	I_a[b]	I_b[b]	I_c[b]	
exp	i) OH	1929.0069	798.4361	741.4388	261.9892	632.9611	681.6193	-
cal		1953.9374	789.5000	738.7142	258.6465	640.1254	684.1333	
		A[a]	B[a]	C[a]	ΔI_a[c]	ΔI_b[c]	ΔI_c[c]	
exp	ii) OD	1927.0625	789.5158	733.6681	0.2644	7.1515	7.2195	To i)
cal		1950.7562	780.6736	730.7637	0.4218	7.2373	7.4432	
		Water HOD5						
		A[a]	B[a]	C[a]	ΔI_a[c]	ΔI_b[c]	ΔI_c[c]	
exp	iii) OH	1906.4806	789.5092	731.1405	3.0956	7.1569	9.6008	To i)
cal		1935.2467	779.0533	727.4160	2.4980	8.5838	10.6260	
exp	iv) OD	1904.2725	780.8608	723.6055	0.3074	7.0896	7.1977	To iii)
cal		1931.7364	770.6106	719.7876	0.4745	7.1071	7.3631	
		Water HOD4						
		A[a]	B[a]	C[a]	ΔI_a[c]	ΔI_b[c]	ΔI_c[c]	
exp	v) OH	1914.6915	776.7687	720.7372	1.9588	17.6561	19.5780	To i)
cal		1943.8342	766.6542	717.4058	1.3443	19.0754	20.3201	
exp	vi) OD	1912.5507	768.4893	713.4935	0.2954	7.0094	7.1189	To v)
cal		1940.2987	758.5311	710.0360	0.4737	7.0594	7.3120	
		Water D_2O						
		A[a]	B[a]	C[a]	ΔI_a[c]	ΔI_b[c]	ΔI_c[c]	
exp	vii) OH	1894.0258	768.1106	711.0510	4.8387	24.9897	29.1300	To i)
cal		1926.3052	756.8588	706.9004	3.7102	27.6068	30.7892	
exp	viii)OD	1891.6444	760.0732	704.0240	0.3359	6.9575	7.0942	To vii)
cal		1922.4525	749.0827	699.8187	0.5258	6.9317	7.2346	

[a] Rotational constants in MHz.

[b] Principal moments of inertia in amu Å^2.

[c] Differences in pricipal moments of inertia to the parent species.

Table S7.29. Percentage errors in the calculated rotational constants of **PFP***G*+*g*+⋯W$_H$ and its deuterated isotopologues species.

Isotopologues	*A /MHz*	(% [a])	*B /MHz*	(% [a])	*C/MHz*	(% [a])
PFP*G*+*g*+⋯H_2O	1730.5	2.8	874.4	-1.9	846.7	-2.0
PFP*G*+*g*+⋯HOD5	1718.9	2.8	859.7	-1.9	835.7	-2.0
PFP*G*+*g*+⋯HOD4	1718.6	2.9	849.9	-2.2	823.8	-2.2
PFP*G*+*g*+⋯D_2O	1707.8	3.1	836.2	-2.1	813.4	-2.2
PFP*G*+*g*+ (OD)⋯H_2O	1725.6	2.8	866.1	-1.8	839.0	-2.0
PFP*G*+*g*+(OD)⋯HOD5	1713.8	2.7	851.8	-1.8	828.3	-2.0
PFP*G*+*g*+ (OD)⋯HOD4	1713.6	2.9	842.0	-2.1	816.8	-2.1
PFP*G*+*g*+(OD)⋯D_2O	1702.6	2.9	828.7	-2.0	806.7	-2.1

[a] The percentage error = 100 *(exp. – calc.) / exp.

Table S7.30. Percentage errors in the calculated rotational constants of **PFP***Tg*+⋯W$_H$ and its deuterated isotopologues species.

Isotopologues	*A /MHz*	(% [a])	*B /MHz*	(% [a])	*C/MHz*	(% [a])
PFP*Tg*+⋯H_2O	1953.9	-1.3	789.5	1.1	738.7	0.4
PFP*Tg*+⋯HOD5	1935.2	-1.5	779.1	1.3	727.4	0.5
PFP*Tg*+⋯HOD4	1943.8	-1.5	766.7	1.3	717.4	0.5
PFP*Tg*+⋯D_2O	1926.3	-1.7	756.9	1.5	706.9	0.6
PFP*Tg*+(OD)⋯H_2O	1950.8	-1.2	780.7	1.1	730.8	0.4
PFP*Tg*+(OD)⋯HOD5	1931.7	-1.4	770.6	1.3	719.8	0.5
PFP*Tg*+(OD)⋯HOD4	1940.3	-1.5	758.5	1.3	710.0	0.5
PFP*Tg*+(OD)⋯D_2O	1922.5	-1.6	749.1	1.4	699.8	0.6

[a] The percentage error = 100 *(exp. – calc.) / exp.

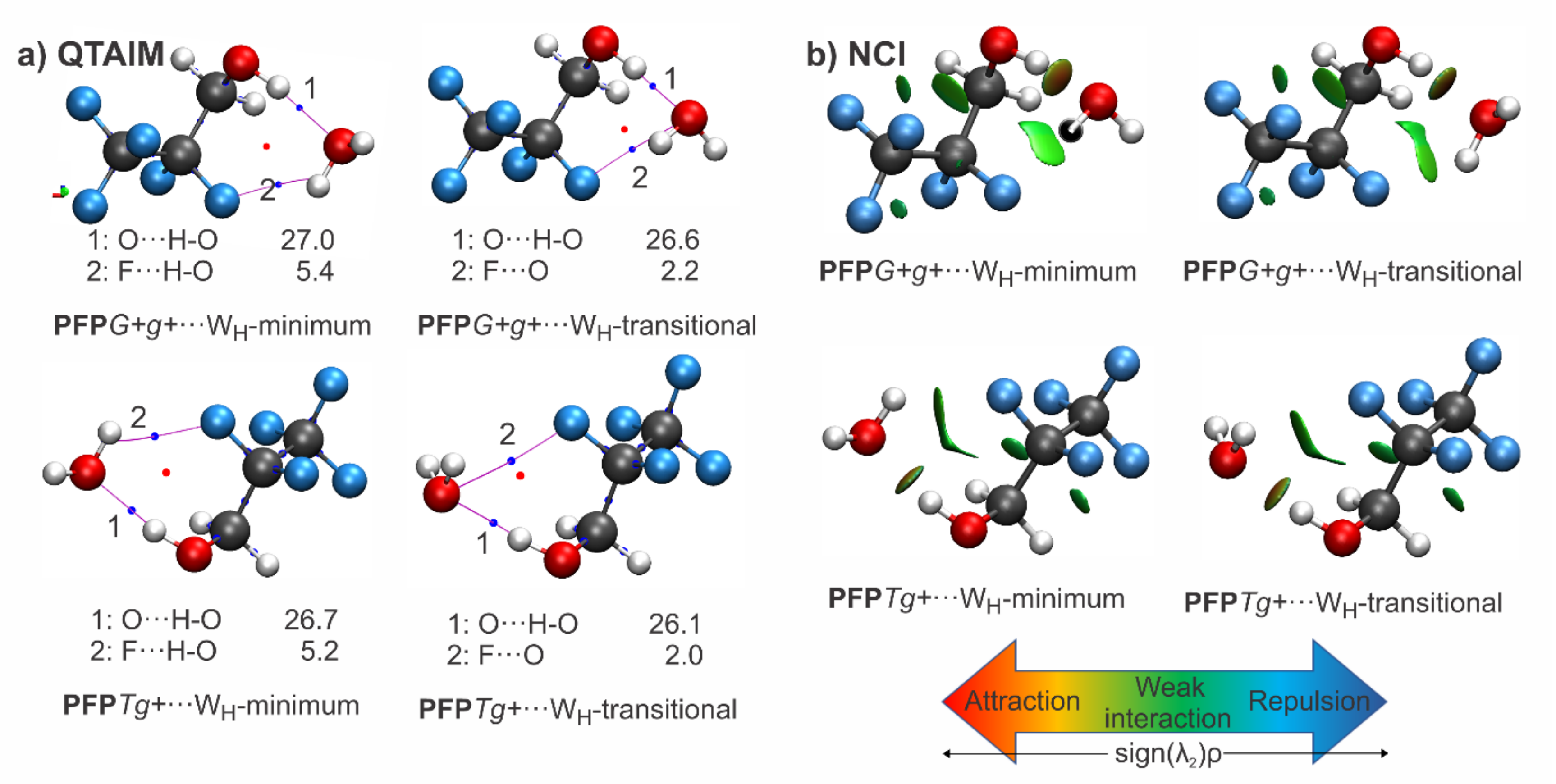

Figure S7.9. The QTAIM and NCI results of the **PFP***G*+*g*+⋯W_H and **PFP***Tg*+⋯W_H conformers and the related water tunneling transition states at the B3LYP-D3(BJ)/def2-QZVP level of theory.

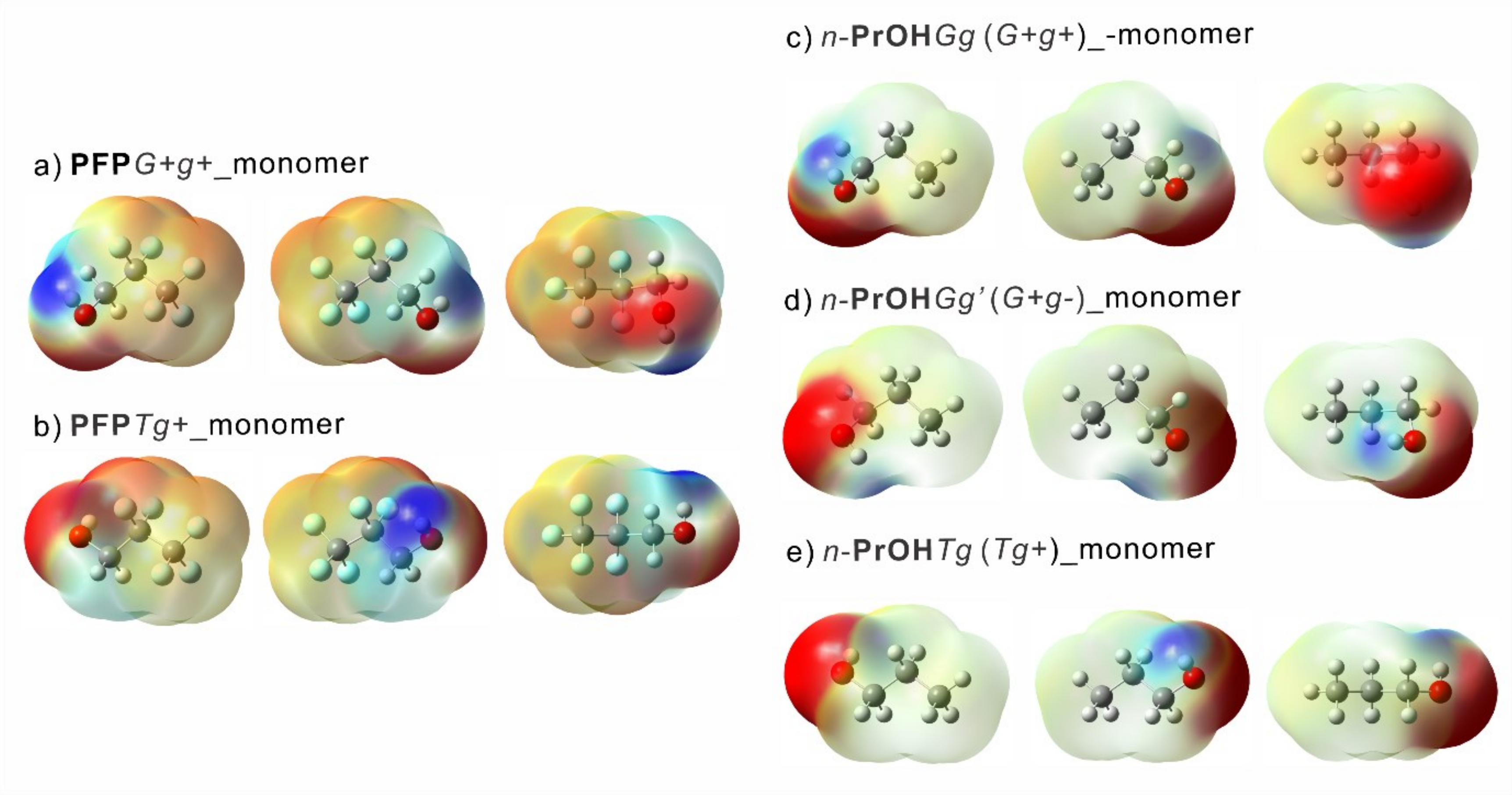

Figure S7.10. The ESP mapped onto a total electron density isosurface at the same value ranges are shown for a) **PFP***G+g+*, b) **PFP***Tg+*, c) n-PrOH*Gg* (*G+g+*) d) n-PrOH*Gg'* (*G+g-*) and e) n-PrOH *Tg* (*Tg+*) calculated at the B3LYP-D3(BJ)/def2-QZVP level of theory, ordering with the PFP and *n*-PrOH monomer stabilities, respectively. Each is shown in three views with the hydroxyl O on left side, with the hydroxyl O on right side, and with the C-C-C chain lying horizontally. Red indicates negative electrostatic potential and blue positive electrostatic potential. Completion of reference 29.

Gaussian 16, Revision C.01, M. J. Frisch, G. W. Trucks, H. B. Schlegel, G. E. Scuseria, M. A. Robb, J. R. Cheeseman, G. Scalmani, V. Barone, G. A. Petersson, H. Nakatsuji, X. Li, M. Caricato, A. V. Marenich, J. Bloino, B. G. Janesko, R. Gomperts, B. Mennucci, H. P. Hratchian, J. V. Ortiz, A. F. Izmaylov, J. L. Sonnenberg, D. Williams-Young, F. Ding, F. Lipparini, F. Egidi, J. Goings, B. Peng, A. Petrone, T. Henderson, D. Ranasinghe, V. G. Zakrzewski, J. Gao, N. Rega, G. Zheng, W. Liang, M. Hada, M. Ehara, K. Toyota, R. Fukuda, J. Hasegawa, M. Ishida, T. Nakajima, Y. Honda, O. Kitao, H. Nakai, T. Vreven, K. Throssell, J. A. Montgomery, Jr., J. E. Peralta, F. Ogliaro, M. J. Bearpark, J. J. Heyd, E. N. Brothers, K. N. Kudin, V. N. Staroverov, T. A. Keith, R. Kobayashi, J. Normand, K. Raghavachari, A. P. Rendell, J. C. Burant, S. S. Iyengar, J. Tomasi, M. Cossi, J. M. Millam, M. Klene, C. Adamo, R. Cammi, J. W. Ochterski, R. L. Martin, K. Morokuma, O. Farkas, J. B. Foresman, and D. J. Fox, Gaussian, Inc., Wallingford CT, 2016.